Disease Mechanisms in Mitochondrial Maintenance Disorders

Kamil Sebastian Sitarz

MSc

Thesis submitted to Newcastle University in candidature for the Degree of Doctor of Philosophy

Institute of Genetic Medicine

Faculty of Medical Sciences

Newcastle University

September 2012

This thesis is dedicated to my beloved wife Agnieszka

and our dearest daughters Zuzia and Gabrysia

for their constant support and unconditional love.

Abstract

OPA1 and MFN2 are two critical mitochondrial membrane proteins required for mitochondrial fusion. *OPA1* mutations account for approximately 60% of cases of autosomal-dominant optic atrophy (DOA) and up to 20% of mutational carriers develop a more severe multi-systemic neurological phenotype (DOA+) in addition to visual failure. *MFN2* mutations result in Charcot-Marie-Tooth disease type 2A (CMT-2A) and in a subgroup of patients, the peripheral neuropathy is complicated by optic atrophy, highlighting a degree of phenotypic overlap with DOA+. *POLG1* encodes the catalytic subunit of DNA polymerase gamma (POLG) and *POLG1*-related diseases are clinically highly heterogeneous, ranging from early-onset Alpers-Huttenlocher syndrome to late-onset isolated chronic progressive external ophthalmoplegia. *OPA1*, *MFN2* and *POLG1* mutations all result in disturbed mitochondrial DNA (mtDNA) maintenance, with both quantitative (depletion) and qualitative (point mutations and deletions) mtDNA abnormalities having been identified in patient tissue samples. In this PhD project, the disease mechanisms underpinning these nuclear mitochondrial disorders have been studied further.

OPA1 and *MFN2* mutations were found to result in significant mtDNA proliferation as a likely compensatory mechanism to impaired mitochondrial oxidative phosphorylation. Using a previously-validated repopulation assay, mtDNA replication in cultured *POLG1*-mutant fibroblasts was severely depressed following a period of ethidium bromide-induced mtDNA depletion. A similar observation was made with *OPA1*-mutant fibroblasts, but this effect was not as marked as for *POLG1*-mutant fibroblasts. Significant reorganisation of the mitochondrial network was also apparent for both groups of mutant fibroblasts.

Although neuromyelitis optica (NMO) shares some clinical features with DOA, genetic variations within *OPA1* are not associated with the risk of developing NMO.

Finally, research into DOA and other mitochondrial optic neuropathies have been severely restricted by the lack of the access to retinal ganglion cells (RGCs), precluding direct studies to be performed on the cell type which is preferentially affected in this group of disorders. To circumvent this limitation, human induced pluripotent stem cell (hiPSC) lines have been generated from patient-derived

fibroblasts harbouring confirmed *OPA1* mutations. The future differentiation of these induced pluripotent stem cell lines into RGCs will hopefully provide a powerful and versatile tool for disease modelling and the development of targeted therapeutic strategies.

Acknowledgements

First and foremost, I owe my sincerest gratitude to my supervisors, Prof. Patrick Chinnery and Dr Rita Horvath for providing me with the opportunity to undertake this PhD project. I am grateful for their thought-provoking guidance, inspiration and continued support over the past three years. It was the greatest pleasure to be a part of their group.

I would like to address my special thanks to Dr Patrick Yu-Wai-Man, who although not being my official supervisor, has provided me with the inspiring suggestions, continual encouragement and invaluable support throughout the entire course of my PhD. I am grateful for all our constructive discussions and the helpful feedback on the drafts of this thesis.

I would like to express my appreciation to all the collaborators I had the pleasure to work with. I owe my gratitude to the members of Prof Majlinda Lako's Stem Cell Group for their continuous willingness to help. At this point, I would like to thank especially Dr Katarzyna Tilgner, for her excellent assistance with the stem cell culture, her patience, and most importantly, for her friendship. My acknowledgements also extend to Dr David Samuels for offering me support with the statistical analyses, and all the members of the Mitochondrial Diagnostic Service (Newcastle upon Tyne) for providing me with the patient tissue samples.

A special mention is also deserved by all my fellow colleagues from the PFC group for making the working environment so friendly. I owe many thanks to Drs Angela Pyle and Gavin Hudson, who have been a great support during my PhD. I would also like to thank Phillippa "Pip" Carling and Gerald "Gerry" Pfeffer, for all these great chats we have had over the much-needed cups of coffee.

I would like to extend my deepest gratitude to my parents for all their love, constant understanding and endless support in every situation of my life.

Lastly, and most importantly, I would like to express my love and appreciation to my wonderful wife, Agnieszka. You gave me the strength to face all the difficulties and you were always by my side during ups and downs. I am so lucky to have you as my best friend, my soul-mate and my wife.

Author's Declaration

This thesis is submitted for the degree of Doctor of Philosophy in Newcastle University. The research detailed inside was performed in the Mitochondrial Research Group within Institute of Genetic Medicine under the supervision and guidance of Prof. Patrick Chinnery and Dr Rita Horvath, between September 2009 and August 2012.

I hereby declare that none of the material presented in this thesis has been previously submitted by me for a degree or any other qualification at this or any other University. Furthermore, it is my own independent work, unless stated otherwise.

Kamil S. Sitarz

List of Contents

Table of Contents

List of Figures

Chapter 1

Chapter 3

Chapter 4

Chapter 5

Chapter 7

Chapter 8

Appendix B.1

Appendix B.2

Appendix C.1

Appendix C.2

List of Tables

Chapter 1

Chapter 3

Chapter 4

Chapter 6

Chapter 7

Chapter 8

Appendix A

List of Publications

1. **Sitarz K.S.**, Almind G.J., Horvath R., Czermin B., Grønskov K., Pyle A., Taylor R.W., Larsen M., Chinnery P.F., Yu-Wai-Man P., 2012. OPA1 mutations induce mtDNA proliferation in leukocytes of patients with dominant optic atrophy. Neurology. 79: 1515-1517.
2. **Sitarz, K.S.**, Yu-Wai-Man, P., Pyle, A., Stewart, J.D., Rautenstrauss, B., Seeman, P., Reilly, M.M., Horvath, R., Chinnery, P.F., 2012. MFN2 mutations cause compensatory mitochondrial DNA proliferation. Brain. 135: 1-3.
3. **Sitarz K.S.**, Yu-Wai-Man P., Hudson G., Jacob A., Boggild M., Horvath R., Chinnery P.F., 2011. Genetic variations within the OPA1 gene are not associated with neuromyelitis optica. Multiple Sclerosis. 18(2): 240-243.
4. **Sitarz K.S.**, Chinnery P.F., Yu-Wai-Man P., 2012. Disorders of the optic nerve in mitochondrial cytopathies: new ideas on pathogenesis and therapeutic targets. Current Neurology and Neuroscience Reports. 12(3): 308-17.
5. Yu-Wai-Man, P., **Sitarz K.S.**, Samuels D.C., Griffiths P.G., Reeve A.K., Bindoff L.A., Horvath R., Chinnery P.F., 2010. OPA1 mutations cause cytochrome c oxidase deficiency due to loss of wild-type mtDNA molecules. Human Molecular Genetics. 19(15): 3043-52.
6. Stewart, J.D., Schoeler, S., **Sitarz, K.S.**, Horvath, R., Hallmann, K., Pyle, A., Yu-Wai-Man, P., Taylor, R.W., Samuels, D.C., Kunz, W.S., Chinnery, P.F., 2011. POLG mutations cause decreased mitochondrial DNA repopulation rates following induced depletion in human fibroblasts. Biochimica et Biophysica Acta. 1812(3): 321-5.

Abbreviations

~	Approximately
µl	Microlitre
µm	Micrometer
µM	Micromole
2D-AGE	Two-dimensional agarose gel electrophoresis
AA	Amino acid
ad	Autosomal dominant
ADP	Adenosine diphosphate
AHS	Alpers-Huttenlocher syndrome
AQP4	Aquaporin-4
ar	Autosomal recessive
ATAD3	ATPase family AAA domain-containing 3
ATP	Adenosine triphosphate
B2M	Beta-2-microglobulin
BER	Base excision repair
BNSU	British Neurological Surveillance Unit
bp	Base pair
CC	Coiled-coil
cDNA	Complementary DNA
CF	Counting fingers
CI	Confidence interval
CMT	Charcot-Marie-Tooth
CNS	Central nervous system
COX	Cytochrome *c* oxidase
CPEO	Chronic progressive external ophthalmoplegia
CREB	cAMP response element-binding protein
Ct	Threshold cycle
DAB	3,3'- diaminobenzidine tetrahydrochloride
DTT	Dithiothreitol
dH_20	Distilled water
DMEM	Dulbecco's Modified Eagle Medium
DMSO	Dimethylsulphoxide

DNA	Deoxyribonucleic acid
dNTP	Deoxyribonucleotide triphosphate
DOA	Dominant optic atrophy
DOA+	Dominant optic atrophy plus
dRP	Deoxyribose phosphate
DRP1	Dynamin-related protein 1
DSB	Double-stranded break
E	Efficiency
EB	Embryoid body
ECC	Embryonal carcinoma cell
EDTA	Ethylenediaminetetraacetic acid
$EF\text{-}G1_{mt}$	Mitochondrial elongation factor G1
$EF\text{-}G2_{mt}$	Mitochondrial elongation factor G2
$EF\text{-}Ts_{mt}$	Mitochondrial elongation factor Ts
$EF\text{-}Tu_{mt}$	Mitochondrial elongation factor Tu
EGC	Embryonic germ cell
ER	Endoplasmic reticulum
ERR	Estrogen-related receptor
ESC	Embryonic stem cell
EtBr	Ethidium bromide
EtOH	Ethanol
FAD	Flavin adenine dinucleotide
$FADH_2$	Reduced flavin adenine dinucleotide
FBS	Fetal bovine serum
FMN	Flavin mononucleotide
GABP	GA-binding protein
GAPDH	Glyceraldehyde 3-phosphate dehydrogenase
GED	GTPase effector domain
GpC	Gapped circle
H^+	Proton
H&E	Haematoxylin and eosin
HBSS	Hank’s Balanced Salt Solution
hESC	Human embryonic stem cell
hFis1	Mitochondrial fission 1
hiPSC	Human induced pluripotent stem cell

HM	Hand movement
HR	Heptad-repeat
HSP	Heavy-strand promoter
HSP	Hereditary spastic paraplegia
H-strand	Heavy-strand
HTG	High tension glaucoma
hUbC	Human ubiquitin C
ICM	Inner cell mass
$IF2_{mt}$	Mitochondrial translation initiation factor 2
$IF3_{mt}$	Mitochondrial translation initiation factor 3
IMM	Inner mitochondrial membrane
IMS	Intermembrane space
iPSC	Induced pluripotent stem cell
IUPAC	International Union of Pure and Applied Chemistry
IVF	*In vitro* fertilisation
kb	kilobase
LHON	Leber hereditary optic neuropathy
LS	Leigh syndrome
LSP	Light-strand promoter
LogMAR	Logarithm of the minimum angle of resolution
l-OPA1	Long-OPA1
L-strand	Light-strand
M	Mole
MEF	Mouse embryonic fibroblast
MELAS	Mitochondrial myopathy, encephalopathy, lactic acidosis, and stroke-like episodes
MEM	Minimum Essential Media
MERRF	Myoclonic epilepsy and ragged red fibres
MFN1	Mitofusin-1
MFN2	Mitofusin-2
MILS	Maternally inherited Leigh syndrome
MIRAS	Mitochondrial recessive ataxia syndrome
MIS	Mitochondrial import sequence
ml	Mililitre
mM	Milimole

MOI	Multiplicity of infection
mPGK	Murine phosphoglycerate kinase
mRNA	Messenger RNA
MRP	Mitochondrial ribosomal protein
mtDNA	Mitochondrial DNA
MTERF1	Mitochondrial transcription terminator factor 1
mtSSB	Mitochondrial single-stranded binding protein
N.A.	Numeric aperture
N/A	Non applicable
NAD^+	Nicotinamide adenine dinucleotide
NADH	Reduced nicotinamide adenine dinucleotide
NARP	Neurogenic weakness, ataxia, and retinitis pigmentosa
NBT	Nitroblue tetrazolium
NCBI	National Centre for Biotechnology Information
nDNA	Nuclear DNA
ng	Nanogram
nM	Nanomole
NMO	Neuromyelitis optica
NRF	Nuclear respiratory factor
NRTI	Nucleoside reverse-transcriptase inhibitor
NS	Non-significant
NTG	Normal tension glaucoma
OD	Oculus deuter
Oh	Heavy-strand origin of replication
OL	Light-strand origin of replication
OMM	Outer mitochondrial membrane
OPA1	Optic atrophy 1
OriZ	Single zone of replication initiation
OS	Oculus sinister
OXPHOS	Oxidative phosphorylation
PAM	Translocase-associated motor
PARL	Presenilin-associated rhomboid like protease
PBS	Phosphate Buffered Solution
PBS	Phosphate buffered solution
PCR	Polymerase chain reaction

PEN	Polyethylene napthalate
PGC	Primordial germ cell
P_i	Inorganic phosphate
PMS	Phenazine methosulphate
POAG	Primary open angle glaucoma
POLG	Catalytic subunit of polymerase γ
POLG2	Accessory subunit of polymerase γ
POLRMT	Mitochondrial RNA polymerase
Polγ	DNA polymerase γ
PPAR	Peroxisome proliferator-activated receptor
PR	Proline-rich
PS	Pearson syndrome
PSF	Point spread function
QH_2	Ubiquinol
qPCR	Quantitative polymerase chain reaction
R^2	Coefficient of determination
RBP	RNA-binding protein
$RF1a_{mt}$	Mitochondrial translation release factor
RFLP	Restriction fragment length polymorphism
RFU	Relative fluorescent unit
RGC	Retinal ganglion cell
RITOLS	Ribonucleotide incorporation throughout the lagging strand
RL	Repopulation level
RNA	Ribonucleic acid
RNFL	Retinal nerve fibre layer
RNS	Reactive nitrogen species
ROCK	Serine/threonine kinase
ROS	Reactive oxygen species
RPE	Retinal pigment epithelium
RRF	Ragged-red fibre
RRF_{mt}	Ribosome recycling factor
rRNA	Ribosomal RNA
RT-PCR	Reverse-transcription polymerase chain reaction
RTT	Rett syndrome
SAM	Sorting and assembly

SANDO	Sensory ataxic neuropathy dysarthria and opthalmoparesis
SD	Standard deviation
SDH	Succinate dehydrogenase; succinate-ubiquinone oxidoreductase
SEM	Standard error of the mean
SeV	Sendai virus
siRNA	Small interfering RNA
SMA	Spinal muscular atrophy
SNP	Single-nucleotide polymorphism
s-OPA1	Short-OPA1
STED	Stimulated emission depletion microscopy
TAE	Tris-acetate EDTA
TCA	Tricarboxylic acid
TFAM	Mitochondrial transcription factor A
TFB1M	Transcription factor B1
TFB2M	Transcription factor B2
TRE	TFAM-responsive element
tRNA	Transfer RNA
U	Unit
UDS	Ultra-deep re-sequencing-by-synthesis
UV	Ultraviolet
v/v	Volume per volume
VA	Visual acuity
VDAC	Voltage dependent anion channels
VPA	Valproic acid
w/v	Weight per volume
$\Delta\Psi m$	Membrane electrical potential

Chapter 1 General Introduction

Table of Contents

1.1 The Mitochondrion

Mitochondria are essential intracellular organelles which form a dynamic network throughout the cell, continuously fusing and breaking apart (Detmer and Chan, 2007). The major function of mitochondria is to supply eukaryotic cells with adequate levels of adenosine triphosphate (ATP) through aerobic respiration, a process referred to as oxidative phosphorylation (OXPHOS). In addition to this fundamental role in energy conversion, mitochondria are involved in numerous other metabolic processes such as β-oxidation of fatty acids, the citric acid cycle, and the biosynthesis of heme, pyrimidines, phospholipids, amino acids and nucleotides (Duchen, 2004; Maechler et al., 2006; McBride et al., 2006; Rossier, 2006). Mitochondria play a distinctive role in the initiation and regulation of apoptosis (Green, 1998), intracellular calcium handling (Gunter et al., 1994; Herrington et al., 1996; Gincel et al., 2001), and the generation of reactive nitrogen species (RNS) and reactive oxygen species (ROS) (Droge, 2002; Balaban et al., 2005). Mitochondria are found within the cytoplasm of most eukaryotic cells and their numbers can vary from a few hundred to several thousand depending on the cell's metabolic requirements (Moyes et al., 1998; Roger and Silberman, 2002).

1.1.1 Origin

According to the endosymbiotic theory, mitochondria evolved from aerobic *Alphaproteobacteria* that were assimilated by primitive glycolytic eubacteria (Margulis, 1971; Lang et al., 1997). The sequencing of human mitochondrial DNA (mtDNA) (Anderson et al., 1981) and the genome of *Alphaproteobacteria* - *Rickettsia prowazekii* (Andersson et al., 1998) have provided solid phylogenomic evidence of a common genetic origin for the mitochondrial and alphaproteobacterial lineages (Gray et al., 1999).

1.1.2 Structure

Each mitochondrion consists of four distinct compartments: an outer mitochondrial membrane (OMM), an inner mitochondrial membrane (IMM), an intermembrane space (IMS), and a matrix contained within the inner mitochondrial membrane (**Figure 1-1**). The outer mitochondrial membrane is a phospholipid bilayer composed

of a number of channel-forming proteins (called porins) or voltage dependent anion channels (VDAC) which form conduits allowing non-specific free diffusion of molecules smaller than 10 kDa. Compared with the outer membrane which has a protein-to-lipid ratio of about 1:1, the inner membrane is more enriched with proteins with a protein-to-lipid ratio of approximately 4:1. This is related to its increased enzymatic and transport functions. The inner membrane lacks porins but it is rich in cardiolipins. These phospholipids are found in mammalian cells almost exclusively within the IMM and they play an essential role in scaffolding enzymatic complexes (Mannella, 2006). Cardiolipins make the inner membrane highly impermeable to most solutes and ions, and therefore molecules from the intermembrane space need to be actively transported into the matrix compartment via specific active transport systems. This transport can be electroneutral, electrogenic, driven by the membrane electrical potential ($\Delta\Psi m$) or a chemical pH difference (Krauss, 2001). In order to increase the effective surface area for ATP production, the inner membrane is compartmentalized into folded structures called cristae (Perkins et al., 1997). The mitochondrial matrix contains soluble enzymes involved in fatty acid β-oxidation and the citric acid cycle. It also encloses mtDNA molecules packed into nucleoids, and the intricate machinery required for mtDNA replication and transcription (Alberts, 1994).

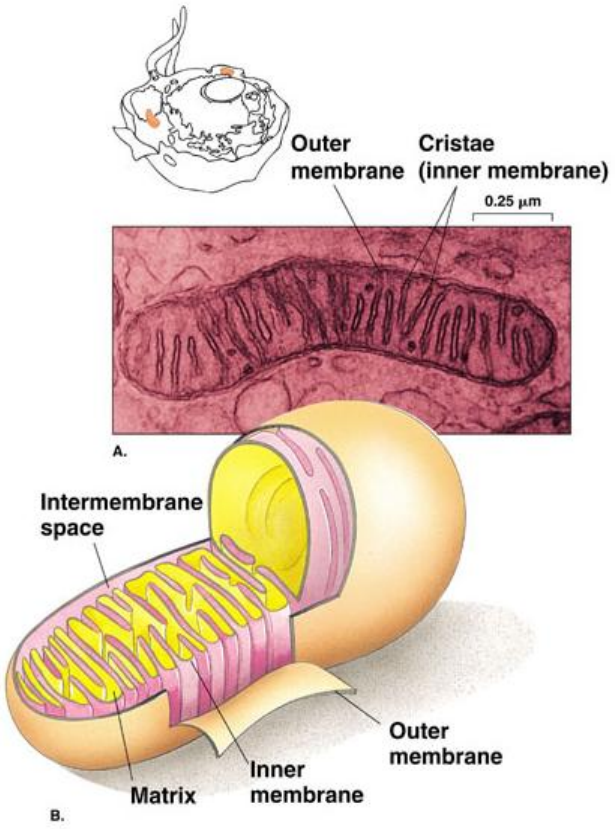

Figure 1-1 General structure of a mitochondrion. (Reproduced from Tobin, 2004).

1.2 Respiratory Chain

Mitochondria are energy-converting organelles that use a transmembrane electrochemical gradient to synthesize ATP molecules from adenosine diphosphate (ADP) and inorganic phosphate (P_i) (Mitchell, 1976). This process is known as oxidative phosphorylation (OXPHOS) and it takes place in the mitochondrial respiratory chain located within the inner mitochondrial membrane. The mitochondrial respiratory chain consists of four transmembrane enzyme complexes (I – IV) and F_OF_1-ATP synthase, usually referred to as complex V (**Figure 1-2**). Each OXPHOS complex is made of multiple subunits which are encoded by both the mitochondrial and nuclear genomes, except for complex II, where all four polypeptide components are nuclear-encoded. Apart from enzymatic complexes, coenzyme Q_{10} and cytochrome *c* also play distinctive roles in OXPHOS, acting as electron carriers between the respiratory chain complexes.

In the initial steps of OXPHOS, NADH (reduced nicotinamide adenine dinucleotide) and $FADH_2$ (reduced flavin adenine dinucleotide) donate electrons to complexes I and II respectively. As these electrons are shuttled along the respiratory chain complexes, energy is released and it is used to pump protons (H^+) from the mitochondrial matrix to the intermembrane space. This electrochemical proton gradient is then used by complex V (ATP synthase) to generate ATP from ADP and P_i.

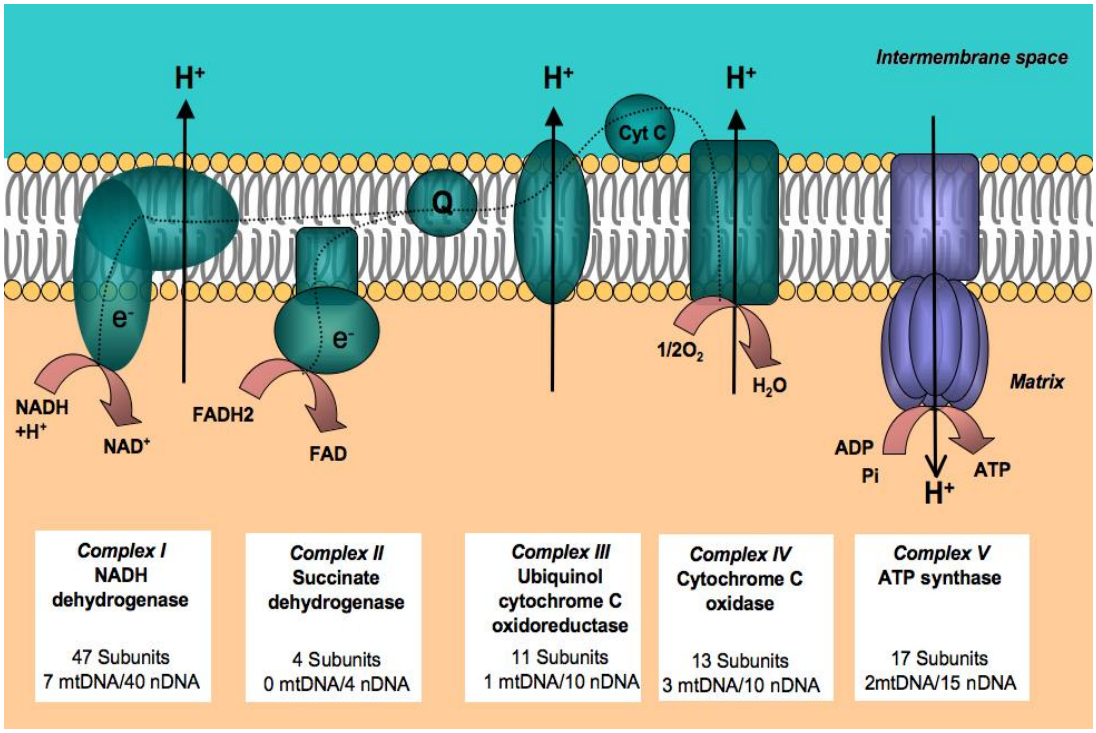

Figure 1-2 Mitochondrial respiratory chain. (Reproduced from Bellance et al., 2009).

1.2.1 Complex I

Complex I (NADH-ubiquinone oxidoreductase) is the largest respiratory chain complex and it consists of 47 subunits, seven of which are mitochondrially-encoded (ND1, ND2, ND3, ND4, ND4L, ND5 and ND6). Complex I contains a co-enzyme, flavin mononucleotide (FMN), and up to nine iron-sulphur clusters involved in the electron transfer (Hinchliffe and Sazanov, 2005). Structurally, complex I has an L-shaped formation with the hydrophobic membrane arm embedded in the IMM and

the hydrophilic peripheral arm protruding into the mitochondrial matrix (Grigorieff, 1999). Complex I is a proton pump and it translocates four protons (H^+) per one molecule of oxidized NADH across the inner membrane, thereby building an electrochemical gradient. Oxidation of NADH to NAD^+ results in the elimination of two electrons which are subsequently transferred to coenzyme Q_{10}, also known as ubiquinone. The electron-rich reduced form of ubiquinone called ubiquinol (QH_2) diffuses within the IMM.

1.2.2 Complex II

Unlike the other OXPHOS complexes, complex II (succinate-ubiquinone oxidoreductase; succinate dehydrogenase; SDH) consists of four subunits (A-D) which are entirely nuclear-encoded (Hatefi and Galante, 1980). Hydrophilic subunits A and B contain a covalently-attached flavin adenine dinucleotide (FAD) coenzyme (subunit A) and three iron-sulfur clusters (subunit B). The remaining two subunits: C and D contain heme groups. Functionally, complex II is responsible for oxidation of succinate to fumarate. Electrons derived from succinate by FAD coenzyme are transferred via three iron-sulfur clusters to finally reduce ubiquinone to ubiquinol. Compared with the process in complex I, this reaction is not accompanied by proton transfer.

1.2.3 Complex III

Complex III (ubiquinol-cytochrome *c* oxidoreductase) consists of eleven subunits; ten of which are nuclear-encoded and only one (cytochrome *b*) is mitochondrially-encoded. Three subunits: cytochrome *b* carrying two haem groups, cytochrome c_1 with a covalently bound haem *c*, and an iron-sulfur protein called a Rieske protein, together form a catalytic core known as the cytochrome bc_1 complex. Complex III is responsible for the mechanism known as the Q cycle, leading to electron transfer from ubiquinol (QH_2) to cytochrome *c*, accompanied by the proton pumping. Finally, two ubiquinols are oxidized to ubiquinones, one ubiquinone is reduced to ubiquinol and two electrons are passed to the two cytochrome *c* molecules. Simultaneously, a proton gradient is built across the inner mitochondrial membrane by the release of four protons from the intermembrane space and the uptake of two protons from the matrix.

1.2.4 Complex IV

Complex IV (cytochrome *c* oxidase; COX) has 13 subunits, three of which are mitochondrial in origin (COX I, COX II and COX III) (Kadenbach et al., 1983). COX is a terminal enzyme of the respiratory chain and acts as a dimer. It is located in the inner membrane, facing both the IMS and the matrix, and consists of two copper centres (Cu_A and Cu_B) and two heme groups (cytochromes *a* and a_3). Complex IV is responsible for molecular oxygen reduction to water and in order for this to occur, four electrons are transferred from cytochrome *c* to the cytochrome a_3-Cu_B binuclear centre, where a rapid oxygen reduction takes place. Subsequently, four protons bind to the reduced oxygen moiety creating two molecules of water. These reactions are accompanied by the translocation of an additional four protons across the inner membrane which builds a proton concentration gradient.

1.2.5 Complex V

Complex V (F_OF_1-ATP synthase) is composed of seventeen subunits, two of which (ATP6 and ATP8) are synthesized in mitochondria. ATP synthase is a large protein complex comprised of two connected rotary motors: F_O which forms a proton channel embedded in the inner mitochondrial membrane, and F_1 which is located in the matrix and catalyses ATP synthesis/hydrolysis. The catalytic F_1 motor is composed of five different protein subunits with the stoichiometry $\alpha_3\beta_3\gamma\delta\varepsilon$ (Abrahams et al., 1994). Three α-subunits and three β-subunits are arranged alternately, creating an $(\alpha\beta)_3$ cylinder around the coiled-coil organization of γ-subunit (Yoshida et al., 2001). The F_O motor is composed of subunits *a*, *b* and *c*, which together form a rotor-stator mechanism (Boyer, 1997). The proton-driven motor is comprised of cylindrically arranged *c*-subunits while the stator is created by an ab_2 complex. The two motors are connected both through the stator, extending between F_Oab_2 and $F_1\alpha_3\beta_3\delta$ complexes, and through the rotor, where F_O *c* ring is linked to the $F_1\gamma\varepsilon$ subunits (Yoshida et al., 2001). ATP synthesis from ADP and P_i occurs along the "binding change mechanism" (Kayalar et al., 1977; Gresser et al., 1982). According to this working model, downhill proton (H^+) translocation through F_O along the previously generated electrochemical potential gradient causes rotation of the F_O rotor and subsequently rotation of the $F_1\gamma\varepsilon$ subunits. The rotary movement

of the γ-subunit is coupled with a conformational change of the β-subunits which constantly cycle between three states: the first "loose" site responsible for binding ADP and P_i, the second "tight" site being in charge of spontaneous ATP formation, and the third "open" state when ATP is released (Gibbons et al., 2000).

1.3 Mitochondrial Genetics

1.3.1 Mitochondrial Genome

Mitochondria are unique in possessing their own genome – a 16,569 base pair (bp)-long, circular, double stranded molecule (**Figure 1-3**) (Anderson et al., 1981). Mitochondrial DNA (mtDNA) molecules are located within the matrix compartment and there are 2-10 copies per mitochondrion. Since eukaryotic cells contain a large number of mitochondria, this results in a high-copy number genome.

The mitochondrial genome is composed of a purine-rich heavy (H) strand and a pyrimidine-rich light (L) strand (Anderson et al., 1981). MtDNA has no introns but it contains a 1.1 kb long non-coding triple-stranded DNA region called the D-loop or control region (Kasamatsu et al., 1971). It encompasses the origin of H-strand replication (O_H), promoter regions for transcription of both the light-strand (LSP) and the heavy-strand (HSP1 and HSP2), as well as the regulatory motifs for mtDNA expression: multiple binding sites for mitochondrial transcription factor A (TFAM), three conserved sequence blocks (CSB1, CSB2, CSB3), and a conserved termination-associated sequence (TAS) (Sbisa et al., 1997; Suissa et al., 2009).

The mitochondrial genome codes for 13 respiratory chain polypeptide subunits, two ribosomal RNAs (12S and 16S rRNAs) and 22 transfer RNAs (tRNAs) (Anderson et al., 1981). The majority of mtDNA-encoded genes are located on the H-strand, with only a single respiratory chain subunit (ND6) and eight tRNA genes placed on the L-strand. All the remaining structural and accessory proteins required for normal mitochondrial function are nuclear-encoded, highlighting the mitochondrion's limited autonomy.

Unlike nuclear DNA (nDNA), mtDNA is strictly maternally inherited (Birky, 1978; Giles et al., 1980) with only one single case report of paternal transmission reported (Schwartz and Vissing, 2002). Sperm mitochondria are labelled with the ubiquitin tags recognized by the oocyte's cytoplasmic destruction machinery which eliminates paternal mitochondria before or during the third embryonic cleavage (Sutovsky et al., 1999).

Mitochondrial and nuclear genomes are also different in terms of their genetic codes (Barrell et al., 1979). Nuclear DNA comprises three stop codons (UAA, UGA, UAG) while mtDNA has only two (AGA and AGG) (Barrell et al., 1979). Furthermore, the nDNA stop codon UGA codes for tryptophan in mtDNA, while AUA, coding for nDNA isoleucine, stands for methionine in the mitochondrial genome (Barrell et al., 1979).

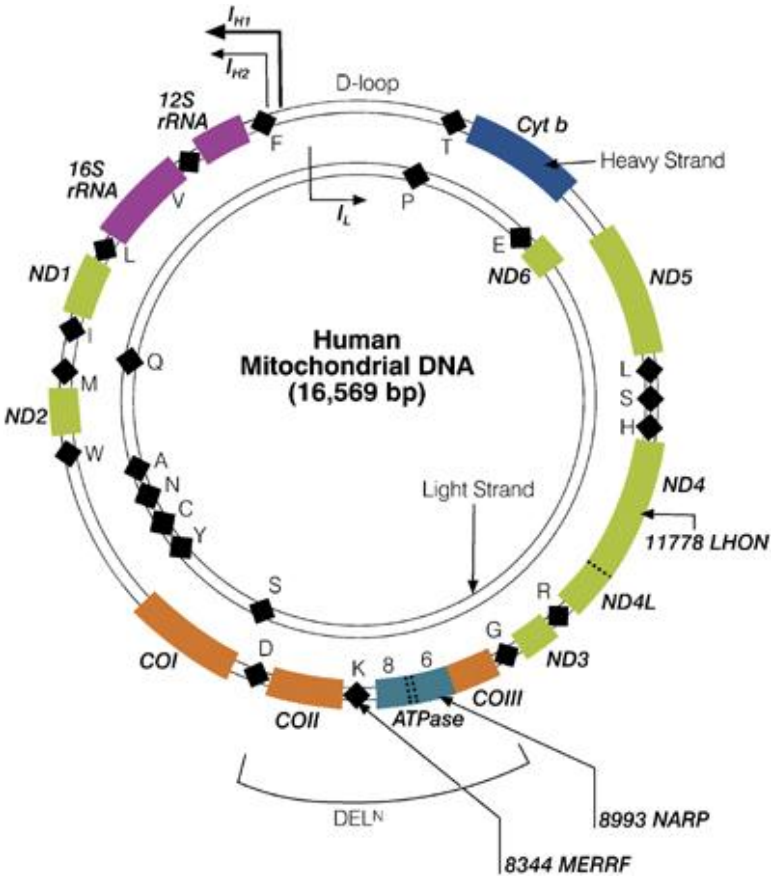

Figure 1-3 The human mitochondrial genome. Heavy strand (H; outer) codes for 12 respiratory chain subunits, 14 tRNAs and two rRNAs. Light strand (L; inner) codes for one respiratory chain subunit (ND6) and eight tRNA genes. (Reproduced from Kyriakouli et al., 2008).

1.3.2 Mitochondrial Haplogroups

As a result of its close proximity to the respiratory chain, mtDNA molecules are permanently exposed to high ROS levels (Raha and Robinson, 2000). Together with the lack of protective histones and the mechanisms allowing for effective repair, as well as a high replication rate favouring the occurrence of replication errors, the mitochondrial genome accumulates mutations drastically faster than the nuclear genome (Howell et al., 1996; Jazin et al., 1998). Through evolution, a large number of benign mtDNA base substitutions, known as single-nucleotide polymorphisms (SNPs), have arisen and these have been inherited successively along maternal lineages (Cann, 2001). Phylogenetic analyses have grouped specific mtDNA sequence polymorphisms with particular haplotypes and groups of these haplotypes can be classified further into major haplogroups (Torroni and Wallace, 1994; Wallace et al., 1999). Human mtDNA haplogroups demonstrate a geographical and a continental localization, and overall 18 major haplogroups have been distinguished (Torroni and Wallace, 1994; Herrnstadt and Howell, 2004). Nine of these haplogroups (H, U, J, T, K, W, I, V, X) are characteristic for individuals of European ancestry, with haplogroup H being the most common (Torroni and Wallace, 1994; Herrnstadt et al., 2002).

1.3.3 Mitochondrial Heteroplasmy

MtDNA is present in cells at a high copy number and these mitochondrial genomes are not always identical. MtDNA can be either homoplasmic, when every mitochondrial genome molecule harbours the same allele, or heteroplasmic, in which case only a sub-population of mtDNA molecules carries a specific allele (Smith et al., 1993; Harding et al., 1995). The majority of pathogenic mtDNA mutations are heteroplasmic and OXPHOS only becomes impaired when the percentage of the mutant mtDNA species exceeds a mutational threshold of 60-80% (Shoubridge et al., 1990; Sciacco et al., 1994; Bua et al., 2006; Durham et al., 2007). Interestingly, the level of heteroplasmy can vary between different tissues of a single individual and this could in part account for the variable tissue-specific phenotypes observed in mitochondrial disease (Chinnery et al., 1999; McFarland et al., 2002b).

1.3.4 Mitochondrial Genetic Bottleneck

The mitochondrial genetic bottleneck has been proposed to explain the rapid segregation of heteroplasmic mtDNA genotypes between generations (Jenuth et al., 1996; Cree et al., 2008). To date three bottleneck mechanisms have been hypothesised. According to the study by *Cao and colleagues*, the level of heteroplasmy transmitted from the mother to an offspring varies significantly as a result of a preferential replication of clusters containing identical mtDNA molecules, so-called homoplasmic segregating units or nucleoids (Cao et al., 2007; Cao et al., 2009). The second model, by *Cree and colleagues*, postulates the rapid genetic drift arises due to a marked reduction in mtDNA copy number during early germ line development, without a need for mtDNA aggregates (Cree et al., 2008). More recently, a third mechanism has been proposed where the genetic bottleneck has been ascribed to the replication of only a subpopulation of mitochondrial genomes, the latter taking place during postnatal folliculogenesis and not during embryonic oogenesis (Wai et al., 2008). Regardless of the actual mechanism, it is likely that the mitochondrial bottleneck has a protective role, reducing deleterious mtDNA mutational load during transmission (Cree et al., 2009).

1.4 Mitochondrial DNA Maintenance

1.4.1 Mitochondrial Nucleoids

The mitochondrial genome was originally considered to be a bare and unprotected structure, unlike nuclear DNA, which is wrapped with protective histones. However, recent studies have revealed that mtDNA is actually protein-coated and packaged into aggregates called nucleoids (Chen and Butow, 2005). The number of nucleoids per mitochondrion is tissue-dependent (Clay Montier et al., 2009) and high-resolution stimulated emission depletion (STED) microscopy has shown that mammalian nucleoids are fairly uniform in size, reaching approximately 100 nm and they usually contain only a single mtDNA molecule (Kukat et al., 2011). Although up-regulation of mtDNA copy number can lead to formation of structurally larger nucleoids (Ylikallio et al., 2010), mtDNA exchange between these individual

nucleoids is limited (Gilkerson et al., 2008). A layered structure of human mitochondrial nucleoids has also been suggested, where both mtDNA replication and transcription occur in the central core of the nucleoid, while translation and complex assembly take place in the peripheral region (Bogenhagen et al., 2008).

Numerous protein components are involved in the structural organisation of nucleoids. Mitochondrial transcription factor A (TFAM) is the main element of mammalian nucleoids (Garrido et al., 2003; Bogenhagen et al., 2008) playing a key role in packaging mtDNA (Alam et al., 2003) and regulating mtDNA copy number (Ekstrand et al., 2004). Several different mtDNA-related components are associated with nucleoids and these include: mitochondrial DNA polymerase γ (polγ), Twinkle helicase, and the mitochondrial single-stranded binding (mtSSB) protein (Garrido et al., 2003; Tyynismaa et al., 2004). In addition to components that participate directly in mtDNA maintenance, other nucleoid-related proteins include human prohibitins 1 and 2. These proteins participate in many essential cellular functions, including apoptosis, cell cycle regulation and signal transduction (Czarnecka et al., 2006). Prohibitins also mediate the structure of mitochondrial cristae and help to organize the inner membrane (Merkwirth and Langer, 2009). Other proteins associated with nucleoids are mitochondrial inner membrane ATAD3 (ATPase family AAA domain-containing 3) protein, which is able to bind to the D-loop region of mtDNA (He et al., 2007), and tumour suppressor protein p53 that interacts with TFAM (Yoshida et al., 2003).

1.4.2 Mitochondrial Genome Replication

Mitochondrial DNA replication is exclusively controlled by nuclear genes. It occurs independently of the cell cycle (Bogenhagen and Clayton, 1977) and its activity may differ between various tissues of the same individual (Wang et al., 1997). The mitochondrial replisome is an assembly of four proteins: polγ, mitochondrial Twinkle helicase, mtSSB and TFAM. Three models of mammalian mtDNA replication have been reported so far (**Figure 1-4**): (i) an asymmetric, strand-displacement mode (Clayton, 1982); (ii) a strand-coupled, bidirectional mode (Holt et al., 2000); and (iii) a ribonucleotide incorporation throughout the lagging strand (RITOLS) mode (Yasukawa et al., 2006).

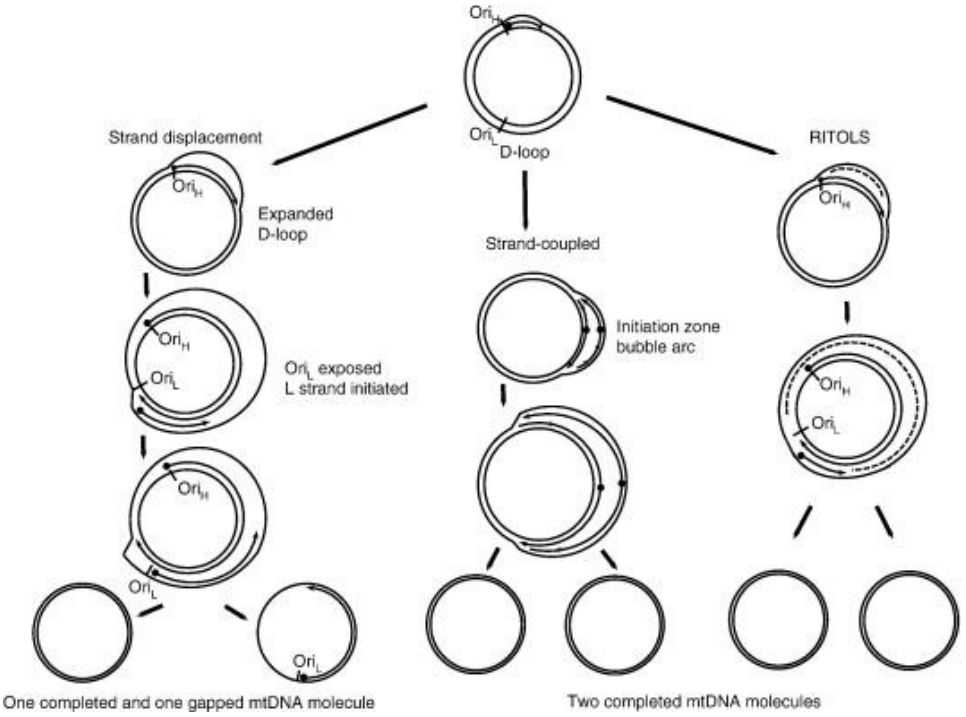

Figure 1-4 Models of mammalian mtDNA replication. (i) Strand-displacement (asymmetric) model (*left* panel): replication is initiated at the H-strand origin of replication (O_H). Displacement of the H-strand leads to an expansion of the D-loop until the L-strand origin of replication (O_L) is revealed. Synthesis of the L-stand is then initiated in the opposite direction. (ii) Strand-coupled (bidirectional) model (*middle* panel): replication is initiated from a single zone of replication initiation (OriZ) and followed by progression of two replication forks around the mtDNA molecule. (iii) RITOLS model (*right* panel): replication of the leading H-strand is similar to the strand-displacement model but the lagging L-strand is initially transcribed as RNA (dashed line) before being replaced by DNA. (Reproduced from Kasiviswanathan et al., 2011).

1.4.2.1 Strand-Displacement Mode

In Clayton's original strand-displacement model (**Figure 1-4**; *left* panel), replication is initiated at the H-strand (heavy-strand) origin of replication (O_H) within the D-loop region (Clayton, 1982). Displacement of the H-strand continues clockwise leading to the expansion of the D-loop until the L-strand (light-strand) origin of replication (O_L) is revealed. Replication of the lagging L-strand begins in the opposite direction when the synthesis of the leading H-strand is almost two-thirds complete. As a result of this asymmetry, one of the daughter mtDNA molecules is entirely synthesized, while the other one still contains an incompletely replicated L-strand and hence is termed a gapped circle (GpC) (Brown et al., 2005).

1.4.2.2 Strand-Coupled Mode

The alternative, bidirectional strand-coupled model of mtDNA replication (**Figure 1-4**; *middle* panel) was presented by *Holt and colleagues* (Holt et al., 2000; Bowmaker et al., 2003). Using two-dimensional agarose gel electrophoresis (2D-AGE), *Holt and colleagues* proposed the occurrence of a simultaneous synthesis of both the heavy and light strands. In this model, bidirectional replication begins within a single zone of replication initiation (OriZ) and it is followed by the expansion of the two replication forks around the mtDNA molecule. As a result, two daughter mtDNA molecules are synthesized concurrently. As suggested by *Holt and colleagues*, a strand-coupled model of mtDNA replication can occur independently or coexist with the original strand-displacement model (Holt et al., 2000).

1.4.2.3 RITOLS Mode

The most recent RITOLS mode (**Figure 1-4**; *right* panel) (Yasukawa et al., 2006) is frequently considered as a modified version of the original strand-displacement model. In principle, both the RITOLS and strand-displacement models expect a major delay between the syntheses of light- and heavy-strands. Compared with the original Clayton's mode, in RITOLS, the lagging strand is initially transcribed as RNA before being replaced by DNA in the maturation stage (Yasukawa et al., 2006).

1.4.3 Mitochondrial DNA Copy Number Regulation

A proper balance between the rates of mitochondrial DNA degradation and synthesis is crucial to maintain a steady-state mtDNA copy number that is adapted to a certain tissue type and its developmental stage (Berk and Clayton, 1974; Clay Montier et al., 2009). Although both mtDNA depletion and proliferation are commonly associated with mitochondrial disease, with mtDNA proliferation often considered a compensatory mechanism, little is known about the exact mechanisms of mtDNA copy number regulation (Clay Montier et al., 2009; Spinazzola and Zeviani, 2009). Several different models trying to clarify the mechanism of mitochondrial DNA copy number regulation have recently been proposed. As suggested by *Clay Montier and colleagues*, mtDNA copy number can be regulated in accordance with the threshold hypothesis (**Figure 1-5**) (Clay Montier et al., 2009). In this model, when mtDNA copy number reaches the lower threshold, unknown factors trigger the up-regulation

of mtDNA replication thereby pushing the copy number back up to its steady-state level. Conversely, when mtDNA copy number gets to the higher threshold, as yet unidentified factors trigger the mechanisms controlling mtDNA degradation, which results in a decrease in the number of mtDNA copies (Clay Montier et al., 2009). Other hypotheses have been proposed where mtDNA copy number is regulated by various mechanisms dependent upon the availability of nucleotides (Tang et al., 2000a), the multiple replication origins (Tang et al., 2000b), or by TFAM modifying the mechanism of mtDNA replication (Pohjoismaki et al., 2006). So far, experimental evidence in support of these models of mtDNA copy number regulation is lacking and further work is needed to elucidate this complex process.

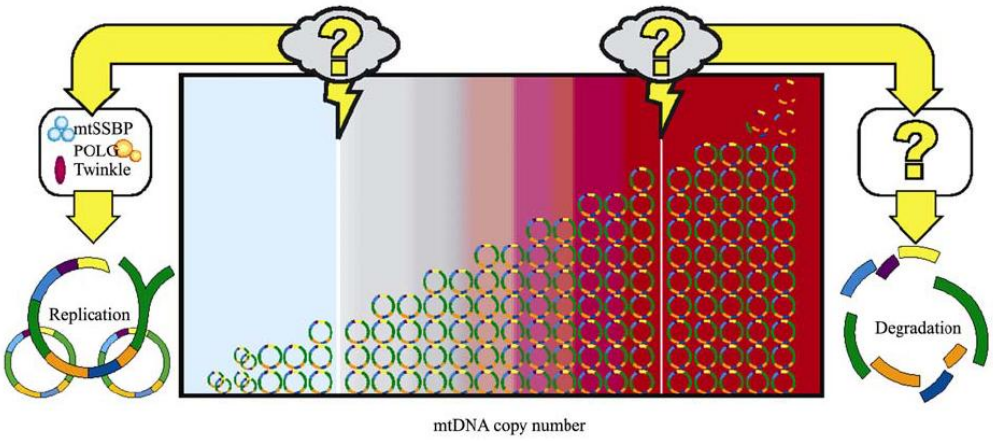

Figure 1-5 Threshold hypothesis of mtDNA copy number control. When mtDNA copy number drops to the lower threshold, unknown factors trigger the up-regulation of mtDNA replication increasing the copy number back to a steady-state level. Respectively, when the higher threshold of mtDNA copy number is reached, yet unidentified factors trigger the mechanisms responsible for mtDNA degradation, to decrease the number of mtDNA copies. (Reproduced from Clay Montier et al., 2009).

1.5 Mitochondrial Transcription

Transcription from the mitochondrial H-strand results in the production of two rRNAs, 12 mRNAs and 14 tRNAs, whereas transcription from the L-strand enables creation of one mRNA and eight tRNAs. The initiation of mtDNA L-strand transcription occurs from a single promoter (LSP). Compared with this, transcription

of the H-strand can arise from two specific and differentially regulated sites - HSP1 and HSP2 (Montoya et al., 1982). The two transcripts available from the H-strand differ from each other both in terms of their initiation and termination sites, as well as frequency of occurrence (Lodeiro et al., 2012). The more common HSP1-initiated transcript consists of two tRNAs ($tRNA^{Phe}$ and $tRNA^{Val}$) and two mitochondrial rRNAs. The HSP2-initiated transcript occurs less frequently and it produces a large, almost genome-length, polycistronic mRNA molecule (Montoya et al., 1983; Lodeiro et al., 2012).

Mitochondrial transcription is controlled by a highly-specialized machinery consisting of a monomeric RNA polymerase (POLRMT) supported by two transcription initiation factors – transcription factor A (TFAM) and transcription factor B2 (TFB2M) (Fisher and Clayton, 1985; Tiranti et al., 1997; Falkenberg et al., 2002; Litonin et al., 2010). Human mitochondria also contain transcription factor B1 (TFB1M), a homologue of the mammalian TFB2M (Falkenberg et al., 2002). However, recent *in vivo* studies have revealed that despite being a crucial methyltransferase responsible for methylation of 12S rRNA, TFB1M is not directly involved in transcription (Metodiev et al., 2009; Litonin et al., 2010).

It was assumed for a long time that the initiation of transcription occurred when TFAM became bound to mtDNA upstream of the promoter sites, which then attracted the POLRMT-TFB2M complex (Bonawitz et al., 2006). According to this model, initiation of transcription required TFAM, POLRMT and TFB2M irrespective of the promoter site (Bonawitz et al., 2006). However, recent studies have shown that mitochondrial transcription can be initiated in a TFAM-independent manner and the absence of TFAM significantly increases transcription observed from HSP1 site, when compared with transcription from LSP promoter site (Shutt et al., 2010). Furthermore, it was shown that transcription from HSP2 requires only POLRMT and TFB2M, whereas TFAM represses transcription by binding to TFAM-responsive elements (TREs) and preventing an efficient connection of POLRMT and TFB2M (Lodeiro et al., 2012).

The mechanisms regulating termination of mtDNA transcription are still under investigation. So far, only mitochondrial transcription terminator factor 1 – MTERF1 (also known as mTERF) has been directly associated with termination of the HSP1

transcript (Kruse et al., 1989; Asin-Cayuela and Gustafsson, 2007). MTERF1 and its three paralogues (MTERF2, MTERF3 and MTERF4) belong to a superfamily of mitochondrial proteins believed to play a crucial role as controllers of mtDNA transcription (Linder et al., 2005; Spahr et al., 2010). As demonstrated recently, MTERF3 can directly interact with the promoter region and it represses the initiation of transcription in mammalian mitochondria (Park et al., 2007).

1.6 Mitochondrial Translation

Mitochondrial translation is still far from being completely understood, mainly due to the absence of an *in vitro* translation system. All mitochondrial ribosomal proteins (MRPs) are nuclear-encoded and they need to be transferred to mitochondria where they form ribosomal complexes together with mitochondrially encoded rRNAs – 12S and 16S (Pietromonaco et al., 1991; O'Brien, 2003). Interestingly, mitochondrial ribosomes (mitoribosomes) contain relatively low amounts of RNA but a reasonably high proportion of protein components, compared with their prokaryotic counterparts (Pietromonaco et al., 1991; O'Brien, 2003; Sharma et al., 2003).

A total of 13 polypeptide respiratory chain subunits are synthesized in mammalian mitochondria (Anderson et al., 1981). Translation is initiated by two initiation factors – mitochondrial initiation factor 2 ($IF2_{mt}$) promoting connection of fMet-tRNA to the small ribosomal subunit (28S) and mitochondrial initiation factor 3 ($IF3_{mt}$) which actively dissociates the 55S ribosome, leading to the release of the 39S subunit and creation of a 28S:$IF3_{mt}$ complex (Liao and Spremulli, 1991; Koc and Spremulli, 2002; Christian et al., 2009; Christian and Spremulli, 2011). The elongation phase is a cyclical process requiring three mitochondrial elongation factors: EF-Tu_{mt}, EF-Ts_{mt} and EF-$G1_{mt}$ (Schwartzbach and Spremulli, 1989; Chung and Spremulli, 1990; Christian and Spremulli, 2011). Termination of translation occurs when one of the four mitochondrial mRNA stop codons (UAA, UAG, AGA or AGG) is encountered. This is facilitated by the release factor $RF1a_{mt}$ which induces the hydrolysis of a freshly generated protein (Soleimanpour-Lichaei et al., 2007). Following successful translation termination, the ribosome is then recycled. So far, two ribosome recycling

factors have been proposed to participate in the recycling process – RRF_{mt} (Rorbach et al., 2008) and $RRF2_{mt}$, known also as $EF\text{-}G2_{mt}$ (Tsuboi et al., 2009) (**Figure 1-6**).

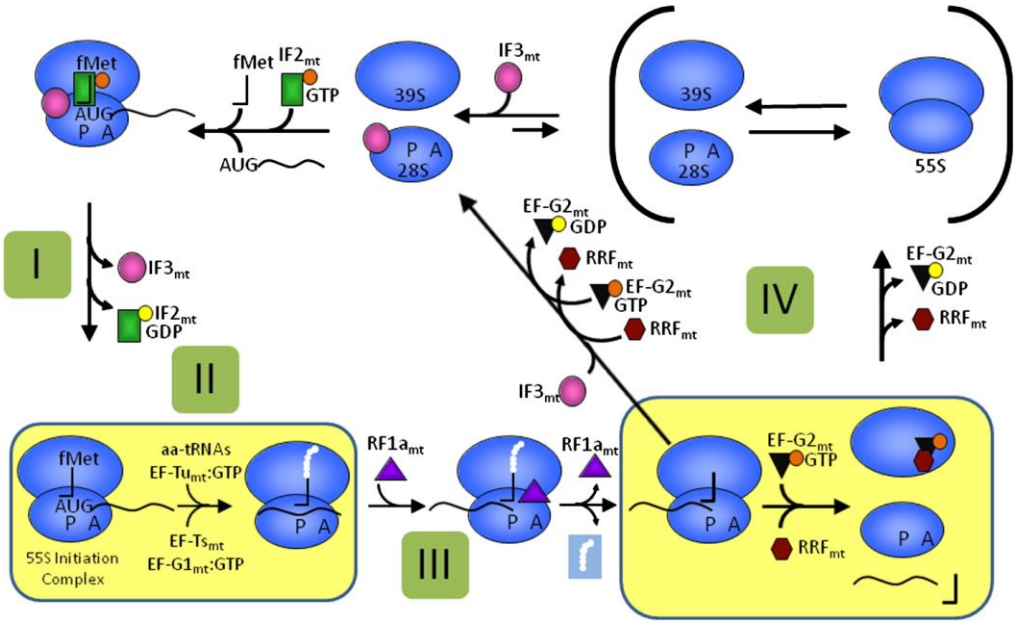

Figure 1-6 Diagram of mitochondrial translation. (I) Protein synthesis initiated by $IF2_{mt}$ and $IF3_{mt}$; (II) Elongation stage requiring $EF\text{-}Tu_{mt}$, $EF\text{-}Ts_{mt}$, and $EF\text{-}G1_{mt}$; (III) Termination carried out by $RF1a_{mt}$; (IV) Ribosome recycling facilitated by RRF_{mt} and $RRF2_{mt}$ (known also as $EF\text{-}G2_{mt}$). (Reproduced from Christian et al., 2009).

1.7 Nuclear-Mitochondrial Interactions

As a consequence of their limited genetic autonomy, mitochondria are heavily dependent on the nuclear genome. Only 13 respiratory chain polypeptides are mtDNA-encoded and the vast majority of mitochondrial proteins (approximately 1500), including those involved in the formation and maintenance of the electron transport chain, mtDNA replication, transcription and translation, are encoded by nuclear genes. These nuclear-encoded proteins are first translated in the cytosol and they are then subsequently targeted to mitochondria (Anderson et al., 1981; Lin et al., 2003; Calvo et al., 2006).

1.7.1 Transcriptional Regulation

Nuclear-encoded DNA-binding transcription factors and their associated coregulators maintain a composite network which controls the activity of mitochondrial gene expression (**Figure 1-7**) (Hock and Kralli, 2009). DNA-binding transcription factors target overlapping but distinct classes of mitochondrial genes, allowing for tissue-specific modulation of dedicated mitochondrial functions (Hock and Kralli, 2009). Two DNA-binding transcription factors, the nuclear respiratory factor-1 (NRF-1) and GA-binding protein (GABP; NRF-2), are involved in the regulation of the OXPHOS system, mtDNA replication and transcription (Virbasius et al., 1993; Scarpulla, 2008). Other DNA-binding factors, such as the peroxisome proliferator-activated receptors (PPARs; PPARα, PPARγ and PPARδ) are involved in the control of lipid metabolism (Evans et al., 2004), whereas estrogen-related receptors (ERRs; ERRα, ERRβ and ERRγ) participate in the regulation of the mitochondrial genes linked to the oxidation of lipids, the OXPHOS system, the tricarboxylic acid (TCA) cycle, mitochondrial import, mitochondrial dynamics and the cell's defence against oxidative stress (Giguere, 2008; Villena and Kralli, 2008; Hock and Kralli, 2009). The remaining DNA-binding factors are: cAMP response element-binding (CREB) protein, which regulates the *CYCS* gene coding for cytochrome *c*; c-Myc, which binds to over a hundred mitochondrial genes including mitochondrial DNA polymerase γ; and finally YY1, which controls various COX genes (Kim et al., 2008; Scarpulla, 2008; Hock and Kralli, 2009).

Nuclear transcriptional coregulators cooperate with multiple DNA-binding factors inducing either their activation (PPARγ coactivator-1 family; PGC-1α, PGC-1β and PRC) or repression (receptor-interacting protein 140; RIP140) (Hock and Kralli, 2009). DNA-binding factors have a dual capacity. They can simultaneously regulate their own expression, e.g. ERRα controls PPARα, NRF-1, GABP, and its own promoter, as well as expression of their coregulators, e.g. PPARγ, PPARδ, ERRγ, and CREB regulate PGC-1α, whereas ERRα controls RIP140 (Huss et al., 2004; Mootha et al., 2004; Villena and Kralli, 2008; Hock and Kralli, 2009).

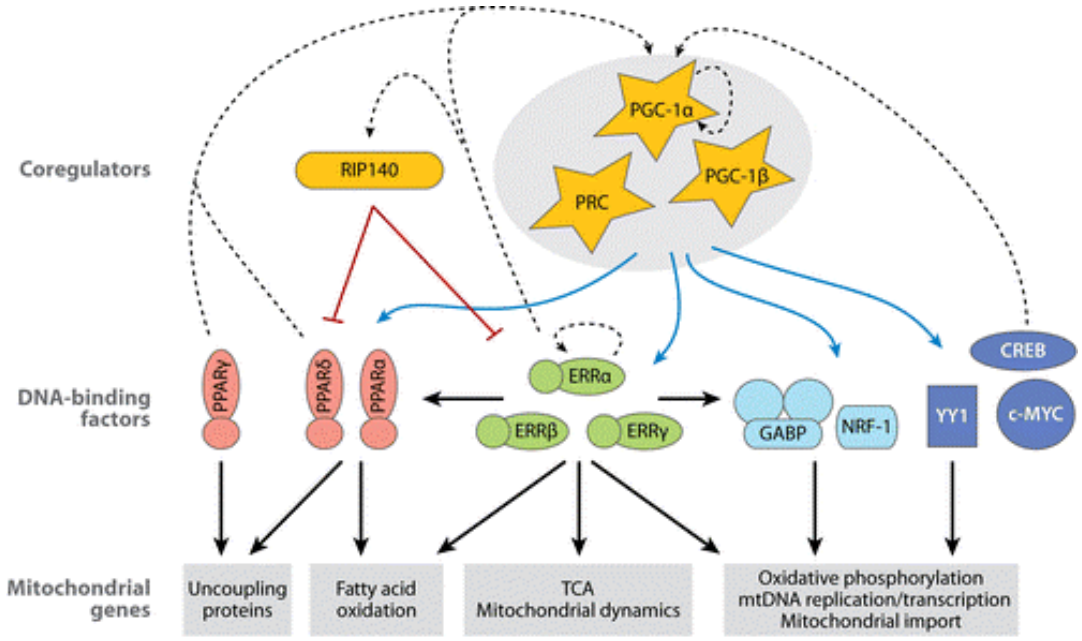

Figure 1-7 The transcriptional network controlling mitochondrial gene expression. DNA-binding factors target overlapping but distinct classes of mitochondrial genes, allowing a tissue-specific modulation of dedicated mitochondrial functions. Coregulators interact with multiple DNA-binding factors inducing either their activation (PGC-1α, PGC-1β and PRC) or repression (RIP140). (Reproduced from Hock and Kralli, 2009).

1.7.2 Post-Transcriptional Regulation

Several post-transcriptional and post-translational mechanisms are linked to the regulation of mitochondrial biogenesis and function (Cannino et al., 2007). RNA-binding proteins such as RBP38, which stabilizes mitochondrial RNA (Sbicego et al., 2003), or LRP130, which binds polyadenylated mRNAs in mitochondria (Mili and Pinol-Roma, 2003), are believed to participate in these intricate nuclear-mitochondrial interactions (Cannino et al., 2007). The reversible process of protein acetylation is another important post-translational modification, which in humans requires a nuclear-encoded SirT3 deacetylase. The latter allows deacetylation of several mitochondrial proteins to proceed efficiently (Schwer et al., 2002). Mitochondrial activity can also be coordinated via the complexes responsible for protein import and assembly (Koehler, 2004; Cannino et al., 2007). TIM23 and the presequence translocase-associated motor (PAM) complexes are involved in the multistep import of pre-proteins into the mitochondrial matrix or IMM (van der Laan et al., 2006). Another important element is the SAM (sorting and assembly

machinery) complex that is crucial for the integration and assembly of the outer membrane proteins (Pfanner et al., 2004).

1.7.3 Mitochondrial-Nuclear Communication

Cross-talk between the mitochondria and the nucleus can be maintained at two levels (Ryan and Hoogenraad, 2007). Firstly, a set of DNA-binding transcription factors and coactivators directly regulate nuclear and mitochondrial gene expression in response to changes in environmental and bioenergetic conditions, such as temperature, caloric intake or exercise (Puigserver et al., 1998; Lin et al., 2003; Norrbom et al., 2004; Ryan and Hoogenraad, 2007) (please refer to **Section 1.7.1**). Secondly, a mechanism known as mitochondrial retrograde signalling utilises multiple factors capable of receiving and transmitting mitochondrial signals to initiate changes in nuclear gene expression, thereby leading to the alteration of the cell's metabolism in response to mitochondrial defects (Butow and Avadhani, 2004; Liu and Butow, 2006). The mitochondrial retrograde signalling has been shown to occur via numerous stimuli e.g. cytosolic changes in Ca^{2+} concentrations in mammalian skeletal myoblasts (Biswas et al., 1999; Amuthan et al., 2002) or translocation of cytochrome *c* oxidase subunit III from mitochondria to the cytosol in the developing rat brain (Cannino et al., 2004; Cannino et al., 2007).

1.8 Mitochondrial Dynamics

Mitochondria are dynamic organelles constantly fusing and breaking apart. It is now clear that the balance between fusion and fission is crucial to maintain a highly-interconnected and stable mitochondrial network (Chen and Chan, 2005). When this delicate balance is perturbed, dramatic changes in mitochondrial network morphology can be observed with detrimental consequences for cell function. Cells with a high fusion-to-fission ratio comprise only few, highly-elongated mitochondria, whereas a low ratio is associated with numerous fragmented mitochondria, these appearing as small, isolated spheres or short rods (Bleazard et al., 1999; Chen et al., 2003). Mitochondria are shuttled within the cell along cytoskeletal tracks, allowing their translocation to locations where they are actively needed (Frederick and Shaw,

2007). This is especially relevant for highly-polarized cells such as neurones and retinal ganglion cells (RGCs) which consist of long axonal segments covering relatively large anatomical distances and hence strongly relying on an effective bidirectional mitochondrial distribution (**Figure 1-8**; **Figure 1-9**) (Hollenbeck and Saxton, 2005; Frederick and Shaw, 2007; Chen and Chan, 2009). The increased interest in mitochondrial dynamics contributed to the discovery of numerous mitochondrial shaping proteins: mitofusin-1 (MFN1), mitofusin-2 (MFN2) and optic atrophy 1 (OPA1), which are key pro-fusion proteins, as well as dynamin-related protein 1 (DRP1) and mitochondrial fission 1 (hFis1), which are key pro-fission proteins (Suen et al., 2008; Liesa et al., 2009).

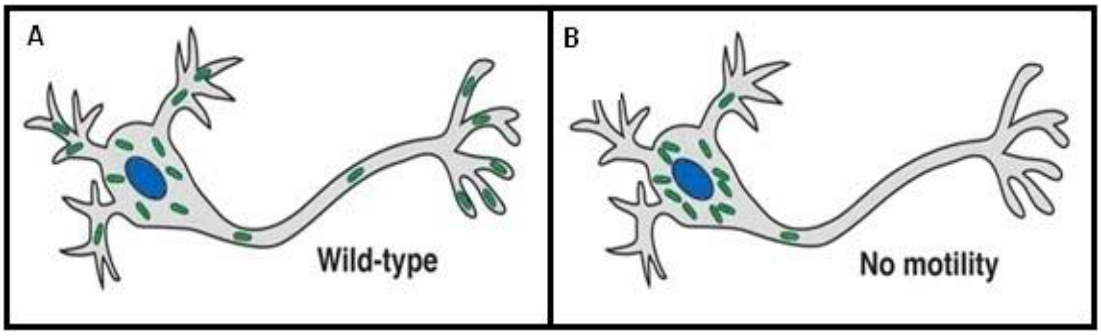

Figure 1-8 Comparison of mitochondrial motility. (A) Wild-type neurones: mitochondria are able to travel from the cell body to the dendritic and axonal terminals; (B) Impaired motility prevents distribution of mitochondria to the periphery. (Reproduced from Chen and Chan, 2009).

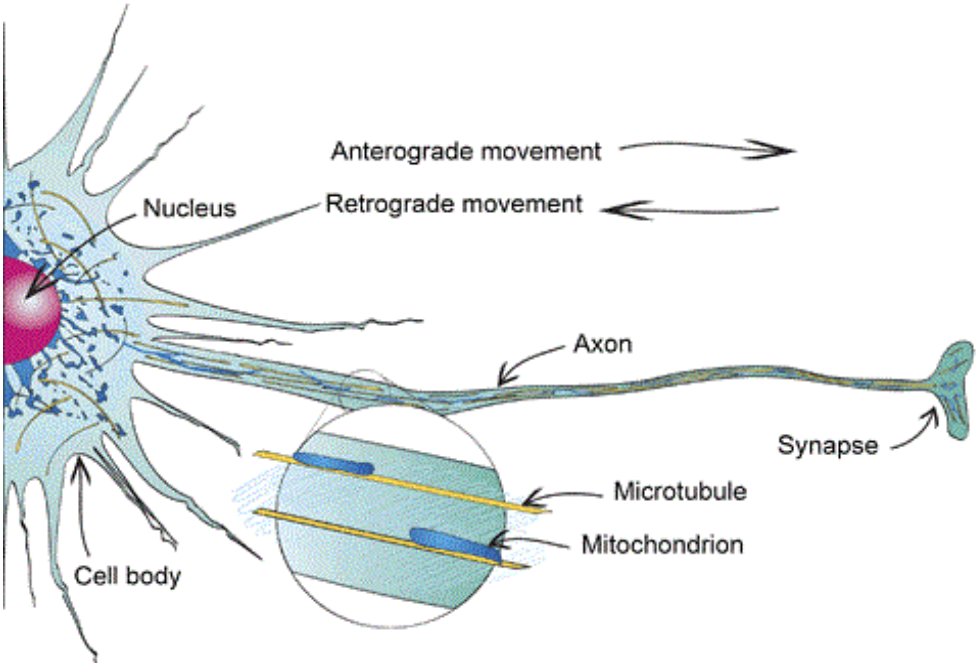

Figure 1-9 Bi-directional movement of mitochondria in neurones. The anterograde transport is responsible for translocating mitochondria from the cell body toward the synapse, whereas retrograde movement returns mitochondria from the peripheral sites. (Reproduced from Frederick and Shaw, 2007).

1.8.1 Functions of Mitochondrial Dynamics

Fusion and fission allow cells to actively and dynamically respond to changes in their surrounding physiological conditions. Fusion enables mitochondrial compartments to mix and functionally complement each other, whereas fission forms organelles that are distinct both in terms of morphology and function (as reviewed in Westermann, 2010). Together, these two processes are essential to maintain normal mitochondrial functions and they are critical for cell survival (**Figure 1-10**).

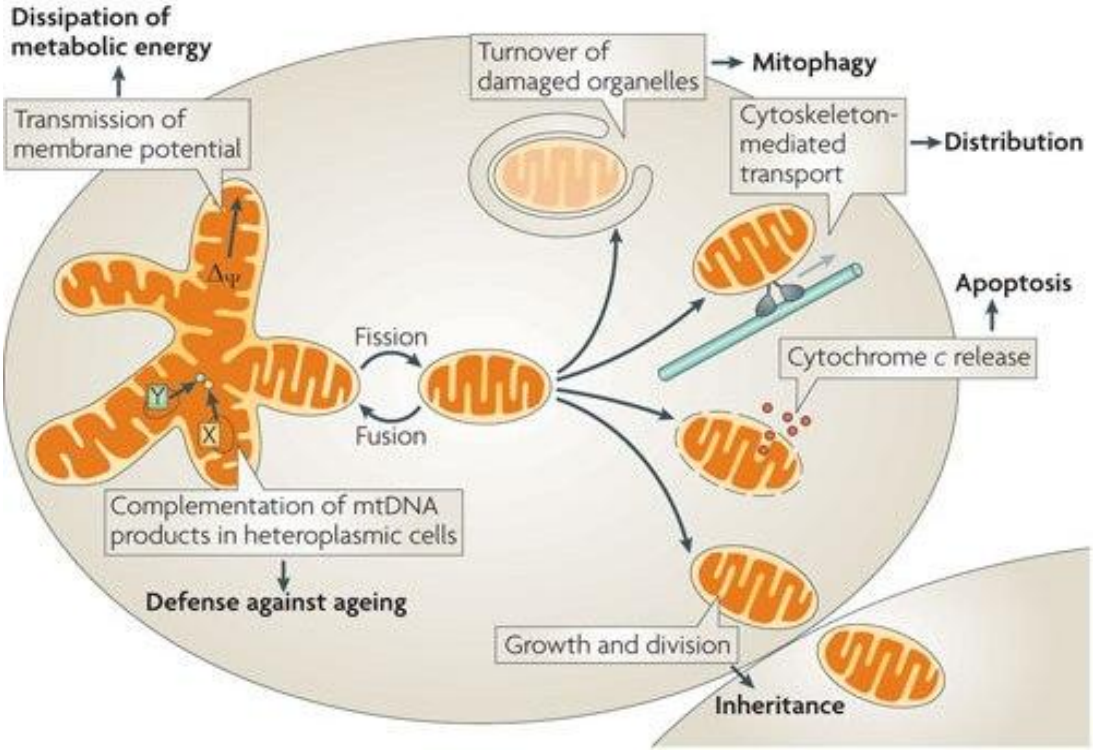

Figure 1-10 Functions of mitochondrial dynamics. Mitochondrial fission is essential for (i) the segregation of mitochondria during cell division, (ii) intracellular cytoskeleton-mediated transport, (iii) turnover of the damaged mitochondria by mitophagy, and (iv) cytochrome *c* release to initiate apoptosis. Mitochondrial fusion is crucial for the dissipation of metabolic energy and complementation of mtDNA in heteroplasmic cells. (Adapted from Westermann, 2010).

1.8.1.1 Mitochondrial Inheritance

The cell's mitochondrial network morphology is dependent upon the cell cycle and fission is responsible for the stochastic partitioning of mitochondria to daughter cells during cell division (Taguchi et al., 2007; Ishihara et al., 2009; Westermann, 2010). Since mitochondrial fission generates highly-fragmented organelles, some of them may lack mtDNA molecules or other essential components. Mitochondrial fusion is therefore critical for the exchange and complementation of impaired or missing mitochondrial components, ensuring their replenishment before the organelle's functionality is lost and allowing OXPHOS to be maintained at an adequate level (Nakada, 2009; Westermann, 2010). Recent studies have suggested the presence of two types of mitochondrial fusion: prolonged complete fusion allowing redistribution of all necessary mitochondrial components, and short-term kiss-and-run transient fusion (**Figure 1-11**) (Liu et al., 2009). The latter effectively facilitates the

redistribution of small solutes, mRNA or proteins, whereas complementation of integral membrane proteins or mtDNA remains restricted (Liu et al., 2009). Although both types of mitochondrial fusion are mediated by the same set of fusion proteins, transient and complete fusions vary in terms of their OPA1 requirements (Liu et al., 2009). If OPA1 levels are inadequate to maintain complete fusion, transient fusion can still be effectively supported (Liu et al., 2009).

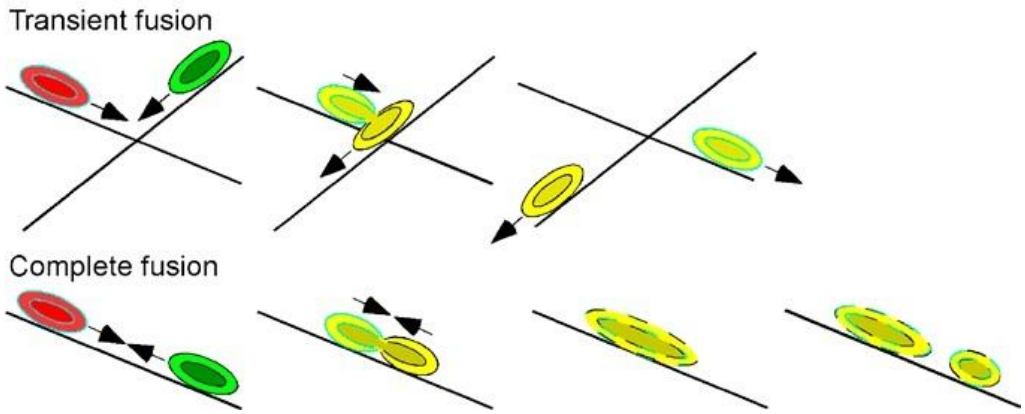

Figure 1-11 Types of mitochondrial fusion. Short-term transient fusion allows quick replenishment of only soluble factors by IMS and matrix exchange whereas prolonged complete fusion allows redistribution of all necessary mitochondrial components. (Reproduced from Liu et al., 2009).

1.8.1.2 Mitochondrial Distribution and Morphology

The fusion and fission machineries allow the mitochondrial network to be shaped according to the specific functional requirements of a particular cell type (**Figure 1-12**) (as reviewed in Westermann, 2010). In neuronal populations, which are good examples of large and extended cell types, fission controls the distribution of mitochondria by splitting the network into transportable units. These can then be further transported along cytoskeletal tracks to sites of higher energy demands (Li et al., 2004; Westermann, 2010). In comparison, in muscle fibres, which are also exceptionally large cells requiring significant amounts of energy, fusion generates enlarged mitochondrial networks, forming electrically coupled systems functioning as intracellular power-transmitting cables (Amchenkova et al., 1988; De Giorgi et al., 2000; Skulachev, 2001). Such a configuration enables transmission of the membrane potential generated in the oxygen-rich areas in the periphery of the muscle fibre to

the oxygen-poor muscle fibre core, thereby allowing ATP synthesis to proceed there (Skulachev, 2001; Westermann, 2012). As shown recently, by forming a hyperfused network, mitochondrial fusion can also act as a protective mechanism that allows a degree of protection against the stress-induced high energy demand or starvation (Tondera et al., 2009; Westermann, 2012). Conversely, in resting cells, which only require a low activity of the mitochondrial respiratory chain, fragmented mitochondria are frequently found (as reviewed in Westermann, 2010).

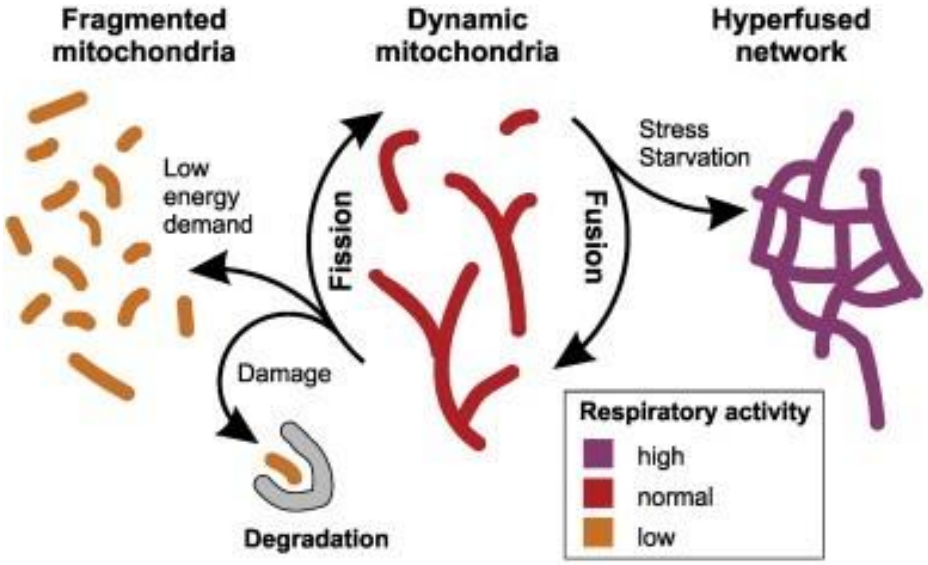

Figure 1-12 Adaptation of mitochondrial morphology to variable respiratory chain activity. Under normal respiratory conditions, mitochondria cyclically undergo fusion and fission. When the cell's energy demand is low, mitochondria prefer a fragmented morphological state whereas exposure to stress or starvation triggers creation of hyperfused mitochondria to optimize mitochondrial function. (Reproduced from Westermann, 2012).

1.8.1.3 Mitochondrial Quality Control and Turnover

Mitochondrial dynamics is believed to play a central role as a quality control mechanism, managing mitochondrial turnover (**Figure 1-13**) (Twig et al., 2008). According to this theory, each mitochondrion cyclically oscillates between two morphological states – an interconnected post-fusion state and a fragmented post-fission state (Twig et al., 2008). Fusion is a brief event and it triggers fission generating daughter mitochondria which either preserve intact membrane potential or

depolarize (Twig et al., 2008). Mitochondria that are unable to restore the membrane potential are unlikely to proceed to a subsequent fusion (Twig et al., 2008). After a few hours in a depolarized and solitary state, these mitochondria are eliminated from the cell by mitochondrial autophagy (mitophagy) (Twig et al., 2008).

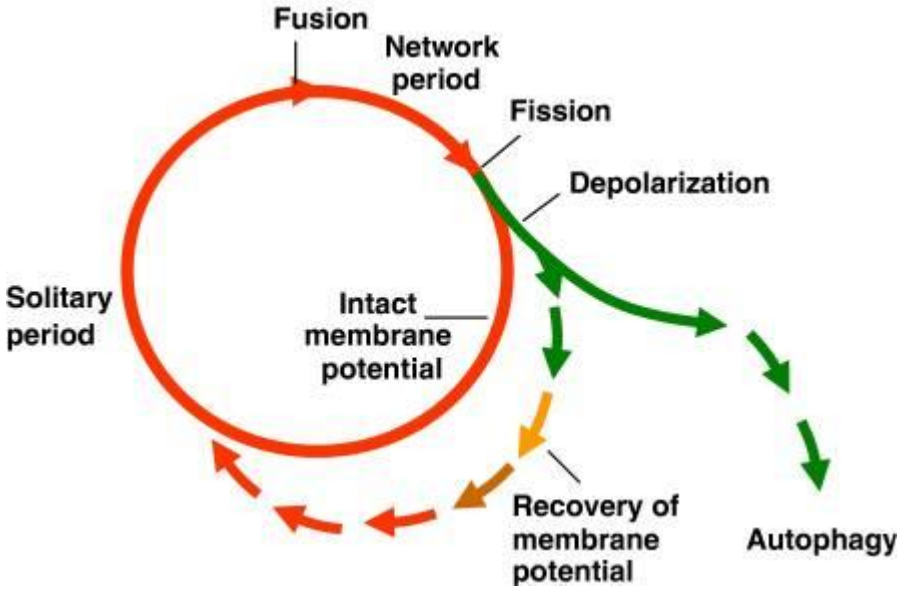

Figure 1-13 Model of mitochondrial life cycle. Mitochondria cyclically oscillate between post-fusion and post-fission states. A brief selective fusion triggers fission that generates daughter mitochondria. These either preserve intact membrane potential *(red line)* or depolarize *(green line)*. Unless membrane potential is restored, the mitochondrion is removed by mitochondrial autophagy (mitophagy). (Reproduced from Twig et al., 2008).

1.8.1.4 Apoptosis

During programmed cell death, mitochondrial fission is a key feature, occurring concomitantly with OMM permeabilization, cristae disorganisation and the successive release of pro-apoptotic factors such as cytochrome *c*, smac/DIABLO, HtrA2/omi, which ultimately leads to procaspase-9 activation (Youle and Karbowski, 2005; Suen et al., 2008; Otera and Mihara, 2012). Both the proapoptotic (Bax/Bak) and antiapoptotic (Bcl-2/Bcl-xL) proteins of the Bcl-2 family play significant roles in the regulation of mitochondrial morphology as part of the intrinsic (mitochondrial) apoptotic pathway (Martinou and Youle, 2011). Once apoptosis is triggered, mitochondrial fission is induced by Bax/Bak activation, which causes a reduction in

mitochondrial fusion followed by an increase in fragmentation, likely through the inhibition of MFN2 (Karbowski et al., 2002; Karbowski et al., 2004; Brooks et al., 2007; Otera and Mihara, 2012). Activation of Bax/Bak also leads to a stable association of DRP1 with the outer mitochondrial membrane, as a consequence of Bax/Bak-dependent SUMO modification of DRP1 (Wasiak et al., 2007; Otera and Mihara, 2012). Although mitochondrial fission is directly correlated with cytochrome *c* release and activation of the apoptotic pathway, the pro-fusion OPA1 protein is capable of regulating the size of mitochondrial cristae junctions, thereby preventing cytochrome *c* molecules from being released and blocking intrinsic apoptotic activation (Frezza et al., 2006; Liesa et al., 2009) (**Figure 1-14**).

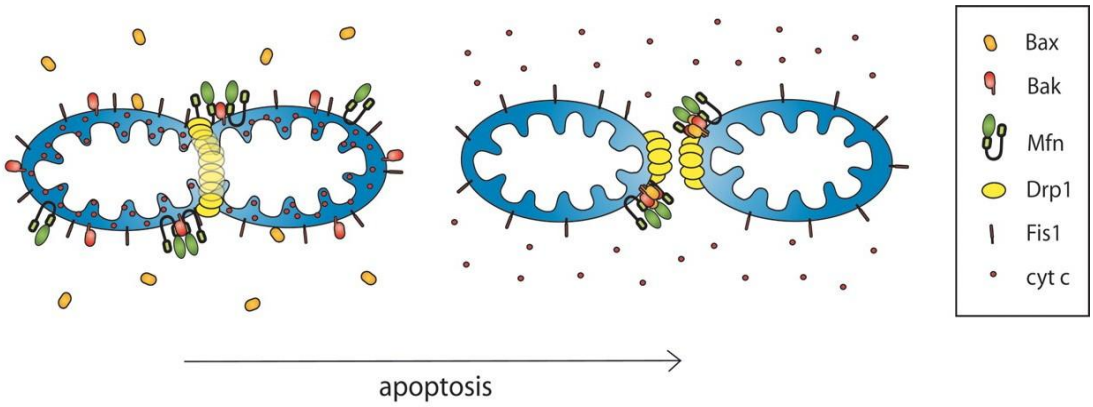

Figure 1-14 Model of apoptosis progression. From *left* to *right*, Bax is translocated to mitochondria where it coalesces with DRP1, MFN2 and Bak. These series of events result in mitochondrial fission and release of cytochrome *c* from mitochondrial cristae. (Reproduced from Suen et al., 2008).

1.8.2 Mitochondrial Fusion

Mitochondrial fusion is a highly coordinated process involving firstly outer membrane and followed by inner membrane fusion (Chen et al., 2003; Cipolat et al., 2004). Three large members of a dynamin-related GTPase superfamily are essential to the fusional process: MFN1, MFN2 and OPA1 (**Figure 1-15**). Mitofusins are responsible for the fusion of the OMM whereas OPA1 facilitates fusion of the IMM (Santel and Fuller, 2001; Chen et al., 2003; Cipolat et al., 2004; Song et al., 2009).

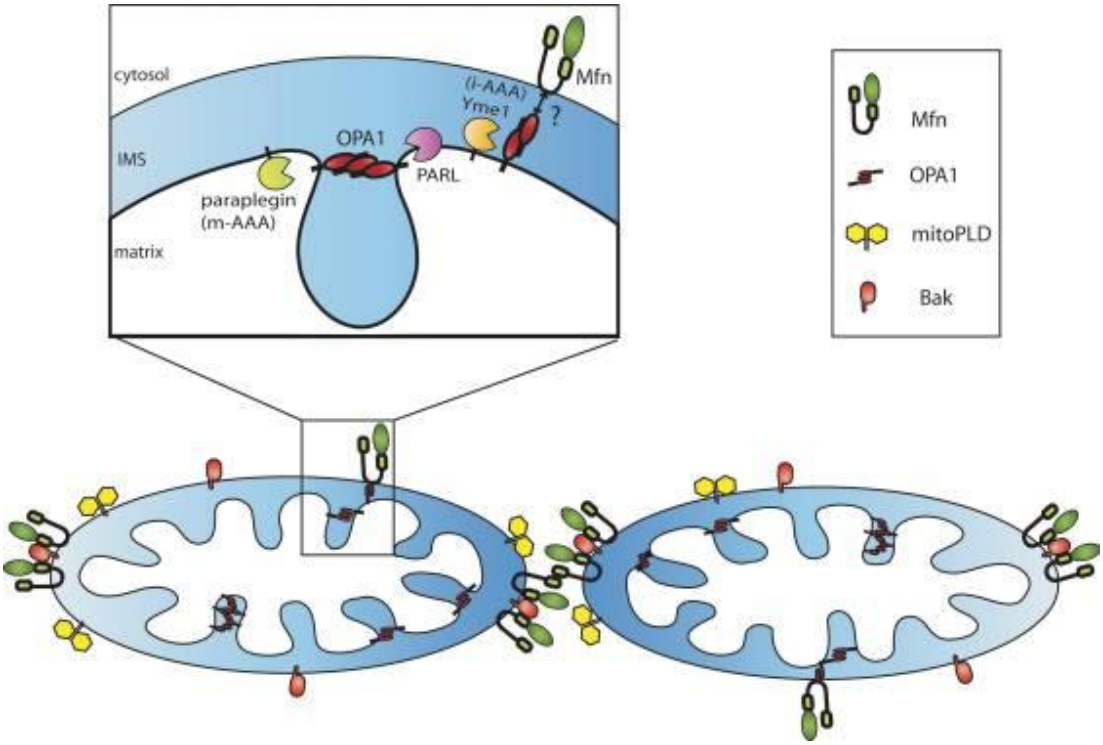

Figure 1-15 Diagram illustrating main proteins involved in fusion of mammalian mitochondria. Mitofusins (MFN1 and MFN2) facilitate OMM fusion while OPA1 controls IMM fusion; mitoPLD (mitochondrial phospholipase D) recruits fusion proteins; mitochondrial proteases: PARL (presenilin-associated rhomboid-like) protease, m-AAA and i-AAA are involved in OPA1 cleavage. (Reproduced from Suen et al., 2008).

1.8.2.1 MFN1 and MFN2

MFN1 and MFN2 are two large GTPases involved in the fusion of the OMM (Chen et al., 2003). Human MFN1 and MFN2 show about 60% homology and a high degree of evolutionary conservation to their yeast homologue Fzo1 (Hermann et al., 1998; Santel and Fuller, 2001; Zorzano, 2010). Both mitofusins are transmembrane proteins integrated in the OMM, with a conserved N-terminal region containing a GTPase-binding domain and a coiled-coil 1 domain (CC1 or heptad-repeat 1; HR1), as well as a C-terminal region consisting of a bipartite transmembrane domain and another coiled-coil domain CC2, also known as the HR2 domain (**Figure 1-16**) (Zorzano, 2010). Both GTPase and HR2 domains face the cytosolic side of the OMM (Rojo et al., 2002; Zorzano, 2010). Mitofusins are capable of forming homo- or heterotypic complexes which mediate tethering between neighbouring mitochondria (Chen et al., 2003; Koshiba et al., 2004; Meeusen et al., 2004).

The central GTPase domain of MFN1 and MFN2 consists of five G motifs (G1 to G5) and these are responsible for binding the phosphate moiety of the GTP molecule (G1), coordinating Mg^{2+} content (G3), activating catalytic activities (G1, G2, G3), and providing a conformation site for GTP binding (G4, G5) (Bourne and McCormick, 1990; Zorzano, 2010). Apart from the GTPase domain, mitofusins contain two coiled-coil domains (CC1 and CC2) tethering adjacent mitochondria and a transmembrane domain (TM). Interestingly, the proline-rich domain (PR) involved in protein-protein interactions is only found in MFN2, being absent in MFN1 (Chen et al., 2003; Zorzano, 2010). MFN2 has been described in more detail in **Section 1.11.3** below.

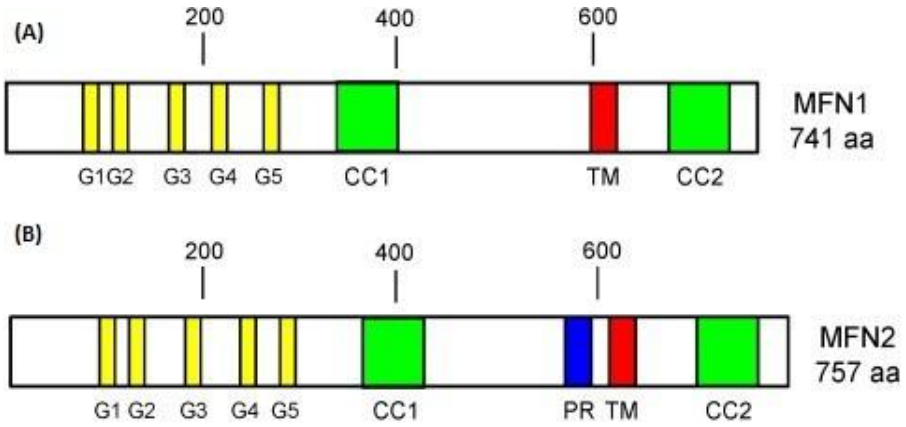

Figure 1-16 MFN1 and MFN2 protein structures - (A) and (B) respectively. GTPase domain motifs (G1 to G5), coiled-coil domains (CC1 and CC2), a transmembrane domain (TM) and a proline-rich domain (PR). (Reproduced from Zorzano, 2010).

1.8.2.2 OPA1

OPA1 is the major protein regulating inner mitochondrial membrane fusion (Meeusen et al., 2004; Meeusen et al., 2006). OPA1 is a dynamin-related GTPase localized within the IMM and it is orthologous to the fungal Msp1 and yeast Mgm1p proteins (Olichon et al., 2002; Landes et al., 2010). In humans, the *OPA1* gene (3q28–q29) is composed of 30 exons; three exons (4, 4b and 5b) are alternatively spliced, resulting in eight specific mRNA isoforms (Delettre et al., 2001; Olichon et al., 2002). As a consequence, the OPA1 protein can range in size from 924 to 1014

amino acids depending on the particular splice variant that is transcribed (Delettre et al., 2001). *OPA1* transcripts are widely expressed in human tissues but they predominate in the brain, retina, heart, and muscle (Alexander et al., 2000; Delettre et al., 2001).

OPA1 consists of: (i) an N-terminal mitochondrial import sequence (MIS) conferring mitochondrial localisation; (ii) a predicted transmembrane region (TM1) associating OPA1 to the inner mitochondrial membrane; (iii) a coiled-coil 1 region (CC1) most likely involved in protein-protein interactions; (iv) a GTPase domain composed of three G motifs (G1, G3 and G4) associated with functions as described for adequate G motifs of mitofusins (please refer to **Section 1.8.2.1** for details); (v) a middle domain, and (vi) a carboxy-terminal coiled-coil domain (CC2), also known as the GTPase effector domain (GED), which is predicted to facilitate interactions between OPA1 and mitofusins (Landes et al., 2010; Zorzano, 2010). Two transmembrane domains (TM2a and TM2b) and an additional coiled-coil region (CC0) are only available in splice variants 4b and 5b (Olichon et al., 2007) (**Figure 1-17**).

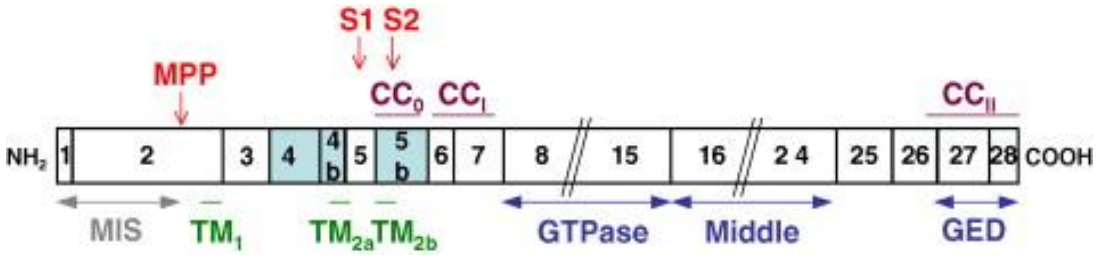

Figure 1-17 *OPA1* gene and protein structure. OPA1 consists of 30 exons (including exons 4b and 5b). The protein domains encoded by particular exons are highlighted below the numbering. MPP, S1 and S2 – proteolytic cleavage sites for Mitochondrial Processing Peptidase (MPP), Paraplegin (S1) and YME1L (S2). (Reproduced from Landes et al., 2010).

OPA1 can exist as long (l-OPA1) and short (s-OPA1) isoforms, depending on the number of proteolytic cleavage sites that get activated (Landes et al., 2010). L-OPA1 isoforms are attached to the IMM while s-OPA1 forms, missing TM1, are believed to be either peripherally anchored to the IMM, diffused within the IMS, or associated with the OMM (Olichon et al., 2002; Satoh et al., 2003; Cipolat et al., 2006; Landes et al., 2010). Formation of the long OPA1 isoforms (l-OPA1) involves cleavage of

the mitochondrial import sequence (MIS) by the mitochondrial processing peptidase (MPP) (Olichon et al., 2002; Satoh et al., 2003; Landes et al., 2010). Short forms are generated by protelolytic cleavage occurring additionally at the S1 and S2 sites, located within exons 5 and 5b, respectively (Ishihara et al., 2006; Song et al., 2007). Three mitochondrial proteases are known to recognize S1 and S2 cleavage sites: (i) presenilin-associated rhomboid-like (PARL) protease, which generates the s-OPA1 isoform, soluble in the IMS (Cipolat et al., 2006), (ii) matrix AAA protease (m-AAA), which forms homo- or heteromeric complexes (containing paraplegin, Afg3L1 and Afg3L2 subunits) capable of cleaving OPA1 at S1 (Ishihara et al., 2006); and finally intermembrane AAA protease (i-AAA) YME1L, which is responsible for cleaving OPA1 at S2 and possibly other sites as well (Griparic et al., 2007; Song et al., 2009). The current view is that the correct balance between long and short isoforms of OPA1 plays an important role in regulating the efficiency of mitochondrial fusion (Song et al., 2007).

Other functions of OPA1 are described in more detail in **Section 1.10.3** below.

1.8.2.3 MitoPLD

Mitochondrial phospholipase D (mitoPLD) is a dimeric enzyme that has recently been proposed to take part in mitochondrial fusion (Choi et al., 2006). MitoPLD binds to the OMM through an amino-terminal transmembrane segment, whereas its catalytic domain faces the cytosol (Jensen and Sesaki, 2006). Following mitofusin-mediated tethering of two mitochondria, mitoPLD places its catalytic domain in the membrane of an adjacent mitochondrion and then it hydrolyses cardiolipin. The cardiolipin then produces phosphatidic acid, which is thought to activate or recruit other fusion proteins or to be a fusogenic lipid itself (Choi et al., 2006; Jensen and Sesaki, 2006; Suen et al., 2008).

1.8.3 Mitochondrial Fission

Mitochondrial fission in mammals requires DRP1. This key protein is recruited from the cytosol to interact with the outer membrane hFis1 protein (Smirnova, 2001; Yoon et al., 2003; Wasiak et al., 2007). DRP1 and hFis1 are the mammalian homologues of the yeast Dnm1 and fis1p, respectively (Bleazard et al., 1999; Fannjiang et al., 2004).

1.8.3.1 DRP1 and hFis1

DRP1 consists of an amino-terminal GTPase domain, a middle domain and a carboxy-terminal GTPase effector domain involved in self-assembly (Westermann, 2010). As a result of alternative splicing in humans, there is a brain-specific DRP1 isoform that contains an additional insertion between the middle region and the GTPase effector domain (Smirnova et al., 1998). Mitochondrial hFis1 is a small outer mitochondrial membrane protein and it consists of a transmembrane domain and a tetratricopeptide (TPR) region (Westermann, 2010). The widely accepted mechanism of mammalian mitochondrial fission assumes hFis1-mediated recruitment of DRP1 from the cytosol and formation of DRP1-hFis1 complexes on the OMM, thereby initiating fission of both the outer and inner mitochondrial membranes (**Figure 1-18**) (Suen et al., 2008; Westermann, 2010). DRP1-hFis1 complexes form spirals at division sites tightly enclosing the mitochondrial tubule, eventually leading to fission (Suen et al., 2008). However, the exact mechanism of mammalian fission is likely to be more complex. For example, recent studies have revealed that DRP1 is capable of assembling on mitochondria without hFis1 (Lee et al., 2004).

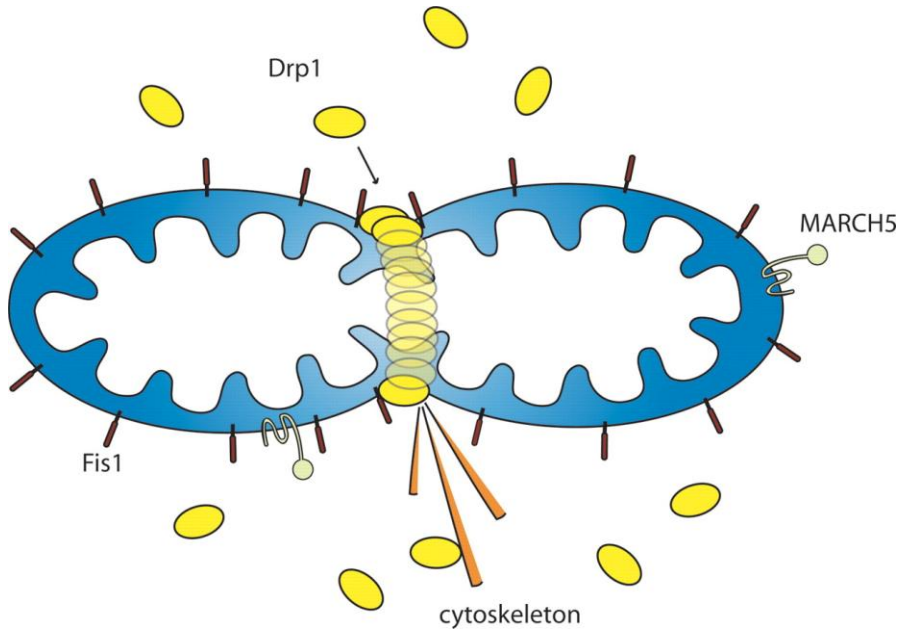

Figure 1-18 Mitochondrial fission machinery. DRP1 is located in the cytosol and it is recruited to the OMM by hFis1 protein. DRP1-hFis1 complexes form spirals at division sites tightly enclosing the mitochondrial tubule and leading to fission of both the outer and inner mitochondrial membranes. (Reproduced from Suen et al., 2008).

1.9 Mitochondrial Genetic Disorders

Mitochondrial cytopathies form a heterogeneous group of human disorders caused by the disturbance of mitochondrial function. Mitochondrial disorders can be classified into two main groups: (i) primary mitochondrial DNA disorders, associated with primary mtDNA point mutations or rearrangements (deletions and duplications), and (ii) nuclear mitochondrial disorders, related to mutations affecting a large number of nuclear genes required for the complex assembly and stability of the mitochondrial machinery. These nuclear mitochondrial disorders are frequently linked to mtDNA instability manifesting as either secondary mtDNA deletions or depletion (Kirkman et al., 2008). Mitochondria are obligate intracellular organelles and they mediate a host of critical cell functions, including energy production through OXPHOS. Unsurprisingly, mitochondrial cytopathies are clinically highly heterogeneous, with patients frequently manifesting a diverse combination of tissue and organ involvement (McFarland et al., 2002b; Sitarz et al., 2012b).

1.9.1 Primary Mitochondrial DNA Disorders

Primary mtDNA disorders can be broadly classified into those secondary to mtDNA point mutations or mtDNA rearrangements (Tuppen et al., 2010). Pathogenic mtDNA point mutations are usually heteroplasmic, but several pathogenic homoplasmic mtDNA variants, often affecting only selected tissues and demonstrating incomplete penetrance, have now been identified (McFarland et al., 2002a; Taylor et al., 2003; Tuppen et al., 2010). The clinical manifestations associated with primary mtDNA mutations are highly variable (**Figure 1-19**), and for some mutations, the age of onset and phenotypic severity usually reflects the mutational load in affected tissues (Tuppen et al., 2010). MtDNA deletions are the most common large-scale genomic rearrangements identified in patients with primary mtDNA disorders. These deletions extend across several critical tRNA and polypeptide-encoding genes, resulting in a significant impairment in OXPHOS and energy production (Schon et al., 1989; Chen et al., 1995; Tuppen et al., 2010).

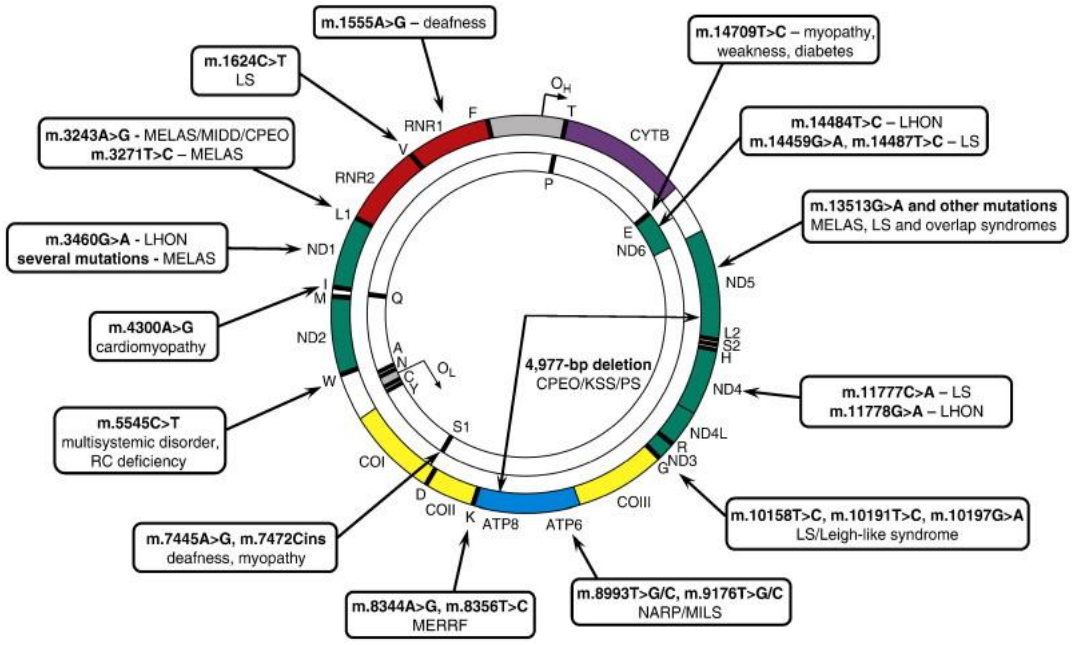

Figure 1-19 Primary mtDNA mutations and their phenotypic manifestations. CPEO - chronic progressive external ophthalmoplegia; LHON - Leber hereditary optic neuropathy; LS - Leigh syndrome; MELAS - mitochondrial myopathy, encephalopathy, lactic acidosis, and stroke-like episodes; MERRF - myoclonic epilepsy and ragged red fibres; MILS - maternally inherited Leigh syndrome; NARP - neurogenic weakness, ataxia, and retinitis pigmentosa; PS - Pearson syndrome. (Reproduced from Tuppen et al., 2010).

1.9.1.1 Leber Hereditary Optic Neuropathy

Leber hereditary optic neuropathy (LHON, OMIM 535000) is the most common primary mitochondrial DNA disorder in the general population, with a minimum prevalence of approximately 1 in 31,000 in the North of England (Yu-Wai-Man et al., 2003). The majority (90-95%) of individuals suffering from LHON harbour one of the three mtDNA point mutations: (i) m.3460G>A (Howell et al., 1991; Huoponen et al., 1991), (ii) m.11778G>A (Wallace et al., 1988) and (iii) m.14484T>C (Johns et al., 1992; Mackey and Howell, 1992). The peak age of onset of visual loss is usually in the second and third decades of life and it is characterized by severe, painless loss of central vision (Johns et al., 1993). Visual loss is bilateral in about 25% of cases, when unilateral, the second eye is usually affected within three months (Yu-Wai-Man et al., 2009; Yu-Wai-Man et al., 2011b). Optic disc pallor becomes evident about six weeks following the onset of visual loss (Yu-Wai-Man et al., 2011b). Pathological cupping of the optic disc is a characteristic feature of established LHON cases, reflecting the irreversible loss of retinal ganglion cell (RGC) axons in the chronic phase of the disease (Yu-Wai-Man et al., 2011b).

LHON is characterized by incomplete penetrance and a marked sex bias, with only about 50% of male carriers and about 10% of female carriers losing vision during their lifetime (Yu-Wai-Man et al., 2011b). The overall prognosis in LHON is poor, even among patients harbouring the m.14484T>C mutation, which carries the best chance for the partial visual recovery (Yu-Wai-Man et al., 2009). LHON is typically a monosymptomatic disease but additional features such as cardiac conduction defects, peripheral neuropathy, dystonia, and myopathy have been reported as occurring more frequently among LHON carriers. In particular, there is a well-reported association between the three primary mtDNA LHON mutations and a multiple sclerosis-like illness, especially among female carriers. Rarer pathogenic mtDNA variants have been linked with more atypical “LHON +” syndromes, where the optic neuropathy segregated with prominent neurological features including spastic dystonia, ataxia, juvenile-onset encephalopathy, and psychiatric disturbances (Yu-Wai-Man et al., 2011b; Sitarz et al., 2012b).

1.9.2 Nuclear Mitochondrial Disorders

Mutations involving nuclear-encoded mitochondrial proteins participating in mtDNA maintenance can result in a decrease in mtDNA copy number, the accumulation of high-levels of somatic mtDNA mutations (point mutations and deletions), or both (**Table 1-1**) (Alberio et al., 2007; Spinazzola and Zeviani, 2009; Yu-Wai-Man et al., 2011b). The recognition of these mtDNA abnormalities in diagnostic samples point towards an underlying nuclear defect and the need for additional targeted molecular investigations (Yu-Wai-Man et al., 2011b). MtDNA depletion is the pathological hallmark found in a number of early-onset nuclear mitochondrial disorders (Yu-Wai-Man et al., 2011b). There is a significant reduction in mtDNA copy number, which can be highly tissue-specific, partly explaining the phenotypic variability of these diseases (Spinazzola et al., 2009). The histochemical investigations of muscle biopsies of individuals with nuclear-mitochondrial disorders frequently reveal the presence of COX-deficient muscle fibres (**Section 1.9.4.1**) (Yu-Wai-Man et al., 2011b). The biochemical COX-defect associated with nuclear genetic mutations involving *OPA1, POLG1* or *POLG2* has been linked to the accumulation of multiple mtDNA deletions, which have clonally expanded above the threshold levels of approximately 70% (Horvath et al., 2006; Amati-Bonneau et al., 2008; Hudson et al., 2008a; Spinazzola and Zeviani, 2009). Multiple mtDNA deletions can accumulate exponentially in post-mitotic tissues of both healthy elderly individuals and in those suffering from neurodegenerative diseases, such as Parkinson disease and Alzheimer's dementia (Cortopassi et al., 1992; Bender et al., 2006; Kraytsberg et al., 2006). Crucially, mtDNA deletions frequently span over critical regions of the mitochondrial genome, resulting in OXPHOS impairment and ultimately leading to cell death and tissue dysfunction (Yu-Wai-Man et al., 2011b).

Table 1-1 Nuclear mitochondrial disorders. (Adapted from Yu-Wai-Man et al., 2011b).

Mutations involving structural subunits of the mitochondrial respiratory chain:
Leigh syndrome: with complex I deficiency – mutations in *NDUFS1, NDUFS2, NDUFS3, NDUFS4, NDUFS6, NDUFS7, NDUFS8, NDUFV1, NDUFV2, NDUFA1, NDUFA8, NDUFA11, ACAD9*; with complex II deficiency – mutations in *SDHA*
Cardiomyopathy and encephalopathy with complex I deficiency – mutations in *NDFUS2*
Optic atrophy and ataxia with complex II deficiency – mutations in *SDHA*
Hypokalaemia and lactic acidosis with complex III deficiency – mutations in *UQCRB*
Mutations involving assembly factors of the mitochondrial respiratory chain:
Leigh syndrome: with COX defect – mutations in *SURF1* and *LRPPRC*; with complex I defect – mutations in *NDUFAF2, C20orf7, C8orf38*
Hepatopathy and ketoacidosis – mutations in *SCO1*
Cardiomyopathy and encephalopathy – mutations in *SCO2*
Leukodystrophy and renal tubulopathy – mutations in *COX10*
Hypertrophic cardiomyopathy – mutations in *COX15*
Encephalopathy, liver failure, and renal tubulopathy with complex III deficiency – mutations in *BCS1L*
Encephalopathy with complex V deficiency – mutations in *ATP12* and *TMEM70*
Nuclear genetic disorders of intra-mitochondrial protein synthesis:
Leigh syndrome – mutations in *MTFMT* and *C12orf65*
Leigh syndrome, liver failure, and lactic acidosis – mutations in *EFG1*
Lactic acidosis and developmental failure – mutations in *MRPS16*
Infantile reversible liver failure – mutations in *TRMU*
Leukodystrophy and polymicrogyria – mutations in *EFTu*
Myopathy and sideroblastic anaemia – mutations in *PUS1* and *YARS2*
Encephalomyopathy and hypertrophic cardiomyopathy – mutations in *EFTs*
Edema, hypotonia, cardiomyopathy, and tubulopathy – mutations in *MRPS22*
Pontocerebellar hypolasia – mutations in *RARS2*

Nuclear genetic disorders of mitochondrial protein import
Mohr-Tranebjaerg syndrome or deafness-dystonia-optic neuronopathy (DDON) syndrome – mutations in *TIMM8A* (*DDP*)
Early-onset dilated cardiomyopathy with ataxia (DCMA) or 3-methylglutaconic aciduria, type V – mutations in *DNAJC19*
Nuclear genetic disorders of mitochondrial DNA maintenance
Chronic progressive external ophthalmoplegia – mutations in *POLG1*, *POLG2*, *PEO1*, *SLC25A4*, *RRM2B*, *TK2* and *OPA1*
Mitochondrial neurogastrointestinal encephalomyopathy – mutations in *TYMP*
Alpers-Huttenlocher syndrome (AHS) – mutations in *POLG1* and *MPV17*
Infantile myopathy and spinal muscular atrophy – mutations in *TK2*
Encephalomyopathy and liver failure – mutations in *DGUOK* and *MPV17*
Hypotonia, renal tubulopathy, and lactic acidosis – mutations in *RRM2B*
Hypotonia, movement disorder and/or Leigh syndrome with methylmalonic aciduria – mutations in *SUCLA2* and *SUCLG1*
Optic atrophy, deafness, chronic progressive external ophthalmoplegia, myopathy, ataxia, and peripheral neuropathy – mutations in *OPA1*
Miscellaneous
Co-enzyme Q10 deficiency – mutations in primary biosynthesis genes *PDSS1*, *PDSS2*, *COQ2*, *COQ6*, *COQ9* and *ADCK3*; secondary Co-enzyme Q10 deficiency – mutations in *ETFDH* and *APTX*
Barth syndrome – mutations in *TAZ*
Sengers syndrome – mutations in *AGK*
Cardiomyopathy and lactic acidosis associated with mitochondrial phosphate carrier deficiency – mutations in *SLC25A3*

Alpers-Huttenlocher syndrome (AHS): epilepsy, cortical blindness, micronodular hepatic cirrhosis, episodic psychomotor regression; Barth syndrome: cardiomyopathy, hypotonia, weakness, and neutropenia; Sengers syndrome – congenital cataract, hypertrophic cardiomyopathy, myopathy and lactic acidosis.

1.9.3 Mitochondrial DNA Deletions

1.9.3.1 Formation

The great majority of mtDNA deletions take place within the major arc of the mitochondrial genome between the two origins of replication (O_H and O_L; please refer to **Section 1.4.2** for details) (Samuels et al., 2004; Bua et al., 2006; Krishnan et al., 2008). Most mtDNA deletions (~ 60%; class I deletions) are flanked by two 13-bp homologous direct repeat sequences, one of which is removed by the deletion process (Samuels et al., 2004). Class II deletions (~ 30% cases) are flanked by imperfect repeats, whereas class III deletions (~ 10% cases) have no direct repeat sequences participating in a deletion process (Samuels et al., 2004).

Several different hypotheses have been suggested to explain the mechanism underlying mtDNA deletion formation (Krishnan et al., 2008). Originally mtDNA deletions were thought to occur through a slipped-strand replication mechanism based on the Clayton's asymmetric strand-displacement replication mode (**Section 1.4.2.1**) (**Figure 1-20**) (Clayton, 1982; Shoffner et al., 1989). However, if replication is the main mechanism behind the formation of mtDNA deletions, then mitotic cells, where mtDNA replication is a more frequent event, should have greater mtDNA deletion loads when compared with post-mitotic tissues (Krishnan et al., 2008). As recently confirmed in human colonic tissue, this is not always the case, hence a different model has been proposed, which explains the generation of mtDNA deletions during the repair of double-stranded breaks (DSBs) within mtDNA molecules (**Figure 1-21**) (Krishnan et al., 2008). According to this theory, single-stranded fragments of mtDNA are generated through 3′→5′ exonuclease activity at double-strand breaks (Krishnan et al., 2008). The 5'- and 3'-repeat fragments can misanneal resulting in degradation of the unbound single strands, ligation of the double strands and ultimately the formation of deleted mtDNA molecules (Krishnan et al., 2008).

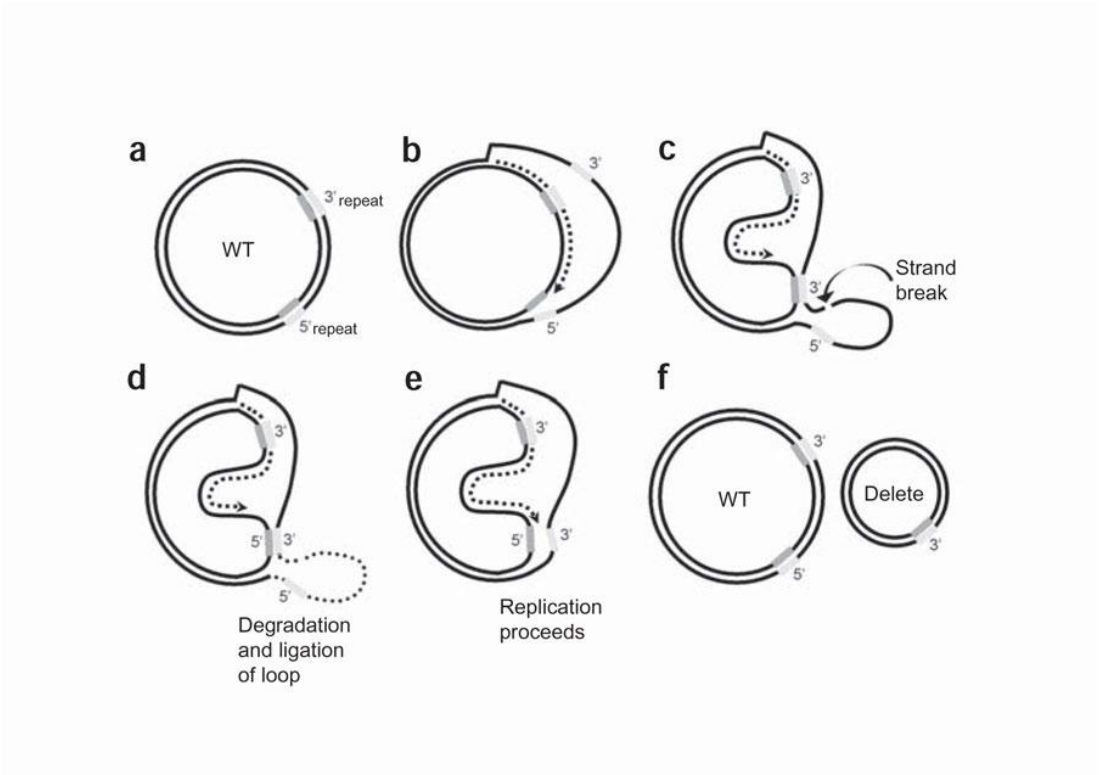

Figure 1-20 Formation of a mtDNA deletion through a slipped-strand model of replication. (a) The mtDNA molecule contains two direct repeats labelled 5′ and 3′; (b) Replication of mtDNA commences at O_H of D-loop, displacing the light strand from the heavy strand; (c) The single-stranded 3′ repeat of the light strand misanneals with the newly exposed single-stranded 5′ repeat of the heavy strand, which generates a downstream, single-stranded and susceptible to strand breaks light-strand loop; (d) The damaged loop is degraded until it reaches the double-stranded regions, and ligation of the free ends of the heavy strand happens; (e) Replication is continued leading to production of a wild-type and a deleted mtDNA molecules (f). (Reproduced from Krishnan et al., 2008).

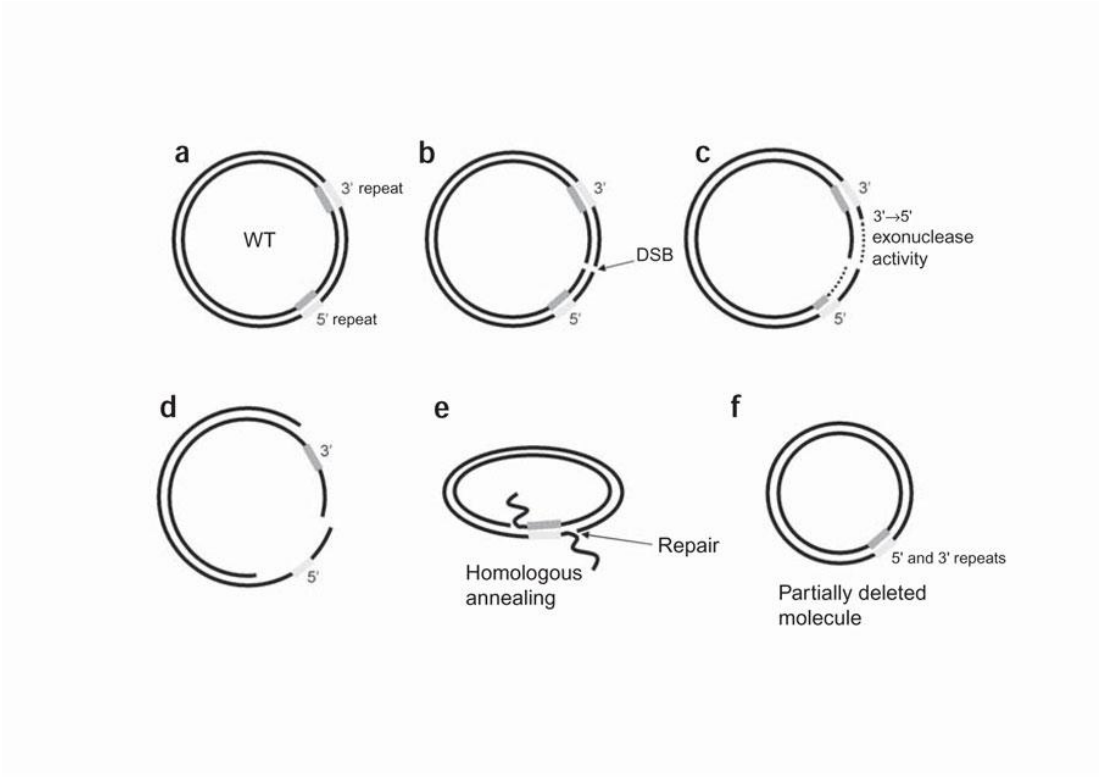

Figure 1-21 Formation of mtDNA deletions during repair of double-stranded breaks. (a) The mtDNA molecule contains two direct repeats labelled 5′ and 3′; (b) A double-stranded break occurs; (c-d) The double-stranded break is susceptible to 3′→5′ exonuclease activity, resulting in production of single strands; (e) The 5′- and 3′-repeat sequences can misanneal, leading to degradation of the unbound single strands, and ligation of the double strands; (f) A deleted mtDNA molecule containing copies of both the 5′ and 3′ repeats, is generated. (Reproduced from Krishnan et al., 2008).

1.9.3.2 Clonal Expansion

Following the formation of a mtDNA deletion, a biochemical defect is only expressed once a mutated mtDNA molecule clonally expands to a level exceeding the critical threshold (Chinnery and Samuels, 1999). Two main mechanisms explaining clonal expansion of mutated mtDNA molecules have been proposed so far: (i) the random genetic drift (Chinnery and Samuels, 1999; Elson et al., 2001) and (ii) an advantageous replication of deleted mtDNA molecules (Fukui and Moraes, 2009; Nicholas et al., 2009).

The random genetic drift theory suggests that relaxed replication of mtDNA, followed by random genetic drift, leads to the clonal expansion of single mutant events during human life (Chinnery and Samuels, 1999; Elson et al., 2001). The

accumulation of mutated mtDNA molecules is balanced by the increase in mitochondrial proliferation acting as a compensatory mechanism to preserve sufficient levels of wild-type mtDNA genomes, allowing normal respiratory chain function (Chinnery and Samuels, 1999; Elson et al., 2001). However, once the mutational level exceeds a defined threshold level, further mitochondrial proliferation results in the replication of the mutated mtDNA molecules at the cost of wild-type genomes, leading to COX-deficiency (Chinnery and Samuels, 1999; Elson et al., 2001). Noteworthy, the ratio between wild-type and mutated mtDNA genomes can be tissue-specific (Durham et al., 2007).

The second model suggests the occurrence of a positive selection for deleted mtDNA species during replication (Fukui and Moraes, 2009; Nicholas et al., 2009). According to this theory, smaller sized, deleted mtDNA molecules are thought to replicate at a higher rate than larger, wild-type mtDNA genomes (Fukui and Moraes, 2009; Nicholas et al., 2009). The level of accumulation of mutated mtDNA species is believed to be inversely proportional to mtDNA deletion size (Diaz and Moraes, 2008; Fukui and Moraes, 2009; Nicholas et al., 2009).

1.9.4 Diagnostic Investigations

Mitochondrial disorders are clinically and genetically heterogeneous and reaching an accurate diagnosis can be a challenging task. If an underlying mitochondrial genetic disorder is suspected, it is advisable to perform molecular investigations directly on the affected tissue, if available. Tissue specificity is an important consideration, e.g. in patients with mtDNA maintenance disorders secondary to nuclear mutations in *POLG1*, mtDNA deletions are usually not detectable in blood, an easily accessible tissue, but they can be identified in post-mitotic tissues such as skeletal muscle (McFarland et al., 2002b). The comprehensive analysis of skeletal muscle specimens using a range of validated histochemical, biochemical and genetic diagnostic tools, is crucial to reach a diagnosis for a large number of patients with suspected mitochondrial disease (**Figure 1-22**) (McFarland et al., 2002b).

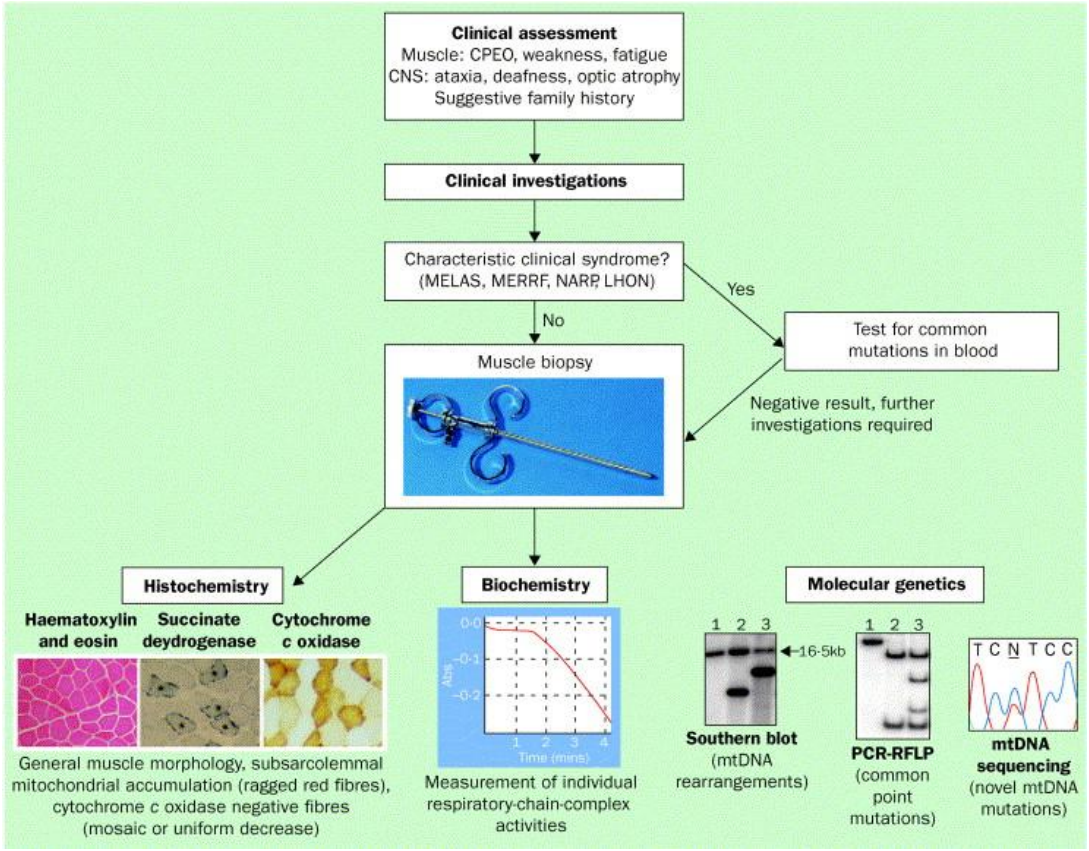

Figure 1-22 Muscle biopsy examinations on patients with suspected mtDNA disorders. (Reproduced from McFarland et al., 2002b).

1.9.4.1 Histochemical Assessment

Mitochondrial histochemical staining performed on skeletal muscle sections is a powerful method of detecting an underlying OXPHOS defect. Numerous well-established staining protocols are commonly used (**Figure 1-23**), involving: (i) haematoxylin and eosin (H&E), (ii) modified Gomori trichrome, (iii) COX and (iv) SDH, as well as (v) myofibrillar ATPase.

H&E stain allows the demonstration of the basic muscle fibre morphology, whereas modified Gomori trichrome stain is performed to reveal abnormal subsarcolemmal accumulation of mitochondria in muscle fibres (so called ragged-red fibres; RRFs). RRFs can also be detected through SDH histochemistry.

Succinate dehydrogenase (SDH; complex II) is encoded entirely by nuclear DNA whereas cytochrome *c* oxidase (COX; complex IV) consists of both mitochondrial- and nuclear-encoded subunits. If mtDNA integrity is compromised e.g. by point

mutations or deletions, this will have a deleterious effect on overall COX activity, whereas SDH activity remains unchanged unless a nuclear defect affects one of its four subunits. Muscle fibres with normal COX activity stain brown (COX-positive) whereas COX-deficient (COX-negative) fibres remain unstained. SDH activity is indicated by the intensity of the blue staining. Following dual COX/SDH staining, COX-negative fibres are highlighted blue whereas COX-positive fibres remain brown in colour. A mosaic pattern of COX-negative muscle fibres is often found in patients suffering from heteroplasmic mtDNA mutations and nuclear mitochondrial disorders characterised by the accumulation of secondary mtDNA deletions (Yu-Wai-Man et al., 2011b). However, some caution is required as COX-negative muscle fibres are not always pathological. It is well established that low levels of COX-negative fibres (1 - 2%) can be detected in skeletal muscle from normal elderly individuals as a result of the age-related clonal expansion of somatic mtDNA deletions (Brierley et al., 1998; Bodyak et al., 2001).

The myofibrillar ATPase staining can be performed to illustrate the distribution of different muscle fibre types, broadly classified as type I (slow contracting, oxidative) or type II (fast contracting, glycolytic/oxidative). ATPase histochemistry allows identification of pathological features such as fibre atrophy or fibre-type grouping, indicative of peripheral neuropathy, a common feature of mitochondrial diseases. In the first step of the ATPase staining protocol, fibres are preincubated with an acid solution (pH ~ 4), which inhibits ATPase activity in fast (type II) fibres. As a result, type I muscle fibres are stained dark brown, whereas type II muscle fibres remain light brown in colour.

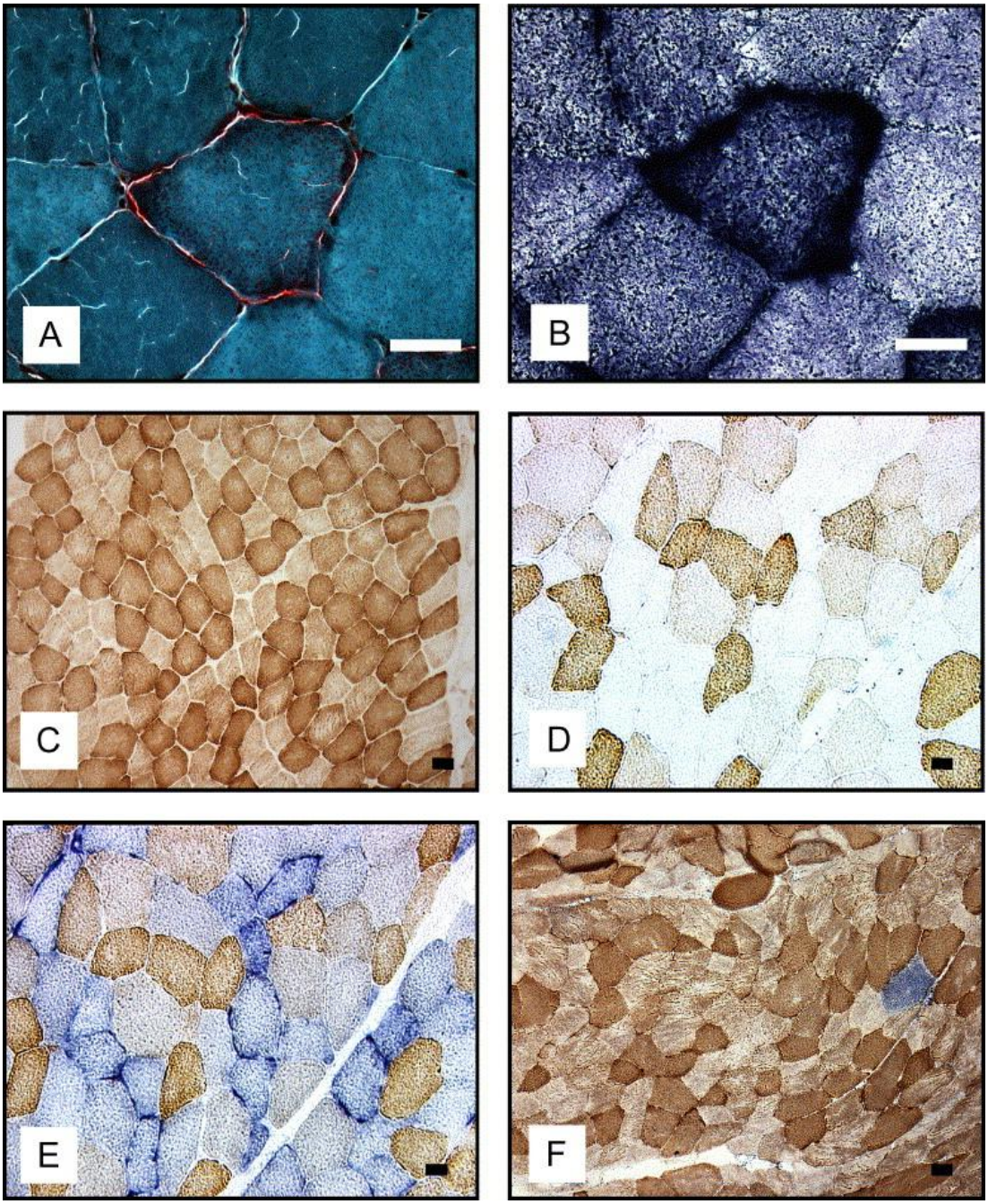

Figure 1-23 Histochemical features of mitochondrial dysfunction. (A) Typical ragged-red muscle fibre revealed by Gomori trichrome staining; (B) Serial section of the muscle fibre shown in (A) following SDH histochemistry; (C) Normal COX staining revealing presence of a mixed population of muscle fibre types (type I – dark, type II - light in colour); (D) Abnormal COX histochemistry from a patient with CPEO, showing a number of COX-deficient fibres; (E) Sequential COX/SDH staining on a serial section of (D), revealing abnormal COX-negative (blue) muscle fibres and normal COX-positive (brown) muscle fibres; (F) Dual COX/SDH histochemistry revealing a single COX-deficient muscle fibre in a section of the ageing muscle. (Reproduced from Taylor et al., 2004).

1.9.4.2 Biochemical Assessment

Measurements of individual respiratory chain complex activities are routinely performed in patients with suspected mitochondrial disease (McFarland et al., 2002b). Ideally, biochemical studies should be carried out on fresh muscle samples, however this is not always possible and frozen muscle sections can be used instead (Taylor et al., 2004). Mitochondrial DNA disorders can be associated either with an isolated defect limited to a single respiratory chain complex or present with a combined deficiency pattern involving several OXPHOS complexes (McFarland et al., 2002b). The majority of combined respiratory chain deficiencies involve complexes: I and IV, I and III, or I, III and IV (Loeffen et al., 2000). Interestingly, combined respiratory chain defects involving complex II (SDH) are relatively rare and if present, affect mostly the muscle tissue (Desnuelle et al., 1989; Vladutiu and Heffner, 2000).

1.9.4.3 Genetic Assessment

Molecular genetic investigation should routinely be carried out for all patients found to have abnormal mitochondrial histochemical and biochemical findings. Even if these tests are negative, consideration should still be given to genetic testing for those patients presenting with clear-cut mitochondrial phenotypes (McFarland et al., 2002b). Patients with clinical manifestations which fit a typical presentation should be referred for screening for the implicated mutations e.g. the m.3243A>G mutation in MELAS or the m.8344A>G mutation in MERRF (McFarland et al., 2002b). Genetic screening is routinely carried out using either restriction fragment length polymorphism (RFLP) assays or with direct polymerase chain reaction (PCR)-based sequencing (McFarland et al., 2002b). Alternatively, DNA samples from patients negative for the most common mtDNA mutations can be subjected to whole mitochondrial genome sequencing (Taylor et al., 2001; McFarland et al., 2002b). However, mtDNA is highly polymorphic and proving pathogenicity for novel variants can be challenging without functional confirmation (McFarland et al., 2002b). If possible, genetic tests should be performed on DNA extracted from an affected tissue, for example, using muscle homogenate DNA in a patient with a myopathy. Unfortunately, despite being highly accessible, blood is not an ideal sample for investigating several mitochondrial disorders as it can contain decreased

levels of some mtDNA mutations, a good illustration being the m.3243A>G (Pyle et al., 2007; Rajasimha et al., 2008).

Mitochondrial disorders associated with mtDNA rearrangements: single deletion, multiple mtDNA deletions, and mtDNA duplications, can be detected using a range of techniques, which include Southern blot, long-range PCR and quantitative real-time PCR assays (Taylor et al., 2004). Southern blotting has long been considered the 'gold standard' technique allowing precise detection and quantification of single mtDNA deletions. However, a limitation is that it may fail to detect low levels of multiple mtDNA deletions (Deschauer et al., 2003; Taylor et al., 2004). Long-range PCR analysis is more sensitive than Southern blotting, however, because it preferentially amplifies smaller mtDNA species, an accurate quantification of the deletion load is not possible (Taylor et al., 2004). Recently, fluorescent-probed real-time PCR assays are more commonly used. This technique is very sensitive and moreover, it requires only small amounts of DNA, allowing quantitative genetic analysis to be performed at a single-cell level (He et al., 2002). Real-time PCR can be used to quantify mtDNA deletion levels as well as mtDNA copy number in individual COX-positive and COX-negative muscle fibres, providing a reliable tool for investigating the mutation threshold required to trigger a biochemical defect (Durham et al., 2005; Durham et al., 2007).

Screening of well-characterised nuclear-encoded genes like *POLG1* or *PEO1*, often allows the identification of the contributory genetic alteration in patients with confirmed multiple mtDNA deletions (Hudson and Chinnery, 2006; Chinnery and Zeviani, 2008). Nevertheless, the underlying genetic basis for a large proportion of suspected nuclear-encoded mitochondrial disorders have yet to be clarified and the development of new high-throughput sequencing techniques, such as exome sequencing, will prove crucial in dissecting the causative genetic defect.

1.10 *OPA1*-Related Disorders

1.10.1 *OPA1* gene

OPA1 mutations are the most common causes of autosomal-dominant optic atrophy (DOA) and they are found in about 60% of patients with a clinical diagnosis of DOA (ADOA; OMIM 165500) (Alexander et al., 2000; Delettre et al., 2000). *OPA1* is a highly polymorphic gene and so far over 200 pathogenic variants have been identified, clustering in the GTPase region and the dynamic central domain (eOPA1 database; http://lbbma.univ-angers.fr/lbbma.php?id=9). For a structural description of the *OPA1* gene and the encoded OPA1 protein, please refer to **Section 1.8.2.2**.

1.10.2 Autosomal-Dominant Optic Atrophy

DOA was first described as a distinct clinical entity by Poul Kjer, a Danish ophthalmologist, in the late 1950's (Kjer, 1959). It has a minimum disease prevalence of 1 in 35,000 in the North of England (Yu-Wai-Man et al., 2010a) and the majority (approximately 60%) of DOA cases are linked to pathogenic mutations within the *OPA1* gene (Cohn et al., 2007). To reduce cost, *OPA1* is routinely sequenced using PCR-based methods, but these techniques are unfortunately unable to detect exonic deletions or duplications. These large-scale rearrangements have been identified in 10-20% of *OPA1*-negative families and additional molecular studies, although not yet widely available, are strongly recommended for probands with a clear-cut DOA phenotype and a strong family history (Fuhrmann et al., 2009; Yu-Wai-Man et al., 2011b; Sitarz et al., 2012b).

DOA is an inherited optic neuropathy characterized by a progressive visual loss starting in early childhood, colour vision abnormalities, visual field defects, and a development of the optic nerve pallor (Votruba, 1998). Similarly to LHON, the primary site of pathology in DOA is the papillomacular bundle and central, centrocecal, and paracentral scotomas are the most common visual field defects (Sitarz et al., 2012b). Histopathological studies of a postmortem eye retrieved from one of the patients showed relative preservation of melanopsin-containing RGCs, the latter accounting for the lack of an afferent pupillary defect in DOA - another clinical peculiarity shared with LHON (La Morgia et al., 2010; Sitarz et al., 2012b). The

optic disc in DOA can look diffusely pale or it can have a characteristic temporal wedge, especially in patients at an early stage of disease when RGC loss remains mostly localized to the papillomacular bundle (**Figure 1-24**) (Fraser et al., 2010; Yu-Wai-Man et al., 2011b; Sitarz et al., 2012b).

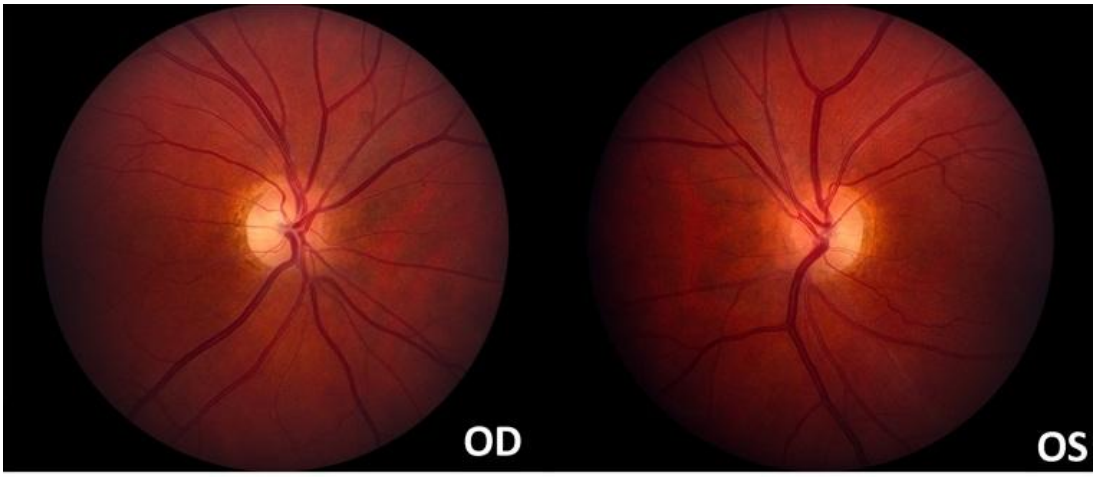

Figure 1-24 Ocular fundus appearance and visual fields in an *OPA1*-mutated patient with dominant optic atrophy (DOA). Temporal wedge of the optic disc pallor can be noticed. OD - *oculus deuter* – right eye; OS – *oculus sinister* – left eye. (Adapted from Fraser et al., 2010).

Although optic nerve dysfunction is the main feature of DOA, it is now well established that up to 20% of *OPA1* carriers will develop additional neuromuscular complications in addition to optic atrophy, so-called DOA+ phenotypes (Yu-Wai-Man et al., 2010b). These more severe syndromal forms of *OPA1* disease are characterised by the development of deafness, ataxia, myopathy, neuropathy and CPEO (Yu-Wai-Man et al., 2010b). Patients with DOA+ phenotypes have higher levels of COX-deficient muscle fibres and mtDNA deletions compared to patients with pure DOA, implicating a direct role for these secondary mtDNA abnormalities in the development of more severe neuromuscular features (Amati-Bonneau et al., 2008). Interestingly, the probability of developing DOA+ phenotype is three times higher with missense *OPA1* mutations targeting the functional GTPase domain of the protein (Yu-Wai-Man et al., 2010b).

1.10.3 Disease Mechanisms

1.10.3.1 Mitochondrial Fusion

As described previously (**Section 1.8.2.2**), OPA1 is responsible for fusion of the IMM (Meeusen et al., 2004; Meeusen et al., 2006). A functional decrease in OPA1 protein level, secondary to pathogenic *OPA1* mutations or the silencing of *OPA1* variants (especially those including exon 4) by small interfering RNAs (siRNAs), induces significant fragmentation of the mitochondrial network (Olichon et al., 2007; Lenaers et al., 2009). The pathological downregulation of *OPA1* expression can dissipate mitochondrial membrane potential, triggering a pro-fission signal, or it can directly affect OPA1 interactions with MFN1 and MFN2, which are essential for the maintenance of an interconnected mitochondrial network (Legros et al., 2002; Cipolat et al., 2004; Guillery et al., 2008). OPA1 pro-fusional activity is essential to maintain both types of mitochondrial fusion, prolonged complete fusion and short-term kiss-and-run transient fusion, thereby allowing exchange and complementation of impaired or missing mitochondrial components (please refer to **Section 1.8.1.1**) (Liu et al., 2009). Overexpression of OPA1 results in excessive mitochondrial elongation (Olichon et al., 2002). This can act as a protective mechanism (Tondera et al., 2009), however, if prolonged, *OPA1* overexpression can trigger cellular senescence as a consequence of ROS over-production and mtDNA damage (Lee et al., 2007; Lenaers et al., 2009).

1.10.3.2 Respiratory Chain Activity

OPA1 plays a key role in mitochondrial OXPHOS as it interacts directly with mitochondrial respiratory chain complexes I, II and III, helping to stabilise these structures (Zanna et al., 2008). It has also been shown that downregulation of OPA1 or overexpression of *OPA1*-mutant alleles can disturb the IMM structure causing uncontrolled proton leakage and dissipation of the membrane potential required for normal mitochondrial respiratory chain function (Olichon et al., 2003).

1.10.3.3 Control of Apoptosis

OPA1 is closely involved in sequestering pro-apoptotic factors such as cytochrome *c* within the cristae, thereby protecting the cell from undergoing apoptosis (Lee et al.,

2004; Olichon et al., 2007). There is experimental data to suggest that different *OPA1* isoforms mediate distinct cellular functions. Crucially, *OPA1* isoforms containing exon 5b are thought to directly control cytochrome *c* release by regulating the tightness of the cristae junctions (Olichon et al., 2007; Lenaers et al., 2009).

1.10.3.4 MtDNA Maintenance

OPA1 mutations have been associated with the accumulation of multiple mtDNA deletions in skeletal muscle (Hudson et al., 2008a). The origin of these deletions and the mechanisms driving their clonal expansion to levels high enough to trigger a biochemical defect, have not yet been elucidated. Based on precipitation studies, some investigators have suggested that OPA1 makes direct physical contact with mtDNA molecules as part of mitochondrial nucleoids (Wang and Bogenhagen, 2006; Elachouri et al., 2011). It has also been shown that cells harbouring *OPA1* mutations show mitochondrial network fragmentation associated with dispersion of nucleoids, resulting in the loss of mtDNA molecules i.e. depletion (Amati-Bonneau et al., 2008).

1.11 *MFN2*-Related Disorders

1.11.1 *MFN2* gene

MFN2 (1p36.22) consists of 19 exons and it codes for a 757 amino acid-long, transmembrane GTPase protein localized to the outer mitochondrial membrane (Rojo et al., 2002; Zorzano, 2010). Missense *MFN2* mutations cause a specific subtype of Charcot-Marie-Tooth (CMT) disease, CMT-2A (OMIM 118210) (Züchner et al., 2004). For a structural description of the *MFN2* gene and MFN2 protein, please refer to **Section 1.8.2.1**.

1.11.2 Charcot-Marie-Tooth 2A

CMT is a heterogeneous group of disorders and it is classified into two main types: type 1 demyelinating form (CMT-1) and type 2 axonal form (CMT-2) (Shy, 2004; Chung et al., 2006). Axonal CMT consists of 9 distinct subtypes (2A, 2B, 2D, 2E, 2F, 2G, 2I, 2K, 2L) and *MFN2* mutations result in the CMT-2A phenotype (**Figure**

1-25) (Chung et al., 2006). CMT-2A is a dominant-inherited neurodegenerative disorder mainly affecting the long peripheral nerves (Züchner et al., 2004). It is characterized by distal muscle weakness and atrophy, mild sensory loss, and normal or near-normal nerve conduction velocities indicative of an axonal peripheral neuropathy (Pareyson, 2004; Chung et al., 2006). Interestingly, optic atrophy is a prominent clinical feature of CMT-2A, clearly implying that MFN2 plays an important role in the maintenance of RGC axonal function and survival (Züchner et al., 2006).

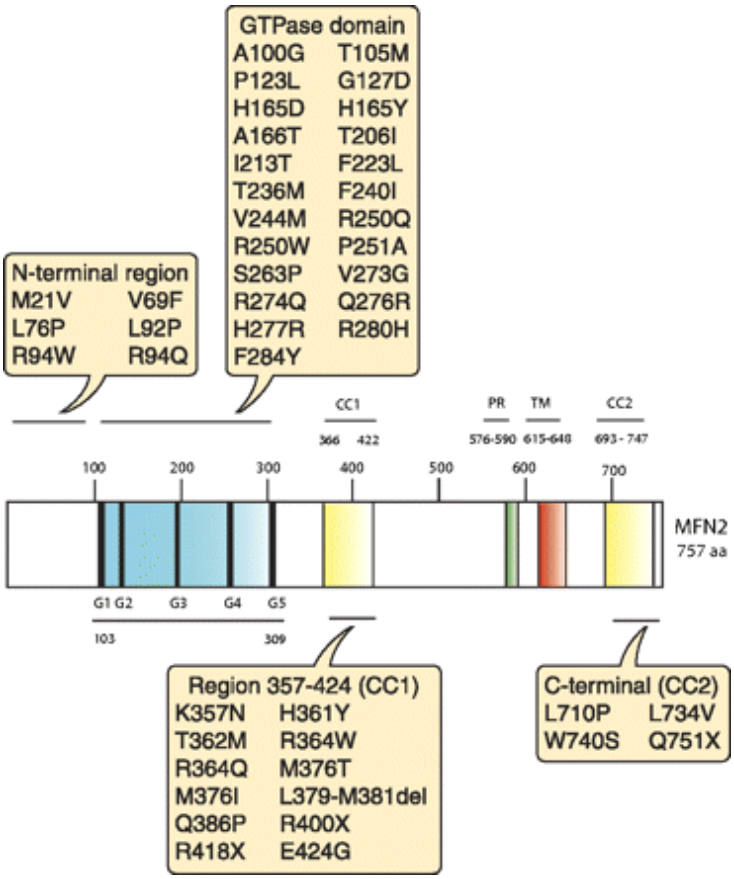

Figure 1-25 *MFN2* mutations confirmed to cause CMT-2A. Genetic disorders are grouped by affected *MFN2* domains. (Reproduced from Liesa et al., 2009).

1.11.3 Disease Mechanisms

MFN2 and its homologue MFN1 share a high degree of structural and functional complementarity with OPA1, all being dynamin GTPase proteins (Chen et al., 2003; Detmer and Chan, 2007). Both MFN1 and MFN2 control fusion of the OMM and they also form homo- or heterotypic complexes which mediate tethering between neighbouring mitochondria (Chen et al., 2003; Koshiba et al., 2004; Meeusen et al., 2004). GTP hydrolysis activity is essential for MFN2-driven mitochondrial fusion (Eura et al., 2003) and mutations within the GTPase domain can either activate this process or inactivate the GTPase domain, thereby blocking fusion (Santel and Fuller, 2001; Chen et al., 2003; Neuspiel et al., 2005; Liesa et al., 2009). Mitofusins form multimeric protein complexes with OPA1 and some *MFN2* mutations can prevent formation of these complexes, thereby inhibiting mitochondrial fusion (Guillery et al., 2008; Liesa et al., 2009).

In addition to OMM fusion, MFN2 regulates mitochondrial membrane potential independently of its role as a pro-fusion protein (Pich et al., 2005). MFN2 also plays a distinct role in mitochondrial oxidative output by regulating the expression of nuclear-encoded mitochondrial respiratory chain subunits and their stable assembly (Pich et al., 2005). MFN2 could also be relevant to mitochondrial axonal transport and the preferential involvement of the long peripheral nerves in CMT (Zorzano, 2010). Recent studies have also confirmed that MFN2 (and not MFN1) is present in the endoplasmic reticulum (ER) where it controls ER morphology and tethering to mitochondria (de Brito and Scorrano, 2008). As a result of its dual function in both mitochondria and the ER, MFN2 regulates calcium homeostasis and it is crucial for the modulation of insulin signalling, as well as maintenance of normal glucose homeostasis (Sebastian et al., 2012). Unsurprisingly, downregulation of *MFN2* has also been linked to ER stress and cellular dysfunction (Ngoh et al., 2012).

1.12 *POLG1*-Related Disorders

1.12.1 DNA Polymerase γ

Polymerase gamma (polγ) is the only mtDNA polymerase and it is a heterotrimeric holoenzyme that consists of a single 140-kDa catalytic subunit (POLG) and a homodimeric 55-kDa accessory subunit (POLG2), encoded by *POLG1* (15q25, OMIM 174763) and *POLG2* (17q, OMIM 604983) genes, respectively (Ito and Braithwaite, 1990; Gray and Wong, 1992; Yakubovskaya et al., 2006). The *POLG1*-encoded catalytic subunit is composed of two distinct functional domains (**Figure 1-26 B**): a C-terminal exonuclease domain (3′→5′ exonuclease activity) and an N-terminal polymerase domain (DNA polymerase activity), separated by the linker region (Kaguni, 2004). Apart from its exonuclease and polymerase activities, the catalytic subunit has also been associated with the 5′- deoxyribose phosphate (dRP) lyase activity involved in the base excision repair (BER) mechanism (Pinz and Bogenhagen, 2000; Kaguni, 2004). Phylogenetic studies confirm a high level of conservation within the catalytic subunit's sequence across species, with conserved active site motifs both in the 3′→5′ exonuclease domain (I, II and III) and in the DNA polymerase domain (A, B and C) (Kaguni, 2004; Chan and Copeland, 2009). The POLG2 accessory subunit is capable of binding DNA with great efficiency during mtDNA replication (Lim et al., 1999) and it plays a role as a maintenance factor regulating the mtDNA content of nucleoids (Di Re et al., 2009).

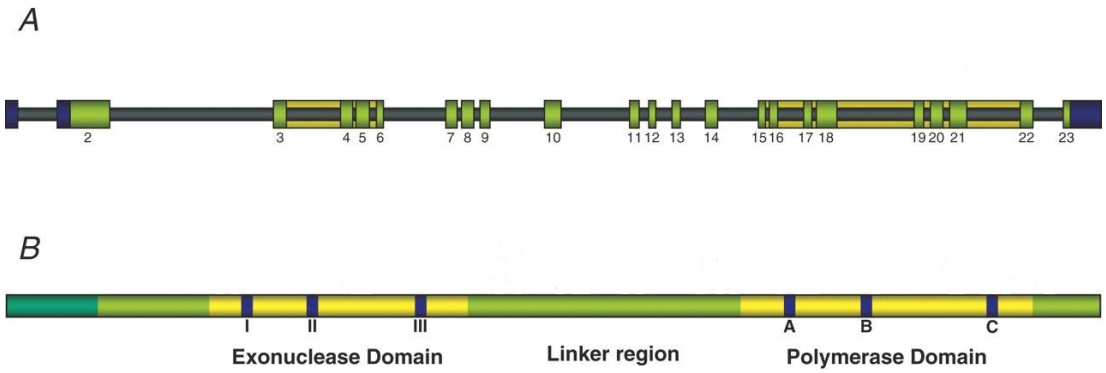

Figure 1-26 *POLG1* gene and the catalytic subunit of polγ (POLG). (A) *POLG1* contains 22 exons encoding the catalytic subunit of polγ. (B) Catalytic subunit of polγ (POLG) consists of two functional domains: C-terminal exonuclease domain and N-terminal polymerase domain, separated by the linker region. Conserved motifs of exonuclease domain (I, II and III) and polymerase domain (A, B and C) are labelled. (Adapted from Horvath et al., 2006).

1.12.2 *POLG1* Mutations and Mitochondrial Disease

Over 150 pathogenic *POLG1* mutations leading to secondary defects of mtDNA maintenance and mitochondrial respiratory chain dysfunction have been identified (**Figure 1-27**) (Chan and Copeland, 2009; Stewart et al., 2009). *POLG1* mutations can lead to both quantitative (depletion) and qualitative (point mutations and deletions) secondary mtDNA abnormalities, and these trigger COX-deficiency at the single cell level in affected tissues (Chan and Copeland, 2009).

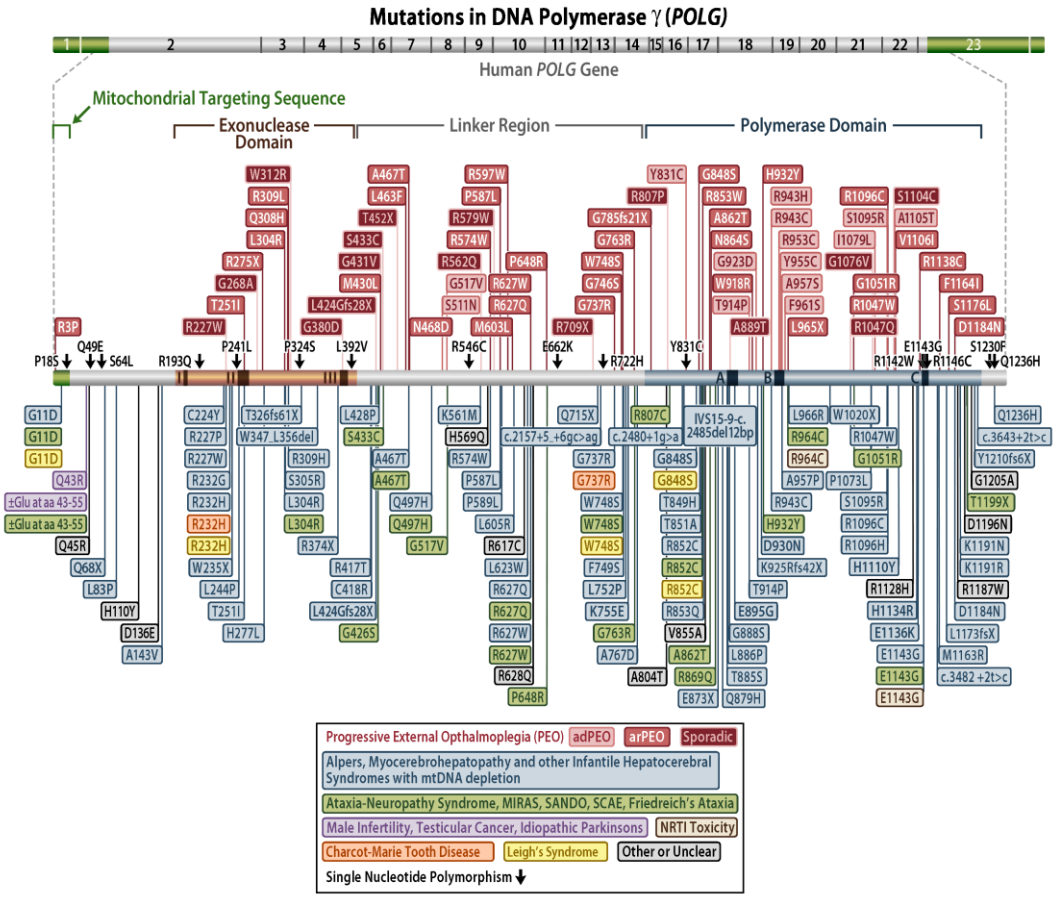

Figure 1-27 Overview of *POLG1* mutations. Reproduced from the Human DNA Polymerase Gamma Mutation Database available at: http://tools.niehs.nih.gov/polg/.

POLG1-related disease is clinically heterogeneous. Pathogenic *POLG1* mutations were first identified in patients with autosomal dominant CPEO (adPEO; OMIM 157640) (Van Goethem et al., 2001), a classical mitochondrial phenotype characterised by bilateral, usually symmetrical, limitation of eye movements (ophthalmoplegia) and droopy upper eyelids (ptosis) (Suomalainen et al., 1997; Van Goethem et al., 2001). Compound heterozygous *POLG1* mutations were subsequently found to cause autosomal recessive CPEO (arPEO; OMIM 258450), this subtype being clinically more heterogeneous and severe compared with adPEO (Bohlega et al., 1996; Van Goethem et al., 2001; Van Goethem et al., 2003). Recessive *POLG1* mutations have also been identified in patients suffering from Alpers-Huttenlocher syndrome (AHS; OMIM 203700) (Davidzon et al., 2005; Nguyen et al., 2005), a disease characterised by severe developmental delay, intractable seizures, liver failure, death in childhood, as well as mtDNA depletion

and decreased POLG activity (Naviaux et al., 1999; Davidzon et al., 2005). *POLG1* mutations are also responsible for a number of other distinct clinical phenotypes, including mitochondrial recessive ataxia syndrome (MIRAS; OMIM 607459) (Hakonen et al., 2005; Tzoulis et al., 2006), sensory ataxic neuropathy dysarthria and opthalmoparesis (SANDO, OMIM 607459), idiopathic parkinsonism and premature ovarian failure (Luoma et al., 2004), and nucleoside reverse-transcriptase inhibitor (NRTI) toxicity (Graziewicz et al., 2006; Hudson and Chinnery, 2006; Copeland, 2008).

1.12.3 Disease Mechanisms

The exact molecular mechanisms by which *POLG1* mutations contribute to the formation and accumulation of mtDNA deletions still remains unclear. Various hypotheses have been put forward including the possibility that *POLG1* mutations affect mtDNA replication by causing structural tertiary changes within POLG, leading to replication errors secondary to slipped H-strand mispairing (Van Goethem et al., 2003). As shown by *Del Bo and colleagues*, mutations involving the *POLG1* exonuclease domain can lead to a reduction in the proof-reading exonuclease activity of POLG, with a deleterious consequence on mtDNA integrity and the subsequent accumulation of pathogenic levels of somatic mtDNA mutations (Del Bo et al., 2003). The significant increase in mtDNA point mutation yield in *POLG1* carriers has recently been confirmed by the ultra-deep re-sequencing-by-synthesis (UDS) assay (Payne et al., 2011).

1.13 Optic Nerve Disorders

Mitochondrial dysfunction has a marked predilection for the optic nerve, a structure composed of the axons of approximately 1.2 million retinal ganglion cells (RGCs). About half of all the patients with confirmed mitochondrial disease will develop some degree of visual loss secondary to optic nerve degeneration. Irrespective of the molecular pathways involved, all mitochondrial optic neuropathies share the same striking set of pathological features – selective degeneration of the RGC layer,

leading to a progressive axonal loss and the onset of visual failure (**Table 1-2**) (Yu-Wai-Man et al., 2011b; Sitarz et al., 2012b).

Table 1-2 Primary inherited optic nerve disorders. (Adapted from Yu-Wai-Man et al., 2011b).

Inheritance	Gene	Phenotype	References
Autosomal dominant	*OPA1*	Isolated optic atrophy and DOA+ phenotypes	(Alexander et al., 2000; Delettre et al., 2000; Yu-Wai-Man et al., 2010b)
	OPA3	Autosomal dominant optic atrophy and cataracts (ADOAC)	(Garcin et al., 1961; Reynier et al., 2004)
	OPA4	Optic atrophy	(Kerrison et al., 1999)
	OPA5	Optic atrophy	(Barbet et al., 2005)
	OPA8	Optic atrophy and sensorineural deafness	(Carelli et al., 2011)
Autosomal recessive	*OPA3*	3-methylglutaconic aciduria type III (Costeff syndrome)	(Anikster et al., 2001)
	OPA6	Optic atrophy	(Barbet et al., 2003)
	OPA7	Optic atrophy	(Hanein et al., 2009)
X-linked	*OPA2*	Optic atrophy	(Assink et al., 1997; Katz et al., 2006)
Mitochondrial	-	LHON and overlapping mitochondrial syndromes	**Table 1-1**

1.13.1 Optic Nerve Anatomy

RGCs are specialised neurones located within the ganglion cell layer of the inner retina (**Figure 1-28**) (Levin, 2006). RGCs receive visual signals from the rod and cone photoreceptors via two different types of intermediate neurons: bipolar and amacrine cells (Levin, 2006). The human retina contains approximately 1.2 million RGCs and each individual cell receives signals from about 100 photoreceptors. The merged information is then relayed along a single axon to the following brain

regions: the lateral geniculate nucleus, the pretectal nucleus, the superior colliculus, or the suprachiasmatic nucleus (Levin, 2006). RGC axons project toward the optic nerve head, where the axons leave the globe to form the optic nerve (**Figure 1-29 B**) (Levin, 2006). The retinal nerve fibre layer is especially dense within the papillomacular region (Levin, 2006). This specific bundle of RGC axons subserves the central 10 degrees of the visual field and it is responsible for high-level discriminatory vision, accounting for the severe visual loss experienced by patients with mitochondrial optic neuropathies (**Figure 1-29 A**) (Levin, 2006).

The efficiency and speed of axonal conduction along the optic nerve is dependent on the presence of an insulating myelin sheath produced by glial oligodendrocytes (Levin, 2006). The intraretinal ganglion cell axons are usually unmyelinated and they acquire a myelin covering behind the lamina cribrosa. This anatomical landmark, marking the transition between myelinated and unmeylinated RGC axon regions, is a multilayered collagen matrix peripherally continuous with the sclera (**Figure 1-29 C**) (Bisaria, 1973; Levin, 2006). Besides oligodendrocytes, the optic nerve is also reliant on another group of glial cells, astrocytes, which are involved in several functions, including ionic homeostasis, potassium transport, glycogen storage and the regulation of neurotransmitters (Levin, 2006).

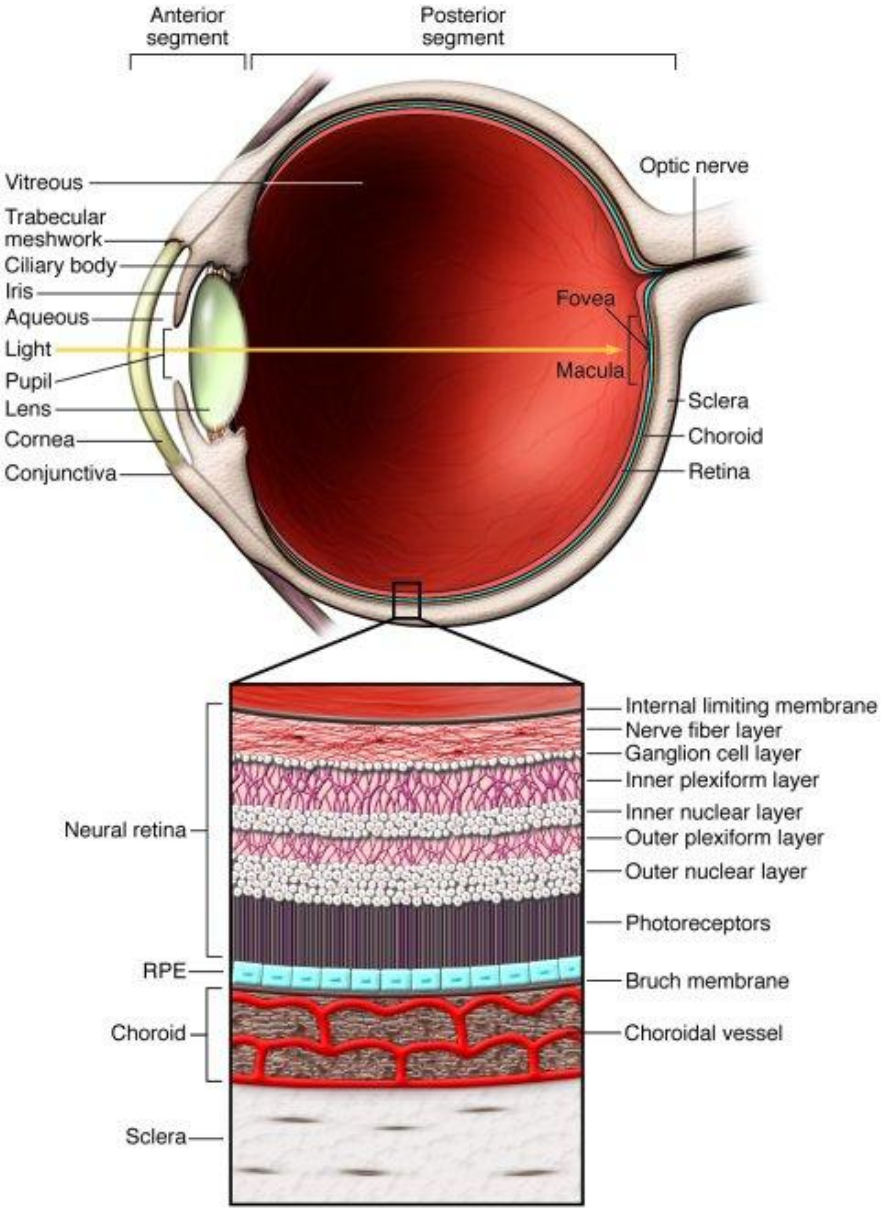

Figure 1-28 Schematic representation of the main anatomical structures of the eye. The insert shows a cross-sectional view of the retina. RPE – retinal pigment epithelium. (Reproduced from Caspi, 2010).

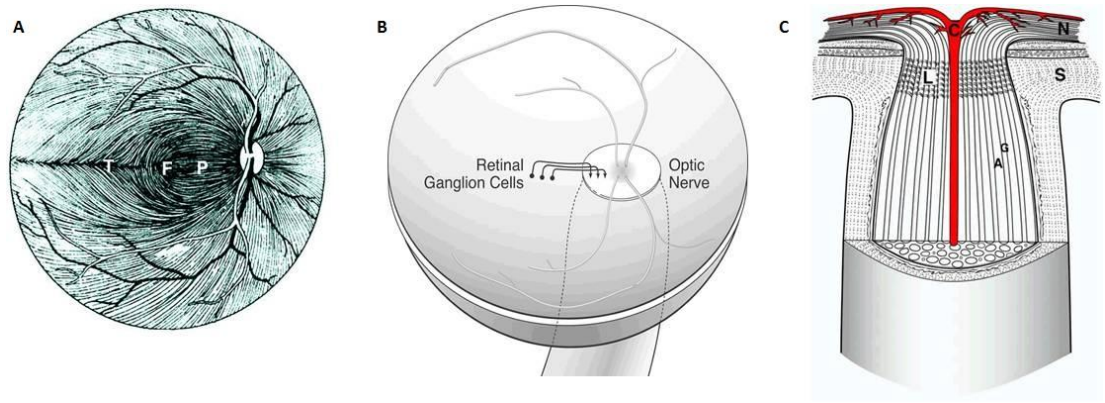

Figure 1-29 Anatomy of the optic nerve. (A) Tracks of retinal ganglion cell (RGC) axons within the retinal nerve fibre layer. Significant accumulation of axons in the area of central vision – papillomacular bundle (F- fovea; P- papillomacular bundle; T-temporal raphe). (B) RGC axons arisen from different locations within the retina are travelling towards the optic disc. (C) Cross-sectional view of the optic nerve head (C- central retinal artery; N- nerve fibre layer; A- bundle of axons within the optic nerve; G- glia; L- lamina cribrosa; S- sclera). (Adapted from Levin, 2006).

1.13.2 Mechanisms Contributing to RGC Loss

The apoptotic loss of RGCs is the final pathological outcome of mitochondrial optic neuropathies. Several disease pathways are likely to contribute to this irreversible process and these have been further detailed below.

1.13.2.1 Mitochondrial Network Dynamics

OPA1 and MFN2 are essential for mitochondrial fusion (**Section 1.8.2; Section 1.10.3.1; Section 1.11.3**). In addition, OPA1 ensures the integrity of the mitochondrial cristae's tight junctions, thereby preventing pro-apoptotic cytochrome *c* molecules from being released into the cytosolic space (**Section 1.10.3.3**) (Lee et al., 2004). Unsurprisingly, the pathological hallmark of *OPA1*- and *MFN2*-mutant fibroblasts is mitochondrial network fragmentation, which not only impairs mitochondrial OXPHOS, but also leads to the uncontrolled release of calcium and cytochrome *c* into an already compromised cellular environment (Amati-Bonneau et al., 2008; Chevrollier et al., 2008; Zanna et al., 2008). Possibly, a similar mechanism may lead to RGCs loss in mitochondrial-related neuropathies.

1.13.2.2 Bioenergetic Failure

Mitochondria regulate OXPHOS and as a result of this tight control, they provide most of the cell's ATP requirements. As described previously (**Section 1.10.3.2**), *OPA1* mutations have a detrimental impact on mitochondrial oxidative output by impairing the assembly and stability of the respiratory chain complexes (Zanna et al., 2008). Although most studies, based on *in vitro* or *in vivo* assays, indicate a significant impairment of complex I activity leading to a reduction in mitochondrial membrane potential and overall ATP synthesis (Yu-Wai-Man et al., 2009), significant decrease in COX activity has also been reported (Chevrollier et al., 2008; Yu-Wai-Man et al., 2010c). This bioenergetic deficit is bound to impact negatively on RGCs, however this by itself cannot solely account for their selective vulnerability in mitochondrial optic neuropathies.

1.13.2.3 Reactive Oxygen Species

The increased susceptibility of RGCs in DOA could be due to an elevation of ROS levels, secondary to the downstream deleterious consequences triggered by *OPA1* mutations. A *drosophila Opa1* (*dOpa1*) model has recently been established where homozygous mutant flies developed a rough and glossy eye phenotype due to the loss of hexagonal lattice cells, with decreased lens and pigment deposition. This genetically engineered *dOpa1* mutation led to a significant increase in ROS levels, providing clear evidence of cellular oxidative stress (Shahrestani et al., 2009; Tang et al., 2009).

1.13.2.4 Disturbed Calcium Handling

MFN2, as described in **Section 1.11.3**, tethers the ER to the mitochondrial network. This ER-mitochondrial interaction is closely involved in the regulation of calcium flux within cells (de Brito and Scorrano, 2008; Sebastian et al., 2012). In CMT-2A neuropathy, this tethering effect is lost with dramatic deleterious consequences on cellular calcium homeostasis (de Brito and Scorrano, 2008; Sebastian et al., 2012). The ER and mitochondrial network are important calcium stores and the dynamic flux between these two compartments buffers against cytosolic calcium spikes that can sensitize the cell to various proapoptotic signals (de Brito and Scorrano, 2008; de Brito and Scorrano, 2009). Similar to the pathomechanism of *MFN2* mutations,

mtDNA point mutations involving complex I and complex IV subunits have also been directly linked with disturbed calcium handling in neuronal populations (Trevelyan et al., 2010). Although speculative, it is tempting to suggest that a similar process is contributing to RGC dysfunction in LHON and DOA (Dayanithi et al., 2010).

1.13.2.5 Somatic mtDNA Defects

Individuals with DOA+ phenotypes have pathological levels of COX-deficient muscle fibres, secondary to the accumulation of high levels of clonally-expanded somatic mtDNA deletions (**Section 1.10.2**) (Amati-Bonneau et al., 2008; Yu-Wai-Man et al., 2010c). OPA1 is likely to be involved in maintaining the integrity of the mitochondrial genome by anchoring the mtDNA replicative machinery (nucleoids) to the IMM (Elachouri et al., 2011). Dominant-negative *OPA1* mutations could therefore lead to the formation of mtDNA deletions by disturbing these delicate physical interactions along the IMM (Elachouri et al., 2011). Patients with DOA+ have more pronounced visual acuities and a significantly thinner retinal nerve fibre layer (RNFL) thickness compared with those who develop only isolated optic atrophy (Yu-Wai-Man et al., 2011a). These clinical observations suggest that the accumulation of somatic mtDNA deletions probably have an incremental detrimental effect on RGC survival.

1.13.3 Selective Vulnerability of RGCs

The preferential involvement of RGC loss in mitochondrial cytopathies could derive from the characteristic anatomy of the optic nerve, the latter acquiring a myelin sheath only behind the lamina cribrosa (Levin, 2006). This transition is marked by a sharp differential gradient with a much higher density of mitochondria and voltage-gated sodium channels in the pre-laminar unmyelinated segment compared with the post-laminar myelinated segment of the optic nerve (**Figure 1-30** and **Figure 1-31**) (Andrews et al., 1999; Bristow et al., 2002). These physiological adaptations facilitate the efficient propagation of the nerve action potentials in the absence of an insulating myelin cover. The pre-laminar region therefore represents a weak link, which is significantly more exposed to the disadvantageous consequences of mitochondrial biochemical defects (Yu-Wai-Man et al., 2011b). The maintenance of

a higher mitochondrial concentration in the pre-laminar region also highlights the central role played by the cytoskeleton, especially the microtubule network, in shuttling and localising mitochondria to appropriate cellular locations (**Figure 1-31**) (**Section 1.8.1.2**). Both mitochondrial respiratory chain defects or a primary disturbance in the cytoskeletal network can therefore lead to impaired axonal transport and ultimately apoptotic RGCs loss (Yu-Wai-Man et al., 2011b).

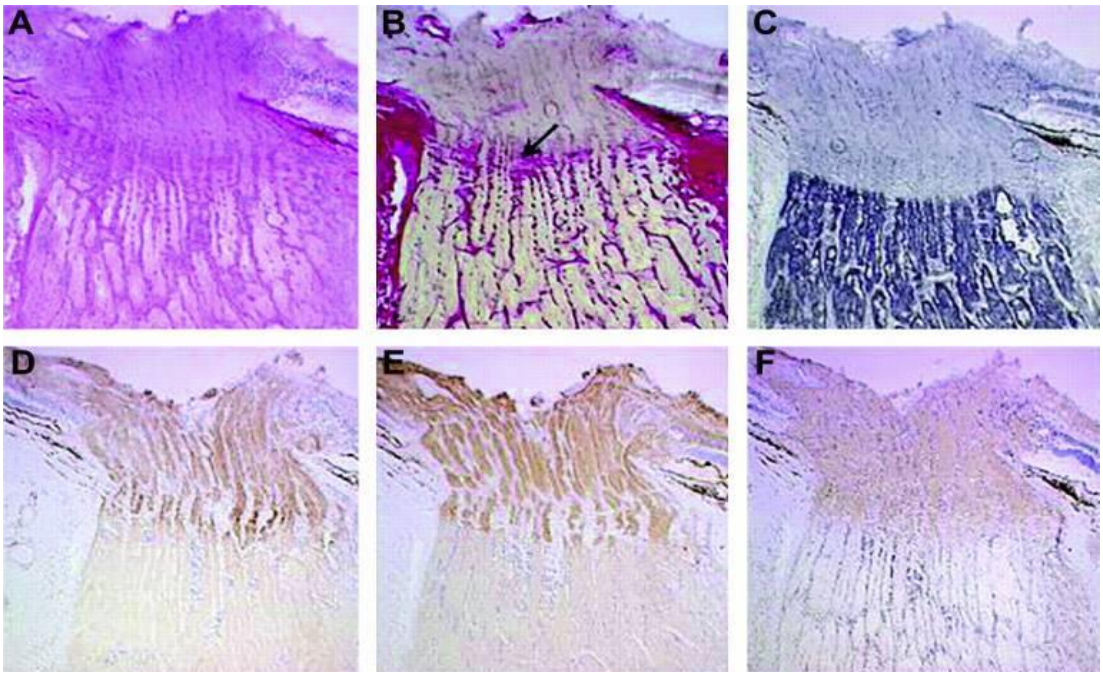

Figure 1-30 Histological, histochemical and immunohistochemistrical investigations performed on serial longitudinal optic nerve sections: (A) haematoxylin and eosin, (B) Van Gieson's preparation for collagen fibres (red; the arrow points towards the lamina cribrosa), (C) Weigert's iron haematoxylin staining for myelin (dark blue), (D) staining for COX activity; darker brown stain confirms higher COX activity in the unmyelinated pre-laminar segment of the optic nerve, (E) immunohistochemistry for COX subunit IV demonstrating a pattern consistent with the level of mitochondrial enzyme activity, (F) immunohistochemistry for Nav 1.1 sodium channels revealing their greater concentration in the pre-laminar region. (Adapted from Barron et al., 2004).

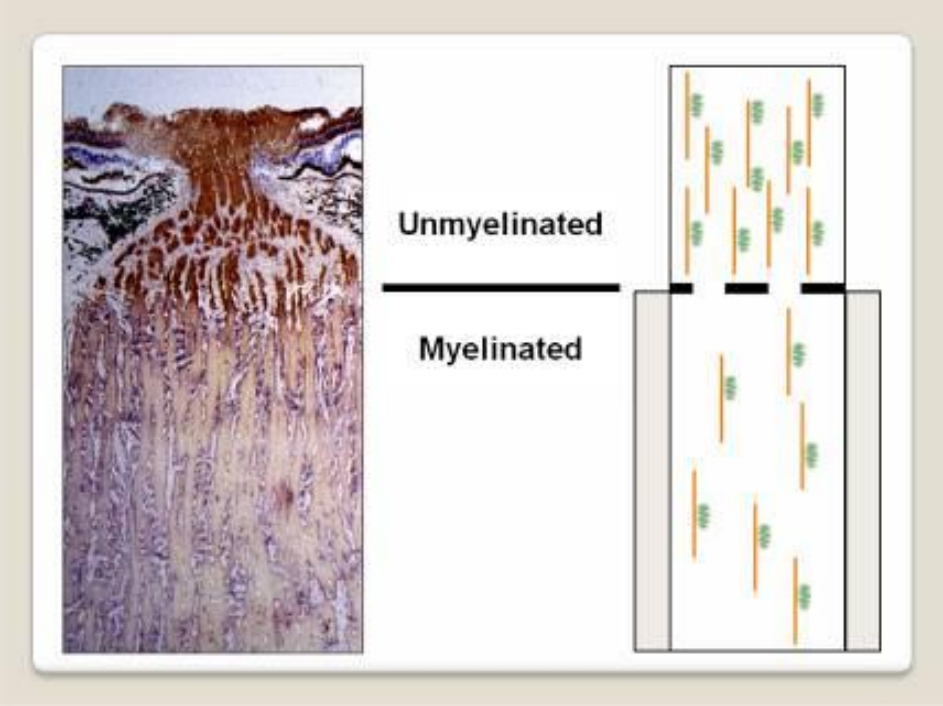

Figure 1-31 Function of the cytoskeletal tracks in maintaining differential densities of mitochondria in pre- and post-laminar cribrosa regions of the optic nerve. The left panel illustrates dual COX/SDH histochemistry on a longitudinal section of the optic nerve. The significantly darker COX staining within the unmyelinated, pre-laminar segment is consistent with a higher mitochondrial density. The right panel is a schematic representation of the dynamic cytoskeletal-mitochondrial interactions within the optic nerve (cytoskeleton in brown; mitochondria in green). (Reproduced from Yu-Wai-Man et al., 2011b).

1.14 Human Induced Pluripotent Stem Cells

1.14.1 Pluripotent Stem Cells

Pluripotent stem cells possess the unique ability to propagate indefinitely, maintaining the capability to spontaneously differentiate into any cell type from all three embryonic germ layers – ectoderm, mesoderm and endoderm (Pera et al., 2000; Hyslop et al., 2005). Several types of pluripotent stem cells have been distinguished depending on their derivation: (i) embryonic stem cells (ESCs), which are derived from the inner cell mass (ICM) of the blastocyst stage of pre-implantation mammalian embryo (Evans and Kaufman, 1981; Thomson et al., 1998); (ii) embryonal carcinoma cells (ECCs) isolated from teratocarcinoma (Stevens, 1967; Kahan and Ephrussi, 1970); (iii) embryonic germ cells (EGCs) derived from the

primordial germ cells (PGCs) of the post-implantation embryo (Resnick et al., 1992); and (iv) induced pluripotent stem cells (iPSCs), which are generated from non-pluripotent adult somatic cells following reprogramming with a set of specific transcription factors (Takahashi and Yamanaka, 2006; Takahashi et al., 2007; Yu et al., 2007). The unique features of pluripotent stem cells allow their use as the cell sources for versatile applications, including basic biological research, disease modelling, drug discovery and screening, as well as regenerative medicine (Hyslop et al., 2005).

Since *Thomason and colleagues* first derived human ESCs (hESCs) from the ICM of an early embryo blastocyst stage, the application of hESCs has been a major focus of biomedical research (Thomson et al., 1998). Initially, five hESC lines were established; three with a normal XY karyotype (H1, H13 and H14), and two with a normal XX karyotype (H7 and H9) (Thomson et al., 1998). Human ESCs are usually obtained either from spare donated embryos that remain after *in vitro* fertilisation (IVF) or from genetically-impaired embryos diagnosed by preimplantation (Thomson et al., 1998; Reubinoff et al., 2000; Pickering et al., 2003). Human ESCs have a distinct morphology typical of primate ESCs, being small and round, with a high nucleus to cytoplasm ratio and prominent nucleoli (Thomson et al., 1998). In addition to these morphological features, hESCs, like all pluripotent stem cells, are capable of unlimited proliferation coupled with the ability to differentiate into virtually all cell types derived from the three primary germ layers (**Figure 1-32**).

Although embryonic stem cell applications carry great potential for modelling and treating human disease, they face a whole host of ethical, biological, and safety concerns. The development of human iPSCs (hiPSCs) is an attractive alternative strategy to overcome the limitations inherent to hESCs (Takahashi et al., 2007). Although various research groups have tried to establish techniques allowing hESCs to be obtained without destroying human embryos or by deriving them from developmentally-arrested embryos at very early stages of development (Zhang et al., 2006), the requirement for human embryonic material is still the leading ethical controversy preventing the widespread clinical and research applications of hESCs. Unlike embryo-derived hESCs, hiPSCs can be artificially created from adult human somatic cells e.g. fibroblasts, by viral-mediated induction of reprogramming factors:

OCT4, *SOX2*, *KLF4* and *c-MYC* (Takahashi et al., 2007) (**Figure 1-32**) or *OCT4*, *SOX2*, *NANOG* and *LIN28* (Yu et al., 2007). Since hiPSCs contain the original donor's genome, they can be used for personalized *in vitro* disease modeling, drug screening and regenerative cell-replacement medicine, without concerns about immunological rejection, the latter remaining a great concern in relation to hESC-mediated therapies (Madonna, 2012).

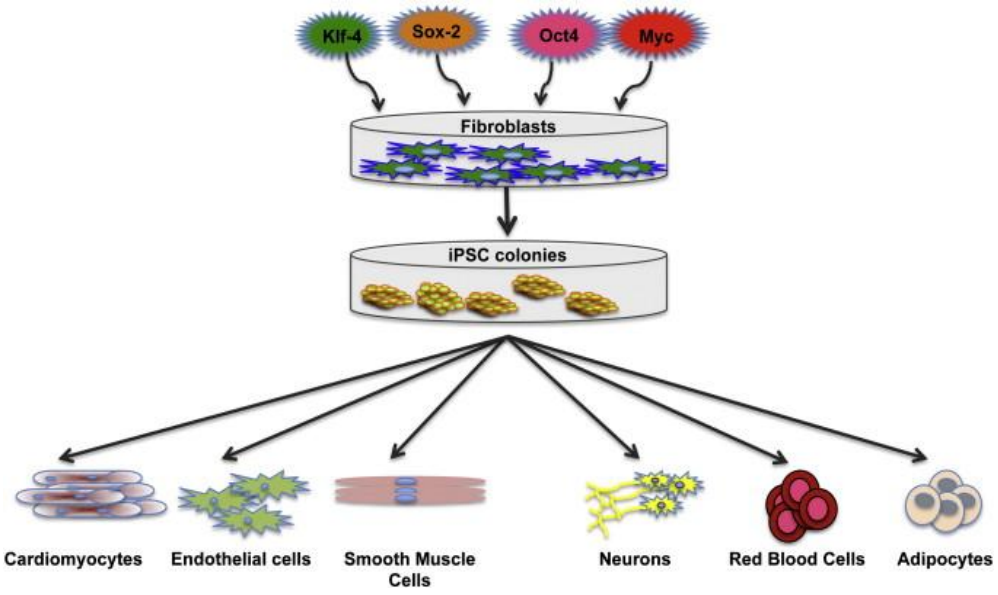

Figure 1-32 Generation of induced pluripotent stem cells. Adult somatic cells (e.g. fibroblasts) are reprogrammed into induced pluripotent stem cells (iPSCs) by over-expression of reprogramming factors (*OCT4*, *SOX2*, KLF4 and c-MYC). The iPSCs can further differentiate into all somatic cell types. (Reproduced from Nsair and MacLellan, 2011).

1.14.2 Comparison of hiPSCs and hESCs

The lack of ethical constraints coupled with the ability to generate patient-tailored cells, is an obvious advantage of hiPSC applications. However, it is essential to assess the degree of similarity between hiPSCs and the current "gold standard" i.e. hESCs. Induced pluripotent and embryonic stem cells are known to share several key properties, including structural morphology, the ability to differentiate into all three germ layers, proliferation rate, pluripotency gene expression profiles, and the ability to form teratomas (Bilic and Izpisua Belmonte, 2012; Puri and Nagy, 2012). Human

ESCs and hiPSCs have also been shown to acquire similar levels of karyotypic abnormalities during expansion and over prolonged tissue culture times (Taapken et al., 2011). Both cell types also manifest almost indistinguishable histone methylation patterns when compared to non-pluripotent cells (Guenther et al., 2010). Recent seminal work has shown that tetraploid complementation with mouse iPSCs have resulted in viable adult mice, providing clear proof of principle that iPSCs have similar powerful developmental potentials to ESCs (Boland et al., 2009; Zhao et al., 2009).

Despite the numerous similarities between hiPSCs and hESCs, there are many differences, such as epigenetic and genetic inconsistencies that have an impact on the pluripotency, differentiation ability, stability and carcinogenicity of hiPSCs compared with hESCs (Bilic and Izpisua Belmonte, 2012). The incomplete silencing of somatic cell-of-origin genes, as well as a decrease in the overall expression of pluripotency genes characteristic of hESCs were observed in some hiPSC lines, supporting the concept of epigenetic memory following reprogramming (Chin et al., 2009; Marchetto et al., 2009). In addition to these epigenetic abnormalities, hiPSCs also accumulate various genomic mutations, including reprogramming-induced deletions of tumour-suppressor genes (Laurent et al., 2011). The dissimilarities between hiPSCs and hESCs are likely to originate from imperfections in the actual reprogramming mechanisms used and it is hoped that the development of new pluripotency inducing techniques may help to unify hiPSC and hESC-based applications (Maekawa et al., 2011; Bilic and Izpisua Belmonte, 2012).

1.14.3 Methods of hiPSC Derivation

Human iPSC lines were first successfully generated by two independent research teams using viral-mediated induction of four transcription factors: *OCT4*, *SOX2*, *KLF4* and *c-MYC* with a retroviral system (Takahashi et al., 2007); and *OCT4*, *SOX2*, *NANOG* and *LIN28* with a lentiviral system (Yu et al., 2007). Since hiPSCs were first created, a number of different reprogramming vectors have been trialled to increase the efficiency and completeness of reprogramming, as well as to reduce genomic insertions of transcription factors and the unpredictable consequences of these random genomic integrations (Drews et al., 2012; Madonna, 2012). The adaptation of small molecular compounds, such as vitamin C or valproic acid (VPA),

have been found to significantly enhance the efficiency of pluripotency induction by mimicking the signalling of transcription factors, thereby decreasing the amount of integrating vectors essential for successful reprogramming (Huangfu et al., 2008; Esteban et al., 2010). Alternatively, single polycistronic vectors, encoding all reprogramming factors, have been used to significantly reduce the number of genomic insertions and to increase reprogramming efficiency (Carey et al., 2009).

The polycistronic lentiviral system contains *loxP* sequences flanking the viral cassette and these can be excised with Cre recombinase (Sommer et al., 2009). In order to produce genetically-unchanged hiPSCs, several alternative transduction vectors have been introduced, including non-integrating adenoviruses (Zhou and Freed, 2009), RNA-based Sendai viruses (Fusaki et al., 2009) and nonviral minicircle DNAs (Jia et al., 2010). More recently, successful reprogramming was achieved using synthetically modified mRNAs (Warren et al., 2010) and mature human ESC-specific microRNAs. This novel approach allows the regulation of gene expression either through the induction of mRNA degradation or by blocking translation of specific mRNA species (Bartel, 2004; Miyoshi et al., 2011). The efficiency of pluripotency induction depends also on the type of somatic cells selected for the reprogramming (Chun et al., 2011). Currently, the majority of hiPSCs have been derived either from the mesodermal (fibroblasts, blood cells) or ectodermal (keratinocytes, melanocytes and neural stem cells) germ layers (Chun et al., 2011).

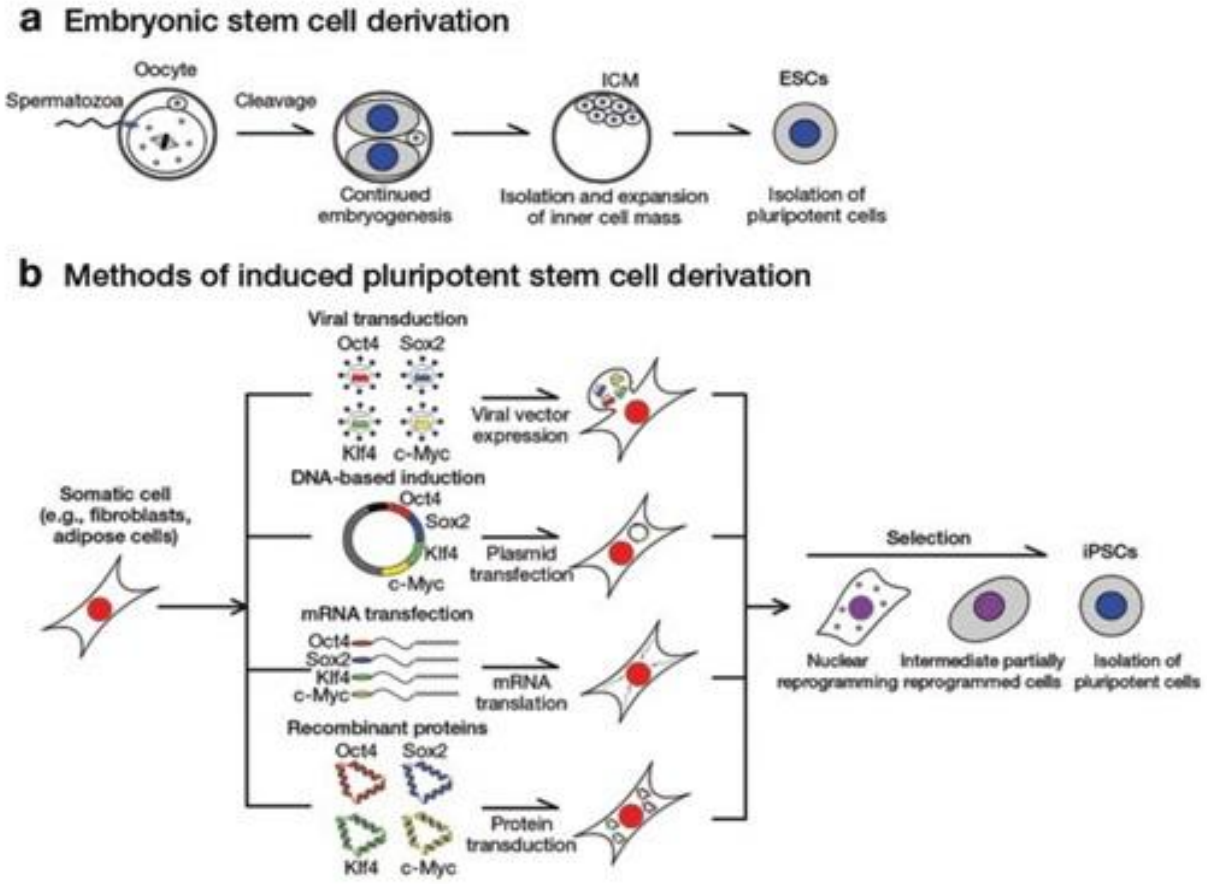

Figure 1-33 Schematic representation of methods used to derive (a) embryonic stem cells (ESCs) and (b) induced pluripotent stem cells (iPSCs). (Adapted from Narsinh et al., 2011).

1.14.4 Applications of hiPSCs

The advent of efficient hiPSC technology should allow the creation of patient- and disease-specific human cells, and these could then be further applied to disease modeling, drug toxicity screening, and personalized cell replacement therapy.

1.14.4.1 Disease Modelling

A number of studies have recently demonstrated the successful generation of *in vitro* disease models using hiPSC-based methodologies. A good example where this strategy has been applied is spinal muscular atrophy (SMA), a neurodegenerative disease leading to the loss of lower motor neurones, which was investigated using hiPSC-derived motor neurones from affected patient fibroblasts (Ebert et al., 2009). Another example is Rett syndrome (RTT), a neurodevelopmental disease characterised by a large spectrum of autistic features, which was studied using neurones derived from affected patients' fibroblasts (Marchetto et al., 2010). Applying hiPSC technology to successfully generate RGCs of patients with various mitochondrial optic neuropathies, harbouring a range of pathogenic mutations is an attractive strategy that would bypass the current lack of access to disease human tissues. These versatile disease models would allow more fundamental research into the underlying mechanisms accounting for the selective degeneration of RGCs in this group of disorders and how this ultimately leads to the onset of visual failure and the development of optic atrophy.

1.14.4.2 Drug Discovery and Screening

Access to high-throughput hiPSC technology offers a great opportunity for reliable and highly-efficient drug screening approaches by using cells with specific disease phenotypes (Chun et al., 2011). Human iPSCs could be used to increase the efficiency of novel drug development and to allow more accurate prediction of drug toxicity (Chun et al., 2011). Hepatotoxicity and cardiotoxicity are leading causes of drug failure during pre-clinical toxicological testing (Chun et al., 2011). Although they lose their functional and phenotypic properties during *in vitro* cell culture, primary human hepatocytes remain the "gold standard" for investigating drug metabolism (Drews et al., 2012). The development of *in vitro* models of both healthy

and disease-specific hepatocytes could therefore allow the faster introduction of more effective and less toxic drugs into clinical practice.

1.14.4.3 Personalized Cell Replacement Therapy

Unlike hESCs, hiPSCs do not pose significant ethical and immunological rejection concerns. They could therefore be used for the purpose of tissue regeneration and organ transplantation (Drews et al., 2012). The field of regenerative medicine is reaching the phase of clinical trials and one such trial has recently been launched by Advanced Cell Technology (http://www.advancedcell.com/clinical-trials/; accessed 17th of July 2012). Its principle was to determine the biosafety and efficacy of subretinal transplantations of hESC-derived retinal pigment epithelium (RPE) cells in patients suffering from two blinding macular disorders: Stargardt's macular dystrophy and dry age-related macular degeneration (Schwartz et al., 2012). Depending on the success of hESC-based trials and future developments in hiPSC technology, the generation of high-quality patient-specific hiPSCs is likely to open a promising area for future translational research into untreatable neurodegenerative disorders, including mitochondrial genetic disorders.

Chapter 2 Research Aims

In my PhD project, I set about exploring the disease mechanisms underlying nuclear disorders of mtDNA maintenance by focusing on three main genes: *OPA1*, *MFN2,* and *POLG1*. To achieve this, I carried out this series of studies with the following aims:

1. To determine whether *OPA1* and *MFN2* mutations affect mtDNA copy number in blood.
2. To investigate if pathogenic *MFN2* mutations result in secondary mtDNA instability in skeletal muscle.
3. To determine whether specific *OPA1* genetic variants are associated with neuromyelitis optica (NMO).
4. To study the pathological consequences of *OPA1* and *POLG1* mutations on mtDNA replication.
5. To quantify the degree of mitochondrial network instability caused by *OPA1* and *POLG1* mutations under physiological conditions and following a period of induced mtDNA depletion.
6. To generate human induced pluripotent stem cells (hiPSCs) from patient-derived *OPA1*-mutant fibroblasts.

Chapter 3 Materials and Methods

Table of Contents

3.1 Genomic DNA Isolation

3.1.1 Genomic DNA Isolation from Cultured Cells

DNA from cultured cells was extracted using DNeasy® Blood & Tissue Kit (Qiagen, Crawley, UK). All centrifugation steps were performed at room temperature and 10,000 rpm unless stated differently. Following the manufacturer's protocol, a cell pellet (maximum of 5 x 10^6 cells) was resuspended in 200µl Phosphate Buffered Solution (PBS; Oxoid, Basingstoke, UK). In order to lyse cells, 20µl of Proteinase K and 200µl of Buffer AL were added, sample was mixed thoroughly by vortexing and incubated at 56°C for 10 minutes. Following that, 200µl of 100% ethanol (EtOH) was added to precipitate each sample. The mixture was then mixed by vortexing and pipetted into the DNeasy® Mini spin-column located in a 2ml collection tube. Each sample was centrifuged for 1 minute and then every spin-column was placed into a fresh collection tube. The old column and the flow-through were discarded. The sample was initially washed with 500µl of Buffer AW1. The column was subsequently centrifuged for 1 minute, the flow-through and collection tube was discarded, and the spin-column was then placed in a new collection tube. The final washing step was carried out by adding 500µl of Buffer AW2 to each sample and centrifuging for 3 minutes at 14,000 rpm to dry the DNeasy® membrane. The spin-column was then placed in a clean 1.5ml tube (Eppendorf, Stevenage, UK) and 100µl of elution Buffer AE was pipetted directly onto the DNeasy® membrane. Following incubation for 1 minute at room temperature, the spin-column was centrifuged for 1 minute to elute the DNA. The concentration of the eluted DNA sample was determined using a NanoDrop™ ND-1000 (NanoDrop Technologies, Wilmington, USA) and the sample was placed at -20°C for long-term storage.

3.1.2 Genomic DNA Isolation from Muscle Homogenate

DNA from muscle homogenate was extracted using Nucleon® Genomic DNA Extraction Kit Hard Tissue (Tepnel Life Sciences, Manchester, UK) following the manufacturer's protocol. All centrifugation steps were performed at room temperature. Initially muscle biopsy was sectioned at 20µm thickness using a Microm™ HM560 cryostat (Thermo Fisher, Schwerte, Germany) and twenty of

these sections were placed in a 1.5ml tube (Eppendorf). To lyse muscle sections, 18µl of Proteinase K (Sigma-Aldrich, Dorset, UK) was added. Sample was then mixed thoroughly by vortexing and incubated overnight at 55°C. Following the incubation, sample was centrifuged at 2,000g for 5 minutes and supernatant was then transferred into a fresh 1.5ml tube (Eppendorf). In order to deproteinize the sample, 100µl of sodium perchlorate was added to the supernatant and mixed manually inverting tube several times. It was followed by adding 600µl of chloroform and manual mixing as before. Finally, 150µl of Nucleon Resin suspension was added, rotary mixed for 5 minutes and centrifuged at 350g for 1 minute. To precipitate DNA, the upper phase was transferred to a fresh 1.5ml tube (Eppendorf) without disturbing the brown Nucleon Resin layer. It was followed by adding 2 volumes of ice cold 100% EtOH and manually inverting several times until the DNA was precipitated. In order to wash the DNA, the sample was centrifuged at 8,000g for 5 minutes to pellet the DNA and the supernatant was then discarded. The washing step was repeated with ice cold 70% EtOH, sample re-centrifuged and the supernatant discarded again. The DNA pellet was then air-dried for 1 hour at 37°C and once all ethanol was evaporated, the sample was resuspended in TE buffer and left to dissolve for 2 hours at 37°C. The concentration of DNA was quantified using NanoDrop™ ND-1000 (NanoDrop Technologies) and the sample was then stored at -20°C.

3.2 RNA Isolation from Cultured Cells

RNA from cultured cells was isolated using RNeasy® Mini Kit (Qiagen) according to the manufacturer's protocol. All centrifugation steps were performed at room temperature at 14,000 rpm. A cell pellet (maximum of 5 x 10^6 cells) was resuspended in 350µl of Buffer RLT and the lysate was then pipetted directly into QIAshredder® homogenizer spin-column (Qiagen) placed in a 2ml collection tube. The spin-column was centrifuged for 2 minutes at 14,000 rpm and 350µl of 70% EtOH was then pipetted and mixed into the homogenized lysate. The resulting mix was transferred into an RNeasy® spin-column already placed in a 2ml collection tube. After centrifuging for 15 seconds, the flow-through was discarded and 700µl of Buffer RW1 was added to the RNeasy® spin-column. This was centrifuged again for 15 seconds to wash the spin-column membrane. After this, the flow-through was

discarded, 500µl of Buffer RPE was added, and the column was centrifuged for further 15 seconds. The flow-through was again removed, 500µl of Buffer RPE was added, and the spin-column centrifuged for 2 minutes. Following flow-through removal, the RNeasy® spin-column was placed in a fresh 1.5ml collection tube (Eppendorf) before the addition of 30µl of RNase-free water directly onto the membrane. After an incubation period of 1 minute at room temperature, the spin-column was finally centrifuged for 1 minute to elute the RNA. The RNA concentration was measured using NanoDrop™ ND-1000 (NanoDrop Technologies) and the sample was then stored at -80°C.

3.3 Polymerase Chain Reaction (PCR)

Polymerase chain reactions (PCRs) were performed using Veriti® 96-well Thermal Cycler (Applied Biosystems, Life Technologies, Paisley, UK) in 96-well plates (Greiner, Stonehouse, UK) or 0.2ml PCR tubes (Eppendorf). Each individual DNA sample (1.5µl; 30ng) was amplified in a 50µl PCR master mix containing: 10X ImmoBuffer (5µl/reaction; Bioline GmbH, London, UK), 2mM dNTPs (dATP, dTTP, dCTP and dGTP; Bioline GmbH) (5µl/reaction; VH Bio, Gateshead, UK), 50mM $MgCl_2$ (1.5µl/reaction; Bioline GmbH), 10µM forward and reverse primers (both 1.25µl/reaction; Sigma-Aldrich), 5U/µl Immolase™ DNA Polymerase (0.25µl/reaction; Bioline GmbH) and dH_2O (34.25µl/reaction).

DNA was amplified under the following cycling conditions: an initial denaturation step at 95°C for 7 minutes, then 30 cycles of denaturation at 95°C for 1 minute, annealing at 58°C for 1 minute, and extension at 72°C for 1 minute. For the last cycle, a final extension step of 10 minutes at 72°C was performed before the sample was cooled to 4°C. PCR products were stored at -20°C.

3.4 Agarose Gel Electrophoresis

The specificity (size) of amplified PCR product was determined by electrophoresis using 2% (w/v) TAE agarose gel with 0.4µg/ml ethidium bromide (EtBr; Sigma-

Aldrich) as an intercalating dye. To prepare a gel, agarose (Helena Biosciences, Gateshead, UK) was first dissolved in 1X TAE buffer (0.04M Tris-acetate, 0.001M EDTA, pH = 8.3; Helena Biosciences) by heating in a microwave and allowed to cool. This was then supplemented with 0.4µg/ml EtBr (Sigma-Aldrich), poured into an electrophoresis tray with a gel comb, and allowed to set. A 5µl aliquot of each amplified PCR product was mixed with 5µl of 2X Orange G loading buffer, consisting of 0.1% (w/v) Orange G (powder; Sigma-Aldrich), 30% (v/v) glycerol (Sigma-Aldrich) and 70% (v/v) dH_2O. This mixture was loaded into a well and then electrophoresed in 1X TAE buffer at a constant voltage of 60-70V. In addition, 5µl of Hyperladder IV (Bioline GmbH) was used as a product size marker. The PCR product bands were visualised by exposure to UV light using an AlphaImager® 2200 system (Alpha Innotech, Kasendorf, Germany).

3.5 Agarose Gel Extraction of PCR Amplicons

DNA amplicons were generated using a standard PCR procedure (**Section 3.3**) and separated on a 1% (w/v) TAE agarose gel (**Section 3.4**). Following separation, bands of the individual DNA samples were scalpel-excised from the agarose gel, placed in a 2ml tube (Eppendorf) and weighed, allowing each tube to hold a maximum of 200mg of gel. To extract DNA, QIAquick® Gel Extraction Kit was used (Qiagen) according to the manufacturer's protocol. All centrifugation steps were carried out at room temperature at 13,000 rpm. Initially, 600µl of Buffer QG was added to each tube and the sample was then incubated for 10 minutes at 50°C. During incubation, samples were mixed by vortexing every 2 minutes to help dissolve the gel. Following incubation, 200µl of isopropanol was added to each tube and then mixed to precipitate the DNA. The resulting solution mix was applied to a QIAquick® spin-column placed in a 2ml collection tube and centrifuged for 1 minute. The flow-through was discarded, 750µl of buffer PE was added to the column, and then centrifugation was carried out for 1 minute. After this step, the spin-column was placed into a clean 2ml collection tube (Eppendorf) and centrifuged for 1 minute to dry the membrane. The spin-column was then placed in a clean 1.5ml tube (Eppendorf) and 30µl of elution Buffer EB was added to the centre of the eluting membrane. After a 1-minute incubation period at room temperature, the spin-column

was centrifuged for 1 minute to elute the extracted DNA. The DNA concentration was determined using NanoDrop™ ND-1000 (NanoDrop Technologies) and the obtained samples were stored at -20°C.

3.6 Sequencing of Nuclear Genes

3.6.1 PCR and Agarose Gel Electrophoresis

PCR products were amplified according to the protocol described in **Section 3.3** using primer pairs containing the universal M13 sequence tag (**Table 3-1**). The amplified PCR products were visualised as described in **Section 3.4**.

3.6.2 ExoSAP-IT Protocol

ExoSAP-IT® (GE Healthcare, Amersham, UK) was added to remove unincorporated dNTPs and primers that could interfere with subsequent sequencing reactions. The ExoSAP-IT® solution contains two hydrolytic enzymes: exonuclease I and shrimp alkaline phosphatase. The clean-up treatment was carried out in 96-well plates (Greiner) in a reaction containing 2µl of ExoSAP-IT® buffer and approximately 20ng of PCR product per well. The mixture was incubated at 37°C for 30 minutes, followed by 15 minutes at 80°C to inactivate hydrolytic enzymes.

3.6.3 BigDye™ Sequencing

The BigDye™ Terminator v3.1 Cycle Sequencing Kit® (Applied Biosystems, Life Technologies) contains all the reagents required for the sequencing reaction. Following ExoSAP-IT® (GE Healthcare) treatment, a mastermix containing 1µl BigDye® Cycle Sequencing RR-100, 2µl of BigDye® Terminator v3.1 5X Sequencing Buffer, 1µl of 0.5µM forward or reverse M13 primer and 9µl dH_2O was added to 7µl of PCR product. The BigDye® cycling protocol had an initial step of 1 minute at 96°C, followed by 25 cycles of 96°C for 10 seconds, 50°C for 5 seconds and 60°C for 4 minutes.

3.6.4 Ethanol Precipitation

Ethanol precipitation was performed to remove unincorporated nucleotides and removal of excess salt. A mixture of 2µl 125mM EDTA (Ethylenediaminetetraacetic acid; Sigma-Aldrich), 2µl 3M sodium acetate (Sigma-Aldrich), and 70µl 100% EtOH was added to each sample. After mixing gently and incubating at room temperature for 20 minutes, the samples were centrifuged at 2060g for 30 minutes. The supernatant was removed, 70µl of 70% EtOH was added, and the plate was centrifuged at 1650g for another 15 minutes. The supernatant was removed and the precipitated products were air-dried in the dark for 10 minutes at room temperature, to allow evaporation of the remaining EtOH before resuspending the pellets.

3.6.5 Resuspension and Sequence Analysis

The precipitated products were resuspended in 10µl Hi-Di® (Applied Biosystems, Life Technologies) before being denatured at 95°C for 2 minutes and then rapidly quenched on ice. BigDye® sequencing was performed on the ABI 3130xl Genetic Analyser (Applied Biosystems, Life Technologies) and the raw data was analysed using SeqScape® v2.1.1 software (Applied Biosystems, Life Technologies). The sequencing results were compared with the corresponding Genbank reference gene sequence (http://www.ncbi.nlm.nih.gov/RefSeq/) and all the identified genetic variants were confirmed by reverse sequencing to exclude any PCR or sequencing errors.

Table 3-1 PCR primers used to amplify the 30 coding exons of the *OPA1* gene. Genbank accession number: NM_015560.2. All primers were incorporated with the universal M13 tags to allow sequencing with a single primer.

Exon	Size (bp)	Forward Primer Sequence (5' – 3')	Reverse Primer Sequence (5' – 3')
1	220	CACTTCCTGGGTCATTCCTG	CACCTGCACATTTTTGGAGA
2	487	TTGCTCTTTTAATGTCATTTCCTTT	CATCCAATTGTATTCCACTACACAA
3	424	TGCTTGTTTGCTGAGACCAC	TGGGCTACTGGGTATTTCTTTT
4	341	GGGTTGTCATGAGGATTAAACAA	AAAAATGTCCTGTTTTTCATTGG
4b	249	TCTCAGACATCTTTGTTTGCTCA	CTGGGGTTTTAAAATTCAGCAT
5	247	TGAAATTCAGCTTAGGCTGTTG	TGGATGTTTTTGTATTTGCTTCTC
5b	271	CTTTGTTGCACCCTTGGTTT	TCCATGAACAGATTGAGGTGA
6	231	AAAAATTTAACTTGCTGTACATTCTGT	CACCTTCCAAATTTTGCTCTG
7	389	TTCCTAATGTTTTCGTAGATGCTTT	CTCCATCCTCCAAGCACATT
8	370	CAGTACAATGATTATGGAAAAACAA	TTGCTTAAGACATTACTTGGAACA
9	266	AAAAACTCAGAGCAGCATTACAAA	TGAACAGGTCTCACTGAAGCA
10+11	477	GCAATGCAGTAGCCCTGTCT	GCAGCAATCTAAACATCAATACCT
12+13	504	AGCGTCTTATCTGAATGGATG	AAAATGAATACGAAGAGAAGGC
14	298	GCTATAATGTAGACACAGGGG	AATAACAAATCCCTATCACAGC
15+16	399	TTTTGCTTTCTAAATTGTATATTACGC	GTGAAAACAGTTCAATTTAAGCTACTC
17	333	AAGAGTGGCTGTTAGCAAGC	TAAATGAACTACCAAGCAACTG
18	347	TACTAAGGGGTCATAGGCG	AGATAACTGCTCCTAGAGATG
19	282	AGCCTAGTCAAAAACCTCCC	GCCAAGGCAACAATAAATCAC
20	340	TAATGATACTTCAGTCAAGCTG	AAGATAGAGGCTGTGATGGG
21	333	CACATCTGTTTGGCTTGAGC	TTAGTCATATAAAGTCTCCTATG
22	296	TTTATGCTGGTTTATATACATGG	TCACTAAAGTTGGATGACTCC
23	300	TGCCTTCATATTGATATAGCAC	ATATTCCTGAGACTGGTCTAG
24	382	AATGTATTTATTAAAATTGAGACTG	ACGCAATCAAAATGACTAAGC
25	246	TACAACTTCTCAGTGTGGTTG	GCATATTTTGACAACTGTTGC
26	286	TTAGGACATATCTACTGGTTC	TTGGGAAGTATTTTGGCATCC
27	360	CTATGACTATGAAAAGTATTAGC	TCAGCCCAGTTCCTTGTAAC
28	241	TACCTCCTGATTTGTGATACC	TACAGCATAAGTGACAAGCAG
M13		TGTAAAACGACGGCCAGT	CAGGAAACAGCTATGACC

3.7 Long-Range PCR of Mitochondrial DNA

Investigation of multiple mtDNA deletions was performed using *TaKaRa LA Taq*^{TM} PCR system (Takara Bio, Otsu, Japan), which contains a mixture of *Taq* Polymerase and a proofreading polymerase, capable of amplifying long DNA templates. For each DNA sample, a 16 kb mtDNA fragment encompassing almost the entire mitochondrial genome was amplified. Long-range PCRs were performed using a Veriti® 96-well Thermal Cycler (Applied Biosystems, Life Technologies) in 96-well plates (Greiner). Each DNA sample (approximately 30ng) was amplified in a 50µl long-range PCR master mix containing Mg^{2+} free 10X LA PCR Buffer II (5µl/reaction; Takara Bio), 2.5mM dNTP Mixture (8µl/reaction; Takara Bio), 10µM forward and reverse primers (both 1.25µl/reaction; Sigma-Aldrich; **Table 3-2**), 5U/µl *TaKaRa LA Taq*^{TM} DNA polymerase (0.5µl/reaction; Takara Bio) and dH_2O (made up to 50µl).

DNA was amplified under the following cycling conditions: an initial denaturation step at 94°C for 1 minute, then 35 cycles of denaturation at 94°C for 30 seconds, annealing at 62°C for 30 seconds, and extension at 68°C for 16 minutes. For the last cycle, a final extension step of 12 minutes at 72°C was performed before cooling the sample to 4°C.

Multiple mtDNA deletions were investigated by separating amplicons on a 0.7% (w/v) TAE agarose gel as described in **Section 3.4**. An aliquot (5µl) of each amplified PCR product was mixed with 5µl 2X Orange G loading buffer (Sigma-Aldrich) and then electrophoresed in 1X TAE buffer at a constant voltage of 30V for 4 hours. To allow the amplified PCR fragments to be sized, 5µl of GeneRuler™ 1 kb Plus DNA Ladder (75-20,000 bp) (Fermentas, St. Leon-Rot, Germany) was placed in one lane to provide a DNA ladder marker. The PCR product bands were visualised following exposure to the UV light source with an AlphaImager® 2200 system (Alpha Innotech).

Table 3-2 Properties of primers used to amplify a 16 kb mtDNA fragment using long-range PCR system. Genbank accession number: NC_012920.1.

	Size (bp)	**Forward Primer Sequence (5' – 3')**	**Reverse Primer Sequence (5' – 3')**
16 kb assay	15433	TTA AAA CTC AAA GGA CCT GGC	AGG GTG ATA GAC CTG TGA TC

3.8 Quantitative Real-Time PCR

Unlike standard PCR, quantitative real-time PCR (qPCR) provides a reliable method of measuring the amount of PCR product being amplified as the reaction progresses. The non-specific fluorescent dye, iQ™ SYBR® green (Bio-Rad, Herts, UK), intercalates with double-stranded DNA and it was used to detect the amplified PCR products. The reaction was run on a MyIQ^{TM} thermocycler (Bio-Rad) and after each cycle, the level of fluorescence was measured by an in-built detector. The iQ5™ optical system software v.2.0 (Bio-Rad) determined the threshold cycle (Ct) when the level of fluorescence exceeded the background level and there was a linear increase in the amplification curve, corresponding to the exponential increase in the amount of amplified product as the PCR reaction proceeded (**Figure 3-1**). All the qPCR preparation steps were performed in a UV-sterilised Aura PCR workstation (Bioair Instruments, Milan, Italy) to avoid any cross-contamination.

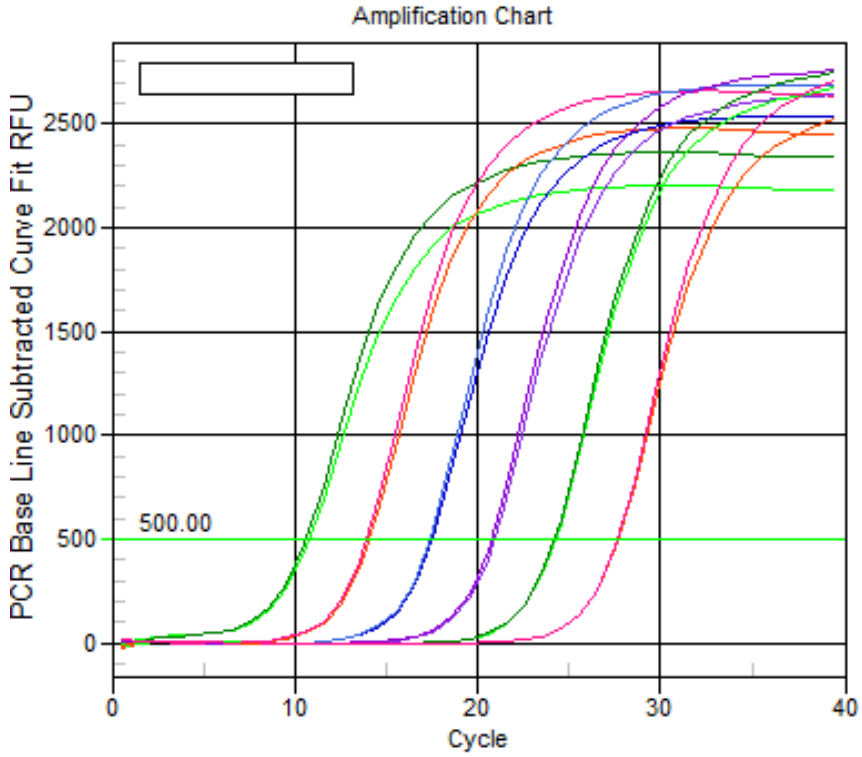

Figure 3-1 Example of the amplification plot of serial dilutions of the B2M template generated by Bio-Rad iQ5™ optical system software v.2.0.

3.8.1 Quantification of MtDNA Copy Number

Quantification of mtDNA copy number was performed using the MyIQ™ thermocycler (Bio-Rad) in 96-well optical plates (Bio-Rad) sealed with Microseal 'B' plate sealers (Bio-Rad). Each DNA sample (approximately 10ng) was amplified in a 25µl qPCR mastermix containing: 1X iQ™ SYBR® Green supermix (12.5µl/reaction; Bio-Rad), 10µM forward and reverse primers (both 0.75µl/reaction; Sigma-Aldrich; **Table 3-3**) and autoclaved nanopure water (9 µl/reaction). For each individual DNA sample, a mitochondrial reference gene (*MTND1*) and a housekeeping nuclear gene (*B2M* or *GAPDH*) were amplified to allow quantification of mtDNA copy number. Additionally, to confirm the efficiency and reliability of the qPCR assay, standard curves with serial dilutions of MTND1 and B2M (or GAPDH) templates were generated (**Figure 3-2**). These templates were produced using a standard PCR protocol (**Table 3-3**) and the amplified fragments were extracted from the agarose gel as described in **Section 3.5**. The number of copies per µl for each template was calculated using the following equation; where C is the template's

concentration [g/µl], Mw is its molecular weight (product length in bp x 2 x 330), and A is Avogadro's constant (6.02 x 10^{23} mol^{-1}):

$$Copies/\mu l = \frac{C}{Mw} \cdot A$$

The qPCR protocol consisted of an initial denaturation phase at 95°C for 3 minutes, then 40 cycles of denaturation at 95°C for 10 seconds, with annealing and extension at 62.5°C for 1 minute. At the end of the cycling protocol, a final denaturation at 95°C for 1 minute was performed. A melting curve was generated to identify all specific and nonspecific PCR products e.g. primer dimers. The melt-curve analysis was performed by detecting the fluorescent signal at each of the 10-second incubation steps during which the sample's temperature rises from 65°C to 95°C in 0.5°C increments (**Figure 3-3**).

Since the qPCR assay assumes a linear relationship between the initial quantity of the template and the Ct value obtained during amplification, the quantification results were taken into consideration only if the amplification efficiency (E) and the coefficient of determination (R^2) were within the optimal ranges: E = 90-105%; R^2 > 0.980 (Nolan et al., 2006).

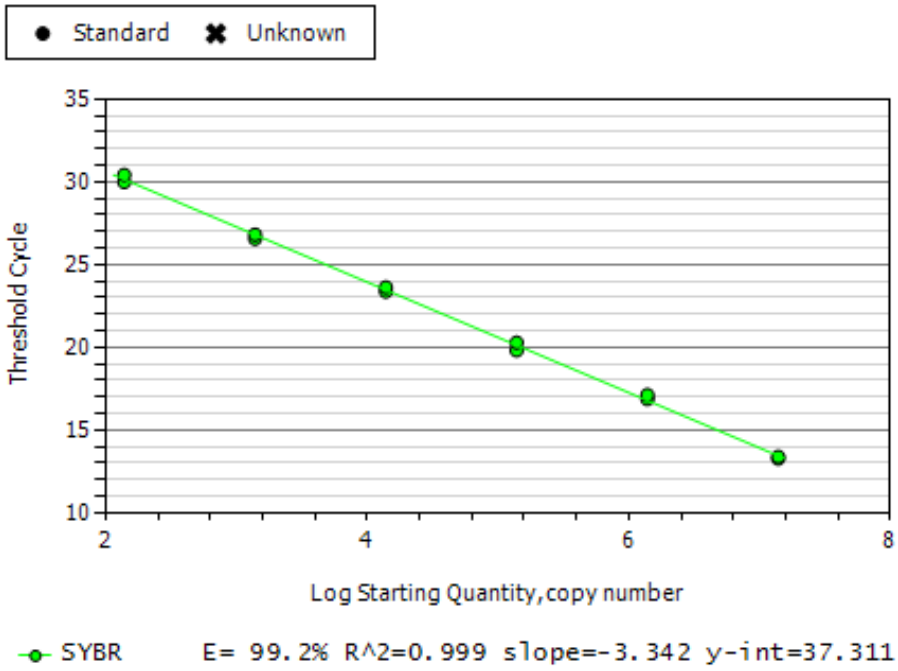

Figure 3-2 Example of a standard curve generated by Bio-Rad iQ5™ optical system software v.2.0 using serial dilutions of the B2M template. (E – amplification efficiency; R^2 – coefficient of determination).

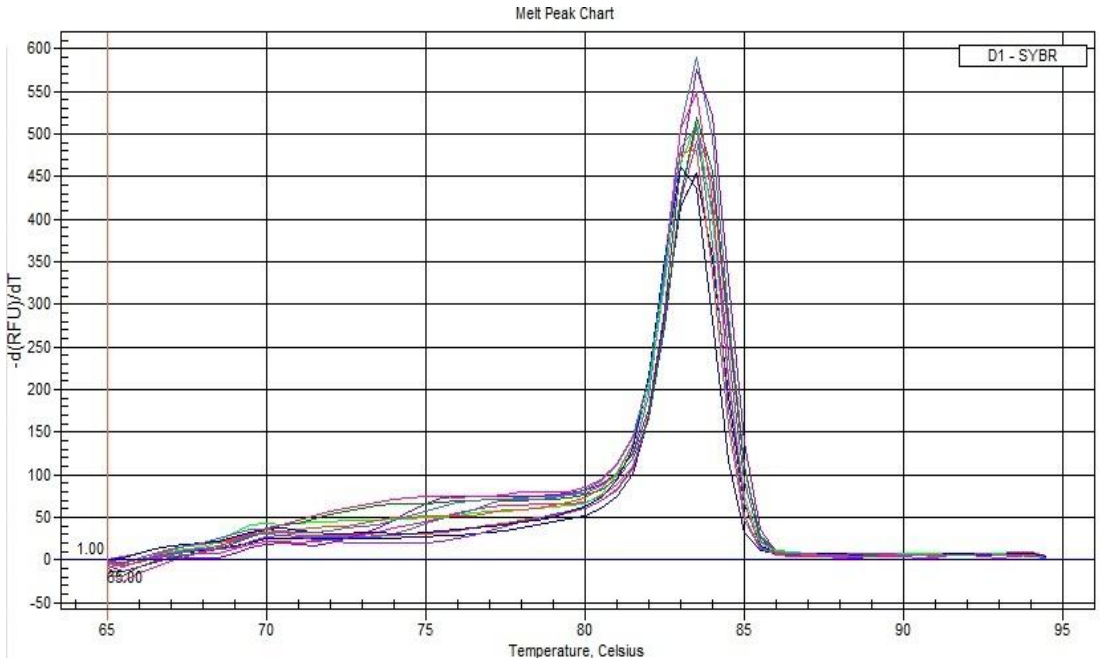

Figure 3-3 Example of a melt-curve analysis performed on serial dilutions of B2M template by Bio-Rad iQ5™ optical system software v.2.0. Fluorescent signal was detected at each incubation step during sample's temperature increase from 65°C to 95°C in 0.5°C increments.

For each analysed DNA sample, Ct values of *MTND1* and *B2M* (or *GAPDH*) were determined in triplicates and their mean values were used for further calculations. The accepted difference between triplicates was up to 0.5 Ct, otherwise the reactions were repeated (Nolan et al., 2006). The analysis was performed using iQ5™ optical system software v.2.0 (Bio-Rad) with a constant fluorescence threshold level set at 500 RFU (relative fluorescence units). Relative mtDNA copy number values were calculated using a delta Ct (ΔCt) method, where delta Ct (ΔCt) was the difference in threshold cycle value (Ct) between *MTND1* and a housekeeping nuclear gene (*B2M* or *GAPDH*). The multiplication factor of 2 is included to account for two copies of the housekeeping nuclear gene per cell nucleus.

$$CopyNumber = 2(2^{-\Delta Ct})$$

Table 3-3 Properties of primers used to generate B2M, GAPDH and MTND1 templates, as well as PCR amplification of housekeeping nuclear genes (*B2M* and *GAPDH*) and a mitochondrial reference gene (*MTND1*). GenBank accession numbers: *B2M* NM_004048.2; *GAPDH* NM_001256799.1; *MTND1* NC_012920.1 ND1.

	Size (bp)	**Forward Primer Sequence (5' – 3')**	**Reverse Primer Sequence (5' – 3')**
Template			
B2M	1092	CGC AAT CTC CAG TGA CAG AA	GCA GAA TAG GCT GCT GTT CC
GAPDH	902	CGA GAT CCC TCC AAA ATC AAG	AGG GGT CTA CAT GGC AAC TG
MTND1	1041	AGG AAC TCG GCA AAT CTT ACC	GTC ATG TGA GAA GAA GCA GG
qPCR			
B2M	231	CAC TGA AAA AGA TGA GTA TGC C	AAC ATT CCC TGA CAA TCC C
GAPDH	102	GGA CCT GAC CTG CCG TCT AG	GTG TAG CCC AGG ATG CCC TTG
MTND1	111	ACG CCA TAA AAC TCT TCA CCA AAG	GGG TTC ATA GTA GAA GAG CGA TGG

3.8.2 Quantification of MtDNA Deletions

MtDNA deletion levels were assessed using a qPCR assay previously optimized in Professor Chinnery's laboratory. This differential *MTND1/MTND4* assay is based on the observation that the *MTND1* gene is rarely involved in large-scale rearrangements, whereas the *MTND4* gene is removed in the majority of reported mtDNA deletions (He et al., 2002). This real-time qPCR protocol was similar to the one described in **Section 3.8.1**, with the primer pairs designed to amplify *MTND1* and *MTND4* fragments (**Table 3-4**) allowing calculation of the total mutant load present. To confirm the efficiency and reliability of this qPCR assay, standard curves were created with serial dilutions of MTND1 and MTND4 templates, generated as described in **Section 3.5**.

For each analysed DNA sample, Ct values of *MTND1* and *MTND4* were determined in triplicates and their mean values were used for further calculations. The accepted difference between triplicates was up to 0.5 Ct, otherwise the reactions were repeated (Nolan et al., 2006). The analysis was performed using MyIQ™ optical system software v.2.0 (Bio-Rad) with a constant fluorescence threshold level of 500 RFU. The relative total (wild-type and mutant) mtDNA copy number was determined from the *MTND1* Ct values, whereas the relative wild-type mtDNA copy number was obtained from the *MTND4* Ct values. The mtDNA deletion level was calculated using the delta Ct method (**Section 3.8.1**) by subtracting the *MTND4* ΔCt value from the *MTND1* ΔCt value.

Table 3-4 Properties of primers used to amplify two mitochondrial regions: *MTND1* and *MTND4*. GenBank accession numbers: *MTND1* NC_012920.1 ND1; *MTND4* NC_012920.1 ND4.

	Size (bp)	Forward Primer Sequence (5' – 3')	Reverse Primer Sequence (5' – 3')
Template			
MTND1	1041	AGG AAC TCG GCA AAT CTT ACC	GTC ATG TGA GAA GAA GCA GG
MTND4	1071	GGC ATT TTG TAG ATG TGG TTT G	AGG AGG AGA ATG GGG GAT AG
qPCR			
MTND1	111	ACG CCA TAA AAC TCT TCA CCA AAG	GGG TTC ATA GTA GAA GAG CGA TGG
MTND4	107	ACC TTG GCT ATC ATC ACC CGA T	AGT GCG ATG AGT AGG GGA AGG

3.9 Reverse-Transcription PCR

Reverse-transcription polymerase chain reaction (RT-PCR) was performed to determine gene transcription at the messenger RNA (mRNA) level. All RT-PCR preparation steps were performed in a UV-sterilised Aura PCR workstation (Bioair Instruments) to avoid any cross-contamination.

3.9.1 First-Strand cDNA Synthesis

First-strand complementary DNA (cDNA) was synthesized from isolated RNA (refer to **Section 3.2** for details) using SuperScript™ III First-Strand Synthesis System for Reverse-Transcription PCR (RT-PCR) (Invitrogen, Life Technologies, Paisley, UK) following the manufacturer's protocol. In order to denature the RNA sample, up to 5µg of RNA was combined in a 0.5ml tube with 1µl of 50µM oligo$(dT)_{20}$, 1µl of 10mM dNTP mix (dATP, dTTP, dCTP and dGTP) and filled up to 10µl with DEPC-treated water. The denaturing mix was then incubated at 65°C for 5 minutes and immediately placed on ice for at least 1 minute. Once the denaturing mix was on ice, the cDNA synthesis mix was prepared. For one reaction, 10µl cDNA synthesis mix was prepared containing: 2µl of 10X RT buffer (200mM Tris-HCl pH = 8.4, 500mM KCl), 4µl of 25mM $MgCl_2$, 2µl of 0.1M DTT (Dithiothreitol), 1µl of RNaseOUT™ (40U/µl) and 1µl of SuperScript™ III RT (200U/µl) combined in the given order.

Following preparation, 10µl of cDNA synthesis mix was added to 10µl of each RNA/primer mixture, mixed gently and collected by brief centrifugation. Once ready, each sample was incubated at 50°C for 50 minutes to synthesise cDNA. This reaction was terminated at 85°C for 5 minutes and sample chilled on ice. To remove any remaining RNA, 1µl of RNase H was added to each tube and incubated for 20 minutes at 37°C. Finally, cDNA synthesis reaction was stored at -20°C.

3.9.2 Quantitative PCR from cDNA Samples

Quantitative PCR on cDNA samples was performed using a MyIQ™ thermocycler (Bio-Rad) in 96-well optical plates (Bio-Rad) sealed with Microseal 'B' plate sealers (Bio-Rad). Each cDNA sample (approximately 10ng) was amplified in a PCR mastermix containing: 1X iQ™ SYBR® green supermix (12.5µl/reaction; Bio-Rad), 10µM forward and reverse primers (both 1.25µl/reaction; Sigma-Aldrich) and autoclaved nanopure water (9µl/reaction).

The PCR protocol consisted of an initial denaturation phase at 95°C for 3 minutes, then 40 cycles of denaturation at 95°C for 10 seconds, with annealing and extension at 62.5°C for 1 minute. At the end of the cycling protocol, a final denaturation at 95°C for 1 minute was performed. Following that, a melting curve was generated to identify all specific and nonspecific PCR products. The melting-curve analysis was performed by detecting fluorescent signal at each of the 10-second incubation steps during the sample's temperature increase from 65°C to 95°C in 0.5°C increments.

The quality of each cDNA sample was assessed by performing quantitative PCR reactions using primers for three widely-expressed housekeeping genes: *GAPDH* and *RPL13A* (**Table 3-5**). The collected qPCR data were assessed with qBASE relative quantification software (http://medgen.ugent.be/qbase/; Ghent University, Belgium), which uses the Ct values obtained for the reference housekeeping genes as the internal controls. This method allowed normalization for variations in the amount and quality of each RNA/cDNA sample that was investigated. The normalized expression levels of various genes were measured by calculating ratios between the quantity of amplified target gene molecules and reference gene molecules. Levels of target gene expression were further used to make comparisons between different samples.

Table 3-5 Properties of primers used to amplify *GAPDH* and *RPL13A* housekeeping reference genes in RT-PCR. GenBank accession numbers: *GAPDH* NM_001256799.1; *RPL13A* NM_001270491.1.

	Size (bp)	Forward Primer Sequence (5' – 3')	Reverse Primer Sequence (5' – 3')
Housekeeping reference genes			
GAPDH	133	CTG ACT TCA ACA GCG ACA CC	ATG AGG TCC ACC ACC CTG T
RPL13A	307	CCT GGA GGA GAA GAG GAA	TTG AGG ACC TCT GTG TAT

3.10 Immunofluorescence

3.10.1 Fixation of Cells

Cells were fixed in 4% (w/v) paraformaldehyde (Sigma-Aldrich) diluted in PBS (Oxoid) by incubating for 20 minutes at room temperature and then washed three times in cold PBS (5 minutes per wash). To detect target proteins expressed intracellularly, cells were additionally permeabilized by incubating with 0.2% (v/v) Triton™ X-100 (Sigma-Aldrich) for 10 minutes at room temperature. Following this step, cells were washed two times in PBS (5 minutes per wash) and stored in PBS (Oxoid) at 4°C for up to one week prior to immunostaining.

3.10.2 Blocking and Incubation with Antibodies

All incubation steps described below were performed at a room temperature in a humidified chamber. To block any unspecific binding of antibodies, cells were incubated in blocking buffer consisting of 1% (w/v) bovine serum albumin (BSA; Sigma-Aldrich) diluted in PBS (Oxoid) for 1 hour. Following the blocking step, the solution was removed and cells were incubated for another hour with a suitable primary antibody diluted to an appropriate concentration in the blocking buffer. The solution was then decanted and cells were washed three times in PBS (5 minutes per wash). Following the last wash, PBS (Oxoid) was removed and the cells were incubated for an hour in the dark with a diluted fluorochrome-conjugated secondary antibody in blocking buffer. After incubation, cells were washed three times in PBS (5 minutes per wash; in the dark) and following the last wash, cells were incubated

for 3 minutes in the dark with 1µg/ml Hoechst 33342 (Molecular Probes, Life Technologies, Paisley, UK) to stain for the nuclei. Cells were then washed in the dark for 5 minutes in PBS (Oxoid) and stored in fresh PBS at 4°C (in the dark). The fluorescent images were obtained using Axiovert 200M microscope (Carl Zeiss, Cambridge, UK) equipped with a digital camera, and analysed with the AxioVision Rel. 4.8 software (Carl Zeiss).

3.11 Mitochondrial Histochemistry

3.11.1 Muscle Biopsy

Muscle biopsies were snap frozen in melting liquid isopentane (-150ºC) and then stored at -80ºC. These were mounted on O.C.T. compound (VWR, Lutterworth, UK) and then serially sectioned at 20µm thickness onto PEN-membrane (Leica, Newcastle upon Tyne, UK) and glass (Fisher Scientific, Loughborough, UK) slides using a Microm™ HM560 cryostat (Fisher Scientific). The serial muscle sections were subsequently stained for COX, SDH, dual COX-SDH, and myofibrillar ATPase activities.

3.11.2 COX/SDH Dual Staining

To stain for cytochrome *c* oxidase (COX) activity, muscle sections were incubated for 35 minutes at 37ºC in medium containing 20% (v/v) 500µM cytochrome *c* (Sigma-Aldrich), 80% (v/v) 3,3'- diaminobenzidine tetrahydrochloride (DAB; Sigma-Aldrich) and a small amount of catalase (Sigma-Aldrich). After incubation, sections were washed twice in PBS (Oxoid; 1 minute per wash). Staining for succinate dehydrogenase (SDH) was performed by incubation for 45 minutes at 37ºC in medium containing 80% (v/v) 1.875mM nitroblue tetrazolium (NBT; Sigma-Aldrich), 10% (v/v) 1.3M sodium succinate (Sigma-Aldrich), 10% (v/v) 2.0mM phenazine methosulphate (PMS; Sigma-Aldrich) and 0.01% (v/v) 100mM sodium azide (Sigma-Aldrich). The incubation was followed by washing twice in PBS (Oxoid; 1 minute per wash).

For dual COX/SDH staining, COX staining was immediately followed by SDH incubation steps. After washing in PBS (Oxoid), muscle sections were dehydrated in a series of graded EtOH solutions: 70%, 95% and 100%. After removing slides from 100% EtOH, the slides were immersed in clean 100% EtOH and left there for 10 minutes. The glass slides were cleared twice in Histo-Clear (VWR) before being mounted in D.P.X. synthetic resin (VWR). The membrane slides were not subjected to Histo-Clear treatment.

3.11.3 ATPase Staining

To stain for ATPase activity, muscle sections were firstly incubated for 30 minutes at room temperature in 0.2M acetate buffer (pH = 4.3) containing 0.2M acetic acid (Sigma-Aldrich) and 0.2M sodium acetate (Sigma-Aldrich). This incubation step was followed by washing 3 times in tap water, and then three times in distilled water. The second incubation step was performed for 45 minutes at 37ºC in medium consisting of ATP disodium salt (Sigma-Aldrich), 0.1M Tris-HCl (Sigma-Aldrich) and 0.08M calcium chloride (Sigma-Aldrich) at an exact pH of 9.5. The slides were then washed twice with 1% calcium chloride (Sigma-Aldrich), followed by incubation in 2% cobalt nitrate (Sigma-Aldrich) for 3 minutes. Afterwards, the slides were washed in three changes of tap water, three changes of distilled water, and developed in 1% ammonium sulphide (Sigma-Aldrich) for 2 minutes. The last step required dehydration through a graded EtOH concentration series: 70%, 95%, and twice in 100%, with the final 100% EtOH immersion lasting 10 minutes. The muscle sections were finally cleared in Histo-Clear (VWR) and mounted in Canada balsam (Sigma-Aldrich).

3.12 Fibroblast Culture

All fibroblast tissue cultures were performed in a class II biohazard hood (Heraeus Herasafe HS-12; Fisher Scientific). In order to maintain stable tissue culture conditions, all culture media were warmed to 37°C in a water bath (JB Aqua 18 Plus; Fisher Scientific) 30 minutes prior to use. All washing steps were performed with PBS (Oxoid).

3.12.1 Tissue Culture Maintenance

Human fibroblasts were cultured in Minimal Essential Medium (MEM) with Earle's salts (Gibco, Life Technologies, Paisley, UK) supplemented with 10% (v/v) heat inactivated fetal bovine serum (FBS; Gibco, Life Technologies), 50U/ml penicillin and 50µg/ml streptomycin (Gibco, Life Technologies), 1X MEM vitamin solution (Gibco, Life Technologies), 1mM sodium pyruvate (Gibco, Life Technologies), 1X non-essential amino acids (Gibco, Life Technologies), 2mM L-glutamine (Gibco, Life Technologies) and 50µg/ml uridine nanopure (Sigma-Aldrich). The cells were grown in suitable tissue culture flasks or plates (Greiner) at 37°C in a humidified cell culture incubator (Heracell 150i, Fisher Scientific) containing 5% CO_2. The cells were monitored on a daily basis with the inverted Leica DM IL microscope (Leica). Once the cells became 90% confluent, they were passaged into a fresh flask. To sub-culture fibroblasts, these were washed once with PBS (Oxoid) and then incubated with 0.05% Trypsin/EDTA (Gibco, Life Technologies) for 5 minutes in a humidified cell culture incubator (37°C, 5% CO_2; Heracell 150i; Fisher Scientific) to detach the cells. The combined Trypsin/EDTA solution was then neutralized by adding 5 volumes of culture medium and the cells were pelleted by centrifugation at 1,200 rpm for five minutes. After removing the supernatant, the cellular pellets obtained were resuspended in medium and reseeded onto fresh flasks/plates in ratios required for specific experimental conditions.

3.12.2 Mycoplasma Detection

Each time a fibroblast cell line was cultured or frozen down, cells were tested for mycoplasma infection using a PCR-based Venor®GeM Mycoplasma Detection Kit (Cambio, Cambridge, UK) following the manufacturer's protocol. PCRs were performed using Veriti® 96-well Thermal Cycler (Applied Biosystems, Life Technologies) in 0.5ml PCR tubes (Eppendorf). All preparation steps were performed on ice. To generate templates for PCR analysis, 100µl of supernatant from each investigated cell line was transferred to a 1.5ml tube (Eppendorf), incubated at 95°C for 5 minutes and briefly centrifuged to pellet cellular debris before adding a PCR mix. The analysed supernatant (2µl) was amplified in a 25µl PCR master mix containing 10X Reaction Buffer (2.5µl/reaction), Primer/Nucleotide Mix

(2.5µl/reaction), Internal control (2.5µl/reaction), 5U/µl DNA Polymerase (0.2µl/reaction) and PCR grade water (15.3µl/reaction). Templates were amplified under the following conditions: an initial denaturation step at 94°C for 10 minutes, then 39 cycles of denaturation at 94°C for 30 seconds, annealing at 55°C for 30 seconds, and extension at 72°C for 30 seconds. Samples were finally cooled to 4°C.

Amplified templates were investigated by separating amplicons on a 1.5% (w/v) TAE agarose gel as described in **Section 3.4**. An aliquot (5µl) of each amplified PCR product was mixed with 5µl of bromophenol blue loading buffer (Sigma-Aldrich), and then electrophoresed in 1X TAE buffer at a constant voltage of 60V for 1 hour. In addition, 5µl of Hyperladder V (Bioline GmbH) was used as a product size marker. The PCR product bands were visualised and compared with a Mycoplasma-positive control (Cambio).

3.12.3 Cell Counting and Viability Assessment

Cell counting was carried out using a haemocytometer chamber (AC1000 Improved Neubauer; Hawksley, Lancing, UK) with Trypan Blue (Sigma-Aldrich) staining for viable cells. This procedure required harvesting fibroblasts as illustrated in **Section 3.12.1**, followed by resuspension of the cell pellet in 1ml of PBS (Oxoid) and the transfer of 100µl of this mixture into a 1.5ml tube (Eppendorf). The suspension was then mixed with 100µl of Trypan Blue (Sigma-Aldrich), which is a blue, vital stain absorbed by damaged or dead cells only. After this step, 15µl of the stained cell suspension was added to two coverslip-sealed haemocytometer chambers. The amount of viable (unstained) and dead (blue in colour) cells were counted in four main corner squares of each haemocytometer chamber. The average count per corner square was then multiplied first by 2, to account for the dilution with Trypan Blue, and then by 10^4 to obtain the number of cells per ml.

3.12.4 Storage of Fibroblasts

3.12.4.1 Cryovial Cryopreservation of Fibroblasts – Freezing

For long-term storage, cells were harvested as described in **Section 3.12.1** and the cell pellet was resuspended in 1ml of the freezing medium (filtered through 0.22µm PES filter; PALL, Portsmouth, UK), containing 70% (v/v) DMEM (Dulbecco's

Modified Eagle Medium; Gibco, Life Technologies) supplemented with 20% (v/v) FBS (Gibco, Life Technologies) and 10% (v/v) dimethylsulphoxide (DMSO; Sigma-Aldrich). Resuspended cells were drop-wise pipetted into a cryovial (Greiner), which then was placed in a Mr. Frosty isopropyl-filled freezing container (Nalgene, Matlock, UK) allowing for a gradual 1°C/min cooling rate. The Mr. Frosty container was placed in a -80°C freezer for 48 hours and after this time, the cryovials were transferred to liquid nitrogen for long-term storage.

3.12.4.2 Cryovial Cryopreservation of Fibroblasts – Thawing

The fibroblast cell lines were placed into culture from frozen cryovials stored in liquid nitrogen storage. Cells were quickly thawed at 37°C (JB Aqua 18 Plus water bath; Fisher Scientific), transferred drop-wise into a 30ml universal container (Fisher Scientific) containing pre-warmed fibroblast medium. The mixture was centrifuged for 5 minutes at 1,200 rpm. The supernatant was aspirated and the cell pellet was resuspended in fresh medium before the cells were seeded in a 25cm^2 flask (Greiner). The medium was changed every 48 hours until the cells reached a confluence of approximately 90% and were ready for another passage.

3.13 Microscopy

Brightfield and fluorescent cell images were captured with an inverted Axiovert 200M microscope (Carl Zeiss) coupled with an AxioCam HRc (Carl Zeiss) digital camera, unless stated otherwise.

3.14 Statistical Analysis

For the purpose of group comparisons statistical analysis was performed using GraphPad™ v.5 statistical software (GraphPad Software, La Jolla, USA). Group comparisons were considered to be statistically non-significant (NS) if the calculated P value was greater than 0.05, significant (*) with P = 0.01 to 0.05, very significant (**) with P = 0.001 to 0.01, and extremely significant (***) when the P value was less than 0.001.

Chapter 4 Disruption of Mitochondrial Fusion and MtDNA Maintenance

Table of Contents

4.1 Introduction

OPA1 and *MFN2* code for two dynamin-like GTPase proteins intrinsically associated with mitochondrial membrane fusion (**Section 1.8.2**). *OPA1* mutations cause autosomal dominant optic atrophy (DOA) (**Section 1.10.2**), and approximately 20% of *OPA1* carriers will develop a more severe form of the disease, DOA+, where the optic atrophy is compounded by additional neurological features, including sensorineural deafness, ataxia, myopathy, and peripheral neuropathy (Yu-Wai-Man et al., 2010b). OPA1 is a multifunctional mitochondrial inner membrane protein (**Section 1.10.3**), and high levels of cytochrome *c* oxidase (COX)-negative muscle fibres have been identified in muscle biopsies from patients manifesting both pure and syndromal DOA phenotypes (Amati-Bonneau et al., 2008; Hudson et al., 2008a). These COX-negative muscle fibres harboured high levels of somatically-acquired mitochondrial DNA deletions and marked mtDNA proliferation was also observed, clearly revealing *OPA1* to be a novel disorder of mtDNA maintenance (Yu-Wai-Man et al., 2010c).

MFN2 mutations typically cause a dominantly-inherited neurodegenerative Charcot-Marie-Tooth type 2A (CMT-2A) disorder (Züchner et al., 2004) (**Section 1.11.2**). Intriguingly, the observed clinical features can overlap with those seen in *OPA1*-related DOA+ phenotypes, with some patients harbouring *MFN2* mutations developing a progressive axonal sensorimotor neuropathy, complicated by optic atrophy, deafness, cerebellar ataxia and proximal myopathy (Rouzier et al., 2012). The presence of COX-deficient fibres and multiple mtDNA deletions in skeletal muscle biopsies suggest that *MFN2* mutations result in disturbed mitochondrial DNA maintenance, similar to *OPA1* mutations (Rouzier et al., 2012).

To further investigate pathological mechanisms associated with disturbed OPA1 and MFN2 function, mtDNA copy number was quantified in blood leukocytes with molecularly-confirmed *OPA1* and *MFN2* mutations.

4.2 Materials and Methods

4.2.1 Patient Cohort

Genomic DNA samples, isolated from the leukocyte fraction of venous blood, were available for the following groups (summarized in **Table 4-1**): (i) individuals harbouring pathogenic *OPA1* mutations (Mean age = 41.3 years, standard deviation (SD) = 18.1 years, range = 3.0-79.0 years, N = 150) from three different populations: British (N = 61), German (N = 40) and Danish (N = 49); (ii) individuals harbouring *MFN2* mutations (N = 58) from three different populations: British (N = 24), German (N = 16) and Czech (N = 18); and (iii) normal healthy controls (Mean age = 55.1 years, SD = 13.1 years, range = 10.0-92.0 years, N = 131) from two different populations: British (N = 87) and German (N = 44). This study had the relevant institutional approval and written informed consent was obtained from all of the subjects involved.

For the list of *OPA1* and *MFN2* mutations identified in our patient cohorts, please refer to **Table A-1** and **Table A-2**, respectively (**Appendix A**).

Table 4-1 Summary of investigated patient cohorts. Individuals with confirmed pathogenic *OPA1* mutations (N = 150) originated from three ethnically diverse subgroups: British (N = 61), German (N = 40) and Danish (N = 49). DNA samples of *MFN2*-affected patients were available from three populations: British (N = 24), German (N = 16) and Czech (N = 18). Control samples were obtained from British (N = 87) and German (N = 44) individuals.

Patient cohort		**N =**
OPA1-positive (N = 150)	British cohort	61
	German cohort	40
	Danish cohort	49
MFN2-positive (N = 58)	British cohort	24
	German cohort	16
	Czech cohort	18
Controls (N = 131)	British cohort	87
	German cohort	44

4.2.2 MtDNA Copy Number Determination

Relative mtDNA copy number was determined using iQ™ SYBR® Green (Bio-Rad) protocol on MyiQ^{TM} real-time PCR detection system (Bio-Rad) with *MTND1* as the mtDNA reference gene and *GAPDH* as the nuclear DNA reference gene (as described in **Section 3.8.1**). MtDNA copy number data for the control cohort were kindly provided by Dr Angela Pyle (Institute of Genetic Medicine, Newcastle University) and Dr Patrick Yu-Wai-Man (Institute of Genetic Medicine, Newcastle University). There was no statistically significant difference in mtDNA content between the British and German normal controls (P = 0.1306; **Figure 4-1 A**).

4.2.3 Detection of Multiple MtDNA Deletions

The presence of multiple mtDNA deletions had previously been investigated in a subgroup of 22 British *OPA1*-positive DNA samples using the long-range PCR protocol described in **Section 3.7**. Multiple mtDNA deletions were not detected in DNA samples extracted from peripheral blood leukocytes. These data were kindly provided by Dr Patrick Yu-Wai-Man (Institute of Genetic Medicine, Newcastle University).

4.2.4 Visual Acuity Assessment

Visual acuity (VA) was measured in the British cohort of *OPA1*-positive patients (N = 61) using a standard Snellen vision chart. For the purpose of statistical analysis, Snellen visual acuity ratios were converted to LogMAR (Logarithm of the minimum angle of resolution) decimal values. A LogMAR value of 0 is equivalent to 20/20 Snellen vision and a value of 1.0 is equivalent to 20/200 Snellen vision, the largest optotype on standard Snellen charts. By convention, patients with visual acuities reduced to counting fingers (CF) are assigned a LogMAR value of 2.0, whilst those with only hand movement (HM) perception are assigned a LogMAR value of 2.3. These data were kindly provided by Dr Patrick Yu-Wai-Man (Institute of Genetic Medicine, Newcastle University), who performed the clinical assessment.

4.2.5 Statistical Analysis

Statistical analysis was performed using GraphPad^{TM} v.4 statistical software (GraphPad Software). Group comparisons were carried out with an unpaired two-tailed Student's t-test with confidence interval (CI) set at 95%.

4.3 Results

4.3.1 *OPA1* Study Group

The analysis of total mtDNA content in three different *OPA1*-positive patient cohorts – British, German and Danish, revealed significantly higher mtDNA copy numbers in peripheral blood leukocytes compared with normal controls (**Figure 4-1 B**, **Figure 4-1 C**, **Figure 4-1 D**). On subgroup analysis, there was no statistically significant difference in mtDNA content between *OPA1*-positive patients harbouring different mutation subtypes (non-significant with Bonferroni correction at P = 0.0199; **Figure 4-2 A**), and when the main functional gene domains were individually compared with each other (non-significant with Bonferroni correction at P = 0.0244; **Figure 4-2 B**). In the British cohort, there was no significant difference in total mtDNA content between patients with pure DOA and DOA+ phenotypes (non-significant with Bonferroni correction at P = 0.0471; **Figure 4-2 C**). No significant correlation was found between visual acuity and mtDNA copy number in the British *OPA1*-mutant group (P = 0.4081; **Figure 4-2 D**).

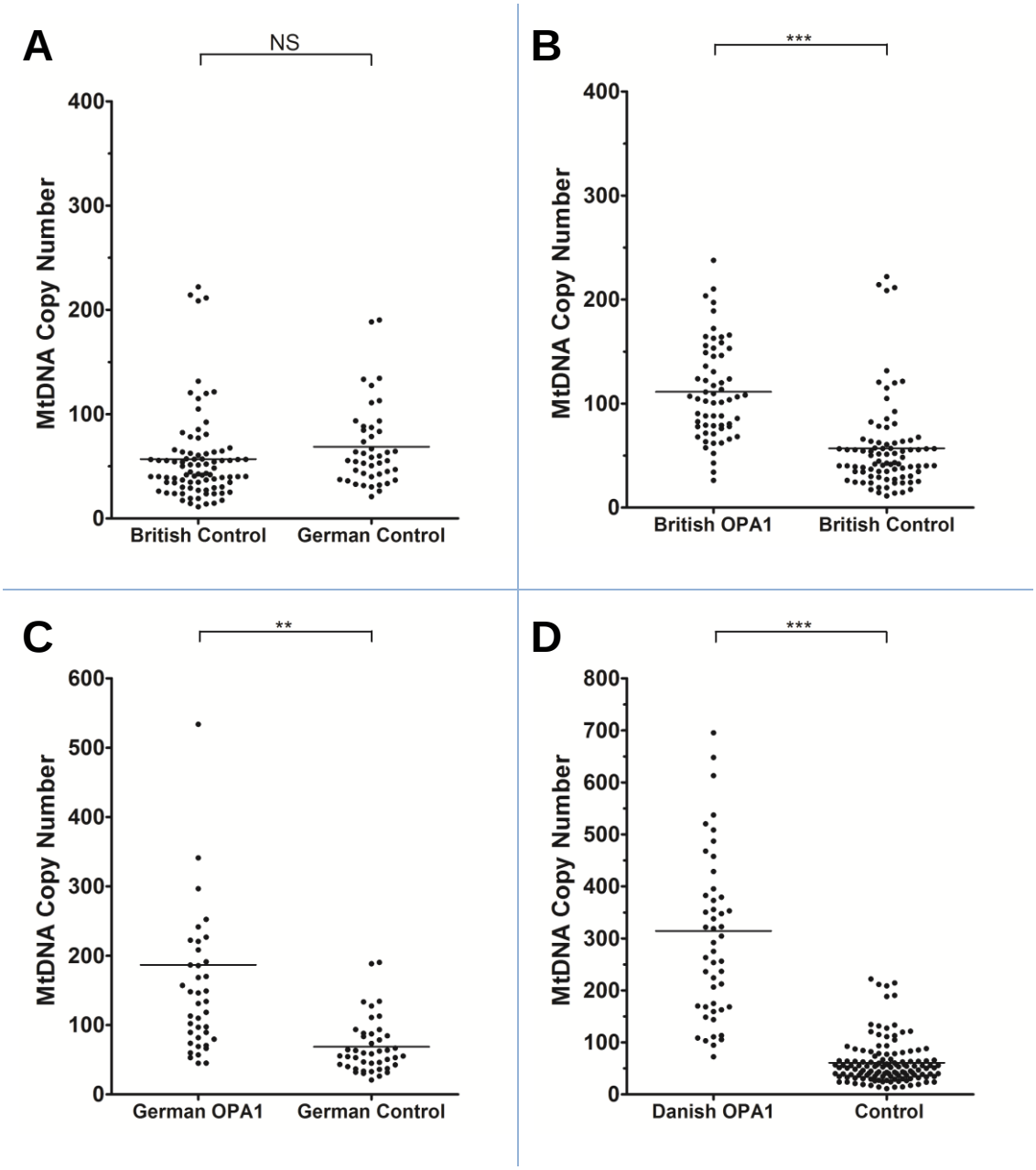

Figure 4-1 Subgroup analysis of total mtDNA content in blood leukocytes of *OPA1*-positive patients. (A) British and German controls (British controls: mean = 56.9, SD = 43.3, N = 87; German controls: mean = 68.7, SD = 39.4, N = 44; NS – not significant at P = 0.1306); (B) British *OPA1*-positive patients (Mean = 111.3, SD = 46.1, N = 61) and British controls (Mean = 56.9, SD = 43.3, N = 87); (C) German *OPA1*-positive patients (Mean = 186.8, SD = 254.1, N = 40) and German controls (Mean = 68.7, SD = 39.4, N = 44); (D) Danish *OPA1*-positive patients (Mean = 314.2, SD = 185.8, N = 49) compared with merged British and German controls (Mean = 60.9, SD = 42.3, N = 131); ** - significant at P value = 0.0031; *** - refers to P value < 0.0001.

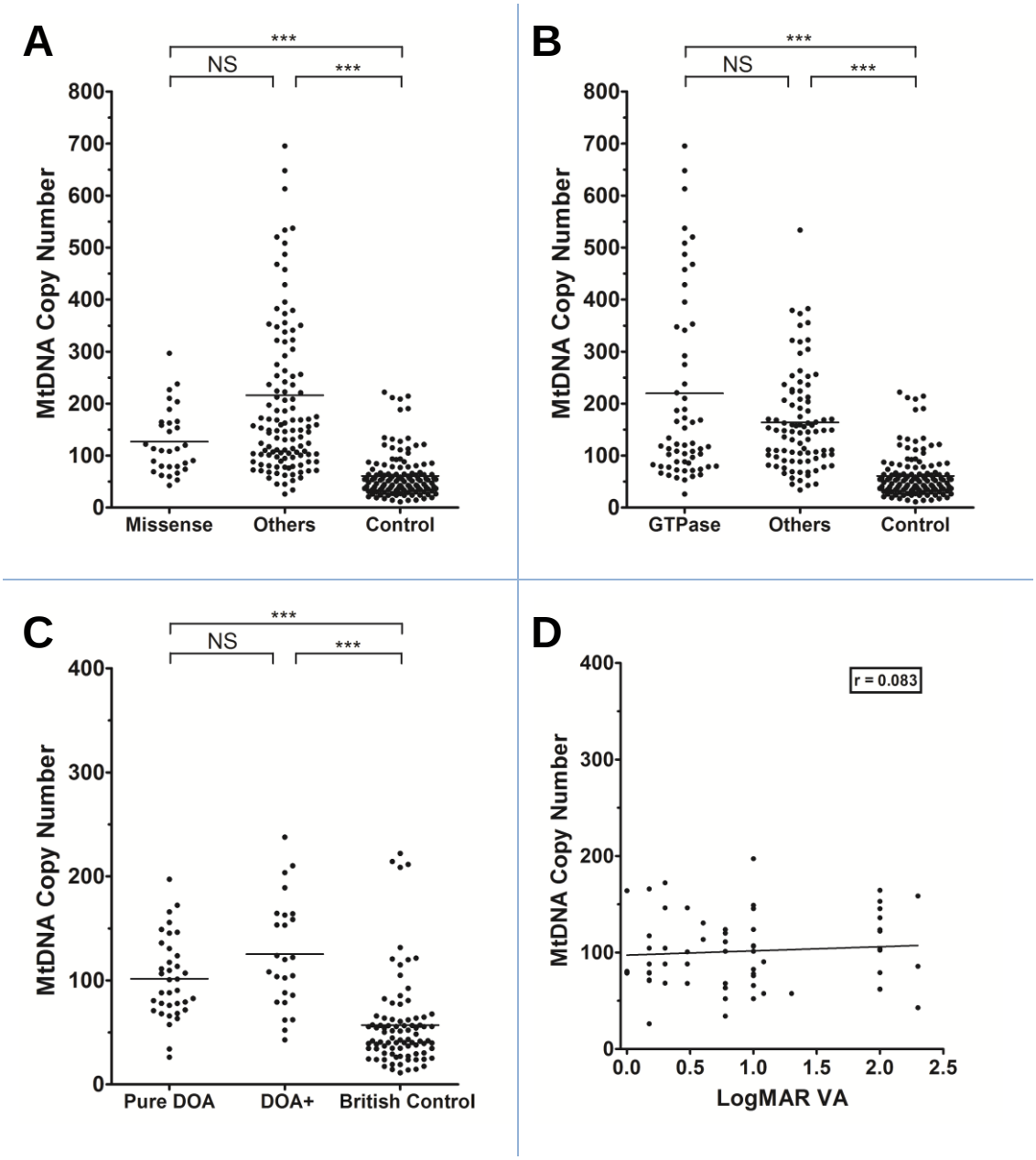

Figure 4-2 Subgroup analysis of total mtDNA content in blood leukocytes of *OPA1*-positive patients. (A) *OPA1* mutational subgroup analysis (missense mutations: mean = 126.8, SD = 62.6, N = 31; other mutational subtypes: mean = 216.1, SD = 208.2, N = 119, NS with Bonferroni correction at P value = 0.0199), (B) *OPA1* functional gene domain analysis (GTPase region: mean = 219.8, SD = 202.6, N = 60; other gene domains: mean = 164.0, SD = 94.0, N = 90, NS with Bonferroni correction at P value = 0.0244); (C) Phenotype subgroup analysis of the British patient cohort (pure DOA subgroup: mean = 101.6, SD = 39.0, N = 36; DOA+ subgroup: mean = 125.3, SD = 52.6, N = 25, NS with Bonferroni correction at P value = 0.0471); (D) Correlation of LogMAR visual acuity (VA) with total mtDNA content in blood leukocytes from British *OPA1*+ve patients (Spearman rank correlation coefficient = 0.083, NS at P value = 0.4081); *** refers to a P value < 0.0001. NS refers to a non-significant P value, with P < 0.0167 being the level of statistical significance after Bonferroni correction for multiple testing.

4.3.2 *MFN2* Study Group

MtDNA copy numbers measured in the blood leukocyte fraction from three independent *MFN2*-positive patient cohorts: British, German and Czech, were significantly higher compared with normal controls (**Figure 4-3 A, Figure 4-3 B, Figure 4-3 C**). No significant difference in total mtDNA content was observed between *MFN2*-positive patients harbouring mutations within GTPase domain and outside this region (P = 0.5957; **Figure 4-3 D**).

Direct comparison of mtDNA content in blood leukocytes from *OPA1*-positive and *MFN2*-positive cohorts revealed no statistical difference between these two disease groups (P = 0.9408; **Figure 4-4**).

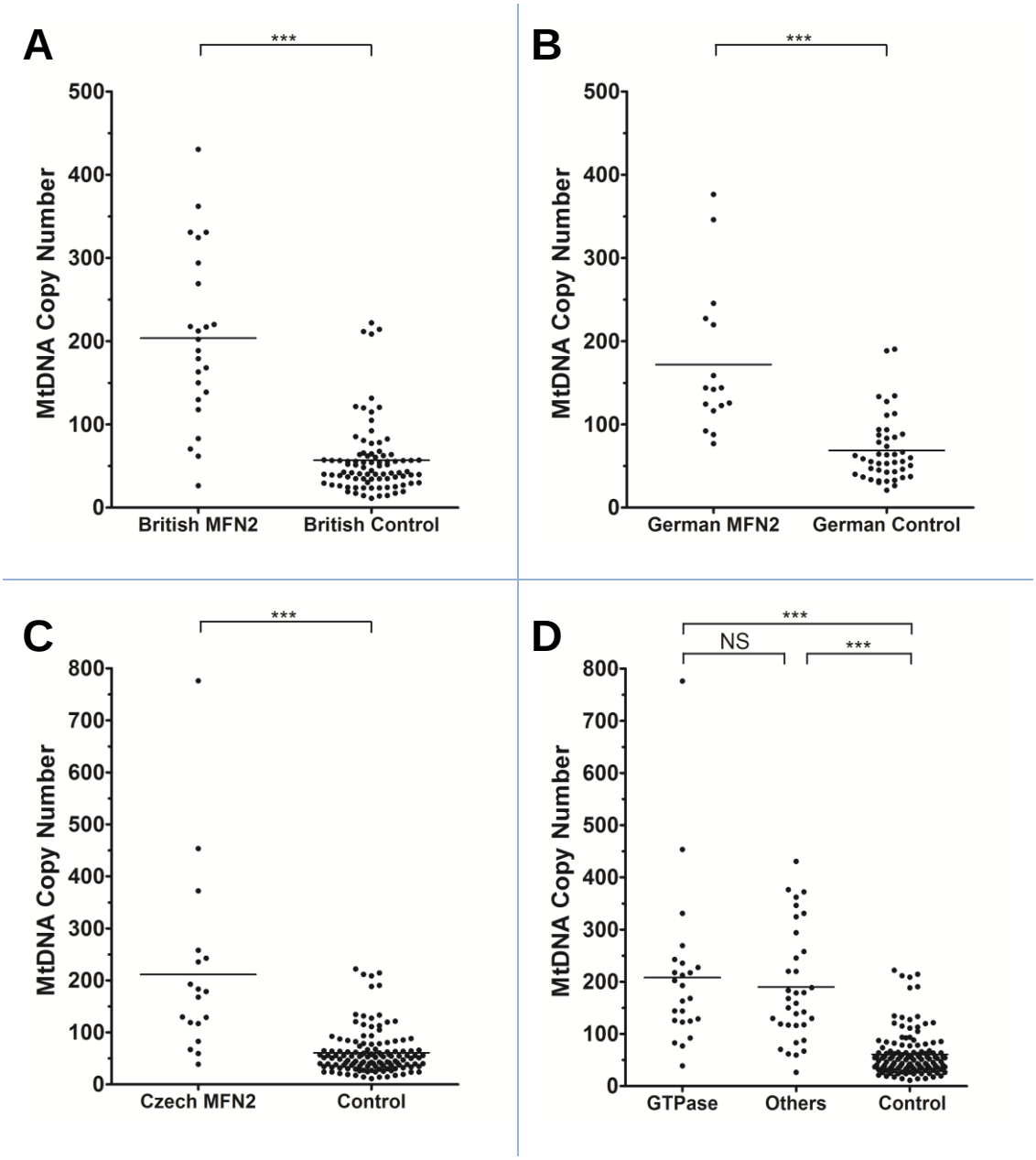

Figure 4-3 Subgroup analysis of total mtDNA content in blood leukocytes of *MFN2*-positive patients. (A) British *MFN2*-positive patients (Mean = 203.7, SD = 103.1, N = 24) and British controls (Mean = 56.9, SD = 43.3, N = 87); (B) German *MFN2*-positive patients (Mean = 171.9, SD = 88.7, N = 16) and German controls (Mean = 68.7, SD = 39.4, N = 44); (C) Czech *MFN2*-positive patients (Mean = 211.3, SD = 177.0, N = 18) compared with merged British and German controls (Mean = 60.9, SD = 42.3, N = 131); (D) *MFN2* functional gene domain analysis (GTPase region: mean = 207.9, SD = 150.2, N = 24; other gene domains: mean = 189.8, SD = 108.2, N = 34, NS at P value = 0.5957; *** - refers to P value < 0.0001.

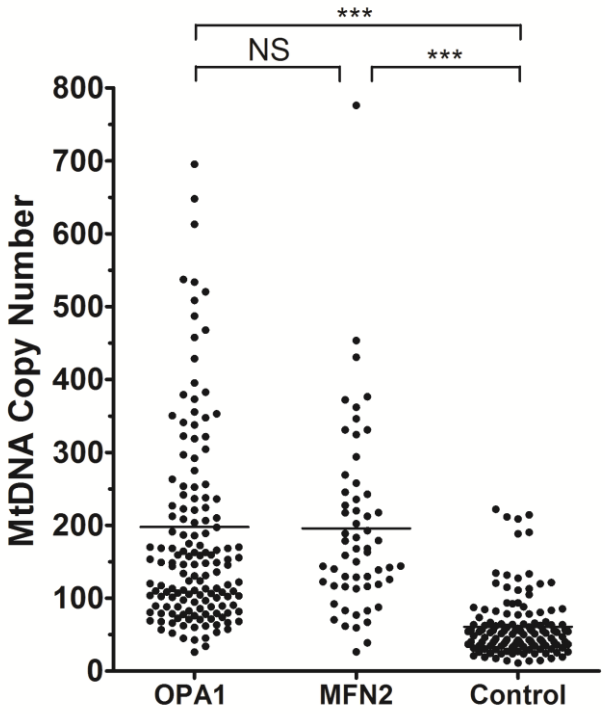

Figure 4-4 Comparison of mtDNA content in blood leukocytes from entire *OPA1*- and *MFN2*-positive patient cohorts. *OPA1*-mutated patients: mean = 197.7, SD = 190.9, N = 150; *MFN2*-mutated patients: mean = 195.7, SD = 126.6, N = 58; NS – non-significant at P = 0.9408; *** - refers to P value < 0.0001.

4.4 Discussion

This study has revealed significant mtDNA proliferation in blood leukocytes of patients harbouring pathogenic *OPA1* and *MFN2* mutations. Compared with control values, there was a two- to five-fold increase in mtDNA content in three independent *OPA1*-positive patient cohorts (British, German and Danish). Similarly, there was a two- to three-fold increase in mtDNA content in three independent *MFN2*-positive patient groups (British, German and Czech). Although it has been previously shown that the differential blood cell count can affect blood-derived mtDNA copy number (Pyle et al., 2010), the consistent increase in mtDNA content observed in both *OPA1* and *MFN2* cohorts across different population groups, strongly suggests that these results are unlikely to have been influenced by this possible confounding factor.

The level of mtDNA proliferation observed in peripheral blood leukocytes of *OPA1*-positive individuals was comparable to the two- to four-fold increase in mtDNA content observed at the single fibre level in skeletal muscle biopsies from *OPA1*-

positive patients (Yu-Wai-Man et al., 2010c). As described previously (**Section 1.10.3.2**), the OPA1 protein plays a key role in the assembly and stability of the respiratory chain complexes and these pathological findings, in both blood and skeletal muscle, are consistent with the detrimental effect of *OPA1* mutations on mitochondrial OXPHOS. In this situation, the increased mtDNA copy number is probably acting as a compensatory bioenergetic mechanism to maintain adequate levels of ATP for normal cellular function (Yu-Wai-Man et al., 2010c). The mtDNA proliferative response in *OPA1*-positive blood leukocytes was not statistically different between patients with pure optic atrophy and those who developed additional neurological complications. Furthermore, irrespective of whether or not *OPA1* carriers developed DOA+ features, there was no significant correlation between total mtDNA copy number and the severity of visual loss. Given the three-fold increased risk of developing DOA+ with missense mutations and those with mutations involving the GTPase catalytic domain, additional subgroup analysis was carried out based on these *OPA1* mutational subtypes (Yu-Wai-Man et al., 2010b). No consistent significant difference in mtDNA copy number was identified, which suggests that this parameter of mitochondrial dysfunction is not associated with clinical severity *per se*, at least in blood leukocytes. Unlike the skeletal muscle, multiple mtDNA deletions were not identified in blood leukocytes from patients with *OPA1* mutations. This is likely related to the relatively short half life of these cells in the blood circulation, their rapid turnover precluding the formation and subsequent clonal expansion of somatic mtDNA abnormalities.

MFN2 and OPA1 mediate mitochondrial membrane fusion synergistically. It is therefore noteworthy that blood leukocytes from patients with *MFN2* mutations demonstrated the same phenomenon observed in tissue samples from patients with *OPA1* mutations i.e. significant mtDNA proliferation. As for *OPA1*-positive patients, this proliferative response in *MFN2*-mutant individuals is probably acting as a compensatory mechanism in response to an underlying cellular bioenergetic crisis (Rouzier et al., 2012). Similar to the *OPA1* patient group, no significant difference in mtDNA proliferation was observed in *MFN2* carriers harbouring mutations within or outside the functional GTPase domain. *MFN2*-related disease is the newest member of an expanding group of nuclear mitochondrial disorders characterised by disturbed

mtDNA maintenance, a process which seems to be intrinsically related to the state of the mitochondrial network (Chen et al., 2010) (**Section 1.11.3**).

The data presented in this chapter have been published following peer review:

1. **Sitarz K.S.**, Almind G.J., Horvath R., Czermin B., Grønskov K., Pyle A., Taylor R.W., Larsen M., Chinnery P.F., Yu-Wai-Man P., 2012. OPA1 mutations induce mtDNA proliferation in leukocytes of patients with dominant optic atrophy. Neurology*: in press*.
2. **Sitarz, K.S.**, Yu-Wai-Man, P., Pyle, A., Stewart, J.D., Rautenstrauss, B., Seeman, P., Reilly, M.M., Horvath, R., Chinnery, P.F., 2012. MFN2 mutations cause compensatory mitochondrial DNA proliferation. Brain. *First published online: April 4, 2012*.

Chapter 5 Investigations of *MFN2*-Positive Muscle Biopsy

Table of Contents

5.1 Introduction

MFN2 mutations cause Charcot-Marie-Tooth type 2A (CMT-2A) (Züchner et al., 2004) and rather intriguingly, the clinical manifestations observed in this disorder can be observed in a subgroup of patients with *OPA1*-related DOA+ phenotypes (Rouzier et al., 2012). *OPA1* mutations have previously been linked with the occurrence of pathological COX-negative muscle fibres, the accumulation of high levels of somatically-acquired mtDNA deletions, and significant mtDNA proliferation (Amati-Bonneau et al., 2008; Hudson et al., 2008a; Yu-Wai-Man et al., 2010c). As detailed previously (**Chapter 4**), blood leukocytes from both *OPA1* and *MFN2* mutant carriers were found to contain significantly higher mtDNA copy numbers compared with those from normal controls (Sitarz et al., 2012a; Sitarz et al., 2012c). It is therefore highly relevant that COX-deficient muscle fibres and multiple mitochondrial DNA deletions have recently been identified in skeletal muscle biopsies from affected family members segregating a pathogenic c.629A>T (p.D210V) *MFN2* missense mutation, clearly implicating disturbed mtDNA maintenance being an important pathogenic mechanism in this family (Rouzier et al., 2012). The main objectives of this study were: (i) to determine whether COX-deficient muscle fibres were present in a skeletal muscle specimen biopsied from one patient with a confirmed *MFN2* mutation (c.1091G>C; p.R364P) within CC1 region; (ii) to investigate whether multiple mtDNA deletions were present in muscle homogenate DNA; and (iii) to quantify mtDNA copy number and the level of mtDNA deletions present in single COX-positive and COX-negative muscle fibres.

5.1.1 Dual COX/SDH Staining

Mitochondrial histochemical staining of skeletal muscle sections is a well-validated, reliable method for detecting impaired OXPHOS. Most diagnostic protocols involve sequential staining to determine the level of activity of two mitochondrial respiratory chain enzymes: succinate dehydrogenase (SDH) for complex II and cytochrome *c* oxidase (COX) for complex IV (**Section 1.9.4.1**). Complex II is entirely nuclear encoded, whereas complex IV consists of subunits encoded by both the nuclear and mitochondrial genomes. If mtDNA integrity is compromised e.g. by point mutations or large-scale deletions, this will have a deleterious effect on overall COX activity, but there will be no detectable loss in SDH activity. Following dual COX/SDH

staining, COX-negative fibres are highlighted blue, whereas COX-positive fibres remain brown in colour (**Figure 5-1**).

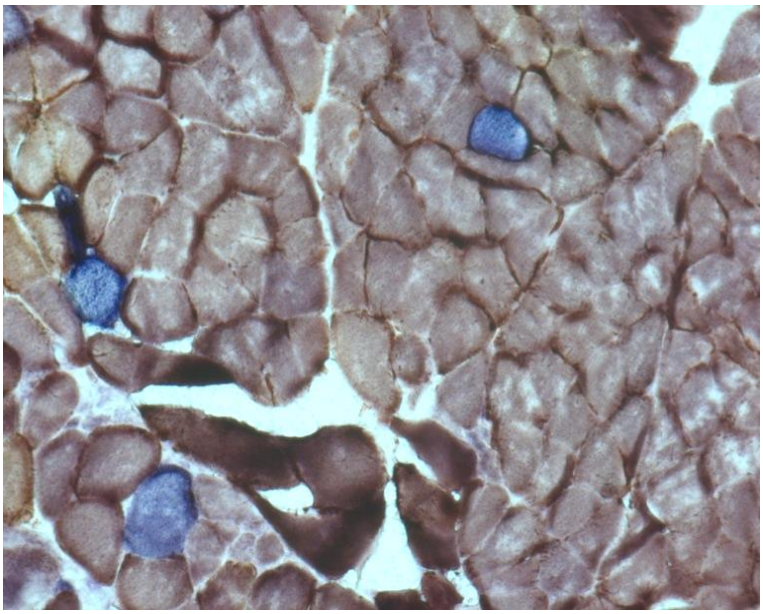

Figure 5-1 Example of dual COX/SDH staining performed on a muscle section. COX-negative fibre highlighted in blue.

5.1.2 Myofibrillar ATPase Staining

Myofibrillar ATPase activity can be used to distinguish between muscle fibre types, which can be broadly classified as type I (slow contracting, oxidative) or type II (fast contracting, glycolytic/oxidative) subtypes. ATPase staining can reveal pathological changes such as muscle fibre atrophy or fibre type grouping, classically seen in patients with peripheral neuropathy. In the first step of the ATPase staining protocol, fibres were preincubated with an acid solution (pH ~ 4), which inhibits ATPase activity in fast (type II) fibres (**Section 1.9.4.1**). As a result, type I muscle fibres were stained dark brown, whereas type II muscle fibres remained light brown (**Figure 5-2**).

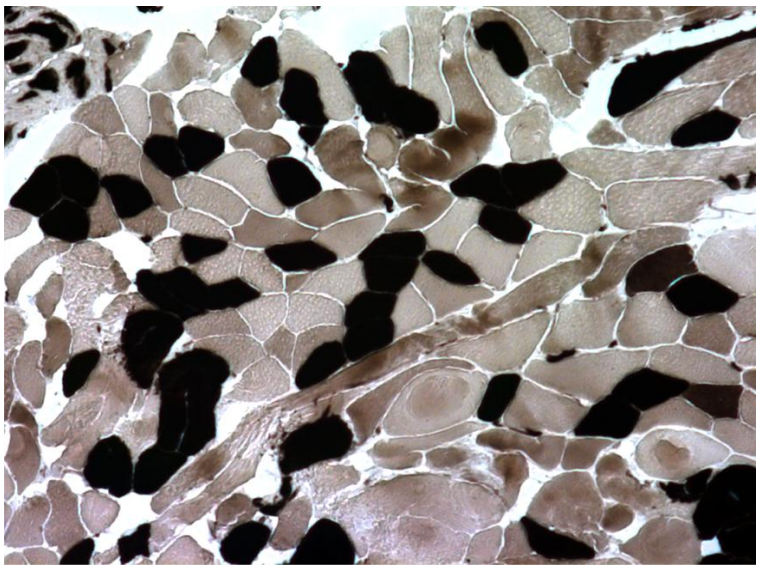

Figure 5-2 Example of ATPase staining performed on a muscle section. Type I muscle fibres are dark brown whereas type II muscle fibres stain light brown.

5.2 Materials and Methods

5.2.1 Tissue Samples

Muscle biopsies from a patient with a confirmed *MFN2* mutation and from a normal healthy individual were investigated in this study. The *MFN2* carrier was a 65-year-old female harbouring a c.1091G>C (p.R364P) missense mutation in CC1 domain, who developed a progressive sensori-motor neuropathy with respiratory muscle involvement. The normal control was a 33-year-old male with no evidence of ocular or neuromuscular pathologies. This study had the relevant institutional approval and written informed consent was obtained from all of the subjects involved.

5.2.2 Mitochondrial Histochemistry

Dual COX/SDH and ATPase histochemical stains were performed on 20µm muscle biopsy sections as described in **Section 3.11.2** and **Section 3.11.3**, respectively.

5.2.3 Long-Range PCR

To detect multiple mtDNA deletions, a 16-kb long-range PCR assay was carried out with the *TaKaRa LA Taq*^{TM} PCR system (Takara Bio) on extracted muscle homogenate DNA, as described in **Section 3.7**.

5.2.4 Single Fibre Analysis

Individual muscle fibres were cut using a LMD 6000™ laser dissecting microscope (Leica) and their cross-sectional areas (µm²) were recorded at the same time. The laser-microdissected muscle fibres were lysed in a Mastercycler^{TM} Gradient System (Eppendorf) for 16 hours at 55ºC, in a 30µl reaction mix containing: 50% (v/v) 1% Tween-20 (Sigma-Aldrich), 10% (v/v) Tris-HCl (Sigma-Aldrich), 1% (v/v) proteinase K (Sigma-Aldrich) and 39% (v/v) dH_2O. This was followed by heat inactivation at 95ºC for 10 minutes. The single-fibre lysates were used for qPCR analysis.

5.2.4.1 Quantification of MtDNA Content and Deletion Level

The mtDNA content of individual muscle fibres was determined using a real-time qPCR (*MTND1*/*B2M*) assay as described in **Section 3.8.1**. The different sizes of muscle fibres could potentially introduce variations in mtDNA content. To account for this, the total mtDNA copy number for each muscle fibre was divided by that fibre's surface area, and the data were presented as the number of mtDNA copies per µm². The level of mtDNA deletions was calculated with a real-time qPCR (*MTND1/MTND4*) assay as detailed in **Section 3.8.2**. The mtDNA content data for four control muscles was kindly provided by Dr Patrick Yu-Wai-Man (Institute of Genetic Medicine, Newcastle University). This normative data set was combined with the results obtained from an additional control muscle biopsy.

5.2.5 Statistical Analysis

Statistical analyses were performed using GraphPad^{TM} v.4 statistical software (GraphPad Software). Group comparisons were carried out with an unpaired two-tailed Student's t-test with confidence interval (CI) set at 95%.

5.3 Results

5.3.1 Mitochondrial Histochemistry

Sequential COX/SDH staining of muscle sections from the *MFN2*-positive patient's biopsy revealed a relatively low level of COX-deficient muscle fibres, estimated at 9/1285 (0.7%) muscle fibres (**Figure 5-3**, **Figure 5-5 A**). Myofibrillar ATPase staining showed clear evidence of muscle fibre atrophy and fibre-type grouping (**Figure 5-4**, **Figure 5-5 B**). No pathological morphological or histochemical changes were noted in control muscle sections, following dual COX/SDH (**Figure 5-6**) and ATPase (**Figure 5-7**) staining.

Figure 5-3 Dual COX/SDH staining in a muscle section from the *MFN2*-positive patient. COX-deficient fibres highlighted in blue.

Figure 5-4 Staining for ATPase activity in a muscle section from the *MFN2*-positive patient. Type I fibres are dark brown, whereas type II fibres are light brown in colour. Fibre-type grouping can be observed in this section with loss of the normal checkerboard appearance.

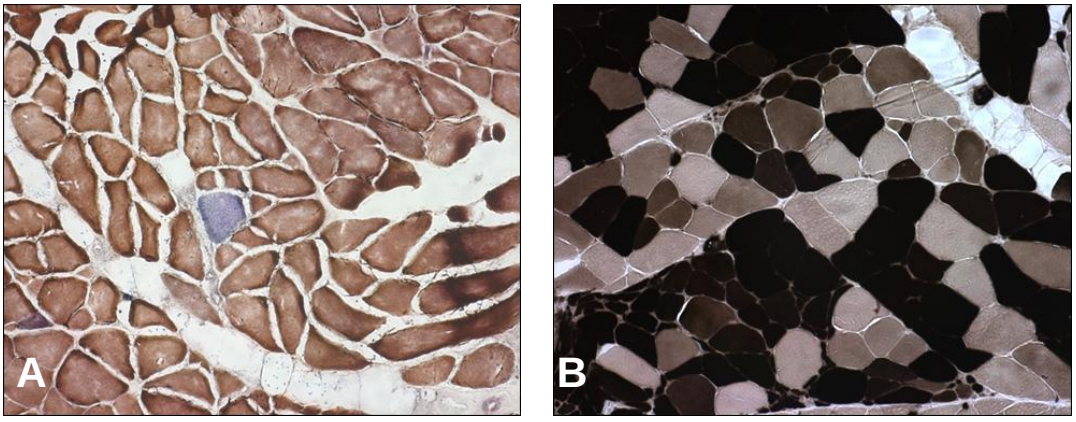

Figure 5-5 Higher magnification views of stained *MFN2*-positive muscle sections revealing: (A) a COX-negative (blue) muscle fibre following dual COX/SDH histochemistry; (B) atrophic muscle fibres and fibre-type grouping following myofibrillar ATPase staining.

Figure 5-6 Dual COX/SDH staining in a muscle section from a normal control individual. No COX-deficient fibres were detected.

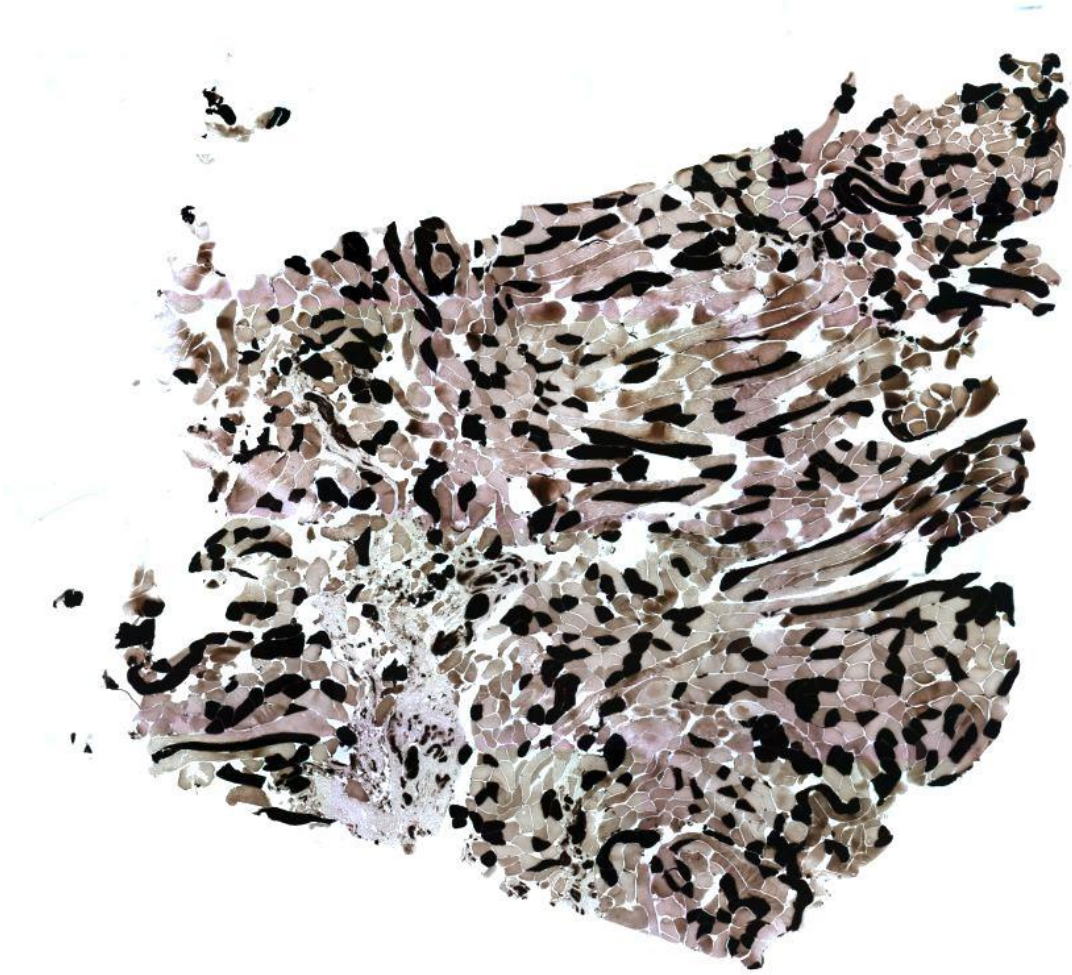

Figure 5-7 Staining for ATPase activity in a muscle section from a normal control individual. Fibre-type grouping and atrophy were not observed.

5.3.2 Detection of Multiple MtDNA Deletions

Multiple mtDNA deletions were not detected in muscle homogenate DNA from the *MFN2*-positive patient (**Figure 5-8**).

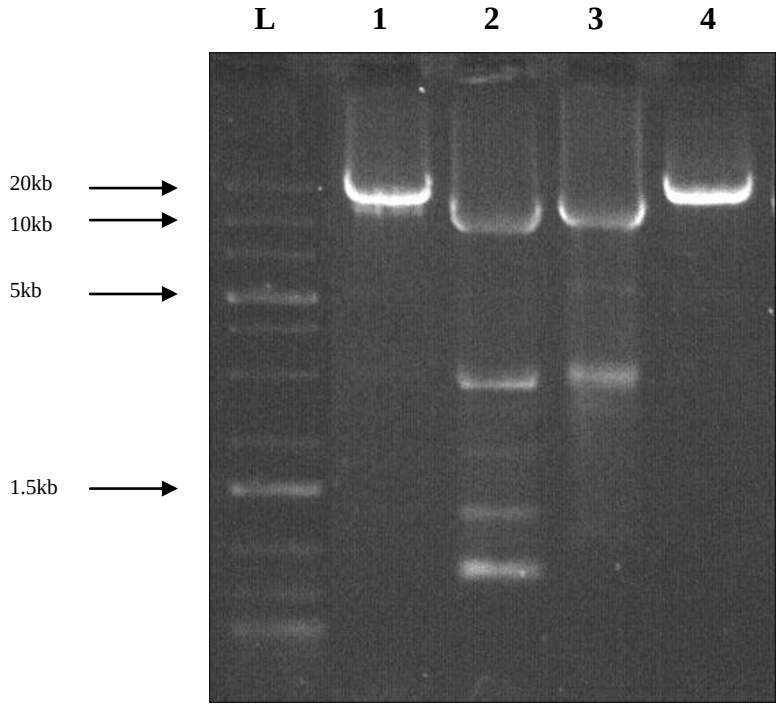

Figure 5-8 Agarose gel revealing no multiple mtDNA deletions detected in total DNA isolated from muscle homogenate of a *MFN2*-positve individual. Legend: L = GeneRuler™ 1 kb Plus DNA Ladder (75-20,000 bp; Fermentas); 1 = *MFN2*-mutated patient; 2 and 3 = positive multiple mtDNA deletion controls; 4 = normal healthy control.

5.3.3 Single Muscle Fibre Analysis

In the *MFN2*-positive muscle biopsy, there was evidence of significant mtDNA proliferation in COX-negative fibres compared with both type I and type II COX-positive fibres (**Figure 5-9 A**). There was no significant difference in mtDNA copy number between different type I and type II COX-positive muscle fibres (P = 0.1827; **Figure 5-9 A**). Four out of eight (50%) COX-negative muscle fibres had mtDNA deletion levels > 70% (**Figure 5-9 B**). Compared with normal control muscle, total mtDNA content was significantly increased in the *MFN2*-positive muscle for both COX-positive type I (P = 0.0328; **Figure 5-10 A**) and COX-positive type II (P < 0.0001; **Figure 5-10 B**) muscle fibres.

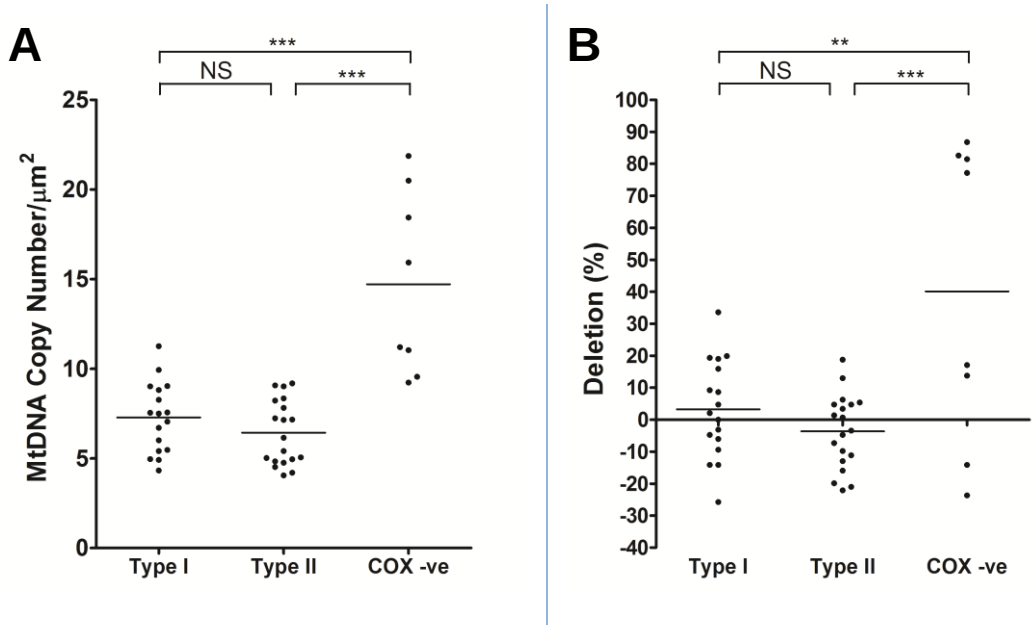

Figure 5-9 Single fibre analysis of a *MFN2*-positive muscle specimen. (A) Comparison of mtDNA content for COX-positive (type I and type II) and COX-negative (COX-ve) fibres (type I: mean = 7.3, SD = 1.9, N = 17; type II: mean = 6.4, SD = 1.8, N = 19; COX-ve: mean = 14.7, SD = 5.1, N = 8); NS - not significant at P = 0.1827; *** - refers to P value < 0.0001. (B) MtDNA deletion levels in different muscle fibre types (type I: mean = 3.2, SD = 15.3, N = 17; type II: mean = -3.7, SD = 11.6, N = 19; COX-ve: mean = 40.1, SD = 46.7, N = 8); NS - non-significant at P = 0.1339; ** - significant at P = 0.0065; *** - refers to P value < 0.0001.

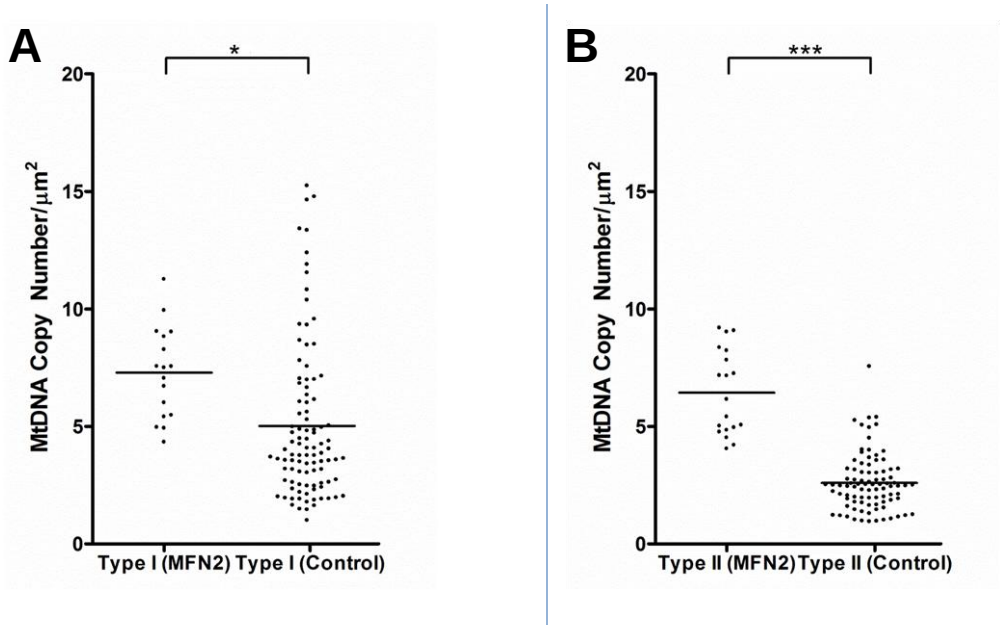

Figure 5-10 Comparison of mtDNA content in type I and type II COX-positive fibres for *MFN2*-positive and control muscle specimens. (A) *MFN2* type I: mean = 7.3, SD = 1.9, N = 17; control type I: mean = 5.4, SD = 3.5, N = 81; * - significant at P = 0.0328. (B) *MFN2* type II: mean = 6.4, SD = 1.8, N = 19; control type II: mean = 2.6, SD = 1.2, N = 90; *** - refers to P value < 0.0001.

5.4 Discussion

The histochemical investigation of a muscle biopsy specimen from a patient harbouring a pathogenic c.1091G>C (p.R364P) mutation has revealed the presence of atrophic muscle fibres and characteristic fibre-type grouping in keeping with an ongoing pathological denervation-reinnervation process. A relatively low level of COX-negative muscle fibres was detected (0.7%), and this could simply reflect the age of the patient, who was 65-years-old when the biopsy was carried out. Up to 1% COX-deficient muscle fibres have been identified in muscle biopsies obtained from healthy, physically-active elderly individuals over the age of 60 years, due to the clonal expansion of somatic mtDNA deletions (Brierley et al., 1998; Bodyak et al., 2001). Single-fibre analysis of the *MFN2*-positive muscle specimen revealed a statistically significant increase in mtDNA copy number in COX-negative muscle fibres compared with both type I and type II COX-positive fibres. Interestingly, significant mtDNA proliferation was also observed in type I and type II COX-positive muscle fibres when compared with muscle fibres from normal control muscle biopsies. This increase in mtDNA copy number could be a compensatory mechanism that helps to maintain adequate levels of ATP production, analogous to the marked mtDNA proliferation observed in muscle biopsies from patients with *OPA1* mutations (Yu-Wai-Man et al., 2010c). More importantly, the observed mtDNA proliferation in the *MFN2*-positive muscle biopsy supports the similar phenomenon detected in blood leukocytes of *MFN2*-mutant carriers (Sitarz et al., 2012c).

Only 50% of COX-negative muscle fibres had deletion levels > 70% i.e. above the generally accepted mutational threshold required to induce a biochemical defect (Shoubridge et al., 1990; Bua et al., 2002; Durham et al., 2007). It is possible that the remaining COX-negative fibres (4/8; 50.0%) harboured small mtDNA deletions, which spared both *MTND1* and *MTND4*, and therefore remained undetectable with the qPCR assay (Bua et al., 2006). Another possibility is that COX-deficiency in these fibres is due to accumulation of high levels of somatic mtDNA point mutations, and not deletions (Del Bo et al., 2003; Wanrooij et al., 2004; Chinnery and Zeviani, 2008; Reeve et al., 2008).

Rouzier and colleagues have recently described a Tunisian family with a progressive multisystem neurological disorder secondary to a novel heterozygous missense mutation in *MFN2* (c.629A>T; p.D210V) (Rouzier et al., 2012). *MFN2* mutations typically cause autosomal-dominant axonal Charcot-Marie-Tooth disease type 2A (CMT2A) (Züchner et al., 2004). Interestingly, the clinical features among mutational carriers in this Tunisian family were more variable, ranging from asymptomatic subclinical disease to an axonal sensorimotor neuropathy complicated by optic atrophy, deafness, cerebellar ataxia, and proximal myopathy (Rouzier et al., 2012). COX-deficient fibres and multiple mtDNA deletions were detected in skeletal muscle biopsies from affected family members, clearly suggesting that the *MFN2* mutation segregating in this family is having a deleterious impact on mtDNA maintenance, ultimately triggering an overt mitochondrial respiratory chain defect and the onset of clinical symptoms. Further studies on a larger number of *MFN2*-positive muscle biopsies are needed to confirm the important findings reported by *Rouzier and colleagues* and the additional observations made in this study.

Chapter 6 Neuromyelitis Optica and Genetic Variations within *OPA1*

Table of Contents

6.1 Introduction

Neuromyelitis optica (NMO), also known as Devic's disease is an idiopathic, autoimmune, demyelinating condition of the central nervous system (CNS) that preferentially affects the optic nerve and spinal cord (Wingerchuk et al., 2007). NMO is a relatively rare cause of CNS demyelination with the prevalence estimated at 0.5 to 1.0 per 100,000 among the white population (Jacob et al., 2009). The discovery of a specific NMO-IgG autoantibody marker against the aquaporin-4 (AQP4) water channel and the consistent presence of longitudinally extensive myelitis on magnetic resonance imaging have further refined the diagnostic criteria for this disorder (Lennon et al., 2004; Wingerchuk, 2006).

Interestingly, NMO shares overlapping clinical features with the more complicated DOA+ variants caused by some pathogenic *OPA1* mutations (**Section 1.10.2**). These observations therefore suggest that some patients diagnosed as having NMO could in fact be harbouring pathogenic *OPA1* mutations, or that the expression of NMO could be influenced by specific *OPA1* single nucleotide polymorphisms (SNPs). The aim of this study was to investigate the role of *OPA1* genetic variants in a cohort of patients with a clinical diagnosis of NMO, supported by consistent magnetic resonance imaging findings and/or positivity for anti-AQP4 antibodies (Wingerchuk, 2006).

6.2 Materials and Methods

6.2.1 Patient Cohort

Genomic DNA samples, extracted from whole blood, were available for the following groups of white British individuals: (i) patients with NMO (N = 32), diagnosed as a part of a British Neurological Surveillance Unit (BNSU) national case ascertainment study. All these patients fulfilled the revised diagnostic criteria for NMO, with clinically and radiologically-confirmed episodes of optic neuritis and transverse myelitis (Wingerchuk, 2006). The clinical characteristics of these patients have been described previously (Hudson et al., 2008b). NMO anti-AQP4 antibodies were detected in 12 of these patients; (ii) patients with primary open angle glaucoma

(POAG; N = 137; mean (SD) age = 71.6 (8.0) years), diagnosed with either the high tension (HTG; N = 67) or normal tension (NTG; N = 70) form of the disease (Yu-Wai-Man et al., 2010d); and (iii) healthy controls (N = 75; mean (SD) age = 79.3 (4.4) years) with no evidence of ophthalmological or neuromuscular disorders. This study had the relevant institutional approval and written informed consent was obtained from all of the subjects involved.

6.2.2 *OPA1* Sequencing

All 30 coding exons and adjacent intronic regions of *OPA1* were amplified by PCR using a set of 27 M13-tagged primer pairs (**Table 3-1**). Sanger sequencing was carried out as described previously (**Section 3.6**). The sequencing results were compared with GenBank *OPA1* reference sequence (accession number NG_011605.1, mRNA transcript variant 1, NM_015560.2), and all identified genetic variants were confirmed by reverse sequencing to exclude PCR and sequencing errors. The significance of the *OPA1* variants found in the NMO cohort was determined by searching online *OPA1* databases: *eOPA1* (http://lbbma.univ-angers.fr/) and NCBI, as well as recent DOA case series reporting novel pathogenic mutations (Yu-Wai-Man et al., 2010a). Bioinformatic analysis and the functional consequence of intronic *OPA1* nucleotide changes were determined using the Fruitfly BDGP predictor software (http://www.fruitfly.org/seq_tools/ splice.html and http://www.fruitfly.org/seq_tools/promoter.html) (Yu-Wai-Man et al., 2010a). The control and glaucoma *OPA1* SNP data used for comparative purposes in this study have been previously published (Yu-Wai-Man et al., 2010d).

6.2.3 Statistical Analysis

The Hardy-Weinberg equilibrium for *OPA1* genotypes was assessed for patient and control groups using the on-line calculator: http://ihg.gsf.de/cgi-bin/hw/hwa1.pl. Allele and genotype SNP frequencies were compared with χ^2 analysis using GraphPad^{TM} v.4 statistical software (GraphPad Software).

6.3 Results

6.3.1 *OPA1* Genotyping

No pathogenic *OPA1* mutations were identified in the NMO cohort. A total of 13 *OPA1* variants were identified. Nine of these had previously been reported as SNPs, whereas the remaining four *OPA1* variants were novel heterozygous changes found in four different patients with NMO (**Table 6-1**). The novel exon 11 (c.1071A>G, p.A357A) and exon 22 (c.2256G>T, p.L752L) variants were synonymous. The two novel intronic variants were not predicted to affect the neighbouring splice donor sites.

6.3.2 *OPA1* SNP Associations

The *OPA1* SNP frequency in the NMO cohort was compared with the following groups: (i) healthy controls, (ii) patients with POAG, and (iii) high tension (HTG) and normal tension (NTG) glaucoma subgroups. No significant allele or genotype associations were detected with the following three *OPA1* SNPs: IVS8+4C>T, IVS8+32T>C and c.473A>G (**Table 6-2**, **Table 6-3**, and **Table 6-4**). Analysis of both the IVS8+4C>T and IVS8+32T>C *OPA1* SNPs did not reveal a significantly increased risk of developing NMO with specific compound genotypes (**Table 6-5**). There was no significant allele or genotype associations for the remaining nine SNPs identified in patients with NMO compared with healthy controls.

Table 6-1 *OPA1* variants identified in the neuromyelitis optica (NMO) cohort. A total of 13 *OPA1* variants were detected. These changes were confirmed by reverse sequencing and then checked against publicly-available databases to determine whether they had previously been reported: (i) the e*OPA1* Database; (ii) the NCBI dbSNP Database; and (iii) the Human Genome Mutation Database.

cDNA	Location	AA change	N =	Homozygous	Heterozygous
c.473A>G	Exon 4	p. N158S	25/32	15/25 (60%)	10/25 (40%)
c.557-19T>C	Intron 4	-	17/32	7/17 (41%)	10/17 (59%)
IVS8+4C>T	Intron 8	-	9/32	2/9 (22%)	7/9 (78%)
IVS8+32T>C	Intron 8	-	17/32	7/17 (41%)	10/17 (59%)
c.1071A>G*	Exon 11	p. A357A	1/32	0/1 (0%)	1/1 (100%)
c.1312+32A>G	Intron 13	-	1/32	0/1 (0%)	1/1 (100%)
c.1589+22T>G*	Intron 16	-	1/32	0/1 (0%)	1/1 (100%)
c.1770+16T>G	Intron 18	-	6/32	0/6 (0%)	6/6 (100%)
c.1770+47T>A*	Intron 18	-	1/32	0/1 (0%)	1/1 (100%)
c.1770+51T>G	Intron 18	-	17/32	7/17 (41%)	10/17 (59%)
c.2109C>T	Exon 21	p.A703A	25/32	15/25 (60%)	10/25 (40%)
c.2256G>T*	Exon 22	p. L752L	1/32	0/1 (0%)	1/1 (100%)
c.2707+25T>A	Intron 26	-	17/32	7/17 (41%)	10/17 (59%)

* = novel *OPA1* variant, AA = amino acid; cDNA = complementary DNA; N = number of NMO patients harbouring the *OPA1* variant.

Table 6-2 Allele and genotype frequencies for the IVS8+4C>T *OPA1* SNP. Both patient and control groups were in Hardy-Weinberg equilibrium at IVS8+4C>T.

	NMO (N = 32)	**Healthy Controls (N = 75)**		**POAG (N = 137)**		**HTG Subgroup (N = 67)**		**NTG Subgroup (N = 70)**	
Allele			**P value**		**P value**		**P value**		**P value**
C	53 (83.0%)	131 (87.3%)		222 (81.0%)		114 (85.1%)		108 (77.1%)	
T	11 (17.0%)	19 (12.7%)	0.395	52 (19.0%)	0.859	20 (14.9%)	0.681	32 (22.9%)	0.460
Genotype			**P value***		**P value***		**P value***		**P value***
CC	23 (72.0%)	59 (78.7%)		90 (65.7%)		49 (73.1%)		41 (58.6%)	
CT	7 (22.0%)	13 (17.3%)		42 (30.7%)		16 (23.9%)		26 (37.1%)	
TT	2 (6.0%)	3 (4.0%)	0.626	5 (3.6%)	0.532	2 (3.0%)	0.614	3 (4.3%)	0.305

* = χ^2 analysis of all three possible genotypes at IVS8+4C>T; HTG = high tension glaucoma; NMO = neuromyelitis optica; NTG = normal tension glaucoma; POAG = primary open angle glaucoma.

Table 6-3 Allele and genotype frequencies for the IVS8+32T>C *OPA1* SNP. Both patient and control groups were in Hardy-Weinberg equilibrium at IVS8+32T>C.

	NMO (N = 32)	**Healthy Controls (N = 75)**		**POAG (N = 137)**		**HTG Subgroup (N = 67)**		**NTG Subgroup (N = 70)**	
Allele			**P value**		**P value**		**P value**		**P value**
T	40 (62.5%)	79 (52.7%)		155 (56.6%)		74 (55.2%)		81 (57.9%)	
C	24 (37.5%)	71 (47.3%)	0.229	119 (43.4%)	0.403	60 (44.8%)	0.359	59 (42.1%)	0.544
Genotype			**P value***		**P value***		**P value***		**P value***
TT	15 (46.9%)	21 (28.0%)		41 (29.9%)		19 (28.4%)		22 (31.4%)	
CT	10 (31.2%)	37 (49.3%)		73 (53.3%)		36 (53.7%)		37 (52.9%)	
CC	7 (21.9%)	17 (22.7%)	0.132	23 (16.8%)	0.075	12 (17.9%)	0.096	11 (15.7%)	0.126

* = χ^2 analysis of all three possible genotypes at IVS8+32T>C; HTG = high tension glaucoma; NMO = neuromyelitis optica; NTG = normal tension glaucoma; POAG = primary open angle glaucoma.

Table 6-4 Allele and genotype frequencies for the c.473A>G *OPA1* SNP. Both patient and control groups were in Hardy-Weinberg equilibrium at c.473A>G.

	NMO (N = 32)	**Healthy Controls (N = 75)**		**POAG (N = 137)**		**HTG Subgroup (N = 67)**		**NTG Subgroup (N = 70)**	
Allele			**P value**		**P value**		**P value**		**P value**
A	24 (37.5%)	75 (50.0%)		128 (46.7%)		65 (48.5%)		63 (45.0%)	
G	40 (62.5%)	75 (50.0%)	0.102	146 (53.3%)	0.380	69 (51.5%)	0.313	77 (55.0%)	0.617
Genotype			**P value***		**P value***		**P value***		**P value***
AA	7 (21.9%)	19 (25.3%)		26 (19.0%)		13 (19.4%)		13 (18.6%)	
AG	10 (31.2%)	37 (49.4%)		76 (55.5%)		39 (58.2%)		37 (52.9%)	
GG	15 (46.9%)	19 (25.3%)	0.080	35 (25.5%)	0.614	15 (22.4%)	0.471	20 (28.5%)	0.840

* = χ^2 analysis of all three possible genotypes at c.473A>G; HTG = high tension glaucoma; NMO = neuromyelitis optica; NTG = normal tension glaucoma; POAG = primary open angle glaucoma.

Table 6-5 Compound genotype frequencies for the IVS8+4C>T and IVS8+32T>C *OPA1* SNPs.

IVS8+4	IVS8+32	NMO	Healthy Controls	P value	Odds ratio	95% CI
TT	TT	2 (6.3%)	3 (4.0%)	0.634	1.600	0.254 - 10.067
CT	TT	5 (15.6%)	2 (2.7%)	0.024*	6.759	1.237 - 36.935
CC	TT	8 (25.0%)	16 (21.3%)	0.801	1.229	0.465 - 3.250
TT	TC	0 (0.0%)	0 (0.0%)	N/A	N/A	N/A
CT	TC	2 (6.3%)	11 (14.7%)	0.336	0.388	0.081 - 1.860
CC	TC	8 (25%)	26 (34.7%)	0.372	0.628	0.248 - 1.594
TT	CC	0 (0.0%)	0 (0.0%)	N/A	N/A	N/A
CT	CC	0 (0.0%)	0 (0.0%)	N/A	N/A	N/A
CC	CC	7 (21.9%)	17 (22.7%)	1.000	0.955	0.352 - 2.590

* = non-significant with Bonferroni correction: $P < 0.008$; N/A = not applicable; CI – confidence interval.

6.4 Discussion

No pathogenic *OPA1* mutations were identified in this well-characterised group of patients with NMO. Although the possibility of large-scale *OPA1* genomic rearrangements cannot be excluded, these are rare in DOA, accounting for less than 1% of singleton cases with suspected inherited optic atrophy (Yu-Wai-Man et al., 2011b). Importantly, *OPA1* mutations have only been reported within the first ten intronic nucleotide positions, making it highly unlikely that the PCR-based sequencing strategy used in this study has missed functional intronic variants influencing mRNA splicing or transcriptional activity (Yu-Wai-Man et al., 2011b). Only one non-synonymous *OPA1* SNP (c.473A>G, p.N158S) was present in patients with NMO, but it is an evolutionarily poorly-conserved amino acid residue. No significant allele and genotype associations were found for c.473A>G and the remaining SNPs identified in the NMO cohort when compared with both healthy controls and patients with POAG. These findings contrast with the recent

observations in POAG, where specific *OPA1* variants at IVS8+4C>T and IVS8+32T>C, have been linked with an increased risk of developing NTG, suggesting a role for *OPA1* in glaucomatous optic nerve degeneration (Aung et al., 2002; Yu-Wai-Man et al., 2010d). NMO is a relatively rare disorder with an estimated prevalence of 0.5 to 1.0 per 100,000 among the white population (Jacob et al., 2009). Although it is possible that a study of 32 patients with NMO might not have been sufficiently powered to detect a small effect, the results of this study suggest that *OPA1* is not a major susceptibility gene in the pathophysiology of this demyelinating CNS disease.

The data presented in this chapter has been published following peer review:

Sitarz K.S., Yu-Wai-Man P., Hudson G., Jacob A., Boggild M., Horvath R., Chinnery P.F., 2011. Genetic variations within the OPA1 gene are not associated with neuromyelitis optica. Multiple Sclerosis. 18(2): 240-243.

Chapter 7 MtDNA Repopulation Assay and Mitochondrial Network Analysis

Table of Contents

7.1 Introduction

OPA1 plays an important role in mtDNA maintenance, with some pathogenic *OPA1* mutations leading to the accumulation of multiple mtDNA deletions (Amati-Bonneau et al., 2008; Hudson et al., 2008a). As shown recently by *Elachouri and colleagues*, the *OPA1*-exon 4b isoform generates a specific 10-kDa N-terminus OPA1 peptide, which contains a domain corresponding to exon 4b (NT-OPA1-exon 4b) (Elachouri et al., 2011). This specific peptide fragment is thought to directly interact with nucleoids, which are located within the mitochondrial matrix compartment, by binding these nucleoids to the IMM, thereby enabling their proper distribution within the mitochondrial network and promoting mtDNA replication (Elachouri et al., 2011). C-terminally truncated *OPA1* alleles result in haploinsufficiency, with a 50% reduction in the protein level, whereas missense mutations affecting the GTPase region are more likely to produce a dysfunctional protein with a dominant-negative effect (Marchbank et al., 2002; Olichon et al., 2007; Amati-Bonneau et al., 2008; Hudson et al., 2008a). In both situations, a disturbance in cristae morphology could disrupt the anchoring of mtDNA molecules to the IMM, with an adverse effect on mitochondrial genome replication (Landes et al., 2010). *OPA1* mutations involving the GTPase domain could also affect the dGTP nucleotide pool, disturbing the delicate balance of nucleotides within the matrix compartment and thus having a detrimental effect on the faithful replication of the mitochondrial genome (Amati-Bonneau et al., 2008). Furthermore, by impairing mitochondrial fusion and the exchange of mitochondrial contents some *OPA1* mutations could prevent defective nucleoids from being repaired or complemented, further contributing to mtDNA instability (Landes et al., 2010).

Both dominant and recessive *POLG1* mutations have been shown to decrease POLG activity resulting in impaired mtDNA replication (Graziewicz et al., 2006). The consequences of pathogenic *POLG1* mutations on mitochondrial genome integrity can be both quantitative (mtDNA depletion) as well as qualitative (mtDNA point mutations and deletions) (Chan and Copeland, 2009). In a recent study by *Stewart and colleagues* a significant decrease in mtDNA repopulation rates was observed in *POLG1*-mutant fibroblasts following ethidium bromide (EtBr)-induced mtDNA depletion (Stewart et al., 2011).

The aims for this study were: (i) to determine the efficiency of mtDNA replication using the same repopulation assay described by *Stewart and colleagues* (Stewart et al., 2011), and (ii) to document the changes in mitochondrial network morphology following EtBr-induced mtDNA depletion and the subsequent mtDNA repopulation phase in fibroblast cell lines harbouring pathogenic *OPA1* or *POLG1* mutations. EtBr is a drug that inhibits mitochondrial transcription and replication in proliferating cells, but it has no effect on nuclear DNA (Leibowitz, 1971; Seidel-Rogol and Shadel, 2002). EtBr prevents [^{3}H]-thymidine incorporation into mtDNA, but not nDNA, and it ultimately leads to the physical breakdown of circular mtDNA molecules (Nass, 1970; Desjardins et al., 1985). Crucially, the effect of EtBr is reversible, so when the drug is removed from the culture medium, cells are able to repopulate their mtDNA population (King and Attardi, 1989). The principle underpinning this assay has previously been used to investigate the mechanisms controlling mtDNA copy number in human osteosarcoma 143B and HeLa cells (Moraes et al., 1999; Seidel-Rogol and Shadel, 2002). A similar experimental protocol has also been used to demonstrate the faster repopulation of smaller deleted mtDNA genomes compared with wild-type mtDNA molecules (Diaz et al., 2002).

A comprehensive quantitative analysis of the mitochondrial network was performed on all investigated cell lines prior to EtBr treatment, at the end of induced mtDNA depletion period, and at the end of subsequent mtDNA repopulation phase. The extent of mitochondrial network fragmentation can vary widely depending on the functional effect of the specific pathogenic *OPA1* mutation (Olichon et al., 2007). A highly fragmented mitochondrial network morphology has previously been observed in fibroblasts from patients harbouring mutations affecting the functional GTPase domain, but not in those harbouring truncated *OPA1* alleles that lead to haploinsufficiency (Olichon et al., 2007; Chevrollier et al., 2012). This pathological mitochondrial network fragmentation has also been documented in *OPA1*-mutant human fibroblasts in response to glycolysis shortage (following culture in glucose-free media) or exogenous oxidative stress (Agier et al., 2012). The aim of this study was therefore to investigate further the pathological consequences of mtDNA depletion on the mitochondrial network in patient-derived fibroblasts harbouring *OPA1* or *POLG1* mutations. The kinetics of mtDNA recovery following EtBr-induced depletion will also provide additional insight into the complexity between

mitochondrial structure-function relationship and how this becomes disrupted by mutations involving OPA1 and POLG proteins, which are intricately involved in mtDNA maintenance.

7.2 Materials and Methods

7.2.1 Cell Lines

Fibroblasts from 17 individuals were selected for this study: (i) eight DOA patients harbouring confirmed *OPA1* mutations (OPA1a – OPA1h; **Table 7-1**); (ii) five patients with confirmed *POLG1* mutations (POLG1a – POLG1e; **Table 7-2**); and (iii) four normal healthy controls with no evidence or family history of neuromuscular disorders (C1 – C4) (**Table 7-2**). The clinical characteristics of the patients included in this study have been detailed further in **Table 7-1** and **Table 7-2**.

Three *OPA1* fibroblast cell lines were derived from affected family members carrying the same *OPA1* nonsense mutation (c.889C>T; p.Q297X) in exon 9. Despite the fact that they harboured the same pathogenic mutation, the mother (OPA1a), the son (OPA1b) and the daughter (OPA1c) had marked differences in disease severity (**Table 7-1**). The OPA1d and OPA1g cell lines were derived from an affected mother (OPA1g) and her affected son (OPA1d), both of them harbouring the same c.1294A>G (p.I432V) missense *OPA1* mutation in exon 13. The OPA1g female patient, who is in her seventies, is clinically asymptomatic, but she had subtle evidence of optic atrophy on optical coherence tomography retinal imaging. The OPA1d male individual suffered from a severe DOA+ phenotype. The two male *OPA1* carriers (OPA1e and OPA1f) were from the same extended pedigree segregating the c.876-878del(TGT) deletion in exon 9, which causes a frameshift at codon 294 and leads to premature protein termination at codon 960 (p.V294fsX667). The OPA1h fibroblasts were derived from a male patient with a c.1516+1G>T splice site mutation.

Three *POLG1*-mutantcell lines (POLG1a, POLG1b and POLG1e) were derived from unrelated patients with Alpers-Huttenlocher syndrome (AHS) secondary to compound heterozygous *POLG1* mutations: (i) POLG1a: c.2243G>C (p.W748S) and

deletion c.3600delT; (ii) POLG1b: c.1399G>A (p.A467T) and c.3311C>T (p.S1104F); (iii) POLG1e: c.2209 G>C (p.G737R) and c.2300 C>A (p.A767N). Alpers-Huttenlocher syndrome is an early-onset, progressive neurodegenerative disorder characterised by intractable epilepsy, developmental delay, and with a subgroup of patients developing limb spasticity, dementia, and liver failure. The remaining two *POLG1*-mutant fibroblast cell lines came from unrelated individuals with mitochondrial recessive ataxia syndrome (MIRAS) secondary to (i) compound heterozygous c.1399 G>A (p.A467T) and c.2243G>C (p.W748S) *POLG1* mutations (POLG1c), and (ii) homozygous c.2243G>C (p.W748S) *POLG1* mutation (POLG1d).

This study had the relevant institutional approval and written informed consent was obtained from all of the subjects involved.

Table 7-1 Clinical phenotype and mutational spectrum of investigated *OPA1* cell lines.

Patient	Age (yrs)	Sex	cDNA	Consequence	Protein Domain Affected	Detailed Clinical Phenotype						
						OA	Deafness	Ataxia	Myopathy	Neuropathy	PEO	Others
OPA1a	50	F	c.889C>T	p.Q297X	-	+	-	-	-	+	-	HSP
OPA1b	23	M	c.889C>T	p.Q297X	-	+	-	-	-	-	-	HSP
OPA1c	28	F	c.889C>T	p.Q297X	-	+	-	-	-	-	-	-
OPA1d	44	M	c.1294A>G	p.I432V	GTPase	+	-	+	+	+	+	-
OPA1e	62	M	c.876–878del(TGT)	p.V294fsX667	-	+	-	-	-	+	-	HSP
OPA1f	43	M	c.876–878del(TGT)	p.V294fsX667	-	+	-	-	-	-	-	-
OPA1g	72	F	c.1294A>G	p.I432V	GTPase	+	-	-	-	-	-	-
OPA1h	39	M	c.1516+1G>T	Splicing defect	-	+	-	-	-	-	-	-

F – female; HSP – hereditary spastic paraplegia; M – male; OA – optic atrophy; PEO – progressive external ophthalmoplegia.

Table 7-2 Properties of investigated cell lines derived from *POLG1*-positive patients and healthy control individuals.

Patient	Age (yrs)	Sex	cDNA	Consequence	Protein Domain Affected	Detailed Clinical Phenotype						
						OA	Epilepsy	Ataxia	Myopathy	Neuropathy	PEO	Others
POLG1a	3	F	c.2243G>C; c.3600delT	p.W748S; c.3600delT	LR; PD	-	+	-	+	N/A	-	AHS
POLG1b	5	M	c.1399G>A; c.3311C>T	p.A467T; p.S1104F	LR; PD	-	+	+	+	N/A	-	AHS
POLG1c	39	M	c.1399 G>A; c.2243G>C	p.A467T; p. W748S	LR	-	-	+	-	+	+	MIRAS
POLG1d	36	M	c.2243G>C; c.2243G>C	p. W748S; p. W748S	LR	-	-	+	-	+	+	MIRAS
POLG1e	1	M	c.2209 G>C; c.2300 C>A	p.G737R; p.A767N	LR	-	+	-	+	N/A	-	AHS
C1	57	F	-	-	-	-	-	-	-	-	-	-
C2	0	M	-	-	-	-	-	-	-	-	-	-
C3	30	F	-	-	-	-	-	-	-	-	-	-
C4	49	M	-	-	-	-	-	-	-	-	-	-

AHS – Alpers-Huttenlocher syndrome; F – female; LR – Linker region; M – male; MIRAS - Mitochondrial recessive ataxia syndrome; PD – Polymerase domain; PEO – progressive external ophthalmoplegia; OA – optic atrophy; N/A – data not available.

7.2.2 Tissue Culture

Fibroblast cell lines were cultured according to the protocol described in **Section 3.12.1**. Cells were maintained at 50-90% confluency with the excess fresh media allowing exponential growth. Culture media were supplemented with uridine to account for the active dihydroorotate hydrogenase loss occurring in the mitochondria lacking mtDNA (Morais et al., 1980; Gregoire et al., 1984). Sodium pyruvate was added as an additional carbon source for energy production. All investigated cell lines were found to be negative for mycoplasma infections when checked using a PCR-based Venor®GeM Mycoplasma Detection Kit (Cambio) (**Section 3.12.2**).

7.2.2.1 Ethidium Bromide Treatment

Ethidium bromide (Sigma-Aldrich) at a concentration of 50ng/ml was added to the fibroblast media to induce mtDNA depletion (Diaz et al., 2002). Cells were grown in EtBr supplemented media for 15 days. Following this period, cells were cultured in normal media for 33 days (**Figure 7-1**). Rates of mtDNA depletion and repopulation were determined by harvesting cells and estimating their mtDNA copy number at days: 0, 6, 12, 18, 24, 30, 36, 42 and 48.

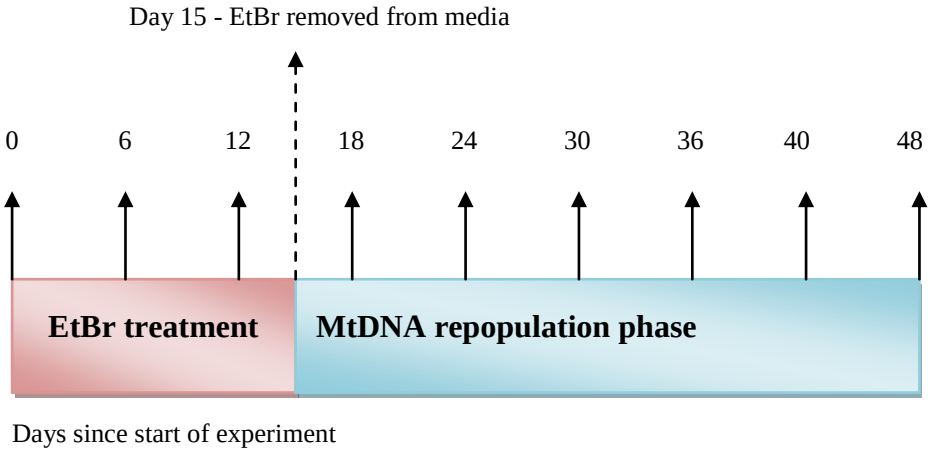

Figure 7-1 Repopulation assay - experimental outline.

For each cell line, EtBr-treated cells were cultured in parallel with untreated controls, in order to correct for normal mtDNA copy number fluctuations. The treated and untreated arms were grown in 6-well plates (Greiner) - 3 wells containing normal media, and 3 wells with EtBr supplemented media (**Figure 7-2**). At each harvesting point, cells were pelleted separately from each well, to allow for independent replicate measurements. For each investigated cell line, mtDNA copy number was determined for two pellets from the EtBr-treated cells, and two pellets from the untreated cells.

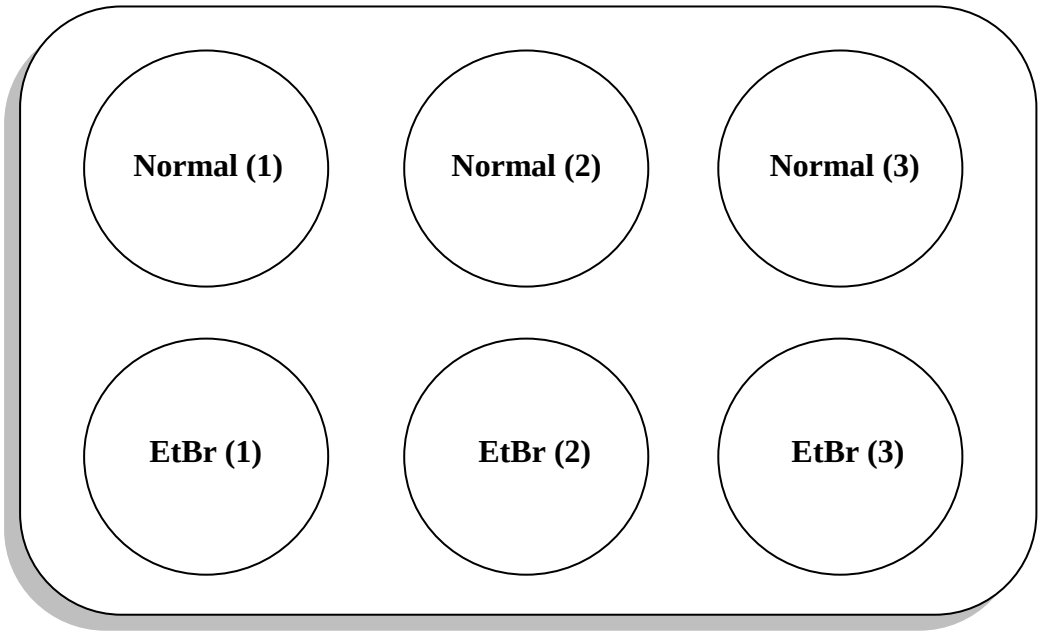

Figure 7-2 Experimental 6-well plate with untreated (Normal) and ethidium bromide treated (EtBr) wells for each fibroblast line.

7.2.3 DNA Extraction from Cell Pellets

For DNA isolation, cells instead of being reseeded, were pipetted into 2ml tubes (Eppendorf) and centrifuged at 12,000 rpm for 3 minutes. Following this, the supernatant was discarded and the obtained pellets were resuspended in PBS (Oxoid), before being centrifuged again at 12,000 rpm for 3 minutes. Finally, PBS (Oxoid) was removed and the pellets stored at -20°C for the future use. DNA from cultured cells was extracted using DNeasy® Blood & Tissue Kit (Qiagen), as described in **Section 3.1.1**.

7.2.4 Quantification of MtDNA Copy Number

The mtDNA copy number was quantified using qPCR-based (*MTND1*/*B2M*) assay, as described in **Section 3.8.1**. The principle of this method is based on the comparison between the relative levels of the mitochondrial *ND1* gene and the nuclear housekeeping *B2M* gene, thereby allowing the cellular mtDNA content to be determined.

7.2.5 MtDNA Repopulation Level Calculation

Repopulation level (RL) at each analysis point was calculated as the ratio between mtDNA copy number for treated ($CN_{treated}$) and untreated ($CN_{untreated}$) cells:

$$RL = \frac{CN_{treated}}{CN_{untreated}}$$

Relative mtDNA copy numbers were determined for two independent pellets from the treated group, and two independent pellets from the untreated group. The final repopulation level (RL_{TOT}) was therefore calculated as the average of four different RL values. To allow for an accurate comparison among various cell lines, the change in mtDNA copy number was determined in relation to the initial mtDNA copy number at day 0.

7.2.6 Mitochondrial Network Analysis

In order to investigate and quantify the mitochondrial network morphology, fibroblasts were seeded at a density of 20,000 cells/well in 12-well plates (Greiner) containing sterilized round 16 mm coverslips (VWR). The cells were allowed to attach during an incubation period of 24-48 hours at 37°C and 5% CO_2 in standard culture medium (as described in **Section 3.12.1**). The medium was then aspirated, after which the cells were washed twice with PBS (Oxoid) before the addition of a staining mix (1ml/well) containing (i) Hank's Balanced Salt Solution (HBSS) buffered with Ca^{2+} and Mg^{2+} (Gibco, Life Technologies), (ii) 100nM MitoTracker® Green (Molecular Probes, Life Technologies), and (iii) 1µg/ml Hoechst 33342

(Molecular Probes, Life Technologies). The cells were incubated in this staining mixture for 30 minutes at 37°C and 5% CO_2 to allow incorporation of the dyes. Following this step, the cells were washed three times in PBS (Oxoid) and then placed in standard culture medium (refer to **Section 3.12.1**) before being visualized with a microscope.

Prior to imaging, each coverslip with the cells attached was removed from a well using sterile tweezers and inverted onto a drop (5µl) of PBS (Oxoid), previously pipetted on a glass slide (Thermo Scientific). Excess PBS was removed, then images of the mitochondrial network and nucleus were captured with an upright epifluorescent widefield Axio Imager.Z1 microscope (Carl Zeiss) equipped with an oil-immersion objective (x63 / N.A.=1.4; Plan APOCHROMAT, Carl Zeiss) and AxioCam HRm digital camera (Carl Zeiss), using AxioVision 4.6 software (Carl Zeiss). The mitochondrial network staining (MitoTracker® Green; Molecular Probes, Life Technologies) was visualized using the green (GFP) channel. The nuclear staining (Hoechst 33342; Molecular Probes, Life Technologies) was detected with the blue (DAPI) channel (**Figure 7-3**). For each individual cell, images were captured as a series of Z-stacks with 20 slices, each 0.2µm apart.

Following acquisition, images were deconvolved with Volocity Software™ (PerkinElmer, Seer Green, UK) (**Figure 7-4**) using a theoretically calculated point spread function (PSF) for each of the dyes. All selected images were iteratively deconvolved until the level of confidence reached 99% or the number of iterations scored 50. The deconvolved images were used for quantitative mitochondrial network analysis using Huygens Essential Software™ (Scientific Volume Imaging, Hilversum, The Netherlands) (**Figure 7-5**) with the following standardised set of parameters: threshold = 10%; seed = 0% and garbage = 30. The quantitative data were further analysed in Excel (Microsoft, Reading, UK) and GraphPad™ v.5 statistical software (GraphPad Software).

Imaging and subsequent mitochondrial network analyses were performed for each individual fibroblast cell line at three time points: (i) at baseline before EtBr addition (day 0); (ii) at the end of the induced period of mtDNA depletion (day 15); and (iii) following a phase of culture in EtBr-free normal medium (day 45). At each sampling point, a minimum of 12 images per cell line were acquired. Following image

deconvolution, mitochondrial network length was quantified for 10 randomly-selected individual cells per each studied fibroblast cell line. The data obtained were used to calculate: (i) the total length of the mitochondrial network per cell (abbreviated as the total length); (ii) the average mitochondrial fragment length (abbreviated as the average length); and (iii) the total number of individual mitochondrial fragments per cell (abbreviated as the number of fragments). The nuclear stain was used as a marker, to only select non-dividing cells for analysis.

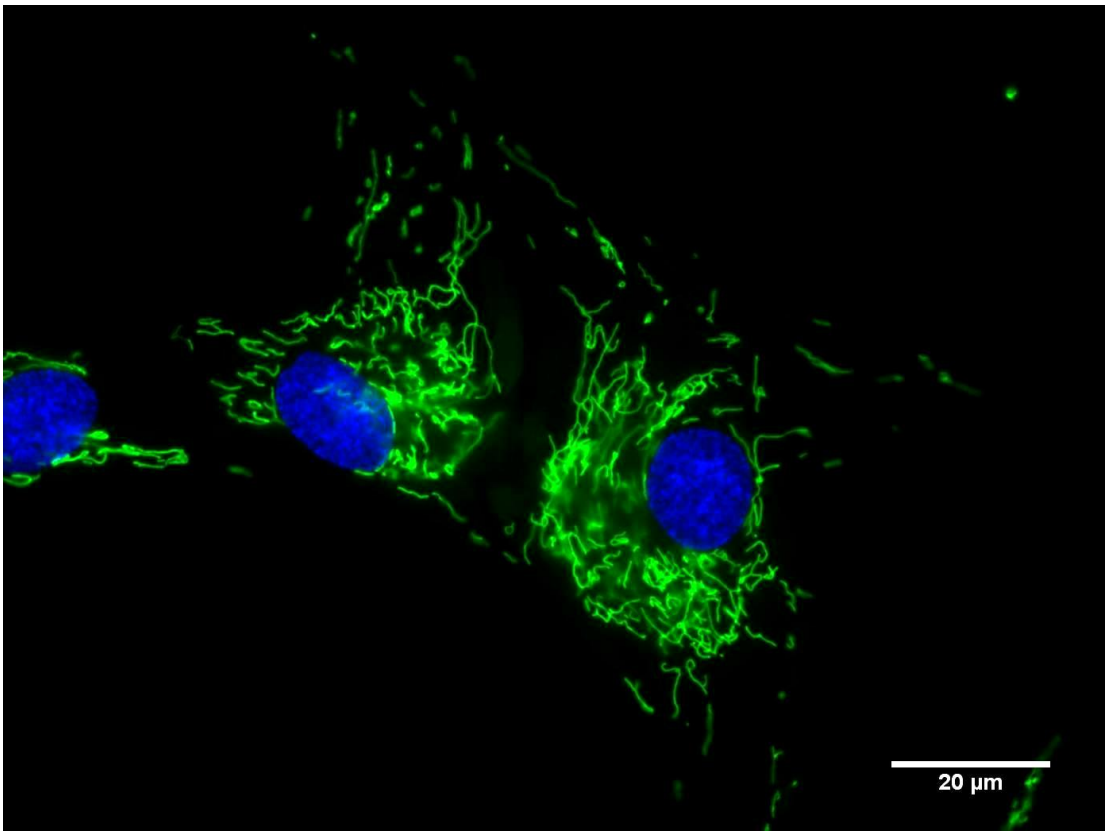

Figure 7-3 Mitochondrial network morphology in control fibroblasts prior to image deconvolution. Staining was performed using MitoTracker™ Green (Molecular Probes, Life Technologies) to delineate the mitochondrial network. The Hoechst 33342 (Molecular Probes, Life Technologies) stain was used to visualise the nucleus.

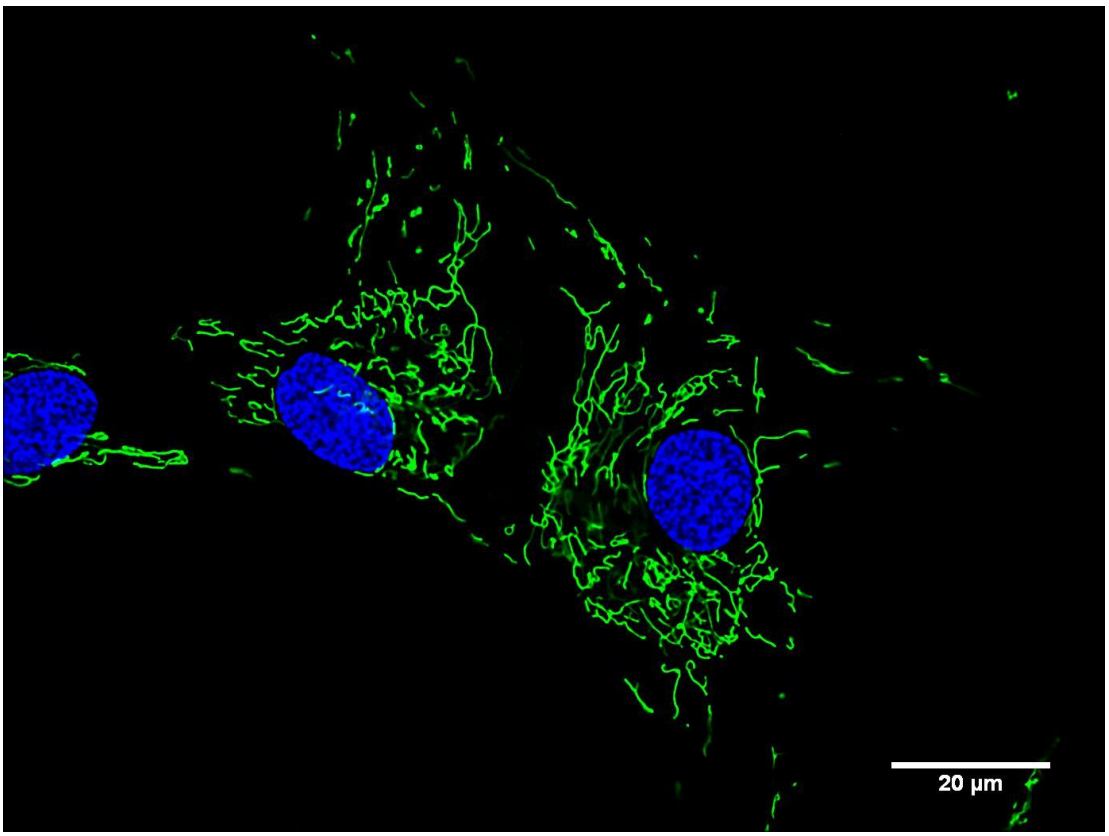

Figure 7-4 Mitochondrial network morphology in control fibroblasts following image deconvolution with Volocity Software™ (PerkinElmer). Staining was performed using MitoTracker™ Green (Molecular Probes, Life Technologies) to define the mitochondrial network. The Hoechst 33342 (Molecular Probes, Life Technologies) stain was used to visualise the nucleus.

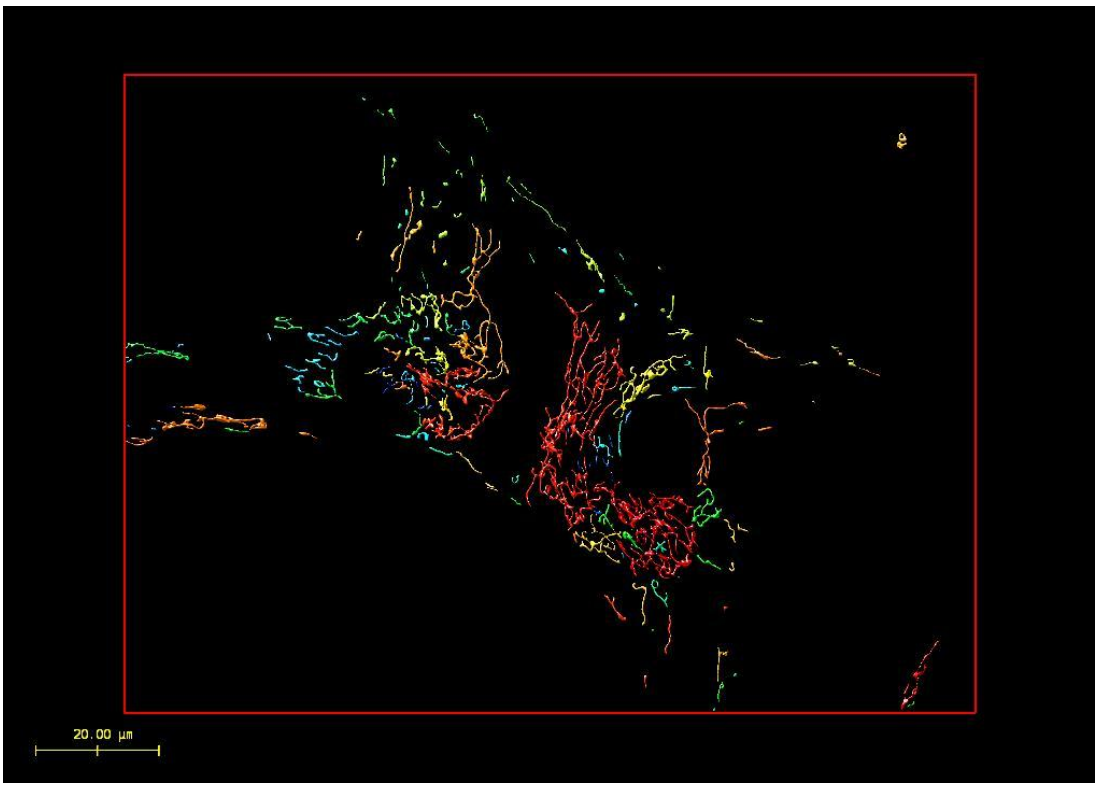

Figure 7-5 Mitochondrial network morphology in control fibroblasts analysed with Huygens Essential Software™ (Scientific Volume Imaging).

7.2.7 Statistical Analysis

Group comparisons were carried out with an unpaired two-tailed Student's t-test using GraphPad™ v.5 statistical software (GraphPad Software).

7.3 Results: Repopulation Assay

Significant EtBr-induced mtDNA depletion was observed within the fibroblasts. However, no visible cell loss was detected during the EtBr-induced mtDNA depletion phase (day 0 to day 15), which implies that the concentration of EtBr was not terminally toxic to the cells. To account for the normal biological fluctuations in mtDNA copy number, each cell line was also cultured in normal media, in the absence of EtBr treatment. For the variation in mtDNA copy number observed in untreated cell lines at each analysis time point from day 0 to day 48, please refer to **Appendix B.1**.

7.3.1 MtDNA Depletion and Repopulation – Control Cell Lines

The mtDNA depletion and repopulation curves for four control cell lines and their mean (abbreviated as the mean control) are presented in **Figure 7-6**. The depletion and subsequent repopulation curve for each individual control line was plotted from the repopulation levels (RL_{TOT}) calculated at each time point from four different RL values (N = 4). The curve for the mean control was constituted from the entire cohort of RL values obtained for all four control cell lines, except days 24 and 36, when data were available only for the three control lines.

Under EtBr culture conditions, significant mtDNA depletion was observed by day 12 in all control cell lines (C1: mean = 0.129, SEM = 0.004; C2: mean = 0.017, SEM = 0.001; C3: mean = 0.012, SEM = 0.0002; C4: mean = 0.037, SEM = 0.011). MtDNA repopulation was observed in three control lines (C1, C3 and C4) as from day 18, and in the C2 control line as from day 24. The mtDNA repopulation rate of the C3 line was significantly lower compared with the other controls until day 42 (mean = 0.535, SEM = 0.025). However, by day 48, all control fibroblast lines repopulated their mtDNA content to the levels observed in untreated cells (C1: mean = 0.949, SEM = 0.079; C2: mean = 1.177, SEM = 0.156; C3: mean = 1.149, SEM = 0.060; C4: mean = 0.944, SEM = 0.045). For subsequent comparisons in this chapter, the mean control will refer to the combined data set for these four control cell lines.

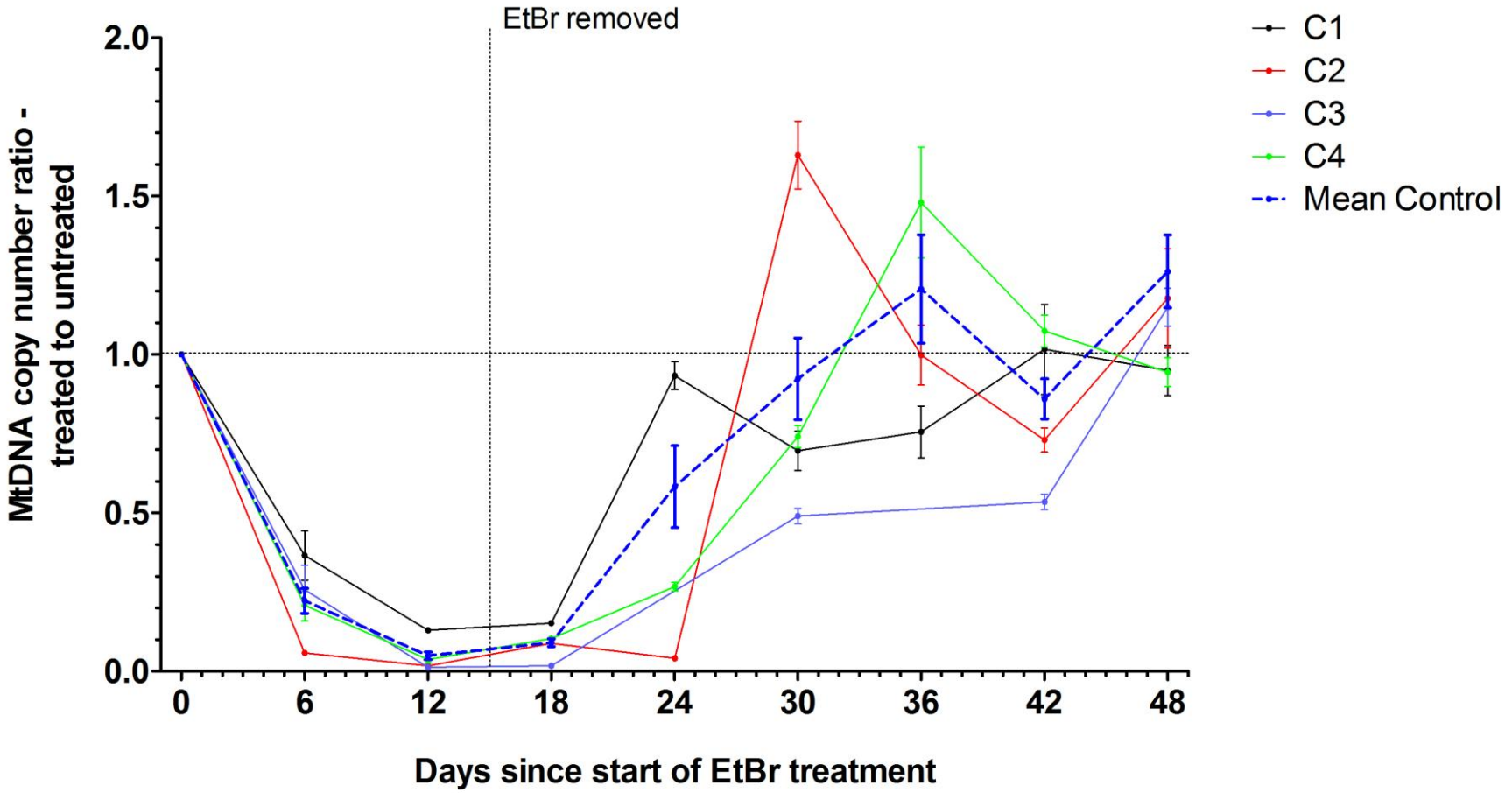

Figure 7-6 MtDNA depletion and repopulation curves of the four individual control lines and the mean control. Each data point represents the average mtDNA copy number ratio of EtBr-treated to untreated cells. The error bars are presented as the standard errors of the mean (SEM).

7.3.2 MtDNA Depletion and Repopulation – *POLG1* Lines

The mtDNA depletion and repopulation curves for the five *POLG1*-positive cell lines (**Figure 7-7**) and their mean (abbreviated as the mean POLG1; **Figure 7-8**) are described below. The curve for the mean POLG1 was constituted from the entire cohort of RL values obtained for all five *POLG1*-positive cell lines, except days 30 and 36 when data were available for four *POLG1* lines only, and days 42 and 48 when results were available for only three *POLG1* cell lines. This was due to the premature post-EtBr treatment death of the POLG1b and POLG1c fibroblast cell lines, despite maintaining optimal cell culture conditions in the repopulation phase and the confirmed absence of mycoplasma infection.

During the mtDNA depletion phase, a significant reduction in mtDNA content was observed in all *POLG1* cell lines by day 12 (**Figure 7-7**). During the repopulation phase, the *POLG1* fibroblast lines repopulated their mtDNA populations to no more than 0.046 (SEM = 0.002) i.e. 4.6% of the baseline values. There were significant differences between the mean POLG1 and the mean control during the whole course of the experimental study (**Figure 7-8**). For subsequent comparisons in this chapter, the mean POLG1 will refer to the combined data set for the five *POLG1* cell lines.

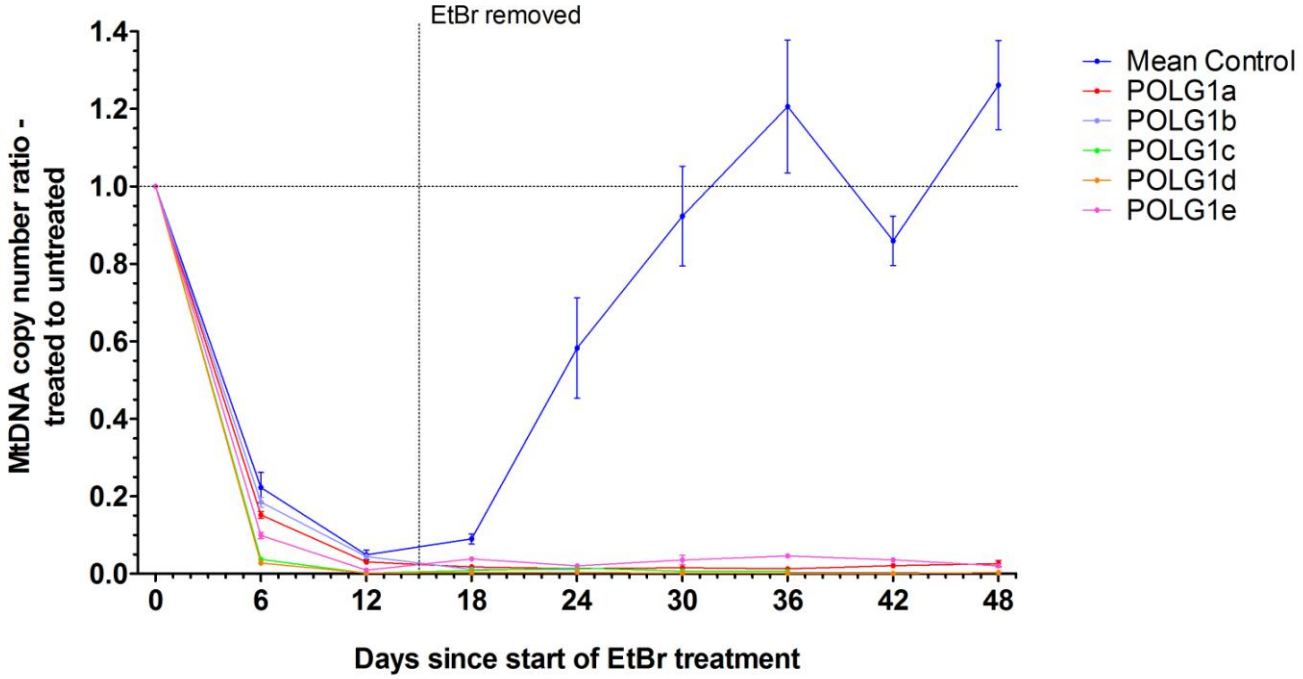

Mean Control vs.	**POLG1a**	0.3909	0.4872	0.0111	0.0226	0.0028	0.0015	**< 0.0001**	**< 0.0001**
	POLG1b	0.6445	0.8603	0.0065	0.0220	N/A	N/A	N/A	N/A
	POLG1c	0.0333	0.0801	0.0051	0.0229	0.0026	0.0014	N/A	N/A
	POLG1d	0.0260	0.0831	0.0033	0.0207	0.0025	0.0014	**< 0.0001**	**< 0.0001**
	POLG1e	0.1417	0.1417	0.0586	0.0242	0.0033	0.0019	**< 0.0001**	**< 0.0001**

Figure 7-7 MtDNA depletion and repopulation curves of the five individual *POLG1* lines. Each data point represents the average mtDNA copy number ratio of EtBr-treated to untreated cells. The error bars are presented as the standard errors of the mean (SEM). Table presents the P values of statistical comparisons made between different *POLG1*-mutant fibroblast lines and the mean control data set. Each column corresponds to the time point on the graph above. The intensity of the red shading correlates with the degree of statistical significance. N/A – data not available due to the death of EtBr-treated cells despite optimal cell culture conditions in the repopulation phase and the confirmed absence of mycoplasma infection.

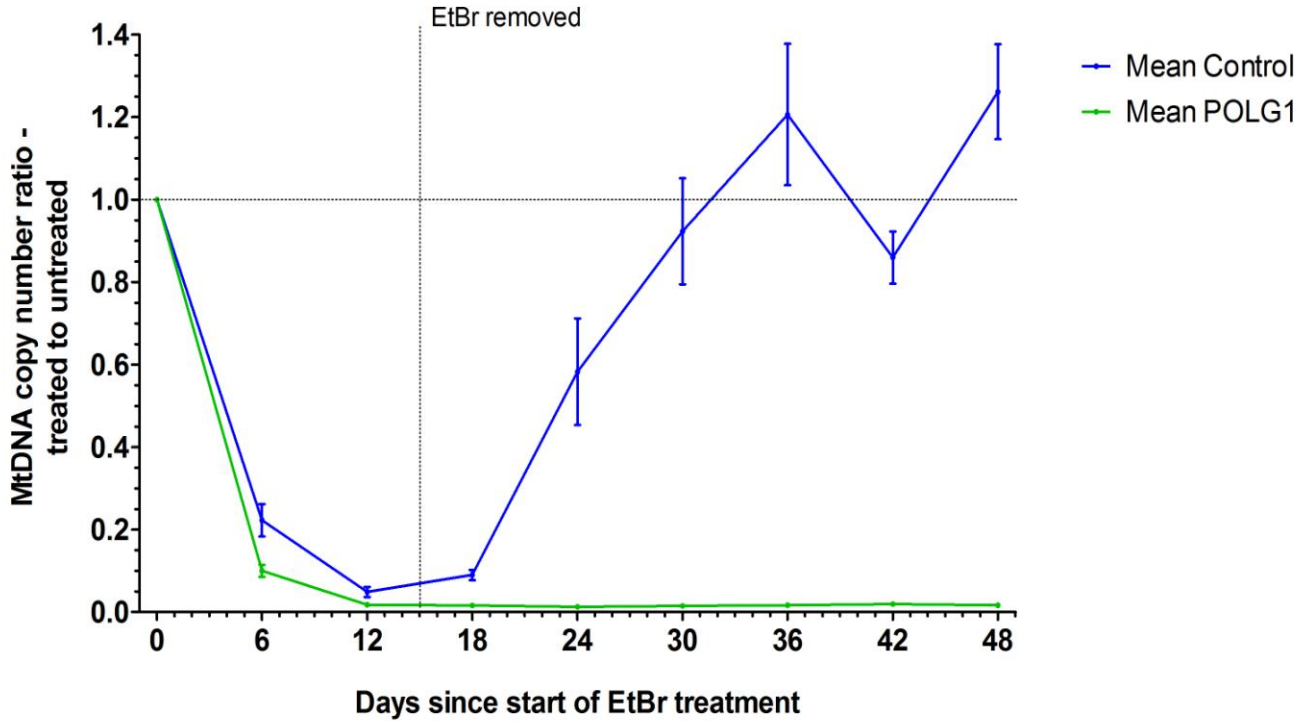

Mean Control vs. Mean POLG1	0.0033	0.0140	**< 0.0001**	**< 0.0001**	**< 0.0001**	**< 0.0001**	**< 0.0001**	**< 0.0001**

Figure 7-8 MtDNA depletion and repopulation curve of the mean POLG1 compared with the mean control. Each data point represents the average mtDNA copy number ratio of EtBr-treated to untreated cells. The error bars are presented as the standard errors of the mean (SEM). Table presents the P values of statistical comparisons made between the mean POLG1 and the mean control data sets. Each column corresponds to the time point on the graph above. The intensity of the red shading correlates with the degree of statistical significance.

7.3.3 MtDNA Depletion and Repopulation – *OPA1* Lines

The mtDNA depletion and repopulation curves for eight individual *OPA1* cell lines (**Figure 7-9** to **Figure 7-16)** and their mean (abbreviated as the mean OPA1; **Figure 7-17**) are presented below. The curves for the mean control and the mean POLG1 have been plotted for comparison.

During mtDNA depletion, a significant reduction in mtDNA content was observed for all *OPA1* cell lines, with a drop in the relative copy number to approximately 0.050 at day 12. There was no significant difference between the *OPA1* patient lines and the mean control. The mtDNA depletion curves for all *OPA1* fibroblasts were however statistically different from the mean POLG1, except for the OPA1b (**Figure 7-10**) and OPA1h (**Figure 7-16**) cell lines at day 6 (P = 0.0551 and P = 0.9434, respectively).

Variability among the individual *OPA1* cell lines was noted during the mtDNA repopulation phase. The OPA1a cell line (**Figure 7-9**) demonstrated only a low level of mtDNA repopulation, with a maximal relative mtDNA copy number of 0.084 (SEM = 0.007) at day 48. The repopulation of this cell line was statistically different from the mean control, during the entire repopulation phase, and from the mean POLG1 from day 24 onwards.

The OPA1b patient line (**Figure 7-10**) reached a maximal mtDNA repopulation level of 0.278 (SEM = 0.047) at day 24. Subsequently, a decrease in the relative mtDNA copy number was observed until day 36 (mean = 0.152, SEM = 0.019), followed by a plateau and a final repopulation level of 0.179 (SEM = 0.001) at day 48. The repopulation of the OPA1b cell line was statistically different from the mean control (except at day 24; P = 0.2003) and the mean POLG1.

The OPA1c cell line (**Figure 7-11**) showed only a low level of mtDNA repopulation, with a maximal relative copy number of 0.059 (SEM = 0.011) at day 24. Following this, the OPA1c cell line plateaued with a relative repopulation level of approximately 0.040. The repopulation of this cell line was significantly different from both the mean control and the mean POLG1 (except at day 18; P = 0.0631).

During the repopulation phase, the OPA1d cell line (**Figure 7-12**) demonstrated an initial gradual increase in its relative mtDNA content to a maximal value of 0.359

(SEM = 0.018) at day 30. This was followed by a decrease until day 42 (mean = 0.251, SEM = 0.021) and a final increase to a repopulation level of 0.426 (SEM = 0.043) at day 48. The repopulation of the OPA1d line was significantly different from the mean control (except at day 24; P = 0.1480) and the mean POLG1.

The OPA1e cell line (**Figure 7-13**) reached the mtDNA repopulation level exceeding 60% by day 30 (mean = 0.627, SEM = 0.020). A decrease in repopulation levels was then observed, which led to a final relative mtDNA copy number of 0.441 (SEM = 0.025) at day 48. The repopulation of the OPA1e cell line was not significantly different from the mean control up to day 30. The OPA1e cell line was however significantly different from the mean POLG1 during the entire study.

The OPA1f cell line (**Figure 7-14**) showed a gradual increase in relative mtDNA copy number until day 30 (mean = 0.353, SEM = 0.054), followed by a decrease to a repopulation level of 0.274 (SEM = 0.004) at day 36, and a subsequent increase to 0.335 (SEM = 0.012) at day 48. The repopulation curve of the OPA1f line was not significantly different from the mean control up to day 24, but it was significantly different from the mean POLG1 during the entire experiment.

The OPA1g cell line (**Figure 7-15**) repopulated its mtDNA content to a maximal level of 0.247 (SEM = 0.002) at day 36, this being followed by a decrease to a final mtDNA copy number of 0.214 (SEM = 0.037) at day 48. The repopulation patterns of the OPA1g line and the mean control were not statistically different until day 24. The OPA1g cell line was however significantly different from the mean POLG1 for all experimental time points during the repopulation phase.

The OPA1h cell line (**Figure 7-16**) demonstrated a relatively low level of repopulation, reaching a maximum of 0.080 (SEM = 0.021) at day 24. This was followed by a decrease in mtDNA repopulation and a final value of 0.053 (SEM = 0.001) was reached at day 48. This cell line was significantly different from the mean control throughout the entire repopulation phase. The OPA1h cell line was significantly different from the mean POLG1, except at days 18 and 36 (P = 0.1040 and P = 0.0611, respectively).

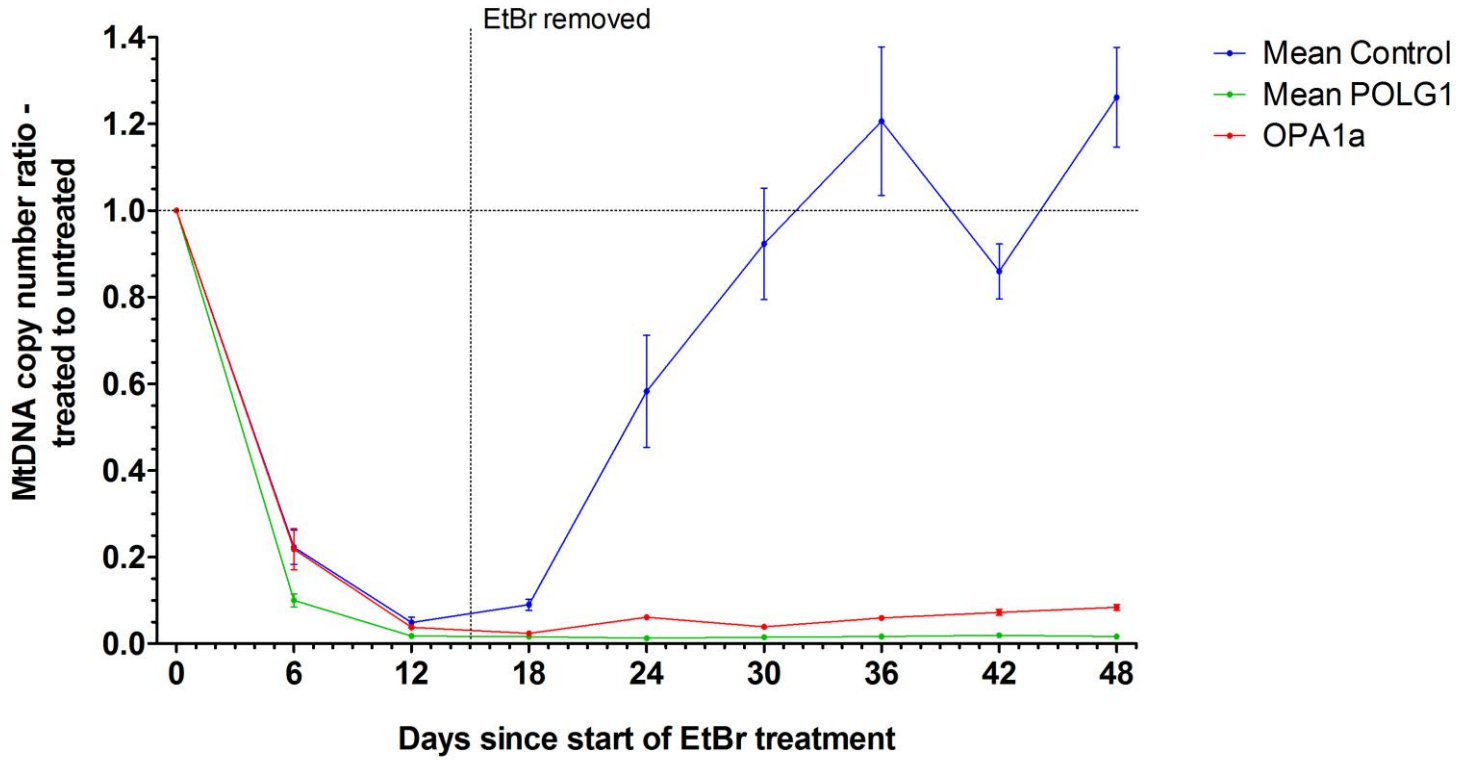

OPA1a vs.	**Mean Control**	0.9581	0.6622	0.0188	0.0348	0.0034	0.0020	**< 0.0001**	**< 0.0001**
	Mean POLG	0.0059	0.0454	0.2416	**< 0.0001**	0.0103	**0.0003**	**< 0.0001**	**< 0.0001**

Figure 7-9 MtDNA depletion and repopulation curve of the OPA1a cell line. Each data point represents the average mtDNA copy number ratio of EtBr-treated to untreated cells. The error bars are presented as the standard errors of the mean (SEM). The table shows the P values for the following statistical comparisons: OPA1a vs. mean control, and OPA1a vs. mean POLG1. Each column corresponds to the time point on the graph above. The intensity of the red shading correlates with the degree of statistical significance.

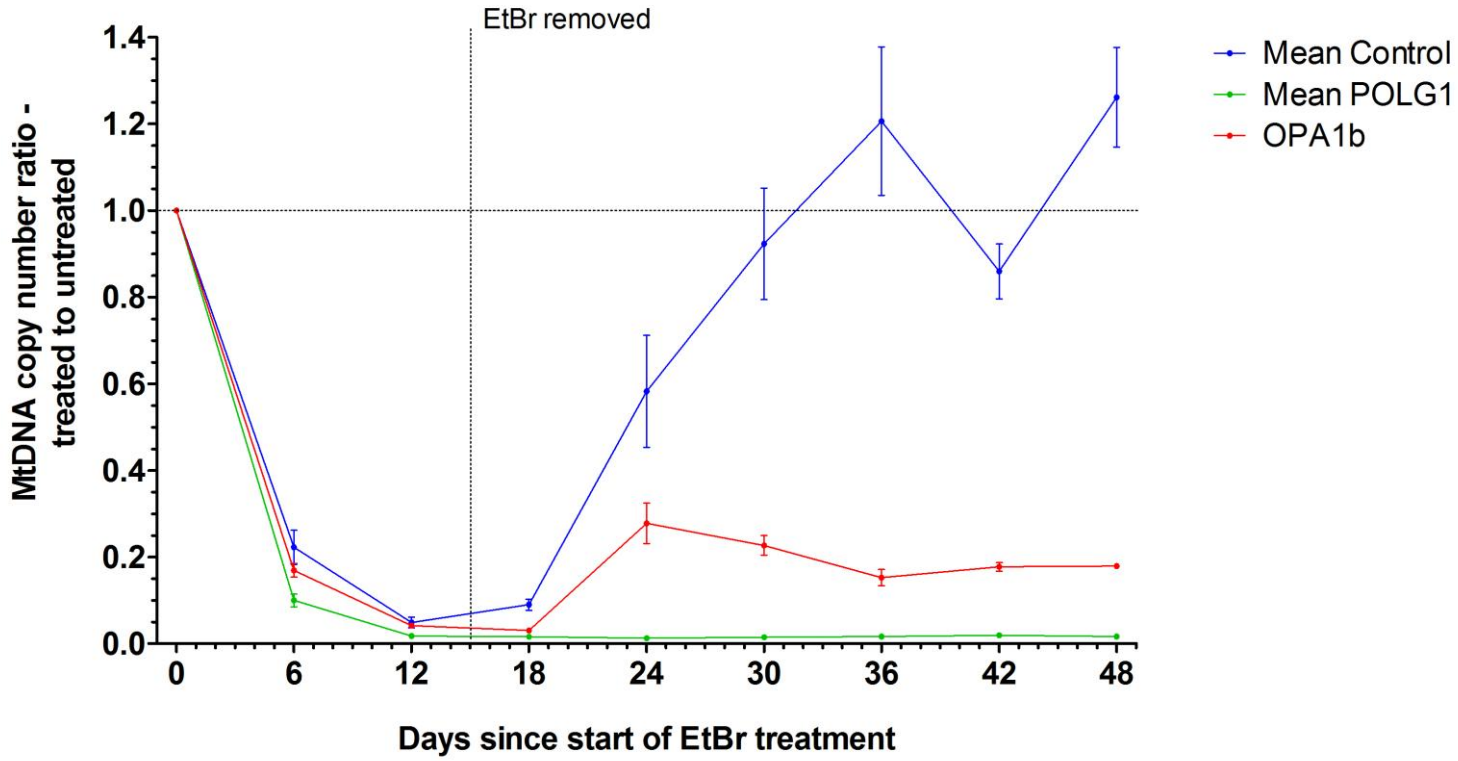

OPA1b vs.	**Mean Control**	0.5192	0.7793	0.0328	0.2003	0.0163	0.0038	**< 0.0001**	**0.0002**
	Mean POLG	0.0551	0.0198	0.0337	**< 0.0001**	**< 0.0001**	**< 0.0001**	**< 0.0001**	**< 0.0001**

Figure 7-10 MtDNA depletion and repopulation curve of the OPA1b cell line. Each data point represents the average mtDNA copy number ratio of EtBr-treated to untreated cells. The error bars are presented as the standard errors of the mean (SEM). The table shows the P values for the following statistical comparisons: OPA1b vs. mean control, and OPA1b vs. mean POLG1. Each column corresponds to the time point on the graph above. The intensity of the red shading correlates with the degree of statistical significance.

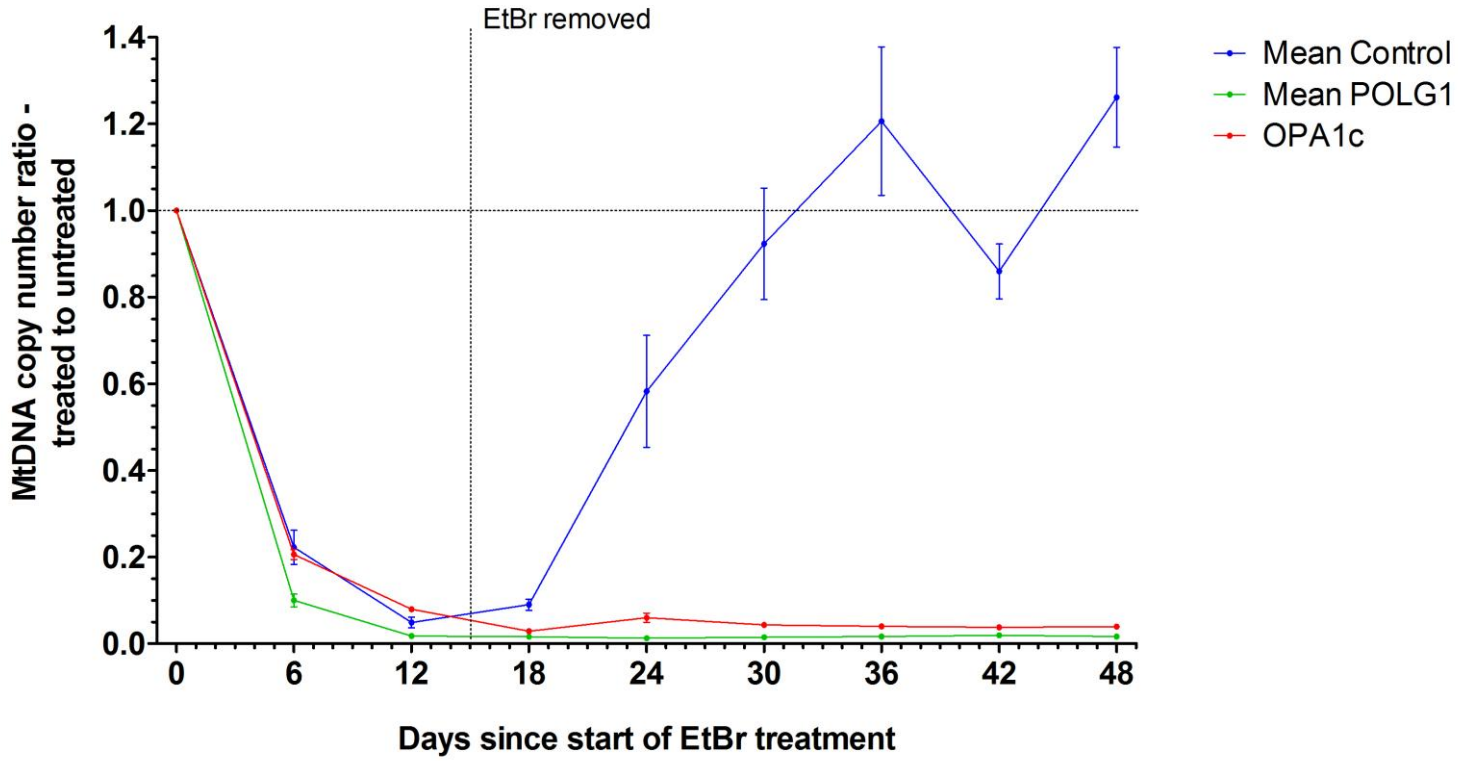

OPA1c vs.	**Mean Control**	0.8394	0.2461	0.0280	0.0344	0.0035	0.0018	**< 0.0001**	**< 0.0001**
	Mean POLG	0.0050	**< 0.0001**	0.0631	**< 0.0001**	0.0040	0.0271	0.0494	0.0068

Figure 7-11 MtDNA depletion and repopulation curve of the OPA1c cell line. Each data point represents the average mtDNA copy number ratio of EtBr-treated to untreated cells. The error bars are presented as the standard errors of the mean (SEM). The table shows the P values for the following statistical comparisons: OPA1c vs. mean control, and OPA1c vs. mean POLG1. Each column corresponds to the time point on the graph above. The intensity of the red shading correlates with the degree of statistical significance.

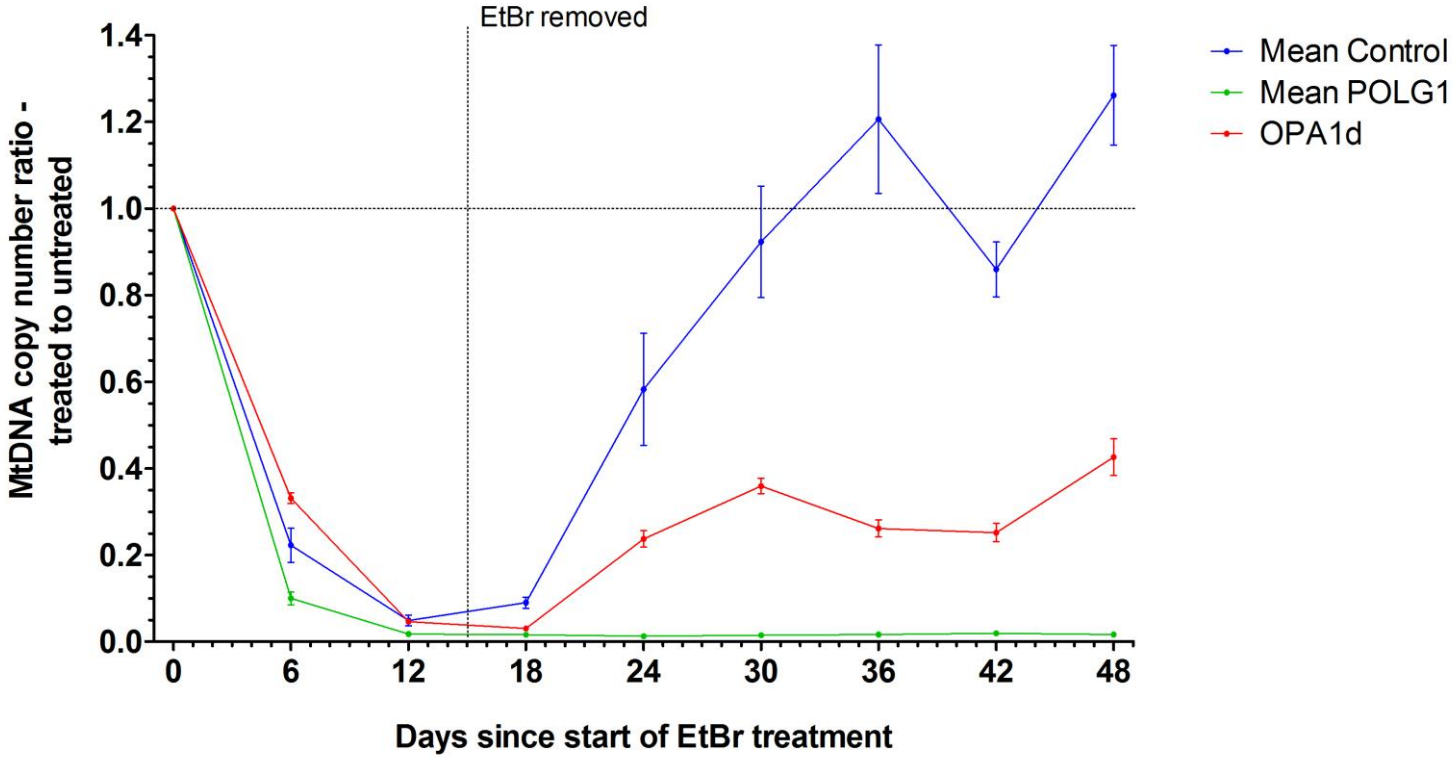

OPA1d vs.	**Mean Control**	0.1922	0.9187	0.0314	0.1480	0.0457	0.0077	**0.0002**	0.0023
	Mean POLG	**< 0.0001**	0.0073	0.0397	**< 0.0001**	**< 0.0001**	**< 0.0001**	**< 0.0001**	**< 0.0001**

Figure 7-12 MtDNA depletion and repopulation curve of the OPA1d cell line. Each data point represents the average mtDNA copy number ratio of EtBr-treated to untreated cells. The error bars are presented as the standard errors of the mean (SEM). The table shows the P values for the following statistical comparisons: OPA1d vs. mean control, and OPA1d vs. mean POLG1. Each column corresponds to the time point on the graph above. The intensity of the red shading correlates with the degree of statistical significance.

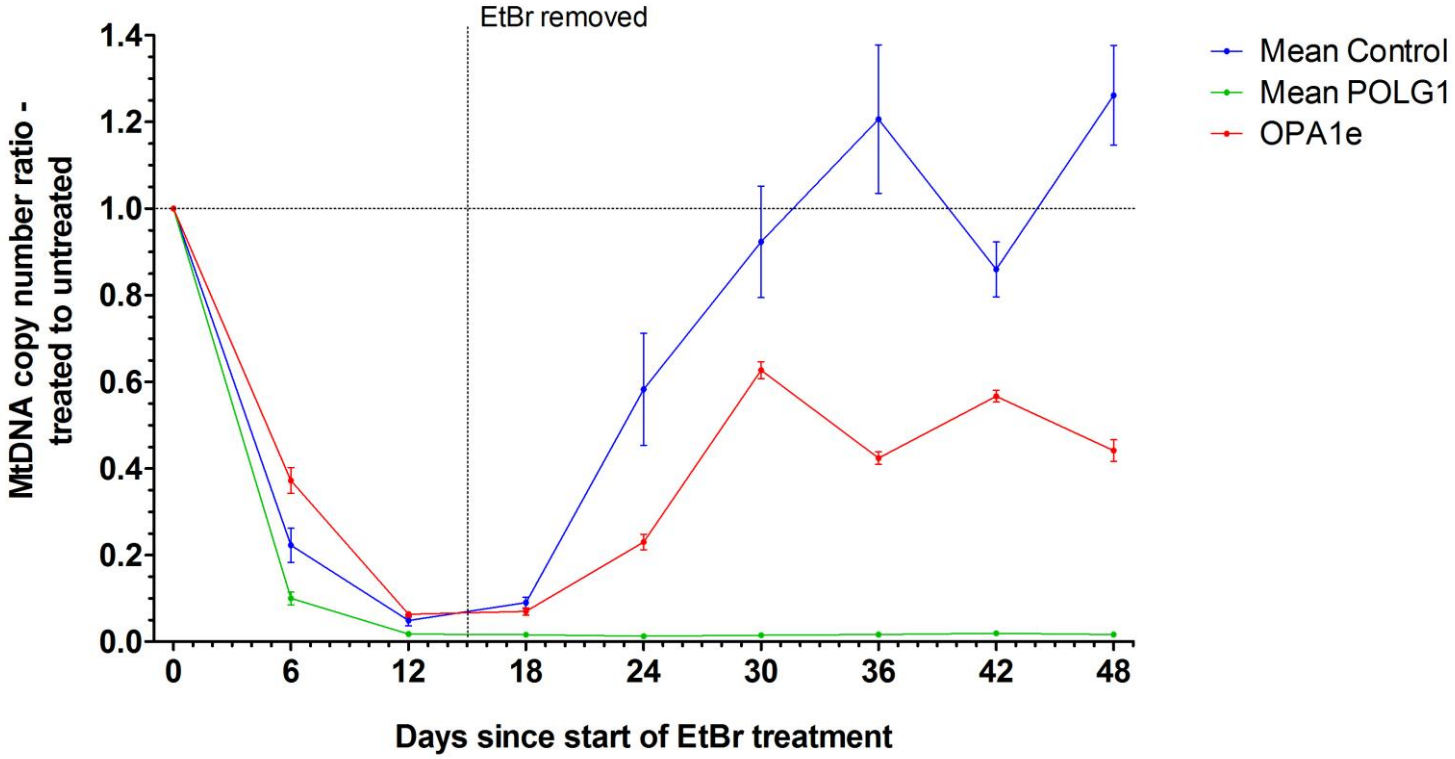

OPA1e vs.	**Mean Control**	0.0824	0.5870	0.4494	0.1400	0.2743	0.0220	0.0363	0.0026
	Mean POLG	**< 0.0001**	**0.0001**	**< 0.0001**	**< 0.0001**	**< 0.0001**	**< 0.0001**	**< 0.0001**	**< 0.0001**

Figure 7-13 MtDNA depletion and repopulation curve of the OPA1e cell line. Each data point represents the average mtDNA copy number ratio of EtBr-treated to untreated cells. The error bars are presented as the standard errors of the mean (SEM). The table shows the P values for the following statistical comparisons: OPA1e vs. mean control, and OPA1e vs. mean POLG1. Each column corresponds to the time point on the graph above. The intensity of the red shading correlates with the degree of statistical significance.

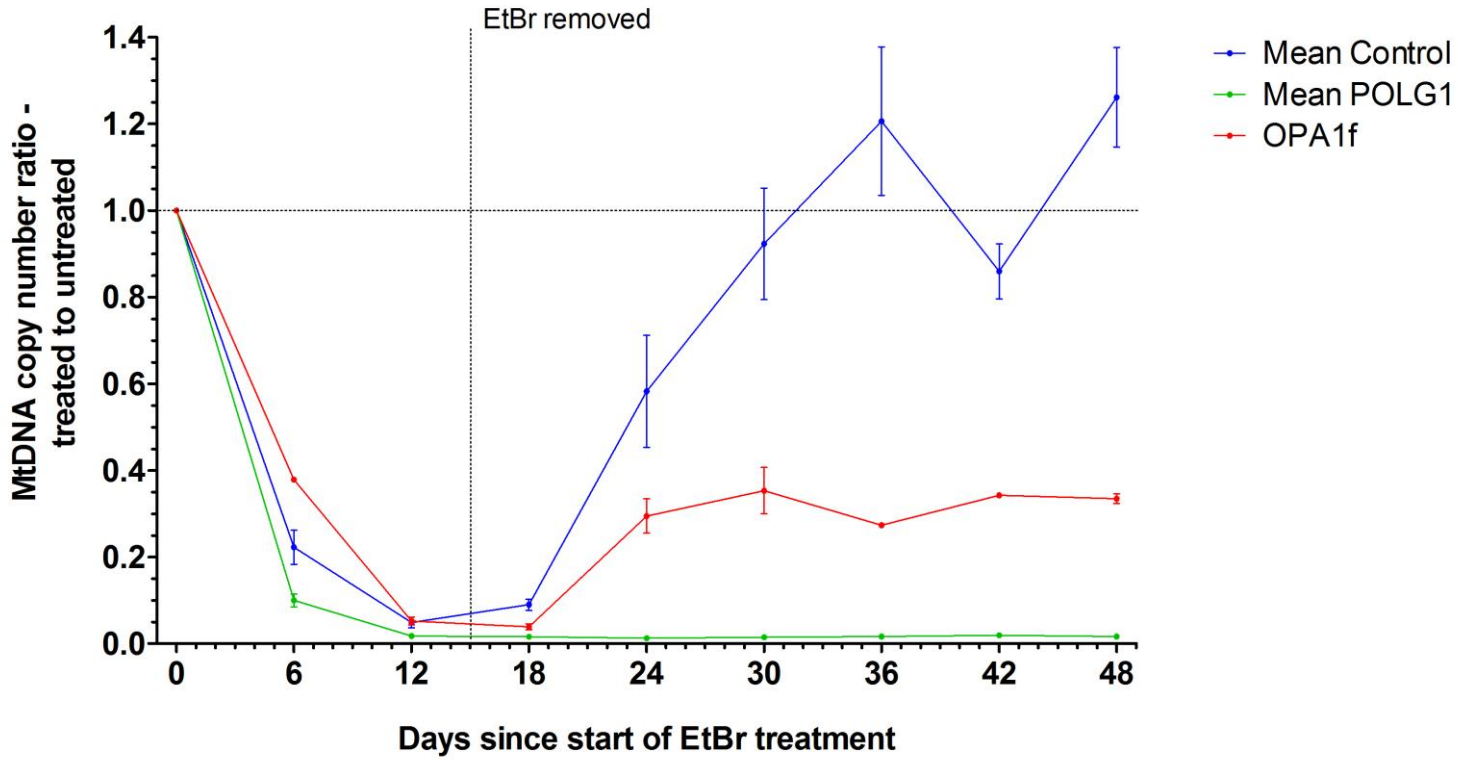

OPA1f vs.	**Mean Control**	0.0672	0.9020	0.0622	0.2247	0.0444	0.0083	**0.0008**	0.0010
	Mean POLG	**< 0.0001**	0.0023	0.0040	**< 0.0001**	**< 0.0001**	**< 0.0001**	**< 0.0001**	**< 0.0001**

Figure 7-14 MtDNA depletion and repopulation curve of the OPA1f cell line. Each data point represents the average mtDNA copy number ratio of EtBr-treated to untreated cells. The error bars are presented as the standard errors of the mean (SEM). The table shows the P values for the following statistical comparisons: OPA1f vs. mean control, and OPA1f vs. mean POLG1. Each column corresponds to the time point on the graph above. The intensity of the red shading correlates with the degree of statistical significance.

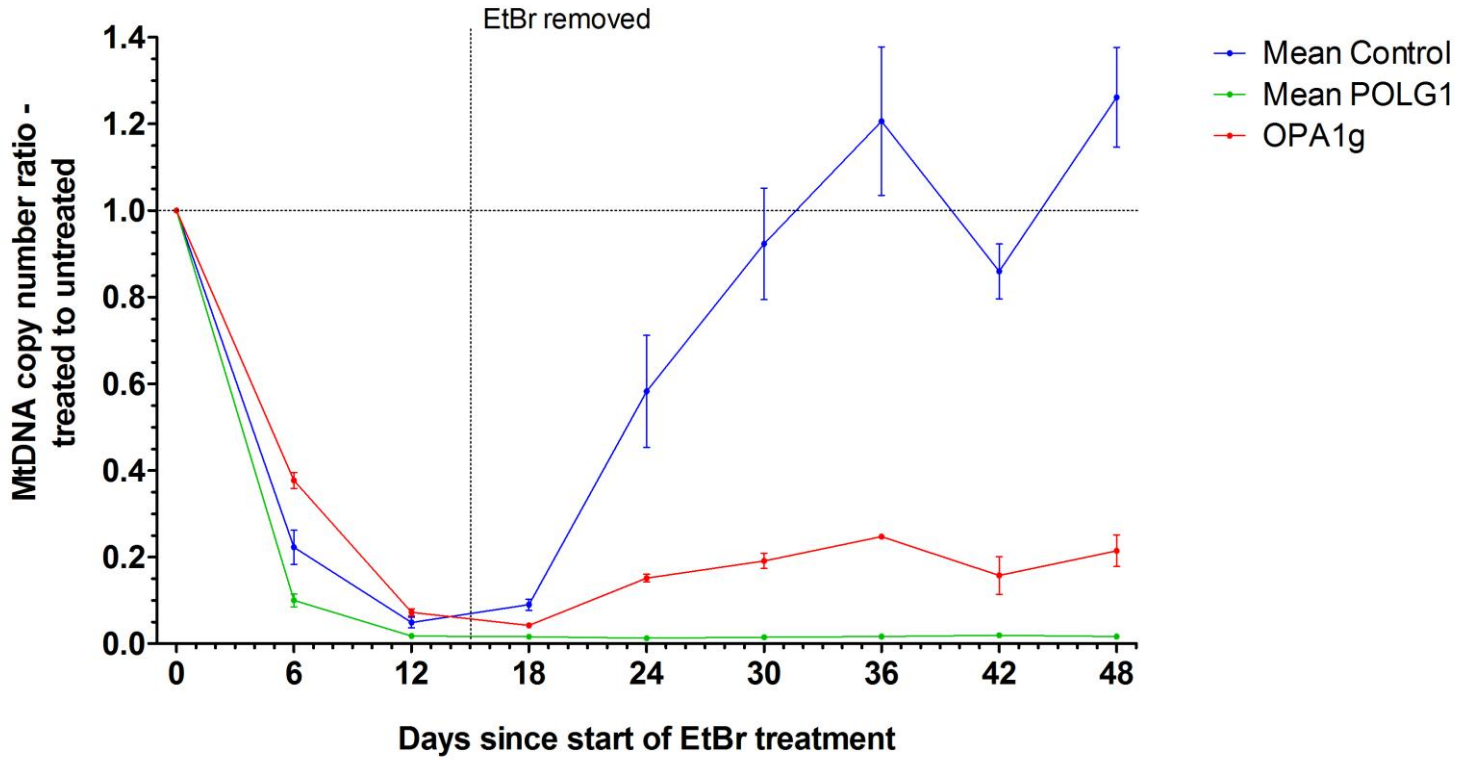

OPA1g vs.	**Mean Control**	0.0712	0.3754	0.0804	0.0751	0.0122	0.0070	**< 0.0001**	**0.0003**
	Mean POLG	**< 0.0001**	**< 0.0001**	**0.0009**	**< 0.0001**	**< 0.0001**	**< 0.0001**	**< 0.0001**	**< 0.0001**

Figure 7-15 MtDNA depletion and repopulation curve of the OPA1g cell line. Each data point represents the average mtDNA copy number ratio of EtBr-treated to untreated cells. The error bars are presented as the standard errors of the mean (SEM). The table shows the P values for the following statistical comparisons: OPA1g vs. mean control, and OPA1g vs. mean POLG1. Each column corresponds to the time point on the graph above. The intensity of the red shading correlates with the degree of statistical significance.

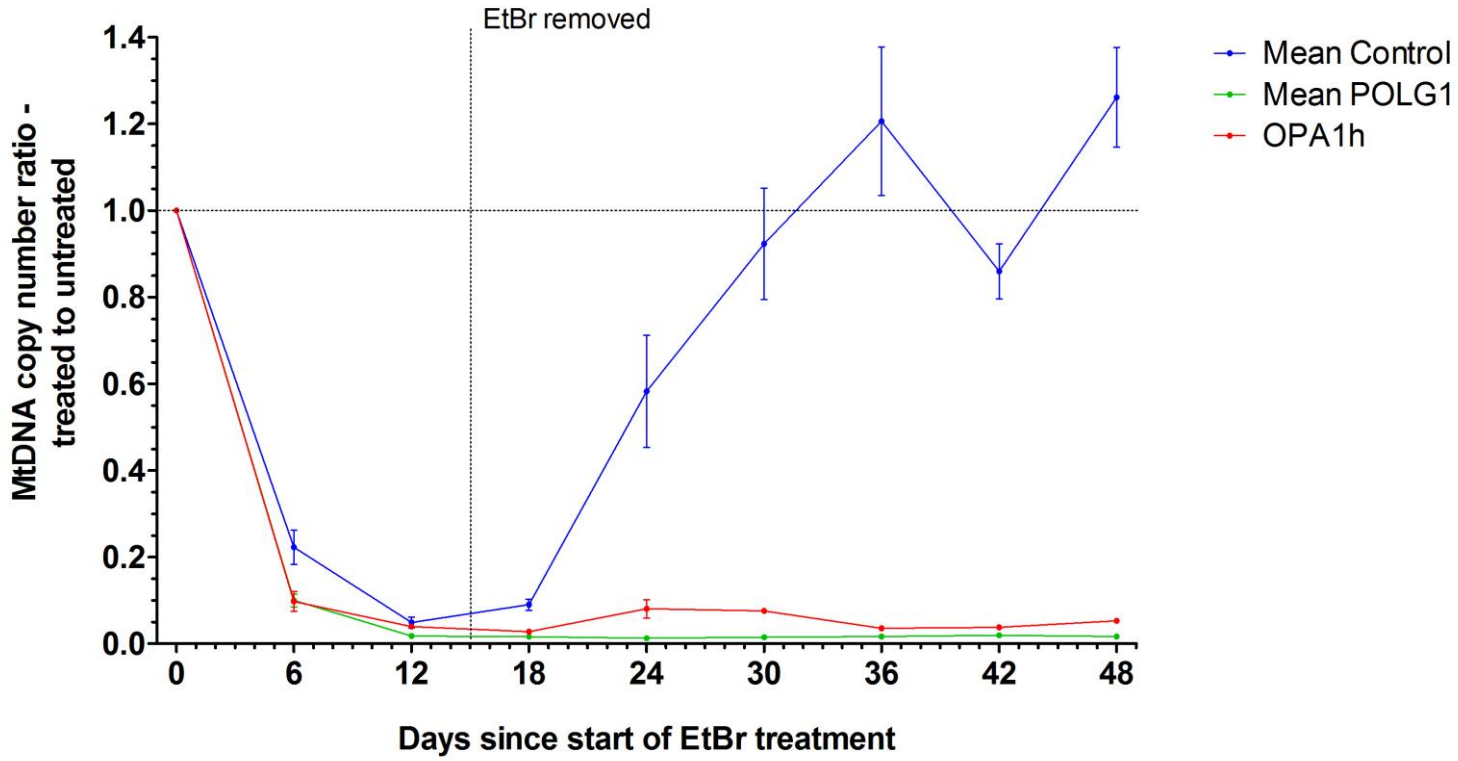

OPA1h vs.	**Mean Control**	0.1403	0.7091	0.0256	0.0413	0.0047	0.0018	**< 0.0001**	**< 0.0001**
	Mean POLG	0.9434	0.0310	0.1040	**< 0.0001**	**< 0.0001**	0.0611	0.0459	**0.0001**

Figure 7-16 MtDNA depletion and repopulation curve of the OPA1h cell line. Each data point represents the average mtDNA copy number ratio of EtBr-treated to untreated cells. The error bars are presented as the standard errors of the mean (SEM). The table shows the P values for the following statistical comparisons: OPA1h vs. mean control, and OPA1h vs. mean POLG1. Each column corresponds to the time point on the graph above. The intensity of the red shading correlates with the degree of statistical significance.

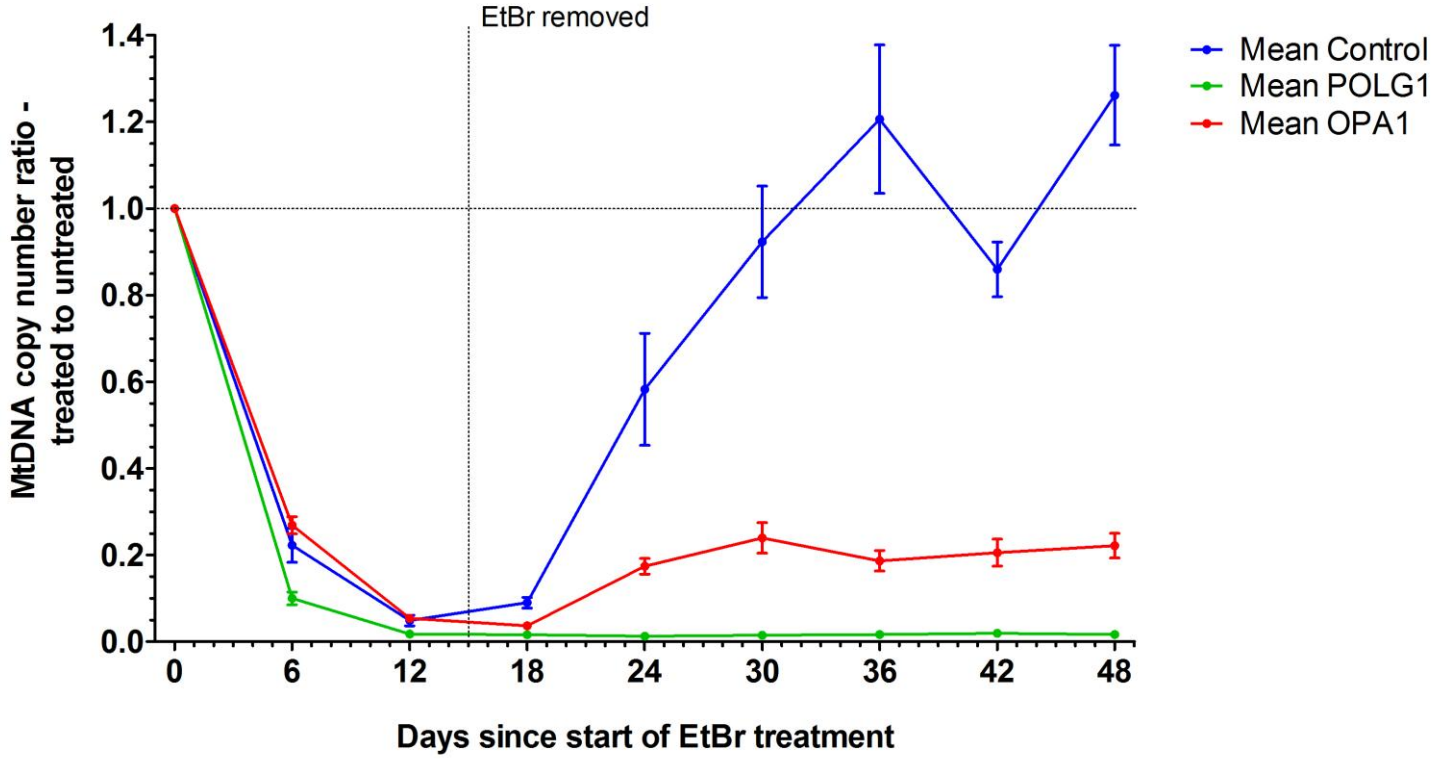

Mean OPA1 vs.	**Mean Control**	0.2435	0.6068	**< 0.0001**	**< 0.0001**	**< 0.0001**	**< 0.0001**	**< 0.0001**	**< 0.0001**
	Mean POLG	**< 0.0001**	**< 0.0001**	**< 0.0001**	**< 0.0001**	**< 0.0001**	**< 0.0001**	**< 0.0001**	**< 0.0001**

Figure 7-17 MtDNA depletion and repopulation curve of the mean OPA1 compared with the mean control and the mean POLG1. Each data point represents the average mtDNA copy number ratio of EtBr-treated to untreated cells. The error bars are presented as the standard errors of the mean (SEM). The table shows the P values for the following statistical comparisons: mean OPA1 vs. mean control, and mean OPA1 vs. mean POLG1. Each column corresponds to the time point on the graph above. The intensity of the red shading correlates with the degree of statistical significance.

7.3.3.1 Subgroup Analysis of *OPA1* Patient Lines

To investigate for possible differences in mtDNA repopulation levels between individual *OPA1* patient lines, the following subgroup analyses were performed based upon: (i) the affected OPA1 functional domain (GTPase vs. non-GTPase; **Figure 7-18**), (ii) the clinical phenotype (pure DOA vs. DOA+; **Figure 7-19**), and (iii) specific familial *OPA1* mutations (**Figure 7-20**).

There were no marked differences in the kinetics of mtDNA depletion and repopulation between the two cell lines harbouring *OPA1* missense mutations involving the GTPase domain compared with the six other *OPA1*-mutant cell lines not involving this functional gene domain exclusively (**Figure 7-18**). At day 48, the GTPase group repopulated to a relative level of 0.320 (SEM = 0.098) comparing with 0.188 (SEM = 0.065) for the non-GTPase cohort, and this difference was of borderline significance (P = 0.0450). The repopulation curves of both the GTPase and non-GTPase groups were statistically different from the mean control and the mean POLG1.

Using this repopulation assay, no significant differences were noted between the *OPA1* subgroups based on their clinical phenotypes (i.e. pure DOA vs. DOA+; **Figure 7-19**). The repopulation curves of both the pure DOA and DOA+ groups were significantly different from the mean control and the mean POLG1 during the whole repopulation phase.

The four familial *OPA1* mutations were compared both with the mean control and the mean POLG1 groups (**Figure 7-20**). During mtDNA depletion phase, the p.Q297X and the splice defect *OPA1* mutation groups behaved in a similar fashion to the mean control. The p.I432V and the p.V294fsX667 *OPA1* mutation groups demonstrated a less profound mtDNA depletion by day 6, which was statistically different from the mean control (P = 0.0303 and P = 0.0133, respectively). All *OPA1* mutation groups were significantly different from the mean POLG1 during the entire depletion phase, except for the OPA1h cell line (splice defect) at day 6 (P = 0.9434). During the mtDNA repopulation phase, all familial *OPA1* mutation groups were significantly different from the mean control as from day 18, except for p.V294fsX66 mutation group, which became significantly different from the mean control only from day 30 onwards. The levels of mtDNA repopulation calculated for

all *OPA1* mutational groups were significantly different from the mean POLG1 during the entre repopulation phase, except for the OPA1h cell line (splice defect) at day 18 (P = 0.1040) and at day 36 (P = 0.0611).

For the statistical comparisons of the different familial *OPA1* mutation groups with each other, please refer to **Figure B-6** in **Appendix B.2**.

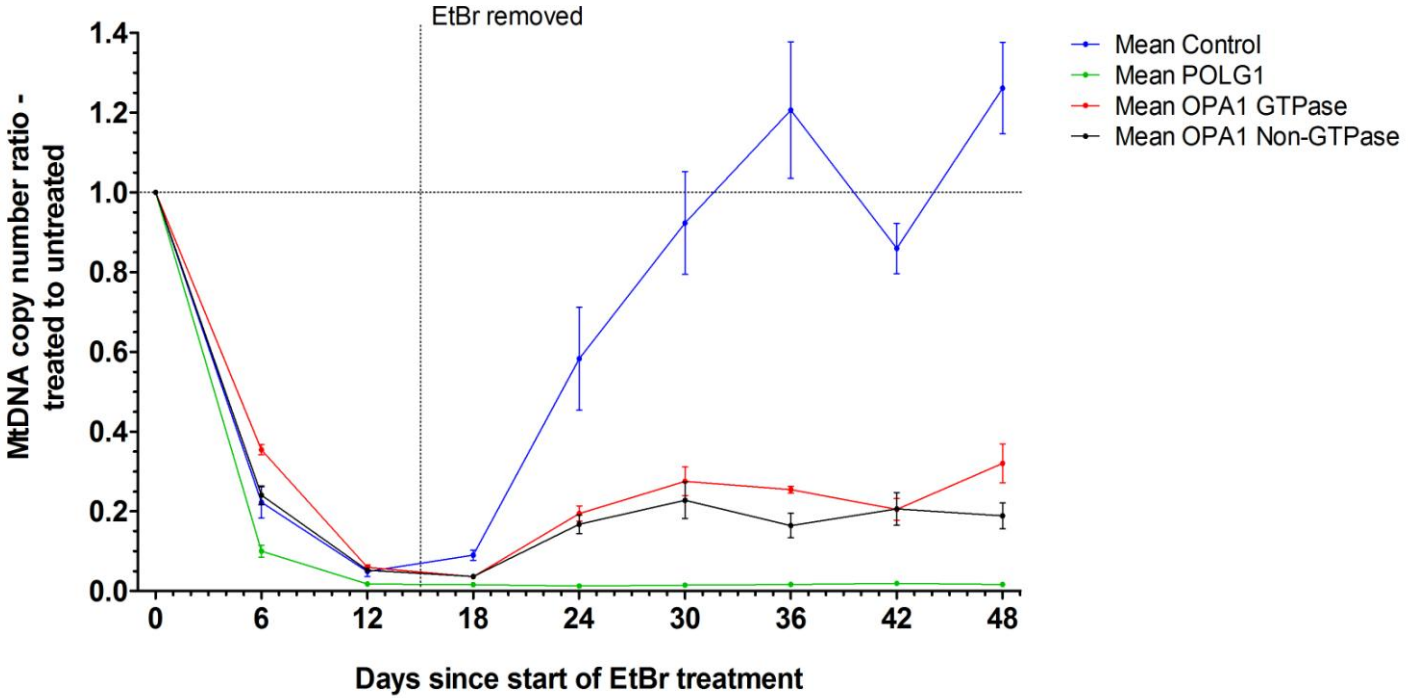

Mean OPA1 GTPase vs.	**Mean control**	0.0303	0.5796	0.0071	0.0263	0.0021	**0.0003**	**< 0.0001**	**< 0.0001**
	Mean POLG1	**< 0.0001**	**< 0.0001**	**0.0004**	**< 0.0001**	**< 0.0001**	**< 0.0001**	**< 0.0001**	**< 0.0001**
Mean OPA1 non-GTPase vs.	**Mean control**	0.6788	0.7662	**< 0.0001**	**0.0001**	**< 0.0001**	**< 0.0001**	**< 0.0001**	**< 0.0001**
	Mean POLG1	**< 0.0001**	**< 0.0001**	**< 0.0001**	**< 0.0001**	**0.0005**	**0.0004**	0.0033	**0.0007**
Mean GTPase vs. Mean non-GTPase		0.0110	0.3460	0.9639	0.5294	0.5668	0.1043	0.9885	0.0450

Figure 7-18 MtDNA depletion and repopulation curves for *OPA1* cell lines involving the GTPase region (N = 2) compared with those carrying mutations outside this functional gene domain (N = 6). Each data point represents the average mtDNA copy number ratio of EtBr-treated to untreated cells. The error bars are presented as the standard errors of the mean (SEM). The table shows the P values for the following statistical comparisons: each *OPA1* subgroup vs. mean control, each *OPA1* subgroup vs. mean POLG1, and *OPA1* subgroups vs. each other. Each column corresponds to the time point on the graph above. The intensity of the red shading correlates with the degree of statistical significance.

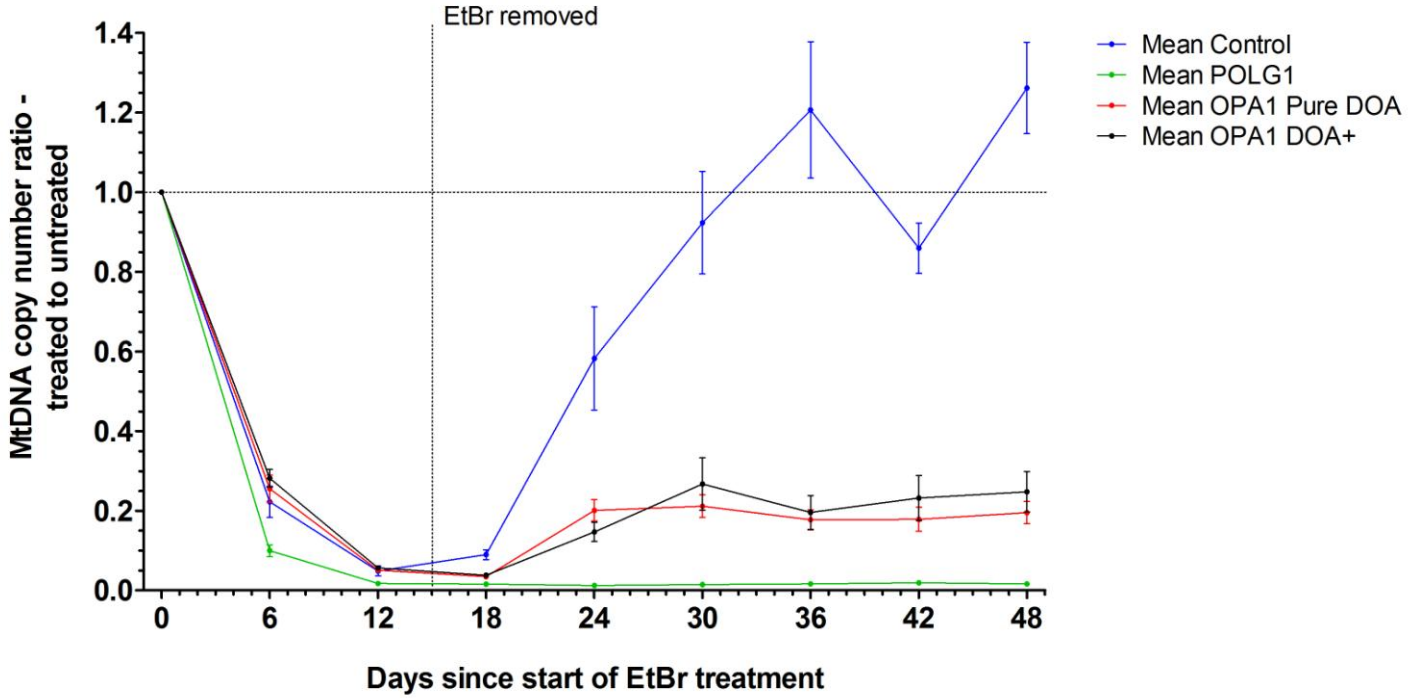

Mean OPA1 Pure DOA vs.	**Mean control**	0.5261	0.8554	**0.0002**	0.0028	**< 0.0001**	**< 0.0001**	**< 0.0001**	**< 0.0001**
	Mean POLG1	**< 0.0001**	**< 0.0001**	**< 0.0001**	**< 0.0001**	**< 0.0001**	**< 0.0001**	**0.0001**	**< 0.0001**
Mean OPA1 DOA+ vs.	**Mean control**	0.1975	0.5672	**0.0006**	**0.0008**	**< 0.0001**	**< 0.0001**	**< 0.0001**	**< 0.0001**
	Mean POLG1	**< 0.0001**	**< 0.0001**	**0.0004**	**< 0.0001**	**0.0006**	**0.0002**	0.0031	**0.0006**
Mean pure DOA vs. Mean DOA+		0.5239	0.4136	0.5625	0.1422	0.4463	0.7061	0.4111	0.3742

Figure 7-19 MtDNA depletion and repopulation curves for *OPA1* lines from patients with pure DOA (N = 4) compared with those with DOA+ (N = 4) phenotypes. Each data point represents the average mtDNA copy number ratio of EtBr-treated to untreated cells. The error bars are presented as the standard errors of the mean (SEM). The table shows the P values for the following statistical comparisons: each *OPA1* subgroup vs. mean control, each *OPA1* subgroup vs. mean POLG1, and *OPA1* subgroups vs. each other. Each column corresponds to the time point on the graph above. The intensity of the red shading correlates with the degree of statistical significance.

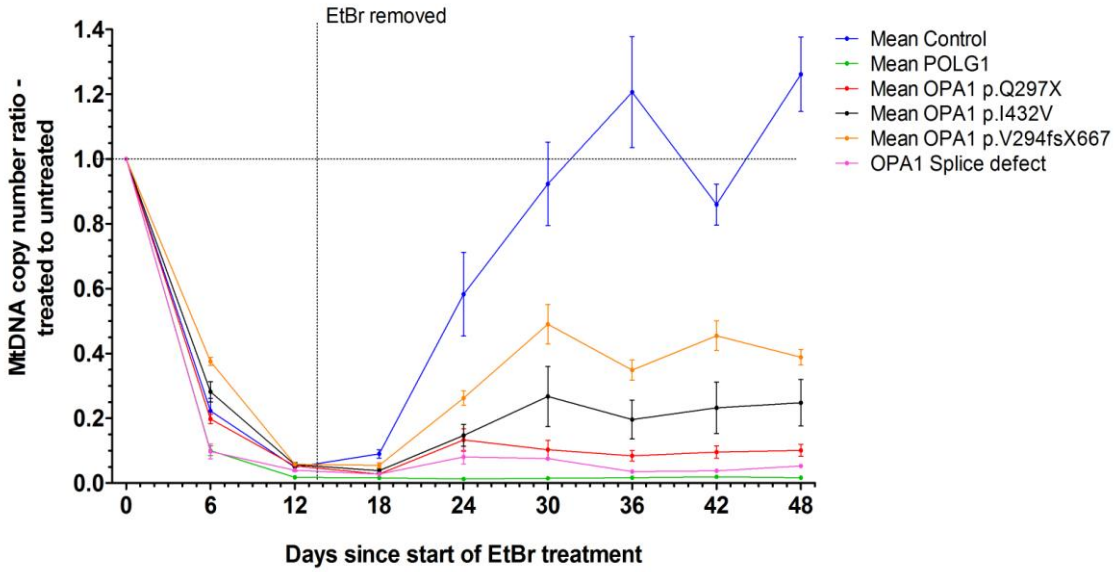

DAY OF STUDY		6	12	18	24	30	36	42	48
Mean Control vs.	OPA1 p.Q297X	0.6071	0.7959	**0.0002**	0.0028	**< 0.0001**	**< 0.0001**	**< 0.0001**	**< 0.0001**
	OPA1 p.I432V	0.0303	0.5796	0.0071	0.0263	0.0021	**0.0003**	**< 0.0001**	**< 0.0001**
	OPA1 p.V294fsX667	0.0133	0.6372	0.0700	0.0615	0.0316	**0.0008**	**0.0004**	**< 0.0001**
	OPA1 Splice	0.1403	0.7091	0.0256	0.0413	0.0047	0.0018	**< 0.0001**	**< 0.0001**
Mean POLG1 vs.	OPA1 p.Q297X	**0.0001**	**< 0.0001**	0.0043	**< 0.0001**	0.0015	**0.0001**	**0.0008**	**0.0002**
	OPA1 p.I432V	**< 0.0001**	**< 0.0001**	**0.0004**	**< 0.0001**	**< 0.0001**	**< 0.0001**	**< 0.0001**	**< 0.0001**
	OPA1 p.V294fsX667	**< 0.0001**	**< 0.0001**	**< 0.0001**	**< 0.0001**	**< 0.0001**	**< 0.0001**	**< 0.0001**	**< 0.0001**
	OPA1 Splice	0.9434	0.0310	0.1040	**< 0.0001**	**< 0.0001**	0.0611	0.0459	**0.0001**

Figure 7-20 MtDNA depletion and repopulation curves for *OPA1* cell lines grouped into familial mutational subgroups: OPA1 p.Q297X (N = 3), OPA1 p.I432V (N = 2), OPA1 p.V294fsX667 (N = 2) and OPA1 splice (N = 1). Each data point represents the average mtDNA copy number ratio of EtBr-treated to untreated cells. The error bars are presented as the standard errors of the mean (SEM). The table shows the P values for the following statistical comparisons: each *OPA1* subgroup vs. mean control and each *OPA1* subgroup vs. mean POLG1. The intensity of the red shading correlates with the degree of statistical significance.

7.4 Results: Mitochondrial Network Analysis

In parallel with the mtDNA repopulation assay, the mitochondrial network was also analysed at three experimental time points: (i) prior to EtBr supplementation (day 0), (ii) at the end of EtBr-induced mtDNA depletion (day 15), and (iii) at the end of the mtDNA repopulation phase (day 45). At each time point, mitochondrial network parameters were quantified for 10 fibroblasts per cell line. The collected data were used to calculate: (i) the total length of the mitochondrial network per cell (abbreviated as the total length; data in µm scale), (ii) the average length of a mitochondrial fragment in a cell (abbreviated as the average length; data in µm scale), and (iii) the total number of mitochondrial fragments per cell (abbreviated as the number of fragments).

7.4.1 Mitochondrial Network in Control Fibroblasts

The total length, the average length and the number of fragments for each of the four independent control cell lines were estimated as the mean values for 10 individual fibroblasts (N = 10). These mitochondrial network parameters for the mean control were calculated from the entire cohort of control cells (N = 40). The analyses for the total length (**Figure 7-21**), the average length (**Figure 7-22**), and the number of fragments (**Figure 7-23**) for the four control fibroblast lines and the mean control, are described further below.

7.4.1.1 Total Mitochondrial Network Length in Control Fibroblasts

There was variability in the total mitochondrial network length calculated for the control cell lines at day 0 (**Figure 7-21 A**). The greatest total length was seen in the C1 line (mean = 369.44, SEM = 34.87), whereas the C2 line (mean = 135.01, SEM = 10.13) showed the smallest value for this parameter. The difference between the C1 and C2 was statistically significant ($P < 0.0001$). By the end of the mtDNA depletion phase (day 15), all the control cell lines had significantly increased the total length of their mitochondrial networks (**Figure 7-21 B**). By day 45, the total length for three control cell lines had decreased to their baseline values (**Figure 7-21 C**). The only exception was the C3 cell line, for which the total length at day 45 was significantly higher compared with day 0 ($P = 0.0341$). The total length for the mean control

(**Figure 7-21 D**) confirmed a significant increase between day 0 (mean = 236.11, SEM = 17.19) and day 15 (mean = 390.17, SEM = 29.84) ($P < 0.0001$), followed by a significant reduction by day 45 ($P = 0.0020$). The total length (mean = 267.68, SEM = 23.72) at day 45 was not significantly different from the value measured at day 0 ($P = 0.2724$).

7.4.1.2 Average Length of Mitochondrial Fragment in Control Fibroblasts

All control cell lines had similar values for the average length of a mitochondrial fragment at day 0, with only the C2 and the C3 lines being significantly different from each other ($P = 0.0407$) (**Figure 7-22 A**). At the end of the mtDNA depletion phase (day 15), all control cell lines, except for C1, showed a significant reduction in the average length of a single mitochondrial fragment (**Figure 7-22 B**). By day 45, all control lines had restored their average lengths to levels that were not significantly different from those at day 0 (**Figure 7-22 C**). In the mean control (**Figure 7-22 D**) there was a significant drop in the average length between day 0 (mean = 3.15, SEM = 0.06) and day 15 (mean = 2.63, SEM = 0.10) ($P = 0.0001$), followed by a significant increase in the average fragment length by day 45 ($P = 0.0016$). At day 45, the average length (mean = 3.17, SEM = 0.09) was not significantly different from the value observed at day 0 ($P = 0.8848$).

7.4.1.3 Total Number of Mitochondrial Fragments in Control Fibroblasts

Variability was also observed in the total number of mitochondrial fragments per cell (**Figure 7-23 A**). The maximum number of fragments at day 0 was detected in the C1 cell line (mean = 115.60, SEM = 11.22), whereas the minimum value was observed in the C2 cell line (mean = 46.60, SEM = 4.51). The difference between the C1 and C2 was statistically significant ($P < 0.0001$). By the end of EtBr-induced mtDNA depletion (day 15), there was a significant increase in the total number of mitochondrial fragments per cell for all four control cell lines (**Figure 7-23 B**). By the end of mtDNA repopulation (day 45), the total number of fragments per cell decreased to the pre-EtBr level for three control lines (**Figure 7-23 C**). The C3 cell line behaved differently, with the number of fragments at day 45 being still significantly higher compared with the baseline i.e. day 0 ($P = 0.0173$). There was a significant increase in the total number of fragments in the mean control (**Figure 7-23 D**) between day 0 (mean = 75.40, SEM = 5.39) and day 15 (mean = 150.04,

SEM = 11.49) ($P < 0.0001$), followed by a significant reduction by day 45 ($P = 0.0005$). The total number of fragments at day 45 (mean = 91.03, SEM = 10.99) was not significantly different from the value observed at day 0 ($P = 0.1727$).

For subsequent comparisons in this chapter, the mean control will refer to the combined data set for the four control cell lines.

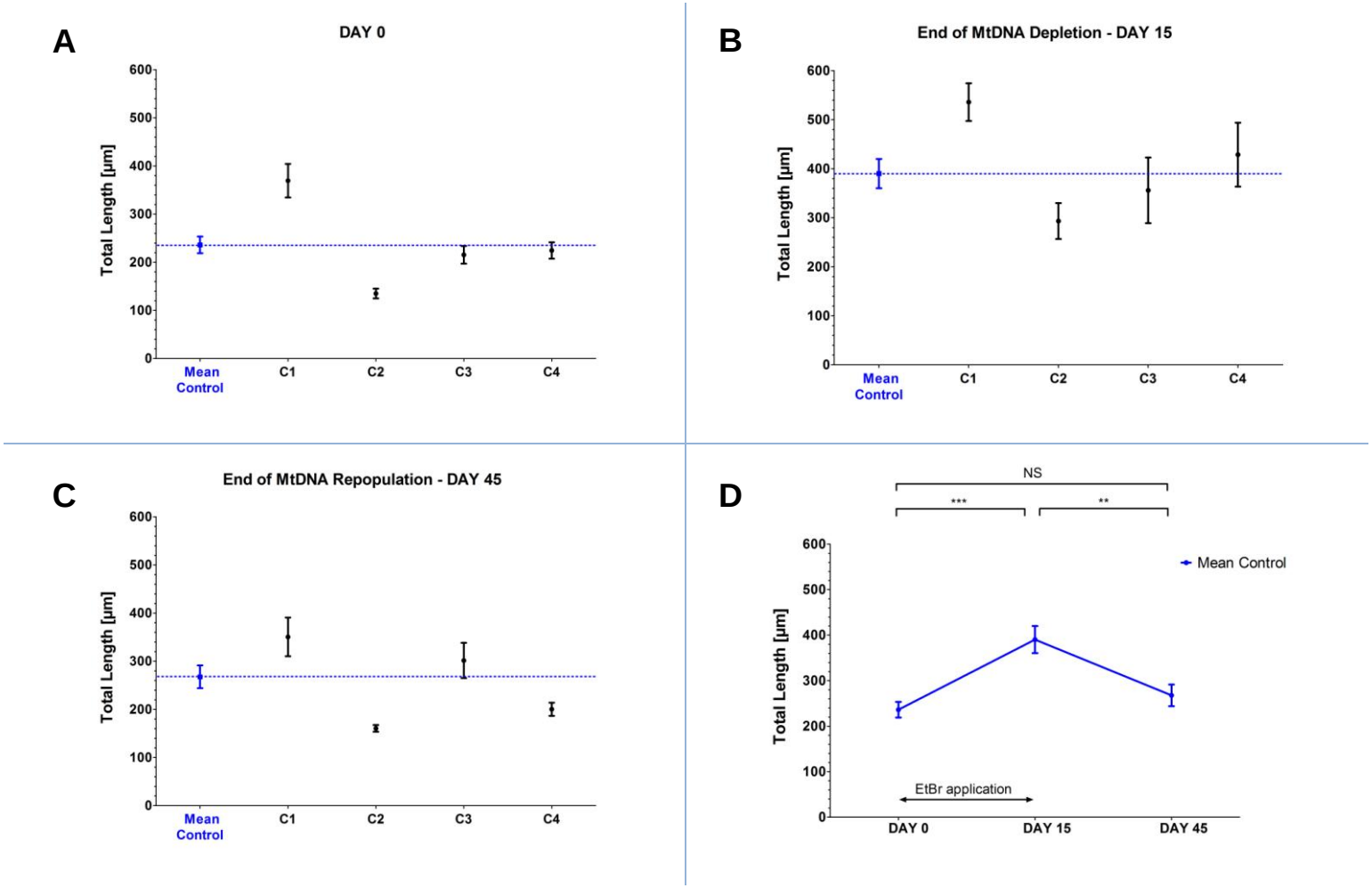

Figure 7-21 Total length of the mitochondrial network per cell in the control fibroblast cell lines: (A) prior to EtBr-treatment (Day 0), (B) at the end of EtBr-induced mtDNA depletion (Day 15), (C) at the end of mtDNA repopulation (Day 45), and (D) at all experimental points in the mean control. Each data point represents the mean total length. The error bars are presented as the standard errors of the mean (SEM). NS – non-significant at P = 0.2724; ** - refers to P value = 0.0020; *** - refers to P value < 0.0001.

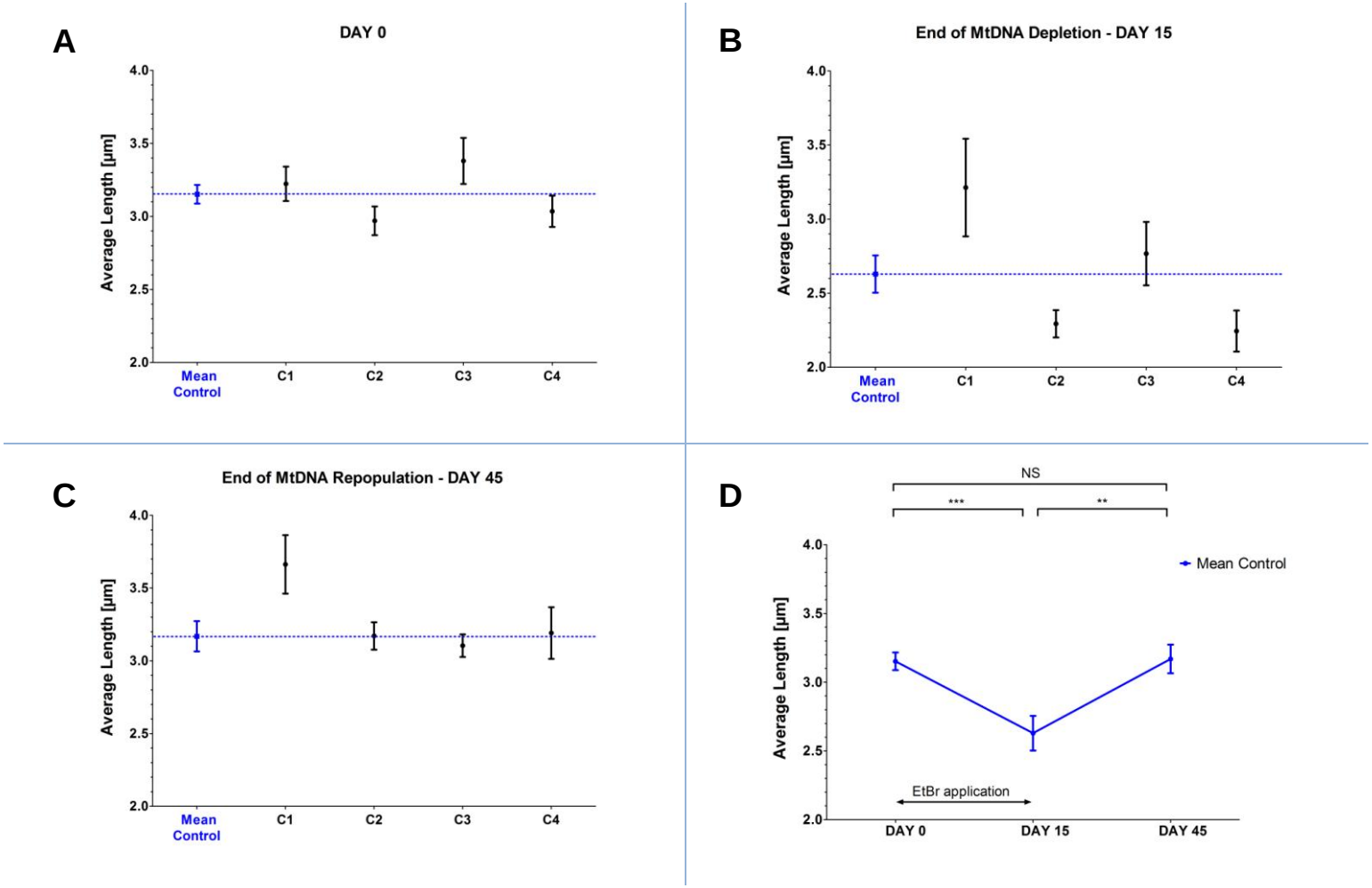

Figure 7-22 Average mitochondrial fragment length in the control fibroblast cell lines: (A) prior to EtBr-treatment (Day 0), (B) at the end of EtBr-induced mtDNA depletion (Day 15), (C) at the end of mtDNA repopulation (Day 45), and (D) at all experimental points in the mean control. Each data point represents the mean average length. The error bars are presented as the standard errors of the mean (SEM). NS – non-significant at P = 0.8848; ** - refers to P value = 0.0016; *** - refers to P value = 0.0001.

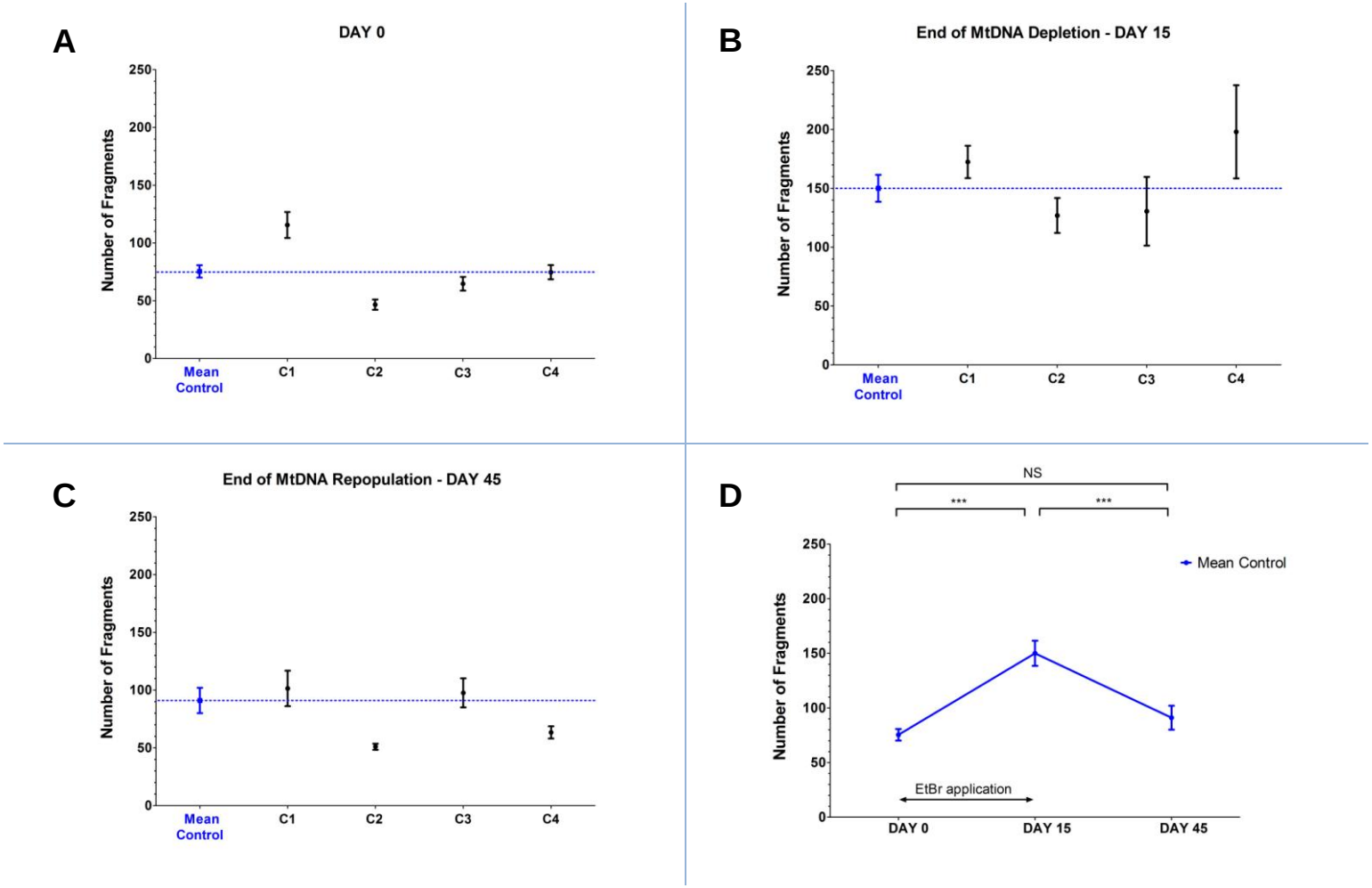

Figure 7-23 Total number of mitochondrial fragments per cell in the control fibroblast cell lines: (A) prior to EtBr-treatment (Day 0), (B) at the end of EtBr-induced mtDNA depletion (Day 15), (C) at the end of mtDNA repopulation (Day 45), and (D) at all experimental points in the mean control. Each data point represents the mean number of fragments. The error bars are presented as the standard errors of the mean (SEM). NS – non-significant at P = 0.1727; *** - refers to P < 0.0001 (day 0 vs. day 15) and P value = 0.0005 (day 15 vs. day 45).

7.4.2 Mitochondrial Network in *POLG1* Fibroblasts

The total length, the average length and the number of fragments for each of the five independent *POLG1* lines were estimated as the mean values for 10 individual fibroblasts (N = 10). These mitochondrial network parameters for the mean POLG1 were calculated from the entire cohort of *POLG1*-mutant cells (N = 50). The only exception was at day 45, when data for only three *POLG1* lines were available. That was caused by the premature death of EtBr-treated POLG1b and POLG1c fibroblasts, despite optimal culture conditions. The analyses of the total length (**Figure 7-24**), the average length (**Figure 7-25**), and the number of fragments (**Figure 7-26**) for individual *POLG1*-mutant fibroblast lines and the mean POLG1, are demonstrated below.

7.4.2.1 Total Mitochondrial Network Length in *POLG1* Fibroblasts

There was variability in the total mitochondrial length calculated for the *POLG1* patient lines at day 0 (**Figure 7-24 A**). The greatest total length was seen in the POLG1b line (mean = 417.79, SEM = 29.38), whereas the smallest values were demonstrated in the POLG1c (mean = 243.18, SEM = 20.97) and the POLG1d (mean = 245.37, SEM = 22.08) lines. By the end of mtDNA depletion (day 15), only the POLG1c and POLG1d lines had significantly increased their total mitochondrial length (**Figure 7-24 B**). By day 45, only the POLG1d line had decreased its total length to the baseline value (**Figure 7-24 C**). The total length for the mean POLG1 (**Figure 7-24 D**) confirmed a significant increase between day 0 (mean = 314.47, SEM = 15.52) and day 15 (mean = 394.13, SEM = 29.07) (P = 0.0180). No significant reduction was then observed by day 45 (P = 0.0991), when the total length (mean = 325.17, SEM = 21.62) was not significantly different from the value measured at day 0 (P = 0.6833).

7.4.2.2 Average Length of Mitochondrial Fragment in *POLG1* Fibroblasts

The average length of mitochondrial fragment at day 0 was similar in four out of the five *POLG1* cell lines, with only the POLG1e line (mean = 2.58, SEM = 0.10) being significantly shorter (**Figure 7-25 A**). By the end of the mtDNA depletion phase (day 15), all *POLG1* fibroblast lines showed a decrease in their average length (**Figure 7-25 B**). By day 45, none of the three *POLG1* patient lines had significantly restored

the average mitochondrial length (**Figure 7-25 C**). The mean POLG1 showed a significant drop in the average length (**Figure 7-25 D**) between day 0 (mean = 3.25, SEM = 0.10) and day 15 (mean = 2.29, SEM = 0.07) ($P < 0.0001$). No significant increase in the average mitochondrial fragment length was then observed by day 45 ($P = 0.2575$). At day 45, the average length (mean = 2.43, SEM = 0.11) was significantly different from the value observed at day 0 ($P < 0.0001$).

7.4.2.3 Total Number of Mitochondrial Fragments in *POLG1* Fibroblasts

The maximum number of mitochondrial fragments per cell at day 0 was presented in the POLG1e line (mean = 126.20, SEM = 16.83), whereas the minimum value was observed in the POLG1c line (mean = 69.40, SEM = 18.40) (**Figure 7-26 A**). By the end of mtDNA depletion phase (day 15), only the POLG1c and POLG1d lines showed significant increase in their number of fragments (**Figure 7-26 B**). By day 45, none of the three *POLG1* lines showed a significant reduction in this parameter (**Figure 7-26 C**). There was a significant increase in number of fragments in the mean POLG1 (**Figure 7-26 D**) between day 0 (mean = 101.46, SEM = 5.97) and day 15 (mean = 168.52, SEM = 13.33) ($P < 0.0001$). No significant reduction was then observed by day 45 ($P = 0.0735$). The total length at day 45 (mean = 138.40, SEM = 10.12) was statistically different from the value observed at day 0 ($P = 0.0012$).

For the comparison of mitochondrial network parameters between individual *POLG1* lines and the mean control, please refer to **Appendix C.1**.

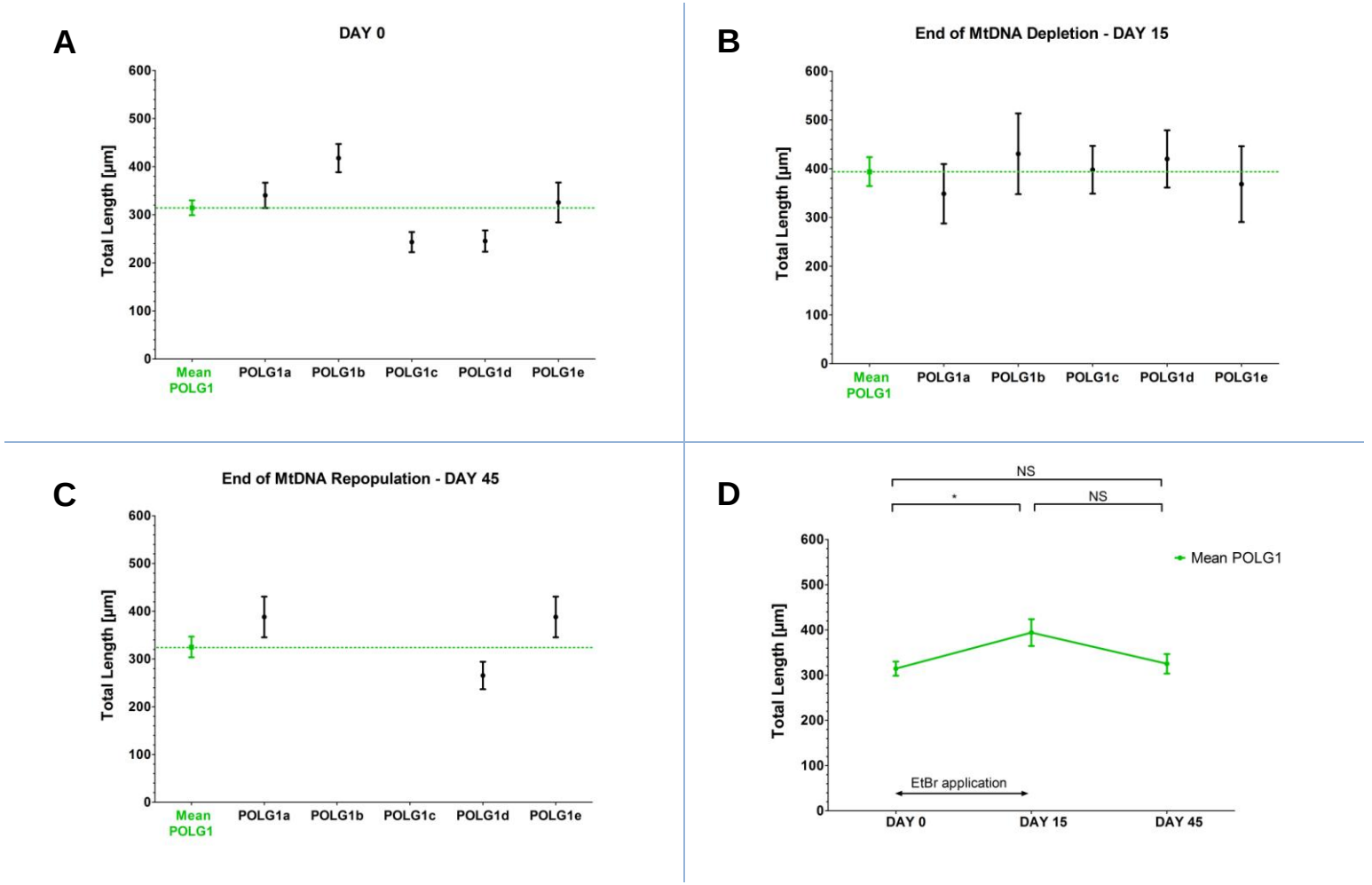

Figure 7-24 Total length of the mitochondrial network per cell in the *POLG1* fibroblast cell lines: (A) prior to EtBr-treatment (Day 0), (B) at the end of EtBr-induced mtDNA depletion (Day 15), (C) at the end of mtDNA repopulation (Day 45), and (D) at all experimental points in the mean POLG1. Each data point represents the mean total length. The error bars are presented as the standard errors of the mean (SEM). NS – non-significant at P = 0.0991 (day 15 vs. day 45) and P value = 0.6833 (day 0 vs. day 45); * - refers to P value = 0.0180. Data points for the POLG1b and POLG1c cell lines were unavailable at day 45 due to the premature death of the POLG1b and the POLG1c EtBr-treated fibroblasts before that sampling point.

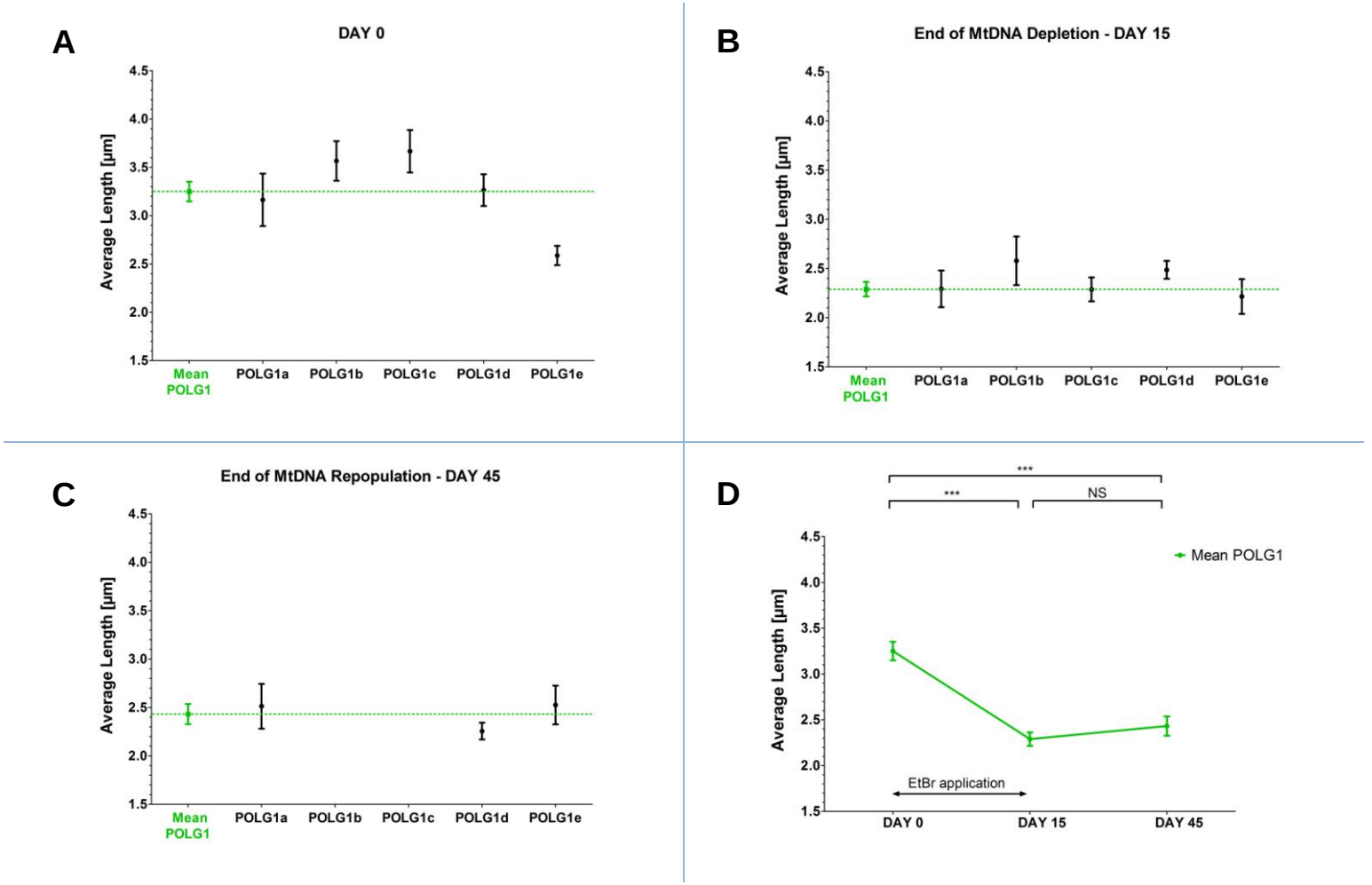

Figure 7-25 Average mitochondrial fragment length in the *POLG1* fibroblast cell lines: (A) prior to EtBr-treatment (Day 0), (B) at the end of EtBr-induced mtDNA depletion (Day 15), (C) at the end of mtDNA repopulation (Day 45), and (D) at all experimental points in the mean POLG1. Each data point represents the mean average length. The error bars are presented as the standard errors of the mean (SEM). NS – non-significant at P = 0.2575; *** - refers to P value < 0.0001. Data points for the POLG1b and POLG1c cell lines were unavailable at day 45 due to the premature death of the POLG1b and the POLG1c EtBr-treated fibroblasts before that sampling point.

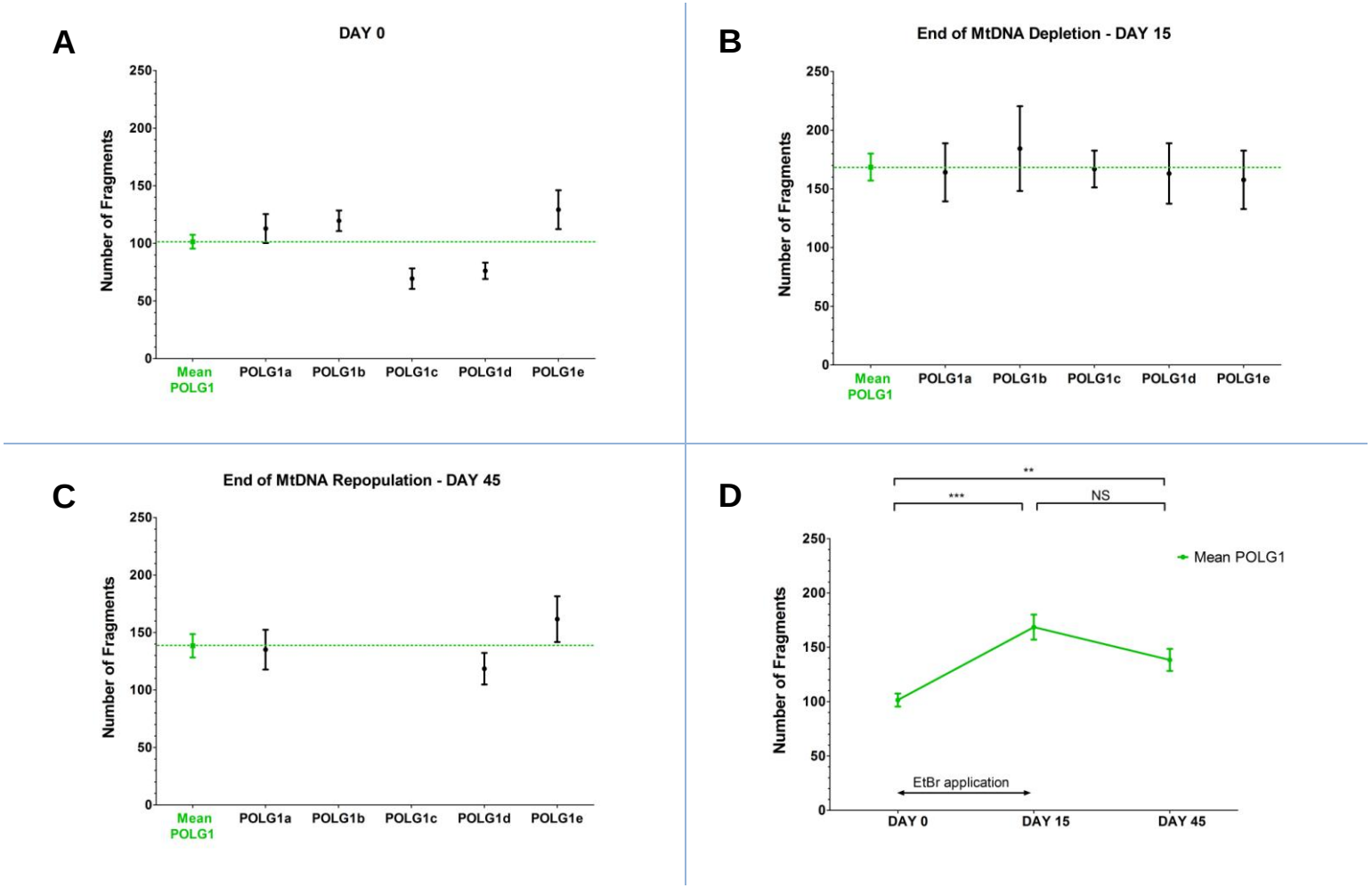

Figure 7-26 Total number of mitochondrial fragments per cell in the *POLG1* fibroblast cell lines: (A) prior to EtBr-treatment (Day 0), (B) at the end of EtBr-induced mtDNA depletion (Day 15), (C) at the end of mtDNA repopulation (Day 45), and (D) at all experimental points in the mean POLG1. Each data point represents the mean number of fragments. The error bars are presented as the standard errors of the mean (SEM). NS – non-significant at P = 0.0735; ** - refers to P value = 0.0012; *** - refers to P < 0.0001. Data points for the POLG1b and POLG1c at day 45 were unavailable due to the premature death of the POLG1b and the POLG1c EtBr-treated fibroblasts before that sampling point.

7.4.3 Mitochondrial Network in *OPA1* Fibroblasts

The total length, the average length and the number of fragments for each of the eight independent *OPA1* cell lines were estimated as the mean values for 10 individual fibroblasts (N = 10). These mitochondrial network parameters for the mean OPA1 were calculated from the entire cohort of *OPA1* cells (N = 80). The analyses of the total length (**Figure 7-27**), the average length (**Figure 7-28**), and the number of fragments (**Figure 7-29**) for the eight *OPA1* fibroblast lines and the mean OPA1, are demonstrated below.

7.4.3.1 Total Mitochondrial Network Length in *OPA1* Fibroblasts

There was variability in the total mitochondrial length calculated for various *OPA1* patient lines at day 0 (**Figure 7-27 A**). The greatest total length was observed in the OPA1f line (mean = 505.32, SEM = 53.26), whereas the OPA1h line (mean = 228.44, SEM = 29.15) showed the lowest value of this parameter. By the end of mtDNA depletion phase (day 15) all *OPA1* lines apart from the OPA1f demonstrated increase in their total lengths (**Figure 7-27 B**). By the end of mtDNA repopulation (day 45), all *OPA1* lines except the OPA1b, decreased their total length (**Figure 7-27 C**). The mean OPA1 (**Figure 7-27 D**) demonstrated a significant increase in the total length between day 0 (mean = 369.31, SEM = 15.59) and day 15 (mean = 452.52, SEM = 22.47) (P = 0.0027), with a subsequent decrease by day 45 (mean = 352.80, SEM = 16.36) (P = 0.0006). The total length at day 45 was not significantly different from the value measured at day 0 (P = 0.4719).

7.4.3.2 Average Length of Mitochondrial Fragment in *OPA1* Fibroblasts

There was variability in the average mitochondrial fragment length calculated for *OPA1* patient lines at day 0 (**Figure 7-28 A**). The maximum average length was demonstrated in the OPA1d line (mean = 3.49, SEM = 0.22), whereas the minimal value was present in the OPA1b line (mean = 2.37, SEM = 0.14). By the end of the mtDNA depletion phase (day 15), a significant reduction in the average length was observed only in the OPA1c and OPA1h lines (P = 0.0002 and P = 0.0202, respectively) (**Figure 7-28 B**). By day 45, the significant increase in the average length was demonstrated for the OPA1c (P < 0.0001), OPA1f (P = 0.0022) and OPA1g (P = 0.0084) lines (**Figure 7-28 C**). The OPA1h was the only cell line which

showed a significant reduction in the average length between days 15 (mean = 2.42, SEM = 0.10) and 45 (mean = 2.07, SEM = 0.11) (P = 0.0301). There was a significant decrease in the average length for the mean OPA1 (**Figure 7-28 D**) between day 0 (mean = 2.91, SEM = 0.08) and day 15 (mean = 2.65, SEM = 0.08) (P = 0.0273). That was followed by a significant increase in the average length by day 45 (mean = 2.98, SEM = 0.09; P = 0.0084). The average length at day 45 was statistically not different from the value measured at day 0 (P = 0.5476).

7.4.3.3 Total Number of Mitochondrial Fragments in *OPA1* Fibroblasts

The variability was observed in the number of fragments calculated for the *OPA1* lines at day 0 (**Figure 7-29 A**). The maximum number of networks was demonstrated in the OPA1f line (mean = 194.80, SEM = 25.10), whereas the minimal value was observed in the OPA1h line (mean = 83.89, SEM = 12.99). By day 15, all *OPA1* lines apart from the OPA1f, showed an increase in their number of fragments (**Figure 7-29 B**), whereas by day 45, all *OPA1* patient lines, apart from the OPA1b, had decreased their number of fragments values (**Figure 7-29 C**). The number of fragments in the mean OPA1 (**Figure 7-29 D**) showed a significant increase between day 0 (mean = 136.04, SEM = 7.05) and day 15 (mean = 177.91, SEM = 8.60) (P = 0.0002). Following that, the number of fragments had significantly decreased by day 45 (mean = 124.12, SEM = 6.46; P < 0.0001). The number of fragments at day 45 was not significantly different from the value measured at day 0 (P = 0.2209).

For the comparison of mitochondrial network parameters between individual *OPA1* lines and the mean control, please refer to **Appendix C.2**.

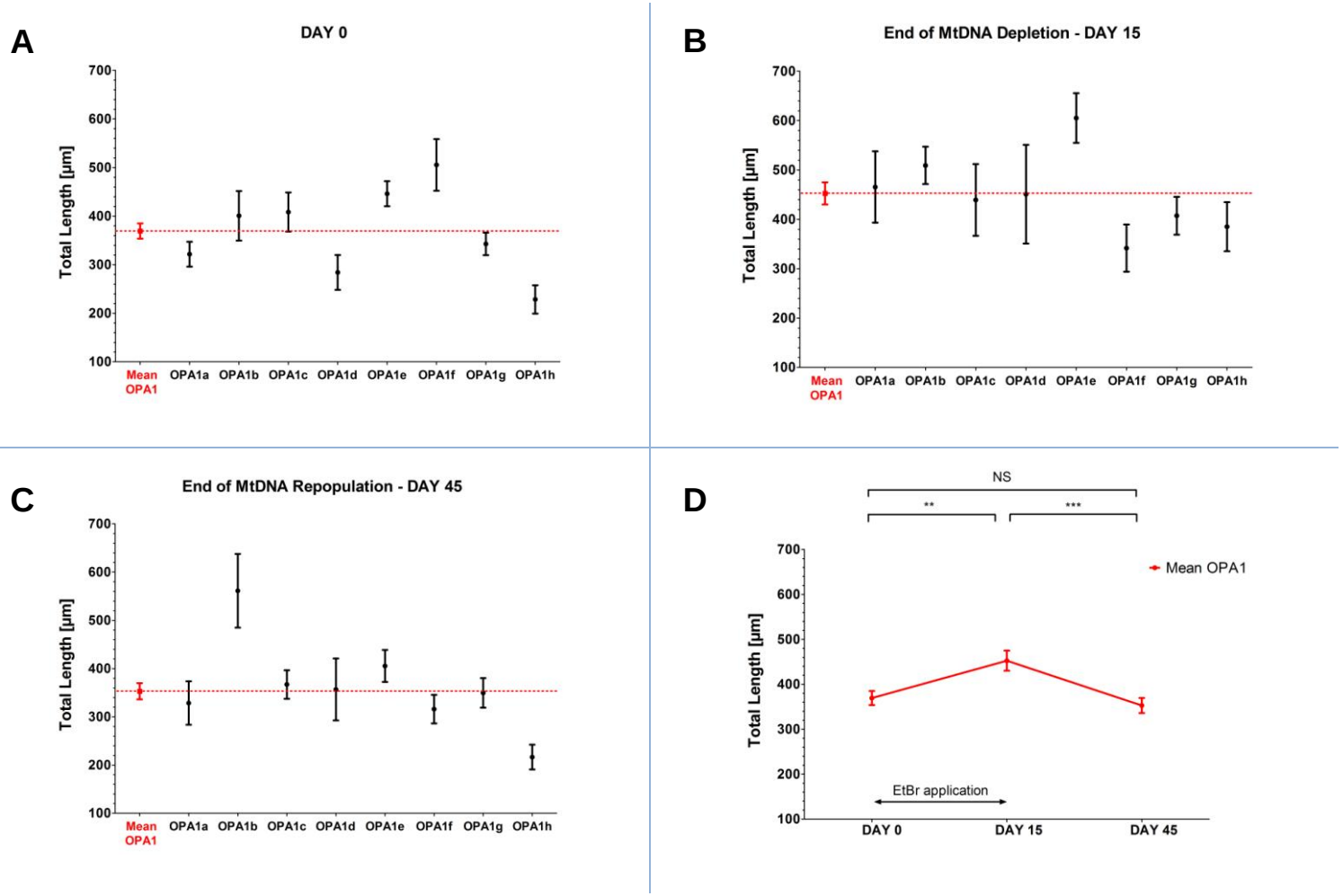

Figure 7-27 Total length of the mitochondrial network per cell in the *OPA1* fibroblast patient lines: (A) prior to EtBr-treatment (Day 0), (B) at the end of EtBr-induced mtDNA depletion (Day 15), (C) at the end of mtDNA repopulation (Day 45), and (D) at all experimental points in the mean OPA1. Each data point represents the mean total length. The error bars are presented as the standard errors of the mean (SEM). NS – non-significant at P = 0.4719; ** - refers to P = 0.0027; *** - refers to P = 0.0006.

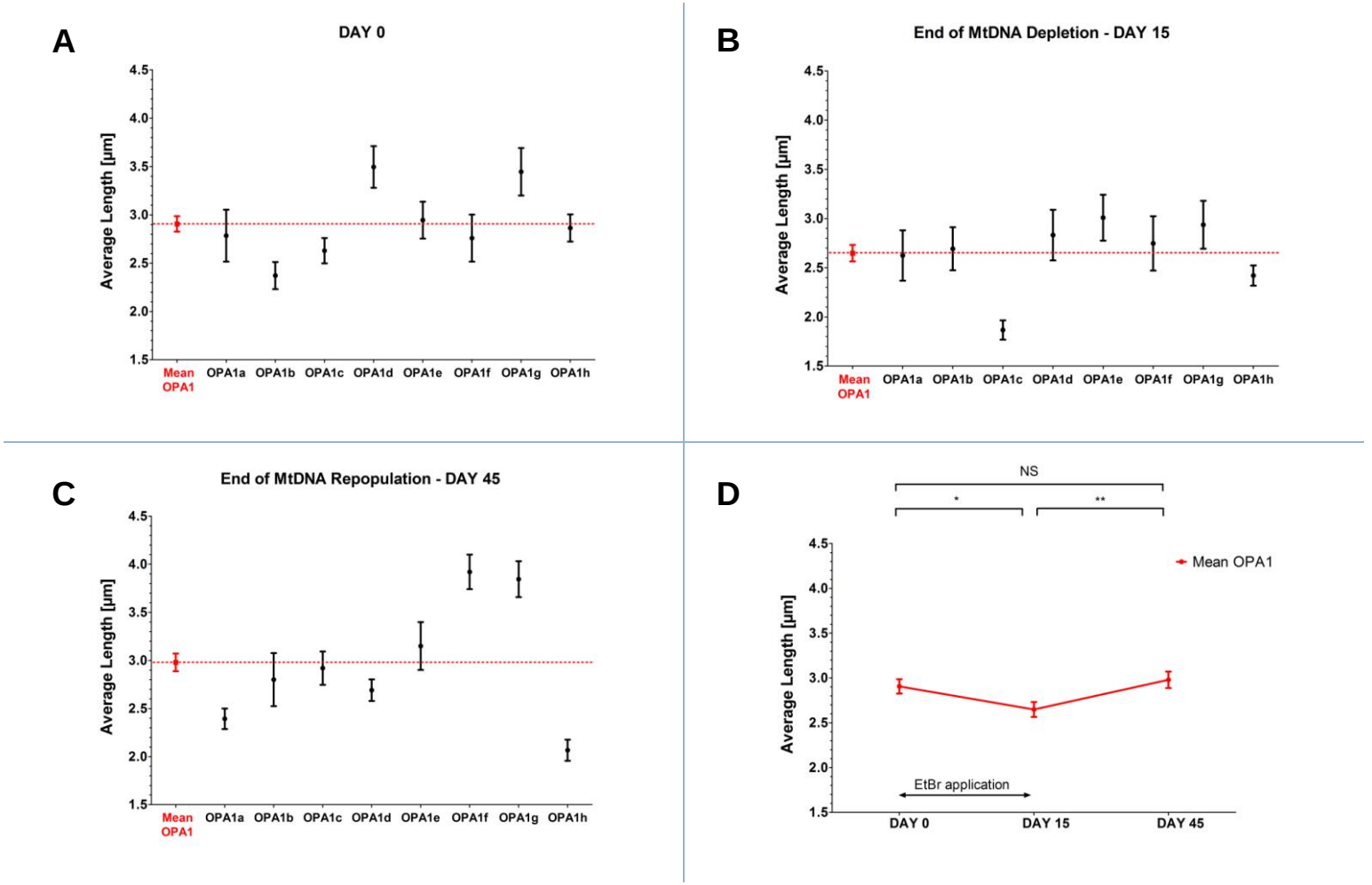

Figure 7-28 Average mitochondrial fragment length in the *OPA1* fibroblast patient lines: (A) prior to EtBr-treatment (Day 0), (B) at the end of EtBr-induced mtDNA depletion (Day 15), (C) at the end of mtDNA repopulation (Day 45), and (D) at all experimental points in the mean OPA1. Each data point represents the mean average length. The error bars are presented as the standard errors of the mean (SEM). NS – non-significant at P = 0.5476; * - refers to P = 0.0273; ** - refers to P = 0.0084.

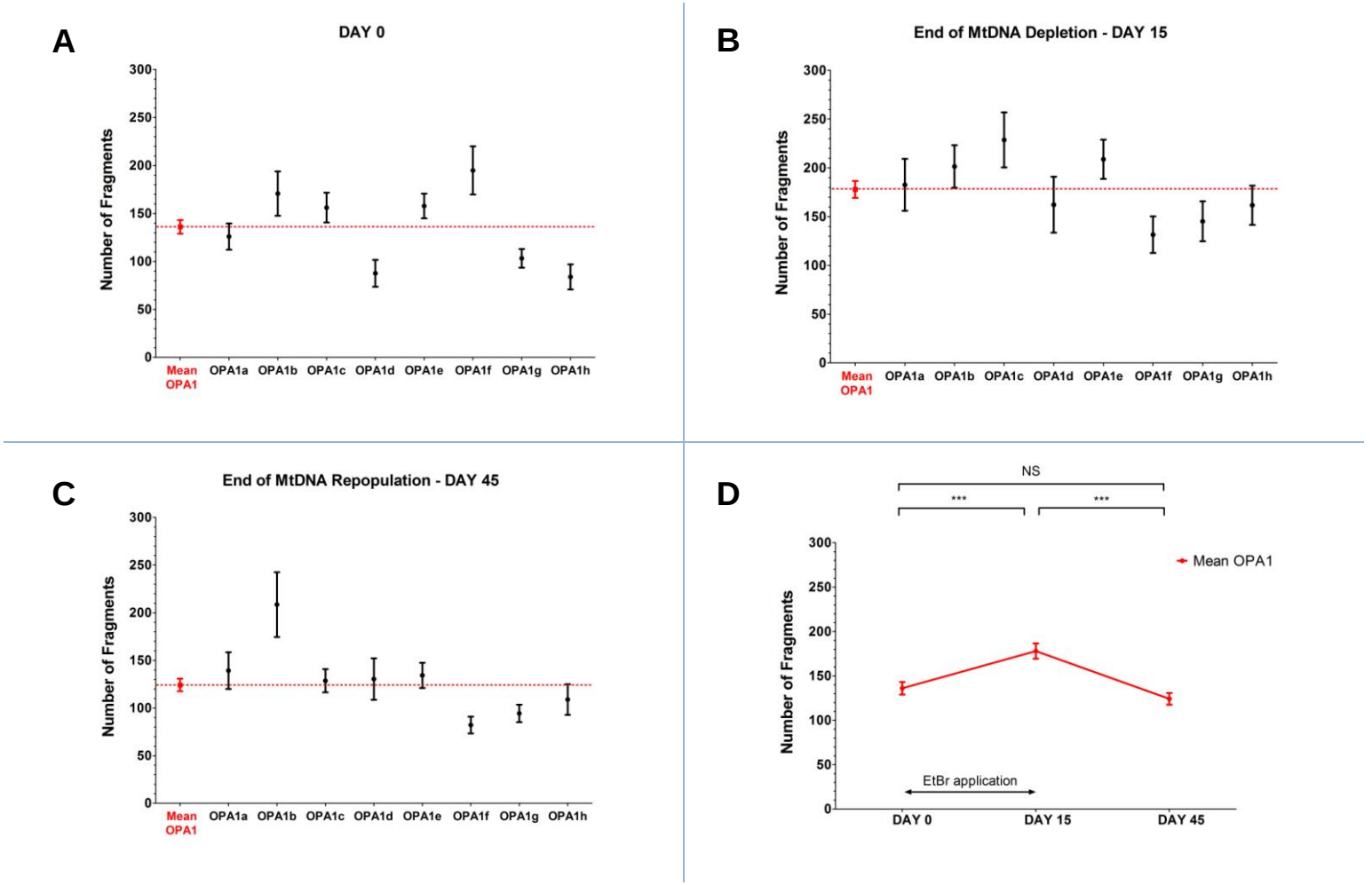

Figure 7-29 Total number of mitochondrial fragments per cell in the *OPA1* fibroblast patient lines : (A) prior to EtBr-treatment (Day 0), (B) at the end of EtBr-induced mtDNA depletion (Day 15), (C) at the end of mtDNA repopulation (Day 45), and (D) at all experimental points in the mean OPA1. Each data point represents the mean number of fragments. The error bars are presented as the standard errors of the mean (SEM). NS – non-significant at P = 0.2209; *** - refers to P = 0.0002 (day 0 vs. day 15) and P < 0.0001 (day 15 vs. day 45).

7.4.4 Mitochondrial Network – Group Comparisons

To investigate the consequence of pathogenic *POLG1* and *OPA1* mutations on mitochondrial network morphology, both patient groups were compared to the mean control in normal culture conditions at the baseline (day 0), after EtBr-induced mtDNA depletion (day 15), and following the 30-day mtDNA repopulation phase (day 45). The comparisons of the total mitochondrial length per cell (**Figure 7-30**), the average mitochondrial fragment length (**Figure 7-31**) and the total number of mitochondrial fragments per cell (**Figure 7-32**) are presented below.

7.4.4.1 Total Mitochondrial Network Length

As demonstrated in **Figure 7-30 A**, the mean POLG1 showed a significant increase in the total mitochondrial length between day 0 (mean = 314.47, SEM = 15.52) and day 15 (mean = 394.13, SEM = 29.07) (P = 0.0180). At day 45, the total length was not significantly different from the value calculated at day 0 (P = 0.6833) and day 15 (P = 0.0991). Compared with the mean control (**Figure 7-30 C**), the total length in the mean POLG1 was significantly greater at day 0 (Mean POLG1: mean = 314.47, SEM = 15.52; Mean control: mean = 236.11, SEM = 17.19; P = 0.0011). Both at day 15 and at day 45, the difference between these two groups was not statistically significant. Similarly to the mean POLG1, the mean OPA1 also demonstrated a significant increase in the total length between day 0 (mean = 369.31, SEM = 15.59) and day 15 (mean = 452.52, SEM = 22.47) (P = 0.0027; **Figure 7-30 B**), and a significant decrease by day 45 (mean = 352.80, SEM = 16.36) (P = 0.0006). The total length for the mean OPA1 at day 45 was not significantly different from the value obtained at day 0 (P = 0.4719). When the mean OPA1 was compared with the mean control (**Figure 7-30 D**), the total mitochondrial length was significantly greater in the mean OPA1, both at day 0 (the mean OPA1: mean = 369.31, SEM = 15.59; the mean control: mean = 236.11, SEM = 17.19; P < 0.0001) and at day 45 (the mean OPA1: mean = 352.80, SEM = 16.40; the mean control: mean = 267.68, SEM = 23.72; P = 0.0064). No significant difference between these two groups was observed at day 15.

7.4.4.2 Average Length of Mitochondrial Fragment

The average mitochondrial length in the mean POLG1 (**Figure 7-31 A**), showed a significant drop between day 0 (mean = 3.25, SEM = 0.10) and day 15 (mean = 2.29, SEM = 0.07) ($P < 0.0001$). No significant increase in average fragment length was observed during the repopulation phase from day 15 at day 45 ($P = 0.2575$). The average length (mean = 2.43, SEM = 0.11) at day 45 was significantly different from the value observed at day 0 ($P < 0.0001$). The comparison of the average length between the mean POLG1 and the mean control (**Figure 7-31 C**) revealed no statistically significant differences between these two groups at day 0. At the end of mtDNA depletion (day 15), the mean POLG1 had significantly smaller average length compared with the mean control (the mean POLG1: mean = 2.29, SEM = 0.07; the mean control: mean = 2.63, SEM = 0.10; $P = 0.0149$). By the end of the mtDNA repopulation phase (day 45), the mean POLG1 remained significantly shorter compared with mean control (the mean POLG1: mean = 2.43, SEM = 0.11; the mean control: mean = 3.17, SEM = 0.09; $P < 0.0001$). Similarly to the *POLG1*-mutant fibroblasts, the mean OPA1 showed a significant decrease in the average length between day 0 (mean = 2.91, SEM = 0.08) and the end of EtBr-induced mtDNA depletion (day 15) (mean = 2.65, SEM = 0.08) ($P = 0.0273$; **Figure 7-31 B**). That was followed by a significant increase in the average length observed in the mean OPA1 by day 45 (mean = 2.98, SEM = 0.09; $P = 0.0084$). The average length for the mean OPA1 at day 45 was not significantly different to the value obtained at day 0 ($P = 0.5476$). The average length in the mean OPA1 was different of borderline significance from the mean control at day 0 (the mean OPA1: mean = 2.91, SEM = 0.08; the mean control: mean = 3.15, SEM = 0.06) ($P = 0.0457$, **Figure 7-31 D**).

7.4.4.3 Total Number of Mitochondrial Fragments

The total number of mitochondrial fragments per cell in the mean POLG1 (**Figure 7-32 A**) increased significantly between day 0 (mean = 101.46, SEM = 5.97) and day 15 (mean = 168.52, SEM = 13.33) ($P < 0.0001$). This increase was maintained until day 45 and there was no significant reduction compared with day 15 ($P = 0.0735$). When compared with the mean control (**Figure 7-32 C**), the total number of mitochondrial fragments per cell in the mean POLG1 was significantly greater both at day 0 (the mean POLG1: mean = 101.46, SEM = 5.97; the mean control: mean =

75.40, SEM = 5.39; P = 0.0021) and at day 45 (the mean POLG1: mean = 138.40, SEM = 10.12; the mean control: mean = 91.03, SEM = 10.99; P = 0.0024). The difference between these two groups was not significant at day 15. Similar to *POLG1*, there was a significant increase in the number of mitochondrial fragments per cell in the mean OPA1 at the end of mtDNA depletion (day 15) (mean = 177.91, SEM = 8.60) compared with day 0 (P = 0.0002) (**Figure 7-32 B**). At day 45, the total number of fragments decreased significantly (mean = 124.12, SEM = 6.46; P < 0.0001), reaching a value that was not significantly different from the baseline at day 0 (P = 0.2209). The total number of fragments was significantly higher in the mean OPA1 compared with the mean control (**Figure 7-32 D**), both prior to EtBr treatment at day 0 (P < 0.0001) and at the end of mtDNA repopulation (day 45) (P = 0.0024). There was no significant difference between the mean OPA1 and the mean control groups at day 15.

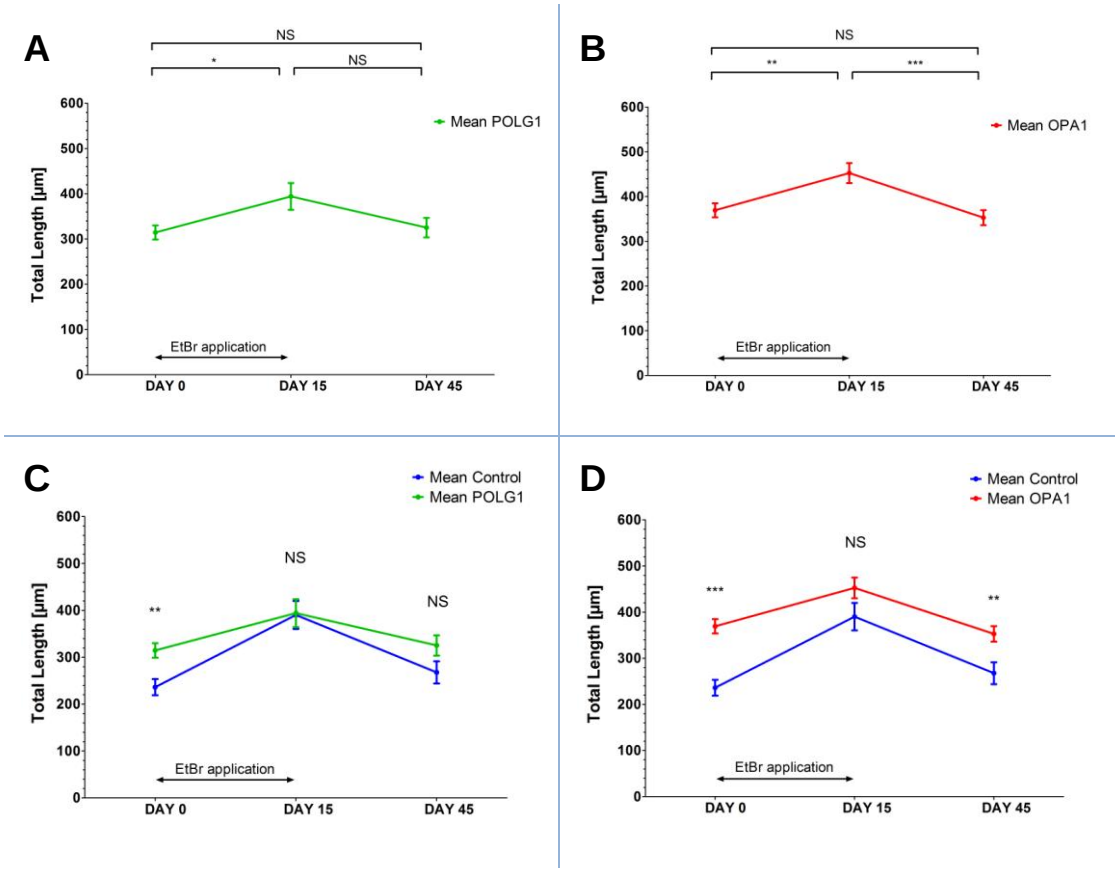

Figure 7-30 Total length of the mitochondrial network per cell: (A) in the mean POLG1, (B) in the mean OPA1, (C) comparison between the mean POLG1 and the mean control, and (D) comparison between the mean OPA1 and the mean control. Each data point represents the mean total length. The error bars are presented as the standard errors of the mean (SEM). The level of statistical significance is indicated for the comparison between: (A) different experimental time points in the mean POLG1, (B) different experimental points in the mean OPA1, (C) the mean POLG1 and the mean control groups at each time point, (D) the mean OPA1 and the mean control groups at each time point.

(A): NS – non-significant at P = 0.0991 (day 15 vs. day 45) and P value = 0.6833 (day 0 vs. day 45); * - refers to P value = 0.0180;

(B): NS – non-significant at P = 0.4719; ** - refers to P = 0.0027; *** - refers to P = 0.0006;

(C): NS – non-significant at P = 0.9310 (day 15) and P = 0.0784 (day 45), ** - refers to P = 0.0011;

(D): NS – non-significant at P = 0.1447, ** - refers to P = 0.0064, *** - refers to P < 0.0001.

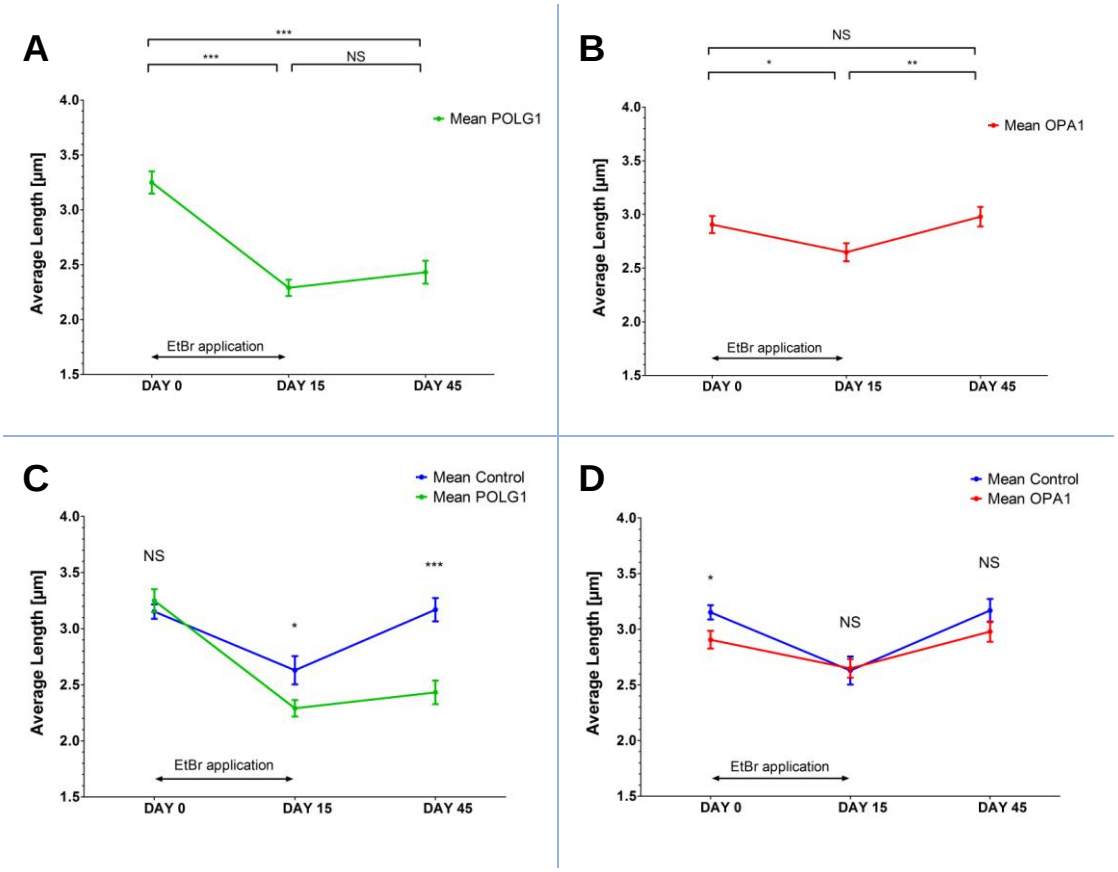

Figure 7-31 Average mitochondrial fragment length: (A) in the mean POLG1, (B) in the mean OPA1, (C) comparison between the mean POLG1 and the mean control, and (D) comparison between the mean OPA1 and the mean control. Each data point represents the mean average length. The error bars are presented as the standard errors of the mean (SEM). The level of statistical significance is indicated for the comparison between: (A) different experimental time points in the mean POLG1, (B) different experimental points in the mean OPA1, (C) the mean POLG1 and the mean control groups at each time point, (D) the mean OPA1 and the mean control groups at each time point.

(A): NS – non-significant at P = 0.2575; *** - refers to P value < 0.0001;

(B): NS – non-significant at P = 0.5476; * - refers to P = 0.0273; ** - refers to P = 0.0084;

(C): NS – non-significant at P = 0.4435, * - refers to P = 0.0149, *** - refers to P < 0.0001;

(D): NS – non-significant at P = 0.9068 (day 15) and P = 0.2375 (day 45), * - refers to P = 0.0457.

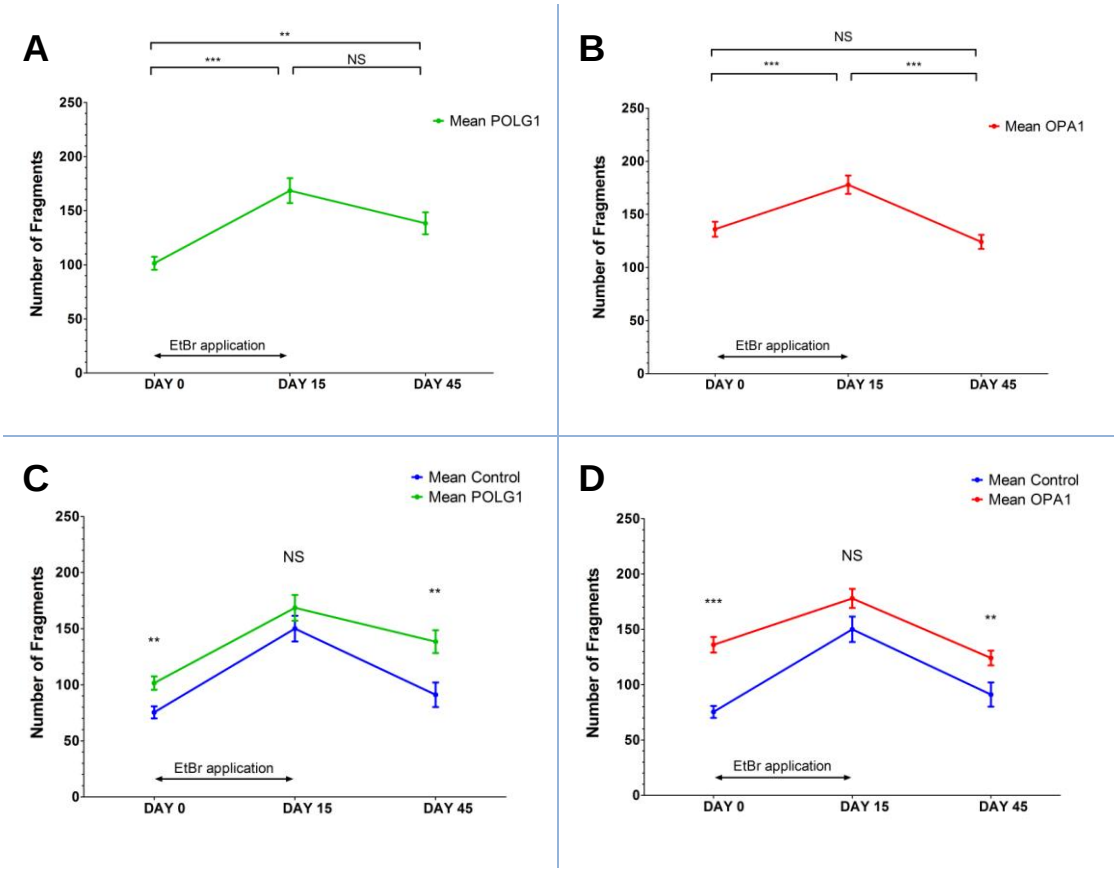

Figure 7-32 Total number of mitochondrial fragments per cell: (A) in the mean POLG1, (B) in the mean OPA1, (C) comparison between the mean POLG1 and the mean control, and (D) comparison between the mean OPA1 and the mean control. Each data point represents the mean number of fragments. The error bars are presented as the standard errors of the mean (SEM). The level of statistical significance is indicated for the comparison between: (A) different experimental time points in the mean POLG1, (B) different experimental points in the mean OPA1, (C) the mean POLG1 and the mean control groups at each time point, (D) the mean OPA1 and the mean control groups at each time point.

(A): NS – non-significant at P = 0.0735; ** - refers to P value = 0.0012; *** - refers to P < 0.0001;

(B): NS – non-significant at P = 0.2209; *** - refers to P = 0.0002 (day 0 vs. day 15) and P < 0.0001 (day 15 vs. day 45);

(C): NS – non-significant at P = 0.2967, ** - refers to P = 0.0021 (day 0) and P = .0024 (day 45);

(D): NS – non-significant at P = 0.0894, ** - refers to P = 0.0099, *** - refers to P < 0.0001.

7.5 Discussion: Repopulation Assay

The aim of this experimental assay was to investigate the kinetics of mtDNA repopulation in *POLG1*, *OPA1* and control fibroblast cell lines following a period of sustained mtDNA depletion secondary to EtBr treatment.

7.5.1 MtDNA Depletion Kinetics

Profound EtBr-induced mtDNA depletion was evident for all the investigated patient and control fibroblast cell lines. No apparent cell loss was observed during the period of EtBr treatment, suggesting that the drug concentration was sufficient to cause loss of mtDNA molecules, without being terminally toxic to the cells. Interestingly, the rate of mtDNA depletion was significantly faster in *POLG1*-mutant fibroblasts lines compared with both the mean control and the mean OPA1 groups (**Figure 7-17**). Mutations in *POLG1* have previously been associated with a reduction in POLG catalytic activity, the latter having a major impact on mtDNA replication (Graziewicz et al., 2006; Copeland, 2008). It is therefore likely that the pathological consequences of the *POLG1* mutations present in these mutant cell lines were further magnified by the addition of EtBr.

7.5.2 MtDNA Repopulation Kinetics

EtBr is a powerful inhibitor of mitochondrial DNA replication and transcription (Nass, 1970; Desjardins et al., 1985). The effect of EtBr is reversible, so when the drug is removed from the culture medium, cells should, in principle, be able to repopulate their mtDNA population (King and Attardi, 1989). However, our repopulation data revealed a clear distinction between *POLG1*, *OPA1* and control cell lines. As expected, control fibroblasts showed a complete recovery in their mtDNA population when compared to the baseline. On the other hand, the rate of mtDNA repopulation following the removal of EtBr was significantly affected in both *POLG1* and *OPA1* cell lines.

MtDNA copy number in *POLG1*-mutant cell lines remained markedly depressed following removal of EtBr, clearly indicating that the presence of the pathogenic *POLG1* mutations was having a detrimental effect on mtDNA replication, preventing any significant recovery from taking place (Graziewicz et al., 2006; Copeland, 2008).

These findings are consistent with the results previously obtained using the same repopulation assay for a cohort of five *POLG1*-mutant fibroblast cell lines (Stewart et al., 2011). It is noteworthy that despite optimal culture conditions, two of the EtBr-treated *POLG1* fibroblast lines (POLG1b, POLG1c) died prematurely during the repopulation phase. It is likely that the severe EtBr-induced mtDNA depletion, coupled with already dysfunctional mtDNA replication machinery, ultimately led to a gradual decline in mtDNA content after each successive cell division. The progressive reduction in respiratory efficiency would then have ultimately triggered cellular apoptosis, leading to growth failure of these two specific *POLG1* cell lines.

This repopulation experiment has also provided additional data linking *OPA1* mutations with impaired mtDNA maintenance. All eight *OPA1* cell lines included in this study showed a reduction in rate of mtDNA repopulation following removal of EtBr when compared with the control fibroblasts. Despite this incomplete recovery, the level of mtDNA repopulation was significantly greater than for the *POLG1*-mutant cell lines. This contrasting observation could be related to the different roles played by the POLG and OPA1 proteins in the complex process that regulates mtDNA replication (Hudson and Chinnery, 2006; Elachouri et al., 2011). *POLG1* mutations directly affect polymerase gamma activity, which is essential for mtDNA replication (Graziewicz et al., 2006; Copeland, 2008). *OPA1* mutations can result in significant disturbance in cristae morphology, which could disrupt the anchoring of mtDNA molecules to the IMM and hence exert a detrimental effect on the faithful and efficient replication of the mitochondrial genome (Landes et al., 2010; Elachouri et al., 2011). No significant difference in the kinetics of mtDNA repopulation was observed between *OPA1* cell lines from patients manifesting both pure DOA and DOA+ clinical phenotypes. The impaired mtDNA repopulation seen in this experimental assay does not therefore correlate with the heterogeneous clinical phenotype observed in human *OPA1* carriers. Similarly, no difference in mtDNA repopulation was observed between missense *OPA1* mutations affecting the GTPase domain compared with those that result in haploinsufficiency. However, this comparison is somewhat limited by the unequal number of cell lines in these two groups (GTPase: N = 2; non-GTPase: N = 6). Rather strikingly, there were obvious differences noted between the different familial *OPA1* mutations. It is tempting to speculate that different *OPA1* mutations have variable deleterious consequences on

the process of mtDNA replication. However, a larger cohort of *OPA1* cell lines is needed to address this hypothesis further.

7.6 Discussion: Mitochondrial Network Analysis

At the baseline (day 0), a significant increase in the total mitochondrial network size was observed in both *POLG1* and *OPA1* mutant fibroblasts compared with the mean control. This remarkable observation could represent a compensatory mechanism to the underlying OXPHOS defect triggered by *POLG1* and *OPA1* mutations in these mutant cell lines. The physical increase in the surface area available for mitochondrial OXPHOS could theoretically balance the reduction in mitochondrial respiratory chain efficiency seen with *POLG1* and *OPA1* mutations. Interestingly, a significant mitochondrial elongation has recently been described by *Agiers and colleagues* in four *OPA1*-mutant fibroblasts, suggesting a compensatory mechanism observed across a broad range of pathogenic *OPA1* mutations (Agier et al., 2012). The marked elevation in the total mitochondrial network size in all fibroblast lines subsequently to EtBr treatment is in keeping with the previous results demonstrating greatly enlarged mitochondrial profiles with few or none cristae, observed in cultured mouse fibroblasts and hamster kidney cells after exposure to EtBr (Nass, 1970). It is therefore tempting to speculate, that the universal compensatory mechanism allows cells to cope with the EtBr-induced stress resulting in mtDNA degradation and subsequent deficit in OXPHOS.

In basal culture conditions (day 0), both *POLG1* and *OPA1* cell lines had a significantly larger number of individual mitochondrial network fragments compared with the mean control. However, this increase needs to be taken in the context of the overall increase in the mitochondrial length. Of note, the average length of a single mitochondrion network fragment in the mean OPA1 (**Figure 7-31**) was slightly shorter compared with the mean control value. However, this difference was of a borderline significance (P = 0.0457). The lack of a dramatic reduction in the average mitochondrial length is not too surprising given that these cells were grown in standard high glucose media, where a deficient mitochondrial OXPHOS mechanism can be bypassed to a certain extent by glycolysis (Robinson et al., 1992; D'Aurelio et

al., 2001). *Zanna and colleagues* have clearly shown that significant mitochondrial network fragmentation in *OPA1*-mutant fibroblasts was only observed in glucose-free media, when cells were forced to rely exclusively on OXPHOS, which was markedly impaired in these fibroblasts (Zanna et al., 2008). At day 15 and day 45 (**Figure 7-31**), the average mitochondrial fragment length for the mean POLG1 was significantly lower compared with the mean control. These results point towards mitochondrial network fragmentation in these *POLG1*-mutant cell lines. Unlike OPA1, POLG is not directly involved in mitochondrial membrane dynamics. It is more likely that the marked impairment in mtDNA repopulation observed in these *POLG1*-mutant cell lines is resulting in a bioenergetic crisis, the latter triggering mitochondrial network fragmentation as a part of the apoptotic cascade that eventually leads to the cell death.

7.7 Concluding Remarks

This series of mtDNA depletion-repopulation experiments has provided convincing data that both *POLG1* and *OPA1* mutations can have a detrimental effect on the capacity of cell to replenish its store of mtDNA molecules following the application of an exogenous stress, in this case EtBr. The striking difference in the kinetics of mtDNA repopulation between these two mutational groups is clearly highlighting diverging pathophysiological mechanisms. This is the first study to objectively measure mitochondrial network morphology in *POLG1*-mutant fibroblasts and future studies are needed to further elucidate how *POLG1* mutations ultimately cause mitochondrial network fragmentation. Mitochondrial elongation is likely to be a common powerful compensatory mechanism and it will be interesting to determine if a similar feature is present in the other mitochondrial maintenance disorders e.g. those linked with *PEO1* and *RRM2B* mutations (Cohen and Naviaux, 2010). Finally, there is a convincing link between mitochondrial network morphology and mtDNA content, with the mitochondrial network fragmentation being a feature of cells that are severely depleted of their mtDNA molecules.

Chapter 8 Generation of hiPSCs from *OPA1*-Mutant Human Fibroblasts

Table of Contents

8.1 Introduction

OPA1 mutations are identified in approximately 60% of patients with a clinical diagnosis of DOA (Alexander et al., 2000; Delettre et al., 2000). This inherited optic neuropathy is characterised by progressive bilateral visual loss starting in early childhood secondary to the preferential loss of RGCs and subsequent degeneration of the optic nerve (Votruba, 1998; Alavi et al., 2009). A greater understanding of the factors underlying this greater vulnerability of RGCs is fundamental to our understanding of *OPA1*-related DOA.

Unlike skin or skeletal muscle, RGCs cannot be biopsied directly without causing irreversible structural damage. There is also a lack of post-mortem disease samples from patients with confirmed *OPA1* mutations. Over the past few years, a number of *OPA1* mouse models have been created to bypass this lack of human tissue samples (Lenaers et al., 2009). Two vertebrate DOA mouse models have been developed, one harbouring a heterozygous nonsense c.1051C>T (p.Q283X) *Opa1* mutation in exon 8, and the other one demonstrating a splicing c.1065+5G>A *Opa1* mutation, leading to exon 10 skipping and in-frame deletion of 27 amino acid residues in the GTPase domain (Alavi et al., 2007; Davies et al., 2007). In both models, the homozygous (*Opa1-/-*) mutant mice were embryonic lethal, whereas heterozygous (*Opa1+/-*) mice revealed a slowly progressive optic neuropathy, replicating the clinical phenotype found in non-syndromic patients with DOA (Davies et al., 2007; Yu-Wai-Man et al., 2011b). The analysis of RGC axons harvested from these heterozygous *Opa1+/-* mice revealed abnormal mitochondria with disorganised cristae structure and an elevated number of autophagosomes (Alavi et al., 2007; White et al., 2009). A third *Opa1* mouse model, harbouring a heterozygous c.2708-2711delTTAG mutation in exon 27, is currently under investigation by *Dr Guy Lenaers and colleagues* (personal communications).

Pluripotent stem cells are able to propagate indefinitely, maintaining the capability to spontaneously differentiate into any cell type from all three embryonic germ layers – ectoderm, mesoderm and endoderm (Pera et al., 2000; Hyslop et al., 2005). The first induced pluripotent stem cells (iPSCs) were generated from somatic cells following transductions with a set of specific transcription factors that are crucial for the maintenance of the pluripotent state (Takahashi and Yamanaka, 2006; Takahashi et

al., 2007; Yu et al., 2007). This seminal discovery has opened up a new frontier in scientific research, with the exciting prospect of creating a range of patient- and disease-specific human cell lines. The application of human iPSC (hiPSC) technology to generate RGCs of patients with *OPA1*-related DOA is an obvious technical innovation that would bypass the current lack of access to diseased human tissues. The aim for this study was therefore to generate hiPSCs from three *OPA1*-mutant human fibroblast lines.

8.2 Materials and Methods

The research in this chapter was carried out in collaboration with Professor Majlinda Lako's Stem Cell Group (Institute of Genetic Medicine, Newcastle University). The techniques used for the derivation of hiPSC lines and subsequent characterisation of their pluripotencial nature have previously been optimised in Professor Lako's group (Armstrong et al., 2010; Jiang et al., 2012).

8.2.1 Fibroblast Patient Lines

Three *OPA1* mutant fibroblast lines (labelled as: P1, P2 and P3) and a single control (labelled as: Control) fibroblast line, were selected for this study (**Table 8-1)**. All these cell lines had previously been investigated in **Chapter 7**. The P1, P2, P3 and Control labels used in this study correspond to the OPA1b, OPA1c, OPA1h and C3, respectively in **Chapter 7**.

Table 8-1 Properties of patient fibroblast cell lines selected for the hiPSCs generation.

Cell Line	Age (yrs)	Sex	cDNA	Consequence	Initial Passage Number	Detailed Clinical Phenotype						
						OA	Deafness	Ataxia	Myopathy	Neuropathy	PEO	Others
P1	23	M	c.889C>T	p.Q297X	4	+	-	-	-	-	-	-
P2	28	F	c.889C>T	p.Q297X	4	+	-	-	-	-	-	HSP
P3	39	M	c.1516+1G>T	Splicing defect	5	+	-	-	-	-	-	-
Control	30	F	-	-	4	-	-	-	-	-	-	-

F – female; HSP – hereditary spastic paraplegia; M – male; OA – optic atrophy; PEO – progressive external ophthalmoplegia.

8.2.2 Derivation of hiPSCs from Human Fibroblasts

The generation and culture of hiPSCs was performed in a class II vertical laminar flow hood (IVF Workstation N24; K-Systems, Birkerød, Denmark) equipped with a fitted dissection microscope (Carl Zeiss). In order to avoid contamination and maintain stable tissue culture conditions, all culture media were initially filtered (filter bottles with PES membrane; Nalgene) and warmed to 37°C (JB Aqua 18 Plus water bath; Fisher Scientific) at least 30 minutes prior to use.

To generate hiPSC lines, mycoplasma-free (details in **Section 3.12.2**) human fibroblasts of low passage numbers from three *OPA1* lines and the control (**Table 8-1**), were seeded in 12-well plates (TPP, Basel, Switzerland) at a density of 20,000 cells/well, 2 wells per a cell line. After 24 hours of incubation, fibroblasts were transduced with a lentiviral 4-in-1 human OSKM polycistronic expression vector containing two *loxP* sites flanking the OSKM expression cassette (**Figure 8-1**) (Allele Biotechnology, San Diego, USA). In this transduction system, all four reprogramming factors (*OCT4, SOX2, KLF4* and *c-MYC*) were expressed from an individual polycistronic transcript into separate polypeptides through the property of 2A "self-cleaving" peptide. To transduce fibroblasts, the transduction medium containing 1ml of fibroblast medium (**Section 3.12.1**), 1µl of reprogramming lentiviruses (multiplicity of infection, MOI = 2) and 1µl polybrene (final concentration of 6µg/ml), was added per well of a 12-well plate and evenly distributed. After 48 hours, transduction medium was replaced by fresh fibroblast medium and this procedure was repeated every 48 hours until day 6. On the sixth day post-transduction, fibroblasts were disaggregated to single cells by trypsynization with 0.05% Trypsin/EDTA (Gibco, Life Technologies), centrifuged for 5 minutes at 200g and each pellet resuspended in 500µl of fibroblast medium. Following that, cells were counted (as in **Section 3.12.3** but without Trypan Blue staining) and seeded into 6-well MEF feeder plates at a density of 15,000 cells per well. The preparation of these MEF feeder plates has been described in **Section 8.2.2.1**. Twenty four hours after re-seeding, fibroblast medium was changed to hESC/hiPSC culture medium containing: 80% Knockout™ DMEM (KO-DMEM; Gibco, Life Technologies), 20% Knockout™ Serum Replacement (Gibco, Life Technologies), 1X non-essential amino acids (Gibco, Life Technologies), 2mM L-glutamine (Gibco,

Life Technologies), 50U/ml penicillin and 50µg/ml streptomycin (Gibco, Life Technologies), and 10ng/ml human basic recombinant fibroblast growth factor (bFGF; Gibco, Life Technologies). The hESC/hiPSC medium was changed every second day until day 14th post-transduction. From thereon, cells were cultured in MEF conditioned medium (as described in **Section 8.2.2.1**), which was changed every 48 hours until the first hiPSC colonies appeared. Newly-generated, morphologically-correct hiPSC colonies were mechanically dissected into pieces and transferred into fresh MEF feeder plates for further expansion before characterisation.

Figure 8-1 Map of a lentiviral 4-in-1 human OSKM polycistronic expression vector with *loxP* sites. Reprogramming factors (*OCT4*, *SOX2*, *KLF4* and *c-MYC*) are expressed from an individual polycistronic transcript into separate polypeptides through the function of 2A "self-cleaving" peptide sites. The cDNAs are flanked by *loxP* sites which allow viral cassette removal using Cre recombinase system. (Adapted from http://www.allelebiotech.com/4-in-1-lentiviral-particles-for-ipscs-generation-human-oskm/).

8.2.2.1 MEF Feeder Plates and MEF Conditioned Medium Preparation

Mitotically-inactivated mouse embryonic fibroblasts (MEFs) were used as feeder cells to support growth and maintain the undifferentiated state of hiPSCs. To prepare MEF feeder plates, 6-well or 4-well plates (TPP) were initially gelatine-coated by adding 0.1% gelatine (Sigma-Aldrich) to each well and then incubated at 37°C for 2 hours. Following this, MEFs mitotically-inactivated with mitomycin-C (MEF CF-1 MITC; Global Stem, Rockville, USA) were thawed, resuspended in pre-warmed fibroblast medium and centrifuged at 200g for 5 minutes. After the supernatant had been aspirated, MEF cells were resuspended in fibroblast medium (**Section 3.12.1**) and counted as in **Section 3.12.3** (no Trypan Blue staining). MEFs were seeded at a density of 130,000 cells/well of a 6-well plate or 37,500 cells/well of a 4-well plate

and incubated overnight. Before placing hiPSCs in MEF feeder plates, the culture medium was changed to hESC/hiPSC medium.

MEF conditioned medium was prepared by seeding MEFs at a density of 5.6 x 10^4 cells per cm^2 of a gelatine-coated flask (TPP) as described above for 4-well and 6-well plates. After overnight incubation, fibroblast medium was replaced by hESC/hiPSC medium (0.33ml per cm^2 of a flask). MEF conditioned medium was collected daily for a maximum period of 10 days. Prior to being added to hiPSCs, the conditioned medium was supplemented with 4ng/ml bFGF (Gibco, Life Technologies), 1X insulin-transferrin-selenium-A (Gibco, Life Technologies) and filtered through a PES membrane into a fresh bottle (Nalgene).

8.2.3 Maintenance and Passaging of hiPSCs

The hiPSC colonies were cultured in an undifferentiated state on MEF feeder layers in hESC/hiPSC medium that was changed every second day. Before each medium change, hiPSC colonies were cleaned with a 21G x 2 inch needle (BD Microlance™ 3; Camlab, Cambridge, UK) or 200µl pipette tip, and any differentiated cells were removed with the aspirated medium. The sub-culture of hiPSC colonies was usually required every 5-7 days, but if for some reasons colonies were not ready to be split, MEF conditioned medium was introduced to prevent hiPSCs differentiation due to insufficient medium supplementation by the old MEF feeders. For sub-culturing, undifferentiated hiPSC colonies were manually cut into smaller pieces, detached and then transferred in 1:3 ratios onto fresh MEF feeders with hESC/hiPSC medium. An alternative method was also used, which involved detaching hiPSC colonies enzymatically by 15-minute incubation at 37°C with 1mg/ml (w/v) collagenase IV in KO-DMEM (both Gibco, Life Technologies). After incubation, the collagenase IV solution was carefully removed and replaced by hESC/hiPSC medium. Colonies were then detached and broken into smaller pieces by pipetting, before being transferred into a 15ml tube (Greiner) containing hESC/hiPSC medium. After centrifugation at 600g for 5 minutes, the supernatant was aspirated and the resulting hiPSC pellet was resuspended in fresh hESC/hiPSC medium prior to transfer onto fresh MEF feeder plates.

8.2.4 Storage of hiPSCs

8.2.4.1 Cryovial Cryopreservation of hiPSCs – Freezing

For long-term storage, whole hiPSC colonies were harvested (manually or enzymatically, as described in **Section 8.2.3**) and centrifuged at 600g for 5 minutes. The cell pellet was resuspended in 0.5ml of the filtered hiPSC freezing medium containing 60% (v/v) hESC/hiPSC medium (**Section 8.2.2**), 20% (v/v) FBS (Gibco, Life Technologies), 20% (v/v) dimethylsulphoxide (DMSO; Sigma-Aldrich) and 0.01% (v/v) Rho-associated coiled-coil forming protein serine/threonine kinase (ROCK) inhibitor (Sigma-Aldrich), the latter protecting cells from apoptosis. Human iPSC colonies were carefully resuspended in freezing medium and then pipetted drop-wise to a cryovial (Greiner), which then was placed in a Mr. Frosty isopropyl-filled freezing container (Nalgene). The freezing container was then placed in a -80ºC freezer for 24 hours and afterwards, the cryovials were transferred to liquid nitrogen for long-term storage.

8.2.4.2 Cryovial Cryopreservation of hiPSCs – Thawing

The hiPSC lines were placed into culture from the frozen cryovials stored in liquid nitrogen. Cells were quickly thawed at 37°C (JB Aqua 18 Plus water bath; Fisher Scientific), transferred drop-wise into a 30ml universal container (Fisher Scientific) with pre-warmed hESC/hiPSC medium (**Section 8.2.2**) and centrifuged for 5 minutes at 200g. The supernatant was aspirated and the hiPSC pellet gently resuspended in fresh hESC/hiPSC medium supplemented with 0.01% (v/v) ROCK inhibitor (Sigma-Aldrich), before the hiPSCs were seeded in a MEF feeder plate with 0.01% (v/v) ROCK inhibitor-supplemented hESC/hiPSC medium. The colonies were cleaned and the medium was changed with fresh hESC/hiPSC medium every 48 hours until the colonies were ready for passage.

8.2.5 *In Vitro* Characterisation of hiPSCs

8.2.5.1 Quantification of Pluripotency Gene Expression Using RT-PCR

All quantitative RT-PCRs were carried out on the first-strand cDNA samples (synthesised as described in **Section 3.9.1**) according to the protocol described in **Section 3.9.2**, with the primer sets listed in **Table 8-2**. The levels of pluripotency marker expression (endogenous and exogenous *c-MYC*) were first quantified in original hiPSC lines still containing viral cassettes to select clones, with the least amount of the viral load, for subsequent Cre-mediated excision (described in **Section 8.2.6**). Following Cre-*loxP* recombination, hiPSC lines were RT-PCR analysed again, to assess final *OCT4* expression levels (refer to **Section 8.2.6.3**). Results of the quantitative RT-PCRs were normalized to *GAPDH* and *RPL13A* expression and compared with the data obtained for the pluripotent H9 hESC line.

Table 8-2 Properties of primers used to amplify endogenous *OCT4*, total *OCT4*, endogenous *c-MYC*, exogenous *c-MYC*, Cre-recombinase gene and *GAPDH*. GenBank accession numbers: *GAPDH* NM_001256799.1; *RPL13A* NM_001270491.1.

Primer Name	Type of Primer	Primer Sequence (5' – 3')
***OCT4* Endogenous (168 bp)**		
OCT4 Endogenous F	Forward	AAG CCC TCA TTT CAC CAG G
OCT4 Endogenous R	Reverse	CTT GGA AGC TTA GCC AGG TC
***OCT4* Total (100 bp)**		
OCT4 Total F	Forward	GAG GAG TCC CAG GAC ATC AA
OCT4 Total R	Reverse	CAT CGG CCT GTG TAT ATC CC
***c-MYC* Endogenous (259bp)**		
c-MYC Endogenous F	Forward	AGC AGA GGA GCA AAA GCT CAT T
c-MYC Endogenous R	Reverse	CCA AAG TCC AAT TTG AGG CAG T
***c-MYC* Exogenous (182bp)**		
c-MYC Exogenous F	Forward	AGC AGA GGA GCA AAA GCT CAT T
c-MYC Exogenous R	Reverse	AAC CTA CAG GTG GGG TCT TTC A
Cre-recombinase gene (113 bp)		
Cre F	Forward	TGT CCG TTT GCC GGT CGT GG
Cre R	Reverse	CAG ACC GCG CGC CTG AAG AT
***GAPDH* (133 bp)**		
GAPDH F	Forward	CTG ACT TCA ACA GCG ACA CC
GAPDH R	Reverse	ATG AGG TCC ACC ACC CTG T
***RPL13A* (307 bp)**		
RPL13A F	Forward	CCT GGA GGA GAA GAG GAA
RPL13A R	Reverse	TTG AGG ACC TCT GTG TAT

8.2.5.2 DNA Sequencing

In order to confirm that *OPA1* mutations present in the original fibroblast lines were retained through the lentiviral-mediated reprogramming procedure, total genomic DNA was extracted from all *OPA1*-affected hiPSC lines, as described in **Section 3.1.1**. The specific *OPA1* mutation was then sequenced, as described in **Section 3.6**.

8.2.5.3 DNA Fingerprinting

To confirm that the generated hiPSC lines were genetically identical to the original fibroblast lines, DNA fingerprinting was performed. Total genomic DNA was extracted from hiPSC lines and the corresponding original fibroblast cell lines as described in **Section 3.1.1**. The extracted DNA samples were amplified with 16 microsatellite markers (Penta E, D18S51, D21S11, TH01, D3S1358, FGA, TPOX, D8S1179, vWA, Amelogenin, Penta D, CSF1PO, D16S539, D7S820, D13S317 and D5S818) using the PowerPlex® 16 HS System (Promega, Southampton, UK) and the fragments were then analysed on the ABI 3130xl sequence analyser (Applied Biosystems, Life Technologies). DNA fingerprinting analysis was performed by Northgene Ltd Company (http://www.paternitytesting.co.uk/) on the DNA samples provided.

8.2.5.4 Karyotype Analysis

To determine whether the viral-mediated reprogramming of human fibroblasts caused any chromosomal abnormalities in the derived hiPSCs, karyotype analysis was performed on all hiPSC lines and the original fibroblast cell lines, using a standard G-banding procedure on 20 metaphase cells. Karyotyping was carried out by the Cytogenetics Laboratory (Northern Genetics Service, Newcastle upon Tyne Hospitals NHS Foundation Trust) on the provided samples.

8.2.5.5 Immunodetection of Pluripotency Markers

For the immunodetection of pluripotency markers, hiPSC lines were cultured in 4-well MEF feeder plates for 4 days to allow sufficient colony expansion. On the fourth day, hiPSCs were fixed to detect cell surface markers (SSEA-4 and TRA-1-81), or fixed and permeabilized to detect intracellular markers (OCT4 and SOX2) of pluripotency, as described in **Section 3.10.1**. Immunostaining was carried out as described in **Section 3.10.2**, using monoclonal fluorochrome-conjugated primary

antibodies listed in **Table 8-3**. The incubation steps were performed in the dark and secondary antibodies were not required.

The fluorescent images were obtained with the inverted Axiovert 200M microscope (Carl Zeiss) equipped with x20 air objective (N.A. = 0.4; Plan APOCHROMAT, Carl Zeiss) and AxioCam HRc digital camera (Carl Zeiss), using AxioVision Rel. 4.8 software (Carl Zeiss). The images were further processed using the public domain ImageJ software (http://rsbweb.nih.gov/ij/).

Table 8-3 Properties of monoclonal fluorochrome-conjugated primary antibodies used for detection of hiPSC pluripotency markers.

Antibody	Fluorochrome	Manufacturer	Species	Dilution
anti OCT4	Fluorescein	R&D Systems, UK (IC1759F)	Rat anti-human IgG_{2B}	1:100
anti SOX2	Alexa Fluor® 488	BD Biosciences, UK (560301)	Mouse anti-human IgG_{2A}	1:100
anti SSEA-4	FITC	BD Biosciences, UK (560126)	Mouse anti-human IgG_3	1:100
anti TRA-1-81	Alexa Fluor® 647	BD Biosciences, UK (560124)	Mouse anti-human IgM	1:100

8.2.6 Cre-*loxP* Recombination System

To remove *loxP*-flanked OSKM polycistronic viral vector from reprogrammed hiPSCs, Cre-*loxP* mediated excision was performed. The Cre-recombinase gene was introduced in a Cre expression plasmid containing puromycin-resistance gene (Plasmid 17408: Puro.Cre empty vector; Addgene) (**Figure 8-2**). Prior to hiPSCs nucleofection with PvuII-linearized plasmid (10µg of plasmid/10^6 hiPSCs; for linearization procedure refer to **Section 8.2.6.1**), hiPSC colonies were harvested (manually or enzymatically, as described in **Section 8.2.3**) and centrifuged at 600g for 5 minutes. The cell pellet was washed once in PBS (Oxoid) and resuspended in 90µl of Nucleofector™ Solution (Amaxa; Lonza, Basel, Switzerland) before being nucleofected with PvuII-linearized plasmid (diluted in 10µl of Nucleofector™ Solution) using programme A23 of an Amaxa® Nucleofector device (Lonza). Following nucleofection, hiPSCs were immediately mixed with pre-warmed hESC/hiPSC medium supplemented with 0.01% (v/v) ROCK inhibitor (Sigma-

Aldrich), before being transferred at high density into a MEF feeder plate. The medium was changed at 48 hours post-nucleofection, and 24 fours later, 0.5 – 1µg/ml puromycin was supplemented to select for hiPSCs that had been successfully nucleofected. Puromycin selection was maintained for 5 days and puromycin-resistant hiPSC colonies were allowed to re-emerge for approximately 7 more days. Selected hiPSC colonies were then transferred to fresh MEF feeder plates and expanded clonally.

To validate successful Cre-mediated excision of *loxP* sites and the generation of viral cassette-free hiPSCs, genomic DNA and RNA were extracted from: (i) puromycin-resistant hiPSC clones, (ii) original (non-nucleofected) hiPSC lines, and (iii) H9 hESC line. DNA and RNA isolations (**Section 3.1.1** and **Section 3.2**, respectively) were performed on manually-harvested cells (as described in **Section 8.2.3**), which were centrifuged at 600g for 5 minutes. The obtained cell pellets were then washed once in PBS (Oxoid). To assess the efficiency of nucleofection, PCR reactions primed to detect the viral cassettes (**Section 8.2.6.2**), and RT-PCRs to determine viral gene expression levels (**Section 8.2.6.3**), were performed.

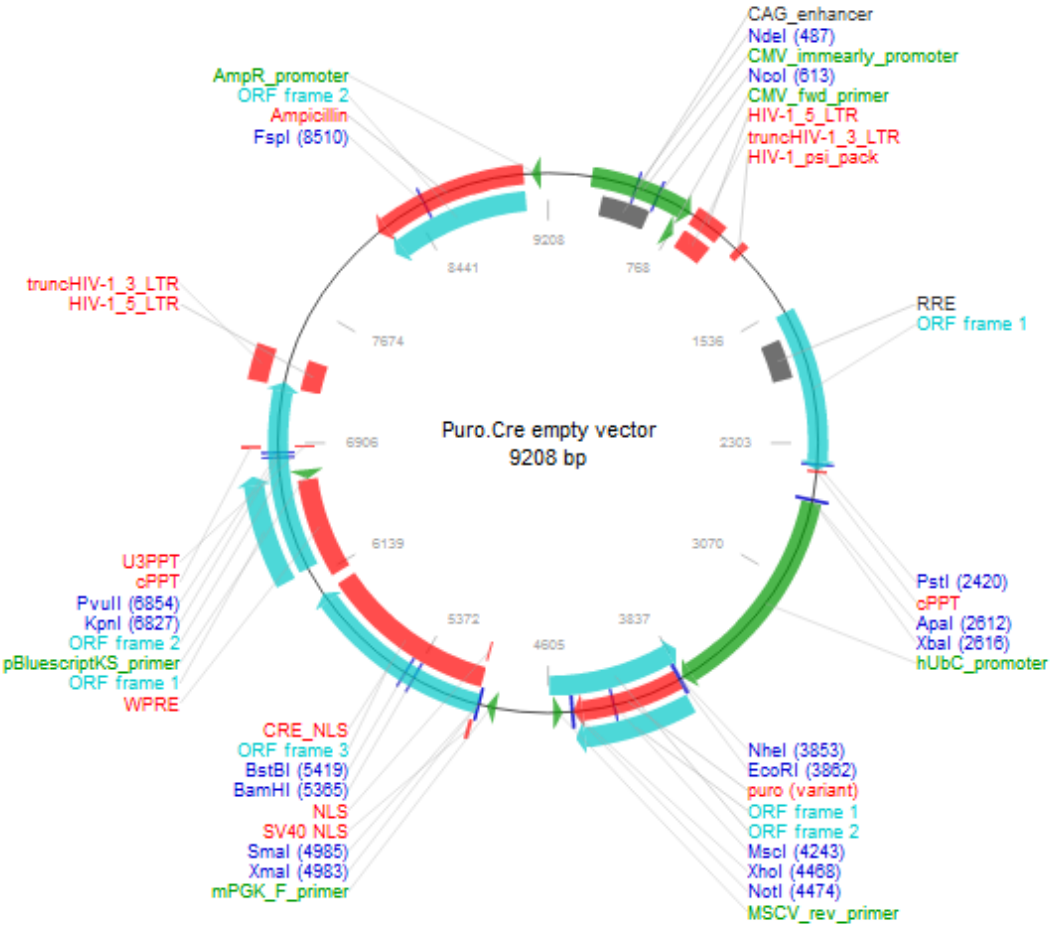

Figure 8-2 Map of the puro – Cre plasmid. (Reproduced from: http://www.addgene.org/browse/sequence/8585/).

8.2.6.1 Puro-Cre Plasmid Linearization

In order to generate stable hiPSC clones post-nucleofection, the puro-Cre plasmids were initially linearized in a PvuII-mediated reaction. Briefly, the plasmids (0.824µg/µl) were incubated overnight at 37°C with PvuII-HF restriction enzyme (4U per 1µg of plasmid; New England Biolabs, Hitchin, UK), 1X Buffer 4 (New England Biolabs) and dH_2O. The next day, the PvuII-HF enzyme was inactivated by incubating for 20 minutes at 80°C. The validation of linearization was assessed by running a 0.7% (w/v) TAE agarose gel and comparing the obtained bands with the band of undigested puro-Cre plasmids (protocol described in **Section 3.4**). Following successful linearization, the digested plasmids were cleaned from the remaining enzymatic reactions using QIAquick™ Gel Extraction Kit (Qiagen) according to the

manufacturer's protocol. In brief, the plasmids in the digestion mixture were initially added to 3 volumes of QG Buffer (Qiagen) and 1 volume of isopropanol, before being applied to QIAquick® spin-columns (up to 10µg of plasmid per column). Further steps were carried out as described in **Section 3.5**.

8.2.6.2 PCR-mediated Viral Cassette Detection

PCRs were performed using the same equipment as described in **Section 3.3**. Each individual DNA sample (30ng) was amplified in a PCR master mix containing: colourless 5X GoTaq® Reaction Buffer (10µl/reaction; Promega), 2mM dNTP Mix (5µl/reaction; VH Bio), 10 µM forward and reverse primers (both 2µl/reaction; Sigma-Aldrich) (**Table 8-4**), 5U/µl GoTaq® DNA Polymerase (0.25µl/reaction; Promega) and dH_2O (filled up to 50 µl/reaction). Each DNA sample was amplified using primers which allowed the detection of: (i) two viral cassette products of different sizes (~250 bp and ~600 bp); (ii) the Cre-recombinase transgene; and (iii) *GAPDH* housekeeping gene as a loading control.

DNA was amplified under the following conditions: an initial denaturation step at 95°C for 2 minutes, then 35 cycles of denaturation at 95°C for 1 minute, annealing at 56°C for 1 minute, and extension at 72°C for 1 minute. For the last cycle, a final extension step of 5 minutes at 72°C was performed before cooling the sample to 4°C. Amplified DNA samples were further validated on the agarose gel as described in **Section 3.4**.

Table 8-4 Properties of primers used to amplify short and long OSKM polycistronic viral vector cassette products, Cre-recombinase gene and *GAPDH*. GenBank accession number: *GAPDH* NM_001256799.1; [1)] product size estimated only approximately as the actual sequence information is considered proprietary by Allele Biotechnology, USA.

Primer Name	Type of Primer	Primer Sequence (5' – 3')
Viral cassette short product (~250 bp[1)])		
EF1α	Forward	TCA AGC CTC AGA CAG TGG TTC
OCT4 Endogenous	Reverse	CTT GGA AGC TTA GCC AGG TC
Viral cassette long product (~ 600bp[1)])		
EF1α	Forward	TCA AGC CTC AGA CAG TGG TTC
OCT4 Total	Reverse	CAT CGG CCT GTG TAT ATC CC
Cre-recombinase gene (113 bp)		
Cre F	Forward	TGT CCG TTT GCC GGT CGT GG
Cre R	Reverse	CAG ACC GCG CGC CTG AAG AT
***GAPDH* (133 bp)**		
GAPDH F	Forward	CTG ACT TCA ACA GCG ACA CC
GAPDH R	Reverse	ATG AGG TCC ACC ACC CTG T

8.2.6.3 Cre-mediated Recombinase Assessment Using RT-PCR

Following first-strand cDNA synthesis (as described in **Section 3.9.1**), RT-PCRs were performed according to the protocol illustrated in **Section 3.9.2** and normalized to *GAPDH* and *RPL13A* expression (all primer sets listed in **Table 8-2**). Quantitative PCRs primed to detect Cre-recombinase transgene were performed to allow a precise assessment of the nucleofection efficiency. The remaining viral contribution to *OCT4* expression was calculated by subtracting the endogenous *OCT4* expression from the total *OCT4* expression.

8.3 Results

8.3.1 Derivation of hiPSCs from Human Fibroblasts

The efficiency of retroviral transduction and the number of morphologically-correct hiPSC colonies generated have been summarized in **Table 8-4**. The hiPSC colonies obtained had morphological characteristics typical of hESCs, with a high cellular density and an elevated nuclear-to-cytoplasmic ratio. The subsequent stages of hiPSC colony formation have been illustrated in **Figure 8-3**.

Table 8-5 The final outcome of the viral-mediated derivation of hiPSCs from all studied fibroblast cell lines.

Cell Line	Efficiency of Transduction	Number of Clones Established
P1	0.00467%	3
P2	0.00600%	2
P3	0.00133%	1
Control	0.14800%	6

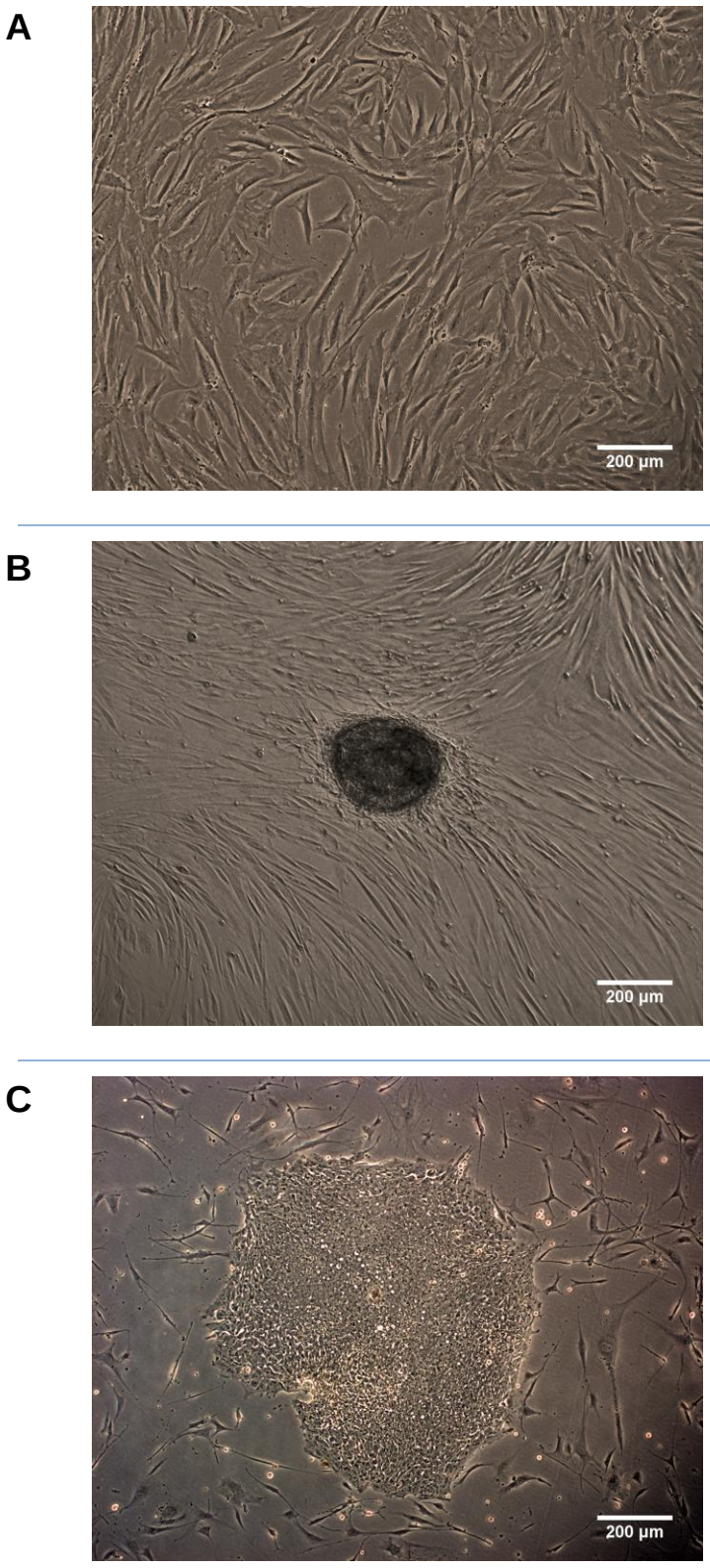

Figure 8-3 Subsequent stages of hiPSCs derivation for the P1 fibroblasts. (A) The morphology of the original fibroblasts. (B) The morphology of primary hiPSC clone at day 21 and (C) at day 42 post-transduction. Brightfield phase contrast images were taken with the Axiovert 200M microscope (Carl Zeiss) equipped with the Plan-Neofluar 5x/0.15 air objective (Carl Zeiss).

8.3.2 *In Vitro* Characterisation of hiPSCs

To allow for a descriptive characterisation, our aim was to clonally expand two independent hiPSC clones from each individual parent fibroblast line. The only exception was the P3 patient line, for which only a single hiPSC line was available. For the P1 line and the control fibroblasts, for which more than two hiPSC clones were available, two were randomly selected for the subsequent analysis. The expanded hiPSC lines were named as follows: (i) P1-1 and P1-2 from the P1 fibroblast line; (ii) P2-1 and P2-2 from the P2 fibroblasts; (iii) P3-1 from the P3 fibroblast line; and (iv) C-1 and C-2 from the control fibroblast line.

8.3.2.1 Quantification of *c-MYC* Expression Using RT-PCR

The RT-PCR analysis was performed on all expanded hiPSC clones to measure the endogenous and exogenous expressions of one of the pluripotency markers used: *c-MYC*. The rationale was to select the hiPSC clone (per patient line) that showed the lower level of exogenous *c-MYC* expression, since the lesser the initial viral load was, the more successful Cre-mediated viral removal could have been. The RT-PCR detection of endogenous and exogenous *c-MYC* transcript expression levels is presented in **Figure 8-4**, with the hESC H9 line used as a control.

The RT-PCR analysis confirmed both the endogenous and the viral/exogenous expression of *c-MYC* transcript in all investigated hiPSC clones (**Figure 8-4)**. As expected, the hESC H9 line, which lacked the polycistronic viral cassette, showed only the endogenous *c-MYC* expression. There was variability in the levels of exogenous *c-MYC* transcripts between the two hiPSC lines originating from the same parent fibroblast line (**Figure 8-4**). For the subsequent experimental stage of characterisation, the hiPSC clone with the lowest viral *c-MYC* expression was selected per original fibroblast line: P1-2, P2-2, P3-1 and C-1 line.

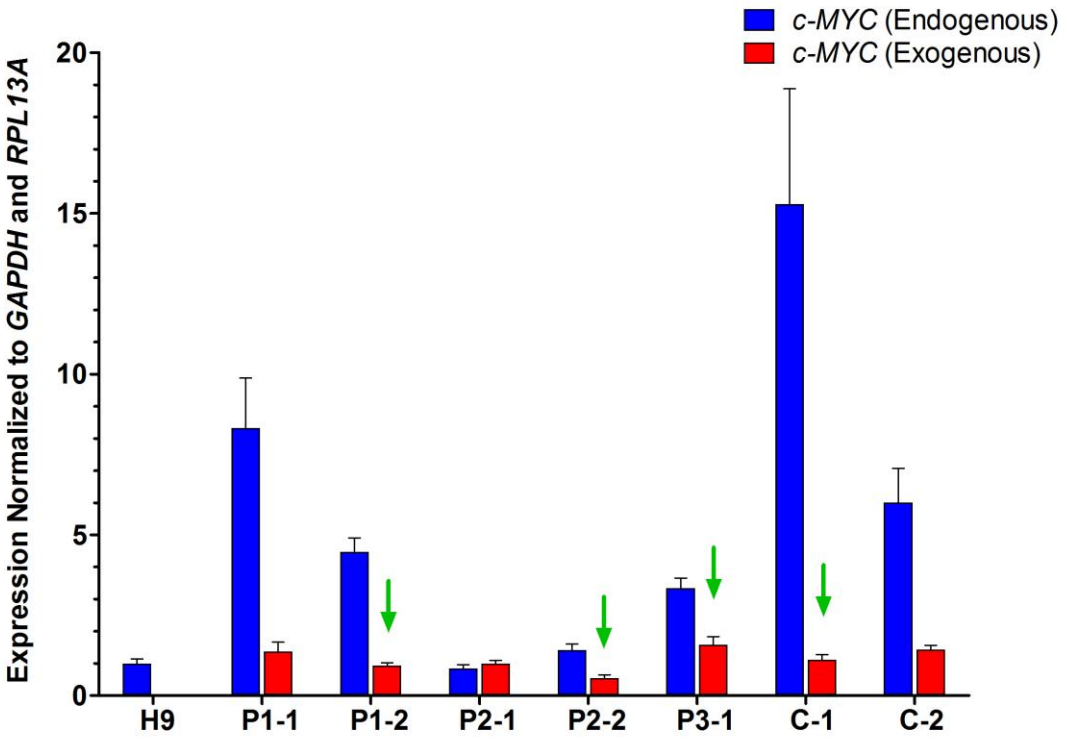

Figure 8-4 Endogenous and exogenous expression patterns of *c-MYC* transcript in hiPSC lines and H9 hESC line. Per each original fibroblast line, the hiPSC clone with the lowest exogenous *c-MYC* expression (indicated with the green arrow) was selected. Expression levels of *c-MYC* transcript are normalized to *GAPDH* and *RPL13A* housekeeping genes and relative to expression in ESC H9 line. The error bars indicate the standard errors of the mean (SEM).

8.3.2.2 *OPA1* Sequencing

Sanger sequencing confirmed that the specific *OPA1* mutations present in the original fibroblast lines were retained in the corresponding generated hiPSC lines: c.889C>T (p.Q297X) in the P1 and P1-2 lines (**Table 8-6**); c.889C>T (p.Q297X) in the P2 and P2-2 lines (**Table 8-7**); c.1516+1G>T (splice defect) in the P3 and P3-1 lines (**Table 8-8**).

Table 8-6 Sequence chromatograms showing the c.889C>T (p.Q297X) heterozygous *OPA1* mutation in the original P1 fibroblasts and the P1-2 hiPSCs. Chromatograms were generated with SeqScape® v2.1.1 software (Applied Biosystems, Life Technologies).

P1 (original fibroblast line)	P1-2 (hiPSC line)
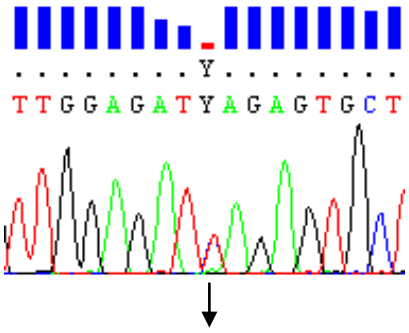 c.889C>T	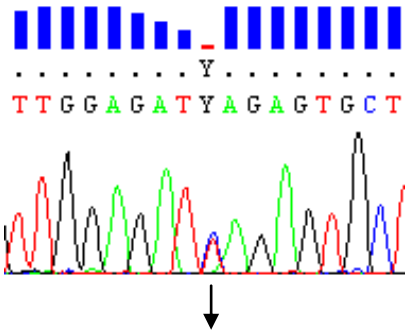 c.889C>T

Y – refers to C or T in IUPAC nucleotide code.

Table 8-7 Sequence chromatograms showing the c.889C>T (p.Q297X) heterozygous *OPA1* mutation in the original P2 fibroblasts and the P2-2 hiPSCs. Chromatograms were generated with SeqScape® v2.1.1 software (Applied Biosystems, Life Technologies).

P2 (original fibroblast line)	P2-2 (hiPSC line)
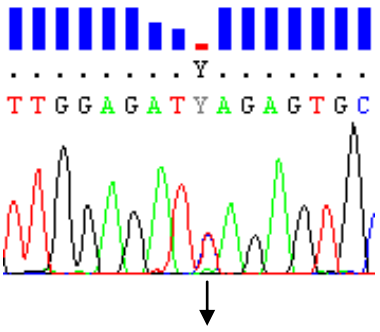 c.889C>T	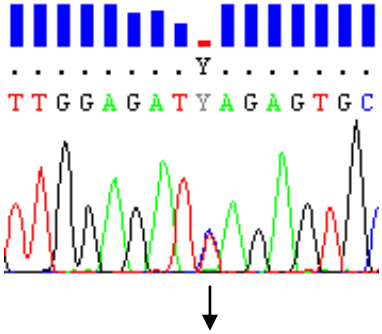 c.889C>T

Y – refers to C or T in IUPAC nucleotide code.

Table 8-8 Sequence chromatograms showing the c.1516+1G>T (splice defect) heterozygous *OPA1* mutation in the original P3 fibroblasts and the P3-1 hiPSCs. Chromatograms were generated with SeqScape® v2.1.1 software (Applied Biosystems, Life Technologies).

P3 (original fibroblast line)	P3-1 (hiPSC line)
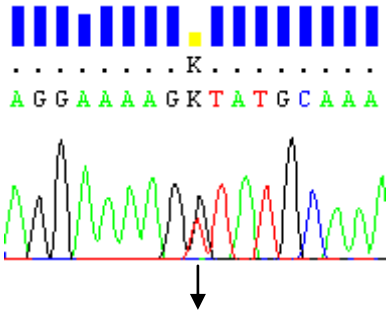 c.1516+1G>T	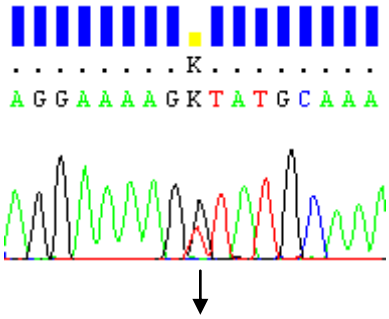 c.1516+1G>T

K – refers to G or T in IUPAC nucleotide code.

8.3.2.3 DNA Fingerprinting

DNA fingerprinting confirmed that all generated hiPSC lines were genetically identical to the original fibroblast lines from which they were derived. Similar allele callings for all 16 different microsatellite markers were obtained for each original fibroblast-hiPSC pair (**Table 8-9**).

Table 8-9 DNA fingerprinting results for each pair of original fibroblast and corresponding hiPSC lines. Specific allele numbers for 16 different microsatellite markers are presented for both chromosomes. Matching results for the original fibroblasts and generated from them hiPSCs indicate their common genotypic background.

Sample	Microsatellite Marker															
	D3S1358	**TH01**	**D21S11**	**D18S51**	**Penta E**	**D5S818**	**D13S317**	**D7S820**	**D16S539**	**CSF1PO**	**Penta D**	**Amelogenin**	**vWA**	**D8S1179**	**TPOX**	**FGA**
Control	15 16	9.3 9.3	29 30	16 20	15 19	10 13	8 11	10 11	12 12	10 11	10 10	X X	16 17	10 14	11 11	20 24
C-1	15 16	9.3 9.3	29 30	16 20	15 19	10 13	8 11	10 11	12 12	10 11	10 10	X X	16 17	10 14	11 11	20 24
P1	16 16	9 9	30 30	16 18	14 18	12 13	8 11	9 10	11 12	10 13	9 12	X Y	17 18	8 10	8 11	20 23
P1-2	16 16	9 9	30 30	16 18	14 18	12 13	8 11	9 10	11 12	10 13	9 12	X Y	17 18	8 10	8 11	20 23
P2	14 16	9 9	30 32.2	16 16	10 15	12 13	9 13	9 10	11 12	11 13	8 11	X X	17 18	10 13	11 11	21 23
P2-2	14 16	9 9	30 32.2	16 16	10 15	12 13	9 13	9 10	11 12	11 13	8 11	X X	17 18	10 13	11 11	21 23
P3	15 17	6 9	30 30.2	14 18	14 18	12 13	8 11	8 12	11 13	12 13	12 13	X Y	18 18	14 16	8 11	21 23
P3-1	15 17	6 9	30 30.2	14 18	14 18	12 13	8 11	8 12	11 13	12 13	12 13	X Y	18 18	14 16	8 11	21 23

8.3.2.4 Karyotype Analysis

The G-banding procedure was performed on all original primary fibroblasts and the derived hiPSC lines. Karyotype analysis of the control fibroblast line revealed the (15;21)(q10;q10) chromosomal translocation in 2/20 metaphase cells, whereas only normal (46, XX) karyotypes were obtained for all 20 metaphase cells from the C-1 hiPSC line (**Figure 8-5**). The P1 fibroblast line showed chromosome 8 trisomy mosaicism (2/20 metaphase cells), whereas the P1-2 hiPSC line revealed just normal (46, XY) karyotypes for all 20 metaphase cells (**Figure 8-6**). Both the P2 fibroblast and P2-2 hiPSC lines had entirely normal (46, XX) karyotypes (**Figure 8-7**). Similarly, the P3 fibroblast and P3-1 hiPSC lines revealed only normal (46, XY) karyotypes for all investigated metaphase cells (**Figure 8-8**).

Figure 8-5 Karyograms of the control fibroblast line and the C-1 hiPSC line. The entire numbered chromosome complement is demonstrated individually for both cell lines. In the control fibroblasts, translocation (15;21)(q10;q10) mosaicism (indicated with red arrows) was observed (2/20 metaphase cells, otherwise normal 46, XX karyotype). The C-1 hiPSC line showed normal 46, XX karyotype in all 20 metaphase cells.

Control (fibroblast line)	**C-1 (hiPSC line)**
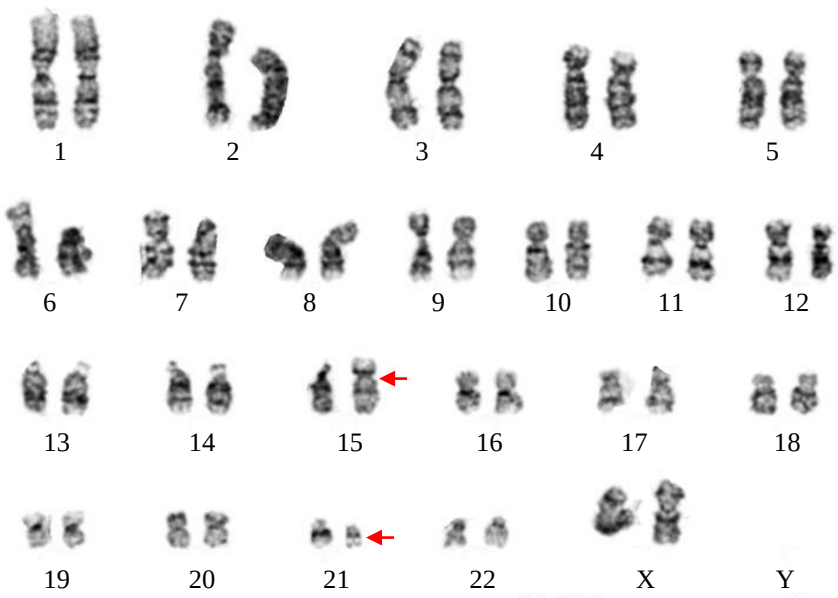	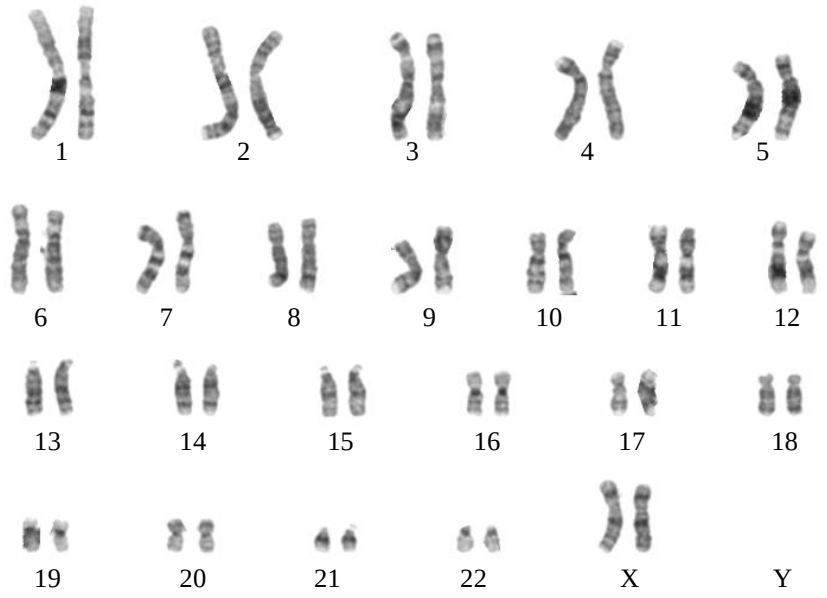
18/20 metaphase cells: 46, XX **2/20 metaphase cells: 46, XX, der(15;21)(q10;q10)**	**20/20 metaphase cells: 46, XX**

Figure 8-6 Karyograms of the P1 fibroblast line and the P1-2 hiPSC line. The entire numbered chromosome complement is demonstrated individually for both cell lines. In the P1 fibroblasts, chromosome 8 trisomy mosaicism (indicated with red arrows) was observed (2/20 metaphase cells, otherwise normal 46, XY karyotype). The P1-2 hiPSC line showed normal 46, XY karyotype in all 20 metaphase cells.

P1 (fibroblast line)	P1-2 (hiPSC line)
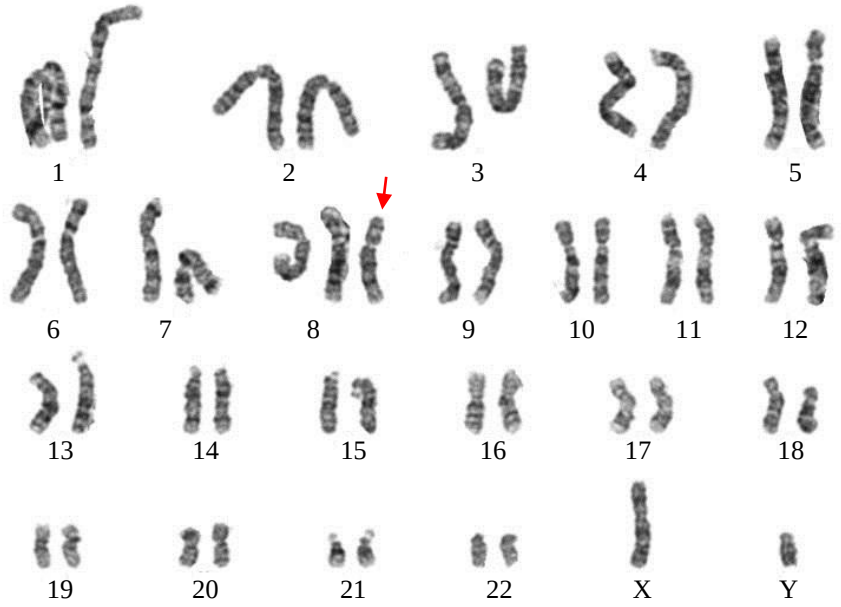	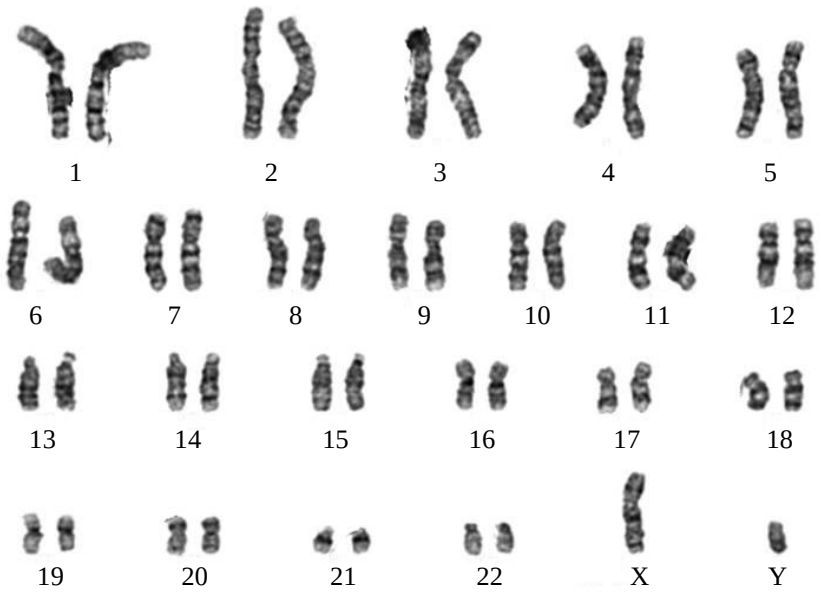
18/20 metaphase cells: 46, XY **2/20 metaphase cells: 46, XY,+8**	**20/20 metaphase cells: 46, XY**

Figure 8-7 Karyograms of the P2 fibroblast line and the P2-2 hiPSC line. The entire numbered chromosome complement is demonstrated individually for both cell lines. The P2 fibroblast and the P2-2 hiPSC lines showed normal 46, XX karyotypes in all metaphase cells.

P2 (fibroblast line)	P2-2 (hiPSC line)
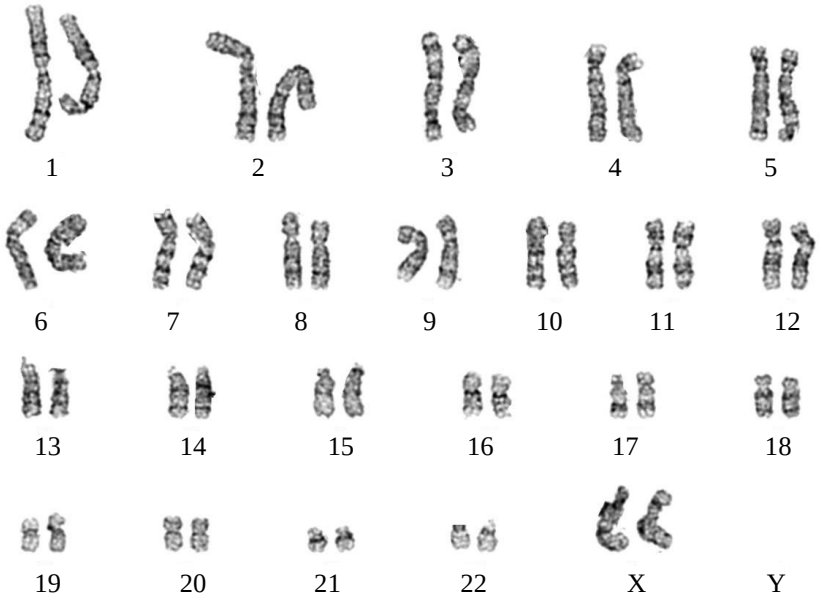	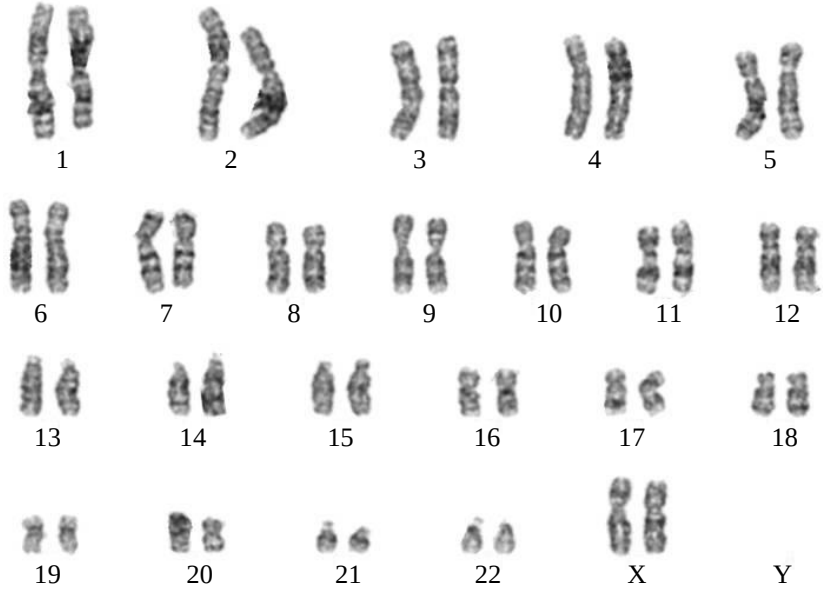
20/20 metaphase cells: 46, XX	**20/20 metaphase cells: 46, XX**

Figure 8-8 Karyograms of the P3 fibroblast line and the P3-1 hiPSC line. The entire numbered chromosome complement is demonstrated individually for both cell lines. The P3 fibroblast and the P3-1 hiPSC lines showed normal 46, XY karyotypes in all metaphase cells.

P3 (fibroblast line)	P3-1 (hiPSC line)
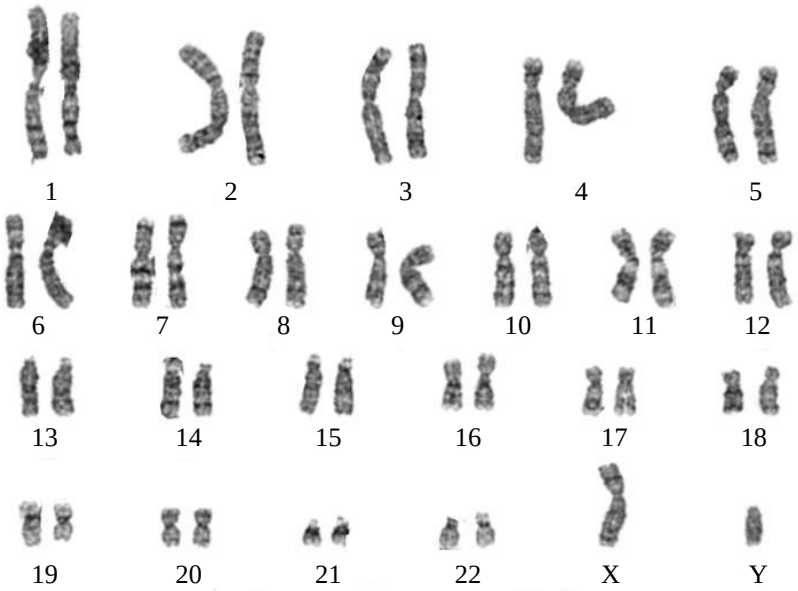	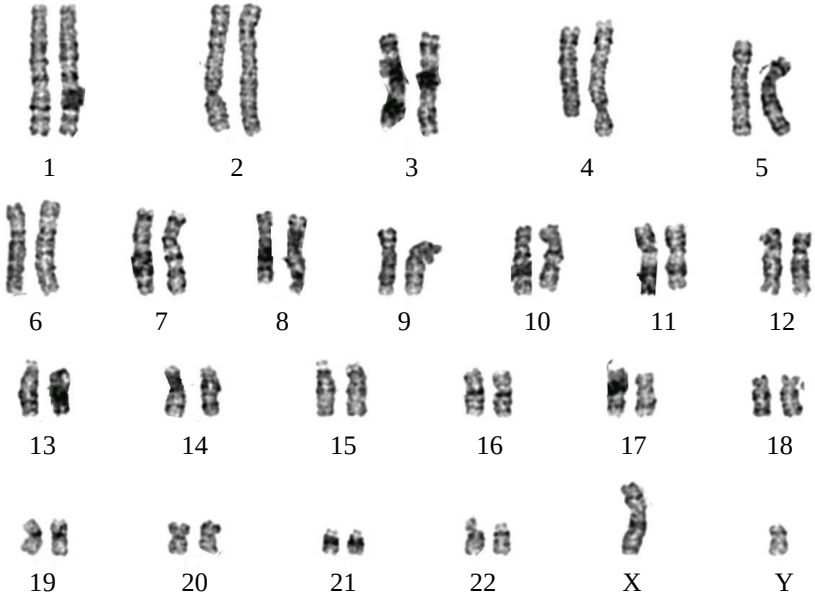
20/20 metaphase cells: 46, XY	**20/20 metaphase cells: 46, XY**

8.3.2.5 Immunodetection of Pluripotency Markers

Immunocytochemical analysis revealed the expected patterns of nuclear expression of OCT4 (**Figure 8-9**) and SOX2 (**Figure 8-10**), as well as the expression of cell surface pluripotency markers SSEA-4 (**Figure 8-11**) and TRA-1-81 (**Figure 8-12**), in all characterised hiPSC lines.

Figure 8-9 Immunocytochemical analysis of hiPSC lines for the expression of OCT4. Nuclei were labelled with Hoechst 33342, whereas OCT4 was detected with fluorescein-conjugated primary antibody. All images were captured with a 20x air objective. Scale bar: 100µm.

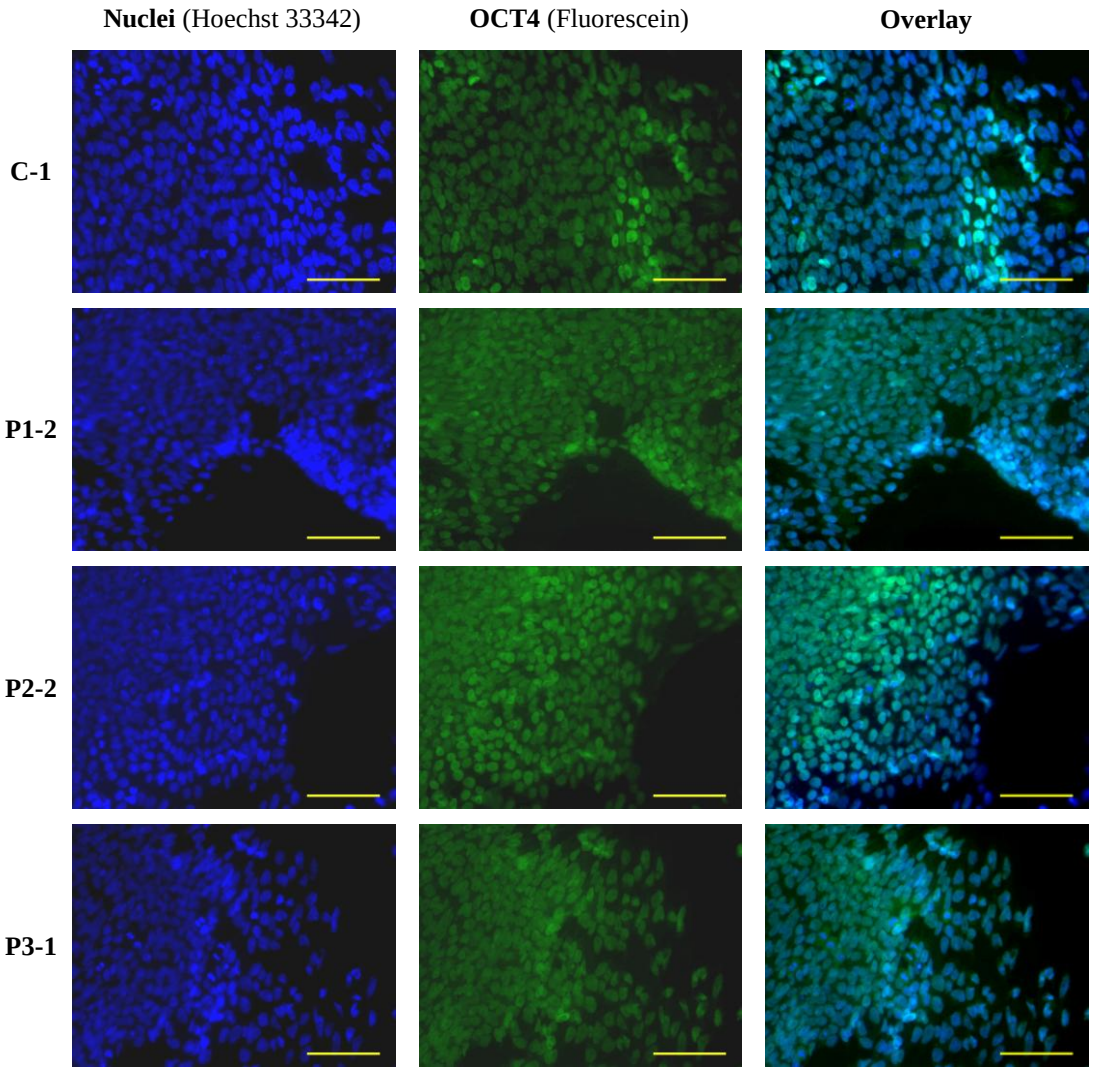

Figure 8-10 Immunocytochemical analysis of hiPSC lines for the expression of SOX2. Nuclei were labelled with Hoechst 33342, whereas SOX2 was detected with Alexa Fluor® 488-conjugated primary antibody. All images were captured with a 20x air objective. Scale bar: 100µm.

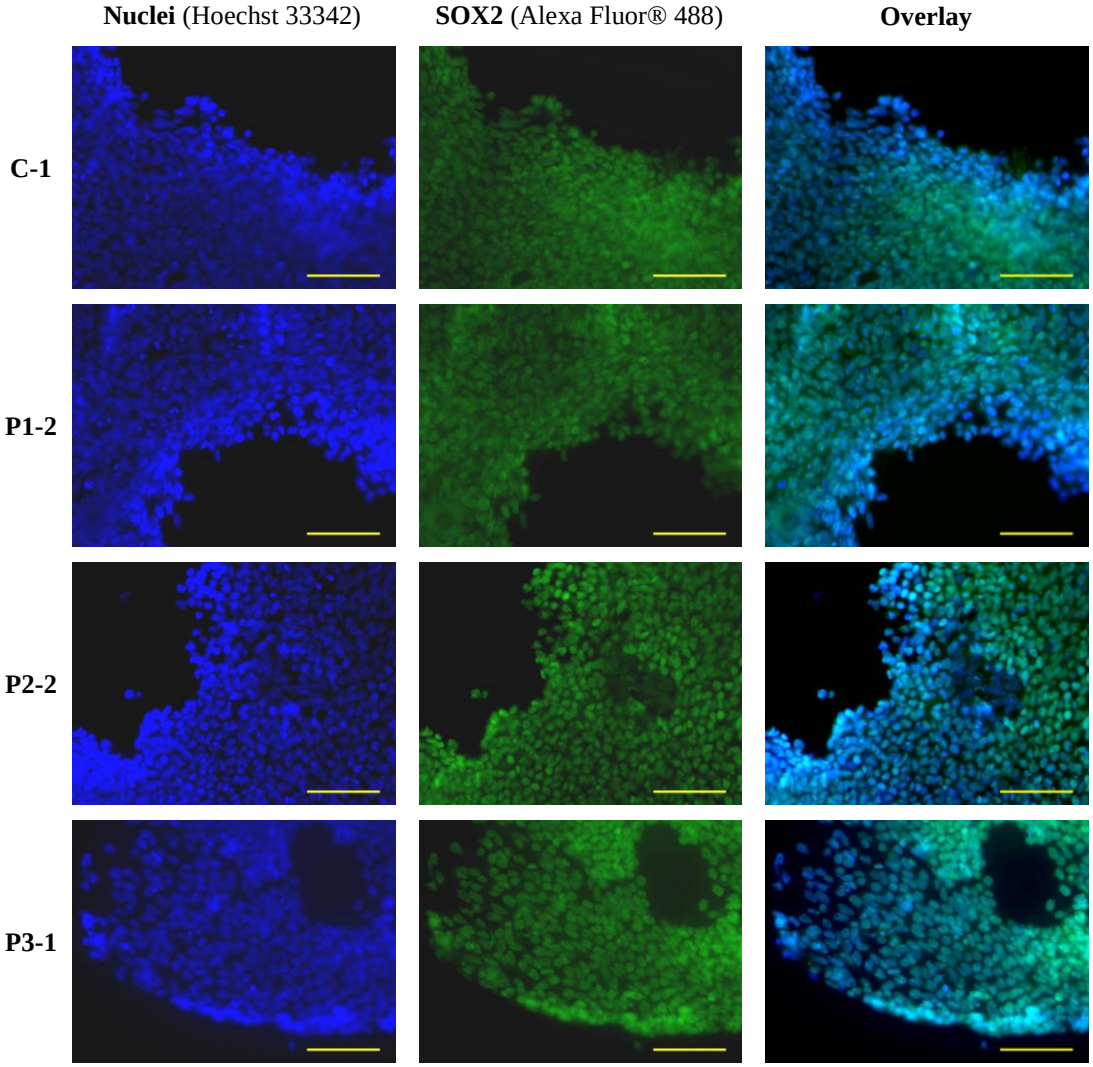

Figure 8-11 Immunocytochemical analysis of hiPSC lines for the expression of SSEA-4. Nuclei were labelled with Hoechst 33342, whereas SSEA-4 was detected with FITC-conjugated primary antibody. All images were captured with a 20x air objective. Scale bar: 100µm.

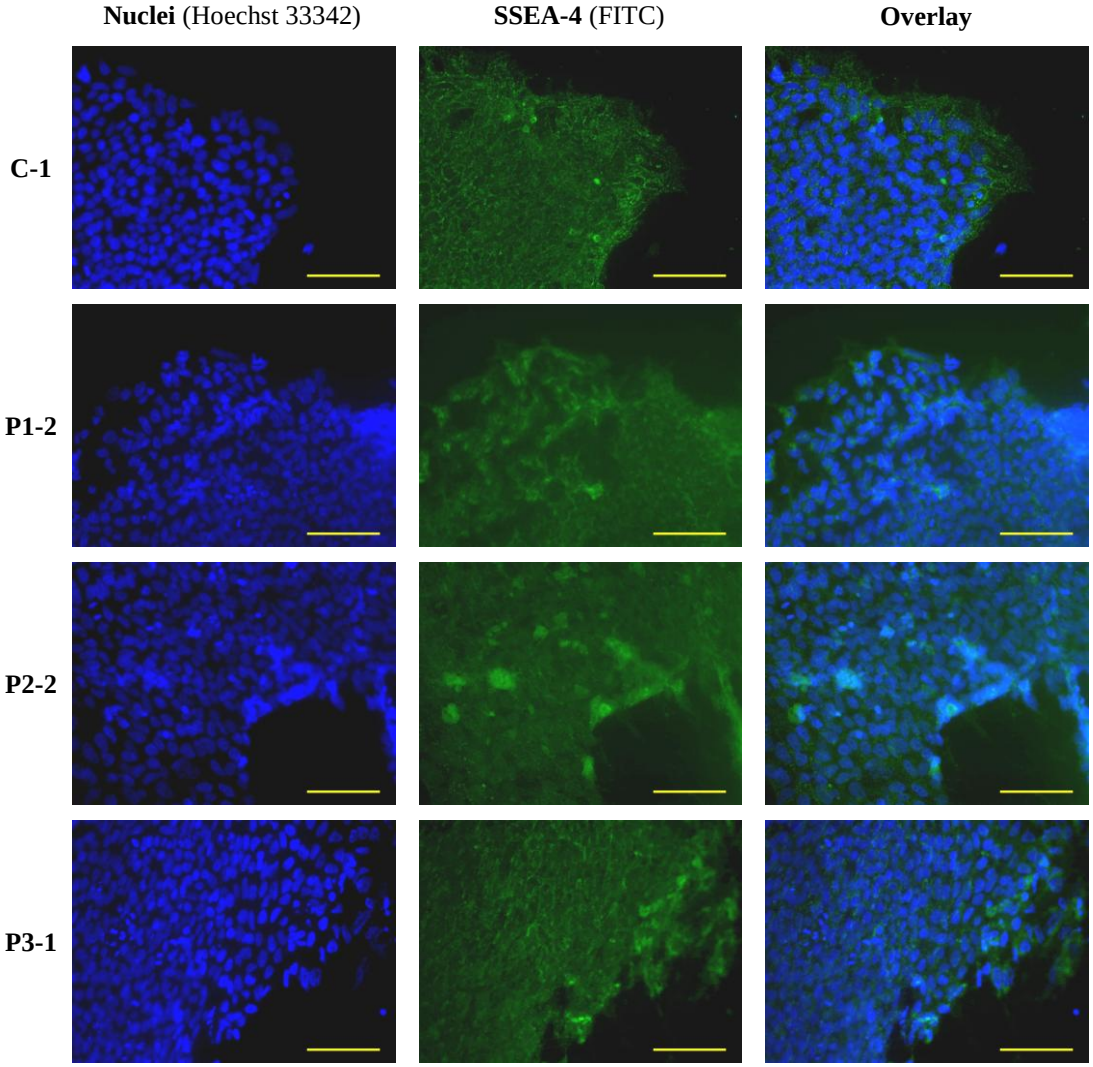

Figure 8-12 Immunocytochemical analysis of hiPSC lines for the expression of TRA-1-81. Nuclei were labelled with Hoechst 33342, whereas TRA-1-81 was detected with Alexa Fluor® 647-conjugated primary antibody. All images were captured with a 20x air objective. Scale bar: 100µm.

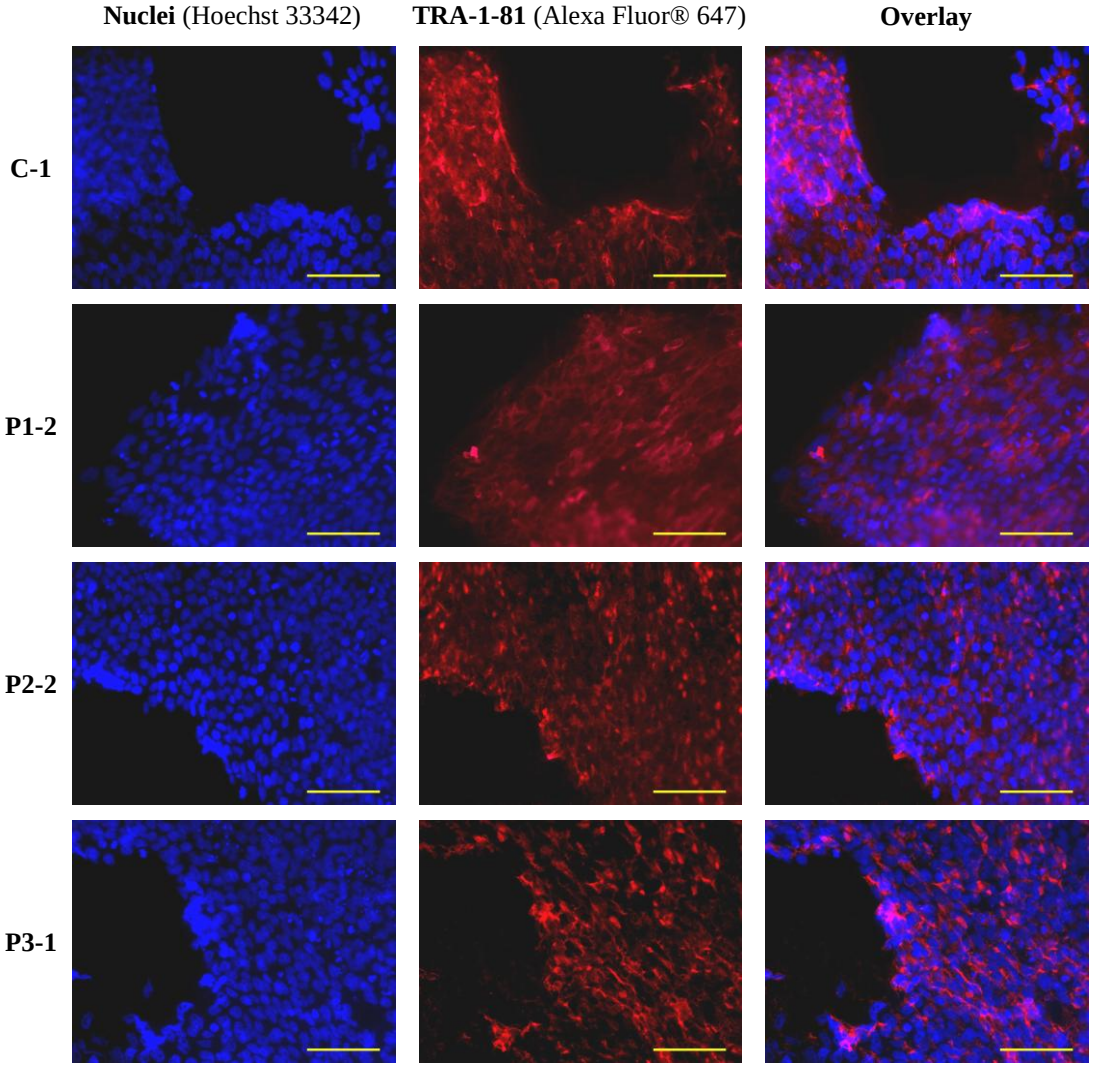

8.3.3 Cre-*loxP* Recombination

To remove *loxP*-flanked OSKM polycistronic viral vector from the selected hiPSC lines (please refer to **Section 8.3.2.1**), Cre-*loxP* mediated excision was performed by nucleofecting hiPSCs with the PvuII-linearized Cre expression plasmid containing puromycin-resistance transgene. After 5 days of selection with puromycin (0.5µg/ml for the first two days; 1µg/ml for the next three days) and a subsequent 7-day period to allow hiPSC colonies to re-emerge, three puromycin-resistant hiPSC clones were established from the P2-2 line, and nine from the C-1 line. Puromycin-resistant hiPSC clones failed to be established for the P1-2 and P3-1 hiPSC lines. The final outcome of the puromycin selection process is summarized in **Table 8-10**.

Table 8-10 The final outcome of the puromycin selection in hiPSC lines nucleofected with the PvuII-linearized Cre expression plasmid containing puromycin-resistance transgene.

Original hiPSC Line	Number of Puromycin-Resistant Clones Established	Numbering of Puromycin-Resistant Clones
P1-2	0	-
P2-2	3	P2-2a; P2-2b; P2-2c
P3-1	0	-
C-1	9	C-1a; C-1b; C-1c; C-1d; C-1e; C-1f; C-1g; C-1h; C-1i;

To determine the efficiency of Cre-*loxP* recombination in each puromycin-resistant hiPSC clone, the presence of the lentiviral OSKM polycistronic cassette was assessed using PCR. Primers designed to amplify the short (~250 kb; **Figure 8-14 A**) and the long (~600 kb; **Figure 8-14 B**) viral cassette products were used (**Figure 8-13**). The viral cassette was also amplified in hiPSC lines before Cre recombination (positive control) and the H9 ESC line (negative control). Consistent results were obtained for the short and long PCR products for all the analysed samples. Both short and long viral cassette amplicons were detected at significant levels in all samples, except the C-1f hiPSC line (abbreviated as 9 in **Figure 8-14**). Of note, the band for

this hiPSC line was however noticeably fainter for the *GAPDH* housekeeping gene (**Figure 8-14 D**). As expected, the viral cassette products were not amplified in the H9 hESC line. PCRs designed to amplify Cre recombinase transgene were performed in all investigated samples and no product bands were detected (**Figure 8-14 D**).

The efficiency of Cre-mediated *loxP* sites excision was further verified with the RT-PCR assay described in **Section 8.2.6.3**. The expression of both the total and endogenous *OCT4* transcripts was determined for the P2-2 hiPSC line (before plasmid nucleofection) and the three puromycin-selected P2-derived hiPSC clones (P2-2a to P2-2c) (**Figure 8-15 A**). Similar measurements were obtained for the C-1 hiPSC line and the nine puromycin-selected C-1-derived hiPSC clones (C-1a to C-1i) (**Figure 8-15 B**). All *OCT4* gene expression levels were calculated relatively to the control H9 hESC line. The viral (exogenous) *OCT4* expression was derived from the difference between the total and the endogenous levels of expression. These differences were not statistically significant for the P2-2b and P2-2c puromycin-resistant hiPSC clones, suggesting successful removal of the viral cassette. To investigate this observation further, expression of Cre recombinase transgene was measured for all puromycin-resistant hiPSC lines (**Figure 8-16**). Significant expression of the Cre transgene was evident only for the P2-2a and P2-2b hiPSC clones. Cre transgene expression was undetectable for the other samples tested.

The P2-2c line was therefore the only one showing significant Cre recombinase transgene expression coupled with the lack of exogenous viral *OCT4* expression.

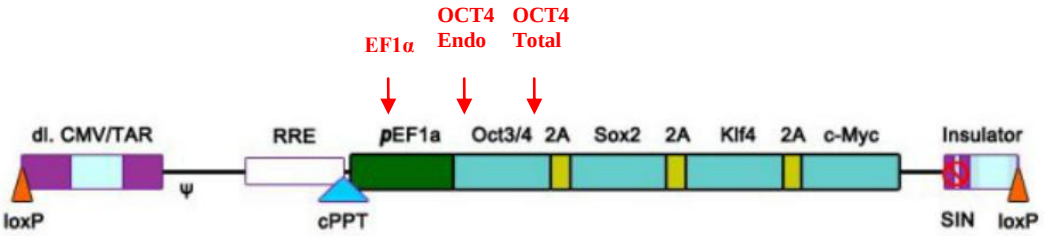

Figure 8-13 Map of a lentiviral 4-in-1 human OSKM polycistronic vector with location of primers used to amplify short and long viral cassette products. Approximate primer positions are indicated with the red arrows. The short viral cassette product was amplified with EF1α (forward) and OCT4 Endo (reverse) primer set. The long product was amplified with EF1α (forward) and OCT4 Total (reverse) primers. (Adapted from http://www.allelebiotech.com/4-in-1-lentiviral-particles-for-ipscs-generation-human-oskm/).

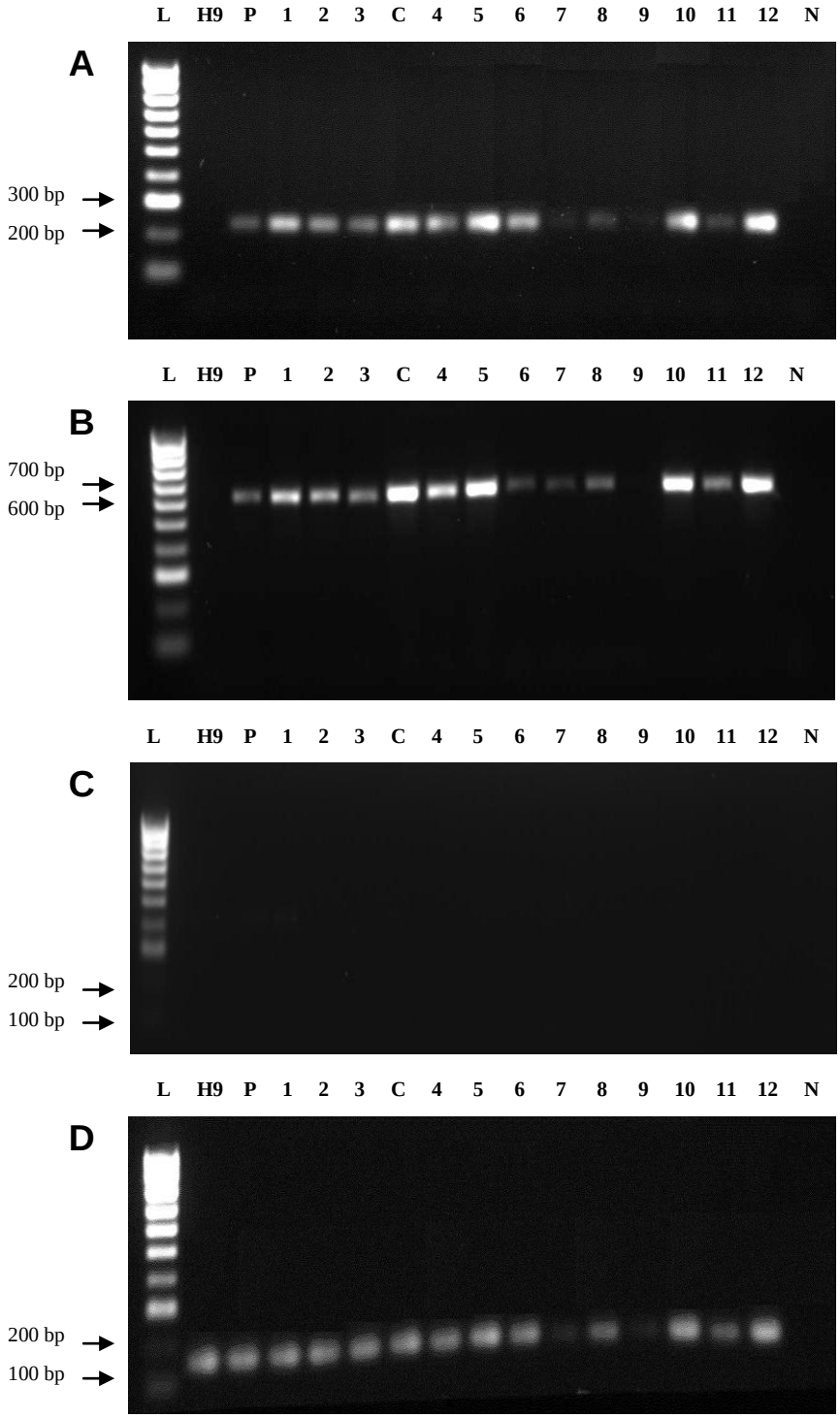

Figure 8-14 PCR-mediated detection of: (A) the short viral cassette product (~250 bp); (B) the long viral cassette product (~600 bp); (C) Cre-recombinase transgene (113 bp); and (D) *GAPDH* housekeeping gene as the loading control (133 bp). Legend: L = Hyperladder IV; H9 = ESC H9 line; P = P2-2 hiPSC line; 1 = P2-2a; 2 = P2-2b; 3 = P2-2c; C = C-1 hiPSC line; 4 = C-1a; 5 = C-1b; 6 = C-1c; 7 = C-1d; 8 = C-1e; 9 = C-1f; 10 = C-1g; 11 = C-1h; 12 = C-1i; N = water.

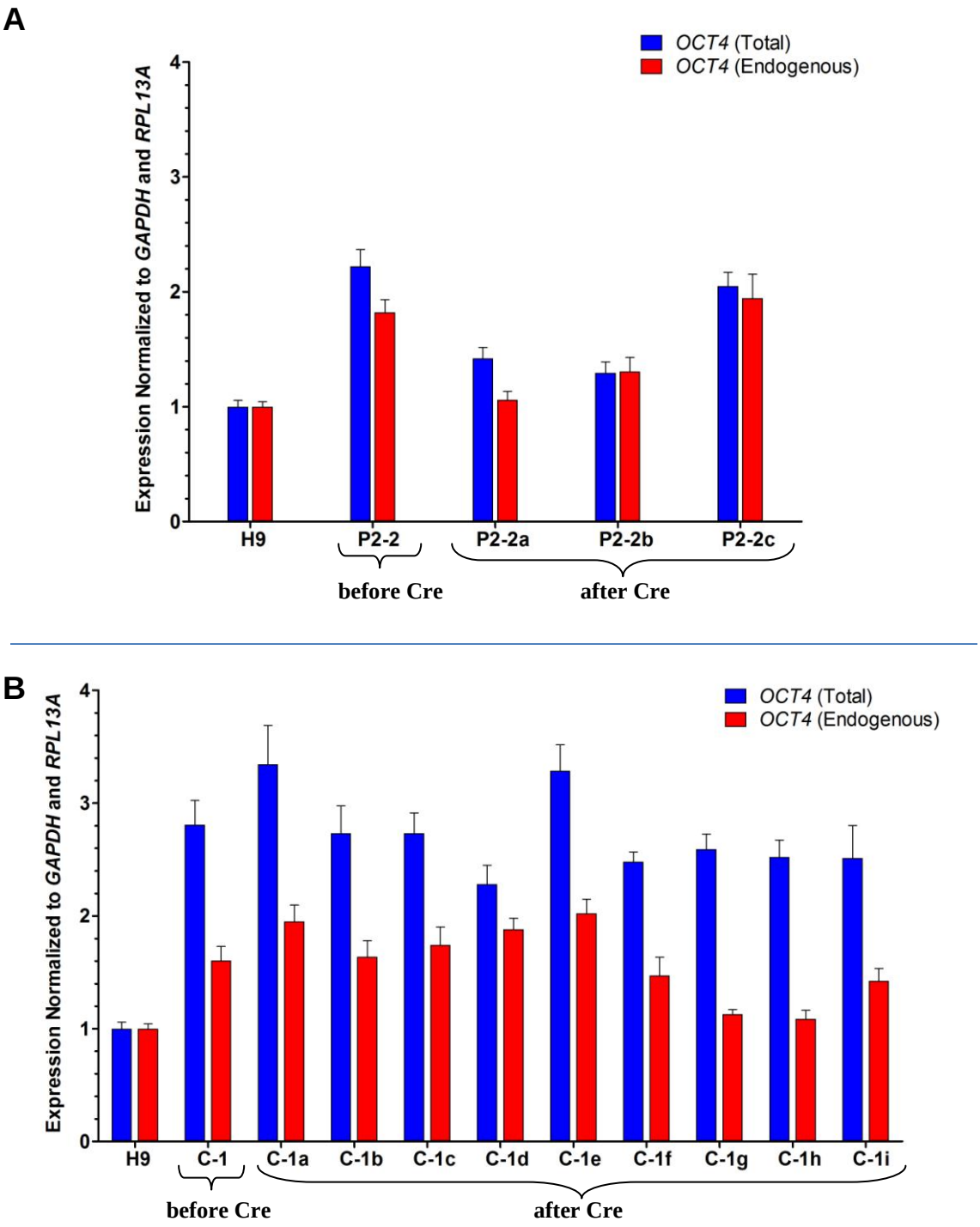

Figure 8-15 Expression levels of total and exogenous *OCT4* transcripts in hiPSC lines and H9 hESC line. (A) The P1 hiPSC lines before and after Cre-mediated *loxP* sites excision; (B) Control hiPSC lines before and after Cre-mediated *loxP* sites excision. Expression levels of *OCT4* transcripts are normalized to *GAPDH* and *RPL13A* housekeeping genes, and calculated relatively to expression in H9 hESC line. The exogenous (viral) *OCT4* expression is estimated from the difference between total and endogenous *OCT4* expression levels. The error bars indicate the standard errors of the mean (SEM).

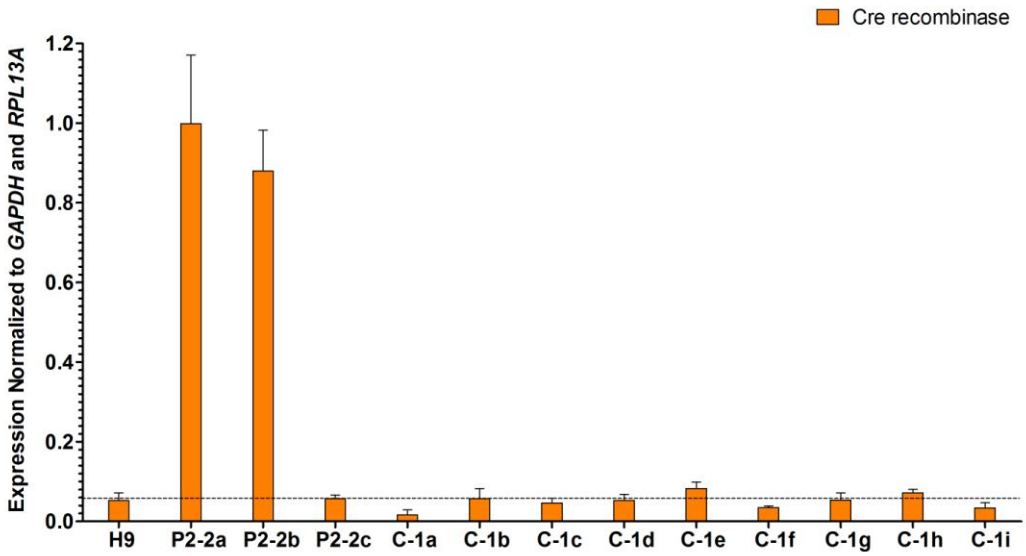

Figure 8-16 Cre recombinase transgene expression in puromycin-resistant hiPSC lines and H9 ESC line. Expression levels of Cre recombinase transgene are normalized to *GAPDH* and *RPL13A* housekeeping genes, and relative to the highest expression demonstrated by the P2-2a hiPSC line. Significant Cre expression levels were observed in the P2-2a and P2-2b hiPSC lines. The expression levels for the remaining samples were calculated from the Ct values > 35 and therefore can be considered within the qPCR assay noise. The error bars indicate the standard errors of the mean (SEM).

8.4 Discussion

We have demonstrated the feasibility of generating and characterising *OPA1*-mutant hiPSC lines using a lentiviral transduction protocol based on the four pluripotency factors (*OCT4*, *SOX2*, *KLF4* and *c-MYC*). The efficiency of viral-mediated reprogramming in this study was similar to those previously reported in other recent studies (Armstrong et al., 2010; Jiang et al., 2012). Although relatively low, the transduction efficiency was sufficient to obtain multiple hiPSC clones from all parental fibroblast lines, with the exception of the P3 line, where only one hiPSC clone was generated (**Table 8-5**). Importantly, all the generated hiPSC clones had the typical morphological features of hESCs. The *in vitro* characterisation of the selected hiPSC lines confirmed that the specific *OPA1* mutations present in the original fibroblast lines were retained through the reprogramming procedure. Based on the fingerprinting analysis, the hiPSC lines had similar DNA profiles to their original fibroblast lines. Karyotype analysis revealed chromosomal abnormalities in 10% of the metaphase cells from the control ((15;21)(q10;q10) translocation) and the P1

(chromosome 8 trisomy) fibroblast lines. However, these chromosomal aberrations were importantly not observed in the hiPSC lines derived from these two fibroblast lines, indicating that they must have originated from the chromosomally-normal parental fibroblasts. These observations agree with the theory suggesting that reprogramming *per se* can exert a selective pressure on the genetically or epigenetically impaired cells of the donor population, resulting in karyotypically-normal hiPSC lines (Kawamura et al., 2009).

All derived hiPSC lines showed characteristic expression of both the nuclear (OCT4, SOX2) and the cell surface (SSEA-4, TRA-1-81) pluripotency markers, similar to previously-published patterns for different fibroblast-derived hiPSCs (Armstrong et al., 2010; Jiang et al., 2012). The significant endogenous and exogenous expression of both *OCT4* and *c-MYC* transcripts confirmed successful viral transduction of these pluripotency genes. Following hiPSC generation, the virally-mediated expression of the pluripotent genes (*OCT4*, *SOX2*, *KLF4* and *c-MYC*) used in this reprogramming protocol has to be suppressed as this can affect the future differentiation properties of the generated hiPSC lines (Soldner et al., 2009; Hu et al., 2010). For example, it has previously been shown that the residual expression of *c-MYC* and *OCT4* transgenes can inhibit the differentiation efficiency of hiPSC lines (Yu et al., 2007; Armstrong et al., 2010). To allow the removal of these viral transgenes, modified lentiviral polycistronic vectors carrying *loxP* sites were used in this study. The elimination of integrated transgenes by the Cre-*loxP*-mediated recombination system should allow the creation of vector-free hiPSCs (Soldner et al., 2009). Following puromycin selection, twelve hiPSC clones were obtained for two original hiPSC lines: C-1 and P-2. Interestingly, although all these hiPSC lines expressed the puromycin resistance transgene, only two of these showed detectable (albeit low) expression of the Cre transgene (P2-2a and P2-2b; **Figure 8-16**). The puromycin resistance and Cre transgenes were under the control of two separate promoters: hUbC (human ubiquitin C) and mPGK (murine phosphoglycerate kinase), respectively (**Figure 8-2**). As studied previously, activities of these two promoters may however be restricted to specific hESC/hiPSC lineages (Norrman et al., 2010). It is therefore conceivable that although the hUbC promoter was active in all puromycin-resistant hiPSC lines, the mPGK promoter could have become methylated in some of them, leading to the lack of Cre transgene expression. The RT-PCR analyses revealed persistent significant expression of the exogenous *OCT4* transcript in all puromycin-selected hiPSCs lines,

with the exception of P2-2b and P2-2c (**Figure 8-15**). Only the P2-2b hiPSC line showed significant Cre transgene expression in conjunction with a reduction in exogenous *OCT4* expression. However, the PCR-based detection used (**Figure 8-14**) still indicated the presence of the viral *OCT4* amplicons in the P2-2b line. The discrepancy between these two assays could be explained by the integration of the lentiviral polycistronic vectors into genomic regions, which after successful reprogramming became tightly-packed heterochromatin. The standard PCR would still detect the viral signature, but being in non-expressed genomic regions, no mRNA transcripts are produced, explaining the lack of detection with the qPCR assay used in this study.

The incomplete excision of the *loxP* flanked transgenes in the selected puromycin-resistant hiPSC lines was also probably due to the high volume of lentiviral integrations, making the complete removal of all these viral cassettes impossible when only relatively low levels of Cre transgene expression were achieved (Soldner et al., 2009). To address this issue, a second round of hiPSCs nucleofection with the puro-Cre plasmids is planned. To enhance the efficiency of this process, the concentration of plasmids will be increased from 10µg to 20µg/10^6 hiPSCs. Following successful removal of the viral vectors, the differentiation capability and developmental potential of the generated hiPSCs will be tested *in vitro*, by generating embryoid bodies (EBs) of all three embryonic germ layers, and *in vivo*, by injecting hiPSCs into mouse kidney capsules and allowing them to form teratomas containing cell types representative of all three primordial germ layers (Yu et al., 2007; Armstrong et al., 2010; Boulting et al., 2011).

Chapter 9 General Discussion

Mitochondria only have limited genetic autonomy and they rely heavily on a complex array of nuclear-encoded mitochondrial proteins for their normal function (Zeviani et al., 2003). The complexity of this synergistic nuclear-mitochondrial interaction is magnified by the multifunctional nature of these nuclear-encoded mitochondrial proteins. The heterogeneous clinical presentation of nuclear mitochondrial disorders remains as yet unexplained, and even more intriguingly, mitochondrial dysfunction seems to have a marked predilection for the optic nerve, causing degeneration of the RGC layer and ultimately progressive blindness (Yu-Wai-Man et al., 2011b). It has become apparent over the past decade that disturbed mitochondrial dynamics represents an important group of human disease, in which optic atrophy again features strongly. The classical example is DOA, a nuclear mitochondrial disorder that disrupts the normal function of OPA1 – a critical inner mitochondrial membrane protein with pro-fusion properties. In this PhD thesis, I have further investigated the disease mechanisms underlying nuclear disorders of mtDNA maintenance by focusing on three main nuclear genes: *OPA1*, *MFN2*, and *POLG1*.

OPA1 and *MFN2* encode dynamin-like GTPase proteins intrinsically associated with the fusion of the IMM and OMM, respectively (Chen et al., 2003; Meeusen et al., 2004; Meeusen et al., 2006). About 20% of *OPA1* mutation carriers will develop a more severe multi-systemic neurological phenotype (DOA+) comprising sensorineural deafness, ataxia, myopathy, and peripheral neuropathy, in addition to progressive visual failure (Yu-Wai-Man et al., 2010b). Besides its critical pro-fusional properties, OPA1 is a multifunctional protein that regulates a number of crucial interrelated cellular processes. These include an integral role in maintaining the assembly and stability of the mitochondrial respiratory chain complexes (Zanna et al., 2008), the regulation of programmed cell death by controlling the release of pro-apoptotic cytochrome *c* molecules (Lee et al., 2004; Olichon et al., 2007), and mtDNA maintenance through a direct physical contact with mtDNA molecules (Wang and Bogenhagen, 2006; Elachouri et al., 2011). *MFN2* mutations typically cause a dominantly-inherited neurodegenerative disorder – CMT-2A (Züchner et al., 2004). Interestingly, the observed clinical features can overlap with those seen in *OPA1*-related DOA+ phenotypes, some affected *MFN2* carriers developing a progressive axonal sensorimotor neuropathy complicated by optic atrophy and other

neurological features such as deafness, cerebellar ataxia and proximal myopathy (Rouzier et al., 2012). *POLG1* encodes the catalytic subunit of DNA polymerase gamma (POLG) and it is the most frequently-identified causative nuclear gene among patients with mtDNA maintenance disorders, accounting for ~25% of all cases (Chinnery and Zeviani, 2008). The disease phenotypes associated with *POLG1* mutations are highly varied, ranging from early-onset AHS to ataxia and late-onset isolated CPEO. A characteristic molecular signature shared by mutations in *OPA1*, *MFN2* and *POLG1* is the disturbed mtDNA maintenance, with clinically affected patients showing both quantitative (depletion) and qualitative (point mutations and deletions) secondary mtDNA abnormalities in a range of tissue samples.

Significant mtDNA proliferation was observed in peripheral blood leukocytes of patients harbouring confirmed pathogenic *OPA1* and *MFN2* mutations (**Chapter 4**). A similar observation was made when measuring mtDNA copy number in single muscle fibres laser-microdissected from a *MFN2*-positive muscle biopsy specimen (**Chapter 5**), with a significant mitochondrial proliferative response being present in both COX-positive and COX-negative muscle fibres. Previous work in our group has shown increased mtDNA copy number in single muscle fibres from biopsy specimens that had been obtained from patients with a range of pathogenic *OPA1* mutations (Yu-Wai-Man et al., 2010c). These consistent experimental observations in two different tissue types and for both *OPA1* and *MFN2* mutations strongly support the current hypothesis that mtDNA proliferation is a normal compensatory cellular response to the underlying fusion and OXPHOS imbalance.

OPA1 mutations result in the accumulation of high levels of COX-deficient muscle fibres in muscle biopsies from patients manifesting both pure optic atrophy and multisystemic DOA+ phenotypes (Amati-Bonneau et al., 2008; Hudson et al., 2008a). The biochemical defect in these COX-deficient muscle fibres is secondary to high levels of somatically-acquired mtDNA deletions (Yu-Wai-Man et al., 2010b; Yu-Wai-Man et al., 2010c). The presence of COX-deficient fibres and multiple mtDNA deletions in skeletal muscle samples from patients with *MFN2* mutations suggests the possibility of shared disease mechanisms precipitating mtDNA instability in both *OPA1* and *MFN2* disease carriers (Rouzier et al., 2012).

A fundamental question remains – is the accumulation of secondary mtDNA deletions in tissues harbouring OPA1 and MFN2 mutations due to a high rate of de novo mutagenesis or is it due to an increased clonal expansion rate? Following the formation of a mtDNA deletion, a biochemical defect is only expressed once the level of the mutated mtDNA species clonally expands to exceed a critical threshold (Chinnery and Samuels, 1999). Crucially, *OPA1* and *MFN2* mutations precipitate mitochondrial network fragmentation and this impairs the effective functional complementation of deleted mtDNA molecules by wild-type genomes, through the normal process of mitochondrial content mixing (Nakada et al., 2009; Chen et al., 2010). Another attractive hypothesis that needs to be tested is whether mitochondrial network fragmentation leads to an increased rate of clonal expansion by reducing the effective number of mtDNA molecules in individual compartments, thereby allowing more rapid segregation of the deleted mtDNA species by random genetic drift (Chinnery and Samuels, 1999; Elson et al., 2001).

Only 50% of COX-negative muscle fibres from the *MFN2*-positive muscle specimen had mtDNA deletion levels above the generally accepted mutational threshold required to induce a biochemical defect (Shoubridge et al., 1990; Bua et al., 2002; Durham et al., 2007) (**Chapter 5**). It is possible that the biochemical defect in these muscle fibres was secondary to the accumulation of high levels of somatic mtDNA point mutations, and not deletions, as it has been described previously for *POLG1*-mutant patient tissues (Del Bo et al., 2003; Wanrooij et al., 2004; Chinnery and Zeviani, 2008; Reeve et al., 2008). The future use of high-throughput next-generation sequencing should allow for a precise characterisation of the range of mtDNA abnormalities (both mutations and deletions) present in tissue samples collected from patients with *OPA1* and *MFN2* mutations, as these could have been missed by the technical limitations inherent to standard methods such as Sanger sequencing and quantitative real-time PCR (Zaragoza et al., 2010).

The effect of *OPA1* and *POLG1* mutations on mtDNA replication efficiency was assessed in patient fibroblast cell lines using a previously-validated EtBr-based mtDNA repopulation assay (**Chapter 7**). Our repopulation data revealed a clear distinction between *POLG1* and *OPA1* mutant cell lines. Following EtBr-induced depletion, the mtDNA content of *POLG1* cell lines remained markedly depressed, a finding which reinforces the central importance of POLG in promoting efficient

mtDNA replication (Graziewicz et al., 2006; Stewart et al., 2011). *OPA1* cell lines also exhibited impaired mtDNA repopulation following EtBr removal. However, *OPA1* cell lines repopulated to ~20% of their baseline values, which was significantly higher compared with *POLG1* cell lines. Interestingly, there were some apparent differences between the various familial *OPA1* mutations, which were not clearly linked to the severity of the clinical phenotype. The basis for the varied clinical presentations of *OPA1* mutations cannot therefore be explained on the basis of the efficiency of mtDNA repopulation following withdrawal of EtBr. The striking difference in the kinetics of mtDNA repopulation between the *OPA1* and *POLG1* mutational groups, highlights the distinct roles played by their respectively encoded proteins in the complex process that regulates mtDNA replication (Hudson and Chinnery, 2006; Elachouri et al., 2011).

To examine the link between mitochondrial network morphology and mtDNA content, a comprehensive quantitative analysis of the mitochondrial network was performed on *OPA1*- and *POLG1*-mutant cell lines (**Chapter 7**). A number of pathogenic *OPA1* mutations have previously been associated with increased fragmentation of the mitochondrial network (Olichon et al., 2007; Zanna et al., 2008; Agier et al., 2012; Chevrollier et al., 2012). A recently published study has also documented increased mitochondrial network fragmentation in *OPA1*-mutant human fibroblasts as a response to glucose deprivation in the culture media or the application of exogenous oxidative stress (Agier et al., 2012). *OPA1*-mutant cell lines investigated in our study did not demonstrate marked fragmentation phenotypes. This finding was probably related to the fact that these cells were cultured in media containing a high glucose content, which allowed for a deficient mitochondrial OXPHOS system to be bypassed, at least to a certain extent, by glycolysis (Robinson et al., 1992; D'Aurelio et al., 2001). In support of this argument, significant mitochondrial network fragmentation in *OPA1* fibroblasts was only observed when cells were forced to rely exclusively on OXPHOS for ATP production e.g. when cultured in glucose-free (galactose) media (Zanna et al., 2008). Our study is the first to objectively quantify mitochondrial network morphology in *POLG1*-mutant fibroblasts. The results revealed marked mitochondrial network fragmentation in *POLG1*-mutant cell lines following EtBr-induced mtDNA depletion. Although speculative, it is likely that this disruption in mitochondrial

network morphology was triggered by a bioenergetic crisis, which was perpetuated by the subsequent failure of mtDNA repopulation on withdrawal of EtBr from the culture media. Interestingly, a significant increase in the total length of the mitochondrial network was observed in both *POLG1* and *OPA1* mutant fibroblasts. This overall elongation of the mitochondrial network could have been triggered by the underlying mitochondrial respiratory chain defect in these mutant cell lines. This physical increase in the surface area available for OXPHOS could, to a certain extent, compensate for the deleterious biochemical consequences of *POLG1* and *OPA1* mutations. It should be noted that both cell size and shape can be crucial factors influencing the overall morphology of the mitochondrial network, and these were not controlled for in our study (Chevrollier et al., 2012). In a series of elegant experiments, *Chevrollier and colleagues* have recently showed that skin fibroblasts can be successfully cultured in micropatterned coverslips, with this technique allowing cell morphology to be standardised. The specific micropattern that was used allowed the cells to spread over a defined surface area, so that they finally adopted equilateral triangular shapes (Chevrollier et al., 2012). It would be interesting to repeat future mtDNA repopulation experiments with additional *POLG1* and *OPA1* mutant cell lines using these micropatterned coverslips, and to see whether the main findings from our current study on the effect of mtDNA depletion on mitochondrial network morphology are replicated.

Neuromyelitis optica (NMO) is an idiopathic, autoimmune, demyelinating condition of the CNS that, rather strikingly, preferentially affects the optic nerve and spinal cord (Wingerchuk et al., 2007). Given that NMO shares overlapping clinical features with *OPA1*-related DOA+ phenotype, our *a priori* hypothesis was that *OPA1* genetic variants could influence the development of NMO. However, we did not find any pathogenic *OPA1* mutations or any specific SNP associations in relation to the risk of developing NMO (**Chapter 6**). It is possible that the relatively small sample size of our study did not have enough statistical power to identify a minor genetic influence. However, NMO is a relatively rare CNS disorder and the major genetic influence of *OPA1* on the development of this demyelinating disease can be excluded.

The lack of access to diseased optic nerve and the technical difficulties in isolating RGCs have been major obstacles in uncovering the disease mechanisms which lead to a progressive visual loss among patients with mitochondrial optic neuropathies. As

an alternative to mouse models, our aim was to generate hiPSC lines harbouring pathogenic *OPA1* mutations, which would then allow the generation of RGCs for the future mechanistic studies. In this thesis, we present data confirming the generation of hiPSC lines from three patient-derived fibroblast lines harbouring two different pathogenic *OPA1* mutations (**Chapter 8**). However, the complete removal of the viral vectors used to induce pluripotency has proven technically challenging. The differentiation of RGCs from these hiPSCs should ideally take place in a viral-free cellular environment, as the residual viral remnants could result in sustained pluripotent gene expression, with possible aberrant consequences for differentiation properties of hiPSCs (Soldner et al., 2009; Hu et al., 2010). If future repeat attempts at clearing the remaining viral transgenes prove unsuccessful, an alternative strategy would involve reprogramming the original *OPA1* fibroblast cell lines using alternative transduction vectors. Since the original Takahashi and Yamanaka's protocol (Takahashi and Yamanaka, 2006; Takahashi et al., 2007) was published, several techniques have been developed to allow for the generation of transgene-free hiPSCs, including non-integrating adenoviruses (Zhou and Freed, 2009), nonviral minicircle DNAs (Jia et al., 2010) and proteins (Kim et al., 2009; Zhou et al., 2009). However, the major disadvantages of these methods are the low transduction efficiency and the requirement for repeated inductions of reprogramming vectors (Ban et al., 2011). An attractive alternative strategy to generate hiPSCs involves the use of Sendai virus (SeV) vectors (Fusaki et al., 2009). These RNA-based viral vectors only replicate within the cytoplasm of infected cells and importantly, they do not integrate into the host genome (Li et al., 2000). SeV vectors have been successfully applied to efficiently generate hiPSCs from human fibroblasts (Fusaki et al., 2009; Macarthur et al., 2012; Nakamura et al., 2012). After successful reprogramming has taken place, the SeV vectors are gradually diluted during the rapid cell division of hiPSCs, and this process is normally completed within eight to twelve passages (Fusaki et al., 2009; Kudva et al., 2012). The generation of RGCs harbouring a range of pathogenic *OPA1* mutations will be a major step in dissecting the fundamental disease mechanisms that precipitate the range of clinical phenotypes seen in patients with DOA. This disease is the most common inherited optic neuropathy in the general population and it causes progressive irreversible blindness from early childhood (Yu-Wai-Man et al., 2011b). The *in vitro* characterisation of

RGCs in both pure DOA and DOA+ disease models will hopefully provide a powerful tool to screen for neuroprotective agents that could prove beneficial to patients affected with this debilitating disorder.

Appendices

Table of Contents

Appendix A

Table A-1 *OPA1* mutations identified in our patient cohort.

Mutation (AA change)	Type	Functional Domain	N =
c.32+1G>A*	Splice	-	4
p.R38_S43del	In-frame Deletion	Basic	2
p.F119X	Nonsense	Basic	2
p.A192GfsX36	Frameshift	Basic	1
p.S210X	Nonsense	Basic	3
p.K212RfsX4	Frameshift	Basic	2
p.K214fsX2	Frameshift	Basic	1
p.R231NfsX21	Frameshift	Basic	2
p.E242X	Nonsense	Basic	2
p.S256R	Missense	Basic	4
p.K262_R290del	In-frame Deletion	Basic	4
p.I265TfsX42	Frameshift	Basic	1
p.V291_K328del	In-frame Deletion	GTPase	20
p.V294fsX667	Frameshift	GTPase	6
p.Q297X	Nonsense	GTPase	3
p.T302P	Missense	GTPase	2
p.L331LfsX3	Frameshift	GTPase	2
c.1065+1G>A*	Splice	-	1
p.L384fsX397	Frameshift	GTPase	2
p.R366X	Nonsense	GTPase	2
p.P400L	Missense	GTPase	1
c.1212+3A>T*	Splice	-	1
p.I432V	Missense	GTPase	3
p.D438V	Missense	GTPase	4
p.D442N	Missense	GTPase	1
p.A443T	Missense	GTPase	2
p.G459E	Missense	GTPase	1

Mutation (AA change)	Type	Functional Domain	N =
p.K468E	Missense	GTPase	2
c.1516+1G>T*	Splice	-	3
p.I515KfsX4	Frameshift	Middle	1
p.S545R	Missense	Middle	3
p.Q563X	Nonsense	Middle	1
p.M555NfsX7	Frameshift	Middle	1
c.1770+2T>G*	Splice	-	1
p.W660X	Nonsense	Middle	1
p.D662VfsX9	Frameshift	Middle	1
p.E671EfsX675	Frameshift	Middle	1
c.2013+1G>C*	Splice	-	1
p.R711X	Nonsense	Middle	1
c.2167-12T>A*	Splice	-	1
p.R733X	Nonsense	Middle	1
p.F747LfsX53	Frameshift	Middle	2
p.E749X	Nonsense	Middle	1
c.2496+1G>T*	Splice	-	1
c.2496+4_2496+5delinsGTAAC*	Splice	-	3
p. L832F	Missense	Middle	1
p.Y841X	Nonsense	Middle	1
p.L872_Q884del	In-frame Deletion	Middle	1
c.2613+1G>A*	Splice	-	5
c.2613+1G>C*	Splice	-	2
p.A888GfsX15	Frameshift	Middle	1
c.2707+1G>C*	Splice	-	3
p. V903GfsX3	Frameshift	Coiled-Coil 2 (CC2)	20
p.R905X	Nonsense	Coiled-Coil 2 (CC2)	7
c.2818+5G>A*	Splice	-	3
p.E947EfsX2	Frameshift	Coiled-Coil 2 (CC2)	1

*The consequences of these splice site *OPA1* mutations on the resulting mRNA transcripts have not yet been determined and deposited on the eOPA1 database (http://lbbma.univangers.fr/lbbma.php?id=9).

Table A-2 *MFN2* mutations identified in our patient cohort.

Mutation (AA change)	Type	Functional Domain	N =
p.E65X	Nonsense	-	3
p.R94W	Missense	-	8
p.R94Q	Missense	-	2
p.A100G	Missense	GTPase	1
p.R104L	Missense	GTPase	3
p.R104W	Missense	GTPase	1
p.T105A	Missense	GTPase	1
p.H165Y	Missense	GTPase	6
p.G202A	Missense	GTPase	4
p.T206I	Missense	GTPase	2
p.T232N	Missense	GTPase	1
p.R250Q	Missense	GTPase	1
p.R259C	Missense	GTPase	1
p.R280H	Missense	GTPase	1
p.G298R	Missense	GTPase	1
p.E308X*	Nonsense	GTPase	1
p.R364W	Missense	Coiled-Coil 1 (CC1)	1
p.R364P	Missense	Coiled-Coil 1 (CC1)	1
p.R364Q	Missense	Coiled-Coil 1 (CC1)	1
p.M376V	Missense	Coiled-Coil 1 (CC1)	1
p.M376I	Missense	Coiled-Coil 1 (CC1)	1
p.A383V	Missense	Coiled-Coil 1 (CC1)	1
p.R468H	Missense	-	2
p.D496G	Missense	-	2
p.R519P*	Missense	-	1
p.L673P	Missense	-	3
p.V705I	Missense	Coiled-Coil 2 (CC2)	2
p.R707W	Missense	Coiled-Coil 2 (CC2)	1
p.R707P	Missense	Coiled-Coil 2 (CC2)	1
p.A716T	Missense	Coiled-Coil 2 (CC2)	1
p.H750P	Missense	-	1
p.Q751X	Nonsense	-	1
p.Y752X	Nonsense	-	1

* One patient harboured two heterozygous *MFN2* mutations.

Appendix B.1

The variation in mtDNA copy number observed in untreated fibroblast cell lines at each analysis time point from day 0 to day 48: (i) control cell lines (**Figure B-1**), (ii) *OPA1* fibroblasts (**Figure B-2** and **Figure B-3**) and (iii) *POLG1* cell lines (**Figure B-4** and **Figure B-5**). The results for each experimental time point were calculated as the average mtDNA copy number obtained from two replicates, relative to the mtDNA copy number at day 0. An average mtDNA copy number value of 1.0 at a specific experimental time point implies a similar mtDNA content to the one measured at the baseline.

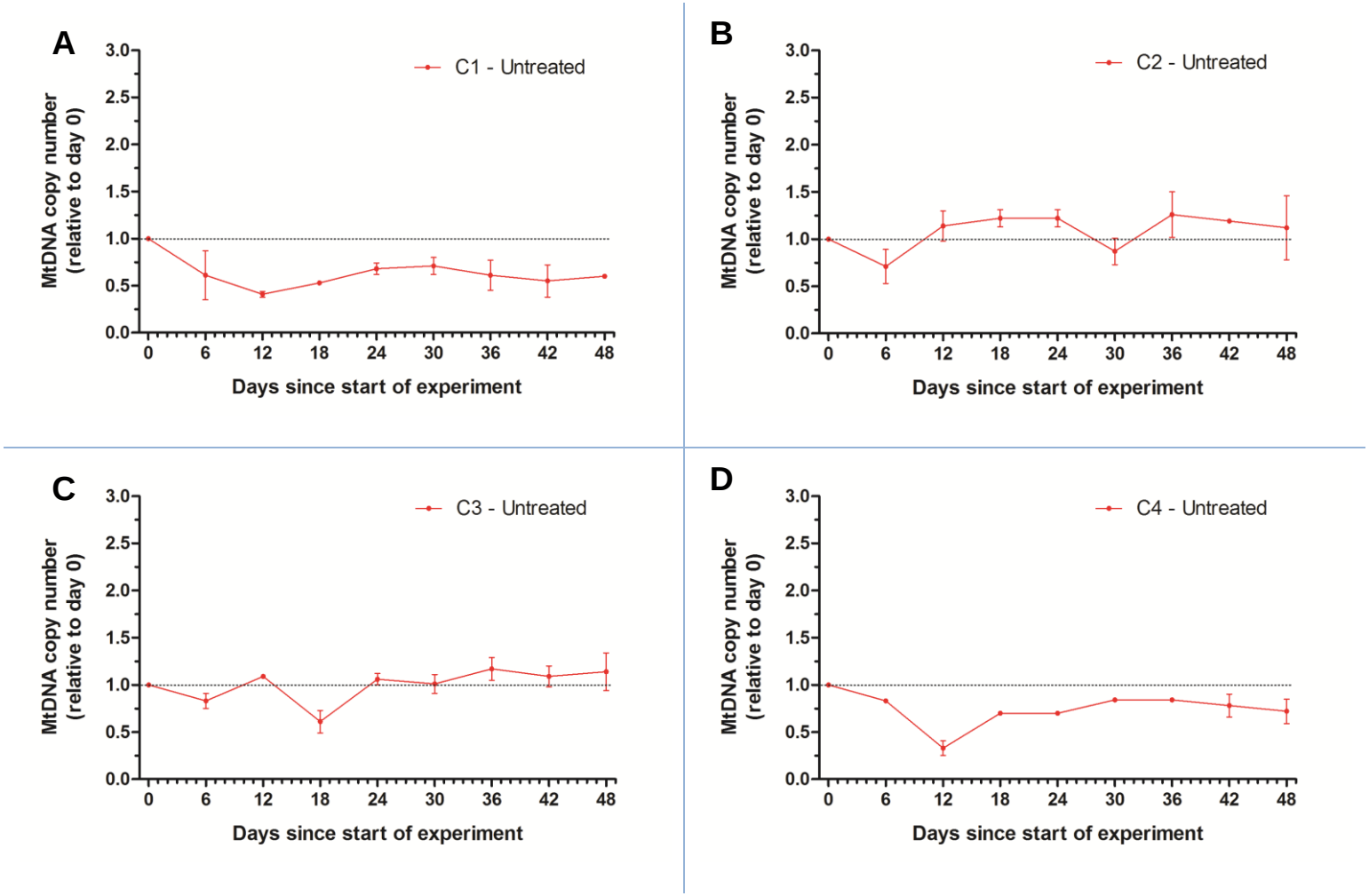

Figure B-1 MtDNA copy number variation in untreated control cell lines: (A) C1, (B) C2, (C) C3, and (D) C4. Each data point represents the average mtDNA copy number relative to the mtDNA copy number at day 0 for two replicates. The error bars are presented as standard deviations (SDs).

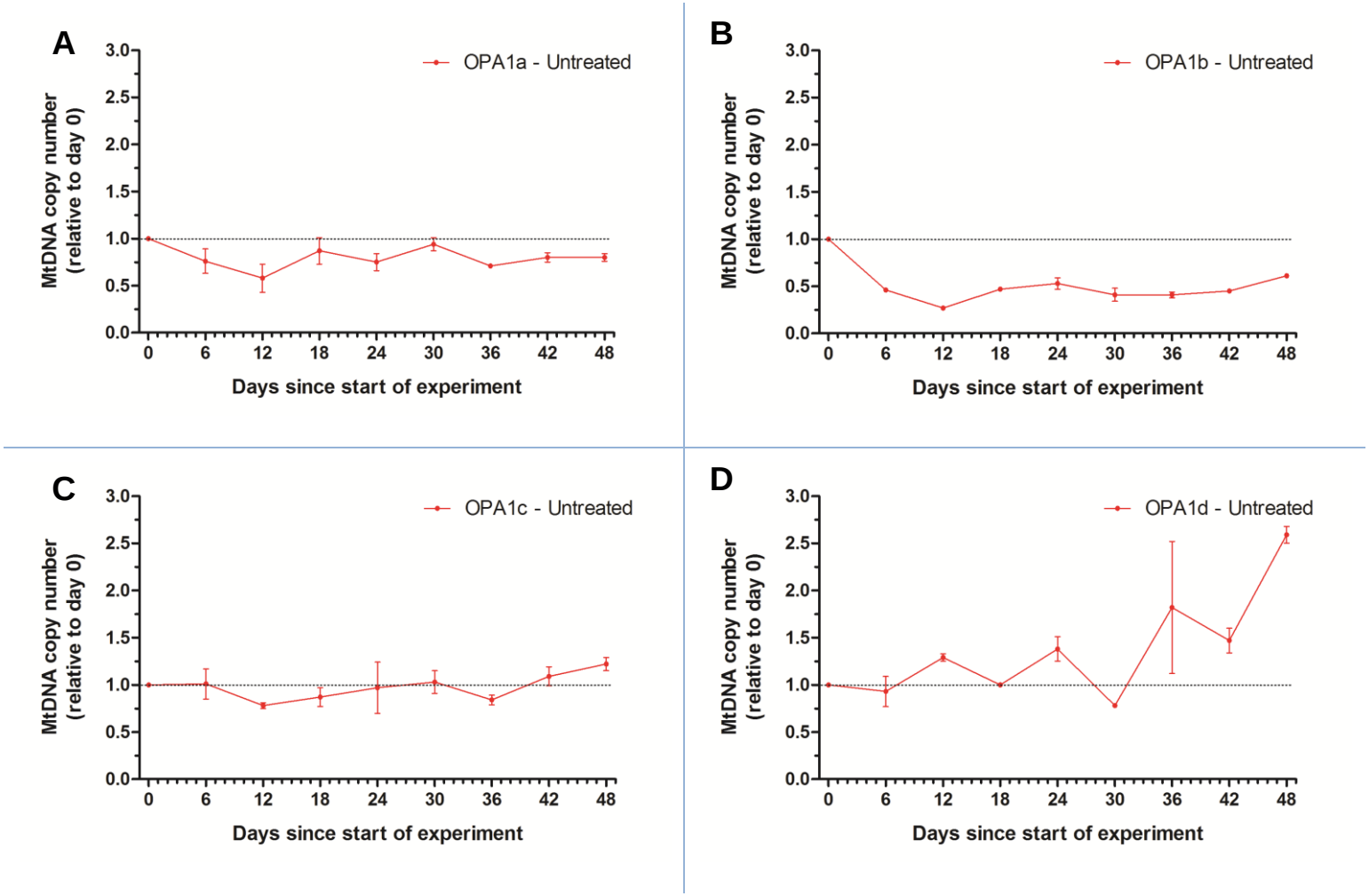

Figure B-2 MtDNA copy number variation in untreated *OPA1* cell lines: (A) OPA1a, (B) OPA1b, (C) OPA1c, and (D) OPA1d. Each data point represents the average mtDNA copy number relative to the mtDNA copy number at day 0 for two replicates. The error bars are presented as standard deviations (SDs).

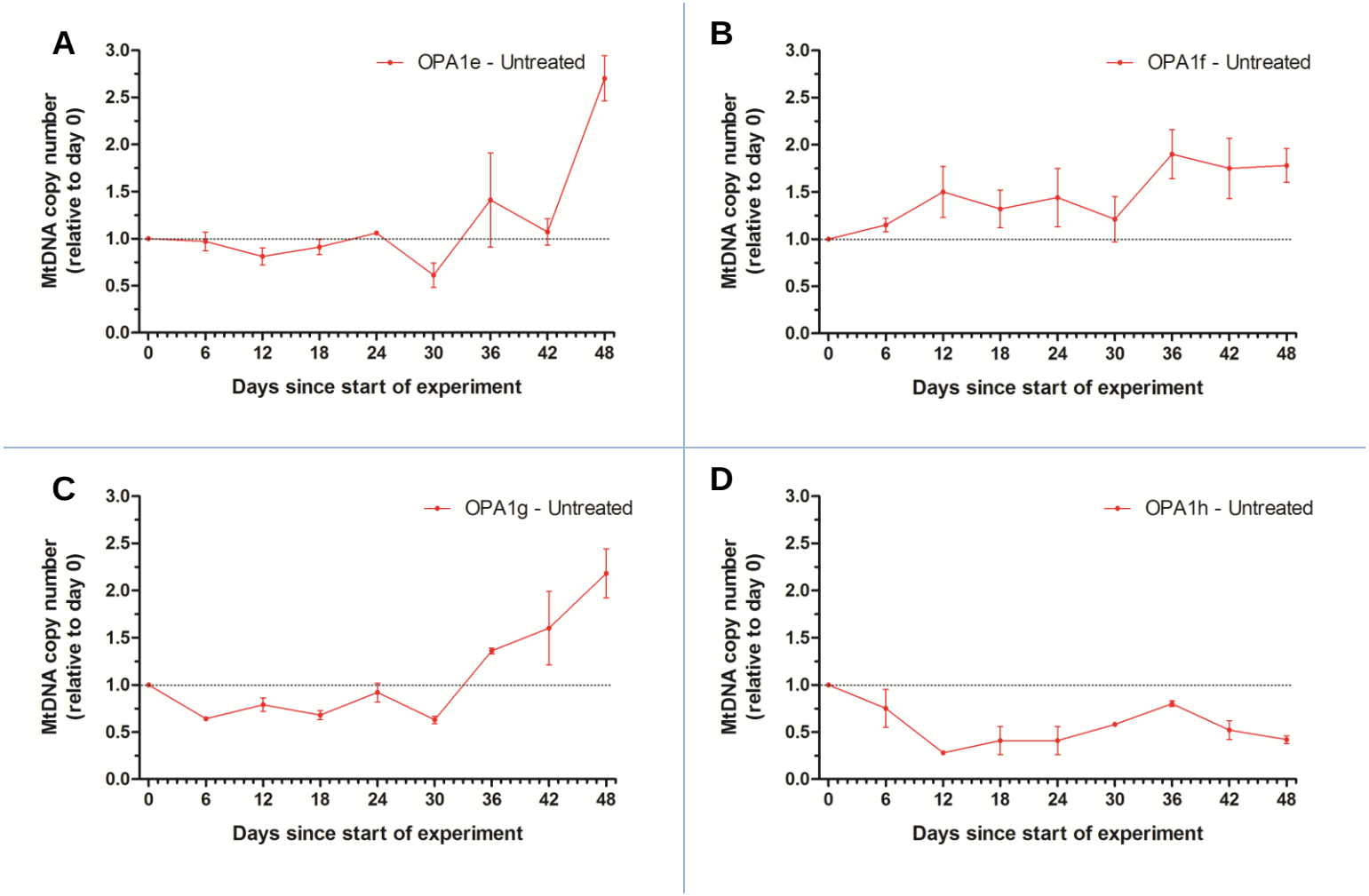

Figure B-3 MtDNA copy number variation in untreated *OPA1* cell lines: (A) OPA1e, (B) OPA1f, (C) OPA1g, and (D) OPA1h. Each data point represents the average mtDNA copy number relative to the mtDNA copy number at day 0 for two replicates. The error bars are presented as standard deviations (SDs).

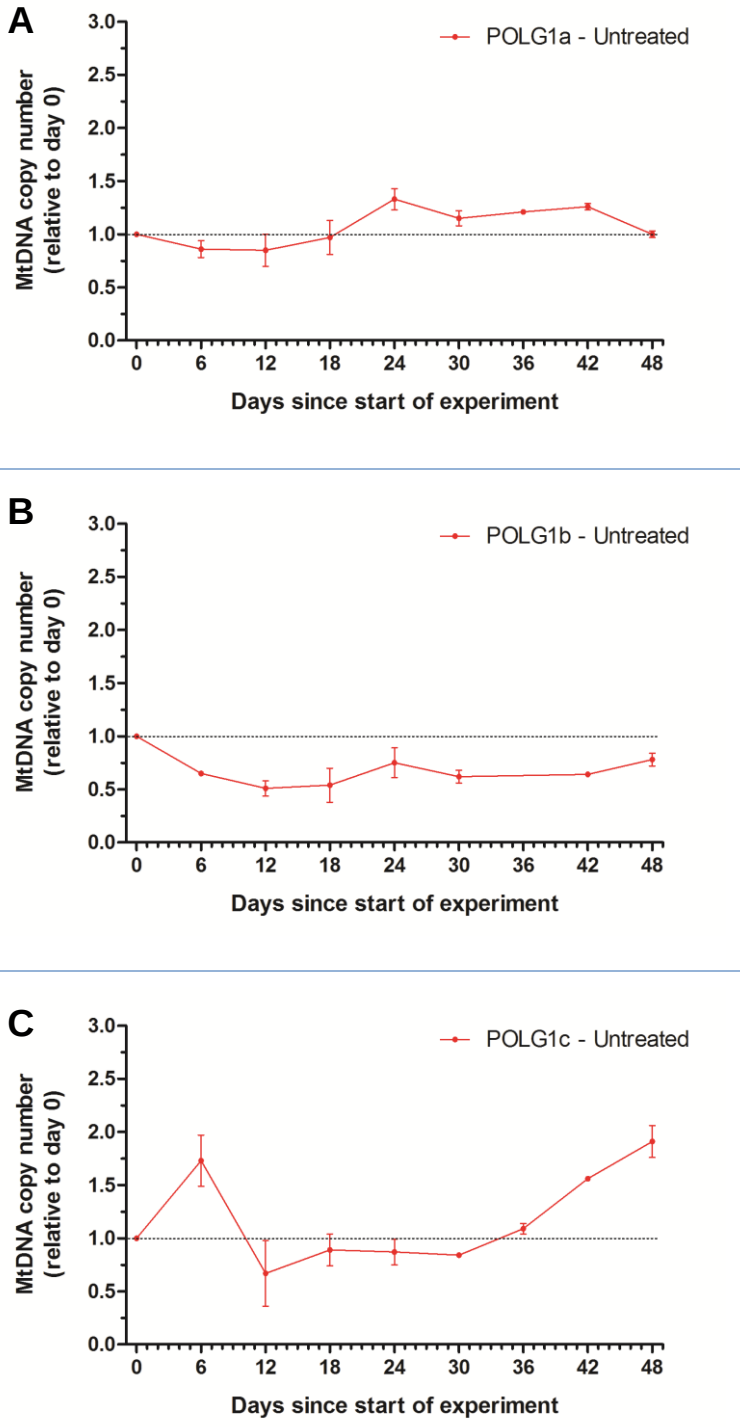

Figure B-4 MtDNA copy number variation in untreated *POLG1* cell lines: (A) POLG1a, (B) POLG1b and (C) POLG1c. Each data point represents the average mtDNA copy number relative to the mtDNA copy number at day 0 for two replicates. The error bars are presented as standard deviations (SDs).

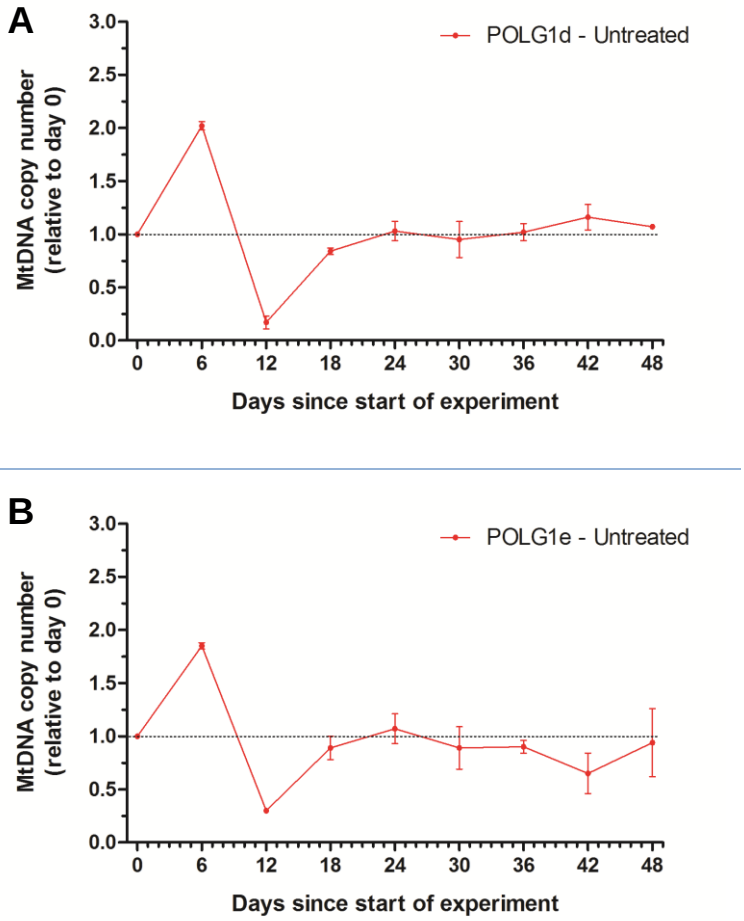

Figure B-5 MtDNA copy number variation in untreated *POLG1* cell lines: (A) POLG1d, and (B) POLG1e. Each data point represents the average mtDNA copy number relative to the mtDNA copy number at day 0 for two replicates. The error bars are presented as standard deviations (SDs).

Appendix B.2

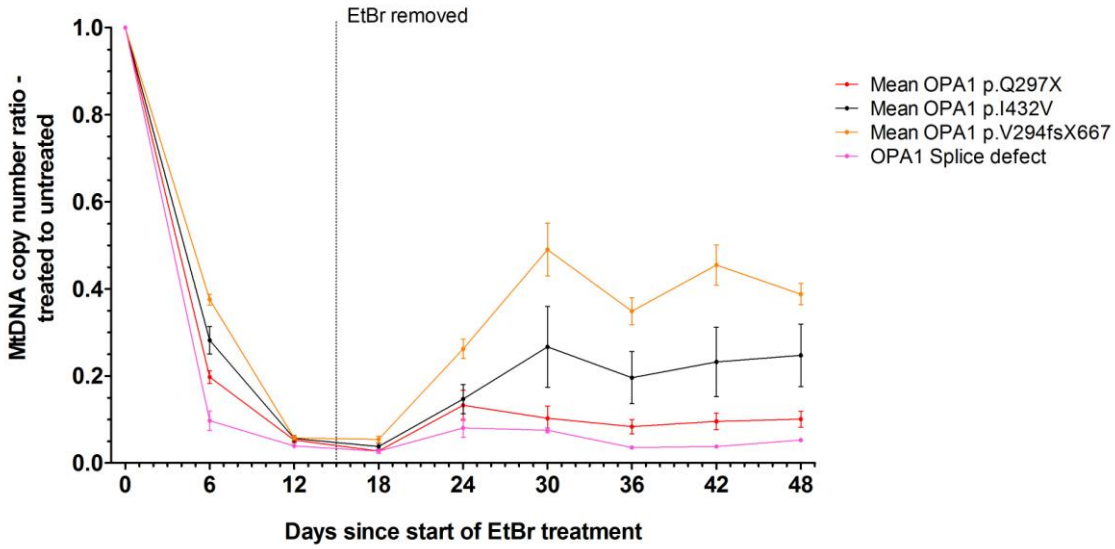

DAY OF STUDY		6	12	18	24	30	36	42	48
OPA1 p.Q297X vs.	OPA1 p.I432V	< 0.0001	0.6030	0.0006	0.0123	< 0.0001	< 0.0001	< 0.0001	< 0.0001
	OPA1 p.V294fsX667	< 0.0001	0.5132	0.0120	0.1963	0.0013	< 0.0001	0.0034	0.0001
	OPA1 Splice	0.0037	0.2419	0.9279	0.4152	0.5946	0.1178	0.1084	0.1687
OPA1 p.I432V vs.	OPA1 p.V294fsX667	0.2547	0.8451	0.0487	0.0375	0.0086	0.0114	0.0004	0.2355
	OPA1 Splice	< 0.0001	0.0680	0.1592	0.0049	0.0033	< 0.0001	0.0019	0.0037
OPA1 Splice vs.	OPA1 p.V294fsX667	< 0.0001	0.0323	0.0432	0.0004	0.0008	< 0.0001	< 0.0001	< 0.0001

Figure B-6 MtDNA depletion and repopulation curves for *OPA1* cell lines grouped into familial mutational subgroups: OPA1 p.Q297X (N = 3), OPA1 p.I432V (N = 2), OPA1 p.V294fsX667 (N = 2) and OPA1 splice (N =1). Each data point represents the average mtDNA copy number ratio of EtBr-treated to untreated cells. The error bars are presented as the standard errors of the mean (SEM). The table presents the P values of the statistical comparisons between all mutational subgroups. The intensity of the red shading correlates with the degree of statistical significance.

Appendix C.1

Mitochondrial network parameters (the total length of the mitochondrial network per cell, the average length of a mitochondrial fragment, and the number of mitochondrial fragments per cell) at each experimental point, in individual *POLG1* lines compared with the mean control. Please refer to **Section 7.4.2** for details.

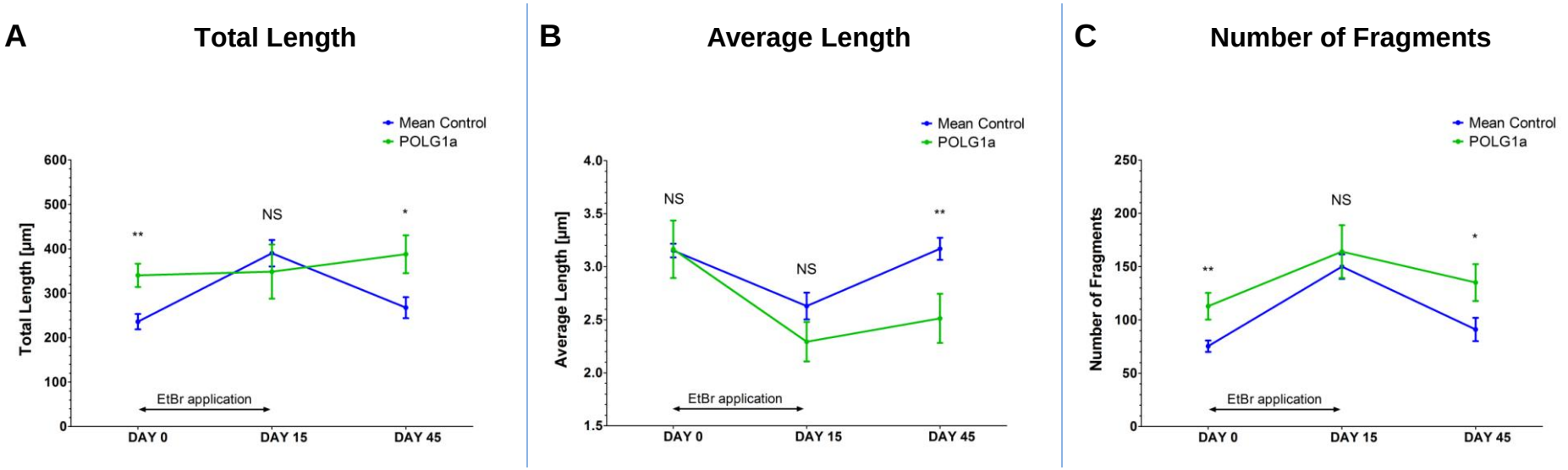

Figure C-1 Comparison of the mitochondrial network parameters between the POLG1a line and the mean control: (A) average total length of the mitochondrial network per cell, (B) average length of a mitochondrial fragment, and (C) average number of mitochondrial fragments per cell. The level of statistical significance at each time point is indicated for the comparison between the POLG1a line and the mean control. Each data point represents the mean value with the error bars representing the standard errors of the mean (SEM).

Total length: NS – non-significant at P = 0.5022, * - refers to P = 0.0162, ** - refers to P = 0.0068;

Average length: NS – non-significant at P = 0.9484 (day 0) and P = 0.1640 (day 15), ** - refers to P = 0.0057;

Number of fragments: NS – non-significant at P = 0.5624, * - refers to P = 0.0473, ** - refers to P = 0.0041.

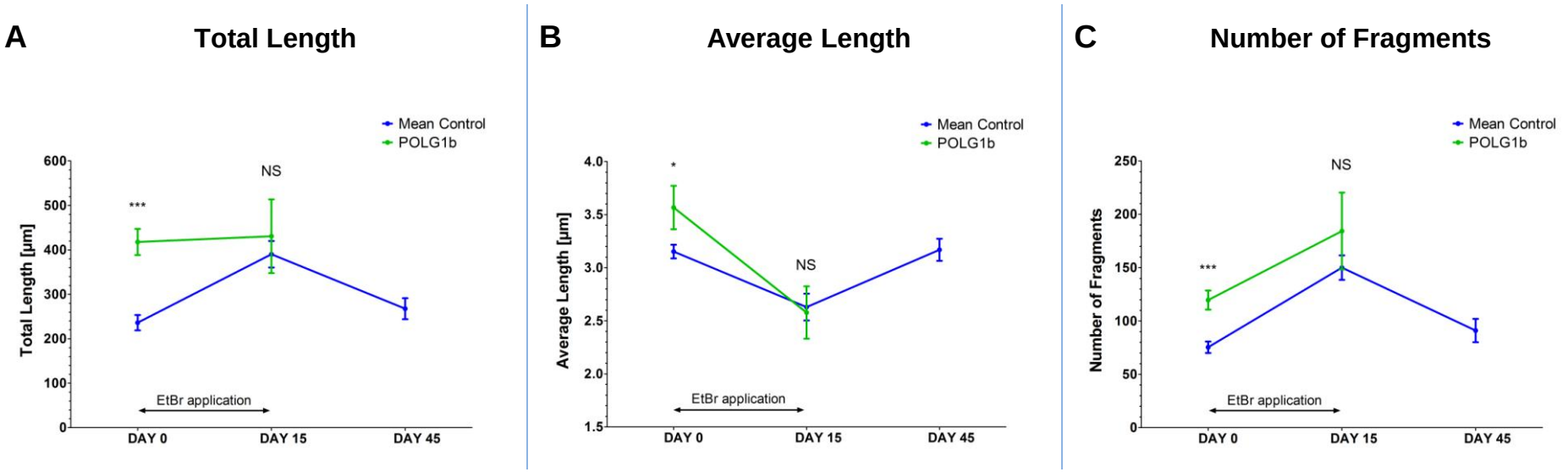

Figure C-2 Comparison of the mitochondrial network parameters between the POLG1b line and the mean control: (A) average total length of the mitochondrial network per cell, (B) average length of a mitochondrial fragment, and (C) average number of mitochondrial fragments per cell. The level of statistical significance at each time point is indicated for the comparison between the POLG1b line and the mean control. Each data point represents the mean value with the error bars representing the standard errors of the mean (SEM). Data points for the POLG1b cell line were unavailable at day 45 due to the premature death of the POLG1b EtBr-treated fibroblasts before that sampling point.

Total length: NS – non-significant at P = 0.5655, *** - refers to P < 0.0001;

Average length: NS – non-significant at P = 0.8427, * - refers to P = 0.0142;

Number of fragments: NS – non-significant at P = 0.2401, *** - refers to P = 0.0004.

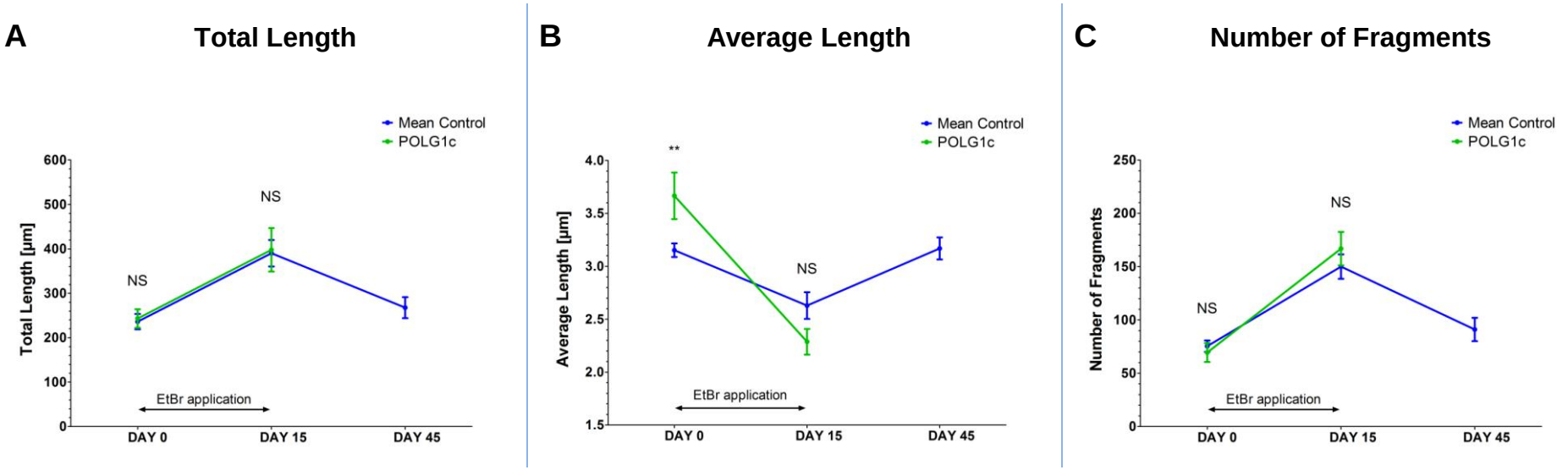

Figure C-3 Comparison of the mitochondrial network parameters between the POLG1c line and the mean control: (A) average total length of the mitochondrial network per cell, (B) average length of a mitochondrial fragment, and (C) average number of mitochondrial fragments per cell. The level of statistical significance at each time point is indicated for the comparison between the POLG1c line and the mean control. Each data point represents the mean value with the error bars representing the standard errors of the mean (SEM Data points for the POLG1c cell line were unavailable at day 45 due to the premature death of the POLG1c EtBr-treated fibroblasts before that sampling point.

Total length: NS – non-significant at P = 0.8454 (day 0) and P = 0.8946 (day 15);

Average length: NS – non-significant at P = 0.1307, ** - refers to P = 0.0035;

Number of fragments: NS – non-significant at P = 0.6098 (day 0) and P = 4314 (day 15).

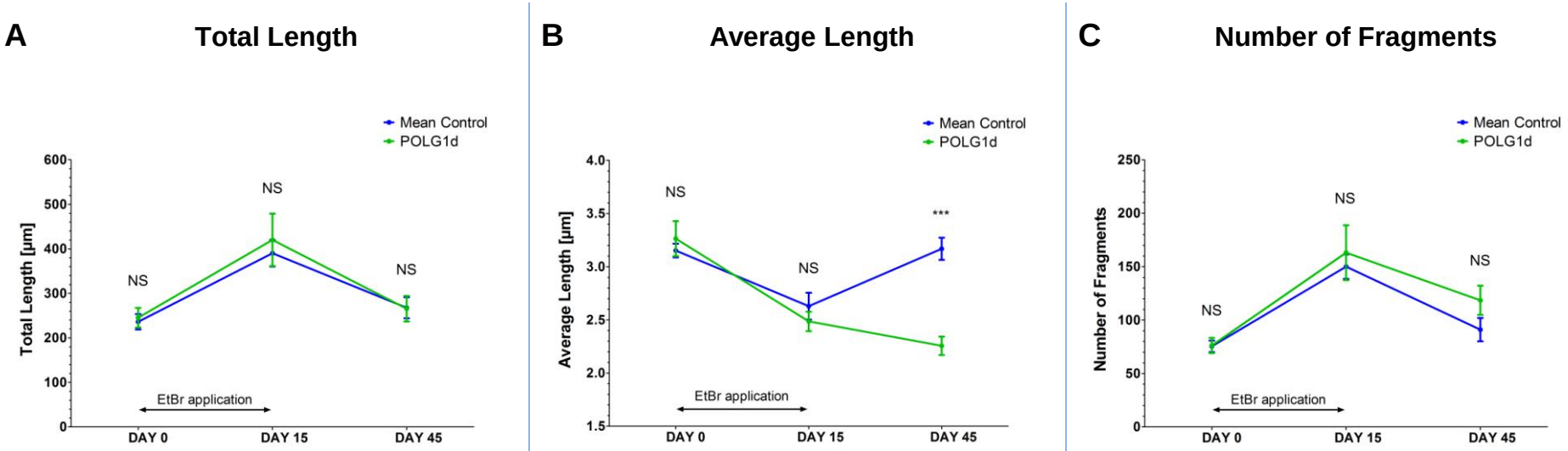

Figure C-4 Comparison of the mitochondrial network parameters between the POLG1d line and the mean control: (A) average total length of the mitochondrial network per cell, (B) average length of a mitochondrial fragment, and (C) average number of mitochondrial fragments per cell. The level of statistical significance at each time point is indicated for the comparison between the POLG1d line and the mean control. Each data point represents the mean value with the error bars representing the standard errors of the mean (SEM).

Total length: NS – non-significant at P = 0.7993 (day 0), P = 0.6402 (day 15) and P = 0.9607 (day 45);

Average length: NS – non-significant at P = 0.4646 (day 0) and P = 0.5535 (day 15), *** - refers to P < 0.0001;

Number of fragments: NS – non-significant at P = 0.9443 (day 0), P = 0.6079 (day 15) and P = 0.1917 (day 45).

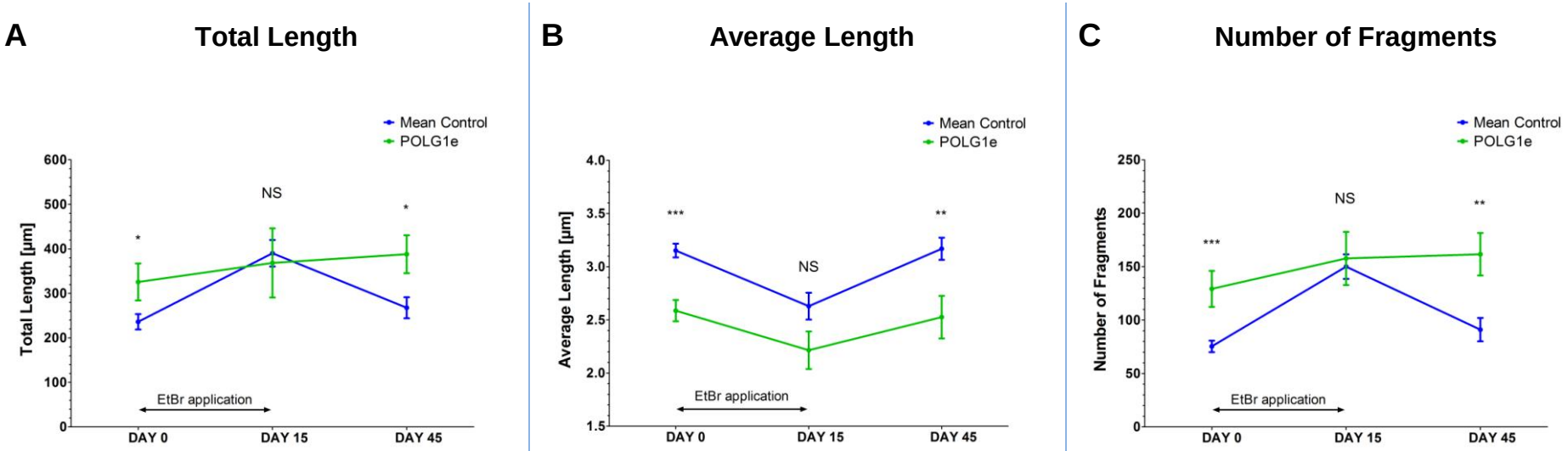

Figure C-5 Comparison of the mitochondrial network parameters between the POLG1e line and the mean control: (A) average total length of the mitochondrial network per cell, (B) average length of a mitochondrial fragment, and (C) average number of mitochondrial fragments per cell. The level of statistical significance at each time point is indicated for the comparison between the POLG1e line and the mean control. Each data point represents the mean value with the error bars representing the standard errors of the mean (SEM).

Total length: NS – non-significant at P = 0.7495, * - refers to P = 0.0300 (day 0) and P = 0.0168 (day 45);

Average length: NS – non-significant at P = 0.0854, ** - refers to P = 0.0047, *** - refers to P = 0.0002;

Number of fragments: NS – non-significant at P = 0.7522, ** - refers to P = 0.0029, *** - refers to P = 0.0002.

Appendix C.2

Mitochondrial network parameters (the total length of the mitochondrial network per cell, the average length of a mitochondrial fragment, and the number of mitochondrial fragments per cell) at each experimental point, in individual *OPA1* lines compared with the mean control. Please refer to **Section 7.4.3** for details.

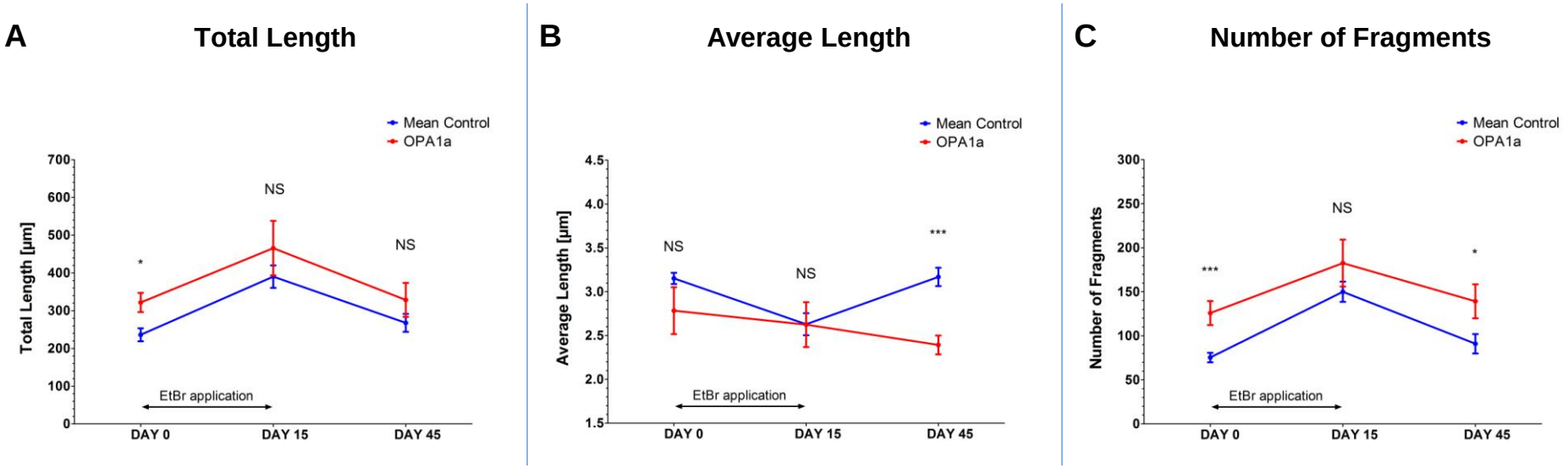

Figure C-6 Comparison of the mitochondrial network parameters between the OPA1a line and the mean control: (A) average total length of the mitochondrial network per cell, (B) average length of a mitochondrial fragment, and (C) average number of mitochondrial fragments per cell. The level of statistical significance at each time point is indicated for the comparison between the OPA1a line and the mean control. Each data point represents the mean value with the error bars representing the standard errors of the mean (SEM).

Total length: NS – non-significant at P = 0.2573 (day 15) and P = 0.2186 (day 45), * - refers to P = 0.0244;

Average length: NS – non-significant at P = 0.0503 (day 0) and P = 0.9847 (day 15), *** - refers to P = 0.0002;

Number of fragments: NS – non-significant at P = 0.1967, * - refers to P = 0.0350, *** - refers to P = 0.0002.

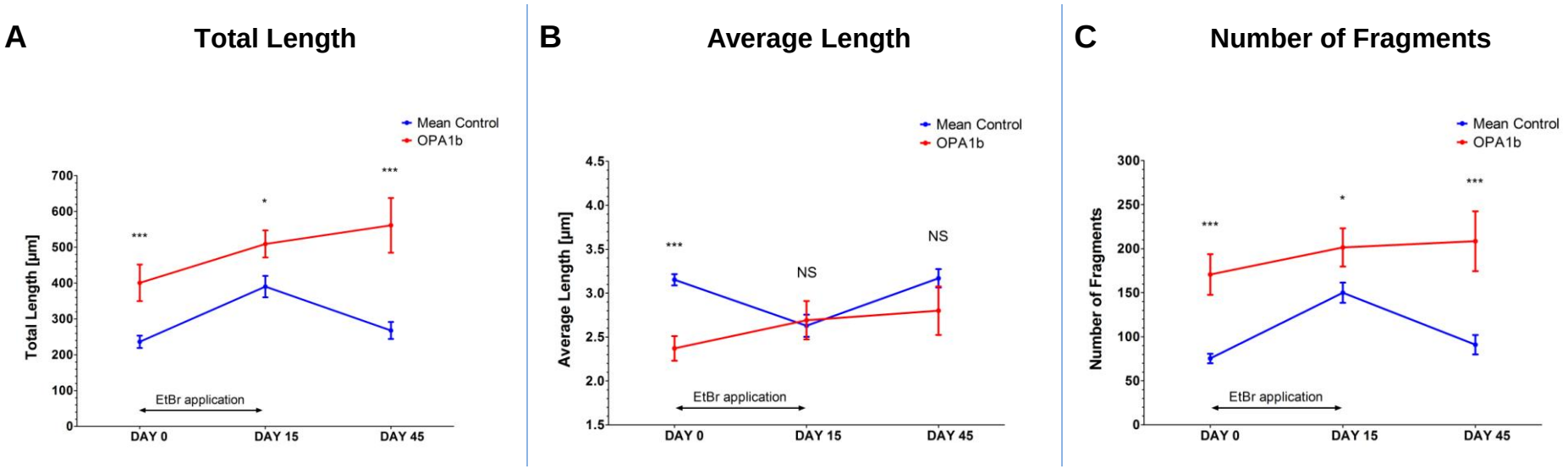

Figure C-7 Comparison of the mitochondrial network parameters between the OPA1b line and the mean control: (A) average total length of the mitochondrial network per cell, (B) average length of a mitochondrial fragment, and (C) average number of mitochondrial fragments per cell. The level of statistical significance at each time point is indicated for the comparison between the OPA1b line and the mean control. Each data point represents the mean value with the error bars representing the standard errors of the mean (SEM).

Total length: * - refers to P = 0.0350, *** - refers to P = 0.0003 (day 0) and P < 0.0001 (day 45);

Average length: NS – non-significant at P = 0.7992 (day 15) and P = 0.1692 (day 45), *** - refers to P < 0.0001;

Number of fragments: * - refers to P = 0.0320, *** - refers to P < 0.0001 (day 0) and P = 0.0002 (day 45).

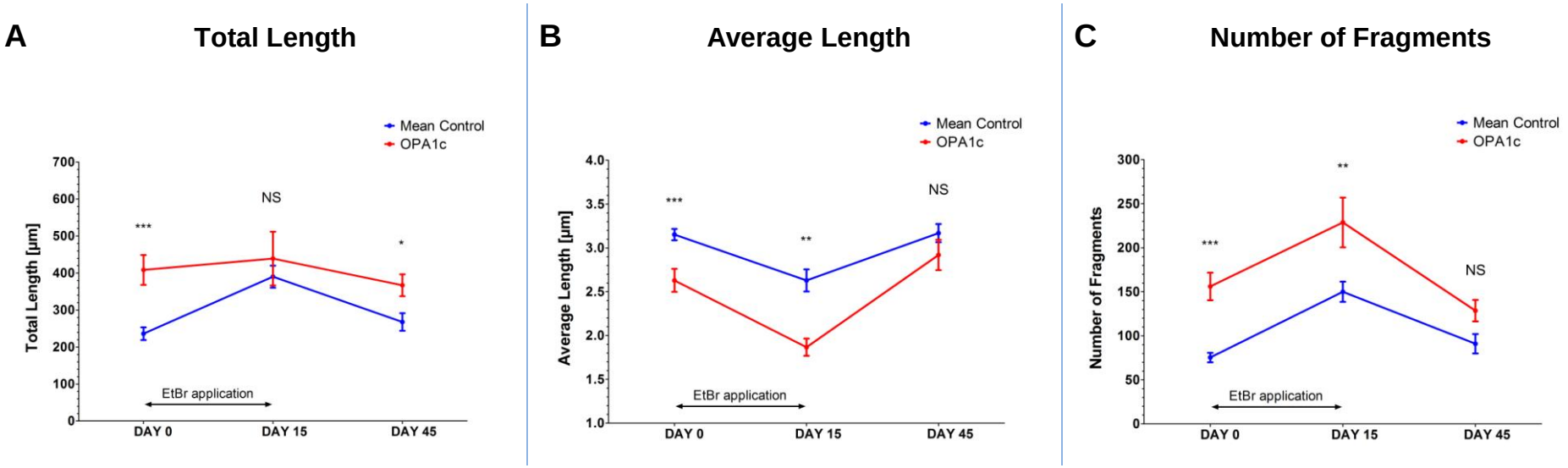

Figure C-8 Comparison of the mitochondrial network parameters between the OPA1c line and the mean control: (A) average total length of the mitochondrial network per cell, (B) average length of a mitochondrial fragment, and (C) average number of mitochondrial fragments per cell. The level of statistical significance at each time point is indicated for the comparison between the OPA1c line and the mean control. Each data point represents the mean value with the error bars representing the standard errors of the mean (SEM).

Total length: NS – non-significant at P = 0.4598, * - refers to P = 0.0321, *** - refers to P < 0.0001;

Average length: NS – non-significant at P = 0.2336, ** - refers to P = 0.0012, *** - refers to P = 0.0007;

Number of fragments: NS – non-significant at P = 0.0727, ** - refers to P = 0.0038, *** - refers to P < 0.0001.

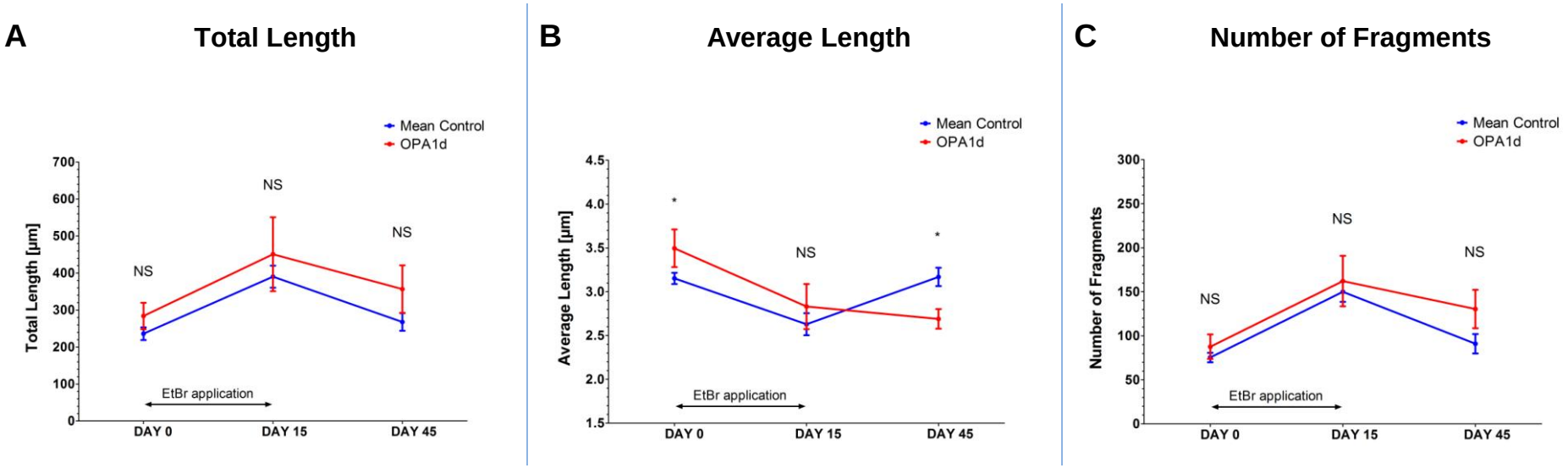

Figure C-9 Comparison of the mitochondrial network parameters between the OPA1d line and the mean control: (A) average total length of the mitochondrial network per cell, (B) average length of a mitochondrial fragment, and (C) average number of mitochondrial fragments per cell. The level of statistical significance at each time point is indicated for the comparison between the OPA1d line and the mean control. Each data point represents the mean value with the error bars representing the standard errors of the mean (SEM).

Total length: NS – non-significant at P = 0.2229 (day 0), P = 0.4379 (day 15) and P = 0.1135 (day 45);

Average length: NS – non-significant at P = 0.4405, * - refers to P = 0.0443 (day 0) and P = 0.0174 (day 45);

Number of fragments: NS – non-significant at P = 0.3445 (day 0), P = 0.6366 (day 15) and P = 0.0915 (day 45).

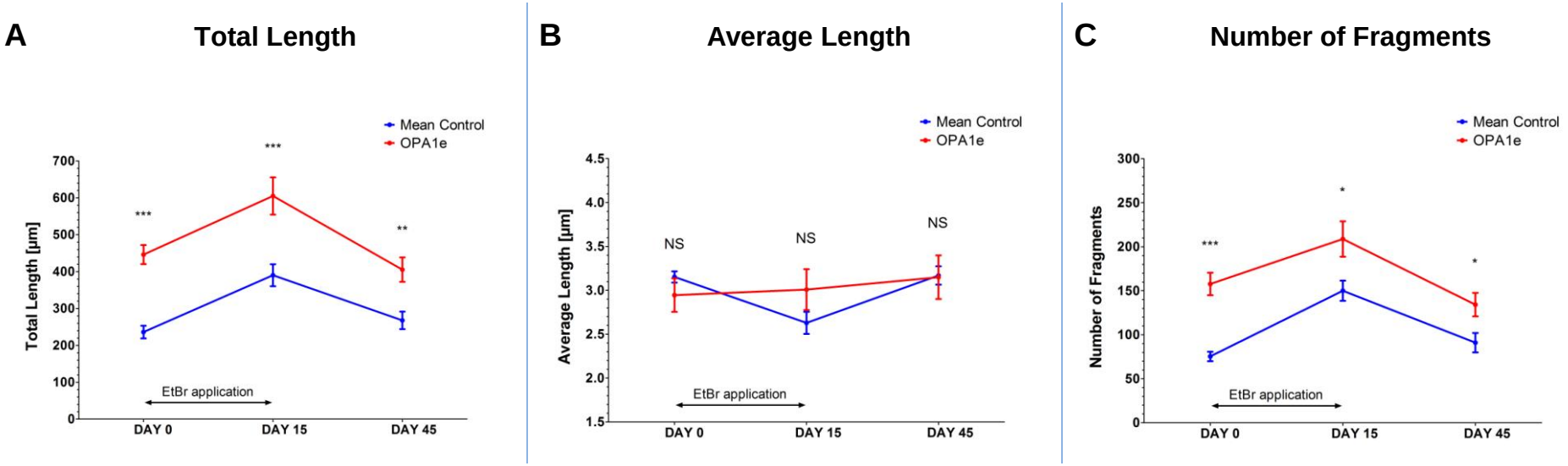

Figure C-10 Comparison of the mitochondrial network parameters between the OPA1e line and the mean control: (A) average total length of the mitochondrial network per cell, (B) average length of a mitochondrial fragment, and (C) average number of mitochondrial fragments per cell. The level of statistical significance at each time point is indicated for the comparison between the OPA1e line and the mean control. Each data point represents the mean value with the error bars representing the standard errors of the mean (SEM).

Total length: ** - refers to P = 0.0044, *** - refers to P < 0.0001 (day 0) and P = 0.0007 (day 15);

Average length: NS – non-significant at P = 0.1990 (day 0), P = 0.1393 (day 15) and P = 0.9311 (day 45);

Number of fragments: * - refers to P = 0.0130 (day 15) and P = 0.0427 (day 45), *** - refers to P < 0.0001.

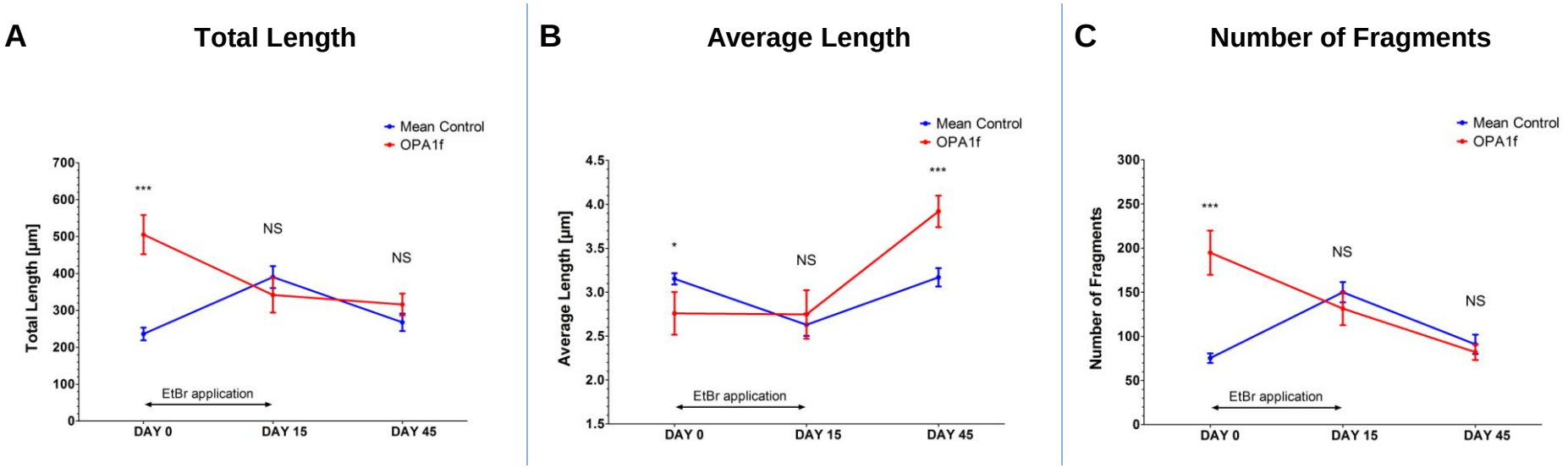

Figure C-11 Comparison of the mitochondrial network parameters between the OPA1f line and the mean control: (A) average total length of the mitochondrial network per cell, (B) average length of a mitochondrial fragment, and (C) average number of mitochondrial fragments per cell. The level of statistical significance at each time point is indicated for the comparison between the OPA1f line and the mean control. Each data point represents the mean value with the error bars representing the standard errors of the mean (SEM).

Total length: NS – non-significant at P = 0.4006 (day 15) and P = 0.6519 (day 45), *** - refers to P < 0.0001;

Average length: NS – non-significant at P = 0.6595, * - refers to P = 0.0294, *** - refers to P = 0.0009;

Number of fragments: NS – non-significant at P = 0.4063 (day 15) and P = 0.6545 (day 45), *** - refers to P < 0.0001.

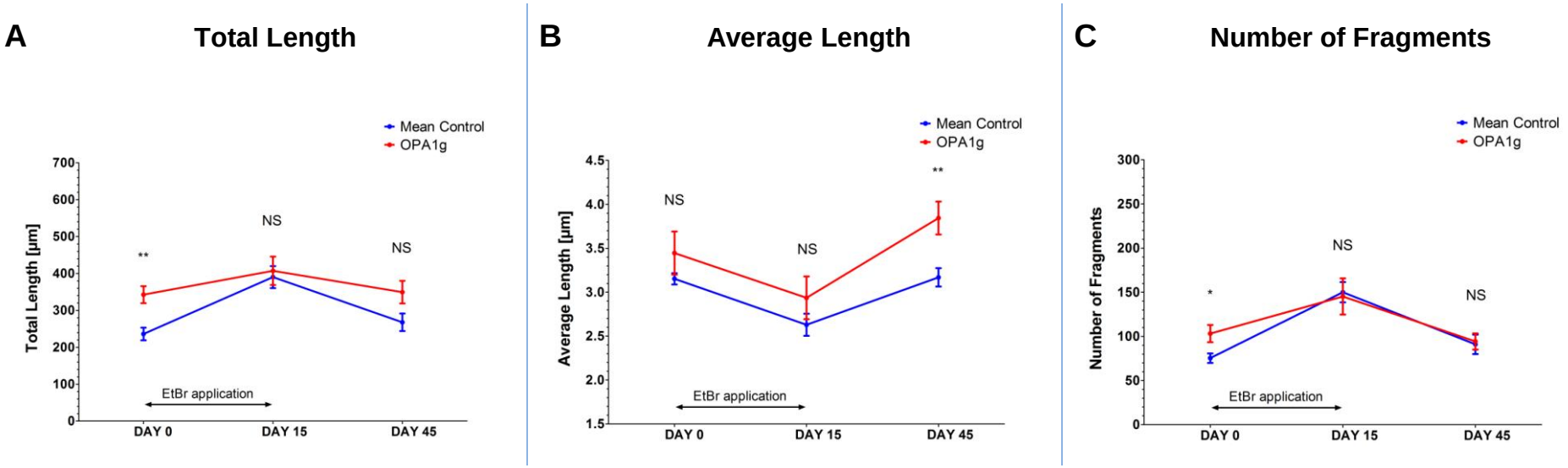

Figure C-12 Comparison of the mitochondrial network parameters between the OPA1g line and the mean control: (A) average total length of the mitochondrial network per cell, (B) average length of a mitochondrial fragment, and (C) average number of mitochondrial fragments per cell. The level of statistical significance at each time point is indicated for the comparison between the OPA1g line and the mean control. Each data point represents the mean value with the error bars representing the standard errors of the mean (SEM).

Total length: NS – non-significant at P = 0.7556 (day 15) and P = 0.0760 (day 45), ** - refers to P = 0.0052;

Average length: NS – non-significant at P = 0.1020 (day 0) and P = 0.2351 (day 15), ** - refers to P = 0.0027;

Number of fragments: NS – non-significant at P = 0.8324 (day 15) and P = 0.8702 (day 45), * - refers to P = 0.0231.

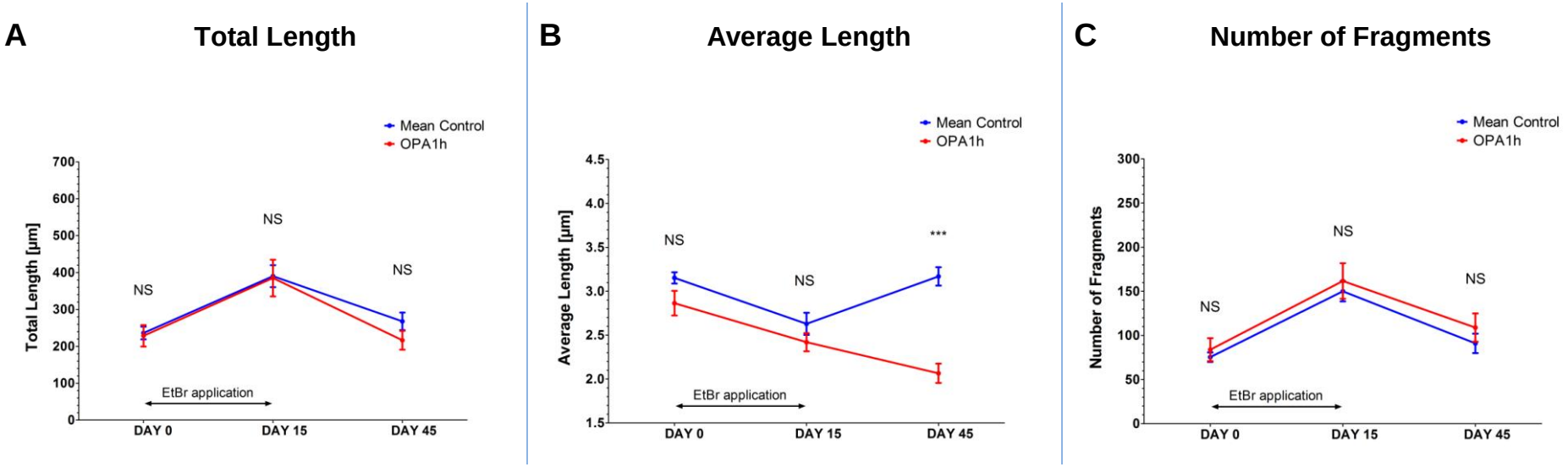

Figure C-13 Comparison of the mitochondrial network parameters between the OPA1h line and the mean control: (A) average total length of the mitochondrial network per cell, (B) average length of a mitochondrial fragment, and (C) average number of mitochondrial fragments per cell. The level of statistical significance at each time point is indicated for the comparison between the OPA1h line and the mean control. Each data point represents the mean value with the error bars representing the standard errors of the mean (SEM).

Total length: NS – non-significant at P = 0.8384 (day 0), P = 0.9297 (day 15) and P = 0.2499 (day 45);

Average length: NS – non-significant at P = 0.0547 (day 0) and P = 0.3436 (day 15), *** - refers to P < 0.0001;

Number of fragments: NS – non-significant at P = 0.5022 (day 0), P = 0.6070 (day 15) and P = 0.4047 (day 45).

Bibliography

Abrahams, J.P., Leslie, A.G., Lutter, R., Walker, J.E., 1994. Structure at 2.8 A resolution of F1-ATPase from bovine heart mitochondria. Nature. 370**,** 621-8.

Agier, V., Oliviero, P., Laine, J., L'Hermitte-Stead, C., Girard, S., Fillaut, S., Jardel, C., Bouillaud, F., Bulteau, A.L., Lombes, A., 2012. Defective mitochondrial fusion, altered respiratory function, and distorted cristae structure in skin fibroblasts with heterozygous OPA1 mutations. Biochim Biophys Acta. 1822**,** 1570-1580.

Alam, T.I., Kanki, T., Muta, T., Ukaji, K., Abe, Y., Nakayama, H., Takio, K., Hamasaki, N., Kang, D., 2003. Human mitochondrial DNA is packaged with TFAM. Nucleic Acids Res. 31**,** 1640-5.

Alavi, M.V., Bette, S., Schimpf, S., Schuettauf, F., Schraermeyer, U., Wehrl, H.F., Ruttiger, L., Beck, S.C., Tonagel, F., Pichler, B.J., Knipper, M., Peters, T., Laufs, J., Wissinger, B., 2007. A splice site mutation in the murine Opa1 gene features pathology of autosomal dominant optic atrophy. Brain. 130**,** 1029-42.

Alavi, M.V., Fuhrmann, N., Nguyen, H.P., Yu-Wai-Man, P., Heiduschka, P., Chinnery, P.F., Wissinger, B., 2009. Subtle neurological and metabolic abnormalities in an Opa1 mouse model of autosomal dominant optic atrophy. Exp Neurol. 220**,** 404-9.

Alberio, S., Mineri, R., Tiranti, V., Zeviani, M., 2007. Depletion of mtDNA: syndromes and genes. Mitochondrion. 7**,** 6-12.

Alberts, B., Bray, D., Lewis, J., Raff, M., Roberts, K. and Watson, J.D., 1994. Molecular Biology of the Cell., Vol., Garland Publishing, New York & London,.

Alexander, C., Votruba, M., Pesch, U.E., Thiselton, D.L., Mayer, S., Moore, A., Rodriguez, M., Kellner, U., Leo-Kottler, B., Auburger, G., Bhattacharya, S.S., Wissinger, B., 2000. OPA1, encoding a dynamin-related GTPase, is mutated in autosomal dominant optic atrophy linked to chromosome 3q28. Nat Genet. 26**,** 211--215.

Amati-Bonneau, P., Valentino, M.L., Reynier, P., Gallardo, M.E., Bornstein, B., Boissi?re, A., Campos, Y., Rivera, H., de la Aleja, J.G., Carroccia, R., Iommarini, L., Labauge, P., Figarella-Branger, D., Marcorelles, P., Furby, A., Beauvais, K., Letournel, F., Liguori, R., Morgia, C.L., Montagna, P., Liguori, M., Zanna, C., Rugolo, M., Cossarizza, A., Wissinger, B., Verny, C., Schwarzenbacher, R., Martín, M.A., Arenas, J., Ayuso, C., Garesse, R., Lenaers, G., Bonneau, D., Carelli, V., 2008. OPA1 mutations induce mitochondrial DNA instability and optic atrophy 'plus' phenotypes. Brain. 131**,** 338--351.

Amchenkova, A.A., Bakeeva, L.E., Chentsov, Y.S., Skulachev, V.P., Zorov, D.B., 1988. Coupling membranes as energy-transmitting cables. I. Filamentous mitochondria in fibroblasts and mitochondrial clusters in cardiomyocytes. J Cell Biol. 107**,** 481-95.

Amuthan, G., Biswas, G., Ananadatheerthavarada, H.K., Vijayasarathy, C., Shephard, H.M., Avadhani, N.G., 2002. Mitochondrial stress-induced calcium signaling, phenotypic changes and invasive behavior in human lung carcinoma A549 cells. Oncogene. 21**,** 7839-49.

Anderson, S., Bankier, A.T., Barrell, B.G., de Bruijn, M.H., Coulson, A.R., Drouin, J., Eperon, I.C., Nierlich, D.P., Roe, B.A., Sanger, F., Schreier, P.H., Smith, A.J., Staden, R., Young, I.G., 1981. Sequence and organization of the human mitochondrial genome. Nature. 290**,** 457--465.

Andersson, S.G., Zomorodipour, A., Andersson, J.O., Sicheritz-Ponten, T., Alsmark, U.C., Podowski, R.M., Naslund, A.K., Eriksson, A.S., Winkler, H.H., Kurland, C.G., 1998. The genome sequence of Rickettsia prowazekii and the origin of mitochondria. Nature. 396**,** 133-40.

Andrews, R.M., Griffiths, P.G., Johnson, M.A., Turnbull, D.M., 1999. Histochemical localisation of mitochondrial enzyme activity in human optic nerve and retina. Br J Ophthalmol. 83**,** 231-5.

Anikster, Y., Kleta, R., Shaag, A., Gahl, W.A., Elpeleg, O., 2001. Type III 3-methylglutaconic aciduria (optic atrophy plus syndrome, or Costeff optic atrophy syndrome): identification of the OPA3 gene and its founder mutation in Iraqi Jews. Am J Hum Genet. 69**,** 1218-24.

Armstrong, L., Tilgner, K., Saretzki, G., Atkinson, S.P., Stojkovic, M., Moreno, R., Przyborski, S., Lako, M., 2010. Human induced pluripotent stem cell lines show stress defense mechanisms and mitochondrial regulation similar to those of human embryonic stem cells. Stem Cells. 28**,** 661-73.

Asin-Cayuela, J., Gustafsson, C.M., 2007. Mitochondrial transcription and its regulation in mammalian cells. Trends Biochem Sci. 32**,** 111-7.

Assink, J.J., Tijmes, N.T., ten Brink, J.B., Oostra, R.J., Riemslag, F.C., de Jong, P.T., Bergen, A.A., 1997. A gene for X-linked optic atrophy is closely linked to the Xp11.4-Xp11.2 region of the X chromosome. Am J Hum Genet. 61**,** 934-9.

Aung, T., Ocaka, L., Ebenezer, N.D., Morris, A.G., Brice, G., Child, A.H., Hitchings, R.A., Lehmann, O.J., Bhattacharya, S.S., 2002. Investigating the association between OPA1 polymorphisms and glaucoma: comparison between normal tension and high tension primary open angle glaucoma. Hum Genet. 110**,** 513-4.

Balaban, R.S., Nemoto, S., Finkel, T., 2005. Mitochondria, oxidants, and aging. Cell. 120**,** 483-95.

Ban, H., Nishishita, N., Fusaki, N., Tabata, T., Saeki, K., Shikamura, M., Takada, N., Inoue, M., Hasegawa, M., Kawamata, S., Nishikawa, S., 2011. Efficient generation of transgene-free human induced pluripotent stem cells (iPSCs) by temperature-sensitive Sendai virus vectors. Proc Natl Acad Sci U S A. 108**,** 14234-9.

Barbet, F., Gerber, S., Hakiki, S., Perrault, I., Hanein, S., Ducroq, D., Tanguy, G., Dufier, J.L., Munnich, A., Rozet, J.M., Kaplan, J., 2003. A first locus for isolated autosomal recessive optic atrophy (ROA1) maps to chromosome 8q. Eur J Hum Genet. 11**,** 966-71.

Barbet, F., Hakiki, S., Orssaud, C., Gerber, S., Perrault, I., Hanein, S., Ducroq, D., Dufier, J.L., Munnich, A., Kaplan, J., Rozet, J.M., 2005. A third locus for dominant optic atrophy on chromosome 22q. J Med Genet. 42**,** e1.

Barrell, B.G., Bankier, A.T., Drouin, J., 1979. A different genetic code in human mitochondria. Nature. 282**,** 189-94.

Barron, M.J., Griffiths, P., Turnbull, D.M., Bates, D., Nichols, P., 2004. The distributions of mitochondria and sodium channels reflect the specific energy requirements and conduction properties of the human optic nerve head. Br J Ophthalmol. 88**,** 286-90.

Bartel, D.P., 2004. MicroRNAs: genomics, biogenesis, mechanism, and function. Cell. 116**,** 281-97.

Bellance, N., Lestienne, P., Rossignol, R., 2009. Mitochondria: from bioenergetics to the metabolic regulation of carcinogenesis. Front Biosci. 14**,** 4015-4034.

Bender, A., Krishnan, K.J., Morris, C.M., Taylor, G.A., Reeve, A.K., Perry, R.H., Jaros, E., Hersheson, J.S., Betts, J., Klopstock, T., Taylor, R.W., Turnbull, D.M., 2006. High levels of mitochondrial DNA deletions in substantia nigra neurons in aging and Parkinson disease. Nat Genet. 38**,** 515-7.

Berk, A.J., Clayton, D.A., 1974. Mechanism of mitochondrial DNA replication in mouse L-cells: asynchronous replication of strands, segregation of circular daughter molecules, aspects of topology and turnover of an initiation sequence. J Mol Biol. 86**,** 801-24.

Bilic, J., Izpisua Belmonte, J.C., 2012. Concise review: Induced pluripotent stem cells versus embryonic stem cells: close enough or yet too far apart? Stem Cells. 30**,** 33-41.

Birky, C.W., 1978. Transmission genetics of mitochondria and chloroplasts. Annu Rev Genet. 12**,** 471-512.

Bisaria, K.K., Narayan, D., 1973. The lamina cribrosa in some mammals - (a histological study). Indian J Ophthalmol. 178-81.

Biswas, G., Adebanjo, O.A., Freedman, B.D., Anandatheerthavarada, H.K., Vijayasarathy, C., Zaidi, M., Kotlikoff, M., Avadhani, N.G., 1999. Retrograde Ca2+ signaling in C2C12 skeletal myocytes in response to mitochondrial genetic and metabolic stress: a novel mode of inter-organelle crosstalk. EMBO J. 18**,** 522-33.

Bleazard, W., McCaffery, J.M., King, E.J., Bale, S., Mozdy, A., Tieu, Q., Nunnari, J., Shaw, J.M., 1999. The dynamin-related GTPase Dnm1 regulates mitochondrial fission in yeast. Nat Cell Biol. 1**,** 298--304.

Bodyak, N.D., Nekhaeva, E., Wei, J.Y., Khrapko, K., 2001. Quantification and sequencing of somatic deleted mtDNA in single cells: evidence for partially duplicated mtDNA in aged human tissues. Hum Mol Genet. 10**,** 17-24.

Bogenhagen, D., Clayton, D.A., 1977. Mouse L cell mitochondrial DNA molecules are selected randomly for replication throughout the cell cycle. Cell. 11**,** 719-27.

Bogenhagen, D.F., Rousseau, D., Burke, S., 2008. The layered structure of human mitochondrial DNA nucleoids. J Biol Chem. 283**,** 3665-75.

Bohlega, S., Tanji, K., Santorelli, F.M., Hirano, M., al-Jishi, A., DiMauro, S., 1996. Multiple mitochondrial DNA deletions associated with autosomal recessive ophthalmoplegia and severe cardiomyopathy. Neurology. 46**,** 1329-34.

Boland, M.J., Hazen, J.L., Nazor, K.L., Rodriguez, A.R., Gifford, W., Martin, G., Kupriyanov, S., Baldwin, K.K., 2009. Adult mice generated from induced pluripotent stem cells. Nature. 461**,** 91-4.

Bonawitz, N.D., Clayton, D.A., Shadel, G.S., 2006. Initiation and beyond: multiple functions of the human mitochondrial transcription machinery. Mol Cell. 24**,** 813-25.

Boulting, G.L., Kiskinis, E., Croft, G.F., Amoroso, M.W., Oakley, D.H., Wainger, B.J., Williams, D.J., Kahler, D.J., Yamaki, M., Davidow, L., Rodolfa, C.T., Dimos, J.T., Mikkilineni, S., MacDermott, A.B., Woolf, C.J., Henderson, C.E., Wichterle, H., Eggan, K., 2011. A functionally characterized test set of human induced pluripotent stem cells. Nat Biotechnol. 29**,** 279-86.

Bourne, H.R., Sanders, D. A., McCormick, F., 1990. The GTPase superfamily: a conserved switch for diverse cell functions. Nature. 348**,** 125-132.

Bowmaker, M., Yang, M.Y., Yasukawa, T., Reyes, A., Jacobs, H.T., Huberman, J.A., Holt, I.J., 2003. Mammalian mitochondrial DNA replicates bidirectionally from an initiation zone. J Biol Chem. 278**,** 50961-9.

Boyer, P.D., 1997. The ATP synthase--a splendid molecular machine. Annu Rev Biochem. 66**,** 717-49.

Brierley, E.J., Johnson, M.A., Lightowlers, R.N., James, O.F., Turnbull, D.M., 1998. Role of mitochondrial DNA mutations in human aging: implications for the central nervous system and muscle. Ann Neurol. 43**,** 217-23.

Bristow, E.A., Griffiths, P.G., Andrews, R.M., Johnson, M.A., Turnbull, D.M., 2002. The distribution of mitochondrial activity in relation to optic nerve structure. Arch Ophthalmol. 120**,** 791-6.

Brooks, C., Wei, Q., Feng, L., Dong, G., Tao, Y., Mei, L., Xie, Z.J., Dong, Z., 2007. Bak regulates mitochondrial morphology and pathology during apoptosis by interacting with mitofusins. Proc Natl Acad Sci U S A. 104**,** 11649-54.

Brown, T.A., Cecconi, C., Tkachuk, A.N., Bustamante, C., Clayton, D.A., 2005. Replication of mitochondrial DNA occurs by strand displacement with alternative light-strand origins, not via a strand-coupled mechanism. Genes Dev. 19**,** 2466-76.

Bua, E., Johnson, J., Herbst, A., Delong, B., McKenzie, D., Salamat, S., Aiken, J.M., 2006. Mitochondrial DNA-deletion mutations accumulate intracellularly to detrimental levels in aged human skeletal muscle fibers. Am J Hum Genet. 79**,** 469-80.

Bua, E.A., McKiernan, S.H., Wanagat, J., McKenzie, D., Aiken, J.M., 2002. Mitochondrial abnormalities are more frequent in muscles undergoing sarcopenia. J Appl Physiol. 92**,** 2617-24.

Butow, R.A., Avadhani, N.G., 2004. Mitochondrial signaling: the retrograde response. Mol Cell. 14**,** 1-15.

Calvo, S., Jain, M., Xie, X., Sheth, S.A., Chang, B., Goldberger, O.A., Spinazzola, A., Zeviani, M., Carr, S.A., Mootha, V.K., 2006. Systematic identification of human mitochondrial disease genes through integrative genomics. Nat Genet. 38**,** 576-82.

Cann, R.L., 2001. Genetic clues to dispersal in human populations: retracing the past from the present. Science. 291**,** 1742-8.

Cannino, G., Di Liegro, C.M., Di Liegro, I., Rinaldi, A.M., 2004. Analysis of cytochrome C oxidase subunits III and IV expression in developing rat brain. Neuroscience. 128**,** 91-8.

Cannino, G., Di Liegro, C.M., Rinaldi, A.M., 2007. Nuclear-mitochondrial interaction. Mitochondrion. 7**,** 359-66.

Cao, L., Shitara, H., Horii, T., Nagao, Y., Imai, H., Abe, K., Hara, T., Hayashi, J., Yonekawa, H., 2007. The mitochondrial bottleneck occurs without reduction of mtDNA content in female mouse germ cells. Nat Genet. 39**,** 386-90.

Cao, L., Shitara, H., Sugimoto, M., Hayashi, J., Abe, K., Yonekawa, H., 2009. New evidence confirms that the mitochondrial bottleneck is generated without reduction of mitochondrial DNA content in early primordial germ cells of mice. PLoS Genet. 5**,** e1000756.

Carelli, V., Schimpf, S., Fuhrmann, N., Valentino, M.L., Zanna, C., Iommarini, L., Papke, M., Schaich, S., Tippmann, S., Baumann, B., Barboni, P., Longanesi, L., Rugolo, M., Ghelli, A., Alavi, M.V., Youle, R.J., Bucchi, L., Carroccia, R., Giannoccaro, M.P., Tonon, C., Lodi, R., Cenacchi, G., Montagna, P., Liguori, R., Wissinger, B., 2011. A clinically complex form of dominant optic atrophy (OPA8) maps on chromosome 16. Hum Mol Genet. 20**,** 1893-905.

Carey, B.W., Markoulaki, S., Hanna, J., Saha, K., Gao, Q., Mitalipova, M., Jaenisch, R., 2009. Reprogramming of murine and human somatic cells using a single polycistronic vector. Proc Natl Acad Sci U S A. 106**,** 157-62.

Caspi, R.R., 2010. A look at autoimmunity and inflammation in the eye. J Clin Invest. 120**,** 3073-83.

Chan, S.S., Copeland, W.C., 2009. DNA polymerase gamma and mitochondrial disease: understanding the consequence of POLG mutations. Biochim Biophys Acta. 1787**,** 312-9.

Chen, Hsiuchen, Detmer, A, S., Ewald, J, A., Griffin, E, E., Fraser, E, S., Chan, C, D., 2003. Mitofusins Mfn1 and Mfn2 coordinately regulate mitochondrial fusion and are essential for embryonic development. J Cell Biol. 160**,** 189-200.

Chen, H., Chan, D.C., 2005. Emerging functions of mammalian mitochondrial fusion and fission. Hum Mol Genet. 14 Spec No. 2**,** R283--R289.

Chen, H., Chan, D.C., 2009. Mitochondrial dynamics--fusion, fission, movement, and mitophagy--in neurodegenerative diseases. Hum Mol Genet. 18**,** R169-76.

Chen, H., Vermulst, M., Wang, Y.E., Chomyn, A., Prolla, T.A., McCaffery, J.M., Chan, D.C., 2010. Mitochondrial fusion is required for mtDNA stability in skeletal muscle and tolerance of mtDNA mutations. Cell. 141**,** 280-9.

Chen, X., Prosser, R., Simonetti, S., Sadlock, J., Jagiello, G., Schon, E.A., 1995. Rearranged mitochondrial genomes are present in human oocytes. Am J Hum Genet. 57**,** 239-47.

Chen, X.J., Butow, R.A., 2005. The organization and inheritance of the mitochondrial genome. Nat Rev Genet. 6**,** 815-25.

Chevrollier, A., Guillet, V., Loiseau, D., Gueguen, N.g., de Crescenzo, M.-A.P., Verny, C., Ferre, M., Dollfus, H.n., Odent, S., Milea, D., Goizet, C., Amati-Bonneau, P., Procaccio, V., Bonneau, D., Reynier, P., 2008. Hereditary optic neuropathies share a common mitochondrial coupling defect. Ann Neurol. 63**,** 794--798.

Chevrollier, A., Cassereau, J., Ferre, M., Alban, J., Desquiret-Dumas, V., Gueguen, N., Amati-Bonneau, P., Procaccio, V., Bonneau, D., Reynier, P., 2012. Standardized mitochondrial analysis gives new insights into mitochondrial dynamics and OPA1 function. Int J Biochem Cell Biol. 44**,** 980-8.

Chin, M.H., Mason, M.J., Xie, W., Volinia, S., Singer, M., Peterson, C., Ambartsumyan, G., Aimiuwu, O., Richter, L., Zhang, J., Khvorostov, I., Ott, V., Grunstein, M., Lavon, N., Benvenisty, N., Croce, C.M., Clark, A.T., Baxter, T., Pyle, A.D., Teitell, M.A., Pelegrini, M., Plath, K., Lowry, W.E., 2009. Induced pluripotent stem cells and embryonic stem cells are distinguished by gene expression signatures. Cell Stem Cell. 5**,** 111-23.

Chinnery, P.F., Samuels, D.C., 1999. Relaxed replication of mtDNA: A model with implications for the expression of disease. Am J Hum Genet. 64**,** 1158-65.

Chinnery, P.F., Zwijnenburg, P.J., Walker, M., Howell, N., Taylor, R.W., Lightowlers, R.N., Bindoff, L., Turnbull, D.M., 1999. Nonrandom tissue distribution of mutant mtDNA. Am J Med Genet. 85**,** 498-501.

Chinnery, P.F., Zeviani, M., 2008. 155th ENMC workshop: polymerase gamma and disorders of mitochondrial DNA synthesis, 21-23 September 2007, Naarden, The Netherlands. Neuromuscul Disord. 18**,** 259-67.

Choi, S.Y., Huang, P., Jenkins, G.M., Chan, D.C., Schiller, J., Frohman, M.A., 2006. A common lipid links Mfn-mediated mitochondrial fusion and SNARE-regulated exocytosis. Nat Cell Biol. 8**,** 1255-62.

Christian, B., Haque, E., Spremulli, L., 2009. Ribosome shifting or splitting: it is all up to the EF-G. Mol Cell. 35**,** 400-2.

Christian, B.E., Spremulli, L.L., 2011. Mechanism of protein biosynthesis in mammalian mitochondria. Biochim Biophys Acta.

Chun, Y.S., Byun, K., Lee, B., 2011. Induced pluripotent stem cells and personalized medicine: current progress and future perspectives. Anat Cell Biol. 44**,** 245-55.

Chung, H.K., Spremulli, L.L., 1990. Purification and characterization of elongation factor G from bovine liver mitochondria. J Biol Chem. 265**,** 21000-4.

Chung, K.W., Kim, S.B., Park, K.D., Choi, K.G., Lee, J.H., Eun, H.W., Suh, J.S., Hwang, J.H., Kim, W.K., Seo, B.C., Kim, S.H., Son, I.H., Kim, S.M., Sunwoo, I.N., Choi, B.O., 2006. Early onset severe and late-onset mild Charcot-Marie-Tooth disease with mitofusin 2 (MFN2) mutations. Brain. 129**,** 2103-18.

Cipolat, S., Martins de Brito, O., Dal Zilio, B., Scorrano, L., 2004. OPA1 requires mitofusin 1 to promote mitochondrial fusion. Proc Natl Acad Sci U S A. 101**,** 15927-32.

Cipolat, S., Rudka, T., Hartmann, D., Costa, V., Serneels, L., Craessaerts, K., Metzger, K., Frezza, C., Annaert, W., D'Adamio, L., Derks, C., Dejaegere, T., Pellegrini, L., D'Hooge, R., Scorrano, L., De Strooper, B., 2006. Mitochondrial rhomboid PARL regulates cytochrome c release during apoptosis via OPA1-dependent cristae remodeling. Cell. 126**,** 163-75.

Clay Montier, L.L., Deng, J.J., Bai, Y., 2009. Number matters: control of mammalian mitochondrial DNA copy number. J Genet Genomics. 36**,** 125-31.

Clayton, D.A., 1982. Replication of animal mitochondrial DNA. Cell. 28**,** 693-705.

Cohen, B.H., Naviaux, R.K., 2010. The clinical diagnosis of POLG disease and other mitochondrial DNA depletion disorders. Methods. 51**,** 364-73.

Cohn, A.C., Toomes, C., Potter, C., Towns, K.V., Hewitt, A.W., Inglehearn, C.F., Craig, J.E., Mackey, D.A., 2007. Autosomal dominant optic atrophy: penetrance and expressivity in patients with OPA1 mutations. Am J Ophthalmol. 143**,** 656-662.

Copeland, W.C., 2008. Inherited mitochondrial diseases of DNA replication. Annu Rev Med. 59**,** 131-46.

Cortopassi, G.A., Shibata, D., Soong, N.W., Arnheim, N., 1992. A pattern of accumulation of a somatic deletion of mitochondrial DNA in aging human tissues. Proc Natl Acad Sci U S A. 89**,** 7370-4.

Cree, L.M., Samuels, D.C., de Sousa Lopes, S.C., Rajasimha, H.K., Wonnapinij, P., Mann, J.R., Dahl, H.H., Chinnery, P.F., 2008. A reduction of mitochondrial DNA molecules during embryogenesis explains the rapid segregation of genotypes. Nat Genet. 40**,** 249-54.

Cree, L.M., Samuels, D.C., Chinnery, P.F., 2009. The inheritance of pathogenic mitochondrial DNA mutations. Biochim Biophys Acta. 1792**,** 1097-102.

Czarnecka, A.M., Campanella, C., Zummo, G., Cappello, F., 2006. Mitochondrial chaperones in cancer: from molecular biology to clinical diagnostics. Cancer Biol Ther. 5**,** 714-20.

D'Aurelio, M., Pallotti, F., Barrientos, A., Gajewski, C.D., Kwong, J.Q., Bruno, C., Beal, M.F., Manfredi, G., 2001. In vivo regulation of oxidative phosphorylation in cells harboring a stop-codon mutation in mitochondrial DNA-encoded cytochrome c oxidase subunit I. J Biol Chem. 276**,** 46925-32.

Davidzon, G., Mancuso, M., Ferraris, S., Quinzii, C., Hirano, M., Peters, H.L., Kirby, D., Thorburn, D.R., DiMauro, S., 2005. POLG mutations and Alpers syndrome. Ann Neurol. 57**,** 921-3.

Davies, V.J., Hollins, A.J., Piechota, M.J., Yip, W., Davies, J.R., White, K.E., Nicols, P.P., Boulton, M.E., Votruba, M., 2007. Opa1 deficiency in a mouse model of autosomal dominant optic atrophy impairs mitochondrial morphology, optic nerve structure and visual function. Hum Mol Genet. 16**,** 1307-18.

Dayanithi, G., Chen-Kuo-Chang, M., Viero, C., Hamel, C., Muller, A., Lenaers, G., 2010. Characterization of Ca2+ signalling in postnatal mouse retinal ganglion cells: involvement of OPA1 in Ca2+ clearance. Ophthalmic Genet. 31**,** 53-65.

de Brito, O.M., Scorrano, L., 2008. Mitofusin 2 tethers endoplasmic reticulum to mitochondria. Nature. 456**,** 605-10.

de Brito, O.M., Scorrano, L., 2009. Mitofusin-2 regulates mitochondrial and endoplasmic reticulum morphology and tethering: the role of Ras. Mitochondrion. 9**,** 222-6.

De Giorgi, F., Lartigue, L., Ichas, F., 2000. Electrical coupling and plasticity of the mitochondrial network. Cell Calcium. 28**,** 365-70.

Del Bo, R., Bordoni, A., Sciacco, M., Di Fonzo, A., Galbiati, S., Crimi, M., Bresolin, N., Comi, G.P., 2003. Remarkable infidelity of polymerase gammaA associated with mutations in POLG1 exonuclease domain. Neurology. 61**,** 903-8.

Delettre, C., Lenaers, G., Griffoin, J.M., Gigarel, N., Lorenzo, C., Belenguer, P., Pelloquin, L., Grosgeorge, J., Turc-Carel, C., Perret, E., Astarie-Dequeker, C., Lasquellec, L., Arnaud, B., Ducommun, B., Kaplan, J., Hamel, C.P., 2000. Nuclear gene OPA1, encoding a mitochondrial dynamin-related protein, is mutated in dominant optic atrophy. Nat Genet. 26**,** 207--210.

Delettre, C., Griffoin, J.M., Kaplan, J., Dollfus, H., Lorenz, B., Faivre, L., Lenaers, G., Belenguer, P., Hamel, C.P., 2001. Mutation spectrum and splicing variants in the OPA1 gene. Hum Genet. 109**,** 584--591.

Deschauer, M., Kiefer, R., Blakely, E.L., He, L., Zierz, S., Turnbull, D.M., Taylor, R.W., 2003. A novel Twinkle gene mutation in autosomal dominant progressive external ophthalmoplegia. Neuromuscul Disord. 13**,** 568-72.

Desjardins, P., Frost, E., Morais, R., 1985. Ethidium bromide-induced loss of mitochondrial DNA from primary chicken embryo fibroblasts. Mol Cell Biol. 5**,** 1163-9.

Desnuelle, C., Birch-Machin, M., Pellissier, J.F., Bindoff, L.A., Ackrell, B.A., Turnbull, D.M., 1989. Multiple defects of the respiratory chain including complex II in a family with myopathy and encephalopathy. Biochem Biophys Res Commun. 163**,** 695-700.

Detmer, S.A., Chan, D.C., 2007. Functions and dysfunctions of mitochondrial dynamics. Nat Rev Mol Cell Biol. 8**,** 870--879.

Di Re, M., Sembongi, H., He, J., Reyes, A., Yasukawa, T., Martinsson, P., Bailey, L.J., Goffart, S., Boyd-Kirkup, J.D., Wong, T.S., Fersht, A.R., Spelbrink,

J.N., Holt, I.J., 2009. The accessory subunit of mitochondrial DNA polymerase gamma determines the DNA content of mitochondrial nucleoids in human cultured cells. Nucleic Acids Res. 37**,** 5701-13.

Diaz, F., Bayona-Bafaluy, M.P., Rana, M., Mora, M., Hao, H., Moraes, C.T., 2002. Human mitochondrial DNA with large deletions repopulates organelles faster than full-length genomes under relaxed copy number control. Nucleic Acids Res. 30**,** 4626-33.

Diaz, F., Moraes, C.T., 2008. Mitochondrial biogenesis and turnover. Cell Calcium. 44**,** 24-35.

Drews, K., Jozefczuk, J., Prigione, A., Adjaye, J., 2012. Human induced pluripotent stem cells-from mechanisms to clinical applications. J Mol Med (Berl).

Droge, W., 2002. Free radicals in the physiological control of cell function. Physiol Rev. 82**,** 47-95.

Duchen, M.R., 2004. Mitochondria in health and disease: perspectives on a new mitochondrial biology. Mol Aspects Med. 25**,** 365-451.

Durham, S.E., Bonilla, E., Samuels, D.C., DiMauro, S., Chinnery, P.F., 2005. Mitochondrial DNA copy number threshold in mtDNA depletion myopathy. Neurology. 65**,** 453-5.

Durham, S.E., Samuels, D.C., Cree, L.M., Chinnery, P.F., 2007. Normal levels of wild-type mitochondrial DNA maintain cytochrome c oxidase activity for two pathogenic mitochondrial DNA mutations but not for m.3243A-->G. Am J Hum Genet. 81**,** 189-95.

Ebert, A.D., Yu, J., Rose, F.F., Jr., Mattis, V.B., Lorson, C.L., Thomson, J.A., Svendsen, C.N., 2009. Induced pluripotent stem cells from a spinal muscular atrophy patient. Nature. 457**,** 277-80.

Ekstrand, M.I., Falkenberg, M., Rantanen, A., Park, C.B., Gaspari, M., Hultenby, K., Rustin, P., Gustafsson, C.M., Larsson, N.G., 2004. Mitochondrial transcription factor A regulates mtDNA copy number in mammals. Hum Mol Genet. 13**,** 935-44.

Elachouri, G., Vidoni, S., Zanna, C., Pattyn, A., Boukhaddaoui, H., Gaget, K., Yu-Wai-Man, P., Gasparre, G., Sarzi, E., Delettre, C., Olichon, A., Loiseau, D., Reynier, P., Chinnery, P.F., Rotig, A., Carelli, V., Hamel, C.P., Rugolo, M., Lenaers, G., 2011. OPA1 links human mitochondrial genome maintenance to mtDNA replication and distribution. Genome Res. 21**,** 12-20.

Elson, J.L., Samuels, D.C., Turnbull, D.M., Chinnery, P.F., 2001. Random intracellular drift explains the clonal expansion of mitochondrial DNA mutations with age. Am J Hum Genet. 68**,** 802-6.

Esteban, M.A., Wang, T., Qin, B., Yang, J., Qin, D., Cai, J., Li, W., Weng, Z., Chen, J., Ni, S., Chen, K., Li, Y., Liu, X., Xu, J., Zhang, S., Li, F., He, W., Labuda, K., Song, Y., Peterbauer, A., Wolbank, S., Redl, H., Zhong, M., Cai, D., Zeng, L., Pei, D., 2010. Vitamin C enhances the generation of mouse and human induced pluripotent stem cells. Cell Stem Cell. 6**,** 71-9.

Eura, Y., Ishihara, N., Yokota, S., Mihara, K., 2003. Two mitofusin proteins, mammalian homologues of FZO, with distinct functions are both required for mitochondrial fusion. J Biochem. 134**,** 333-44.

Evans, M.J., Kaufman, M.H., 1981. Establishment in culture of pluripotential cells from mouse embryos. Nature. 292**,** 154-6.

Evans, R.M., Barish, G.D., Wang, Y.X., 2004. PPARs and the complex journey to obesity. Nat Med. 10**,** 355-61.

Falkenberg, M., Gaspari, M., Rantanen, A., Trifunovic, A., Larsson, N.G., Gustafsson, C.M., 2002. Mitochondrial transcription factors B1 and B2 activate transcription of human mtDNA. Nat Genet. 31**,** 289-94.

Fannjiang, Y., Cheng, W.C., Lee, S.J., Qi, B., Pevsner, J., McCaffery, J.M., Hill, R.B., Basanez, G., Hardwick, J.M., 2004. Mitochondrial fission proteins regulate programmed cell death in yeast. Genes Dev. 18**,** 2785-97.

Fisher, R.P., Clayton, D.A., 1985. A transcription factor required for promoter recognition by human mitochondrial RNA polymerase. Accurate initiation at the heavy- and light-strand promoters dissected and reconstituted in vitro. J Biol Chem. 260**,** 11330-8.

Fraser, J.A., Biousse, V., Newman, N.J., 2010. The neuro-ophthalmology of mitochondrial disease. Surv Ophthalmol. 55**,** 299-334.

Frederick, R.L., Shaw, J.M., 2007. Moving mitochondria: establishing distribution of an essential organelle. Traffic. 8**,** 1668-75.

Frezza, C., Cipolat, S., Martins de Brito, O., Micaroni, M., Beznoussenko, G.V., Rudka, T., Bartoli, D., Polishuck, R.S., Danial, N.N., De Strooper, B., Scorrano, L., 2006. OPA1 controls apoptotic cristae remodeling independently from mitochondrial fusion. Cell. 126**,** 177-89.

Fuhrmann, N., Alavi, M.V., Bitoun, P., Woernle, S., Auburger, G., Leo-Kottler, B., Yu-Wai-Man, P., Chinnery, P., Wissinger, B., 2009. Genomic rearrangements in OPA1 are frequent in patients with autosomal dominant optic atrophy. J Med Genet. 46**,** 136-44.

Fukui, H., Moraes, C.T., 2009. Mechanisms of formation and accumulation of mitochondrial DNA deletions in aging neurons. Hum Mol Genet. 18**,** 1028-36.

Fusaki, N., Ban, H., Nishiyama, A., Saeki, K., Hasegawa, M., 2009. Efficient induction of transgene-free human pluripotent stem cells using a vector based on Sendai virus, an RNA virus that does not integrate into the host genome. Proc Jpn Acad Ser B Phys Biol Sci. 85**,** 348-62.

Garcin, R., Raverdy, P., Delthil, S., Man, H.X., Chimenes, H., 1961. [On a heredo-familial disease combining cataract, optic atrophy, extrapyramidal symptoms and certain defects of Friedreich's disease. (Its nosological position in relation to the Behr's syndrome, the Marinesco-Sjogren syndrome and Friedreich's disease with ocular symptoms]. Rev Neurol (Paris). 104**,** 373-9.

Garrido, N., Griparic, L., Jokitalo, E., Wartiovaara, J., van der Bliek, A.M., Spelbrink, J.N., 2003. Composition and dynamics of human mitochondrial nucleoids. Mol Biol Cell. 14**,** 1583-96.

Gibbons, C., Montgomery, M.G., Leslie, A.G., Walker, J.E., 2000. The structure of the central stalk in bovine F(1)-ATPase at 2.4 A resolution. Nat Struct Biol. 7**,** 1055-61.

Giguere, V., 2008. Transcriptional control of energy homeostasis by the estrogen-related receptors. Endocr Rev. 29**,** 677-96.

Giles, R.E., Blanc, H., Cann, H.M., Wallace, D.C., 1980. Maternal inheritance of human mitochondrial DNA. Proc Natl Acad Sci U S A. 77**,** 6715-9.

Gilkerson, R.W., Schon, E.A., Hernandez, E., Davidson, M.M., 2008. Mitochondrial nucleoids maintain genetic autonomy but allow for functional complementation. J Cell Biol. 181**,** 1117-28.

Gincel, D., Zaid, H., Shoshan-Barmatz, V., 2001. Calcium binding and translocation by the voltage-dependent anion channel: a possible regulatory mechanism in mitochondrial function. Biochem J. 358**,** 147-55.

Gray, H., Wong, T.W., 1992. Purification and identification of subunit structure of the human mitochondrial DNA polymerase. J Biol Chem. 267**,** 5835-41.

Gray, M.W., Burger, G., Lang, B.F., 1999. Mitochondrial evolution. Science. 283**,** 1476-81.

Graziewicz, M.A., Longley, M.J., Copeland, W.C., 2006. DNA polymerase gamma in mitochondrial DNA replication and repair. Chem Rev. 106**,** 383-405.

Green, D.R., 1998. Apoptotic pathways: the roads to ruin. Cell. 94**,** 695-8.

Gregoire, M., Morais, R., Quilliam, M.A., Gravel, D., 1984. On auxotrophy for pyrimidines of respiration-deficient chick embryo cells. Eur J Biochem. 142**,** 49-55.

Gresser, M.J., Myers, J.A., Boyer, P.D., 1982. Catalytic site cooperativity of beef heart mitochondrial F1 adenosine triphosphatase. Correlations of initial velocity, bound intermediate, and oxygen exchange measurements with an alternating three-site model. J Biol Chem. 257**,** 12030-8.

Grigorieff, N., 1999. Structure of the respiratory NADH:ubiquinone oxidoreductase (complex I). Curr Opin Struct Biol. 9**,** 476-83.

Griparic, L., Kanazawa, T., van der Bliek, A.M., 2007. Regulation of the mitochondrial dynamin-like protein Opa1 by proteolytic cleavage. J Cell Biol. 178**,** 757-64.

Guenther, M.G., Frampton, G.M., Soldner, F., Hockemeyer, D., Mitalipova, M., Jaenisch, R., Young, R.A., 2010. Chromatin structure and gene expression programs of human embryonic and induced pluripotent stem cells. Cell Stem Cell. 7**,** 249-57.

Guillery, O., Malka, F., Landes, T., Guillou, E., Blackstone, C., Lombes, A., Belenguer, P., Arnoult, D., Rojo, M., 2008. Metalloprotease-mediated OPA1 processing is modulated by the mitochondrial membrane potential. Biol Cell. 100**,** 315-25.

Gunter, T.E., Gunter, K.K., Sheu, S.S., Gavin, C.E., 1994. Mitochondrial calcium transport: physiological and pathological relevance. Am J Physiol. 267**,** C313-39.

Hakonen, A.H., Heiskanen, S., Juvonen, V., Lappalainen, I., Luoma, P.T., Rantamaki, M., Goethem, G.V., Lofgren, A., Hackman, P., Paetau, A., Kaakkola, S., Majamaa, K., Varilo, T., Udd, B., Kaariainen, H., Bindoff, L.A., Suomalainen, A., 2005. Mitochondrial DNA polymerase W748S mutation: a common cause of autosomal recessive ataxia with ancient European origin. Am J Hum Genet. 77**,** 430-41.

Hanein, S., Perrault, I., Roche, O., Gerber, S., Khadom, N., Rio, M., Boddaert, N., Jean-Pierre, M., Brahimi, N., Serre, V., Chretien, D., Delphin, N., Fares-Taie, L., Lachheb, S., Rotig, A., Meire, F., Munnich, A., Dufier, J.L., Kaplan, J., Rozet, J.M., 2009. TMEM126A, encoding a mitochondrial protein, is mutated in autosomal-recessive nonsyndromic optic atrophy. Am J Hum Genet. 84**,** 493-8.

Harding, A.E., Sweeney, M.G., Govan, G.G., Riordan-Eva, P., 1995. Pedigree analysis in Leber hereditary optic neuropathy families with a pathogenic mtDNA mutation. Am J Hum Genet. 57**,** 77-86.

Hatefi, Y., Galante, Y.M., 1980. Isolation of cytochrome b560 from complex II (succinateubiquinone oxidoreductase) and its reconstitution with succinate dehydrogenase. J Biol Chem. 255**,** 5530-7.

He, J., Mao, C.C., Reyes, A., Sembongi, H., Di Re, M., Granycome, C., Clippingdale, A.B., Fearnley, I.M., Harbour, M., Robinson, A.J., Reichelt, S., Spelbrink, J.N., Walker, J.E., Holt, I.J., 2007. The AAA+ protein ATAD3 has displacement loop binding properties and is involved in mitochondrial nucleoid organization. J Cell Biol. 176**,** 141-6.

He, L., Chinnery, P.F., Durham, S.E., Blakely, E.L., Wardell, T.M., Borthwick, G.M., Taylor, R.W., Turnbull, D.M., 2002. Detection and quantification of mitochondrial DNA deletions in individual cells by real-time PCR. Nucleic Acids Res. 30**,** e68.

Hermann, G.J., Thatcher, J.W., Mills, J.P., Hales, K.G., Fuller, M.T., Nunnari, J., Shaw, J.M., 1998. Mitochondrial fusion in yeast requires the transmembrane GTPase Fzo1p. J Cell Biol. 143**,** 359--373.

Herrington, J., Park, Y.B., Babcock, D.F., Hille, B., 1996. Dominant role of mitochondria in clearance of large Ca2+ loads from rat adrenal chromaffin cells. Neuron. 16**,** 219-28.

Herrnstadt, C., Elson, J.L., Fahy, E., Preston, G., Turnbull, D.M., Anderson, C., Ghosh, S.S., Olefsky, J.M., Beal, M.F., Davis, R.E., Howell, N., 2002. Reduced-median-network analysis of complete mitochondrial DNA coding-region sequences for the major African, Asian, and European haplogroups. Am J Hum Genet. 70**,** 1152-71.

Herrnstadt, C., Howell, N., 2004. An evolutionary perspective on pathogenic mtDNA mutations: haplogroup associations of clinical disorders. Mitochondrion. 4**,** 791-8.

Hinchliffe, P., Sazanov, L.A., 2005. Organization of iron-sulfur clusters in respiratory complex I. Science. 309**,** 771-4.

Hock, M.B., Kralli, A., 2009. Transcriptional control of mitochondrial biogenesis and function. Annu Rev Physiol. 71**,** 177-203.

Hollenbeck, P.J., Saxton, W.M., 2005. The axonal transport of mitochondria. J Cell Sci. 118**,** 5411-5419.

Holt, I.J., Lorimer, H.E., Jacobs, H.T., 2000. Coupled leading- and lagging-strand synthesis of mammalian mitochondrial DNA. Cell. 100**,** 515-24.

Horvath, R., Hudson, G., Ferrari, G., Futterer, N., Ahola, S., Lamantea, E., Prokisch, H., Lochmuller, H., McFarland, R., Ramesh, V., Klopstock, T., Freisinger, P., Salvi, F., Mayr, J.A., Santer, R., Tesarova, M., Zeman, J., Udd, B., Taylor, R.W., Turnbull, D., Hanna, M., Fialho, D., Suomalainen, A., Zeviani, M., Chinnery, P.F., 2006. Phenotypic spectrum associated with mutations of the mitochondrial polymerase gamma gene. Brain. 129**,** 1674-84.

Howell, N., Bindoff, L.A., McCullough, D.A., Kubacka, I., Poulton, J., Mackey, D., Taylor, L., Turnbull, D.M., 1991. Leber hereditary optic neuropathy: identification of the same mitochondrial ND1 mutation in six pedigrees. Am J Hum Genet. 49**,** 939-50.

Howell, N., Kubacka, I., Mackey, D.A., 1996. How rapidly does the human mitochondrial genome evolve? Am J Hum Genet. 59**,** 501-9.

Hu, B.Y., Weick, J.P., Yu, J., Ma, L.X., Zhang, X.Q., Thomson, J.A., Zhang, S.C., 2010. Neural differentiation of human induced pluripotent stem cells follows developmental principles but with variable potency. Proc Natl Acad Sci U S A. 107**,** 4335-40.

Huangfu, D., Osafune, K., Maehr, R., Guo, W., Eijkelenboom, A., Chen, S., Muhlestein, W., Melton, D.A., 2008. Induction of pluripotent stem cells from primary human fibroblasts with only Oct4 and Sox2. Nat Biotechnol. 26**,** 1269-75.

Hudson, G., Chinnery, P.F., 2006. Mitochondrial DNA polymerase-gamma and human disease. Hum Mol Genet. 15 Spec No 2**,** R244-52.

Hudson, G., Amati-Bonneau, P., Blakely, E.L., Stewart, J.D., He, L., Schaefer, A.M., Griffiths, P.G., Ahlqvist, K., Suomalainen, A., Reynier, P., McFarland, R., Turnbull, D.M., Chinnery, P.F., Taylor, R.W., 2008a. Mutation of OPA1 causes dominant optic atrophy with external ophthalmoplegia, ataxia, deafness and multiple mitochondrial DNA deletions: a novel disorder of mtDNA maintenance. Brain. 131**,** 329--337.

Hudson, G., Mowbray, C., Elson, J.L., Jacob, A., Boggild, M., Torroni, A., Chinnery, P.F., 2008b. Does mitochondrial DNA predispose to neuromyelitis optica (Devic's disease)? Brain. 131**,** e93.

Huoponen, K., Vilkki, J., Aula, P., Nikoskelainen, E.K., Savontaus, M.L., 1991. A new mtDNA mutation associated with Leber hereditary optic neuroretinopathy. Am J Hum Genet. 48**,** 1147-53.

Huss, J.M., Torra, I.P., Staels, B., Giguere, V., Kelly, D.P., 2004. Estrogen-related receptor alpha directs peroxisome proliferator-activated receptor alpha signaling in the transcriptional control of energy metabolism in cardiac and skeletal muscle. Mol Cell Biol. 24**,** 9079-91.

Hyslop, L.A., Armstrong, L., Stojkovic, M., Lako, M., 2005. Human embryonic stem cells: biology and clinical implications. Expert Rev Mol Med. 7**,** 1-21.

Ishihara, N., Fujita, Y., Oka, T., Mihara, K., 2006. Regulation of mitochondrial morphology through proteolytic cleavage of OPA1. EMBO J. 25**,** 2966-77.

Ishihara, N., Nomura, M., Jofuku, A., Kato, H., Suzuki, S.O., Masuda, K., Otera, H., Nakanishi, Y., Nonaka, I., Goto, Y., Taguchi, N., Morinaga, H., Maeda, M., Takayanagi, R., Yokota, S., Mihara, K., 2009. Mitochondrial fission factor Drp1 is essential for embryonic development and synapse formation in mice. Nat Cell Biol. 11**,** 958-66.

Ito, J., Braithwaite, D.K., 1990. Yeast mitochondrial DNA polymerase is related to the family A DNA polymerases. Nucleic Acids Res. 18**,** 6716.

Jacob, A., Das, K., Boggild, M., 2009. Estimating the incidence and prevalence of neuromyelitis optica in the UK: extrapolating data from Merseyside. Journal of Neurology, Neurosurgery and Psychiatry with Practical Neurology. 80.

Jazin, E., Soodyall, H., Jalonen, P., Lindholm, E., Stoneking, M., Gyllensten, U., 1998. Mitochondrial mutation rate revisited: hot spots and polymorphism. Nat Genet. 18**,** 109-10.

Jensen, R.E., Sesaki, H., 2006. Ahead of the curve: mitochondrial fusion and phospholipase D. Nat Cell Biol. 8**,** 1215-7.

Jenuth, J.P., Peterson, A.C., Fu, K., Shoubridge, E.A., 1996. Random genetic drift in the female germline explains the rapid segregation of mammalian mitochondrial DNA. Nat Genet. 14**,** 146-51.

Jia, F., Wilson, K.D., Sun, N., Gupta, D.M., Huang, M., Li, Z., Panetta, N.J., Chen, Z.Y., Robbins, R.C., Kay, M.A., Longaker, M.T., Wu, J.C., 2010. A nonviral minicircle vector for deriving human iPS cells. Nat Methods. 7**,** 197-9.

Jiang, Y., Cowley, S.A., Siler, U., Melguizo, D., Tilgner, K., Browne, C., Dewilton, A., Przyborski, S., Saretzki, G., James, W.S., Seger, R.A., Reichenbach, J., Lako, M., Armstrong, L., 2012. Derivation and functional analysis of patient-specific induced pluripotent stem cells as an in vitro model of chronic granulomatous disease. Stem Cells. 30**,** 599-611.

Johns, D.R., Neufeld, M.J., Park, R.D., 1992. An ND-6 mitochondrial DNA mutation associated with Leber hereditary optic neuropathy. Biochem Biophys Res Commun. 187**,** 1551-7.

Johns, D.R., Heher, K.L., Miller, N.R., Smith, K.H., 1993. Leber's hereditary optic neuropathy. Clinical manifestations of the 14484 mutation. Arch Ophthalmol. 111**,** 495-8.

Kadenbach, B., Jarausch, J., Hartmann, R., Merle, P., 1983. Separation of mammalian cytochrome c oxidase into 13 polypeptides by a sodium dodecyl sulfate-gel electrophoretic procedure. Anal Biochem. 129**,** 517-21.

Kaguni, L.S., 2004. DNA polymerase gamma, the mitochondrial replicase. Annu Rev Biochem. 73**,** 293-320.

Kahan, B.W., Ephrussi, B., 1970. Developmental potentialities of clonal in vitro cultures of mouse testicular teratoma. J Natl Cancer Inst. 44**,** 1015-36.

Karbowski, M., Lee, Y.J., Gaume, B., Jeong, S.Y., Frank, S., Nechushtan, A., Santel, A., Fuller, M., Smith, C.L., Youle, R.J., 2002. Spatial and temporal

association of Bax with mitochondrial fission sites, Drp1, and Mfn2 during apoptosis. J Cell Biol. 159**,** 931-8.

Karbowski, M., Arnoult, D., Chen, H., Chan, D.C., Smith, C.L., Youle, R.J., 2004. Quantitation of mitochondrial dynamics by photolabeling of individual organelles shows that mitochondrial fusion is blocked during the Bax activation phase of apoptosis. J Cell Biol. 164**,** 493-9.

Kasamatsu, H., Robberson, D.L., Vinograd, J., 1971. A novel closed-circular mitochondrial DNA with properties of a replicating intermediate. Proc Natl Acad Sci U S A. 68**,** 2252-7.

Kasiviswanathan, R., Collins, T.R., Copeland, W.C., 2011. The interface of transcription and DNA replication in the mitochondria. Biochim Biophys Acta.

Katz, B.J., Zhao, Y., Warner, J.E., Tong, Z., Yang, Z., Zhang, K., 2006. A family with X-linked optic atrophy linked to the OPA2 locus Xp11.4-Xp11.2. Am J Med Genet A. 140**,** 2207-11.

Kawamura, T., Suzuki, J., Wang, Y.V., Menendez, S., Morera, L.B., Raya, A., Wahl, G.M., Izpisua Belmonte, J.C., 2009. Linking the p53 tumour suppressor pathway to somatic cell reprogramming. Nature. 460**,** 1140-4.

Kayalar, C., Rosing, J., Boyer, P.D., 1977. An alternating site sequence for oxidative phosphorylation suggested by measurement of substrate binding patterns and exchange reaction inhibitions. J Biol Chem. 252**,** 2486-91.

Kerrison, J.B., Arnould, V.J., Ferraz Sallum, J.M., Vagefi, M.R., Barmada, M.M., Li, Y., Zhu, D., Maumenee, I.H., 1999. Genetic heterogeneity of dominant optic atrophy, Kjer type: Identification of a second locus on chromosome 18q12.2-12.3. Arch Ophthalmol. 117**,** 805-10.

Kim, D., Kim, C.H., Moon, J.I., Chung, Y.G., Chang, M.Y., Han, B.S., Ko, S., Yang, E., Cha, K.Y., Lanza, R., Kim, K.S., 2009. Generation of human induced pluripotent stem cells by direct delivery of reprogramming proteins. Cell Stem Cell. 4**,** 472-6.

Kim, J., Lee, J.H., Iyer, V.R., 2008. Global identification of Myc target genes reveals its direct role in mitochondrial biogenesis and its E-box usage in vivo. PLoS One. 3**,** e1798.

King, M.P., Attardi, G., 1989. Human cells lacking mtDNA: repopulation with exogenous mitochondria by complementation. Science. 246**,** 500-3.

Kirkman, M.A., Yu-Wai-Man, P., Chinnery, P.F., 2008. The clinical spectrum of mitochondrial genetic disorders. Clin Med. 8**,** 601-6.

Kjer, P., 1959. Infantile optic atrophy with dominant mode of inheritance: a clinical and genetic study of 19 Danish families. Acta Ophthalmol Suppl. 164**,** 1-147.

Koc, E.C., Spremulli, L.L., 2002. Identification of mammalian mitochondrial translational initiation factor 3 and examination of its role in initiation complex formation with natural mRNAs. J Biol Chem. 277**,** 35541-9.

Koehler, C.M., 2004. New developments in mitochondrial assembly. Annu Rev Cell Dev Biol. 20**,** 309-35.

Koshiba, T., Detmer, S.A., Kaiser, J.T., Chen, H., McCaffery, J.M., Chan, D.C., 2004. Structural basis of mitochondrial tethering by mitofusin complexes. Science. 305**,** 858-62.

Krauss, S., 2001. Mitochondria: Structure and Role in Respiration. Vol., ed.^eds. ENCYCLOPEDIA OF LIFE SCIENCES / Nature Publishing Group.

Kraytsberg, Y., Kudryavtseva, E., McKee, A.C., Geula, C., Kowall, N.W., Khrapko, K., 2006. Mitochondrial DNA deletions are abundant and cause functional impairment in aged human substantia nigra neurons. Nat Genet. 38**,** 518-20.

Krishnan, K.J., Reeve, A.K., Samuels, D.C., Chinnery, P.F., Blackwood, J.K., Taylor, R.W., Wanrooij, S., Spelbrink, J.N., Lightowlers, R.N., Turnbull, D.M., 2008. What causes mitochondrial DNA deletions in human cells? Nat Genet. 40**,** 275-9.

Kruse, B., Narasimhan, N., Attardi, G., 1989. Termination of transcription in human mitochondria: identification and purification of a DNA binding protein factor that promotes termination. Cell. 58**,** 391-7.

Kudva, Y.C., Ohmine, S., Greder, L.V., Dutton, J.R., Armstrong, A., De Lamo, J.G., Khan, Y.K., Thatava, T., Hasegawa, M., Fusaki, N., Slack, J.M.W., Ikeda, Y., 2012. Transgene-Free Disease-Specific Induced Pluripotent Stem Cells from Patients with Type 1 and Type 2 Diabetes. Stem Cells Translational Medicine. doi: 10.5966/sctm.2011-0044.

Kukat, C., Wurm, C.A., Spahr, H., Falkenberg, M., Larsson, N.G., Jakobs, S., 2011. Super-resolution microscopy reveals that mammalian mitochondrial nucleoids have a uniform size and frequently contain a single copy of mtDNA. Proc Natl Acad Sci U S A. 108**,** 13534-9.

Kyriakouli, D.S., Boesch, P., Taylor, R.W., Lightowlers, R.N., 2008. Progress and prospects: gene therapy for mitochondrial DNA disease. Gene Ther. 15**,** 1017-23.

La Morgia, C., Ross-Cisneros, F.N., Sadun, A.A., Hannibal, J., Munarini, A., Mantovani, V., Barboni, P., Cantalupo, G., Tozer, K.R., Sancisi, E., Salomao, S.R., Moraes, M.N., Moraes-Filho, M.N., Heegaard, S., Milea, D., Kjer, P., Montagna, P., Carelli, V., 2010. Melanopsin retinal ganglion cells are resistant to neurodegeneration in mitochondrial optic neuropathies. Brain. 133**,** 2426-38.

Landes, T., Leroy, I., Bertholet, A., Diot, A., Khosrobakhsh, F., Daloyau, M., Davezac, N., Miquel, M.-C., Courilleau, D., Guillou, E., Olichon, A., Lenaers, G., Arnauné-Pelloquin, L., Emorine, L.J., Belenguer, P., 2010. OPA1 (dys)functions. Semin Cell Dev Biol.

Lang, B.F., Burger, G., O'Kelly, C.J., Cedergren, R., Golding, G.B., Lemieux, C., Sankoff, D., Turmel, M., Gray, M.W., 1997. An ancestral mitochondrial DNA resembling a eubacterial genome in miniature. Nature. 387**,** 493-7.

Laurent, L.C., Ulitsky, I., Slavin, I., Tran, H., Schork, A., Morey, R., Lynch, C., Harness, J.V., Lee, S., Barrero, M.J., Ku, S., Martynova, M., Semechkin, R., Galat, V., Gottesfeld, J., Izpisua Belmonte, J.C., Murry, C., Keirstead, H.S., Park, H.S., Schmidt, U., Laslett, A.L., Muller, F.J., Nievergelt, C.M., Shamir, R., Loring, J.F., 2011. Dynamic changes in the copy number of pluripotency

and cell proliferation genes in human ESCs and iPSCs during reprogramming and time in culture. Cell Stem Cell. 8**,** 106-18.

Lee, S., Jeong, S.Y., Lim, W.C., Kim, S., Park, Y.Y., Sun, X., Youle, R.J., Cho, H., 2007. Mitochondrial fission and fusion mediators, hFis1 and OPA1, modulate cellular senescence. J Biol Chem. 282**,** 22977-83.

Lee, Y.J., Jeong, S.Y., Karbowski, M., Smith, C.L., Youle, R.J., 2004. Roles of the mammalian mitochondrial fission and fusion mediators Fis1, Drp1, and Opa1 in apoptosis. Mol Biol Cell. 15**,** 5001-11.

Legros, F., Lombes, A., Frachon, P., Rojo, M., 2002. Mitochondrial fusion in human cells is efficient, requires the inner membrane potential, and is mediated by mitofusins. Mol Biol Cell. 13**,** 4343-54.

Leibowitz, R.D., 1971. The effect of ethidium bromide on mitochondrial DNA synthesis and mitochondrial DNA structure in HeLa cells. J Cell Biol. 51**,** 116-22.

Lenaers, G., Reynier, P., Elachouri, G., Soukkarieh, C., Olichon, A., Belenguer, P., Baricault, L., Ducommun, B., Hamel, C., Delettre, C., 2009. OPA1 functions in mitochondria and dysfunctions in optic nerve. Int J Biochem Cell Biol. 41**,** 1866-74.

Lennon, V.A., Wingerchuk, D.M., Kryzer, T.J., Pittock, S.J., Lucchinetti, C.F., Fujihara, K., Nakashima, I., Weinshenker, B.G., 2004. A serum autoantibody marker of neuromyelitis optica: distinction from multiple sclerosis. Lancet. 364**,** 2106-12.

Levin, L.A., 2006. Chapter 21 "Physiology of the Optic Nerve". In: Duane's Ophthalmology. Vol., ed.^eds.

Li, H.O., Zhu, Y.F., Asakawa, M., Kuma, H., Hirata, T., Ueda, Y., Lee, Y.S., Fukumura, M., Iida, A., Kato, A., Nagai, Y., Hasegawa, M., 2000. A cytoplasmic RNA vector derived from nontransmissible Sendai virus with efficient gene transfer and expression. J Virol. 74**,** 6564-9.

Li, Z., Okamoto, K., Hayashi, Y., Sheng, M., 2004. The importance of dendritic mitochondria in the morphogenesis and plasticity of spines and synapses. Cell. 119**,** 873-87.

Liao, H.X., Spremulli, L.L., 1991. Initiation of protein synthesis in animal mitochondria. Purification and characterization of translational initiation factor 2. J Biol Chem. 266**,** 20714-9.

Liesa, M., Palacin, M., Zorzano, A., 2009. Mitochondrial dynamics in mammalian health and disease. Physiol Rev. 89**,** 799-845.

Lim, S.E., Longley, M.J., Copeland, W.C., 1999. The mitochondrial p55 accessory subunit of human DNA polymerase gamma enhances DNA binding, promotes processive DNA synthesis, and confers N-ethylmaleimide resistance. J Biol Chem. 274**,** 38197-203.

Lin, J., Tarr, P.T., Yang, R., Rhee, J., Puigserver, P., Newgard, C.B., Spiegelman, B.M., 2003. PGC-1beta in the regulation of hepatic glucose and energy metabolism. J Biol Chem. 278**,** 30843-8.

Linder, T., Park, C.B., Asin-Cayuela, J., Pellegrini, M., Larsson, N.G., Falkenberg, M., Samuelsson, T., Gustafsson, C.M., 2005. A family of putative transcription termination factors shared amongst metazoans and plants. Curr Genet. 48**,** 265-9.

Litonin, D., Sologub, M., Shi, Y., Savkina, M., Anikin, M., Falkenberg, M., Gustafsson, C.M., Temiakov, D., 2010. Human mitochondrial transcription revisited: only TFAM and TFB2M are required for transcription of the mitochondrial genes in vitro. J Biol Chem. 285**,** 18129-33.

Liu, X., Weaver, D., Shirihai, O., Hajnóczky, G., 2009. Mitochondrial 'kiss-and-run': interplay between mitochondrial motility and fusion-fission dynamics. EMBO J. 28**,** 3074--3089.

Liu, Z., Butow, R.A., 2006. Mitochondrial retrograde signaling. Annu Rev Genet. 40**,** 159-85.

Lodeiro, M.F., Uchida, A., Bestwick, M., Moustafa, I.M., Arnold, J.J., Shadel, G.S., Cameron, C.E., 2012. Transcription from the second heavy-strand promoter of human mtDNA is repressed by transcription factor A in vitro. Proc Natl Acad Sci U S A. 109**,** 6513-8.

Loeffen, J.L., Smeitink, J.A., Trijbels, J.M., Janssen, A.J., Triepels, R.H., Sengers, R.C., van den Heuvel, L.P., 2000. Isolated complex I deficiency in children: clinical, biochemical and genetic aspects. Hum Mutat. 15**,** 123-34.

Luoma, P., Melberg, A., Rinne, J.O., Kaukonen, J.A., Nupponen, N.N., Chalmers, R.M., Oldfors, A., Rautakorpi, I., Peltonen, L., Majamaa, K., Somer, H., Suomalainen, A., 2004. Parkinsonism, premature menopause, and mitochondrial DNA polymerase gamma mutations: clinical and molecular genetic study. Lancet. 364**,** 875-82.

Macarthur, C.C., Fontes, A., Ravinder, N., Kuninger, D., Kaur, J., Bailey, M., Taliana, A., Vemuri, M.C., Lieu, P.T., 2012. Generation of human-induced pluripotent stem cells by a nonintegrating RNA Sendai virus vector in feeder-free or xeno-free conditions. Stem Cells Int. 2012**,** 564612.

Mackey, D., Howell, N., 1992. A variant of Leber hereditary optic neuropathy characterized by recovery of vision and by an unusual mitochondrial genetic etiology. Am J Hum Genet. 51**,** 1218-28.

Madonna, R., 2012. Human-Induced Pluripotent Stem Cells: In Quest of Clinical Applications. Mol Biotechnol.

Maechler, P., Carobbio, S., Rubi, B., 2006. In beta-cells, mitochondria integrate and generate metabolic signals controlling insulin secretion. Int J Biochem Cell Biol. 38**,** 696-709.

Maekawa, M., Yamaguchi, K., Nakamura, T., Shibukawa, R., Kodanaka, I., Ichisaka, T., Kawamura, Y., Mochizuki, H., Goshima, N., Yamanaka, S., 2011. Direct reprogramming of somatic cells is promoted by maternal transcription factor Glis1. Nature. 474**,** 225-9.

Mannella, C.A., 2006. Structure and dynamics of the mitochondrial inner membrane cristae. Biochim Biophys Acta. 1763**,** 542-8.

Marchbank, N.J., Craig, J.E., Leek, J.P., Toohey, M., Churchill, A.J., Markham, A.F., Mackey, D.A., Toomes, C., Inglehearn, C.F., 2002. Deletion of the OPA1 gene in a dominant optic atrophy family: evidence that haploinsufficiency is the cause of disease. J Med Genet. 39**,** e47.

Marchetto, M.C., Yeo, G.W., Kainohana, O., Marsala, M., Gage, F.H., Muotri, A.R., 2009. Transcriptional signature and memory retention of human-induced pluripotent stem cells. PLoS One. 4**,** e7076.

Marchetto, M.C., Carromeu, C., Acab, A., Yu, D., Yeo, G.W., Mu, Y., Chen, G., Gage, F.H., Muotri, A.R., 2010. A model for neural development and treatment of Rett syndrome using human induced pluripotent stem cells. Cell. 143**,** 527-39.

Margulis, L., 1971. Symbiosis and evolution. Sci Am. 225**,** 48-57.

Martinou, J.C., Youle, R.J., 2011. Mitochondria in apoptosis: Bcl-2 family members and mitochondrial dynamics. Dev Cell. 21**,** 92-101.

McBride, H.M., Neuspiel, M., Wasiak, S., 2006. Mitochondria: more than just a powerhouse. Curr Biol. 16**,** R551-60.

McFarland, R., Clark, K.M., Morris, A.A., Taylor, R.W., Macphail, S., Lightowlers, R.N., Turnbull, D.M., 2002a. Multiple neonatal deaths due to a homoplasmic mitochondrial DNA mutation. Nat Genet. 30**,** 145-6.

McFarland, R., Taylor, R.W., Turnbull, D.M., 2002b. The neurology of mitochondrial DNA disease. Lancet Neurol. 1**,** 343-51.

Meeusen, S., McCaffery, J.M., Nunnari, J., 2004. Mitochondrial fusion intermediates revealed in vitro. Science. 305**,** 1747--1752.

Meeusen, S., DeVay, R., Block, J., Cassidy-Stone, A., Wayson, S., McCaffery, J.M., Nunnari, J., 2006. Mitochondrial inner-membrane fusion and crista maintenance requires the dynamin-related GTPase Mgm1. Cell. 127**,** 383-95.

Merkwirth, C., Langer, T., 2009. Prohibitin function within mitochondria: essential roles for cell proliferation and cristae morphogenesis. Biochim Biophys Acta. 1793**,** 27-32.

Metodiev, M.D., Lesko, N., Park, C.B., Camara, Y., Shi, Y., Wibom, R., Hultenby, K., Gustafsson, C.M., Larsson, N.G., 2009. Methylation of 12S rRNA is necessary for in vivo stability of the small subunit of the mammalian mitochondrial ribosome. Cell Metab. 9**,** 386-97.

Mili, S., Pinol-Roma, S., 2003. LRP130, a pentatricopeptide motif protein with a noncanonical RNA-binding domain, is bound in vivo to mitochondrial and nuclear RNAs. Mol Cell Biol. 23**,** 4972-82.

Mitchell, P., 1976. Vectorial chemistry and the molecular mechanics of chemiosmotic coupling: power transmission by proticity. Biochem Soc Trans. 4**,** 399-430.

Miyoshi, N., Ishii, H., Nagano, H., Haraguchi, N., Dewi, D.L., Kano, Y., Nishikawa, S., Tanemura, M., Mimori, K., Tanaka, F., Saito, T., Nishimura, J., Takemasa, I., Mizushima, T., Ikeda, M., Yamamoto, H., Sekimoto, M., Doki,

Y., Mori, M., 2011. Reprogramming of mouse and human cells to pluripotency using mature microRNAs. Cell Stem Cell. 8**,** 633-8.

Montoya, J., Christianson, T., Levens, D., Rabinowitz, M., Attardi, G., 1982. Identification of initiation sites for heavy-strand and light-strand transcription in human mitochondrial DNA. Proc Natl Acad Sci U S A. 79**,** 7195-9.

Montoya, J., Gaines, G.L., Attardi, G., 1983. The pattern of transcription of the human mitochondrial rRNA genes reveals two overlapping transcription units. Cell. 34**,** 151-9.

Mootha, V.K., Handschin, C., Arlow, D., Xie, X., St Pierre, J., Sihag, S., Yang, W., Altshuler, D., Puigserver, P., Patterson, N., Willy, P.J., Schulman, I.G., Heyman, R.A., Lander, E.S., Spiegelman, B.M., 2004. Erralpha and Gabpa/b specify PGC-1alpha-dependent oxidative phosphorylation gene expression that is altered in diabetic muscle. Proc Natl Acad Sci U S A. 101**,** 6570-5.

Moraes, C.T., Kenyon, L., Hao, H., 1999. Mechanisms of human mitochondrial DNA maintenance: the determining role of primary sequence and length over function. Mol Biol Cell. 10**,** 3345-56.

Morais, R., Gregoire, M., Jeannotte, L., Gravel, D., 1980. Chick embryo cells rendered respiration-deficient by chloramphenicol and ethidium bromide are auxotrophic for pyrimidines. Biochem Biophys Res Commun. 94**,** 71-7.

Moyes, C.D., Battersby, B.J., Leary, S.C., 1998. Regulation of muscle mitochondrial design. J Exp Biol. 201**,** 299-307.

Nakada, K., Sato, A., ichi Hayashi, J., 2009. Mitochondrial functional complementation in mitochondrial DNA-based diseases. Int J Biochem Cell Biol. 41**,** 1907--1913.

Nakada, K., Sato, Akitsugu, Hayashi, Jun ichi, 2009. Mitochondrial functional complementation in mitochondrial DNA-based diseases. Int J Biochem Cell Biol. 41**,** 1907-1913.

Nakamura, N., Saeki, K., Mitsumoto, M., Matsuyama, S., Nishio, M., Hasegawa, M., Miyagawa, Y., Ohkita, H., Kiyokawa, N., Toyoda, M., Akutsu, H., Umezawa, A., Yuo, A., 2012. Feeder-free and serum-free production of hepatocytes, cholangiocytes, and their proliferating progenitors from human pluripotent stem cells: application to liver-specific functional and cytotoxic assays. Cell Reprogram. 14**,** 171-85.

Narsinh, K.H., Plews, J., Wu, J.C., 2011. Comparison of human induced pluripotent and embryonic stem cells: fraternal or identical twins? Mol Ther. 19**,** 635-8.

Nass, M.M., 1970. Abnormal DNA patterns in animal mitochondria: ethidium bromide-induced breakdown of closed circular DNA and conditions leading to oligomer accumulation. Proc Natl Acad Sci U S A. 67**,** 1926-33.

Naviaux, R.K., Nyhan, W.L., Barshop, B.A., Poulton, J., Markusic, D., Karpinski, N.C., Haas, R.H., 1999. Mitochondrial DNA polymerase gamma deficiency and mtDNA depletion in a child with Alpers' syndrome. Ann Neurol. 45**,** 54-8.

Neuspiel, M., Zunino, R., Gangaraju, S., Rippstein, P., McBride, H., 2005. Activated mitofusin 2 signals mitochondrial fusion, interferes with Bax activation, and

reduces susceptibility to radical induced depolarization. J Biol Chem. 280**,** 25060-70.

Ngoh, G.A., Papanicolaou, K.N., Walsh, K., 2012. Loss of mitofusin 2 promotes endoplasmic reticulum stress. J Biol Chem. 287**,** 20321-32.

Nguyen, K.V., Ostergaard, E., Ravn, S.H., Balslev, T., Danielsen, E.R., Vardag, A., McKiernan, P.J., Gray, G., Naviaux, R.K., 2005. POLG mutations in Alpers syndrome. Neurology. 65**,** 1493-5.

Nicholas, A., Kraytsberg, Y., Guo, X., Khrapko, K., 2009. On the timing and the extent of clonal expansion of mtDNA deletions: evidence from single-molecule PCR. Exp Neurol. 218**,** 316-9.

Nolan, T., Hands, R.E., Bustin, S.A., 2006. Quantification of mRNA using real-time RT-PCR. Nat Protoc. 1**,** 1559-82.

Norrbom, J., Sundberg, C.J., Ameln, H., Kraus, W.E., Jansson, E., Gustafsson, T., 2004. PGC-1alpha mRNA expression is influenced by metabolic perturbation in exercising human skeletal muscle. J Appl Physiol. 96**,** 189-94.

Norrman, K., Fischer, Y., Bonnamy, B., Wolfhagen Sand, F., Ravassard, P., Semb, H., 2010. Quantitative comparison of constitutive promoters in human ES cells. PLoS One. 5**,** e12413.

Nsair, A., MacLellan, W.R., 2011. Induced pluripotent stem cells for regenerative cardiovascular therapies and biomedical discovery. Adv Drug Deliv Rev. 63**,** 324-30.

O'Brien, T.W., 2003. Properties of human mitochondrial ribosomes. IUBMB Life. 55**,** 505-13.

Olichon, A., Emorine, L.J., Descoins, E., Pelloquin, L., Brichese, L., Gas, N., Guillou, E., Delettre, C., Valette, A., Hamel, C.P., Ducommun, B., Lenaers, G., Belenguer, P., 2002. The human dynamin-related protein OPA1 is anchored to the mitochondrial inner membrane facing the inter-membrane space. FEBS Lett. 523**,** 171-176.

Olichon, A., Baricault, L., Gas, N., Guillou, E., Valette, A., Belenguer, P., Lenaers, G., 2003. Loss of OPA1 perturbates the mitochondrial inner membrane structure and integrity, leading to cytochrome c release and apoptosis. J Biol Chem. 278**,** 7743-7746.

Olichon, A., Landes, T., Arnauné-Pelloquin, L., Emorine, L.J., Mils, V., Guichet, A.s., Delettre, C., Hamel, C., Amati-Bonneau, P., Bonneau, D., Reynier, P., Lenaers, G., Belenguer, P., 2007. Effects of OPA1 mutations on mitochondrial morphology and apoptosis: relevance to ADOA pathogenesis. J Cell Physiol. 211**,** 423--430.

Otera, H., Mihara, K., 2012. Mitochondrial dynamics: functional link with apoptosis. Int J Cell Biol. 2012**,** 821676.

Pareyson, D., 2004. Differential diagnosis of Charcot-Marie-Tooth disease and related neuropathies. Neurol Sci. 25**,** 72-82.

Park, C.B., Asin-Cayuela, J., Camara, Y., Shi, Y.H., Pellegrini, M., Gaspari, M., Wibom, R., Hultenby, K., Erdjument-Bromage, H., Tempst, P., Falkenberg,

M., Gustafsson, C.M., Larsson, N.G., 2007. MTERF3 is a negative regulator of mammalian mtDNA transcription. Cell. 130**,** 273-285.

Payne, B.A., Wilson, I.J., Hateley, C.A., Horvath, R., Santibanez-Koref, M., Samuels, D.C., Price, D.A., Chinnery, P.F., 2011. Mitochondrial aging is accelerated by anti-retroviral therapy through the clonal expansion of mtDNA mutations. Nat Genet. 43**,** 806-10.

Pera, M.F., Reubinoff, B., Trounson, A., 2000. Human embryonic stem cells. J Cell Sci. 113 (Pt 1)**,** 5-10.

Perkins, G., Renken, C., Martone, M.E., Young, S.J., Ellisman, M., Frey, T., 1997. Electron tomography of neuronal mitochondria: three-dimensional structure and organization of cristae and membrane contacts. J Struct Biol. 119**,** 260-72.

Pfanner, N., Wiedemann, N., Meisinger, C., Lithgow, T., 2004. Assembling the mitochondrial outer membrane. Nat Struct Mol Biol. 11**,** 1044-8.

Pich, S., Bach, D., Briones, P., Liesa, M., Camps, M., Testar, X., Palacín, M., Zorzano, A., 2005. The Charcot-Marie-Tooth type 2A gene product, Mfn2, up-regulates fuel oxidation through expression of OXPHOS system. Hum Mol Genet. 14**,** 1405--1415.

Pickering, S.J., Braude, P.R., Patel, M., Burns, C.J., Trussler, J., Bolton, V., Minger, S., 2003. Preimplantation genetic diagnosis as a novel source of embryos for stem cell research. Reprod Biomed Online. 7**,** 353-64.

Pietromonaco, S.F., Denslow, N.D., O'Brien, T.W., 1991. Proteins of mammalian mitochondrial ribosomes. Biochimie. 73**,** 827-35.

Pinz, K.G., Bogenhagen, D.F., 2000. Characterization of a catalytically slow AP lyase activity in DNA polymerase gamma and other family A DNA polymerases. J Biol Chem. 275**,** 12509-14.

Pohjoismaki, J.L., Wanrooij, S., Hyvarinen, A.K., Goffart, S., Holt, I.J., Spelbrink, J.N., Jacobs, H.T., 2006. Alterations to the expression level of mitochondrial transcription factor A, TFAM, modify the mode of mitochondrial DNA replication in cultured human cells. Nucleic Acids Res. 34**,** 5815-28.

Puigserver, P., Wu, Z., Park, C.W., Graves, R., Wright, M., Spiegelman, B.M., 1998. A cold-inducible coactivator of nuclear receptors linked to adaptive thermogenesis. Cell. 92**,** 829-39.

Puri, M.C., Nagy, A., 2012. Concise review: Embryonic stem cells versus induced pluripotent stem cells: the game is on. Stem Cells. 30**,** 10-4.

Pyle, A., Taylor, R.W., Durham, S.E., Deschauer, M., Schaefer, A.M., Samuels, D.C., Chinnery, P.F., 2007. Depletion of mitochondrial DNA in leucocytes harbouring the 3243A->G mtDNA mutation. J Med Genet. 44**,** 69-74.

Pyle, A., Burn, D.J., Gordon, C., Swan, C., Chinnery, P.F., Baudouin, S.V., 2010. Fall in circulating mononuclear cell mitochondrial DNA content in human sepsis. Intensive Care Med. 36**,** 956-62.

Raha, S., Robinson, B.H., 2000. Mitochondria, oxygen free radicals, disease and ageing. Trends Biochem Sci. 25**,** 502-8.

Rajasimha, H.K., Chinnery, P.F., Samuels, D.C., 2008. Selection against pathogenic mtDNA mutations in a stem cell population leads to the loss of the 3243A-->G mutation in blood. Am J Hum Genet. 82**,** 333-43.

Reeve, A.K., Krishnan, K.J., Turnbull, D., 2008. Mitochondrial DNA mutations in disease, aging, and neurodegeneration. Ann N Y Acad Sci. 1147**,** 21-9.

Resnick, J.L., Bixler, L.S., Cheng, L., Donovan, P.J., 1992. Long-term proliferation of mouse primordial germ cells in culture. Nature. 359**,** 550-1.

Reubinoff, B.E., Pera, M.F., Fong, C.Y., Trounson, A., Bongso, A., 2000. Embryonic stem cell lines from human blastocysts: somatic differentiation in vitro. Nat Biotechnol. 18**,** 399-404.

Reynier, P., Amati-Bonneau, P., Verny, C., Olichon, A., Simard, G., Guichet, A., Bonnemains, C., Malecaze, F., Malinge, M.C., Pelletier, J.B., Calvas, P., Dollfus, H., Belenguer, P., Malthiery, Y., Lenaers, G., Bonneau, D., 2004. OPA3 gene mutations responsible for autosomal dominant optic atrophy and cataract. J Med Genet. 41**,** e110.

Robinson, B.H., Petrova-Benedict, R., Buncic, J.R., Wallace, D.C., 1992. Nonviability of cells with oxidative defects in galactose medium: a screening test for affected patient fibroblasts. Biochem Med Metab Biol. 48**,** 122-6.

Roger, A.J., Silberman, J.D., 2002. Cell evolution: mitochondria in hiding. Nature. 418**,** 827-9.

Rojo, Manuel, Legros, Frédéric, Chateau, Danielle, Lombès, Anne, 2002. Membrane topology and mitochondrial targeting of mitofusins, ubiquitous mammalian homologs of the transmembrane GTPase Fzo. J Cell Sci. 115**,** 1663-1674.

Rorbach, J., Richter, R., Wessels, H.J., Wydro, M., Pekalski, M., Farhoud, M., Kuhl, I., Gaisne, M., Bonnefoy, N., Smeitink, J.A., Lightowlers, R.N., Chrzanowska-Lightowlers, Z.M., 2008. The human mitochondrial ribosome recycling factor is essential for cell viability. Nucleic Acids Res. 36**,** 5787-99.

Rossier, M.F., 2006. T channels and steroid biosynthesis: in search of a link with mitochondria. Cell Calcium. 40**,** 155-64.

Rouzier, C., Bannwarth, S., Chaussenot, A., Chevrollier, A., Verschueren, A., Bonello-Palot, N., Fragaki, K., Cano, A., Pouget, J., Pellissier, J.F., Procaccio, V., Chabrol, B., Paquis-Flucklinger, V., 2012. The MFN2 gene is responsible for mitochondrial DNA instability and optic atrophy 'plus' phenotype. Brain. 135**,** 23-34.

Ryan, M.T., Hoogenraad, N.J., 2007. Mitochondrial-nuclear communications. Annu Rev Biochem. 76**,** 701-22.

Samuels, D.C., Schon, E.A., Chinnery, P.F., 2004. Two direct repeats cause most human mtDNA deletions. Trends Genet. 20**,** 393-8.

Santel, A., Fuller, M.T., 2001. Control of mitochondrial morphology by a human mitofusin. J Cell Sci. 114**,** 867--874.

Satoh, M., Hamamoto, T., Seo, N., Kagawa, Y., Endo, H., 2003. Differential sublocalization of the dynamin-related protein OPA1 isoforms in mitochondria. Biochem Biophys Res Commun. 300**,** 482-93.

Sbicego, S., Alfonzo, J.D., Estevez, A.M., Rubio, M.A., Kang, X., Turck, C.W., Peris, M., Simpson, L., 2003. RBP38, a novel RNA-binding protein from trypanosomatid mitochondria, modulates RNA stability. Eukaryot Cell. 2**,** 560-8.

Sbisa, E., Tanzariello, F., Reyes, A., Pesole, G., Saccone, C., 1997. Mammalian mitochondrial D-loop region structural analysis: identification of new conserved sequences and their functional and evolutionary implications. Gene. 205**,** 125-40.

Scarpulla, R.C., 2008. Transcriptional paradigms in mammalian mitochondrial biogenesis and function. Physiol Rev. 88**,** 611-38.

Schon, E.A., Rizzuto, R., Moraes, C.T., Nakase, H., Zeviani, M., DiMauro, S., 1989. A direct repeat is a hotspot for large-scale deletion of human mitochondrial DNA. Science. 244**,** 346-9.

Schwartz, M., Vissing, J., 2002. Paternal inheritance of mitochondrial DNA. N Engl J Med. 347**,** 576-80.

Schwartz, S.D., Hubschman, J.P., Heilwell, G., Franco-Cardenas, V., Pan, C.K., Ostrick, R.M., Mickunas, E., Gay, R., Klimanskaya, I., Lanza, R., 2012. Embryonic stem cell trials for macular degeneration: a preliminary report. Lancet. 379**,** 713-20.

Schwartzbach, C.J., Spremulli, L.L., 1989. Bovine mitochondrial protein synthesis elongation factors. Identification and initial characterization of an elongation factor Tu-elongation factor Ts complex. J Biol Chem. 264**,** 19125-31.

Schwer, B., North, B.J., Frye, R.A., Ott, M., Verdin, E., 2002. The human silent information regulator (Sir)2 homologue hSIRT3 is a mitochondrial nicotinamide adenine dinucleotide-dependent deacetylase. J Cell Biol. 158**,** 647-57.

Sciacco, M., Bonilla, E., Schon, E.A., DiMauro, S., Moraes, C.T., 1994. Distribution of wild-type and common deletion forms of mtDNA in normal and respiration-deficient muscle fibers from patients with mitochondrial myopathy. Hum Mol Genet. 3**,** 13-9.

Sebastian, D., Hernandez-Alvarez, M.I., Segales, J., Sorianello, E., Munoz, J.P., Sala, D., Waget, A., Liesa, M., Paz, J.C., Gopalacharyulu, P., Oresic, M., Pich, S., Burcelin, R., Palacin, M., Zorzano, A., 2012. Mitofusin 2 (Mfn2) links mitochondrial and endoplasmic reticulum function with insulin signaling and is essential for normal glucose homeostasis. Proc Natl Acad Sci U S A. 109**,** 5523-8.

Seidel-Rogol, B.L., Shadel, G.S., 2002. Modulation of mitochondrial transcription in response to mtDNA depletion and repletion in HeLa cells. Nucleic Acids Res. 30**,** 1929-34.

Shahrestani, P., Leung, H.T., Le, P.K., Pak, W.L., Tse, S., Ocorr, K., Huang, T., 2009. Heterozygous mutation of Drosophila Opa1 causes the development of multiple organ abnormalities in an age-dependent and organ-specific manner. PLoS One. 4**,** e6867.

Sharma, M.R., Koc, E.C., Datta, P.P., Booth, T.M., Spremulli, L.L., Agrawal, R.K., 2003. Structure of the mammalian mitochondrial ribosome reveals an expanded functional role for its component proteins. Cell. 115**,** 97-108.

Shoffner, J.M., Lott, M.T., Voljavec, A.S., Soueidan, S.A., Costigan, D.A., Wallace, D.C., 1989. Spontaneous Kearns-Sayre/chronic external ophthalmoplegia plus syndrome associated with a mitochondrial DNA deletion: a slip-replication model and metabolic therapy. Proc Natl Acad Sci U S A. 86**,** 7952-6.

Shoubridge, E.A., Karpati, G., Hastings, K.E., 1990. Deletion mutants are functionally dominant over wild-type mitochondrial genomes in skeletal muscle fiber segments in mitochondrial disease. Cell. 62**,** 43-9.

Shutt, T.E., Lodeiro, M.F., Cotney, J., Cameron, C.E., Shadel, G.S., 2010. Core human mitochondrial transcription apparatus is a regulated two-component system in vitro. Proc Natl Acad Sci U S A. 107**,** 12133-8.

Shy, M.E., 2004. Charcot-Marie-Tooth disease: an update. Curr Opin Neurol. 17**,** 579-85.

Sitarz, K.S., Almind, G.J., Horvath, R., Czermin, B., Grønskov, K., Pyle, A., Taylor, R.W., Larsen, M., Chinnery, P.F., Yu-Wai-Man, P., 2012a. OPA1 mutations induce mtDNA proliferation in leukocytes of patients with dominant optic atrophy. Neurology. *In press*.

Sitarz, K.S., Chinnery, P.F., Yu-Wai-Man, P., 2012b. Disorders of the optic nerve in mitochondrial cytopathies: new ideas on pathogenesis and therapeutic targets. Curr Neurol Neurosci Rep. 12**,** 308-17.

Sitarz, K.S., Yu-Wai-Man, P., Pyle, A., Stewart, J.D., Rautenstrauss, B., Seeman, P., Reilly, M.M., Horvath, R., Chinnery, P.F., 2012c. MFN2 mutations cause compensatory mitochondrial DNA proliferation. Brain.

Skulachev, V.P., 2001. Mitochondrial filaments and clusters as intracellular power-transmitting cables. Trends Biochem Sci. 26**,** 23-9.

Smirnova, E., Shurland, D.L., Ryazantsev, S.N., van der Bliek, A.M., 1998. A human dynamin-related protein controls the distribution of mitochondria. J Cell Biol. 143**,** 351-8.

Smirnova, E., Griparic, L., Shurland, D. L., van, A. M., 2001. Dynamin-related protein Drp1 is required for mitochondrial division in mammalian cells. Mol Biol Cell. 12**,** 2245-2256.

Smith, P.R., Cooper, J.M., Govan, G.G., Harding, A.E., Schapira, A.H., 1993. Smoking and mitochondrial function: a model for environmental toxins. Q J Med. 86**,** 657-60.

Soldner, F., Hockemeyer, D., Beard, C., Gao, Q., Bell, G.W., Cook, E.G., Hargus, G., Blak, A., Cooper, O., Mitalipova, M., Isacson, O., Jaenisch, R., 2009. Parkinson's disease patient-derived induced pluripotent stem cells free of viral reprogramming factors. Cell. 136**,** 964-77.

Soleimanpour-Lichaei, H.R., Kuhl, I., Gaisne, M., Passos, J.F., Wydro, M., Rorbach, J., Temperley, R., Bonnefoy, N., Tate, W., Lightowlers, R., Chrzanowska-Lightowlers, Z., 2007. mtRF1a is a human mitochondrial translation release

factor decoding the major termination codons UAA and UAG. Mol Cell. 27**,** 745-57.

Sommer, C.A., Stadtfeld, M., Murphy, G.J., Hochedlinger, K., Kotton, D.N., Mostoslavsky, G., 2009. Induced pluripotent stem cell generation using a single lentiviral stem cell cassette. Stem Cells. 27**,** 543-9.

Song, Zhiyin, Ghochani, Mariam, McCaffery, Michael, J., Frey, G, T., Chan, C, D., 2009. Mitofusins and OPA1 mediate sequential steps in mitochondrial membrane fusion. Mol Biol Cell. 20**,** 3525-3532.

Song, Z., Chen, H., Fiket, M., Alexander, C., Chan, D.C., 2007. OPA1 processing controls mitochondrial fusion and is regulated by mRNA splicing, membrane potential, and Yme1L. J Cell Biol. 178**,** 749--755.

Spahr, H., Samuelsson, T., Hallberg, B.M., Gustafsson, C.M., 2010. Structure of mitochondrial transcription termination factor 3 reveals a novel nucleic acid-binding domain. Biochem Biophys Res Commun. 397**,** 386-90.

Spinazzola, A., Invernizzi, F., Carrara, F., Lamantea, E., Donati, A., Dirocco, M., Giordano, I., Meznaric-Petrusa, M., Baruffini, E., Ferrero, I., Zeviani, M., 2009. Clinical and molecular features of mitochondrial DNA depletion syndromes. J Inherit Metab Dis. 32**,** 143-58.

Spinazzola, A., Zeviani, M., 2009. Mitochondrial diseases: a cross-talk between mitochondrial and nuclear genomes. Adv Exp Med Biol. 652**,** 69-84.

Stevens, L.C., 1967. Origin of testicular teratomas from primordial germ cells in mice. J Natl Cancer Inst. 38**,** 549-52.

Stewart, J.D., Tennant, S., Powell, H., Pyle, A., Blakely, E.L., He, L., Hudson, G., Roberts, M., du Plessis, D., Gow, D., Mewasingh, L.D., Hanna, M.G., Omer, S., Morris, A.A., Roxburgh, R., Livingston, J.H., McFarland, R., Turnbull, D.M., Chinnery, P.F., Taylor, R.W., 2009. Novel POLG1 mutations associated with neuromuscular and liver phenotypes in adults and children. J Med Genet. 46**,** 209-14.

Stewart, J.D., Schoeler, S., Sitarz, K.S., Horvath, R., Hallmann, K., Pyle, A., Yu-Wai-Man, P., Taylor, R.W., Samuels, D.C., Kunz, W.S., Chinnery, P.F., 2011. POLG mutations cause decreased mitochondrial DNA repopulation rates following induced depletion in human fibroblasts. Biochim Biophys Acta. 1812**,** 321-5.

Suen, D.F., Norris, K.L., Youle, R.J., 2008. Mitochondrial dynamics and apoptosis. Genes Dev. 22**,** 1577-90.

Suissa, S., Wang, Z., Poole, J., Wittkopp, S., Feder, J., Shutt, T.E., Wallace, D.C., Shadel, G.S., Mishmar, D., 2009. Ancient mtDNA genetic variants modulate mtDNA transcription and replication. PLoS Genet. 5**,** e1000474.

Suomalainen, A., Majander, A., Wallin, M., Setala, K., Kontula, K., Leinonen, H., Salmi, T., Paetau, A., Haltia, M., Valanne, L., Lonnqvist, J., Peltonen, L., Somer, H., 1997. Autosomal dominant progressive external ophthalmoplegia with multiple deletions of mtDNA: clinical, biochemical, and molecular genetic features of the 10q-linked disease. Neurology. 48**,** 1244-53.

Sutovsky, P., Moreno, R.D., Ramalho-Santos, J., Dominko, T., Simerly, C., Schatten, G., 1999. Ubiquitin tag for sperm mitochondria. Nature. 402**,** 371-2.

Taapken, S.M., Nisler, B.S., Newton, M.A., Sampsell-Barron, T.L., Leonhard, K.A., McIntire, E.M., Montgomery, K.D., 2011. Karyotypic abnormalities in human induced pluripotent stem cells and embryonic stem cells. Nat Biotechnol. 29**,** 313-4.

Taguchi, N., Ishihara, N., Jofuku, A., Oka, T., Mihara, K., 2007. Mitotic phosphorylation of dynamin-related GTPase Drp1 participates in mitochondrial fission. J Biol Chem. 282**,** 11521-9.

Takahashi, K., Yamanaka, S., 2006. Induction of pluripotent stem cells from mouse embryonic and adult fibroblast cultures by defined factors. Cell. 126**,** 663-76.

Takahashi, K., Tanabe, K., Ohnuki, M., Narita, M., Ichisaka, T., Tomoda, K., Yamanaka, S., 2007. Induction of pluripotent stem cells from adult human fibroblasts by defined factors. Cell. 131**,** 861-72.

Tang, S., Le, P.K., Tse, S., Wallace, D.C., Huang, T., 2009. Heterozygous mutation of Opa1 in Drosophila shortens lifespan mediated through increased reactive oxygen species production. PLoS One. 4**,** e4492.

Tang, Y., Schon, E.A., Wilichowski, E., Vazquez-Memije, M.E., Davidson, E., King, M.P., 2000a. Rearrangements of human mitochondrial DNA (mtDNA): new insights into the regulation of mtDNA copy number and gene expression. Mol Biol Cell. 11**,** 1471-85.

Tang, Y., Manfredi, G., Hirano, M., Schon, E.A., 2000b. Maintenance of human rearranged mitochondrial DNAs in long-term cultured transmitochondrial cell lines. Mol Biol Cell. 11**,** 2349-58.

Taylor, R.W., Taylor, G.A., Durham, S.E., Turnbull, D.M., 2001. The determination of complete human mitochondrial DNA sequences in single cells: implications for the study of somatic mitochondrial DNA point mutations. Nucleic Acids Res. 29**,** E74-4.

Taylor, R.W., Giordano, C., Davidson, M.M., d'Amati, G., Bain, H., Hayes, C.M., Leonard, H., Barron, M.J., Casali, C., Santorelli, F.M., Hirano, M., Lightowlers, R.N., DiMauro, S., Turnbull, D.M., 2003. A homoplasmic mitochondrial transfer ribonucleic acid mutation as a cause of maternally inherited hypertrophic cardiomyopathy. J Am Coll Cardiol. 41**,** 1786-96.

Taylor, R.W., Schaefer, A.M., Barron, M.J., McFarland, R., Turnbull, D.M., 2004. The diagnosis of mitochondrial muscle disease. Neuromuscul Disord. 14**,** 237-45.

Thomson, J.A., Itskovitz-Eldor, J., Shapiro, S.S., Waknitz, M.A., Swiergiel, J.J., Marshall, V.S., Jones, J.M., 1998. Embryonic stem cell lines derived from human blastocysts. Science. 282**,** 1145-7.

Tiranti, V., Savoia, A., Forti, F., D'Apolito, M.F., Centra, M., Rocchi, M., Zeviani, M., 1997. Identification of the gene encoding the human mitochondrial RNA polymerase (h-mtRPOL) by cyberscreening of the Expressed Sequence Tags database. Hum Mol Genet. 6**,** 615-25.

Tobin, J.D., 2004. Asking About Life, Vol., Cengage Learning.

Tondera, D., Grandemange, S., Jourdain, A., Karbowski, M., Mattenberger, Y., Herzig, S., Da Cruz, S., Clerc, P., Raschke, I., Merkwirth, C., Ehses, S., Krause, F., Chan, D.C., Alexander, C., Bauer, C., Youle, R., Langer, T., Martinou, J.C., 2009. SLP-2 is required for stress-induced mitochondrial hyperfusion. EMBO J. 28**,** 1589-600.

Torroni, A., Wallace, D.C., 1994. Mitochondrial DNA variation in human populations and implications for detection of mitochondrial DNA mutations of pathological significance. J Bioenerg Biomembr. 26**,** 261-71.

Trevelyan, A.J., Kirby, D.M., Smulders-Srinivasan, T.K., Nooteboom, M., Acin-Perez, R., Enriquez, J.A., Whittington, M.A., Lightowlers, R.N., Turnbull, D.M., 2010. Mitochondrial DNA mutations affect calcium handling in differentiated neurons. Brain. 133**,** 787-96.

Tsuboi, M., Morita, H., Nozaki, Y., Akama, K., Ueda, T., Ito, K., Nierhaus, K.H., Takeuchi, N., 2009. EF-G2mt is an exclusive recycling factor in mammalian mitochondrial protein synthesis. Mol Cell. 35**,** 502-10.

Tuppen, H.A., Blakely, E.L., Turnbull, D.M., Taylor, R.W., 2010. Mitochondrial DNA mutations and human disease. Biochim Biophys Acta. 1797**,** 113-28.

Twig, G., Elorza, A., Molina, A.J., Mohamed, H., Wikstrom, J.D., Walzer, G., Stiles, L., Haigh, S.E., Katz, S., Las, G., Alroy, J., Wu, M., Py, B.F., Yuan, J., Deeney, J.T., Corkey, B.E., Shirihai, O.S., 2008. Fission and selective fusion govern mitochondrial segregation and elimination by autophagy. EMBO J. 27**,** 433-46.

Tyynismaa, H., Sembongi, H., Bokori-Brown, M., Granycome, C., Ashley, N., Poulton, J., Jalanko, A., Spelbrink, J.N., Holt, I.J., Suomalainen, A., 2004. Twinkle helicase is essential for mtDNA maintenance and regulates mtDNA copy number. Hum Mol Genet. 13**,** 3219-27.

Tzoulis, C., Engelsen, B.A., Telstad, W., Aasly, J., Zeviani, M., Winterthun, S., Ferrari, G., Aarseth, J.H., Bindoff, L.A., 2006. The spectrum of clinical disease caused by the A467T and W748S POLG mutations: a study of 26 cases. Brain. 129**,** 1685-92.

van der Laan, M., Rissler, M., Rehling, P., 2006. Mitochondrial preprotein translocases as dynamic molecular machines. FEMS Yeast Res. 6**,** 849-61.

Van Goethem, G., Dermaut, B., Lofgren, A., Martin, J.J., Van Broeckhoven, C., 2001. Mutation of POLG is associated with progressive external ophthalmoplegia characterized by mtDNA deletions. Nat Genet. 28**,** 211-2.

Van Goethem, G., Martin, J.J., Dermaut, B., Lofgren, A., Wibail, A., Ververken, D., Tack, P., Dehaene, I., Van Zandijcke, M., Moonen, M., Ceuterick, C., De Jonghe, P., Van Broeckhoven, C., 2003. Recessive POLG mutations presenting with sensory and ataxic neuropathy in compound heterozygote patients with progressive external ophthalmoplegia. Neuromuscul Disord. 13**,** 133-42.

Villena, J.A., Kralli, A., 2008. ERRalpha: a metabolic function for the oldest orphan. Trends Endocrinol Metab. 19**,** 269-76.

Virbasius, J.V., Virbasius, C.A., Scarpulla, R.C., 1993. Identity of GABP with NRF-2, a multisubunit activator of cytochrome oxidase expression, reveals a cellular role for an ETS domain activator of viral promoters. Genes Dev. 7**,** 380-92.

Vladutiu, G.D., Heffner, R.R., 2000. Succinate dehydrogenase deficiency. Arch Pathol Lab Med. 124**,** 1755-8.

Votruba, M., Fitzke, F. W., Holder, G. E., Carter, A., Bhattacharya, S. S., Moore, A. T., 1998. Clinical features in affected individuals from 21 pedigrees with dominant optic atrophy. Arch Ophthalmol. 116**,** 351-358.

Wai, T., Teoli, D., Shoubridge, E.A., 2008. The mitochondrial DNA genetic bottleneck results from replication of a subpopulation of genomes. Nat Genet. 40**,** 1484-8.

Wallace, D.C., Singh, G., Lott, M.T., Hodge, J.A., Schurr, T.G., Lezza, A.M., Elsas, L.J., 2nd, Nikoskelainen, E.K., 1988. Mitochondrial DNA mutation associated with Leber's hereditary optic neuropathy. Science. 242**,** 1427-30.

Wallace, D.C., Brown, M.D., Lott, M.T., 1999. Mitochondrial DNA variation in human evolution and disease. Gene. 238**,** 211-30.

Wang, G.J., Nutter, L.M., Thayer, S.A., 1997. Insensitivity of cultured rat cortical neurons to mitochondrial DNA synthesis inhibitors: evidence for a slow turnover of mitochondrial DNA. Biochem Pharmacol. 54**,** 181-7.

Wang, Y., Bogenhagen, D.F., 2006. Human mitochondrial DNA nucleoids are linked to protein folding machinery and metabolic enzymes at the mitochondrial inner membrane. J Biol Chem. 281**,** 25791--25802.

Wanrooij, S., Luoma, P., van Goethem, G., van Broeckhoven, C., Suomalainen, A., Spelbrink, J.N., 2004. Twinkle and POLG defects enhance age-dependent accumulation of mutations in the control region of mtDNA. Nucleic Acids Res. 32**,** 3053-64.

Warren, L., Manos, P.D., Ahfeldt, T., Loh, Y.H., Li, H., Lau, F., Ebina, W., Mandal, P.K., Smith, Z.D., Meissner, A., Daley, G.Q., Brack, A.S., Collins, J.J., Cowan, C., Schlaeger, T.M., Rossi, D.J., 2010. Highly efficient reprogramming to pluripotency and directed differentiation of human cells with synthetic modified mRNA. Cell Stem Cell. 7**,** 618-30.

Wasiak, S., Zunino, R., McBride, H.M., 2007. Bax/Bak promote sumoylation of DRP1 and its stable association with mitochondria during apoptotic cell death. J Cell Biol. 177**,** 439-50.

Westermann, B., 2010. Mitochondrial fusion and fission in cell life and death. Nat Rev Mol Cell Biol. 11**,** 872-84.

Westermann, B., 2012. Bioenergetic role of mitochondrial fusion and fission. Biochim Biophys Acta.

White, K.E., Davies, V.J., Hogan, V.E., Piechota, M.J., Nichols, P.P., Turnbull, D.M., Votruba, M., 2009. OPA1 deficiency associated with increased autophagy in retinal ganglion cells in a murine model of dominant optic atrophy. Invest Ophthalmol Vis Sci. 50**,** 2567-71.

Wingerchuk, D.M., 2006. Neuromyelitis optica. Int MS J. 13**,** 42--50.

Wingerchuk, D.M., Lennon, V.A., Lucchinetti, C.F., Pittock, S.J., Weinshenker, B.G., 2007. The spectrum of neuromyelitis optica. Lancet Neurol. 6**,** 805-15.

Yakubovskaya, E., Chen, Z., Carrodeguas, J.A., Kisker, C., Bogenhagen, D.F., 2006. Functional human mitochondrial DNA polymerase gamma forms a heterotrimer. J Biol Chem. 281**,** 374-82.

Yasukawa, T., Reyes, A., Cluett, T.J., Yang, M.Y., Bowmaker, M., Jacobs, H.T., Holt, I.J., 2006. Replication of vertebrate mitochondrial DNA entails transient ribonucleotide incorporation throughout the lagging strand. EMBO J. 25**,** 5358-71.

Ylikallio, E., Tyynismaa, H., Tsutsui, H., Ide, T., Suomalainen, A., 2010. High mitochondrial DNA copy number has detrimental effects in mice. Hum Mol Genet. 19**,** 2695-705.

Yoon, Yisang, Krueger, W, E., Oswald, J, B., McNiven, A, M., 2003. The mitochondrial protein hFis1 regulates mitochondrial fission in mammalian cells through an interaction with the dynamin-like protein DLP1. Mol Cell Biol. 23**,** 5409-5420.

Yoshida, M., Muneyuki, E., Hisabori, T., 2001. ATP synthase--a marvellous rotary engine of the cell. Nat Rev Mol Cell Biol. 2**,** 669-77.

Yoshida, Y., Izumi, H., Torigoe, T., Ishiguchi, H., Itoh, H., Kang, D., Kohno, K., 2003. P53 physically interacts with mitochondrial transcription factor A and differentially regulates binding to damaged DNA. Cancer Res. 63**,** 3729-34.

Youle, R.J., Karbowski, M., 2005. Mitochondrial fission in apoptosis. Nat Rev Mol Cell Biol. 6**,** 657-63.

Yu-Wai-Man, P., Griffiths, P.G., Brown, D.T., Howell, N., Turnbull, D.M., Chinnery, P.F., 2003. The epidemiology of Leber hereditary optic neuropathy in the North East of England. Am J Hum Genet. 72**,** 333-9.

Yu-Wai-Man, P., Griffiths, P.G., Hudson, G., Chinnery, P.F., 2009. Inherited mitochondrial optic neuropathies. J Med Genet. 46**,** 145--158.

Yu-Wai-Man, P., Griffiths, P.G., Burke, A., Sellar, P.W., Clarke, M.P., Gnanaraj, L., Ah-Kine, D., Hudson, G., Czermin, B., Taylor, R.W., Horvath, R., Chinnery, P.F., 2010a. The Prevalence and Natural History of Dominant Optic Atrophy Due to OPA1 Mutations. Ophthalmology.

Yu-Wai-Man, P., Griffiths, P.G., Gorman, G.S., Lourenco, C.M., Wright, A.F., Auer-Grumbach, M., Toscano, A., Musumeci, O., Valentino, M.L., Caporali, L., Lamperti, C., Tallaksen, C.M., Duffey, P., Miller, J., Whittaker, R.G., Baker, M.R., Jackson, M.J., Clarke, M.P., Dhillon, B., Czermin, B., Stewart, J.D., Hudson, G., Reynier, P., Bonneau, D., Marques, W., Jr., Lenaers, G., McFarland, R., Taylor, R.W., Turnbull, D.M., Votruba, M., Zeviani, M., Carelli, V., Bindoff, L.A., Horvath, R., Amati-Bonneau, P., Chinnery, P.F., 2010b. Multi-system neurological disease is common in patients with OPA1 mutations. Brain. 133**,** 771-86.

Yu-Wai-Man, P., Sitarz, K.S., Samuels, D.C., Griffiths, P.G., Reeve, A.K., Bindoff, L.A., Horvath, R., Chinnery, P.F., 2010c. OPA1 mutations cause cytochrome

c oxidase deficiency due to loss of wild-type mtDNA molecules. Hum Mol Genet. 19**,** 3043-52.

Yu-Wai-Man, P., Stewart, J.D., Hudson, G., Andrews, R.M., Griffiths, P.G., Birch, M.K., Chinnery, P.F., 2010d. OPA1 increases the risk of normal but not high tension glaucoma. J Med Genet. 47**,** 120-5.

Yu-Wai-Man, P., Bailie, M., Atawan, A., Chinnery, P.F., Griffiths, P.G., 2011a. Pattern of retinal ganglion cell loss in dominant optic atrophy due to OPA1 mutations. Eye (Lond). 25**,** 596-602.

Yu-Wai-Man, P., Griffiths, P.G., Chinnery, P.F., 2011b. Mitochondrial optic neuropathies - disease mechanisms and therapeutic strategies. Prog Retin Eye Res. 30**,** 81-114.

Yu, J., Vodyanik, M.A., Smuga-Otto, K., Antosiewicz-Bourget, J., Frane, J.L., Tian, S., Nie, J., Jonsdottir, G.A., Ruotti, V., Stewart, R., Slukvin, II, Thomson, J.A., 2007. Induced pluripotent stem cell lines derived from human somatic cells. Science. 318**,** 1917-20.

Zanna, C., Ghelli, A., Porcelli, A.M., Karbowski, M., Youle, R.J., Schimpf, S., Wissinger, B., Pinti, M., Cossarizza, A., Vidoni, S., Valentino, M.L., Rugolo, M., Carelli, V., 2008. OPA1 mutations associated with dominant optic atrophy impair oxidative phosphorylation and mitochondrial fusion. Brain. 131**,** 352--367.

Zaragoza, M.V., Fass, J., Diegoli, M., Lin, D., Arbustini, E., 2010. Mitochondrial DNA variant discovery and evaluation in human Cardiomyopathies through next-generation sequencing. PLoS One. 5**,** e12295.

Zeviani, M., Spinazzola, A., Carelli, V., 2003. Nuclear genes in mitochondrial disorders. Curr Opin Genet Dev. 13**,** 262-70.

Zhang, X., Stojkovic, P., Przyborski, S., Cooke, M., Armstrong, L., Lako, M., Stojkovic, M., 2006. Derivation of human embryonic stem cells from developing and arrested embryos. Stem Cells. 24**,** 2669-76.

Zhao, X.Y., Li, W., Lv, Z., Liu, L., Tong, M., Hai, T., Hao, J., Guo, C.L., Ma, Q.W., Wang, L., Zeng, F., Zhou, Q., 2009. iPS cells produce viable mice through tetraploid complementation. Nature. 461**,** 86-90.

Zhou, H., Wu, S., Joo, J.Y., Zhu, S., Han, D.W., Lin, T., Trauger, S., Bien, G., Yao, S., Zhu, Y., Siuzdak, G., Scholer, H.R., Duan, L., Ding, S., 2009. Generation of induced pluripotent stem cells using recombinant proteins. Cell Stem Cell. 4**,** 381-4.

Zhou, W., Freed, C.R., 2009. Adenoviral gene delivery can reprogram human fibroblasts to induced pluripotent stem cells. Stem Cells. 27**,** 2667-74.

Zorzano, A., Liesa, Marc, Sebastián, David, Segalés, Jessica, Palacín, Manuel, 2010. Mitochondrial fusion proteins: Dual regulators of morphology and metabolism. Semin Cell Dev Biol.

Züchner, S., Mersiyanova, I.V., Muglia, M., Bissar-Tadmouri, N., Rochelle, J., Dadali, E.L., Zappia, M., Nelis, E., Patitucci, A., Senderek, J., Parman, Y., Evgrafov, O., Jonghe, P.D., Takahashi, Y., Tsuji, S., Pericak-Vance, M.A., Quattrone, A., Battaloglu, E., Polyakov, A.V., Timmerman, V., Schröder,

J.M., Vance, J.M., Battologlu, E., 2004. Mutations in the mitochondrial GTPase mitofusin 2 cause Charcot-Marie-Tooth neuropathy type 2A. Nat Genet. 36**,** 449--451.

Züchner, S., De Jonghe, P., Jordanova, A., Claeys, K.G., Guergueltcheva, V., Cherninkova, S., Hamilton, S.R., Van Stavern, G., Krajewski, K.M., Stajich, J., Tournev, I., Verhoeven, K., Langerhorst, C.T., de Visser, M., Baas, F., Bird, T., Timmerman, V., Shy, M., Vance, J.M., 2006. Axonal neuropathy with optic atrophy is caused by mutations in mitofusin 2. Ann Neurol. 59**,** 276-81.

Publications

Clinical/Scientific Notes

Kamil S. Sitarz, MSc
Gitte J. Almind, MD
Rita Horvath, MD, PhD
Birgit Czermin, PhD
Karen Grønskov, PhD
Angela Pyle, PhD
Robert W. Taylor, PhD, FRCPath
Michael Larsen, MD, DMSc
Patrick F. Chinnery, PhD, FRCP
Patrick Yu-Wai-Man, PhD, FRCOphth

OPA1 MUTATIONS INDUCE mtDNA PROLIFERATION IN LEUKOCYTES OF PATIENTS WITH DOMINANT OPTIC ATROPHY

OPA1 mutations cause autosomal dominant optic atrophy (DOA), a debilitating mitochondrial optic neuropathy characterized by irreversible loss of retinal ganglion cells (RGCs) and progressive visual failure starting in early childhood.[1] Interestingly, ~20% of *OPA1* carriers will develop a more severe form of the disease, DOA+, where the optic atrophy is compounded by additional neurologic features.[1] *OPA1* is a multifunctional mitochondrial inner membrane protein, and rather unexpectedly, high levels of cytochrome *c* oxidase (COX)-negative muscle fibers were recently identified in biopsy specimens from patients manifesting both the pure and syndromal phenotypes.[2,3] These COX-negative muscle fibers harbored high levels of somatically acquired mitochondrial DNA (mtDNA) deletions and marked mtDNA proliferation was also observed, clearly revealing *OPA1* to be a novel disorder of mtDNA maintenance.[4] To further investigate this key pathologic mechanism, mtDNA copy number was quantified in blood leukocytes from 3 independent patient cohorts with molecularly confirmed *OPA1* mutations.

Methods. Using different extraction protocols (Method e-1 on the *Neurology*® Web site at www.neurology.org), total genomic DNA was isolated from the leukocyte fraction of venous blood from 3 groups of patients harboring pathogenic *OPA1* mutations: 1) British cohort (n = 61), 2) German cohort (n = 40), and 3) Danish cohort (n = 49). Relative mtDNA copy number was determined using the MyiQ™ real-time PCR detection system (BioRad, Hercules, CA).[5] The presence of multiple mtDNA deletions was investigated in a subgroup of 22 British *OPA1*-positive DNA samples using long-range PCR.[1] Visual acuity was measured using a standard Snellen vision chart (Method e-2).

Standard protocol approvals, registrations, and patient consents. This study had the relevant institutional ethical approval and complied with the Declaration of Helsinki.

Results. Blood leukocytes from British *OPA1*-positive patients had significantly higher mtDNA copy numbers compared with controls (figure 1A). In the British cohort, there was no significant difference in total mtDNA content between patients with pure DOA and DOA+ phenotypes (figure 1B). There was no significant correlation between patients' visual acuity and mtDNA copy number in blood leukocytes (figure 1C). There was evidence of significant mtDNA proliferation in blood leukocytes from German *OPA1*-positive patients (figure 1D) and Danish *OPA1*-positive patients (figure e-1). On subgroup analysis, there was no significant difference in total mtDNA content between patients with different *OPA1* mutation subtypes (figure e-2). Multiple mtDNA deletions were not detected in blood leukocytes.

Discussion. This study has revealed significant mtDNA proliferation in blood leukocytes harboring pathogenic *OPA1* mutations in 3 independent patient cohorts. The degree of mtDNA proliferation in blood was comparable to the 2- to 4-fold increase in mtDNA content observed at the single fiber level in skeletal muscle biopsies from *OPA1*-positive patients.[4] The OPA1 protein plays a key role in the assembly and stability of the respiratory chain complexes and these pathologic findings, in both blood and skeletal muscle, are consistent with the detrimental effect of *OPA1* mutations on mitochondrial oxidative phosphorylation, the increased mtDNA copy number probably acting as a compensatory bioenergetic mechanism.[4] OPA1 mediates mitochondrial membrane fusion in tandem with mitofusin 2 (MFN2), which is dysfunctional in the most common, autosomal dominant, axonal form of Charcot-Marie-Tooth disease (CMT2A).[6] It is therefore noteworthy that *MFN2* mutations also triggered a significant mtDNA proliferative response in blood, supporting our observation for *OPA1* mutations.[6] Unlike skeletal muscle, multiple mtDNA deletions were not identified in blood leukocytes from patients with *OPA1* mutations. This is likely related to the relatively short half-life of those cells in the circulation, their rapid turnover precluding the formation and subsequent clonal expansion of somatic mtDNA abnormalities.

The mtDNA proliferative response in *OPA1*-positive blood leukocytes was not statistically different between patients with pure optic atrophy and

See page 1517

Supplemental data at www.neurology.org

Figure 1 MtDNA copy number analysis

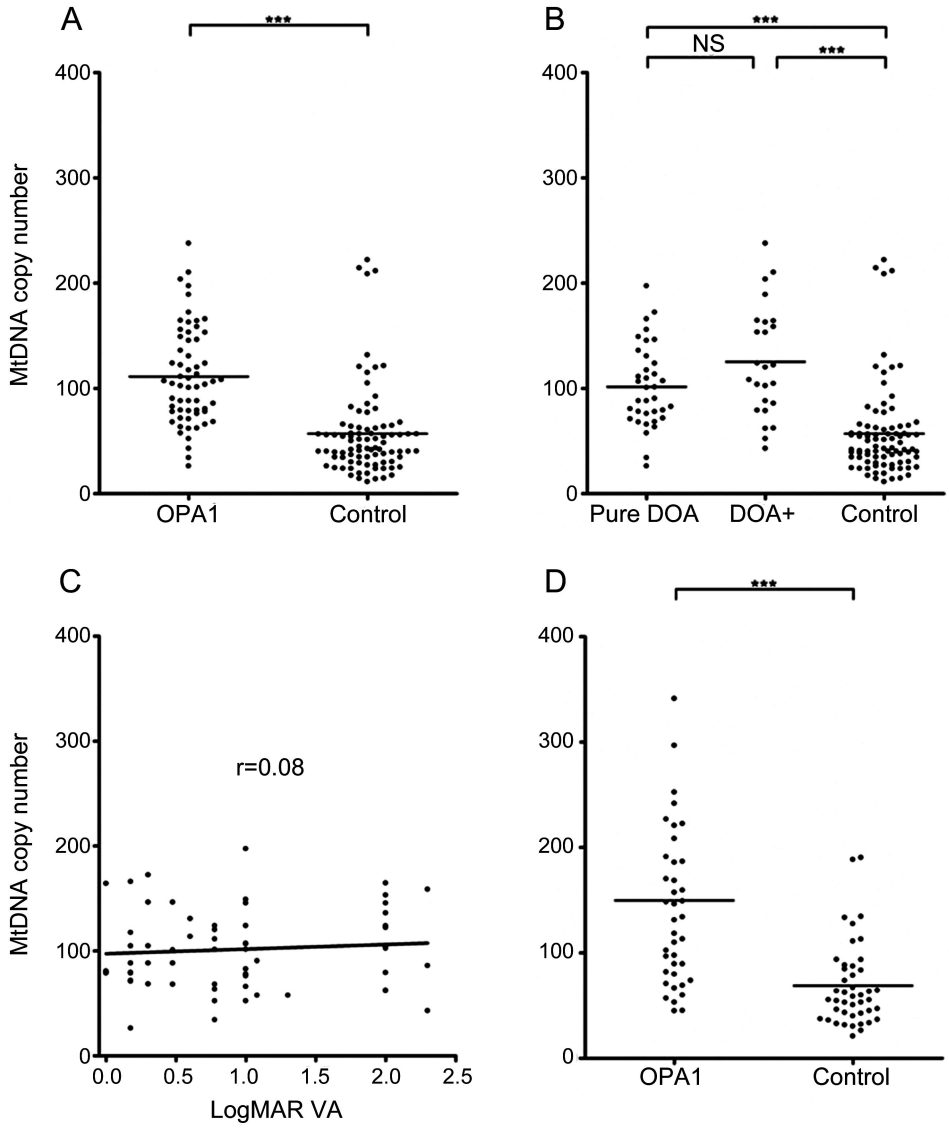

(A) Comparison of total mtDNA content in blood leukocytes from the British cohort (*OPA1*-positive patients: mean = 111.3, SD = 46.1, n = 61; controls: mean = 56.9, SD = 43.3, n = 87). (B) Phenotype subgroup analysis of the British patient cohort (pure dominant optic atrophy subgroup: mean = 101.6, SD = 39.0, n = 36; DOA+ subgroup: mean = 125.3, SD = 52.6, n = 25, NS with Bonferroni correction at p value = 0.0471). (C) Correlation of logMAR visual acuity (VA) with total mtDNA content in blood leukocytes from British *OPA1*-positive patients (Spearman rank correlation coefficient = 0.08, NS at p value = 0.4081). (D) Comparison of total mtDNA content in blood leukocytes from the German cohort (*OPA1*-positive patients: mean = 149.8, SD = 95.0, n = 40; controls: mean = 68.7, SD = 39.4, n = 44). Statistical analysis was performed using GraphPad™ v.4 statistical software (San Diego, CA). Group comparisons were made with the unpaired t test. The relationship between logMAR VA and total mtDNA content level was assessed with Spearman rank correlation coefficient. ***$p < 0.0001$. NS refers to a nonsignificant p value, with $p < 0.0167$ being the threshold level for statistical significance after Bonferroni correction for multiple testing.

those who developed additional neurologic complications. Furthermore, irrespective of whether or not *OPA1* mutation carriers developed DOA+ features, there was no correlation between absolute mtDNA copy number and the severity of visual loss. Given the 3-fold increased risk of developing DOA+ with missense mutations and those mutations involving the GTPase catalytic domain, additional subgroup analysis was carried out based on these *OPA1* mutational subtypes.[1] No consistent significant difference in mtDNA copy number was identified, which suggests that this parameter of mitochondrial dysfunction is not associated with clinical severity per se, at least in blood leukocytes. Paradoxically, a previous study found relative mtDNA depletion in blood samples collected from patients with DOA. However, only 8 *OPA1*-positive cases were included and the observed reduction in mtDNA copy number was relatively small,

~25% of the mean control value.[7] Further work is needed to clarify the still poorly understood pathways linking *OPA1* mutations with mtDNA instability and ultimately RGC loss in DOA.

From the Institute of Genetic Medicine (K.S.S., R.H., A.P., P.F.C., P.Y.-W.-M.) and Institute for Ageing and Health (R.W.T.), Wellcome Trust Centre for Mitochondrial Research, Newcastle University, Newcastle upon Tyne, UK; Center for Applied Human Molecular Genetics (G.J.A., K.G.), Kennedy Center, Glostrup, Denmark; Departments of Neurology (R.H., P.F.C.) and Ophthalmology (P.Y.-W.-M.), Royal Victoria Infirmary, Newcastle upon Tyne, UK; Medical Genetics Center (B.C.), Munich, Germany; Department of Ophthalmology (M.L.), Glostrup Hospital, Glostrup; and Faculty of Health Sciences (M.L.), University of Copenhagen, Copenhagen, Denmark.

Author contributions: Kamil S. Sitarz: drafting/revising the manuscript for content, including medical writing for content, analysis or interpretation of data, acquisition of data, statistical analysis. Gitte J. Almind: drafting/revising the manuscript for content, including medical writing for content, analysis or interpretation of data, acquisition of data, statistical analysis. Rita Horvath: drafting/revising the manuscript for content, including medical writing for content, analysis or interpretation of data, study supervision or coordination. Birgit Czermin: drafting/revising the manuscript for content, including medical writing for content, analysis or interpretation of data. Karen Grønskov: drafting/revising the manuscript for content, including medical writing for content, analysis or interpretation of data. Angela Pyle: drafting/revising the manuscript for content, including medical writing for content, analysis or interpretation of data, acquisition of data. Robert W. Taylor: drafting/revising the manuscript for content, including medical writing for content, analysis or interpretation of data. Michael Larsen: drafting/revising the manuscript for content, including medical writing for content, analysis or interpretation of data. Patrick F. Chinnery: drafting/revising the manuscript for content, including medical writing for content, analysis or interpretation of data, study supervision or coordination, obtaining funding. Patrick Yu-Wai-Man: drafting/revising the manuscript for content, including medical writing for content, analysis or interpretation of data, study supervision or coordination, obtaining funding.

Study funding: P.Y.-W.-M. is a Medical Research Council (MRC, UK) Clinician Scientist. R.H. is supported by the Academy of Medical Sciences (UK) and by the MRC (UK). R.W.T. is funded by the Wellcome Trust and the UK NHS Highly Specialised Services Group. P.F.C. is a Wellcome Trust Senior Fellow in Clinical Science and a UK National Institute of Health Senior Investigator who also receives funding from the MRC (UK), Parkinson's UK, the Association Française contre les Myopathies, and the UK NIHR Biomedical Research Centre for Ageing and Age-related disease award to the Newcastle upon Tyne Hospitals NHS Foundation Trust.

Disclosure: The authors report no disclosures relevant to the manuscript. ***Go to Neurology.org for full disclosures.***

Correspondence & reprint requests to Dr. Yu-Wai-Man: Patrick.Yu-Wai-Man@ncl.ac.uk

Received January 26, 2012. Accepted in final form May 23, 2012.

1. Yu-Wai-Man P, Griffiths PG, Gorman GS, et al. Multisystem neurological disease is common in patients with *OPA1* mutations. Brain 2010;133:771–786.
2. Amati-Bonneau P, Valentino ML, Reynier P, et al. *OPA1* mutations induce mitochondrial DNA instability and optic atrophy plus phenotypes. Brain 2008;131:338–351.
3. Hudson G, Amati-Bonneau P, Blakely EL, et al. Mutation of *OPA1* causes dominant optic atrophy with external ophthalmoplegia, ataxia, deafness and multiple mitochondrial DNA deletions: a novel disorder of mtDNA maintenance. Brain 2008;131:329–337.
4. Yu-Wai-Man P, Sitarz KS, Samuels DC, et al. *OPA1* mutations cause cytochrome c oxidase deficiency due to loss of wild-type mtDNA molecules. Hum Molec Genet 2010;19:3043–3052.
5. Pyle A, Burn DJ, Gordon C, et al. Fall in circulating mononuclear cell mitochondrial DNA content in human sepsis. Intens Care Med 2010;36:956–962.
6. Sitarz KS, Yu-Wai-Man P, Pyle A, et al. *MFN2* mutations cause compensatory mitochondrial DNA proliferation. Brain 2012;135:e219.
7. Kim JY, Hwang JM, Ko HS, et al. Mitochondrial DNA content is decreased in autosomal dominant optic atrophy. Neurology 2005;64:966–972.

Luisa Iommarini, PhD
Alessandra Maresca, PhD
Leonardo Caporali, BSc
Maria Lucia Valentino, MD
Rocco Liguori, MD
Carla Giordano, MD, PhD
Valerio Carelli, MD, PhD

REVISITING THE ISSUE OF MITOCHONDRIAL DNA CONTENT IN OPTIC MITOCHONDRIOPATHIES

Involvement of the visual system in mitochondrial diseases, in particular of retinal ganglion cells (RGCs) and the optic nerve, is very common and has been defined "optic mitochondriopathies."[1] The prototype is Leber hereditary optic neuropathy (LHON, OMIM 535000), the first disease to be associated with a mitochondrial DNA (mtDNA) point mutation and now considered the most frequent mitochondrial disease.[2] LHON has been joined by dominant optic atrophy (DOA, OMIM 165500) Kjer type, which in a large set of cases is associated with heterozygous mutations in the nuclear gene *OPA1* encoding for a mitochondrial fusion protein.[2] Both disorders have features in common: clinically the preferential involvement of the papillomacular bundle and central vision, biochemically a defective respiratory chain and an increased propensity toward apoptosis.[2]

Furthermore, the shared selectivity for RGCs and the associated optic nerve has been related to the peculiar arrangement of this axonal system, which is nonmyelinated and very energy dependent in the retina, and only posterior to the anatomic constrain of the lamina cribrosa becomes myelinated and less energy dependent.[2] It has been hypothesized that this anatomic peculiarity imposes a fine tuning of the uneven mitochondrial distribution within the system, particularly abundant in the nonmyelinated section. Thus, either through an energy failure or an impaired fusion of mitochondria, this distribution may become abnormal and lead to loss of RGCs viability.[2] It has been reported that the mtDNA content of blood cells was significantly lower in *OPA1* mutant cases of DOA compared to controls, providing an indirect

See page 1515

doi:10.1093/brain/aws049 Brain 2012: 135; 1–3 | e219

BRAIN
A JOURNAL OF NEUROLOGY

LETTER TO THE EDITOR

MFN2 mutations cause compensatory mitochondrial DNA proliferation

Kamil S. Sitarz,[1] Patrick Yu-Wai-Man,[1,2] Angela Pyle,[1] Joanna D. Stewart,[1,3] Bernd Rautenstrauss,[4] Pavel Seeman,[5] Mary M. Reilly,[6] Rita Horvath[1,7] and Patrick F. Chinnery[1,7]

1 Wellcome Trust Centre for Mitochondrial Research, Institute of Genetic Medicine, Newcastle University, Newcastle upon Tyne, NE1 3BZ, UK
2 Department of Ophthalmology, Royal Victoria Infirmary, Newcastle upon Tyne, NE1 4LP, UK
3 IfADo – Leibniz Research Centre for Working Environment and Human Factors, Dortmund, Germany
4 Friedrich-Baur Institute, Ludwig Maximilian University, Munich, Germany
5 Department of Child Neurology, DNA Laboratory, Charles University, 2nd School of Medicine and University Hospital Motol, Prague, Czech Republic
6 MRC Centre for Neuromuscular Diseases, UCL Institute of Neurology, Queen Square, London, WC1N 3BG, UK
7 Department of Neurology, Royal Victoria Infirmary, Newcastle upon Tyne, NE1 4LP, UK

Correspondence to: Dr Patrick Yu-Wai-Man,
Wellcome Trust Centre for Mitochondrial Research,
Institute of Genetic Medicine,
Newcastle University,
Newcastle upon Tyne,
NE1 3BZ, UK
E-mail: patrick.yu-wai-man@ncl.ac.uk

Sir, We read with great interest the report of a Tunisian family by Rouzier *et al*. (2011) describing the neurological disorder linked to a novel heterozygous missense mutation in *MFN2* (1p36.2) (Rouzier *et al*., 2011). *MFN2* mutations typically cause autosomal dominant axonal Charcot–Marie–Tooth disease (CMT2A, OMIM 609260), with peripheral nerve degeneration occasionally associated with visual failure and optic atrophy (Zuchner *et al*., 2004, 2006). Interestingly, the clinical manifestations among mutational carriers in this Tunisian family were even more variable, ranging from asymptomatic subclinical disease to an axonal sensorimotor neuropathy complicated by optic atrophy, deafness, cerebellar ataxia and proximal myopathy. Furthermore, the intriguing finding of cytochrome *c* oxidase (COX)-deficient fibres and multiple mitochondrial DNA deletions in skeletal muscle biopsies suggest that *MFN2* mutations can result in disturbed mitochondrial DNA maintenance and an overt respiratory chain defect, in addition to marked fragmentation of the mitochondrial network. These deleterious consequences are strikingly reminiscent of the pathological features recently highlighted in *Brain* for autosomal dominant optic atrophy due to *OPA1* mutations (Amati-Bonneau *et al*., 2008; Hudson *et al*., 2008; Yu-Wai-Man *et al*., 2010*a*). Here, we provide additional evidence that *MFN2*-associated neuropathy is a novel disorder of mitochondrial DNA maintenance in a study of 58 probands with CMT2A and confirmed *MFN2* mutations (Table 1), compared with 131 age-matched normal controls.

Total genomic DNA was extracted from the leucocyte fraction of venous blood samples. The average cellular mitochondrial DNA content was quantified with a SYBR Green^{TM} quantitative polymerase chain reaction assay on a MyiQ^{TM} real-time polymerase chain reaction detection system (Biorad), with *MTND1* as the mitochondrial template and *GAPDH* as the nuclear-encoded housekeeping template (Yu-Wai-Man *et al*., 2010*a*). Relative mitochondrial DNA copy number was derived from the difference in threshold cycle (C_t) values obtained for *MTND1* and *GAPDH* using the $2(2_t^{-\Delta}C)$ equation to account for two copies of *GAPDH* per cell nucleus.

Mitochondrial DNA levels in the *MFN2* group [mean mitochondrial DNA copy number = 195.7, standard deviation (SD) = 126.6, $n = 58$] were significantly higher compared with controls (mean mitochondrial DNA copy number = 60.9, SD = 42.3, $n = 131$,

Advance Access publication April 4, 2012

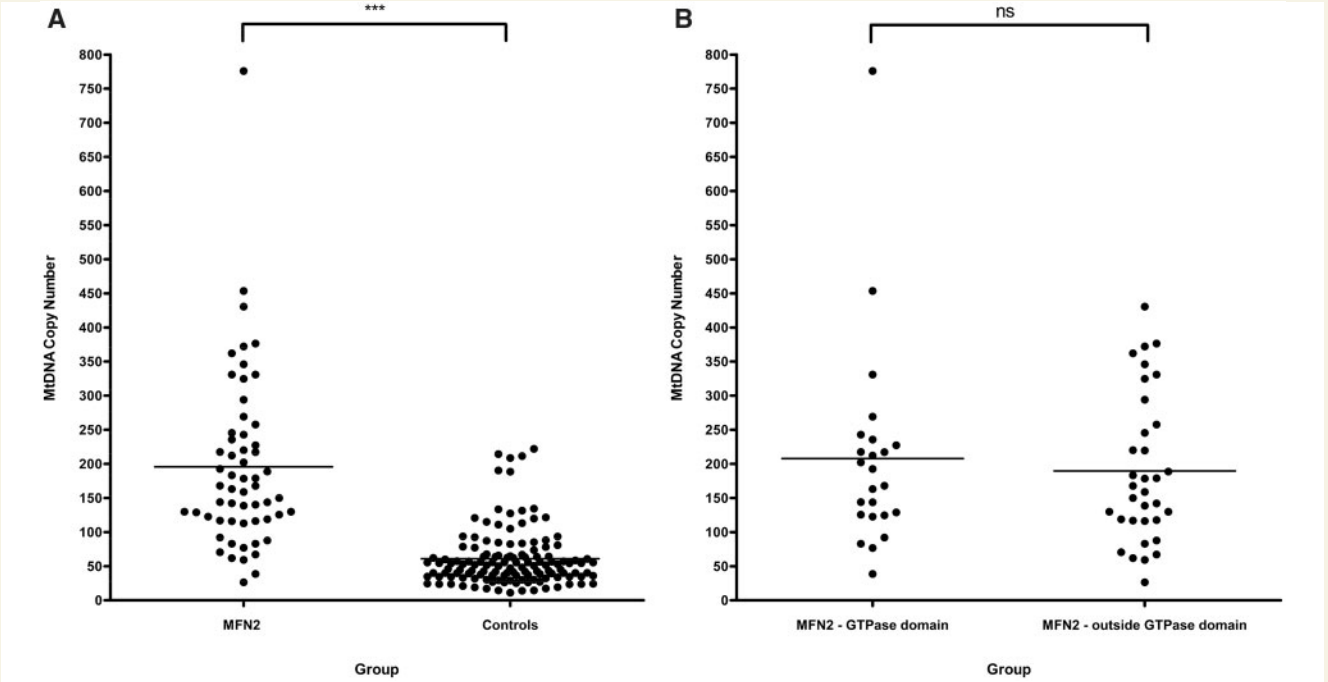

Figure 1 Comparison of mitochondrial DNA (MtDNA) blood copy number: (**A**) *MFN2* mutational carriers compared with age-matched normal controls; (**B**) patients harbouring *MFN2* mutations within the GTPase domain (mean mitochondrial DNA copy number = 207.9, SD = 150.2, *n = 0 24*) compared with those located outside this region (mean mitochondrial DNA copy number = 189.8, SD = 108.2, *n* = 34); ***$P < 0.0001$; ns = not significant at $P = 0.5957$.

$P < 0.0001$) (Fig. 1A). Given the suggestion by Rouzier *et al.* (2011) that *MFN2* mutations involving the functional GTPase domain were more likely to precipitate the severe multi-system phenotype documented in their family, we performed a subgroup analysis based on whether or not patients in our cohort harboured mutations within the highly conserved GTPase gene region. No significant difference was found between these two distinct mutational subgroups ($P = 0.5957$) (Fig. 1B).

Although we have previously shown that variation in the differential blood cell count can affect blood-derived mitochondrial DNA copy number (Pyle *et al.*, 2010), the 3-fold increase in mitochondrial DNA content detected in our *MFN2* cohort was substantially greater than the error attributable to this possible confounding factor. Mitochondrial proliferation is a well-recognized important diagnostic feature in skeletal muscle of patients with a range of mitochondrial cytopathies (Taylor *et al.*, 2004; Aure *et al.*, 2006). This compensatory mechanism is thought to occur in response to an underlying cellular bioenergetic crisis (the 'sick mitochondrion hypothesis'), which leads to the classical 'ragged-red fibre' appearance on Gomori Trichrome or succinate dehydrogenase staining (Chinnery and Samuels, 1999; Capps *et al.*, 2003; Durham *et al.*, 2007). In this study, we have demonstrated the same phenomenon in blood leucocytes derived from patients with *MFN2* mutations. Although Rouzier *et al.* (2011) determined mitochondrial DNA copy number in four skeletal muscle biopsies, they only report on the absence of mitochondrial DNA depletion in homogenate muscle extracts (Table 1). Pathologically increased mitochondrial DNA levels have been detected in laser-microdissected single skeletal muscle fibres from patients with *OPA1* mutations, this effect being particularly marked in COX-deficient muscle fibres (Yu-Wai-Man *et al.*, 2010*b*). Given the overlapping clinical, histological and molecular characteristics observed in these two primary disorders of mitochondrial dynamics, it would be of great interest to know whether mitochondrial DNA proliferation was also present in muscle fibres from patients with *MFN2* mutations, especially in the two biopsies noted to have ragged-red fibres.

MFN2 is the newest member of an expanding group of nuclear mitochondrial disorders characterized by disturbed mitochondrial DNA maintenance, a process which, increasingly, seems to be intrinsically related to the state of the mitochondrial network (Chen *et al.*, 2010; Elachouri *et al.*, 2011). Our observation that *MFN2* mutations cause mitochondrial proliferation in blood adds weight to the novel disease mechanism reported by Rouzier *et al.* (2011). Future work is needed to disentangle the complex interplay between disturbed mitochondrial fusion and fission, mitochondrial DNA instability and the eventual development of both neurological and visual deficits in patients with CMT2A and *MFN2* mutations.

Table 1 ***MFN2*** **mutations identified in our patient cohort**

Mutation	Type	Functional domain	Number of patients
p.Glu65Stop	Nonsense	–	3
p.Arg94Trp	Missense	–	8
p.Arg94Gln	Missense	–	2
p.Ala100Gly	Missense	GTPase	1
p.Arg104Leu	Missense	GTPase	3
p.Arg104Trp	Missense	GTPase	1
p.Thr105Ala	Missense	GTPase	1
p.His165Tyr	Missense	GTPase	6
p.Gly202Ala	Missense	GTPase	4
p.Thr206Ile	Missense	GTPase	2
p.Thr232Asn	Missense	GTPase	1
p.Arg250Gln	Missense	GTPase	1
p.Arg259Cys	Missense	GTPase	1
p.Arg280His	Missense	GTPase	1
p.Gly298Arg	Missense	GTPase	1
p.Glu308Stop[a]	Nonsense	GTPase	1
p.Arg364Trp	Missense	Coiled-Coil 1 (CC1)	1
p.Arg364Pro	Missense	Coiled-Coil 1 (CC1)	1
p.Arg364Gln	Missense	Coiled-Coil 1 (CC1)	1
p.Met376Val	Missense	Coiled-Coil 1 (CC1)	1
p.Met376Ile	Missense	Coiled-Coil 1 (CC1)	1
p.Ala383Val	Missense	Coiled-Coil 1 (CC1)	1
p.Arg468His	Missense	–	2
p.Asp496Gly	Missense	–	2
p.Arg519Pro[a]	Missense	–	1
p.Leu673Pro	Missense	–	3
p.Val705Ile	Missense	Coiled-Coil 2 (CC2)	2
p.Arg707Trp	Missense	Coiled-Coil 2 (CC2)	1
p.Arg707Pro	Missense	Coiled-Coil 2 (CC2)	1
p.Ala716Thr	Missense	Coiled-Coil 2 (CC2)	1
p.His750Pro	Missense	–	1
p.Gln751Stop	Nonsense	–	1
p.Tyr752Stop	Nonsense	–	1

[a]One patient harboured two heterozygous *MFN2* mutations.

Funding

P.Y.W.M. is a Medical Research Council (MRC, UK) Clinician Scientist. R.H. is supported by the Academy of Medical Sciences (UK) and by the MRC (UK). P.S. is funded by IGA MH CR No 10554-3. P.F.C. is a Wellcome Trust Senior Fellow in Clinical Science and a UK National Institute of Health Senior Investigator who also receives funding from the MRC (UK), Parkinson's UK, the Association Francaise contre les Myopathies, and the UK NIHR Biomedical Research Centre for Ageing and Age-related Disease award to the Newcastle upon Tyne Hospitals NHS Foundation Trust.

References

Amati-Bonneau P, Valentino ML, Reynier P, Gallardo ME, Bornstein B, Boissiere A, et al. *OPA1* mutations induce mitochondrial DNA instability and optic atrophy plus phenotypes. Brain 2008; 131: 338–51.

Aure K, Fayet G, Lacene E, Romero NB, Lombes A. Apoptosis in mitochondrial myopathies is linked to mitochondrial proliferation. Brain 2006; 129: 1249–59.

Capps GJ, Samuels DC, Chinnery PF. A model of the nuclear control of mitochondrial DNA replication. J Theor Biol 2003; 221: 565–83.

Chen HC, Vermulst M, Wang YE, Chomyn A, Prolla TA, McCaffery JM, et al. Mitochondrial fusion is required for mtDNA stability in skeletal muscle and tolerance of mtDNA mutations. Cell 2010; 141: 280–9.

Chinnery PF, Samuels DC. Relaxed replication of mtDNA: a model with implications for the expression of disease. Am J Hum Genet 1999; 64: 1158–65.

Durham SE, Samuels DC, Cree LM, Chinnery PF. Normal levels of wild-type mitochondrial DNA maintain cytochrome c oxidase activity for two pathogenic mitochondrial DNA mutations but not for m.3243A -> G. Am J Hum Genet 2007; 81: 189–95.

Elachouri G, Vidoni S, Zanna C, Pattyn A, Boukhaddaoui H, Gaget K, et al. *OPA1* links human mitochondrial genome maintenance to mtDNA replication and distribution. Genome Res 2011; 21: 12–20.

Hudson G, Amati-Bonneau P, Blakely EL, Stewart JD, He LP, Schaefer AM, et al. Mutation of *OPA1* causes dominant optic atrophy with external ophthalmoplegia, ataxia, deafness and multiple mitochondrial DNA deletions: a novel disorder of mtDNA maintenance. Brain 2008; 131: 329–37.

Pyle A, Burn DJ, Gordon C, Swan C, Chinnery PF, Baudouin SV. Fall in circulating mononuclear cell mitochondrial DNA content in human sepsis. Intensive Care Med 2010; 36: 956–62.

Rouzier C, Bannwarth S, Chaussenot A, Chevrollier A, Verschueren A, Bonello-Palot N, et al. The *MFN2* gene is responsible for mitochondrial DNA instability and optic atrophy 'plus' phenotype. Brain 2011; 135: 23–34.

Taylor RW, Schaefer AM, Barron MJ, McFarland R, Turnbull DM. The diagnosis of mitochondrial muscle disease. Neuromuscul Disord 2004; 14: 237–45.

Yu-Wai-Man P, Griffiths PG, Gorman GS, Lourenco CM, Wright AF, Auer-Grumbach M, et al. Multi-system neurological disease is common in patients with *OPA1* mutations. Brain 2010a; 133: 771–86.

Yu-Wai-Man P, Sitarz KS, Samuels DC, Griffiths PG, Reeve AK, Bindoff LA, et al. *OPA1* mutations cause cytochrome c oxidase deficiency due to loss of wild-type mtDNA molecules. Human Molecular Genetics 2010b; 19: 3043–52.

Zuchner S, De Jonghe P, Jordanova A, Claeys KG, Guergueltcheva V, Cherninkova S, et al. Axonal neuropathy with optic atrophy is caused by mutations in mitofusin 2. Ann Neurol 2006; 59: 276–81.

Zuchner S, Mersiyanova IV, Muglia M, Bissar-Tadmouri N, Rochelle J, Dadali EL, et al. Mutations in the mitochondrial GTPase mitofusin 2 cause Charcot-Marie-Tooth neuropathy type 2A. Nat Genet 2004; 36: 449–51.

Multiple Sclerosis Journal
http://msj.sagepub.com/

Genetic variations within the *OPA1* gene are not associated with neuromyelitis optica

Kamil S Sitarz, Patrick Yu-Wai-Man, Gavin Hudson, Anu Jacob, Mike Boggild, Rita Horvath and Patrick F Chinnery

Mult Scler 2012 18: 240 originally published online 9 August 2011
DOI: 10.1177/1352458511416838

The online version of this article can be found at:
http://msj.sagepub.com/content/18/2/240

Published by:
SAGE
http://www.sagepublications.com

MULTIPLE SCLEROSIS JOURNAL | MSJ

Multiple Sclerosis Journal
18(2) 240–243

DOI: 10.1177/1352458511416838
msj.sagepub.com
SAGE

Genetic variations within the *OPA1* gene are not associated with neuromyelitis optica

Kamil S Sitarz[1], Patrick Yu-Wai-Man[1,2], Gavin Hudson[1], Anu Jacob[3], Mike Boggild[3], Rita Horvath[1] and Patrick F Chinnery[1]

Abstract

Neuromyelitis optica (NMO) is an idiopathic demyelinating disease which predominantly affects the optic nerve and spinal cord. Multiplex NMO pedigrees have been reported but the genetic risk factors conferring this increased familial susceptibility have not yet been determined. *OPA1* mutations have recently been identified in families with progressive visual failure and spastic paraparesis, raising the possibility that *OPA1* genetic variants could contribute to the aetiology of NMO. We therefore screened for *OPA1* in 32 patients with NMO. No pathogenic mutations were found, and none of the 13 single-nucleotide polymorphisms identified were associated with an increased risk of developing NMO.

Keywords

demyelination, Devic's disease, dominant optic atrophy, mitochondria, neuromyelitis optica, *OPA1*

Date received: 30th March 2011; accepted: 21st June 2011

Introduction

Neuromyelitis optica (NMO), also known as Devic's disease, is an idiopathic inflammatory demyelinating disease of the central nervous system (CNS) that preferentially targets the optic nerve and spinal cord.[1] The discovery of a specific NMO-IgG autoantibody marker against the aquaporin-4 (AQP4) water channel and the consistent presence of longitudinally extensive myelitis on magnetic resonance imaging have further refined the diagnostic criteria for this disorder.[2] Recent clinicopathological studies have also revealed striking differences between NMO and prototypic multiple sclerosis (MS), establishing them as two distinct disease entities.[3] Compared with MS, NMO is a relatively rare cause of CNS demyelination and the prevalence has been estimated at 0.5 to 1.0 per 100,000 among the white population.[4]

The localized pathology observed within the optic nerve and spinal cord in NMO is intriguing and it is reminiscent of the more complicated phenotypes we have recently described in a subgroup of patients harbouring pathogenic *OPA1* mutations: the major causative gene for autosomal dominant optic atrophy (DOA; OMIM 165500).[5] The cardinal feature of DOA is progressive visual failure secondary to the focal loss of retinal ganglion cell (RGC) axons and optic nerve demyelination. However, up to 20% of *OPA1* mutational carriers will develop multi-system organ involvement in later life, with a predilection for the neuraxis.[6] In two of these families with DOA+, the *OPA1* mutation segregated with both optic atrophy and a severe progressive form of spastic paraplegia.[6] Transcranial magnetic stimulation has also revealed subclinical demyelination of the corticospinal tract in patients

[1]Mitochondrial Research Group, Institute of Genetic Medicine, Newcastle University, UK.
[2]Department of Ophthalmology, Royal Victoria Infirmary, Newcastle upon Tyne, UK.
[3]The Walton Centre for Neurology and Neurosurgery, Liverpool, UK.

Corresponding author:
Dr Patrick Yu-Wai Man, Institute of Genetic Medicine, Newcastle University, Newcastle upon Tyne NE1 3BZ, UK
Email: patrick.yu-wai-man@ncl.ac.uk

with pure DOA, further highlighting the increased susceptibility of long neuronal pathways, including RGC axons, in *OPA1* disease.[7] In one British and one French *OPA1*-positive family, the probands developed an MS-like illness, strikingly similar to the association between the primary mitochondrial DNA mutations causing Leber hereditary optic neuropathy and demyelination (Harding's disease).[6] OPA1 is an inner mitochondrial membrane protein, reinforcing the emerging links between mitochondrial dysfunction, oligodendrocyte survival, and neurodegeneration.[5] Interestingly, multi-generational NMO pedigrees have been reported with clinical features indistinguishable from the more common sporadic variant.[8] Candidate gene analysis has excluded pathogenic *AQP4* mutations and the major genetic risk determinants in these familial cases remain to the determined.[8,9] Our clinical observations relating to DOA+ therefore imply that some patients diagnosed with NMO could be harbouring pathogenic *OPA1* mutations, or that the expression of NMO could be influenced by specific *OPA1* single-nucleotide polymorphisms (SNPs). To investigate these hypotheses, we screened a large case series of patients with NMO for possible disease-modifying *OPA1* genetic variants.

Patients and methods

Study groups

Genomic DNA samples, extracted from whole blood, were available from the following groups of white British subjects: (i) patients with NMO ($N = 32$), identified as part of a British Neurological Surveillance Unit (BNSU) national case ascertainment study. All these patients fulfilled the revised diagnostic criteria,[2] with clinically and radiologically confirmed episodes of optic neuritis and transverse myelitis.[4,9] NMO anti-AQP4 antibodies were detected in 12 of these patients; (ii) patients with primary open angle glaucoma (POAG; $N = 137$), diagnosed with either the high tension (HTG; $N = 67$) or normal tension (NTG; $N = 70$) form of the disease;[10] and (iii) healthy controls ($N = 75$) with no evidence of ophthalmological or neuromuscular disorders. This study had the relevant institutional approval and written informed consent was obtained from all of the subjects involved.

OPA1 genotyping

The entire coding region of the *OPA1* gene, including flanking exon–intron boundaries, was amplified by the polymerase chain reaction (PCR), using a set of 27 M13-tagged primer pairs, which is available on request. PCR products were sequenced using BigDye™ terminator cycle chemistries on an ABI3100 Genetic Analyser (Applied Biosystems, UK). The sequence electropherograms obtained were compared with the Genbank *OPA1* reference sequence (accession number NG_011605.1, mRNA transcript variant 1, NM_015560.2), using SeqScape™ software v2.6 (Applied Biosystems, UK).

Statistical analysis

The Hardy–Weinberg equilibrium for *OPA1* genotypes was assessed for patient and control groups (http://ihg.gsf.de/cgi-bin/hw/hwa1.pl). Allele and genotype SNP frequencies were compared with χ^2 analysis using GraphPad™ v.4 statistical software (San Diego, CA).

Results

OPA1 variants identified

No pathogenic *OPA1* mutations were identified in the NMO cohort. A total of 13 *OPA1* variants were identified, and of these, nine were previously reported SNPs (Table 1). The remaining four variants were novel heterozygous changes found in four different patients with NMO. The exon 11 (c.1071A > G, p.A357A) and exon 22 (c.2256G > T, p.L752L) variants were synonymous, and the two novel intronic variants were not predicted to affect the neighbouring splice donor sites.

SNP associations

The SNP frequency in the NMO cohort was compared with healthy controls and the POAG group. No significant allele or genotype associations were detected with the following three *OPA1* SNPs: c.473A > G, IVS8 + 4c > t, and IVS8 + 32t > c (Online e-Tables 1, 2, and 3). Analysis of both the IVS8 + 4c > t and IVS8 + 32t > c SNPs showed no significantly increased risk of developing NMO with specific compound genotypes (Online e-Table 4). There was no significant allele or genotype associations for the remaining SNPs identified in patients with NMO compared with healthy controls (data not shown). Further subgroup analysis did not reveal any significant *OPA1* SNP association between: (i) anti-AQP4 antibody-seropositive NMO patients and controls; (ii) anti-AQP4 antibody-seronegative NMO patients and controls; and (iii) anti-AQP4 antibody-seropositive and antibody-seronegative NMO patients (data not shown).

Discussion

No pathogenic *OPA1* mutations were identified in this well-characterized group of patients with NMO.

Table 1. *OPA1* variants identified in the neuromyelitis optica (NMO) cohort

cDNA	Location	AA change	*N*	Homozygous	Heterozygous
c.473A > G	Exon 4	p.N158S	25/32	15/25 (60%)	10/25 (40%)
c.557-19t > c	Intron 4	-	17/32	7/17 (41%)	10/17 (59%)
IVS8 + 4c > t	Intron 8	-	9/32	2/9 (22%)	7/9 (78%)
IVS8 + 32t > c	Intron 8	-	17/32	7/17 (41%)	10/17 (59%)
c.1071A > G*	Exon 11	p.A357A	1/32	0/1 (0%)	1/1 (100%)
c.1312 + 32a > g	Intron 13	-	1/32	0/1 (0%)	1/1 (100%)
c.1589 + 22t > g*	Intron 16	-	1/32	0/1 (0%)	1/1 (100%)
c.1770 + 16t > g	Intron 18	-	6/32	0/6 (0%)	6/6 (100%)
c.1770 + 47t > a*	Intron 18	-	1/32	0/1 (0%)	1/1 (100%)
c.1770 + 51t > g	Intron 18	-	17/32	7/17 (41%)	10/17 (59%)
c.2109C > T	Exon 21	p.A703A	25/32	15/25 (60%)	10/25 (40%)
c.2256G > T*	Exon 22	p.L752L	1/32	0/1 (0%)	1/1 (100%)
c.2707 + 25t > a	Intron 26	-	17/32	7/17 (41%)	10/17 (59%)

*Novel *OPA1* variant.
AA, amino acid; cDNA, complementary DNA; *N*, number of NMO patients harbouring the *OPA1* variant.
Identified *OPA1* variants were confirmed by reverse sequencing and checked against available databases to determine whether they had previously been reported: (i) the e*OPA1* Database; (ii) the NCBI dbSNP Database; and (iii) the Human Genome Mutation Database.

Although we cannot exclude the possibility of large-scale *OPA1* genomic rearrangements, the latter are rare in DOA, accounting for less than 1% of singleton cases with suspected inherited optic atrophy.[5] *OPA1* mutations have only been reported within the first 10 intronic nucleotide positions, making it also unlikely that our PCR-based sequencing strategy has missed functional intronic variants influencing mRNA splicing or transcriptional activity.[5] Only one non-synonymous *OPA1* SNP (c.473A > G, p.N158S) was present in patients with NMO, but it is an evolutionarily poorly conserved amino acid residue. No significant allele and genotype associations were found for c.473A > G and the remaining SNPs identified in this NMO cohort when compared with both healthy controls and patients with POAG. Our findings contrast with recent observations in POAG, where specific *OPA1* variants at IVS8 + 4c > t and IVS8 + 32t > c have been linked with an increased risk of developing NTG, suggesting a role for *OPA1* in glaucomatous optic nerve degeneration.[10] Theoretically, these two intronic SNPs could still exert a minor influence on the expression of the NMO disease phenotype. However, NMO is a relatively rare form of CNS demyelination, and the sample size required to demonstrate these more subtle genetic modulatory effects will prove challenging.

Funding

PYWM is a Medical Research Council (MRC) Clinical Research Fellow in Neuro-Ophthalmology and PFC is a Wellcome Trust Senior Fellow in Clinical Science. PFC also receives funding from Parkinson's UK, the MRC Translational Muscle Centre, and the UK NIHR Biomedical Research Centre in Ageing and Age-related Disease.

Conflict of interest statement

The authors declare no conflicts of interest in preparing this article.

References

1. Wingerchuk DM, Lennon VA, Lucchinetti CF, et al. The spectrum of neuromyelitis optica. *Lancet Neurol* 2007; 6: 805–815.
2. Wingerchuk DM, Lennon VA, Pittock SJ, et al. Revised diagnostic criteria for neuromyelitis optica. *Neurology* 2006; 66: 1485–1489.
3. Compston A. Complexity and heterogeneity in demyelinating disease. *Brain* 2007; 130: 1178–1180.
4. Jacob A, Das K and Boggild M. Estimating the incidence and prevalence of neuromyelitis optica in the UK: extrapolating data from Merseyside. *J Neurol Neurosurg Psychiatry* 2009; 80: e1.
5. Yu-Wai-Man P, Griffiths PG and Chinnery PF. Mitochondrial optic neuropathies - disease mechanisms and therapeutic strategies. *Prog Retinal Eye Res* 2011; 30: 81–114.
6. Yu-Wai-Man P, Griffiths PG, Gorman GS, et al. Multi-system neurological disease is common in patients with OPA1 mutations. *Brain* 2010; 133: 771–786.
7. Baker MR, Fisher KM, Whittaker RG, Griffiths PG, Yu-Wai-Man P and Chinnery PF. Subclinical multi-system neurological disease in "pure" OPA1

autosomal dominant optic atrophy. *Neurology* 2011; in press.
8. Wingerchuk DM. Neuromyelitis optica: effect of gender. *J Neurol Sci* 2009; 286: 18–23.
9. Hudson G, Mowbray C, Elson JL, et al. Does mitochondrial DNA predispose to neuromyelitis optica (Devic's disease)? *Brain* 2008; 131: e93.
10. Yu-Wai-Man P, Stewart JD, Hudson G, et al. OPA1 increases the risk of normal but not high tension glaucoma. *J Med Genet* 2010; 47: 120–125.

Curr Neurol Neurosci Rep (2012) 12:308–317
DOI 10.1007/s11910-012-0260-0

NEURO-OPHTHALMOLOGY (G PLANT, SECTION EDITOR)

Disorders of the Optic Nerve in Mitochondrial Cytopathies: New Ideas on Pathogenesis and Therapeutic Targets

Kamil S. Sitarz · Patrick F. Chinnery · Patrick Yu-Wai-Man

Published online: 4 March 2012

Abstract Mitochondrial cytopathies are a heterogeneous group of human disorders triggered by disturbed mitochondrial function. This can be due to primary mitochondrial DNA mutations or nuclear defects affecting key components of the mitochondrial machinery. Optic neuropathy is a frequent disease manifestation and the degree of visual failure can be profound, with a severe impact on the patient's quality of life. This review focuses on the major mitochondrial disorders exhibiting optic nerve involvement, either as the defining clinical feature or as an additional component of a more extensive phenotype. Over the past decade, significant progress has been achieved in our basic understanding of Leber hereditary optic neuropathy and autosomal-dominant optic atrophy—the two classical paradigms for these mitochondrial optic neuropathies. There are currently limited treatments for these blinding ocular disorders and, ultimately, the aim is to translate these major advances into tangible benefits for patients and their families.

Keywords Dominant optic atrophy · Haplogroup · Hereditary spastic paraplegia, Heteroplasmy · Idebenone · Leber hereditary optic neuropathy · Mitochondrial DNA · Mitofusin · Multiple sclerosis · Neuroprotection · Retinal ganglion cell · Optic nerve · Mitochondrial cytopathies

K. S. Sitarz · P. F. Chinnery · P. Yu-Wai-Man
Wellcome Trust Centre for Mitochondrial Research, Institute of Genetic Medicine, Newcastle University, Newcastle, UK

P. Yu-Wai-Man
Department of Ophthalmology, Royal Victoria Infirmary, Newcastle upon Tyne, UK

P. Yu-Wai-Man (✉)
Wellcome Trust Centre for Mitochondrial Research, Institute of Genetic Medicine, Centre for Life, Newcastle University, Newcastle upon Tyne NE1 3BZ, UK
e-mail: Patrick.Yu-Wai-Man@ncl.ac.uk

Introduction

Mitochondria are found in all nucleated cells and reflecting this ubiquitous presence, patients with mitochondrial cytopathies often manifest a diverse combination of tissue and organ involvement [1]. However, for reasons that still remain unclear, mitochondrial dysfunction has a marked predilection for the optic nerve, the latter being affected in about half of all patients with confirmed mitochondrial disease (Fig. 1). Irrespective of the molecular pathways involved, remarkably, these mitochondrial optic neuropathies all share the same pathological features—selective degeneration of the retinal ganglion cell (RGC) layer, leading to progressive axonal loss and the onset of visual failure [2]. In this review, recent advances in our understanding of this important group of disorders are discussed, in addition to promising therapeutic strategies.

Leber Hereditary Optic Neuropathy

Epidemiology

Leber hereditary optic neuropathy (LHON, OMIM 535000) is named after Theodore Leber (1840–1917), a German ophthalmologist who was the first to describe the key features of this disorder [3]. LHON is the most common of the primary mitochondrial DNA (mtDNA) disorders and the minimum prevalence has been estimated at 1 in 31,000 in the North of England (Fig. 1) [4]. Epidemiological studies from the Netherlands and Finland have reported comparable

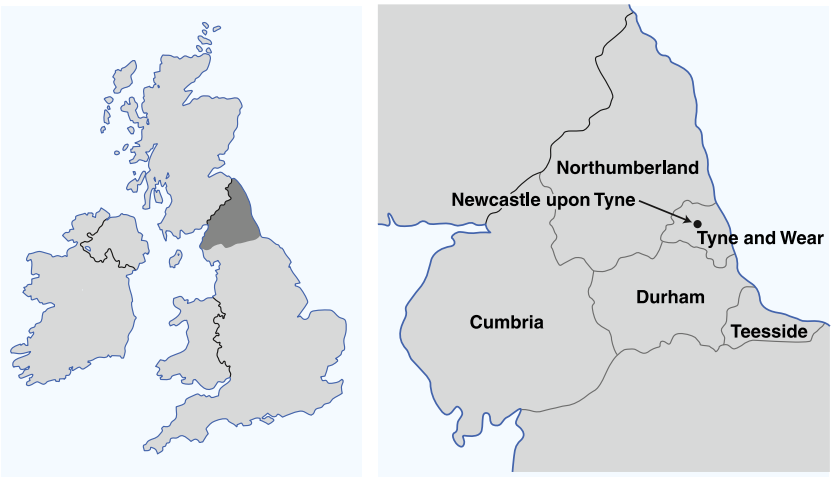

Figure 1 Mitochondrial disease in the North of England. (Adapted from Yu-Wai-Man et al. [2] and Schaefer et al. [50])

Disorder	Minimum prevalence
Mitochondrial genetic disorders	1 in 5000
Leber hereditary optic neuropathy	1 in 31,000
Autosomal-dominant optic atrophy	1 in 35,000
Optic neuropathy in mitochondrial cytopathies	1 in 10,000

figures of 1 in 39,000 and 1 in 50,000, respectively. In one Australian study, 2% of individuals on the National Blind Registry had optic atrophy secondary to LHON, highlighting the significant socioeconomic burden of this inherited optic nerve disorder. Three mtDNA point mutations—m.3460 G>A, m.11778 G>A, and m.14484 T>C—account for the vast majority (~90%) of LHON cases and, for this reason, they are often referred to as "primary" (Table 1) [3, 5].

Clinical Manifestations

Typically, disease conversion in LHON is characterized by acute or subacute central visual loss in one eye, followed 2 to 4 months later by the fellow eye [3, 5]. Unilateral optic nerve involvement in LHON is exceptionally rare and another underlying pathological process should be actively excluded in these atypical cases. Bilateral simultaneous onset probably occurs in about 25% of patients, although it can be difficult for some individuals to accurately report whether visual loss had been ongoing in one eye prior to the fellow eye being affected. The peak age of onset is in the second and third decades of life and it is unusual for symptoms to develop beyond 50 years of age.

The initial visual loss in LHON is severe and it usually plateaus over the next 6 months, with most patients achieving visual acuities of 20/200 or worse [3, 5]. There is an associated dense central or centrocecal scotoma and color vision is significantly impaired. The pupillary light reflexes are relatively preserved and this rather surprising feature has recently been ascribed to a special class of melanopsin-containing RGCs that are more resistant to the mtDNA LHON mutations [6••]. In the acute phase, classically, there is optic disc hyperemia, peripapillary telangiectatic vessels, vascular tortuosity, and retinal nerve fiber layer (RNFL) edema secondary to axonal stasis. In a proportion (20% to 40%) of LHON carriers undergoing disease conversion, the optic discs can look entirely normal, followed 6 weeks later by the development of neuroretinal rim pallor [5]. Pathological cupping of the optic disc is also a recognized feature of longstanding LHON cases, reflecting the ongoing loss of RGC axons in the chronic phase of the disease. The overall prognosis in LHON is poor, even among patients harboring the m.14484 T>C mutation, which carries the best chance for partial visual recovery [5]. If it occurs, a slow improvement in visual parameters can be expected within the first year, although more delayed visual recovery has been reported.

Syndromal LHON Phenotypes

LHON is typically a monosymptomatic disease but additional features such as cardiac conduction defects, peripheral neuropathy, dystonia, and myopathy have been reported as occurring more frequently among LHON carriers. In particular, there is a well-reported association between the three primary mtDNA LHON mutations and a multiple sclerosis–like illness, especially among female carriers. Rarer pathogenic mtDNA variants have been linked with more atypical "LHON +" syndromes, where the optic neuropathy segregated with prominent neurological features including spastic dystonia, ataxia, juvenile-onset encephalopathy, and psychiatric disturbances [2].

Table 1 mtDNA variants associated with LHON

	Mitochondrial gene	Nucleotide change
Common variants (~ 90%)	*MTND1*	m.3460 G>A[a]
	MTND4	m.11778 G>A[a]
	MTND6	m.14484 T>C[a]
Rare variants (~ 10%)	*MTND1*	m.3376 G>A, m.3635 G>A[a], m.3697 G>A, m.3700 G>A, m.3733 G>A[a], m.4025 C>T, m.4160 T>C, m.4171 C>A[a]
	MTND2	m.4640 C>A, m.5244 G>A
	MTND3	m.10237 T>C
	MTND4	m.11696 G>A, m.11253 T>C
	MTND4L	m.10663 T>C[a]
	MTND5	m.12811 T>C, m.12848 C>T, m.13637 A>G, m.13730 G>A
	MTND6	m.14325 T>C, m.14568 C>T, m.14459 G>A[a], m.14729 G>A, m.14482 C>A[a], m.14482 C>G[a], m.14495 A>G[a], m.14498 C>T, m.14568 C>T[a], m.14596 A>T
	MTATP6	m.9101 T>C
	MTCO3	m.9804 G>A
	MTCYB	m.14831 G>A

Over 70% of LHON carriers harbor the m.11778 G>A mutation, but as a result of a founder event, the m.14484 T>C mutation has been identified in nearly 90% of all affected patients of French Canadian descent [3, 5]. In most laboratories worldwide, the diagnostic protocol involves screening for the three "primary" LHON mutations in the first instance. As full mitochondrial genome sequencing remains time consuming and expensive, this is only indicated if the initial LHON screen is negative and there is a strong clinical suspicion

[a] These mtDNA variants are definitely pathogenic. They have been identified in two or more independent LHON pedigrees, showing segregation with affected disease status. The remaining putative LHON mutations have been found in singleton cases or in a single family, and additional evidence is required before pathogenicity can be irrefutably ascribed

LHON Leber hereditary optic neuropathy; *mtDNA* mitochondrial DNA

Disease Modifiers

LHON is characterized by incomplete penetrance and a marked sex bias, with only about 50% of male carriers and about 10% of female carriers losing vision during their lifetime. The pathological consequences of the mtDNA LHON mutations are clearly being influenced by other disease modifiers, and these can be classified into four main groups: 1) the mitochondrial genetic background, 2) nuclear susceptibility genes, 3) hormonal differences, and 4) environmental triggers.

As mitochondria have a high copy number genome, LHON carriers can be homoplasmic (100% mutant) for the mtDNA mutation, or heteroplasmic with a combination of both the wild-type and mutant mtDNA species. Although the risk of visual loss is minimal at heteroplasmy levels below 60%, this observation cannot account for the bulk of unaffected LHON carriers, most of whom are homoplasmic mutant and therefore beyond this biochemical threshold [7]. MtDNA is highly polymorphic and during human evolution, ancient mtDNA variants have clustered together in specific combinations known as haplogroups. As mtDNA haplogroups influence mitochondrial oxidative phosphorylation, these more subtle variations could magnify or lessen the impact of the LHON mutation on RGC survival. In a large study involving 159 Caucasian LHON pedigrees, haplogroup J was associated with a significantly increased risk of visual loss among m.11778 G>A and m.14484 T>C carriers, whereas m.3460 G>A carriers were more likely to become affected on a haplogroup K background [8]. Haplogroup H had a protective effect but only among individuals harboring the m.11778 G>A mutation. Haplogroup associations have been reported in other ethnic groups, supporting a contributory role for the mtDNA background in influencing LHON penetrance [9].

The predilection for males to lose vision in LHON cannot be explained by mitochondrial genetics and a visual loss susceptibility gene on the X chromosome has long been suspected, the so-called two-locus disease model [10]. Although such an X-linked disease modifier gene has yet to be formally identified, three independent linkage studies have revealed overlapping candidate regions, providing strong evidence for its existence [11–13]. Another obvious factor to account for the observed male bias in LHON is a protective influence conferred by female sex hormones. This hypothesis was recently investigated using LHON cybrid cell lines, and interestingly, treatment with 17β-estradiol resulted in reduced reactive oxygen species (ROS) levels, increased activity of the antioxidant enzyme superoxide dismutase, and more efficient mitochondrial biogenesis [14•].

Various environmental factors have been implicated in precipitating visual loss among LHON carriers including head trauma, industrial toxins, and drugs with mitochondrial toxic effects [15]. The evidence for these environmental triggers is largely anecdotal, but a recent multicenter study of 125 LHON pedigrees has provided convincing evidence for an increased risk of visual failure among smokers, and to a lesser extent, heavy drinkers [16•].

Mitochondrial Encephalomyopathies

The mitochondrial encephalomyopathies encompass several distinct phenotypes such as mitochondrial encephalomyopathy, lactic acidosis, and stroke-like episodes (MELAS), myoclonic epilepsy and ragged-red fibers (MERRF), maternally inherited Leigh syndrome (MILS), mitochondrial neurogastrointestinal encephalomyopathy (MNGIE), and the Kearns-Sayre syndrome (KSS) [1,

17]. Although variable and not a disease-defining feature, the occurrence of optic atrophy is well described in this group of patients, exacerbating the already considerable disease burden [18]. Additional studies are required to determine the true prevalence of both clinical and subclinical optic neuropathy in these mitochondrial encephalomyopathies, and whether specific mtDNA mutations or phenotypes are linked with an increased risk of optic nerve involvement.

Nuclear Mitochondrial Disorders

Autosomal-Dominant Optic Atrophy

Epidemiology

Frederick Batten (1865–1918), a pediatric neurologist, is credited with the first report of autosomal-dominant optic atrophy (DOA) in one British family. The characteristic features were described in greater detail by Poul Kjer in a large cohort of Danish families, establishing DOA as a distinct clinical entity from LHON [3]. The prevalence of DOA was estimated at 1 in 35,000 in the North of England (Fig. 1), but additional families have since been identified and the true figure is likely to be much higher (Yu-Wai-Man, Unpublished data).

Disease Genes and Candidate Loci

Between 50% and 60% of families with DOA harbor pathogenic mutations in *OPA1*, which codes for a mitochondrial inner membrane protein (Table 2) [3, 5]. *OPA1* is highly polymorphic and over 200 pathogenic variants have been identified, clustering in the GTPase region and the dynamic central domain. To minimize cost, *OPA1* is routinely sequenced using polymerase chain reaction–based methods, which will not detect exonic deletions or duplications. These large-scale rearrangements have been identified in 10% to 20% of *OPA1*-negative families, and these additional molecular studies, although not yet widely available, are recommended for probands with a clear-cut DOA phenotype and a strong family history [2].

Mutations in *OPA3* were first described in Iraqi-Jewish families with autosomal-recessive type III 3-methylglutaconic aciduria (Costeff syndrome), a progressive neurodegenerative disorder with early-onset optic atrophy, hypotonia, ataxia, extrapyramidal dysfunction, and cognitive decline [19]. Heterozygous *OPA3* mutations were subsequently reported in two French families with a dominantly inherited form of optic atrophy associated with premature cataract formation (ADOAC) [20]. Similar to *OPA1*, *OPA3* has a mitochondrial-targeting domain and it was initially considered to be a mitochondrial inner membrane protein. However, a recent study has suggested instead that *OPA3* localizes to the mitochondrial outer membrane, with its C-terminus facing the cytosol [21]. The causative genetic defects in the remaining families with DOA have not yet been identified, although a number of candidate loci have been reported (Table 2).

Visual Function and Disease Progression

Visual loss in DOA is bilateral and symmetrical with the majority patients reporting subnormal vision from early childhood. There is a wide intra- and inter-familial variability in disease severity, with visual acuities ranging from 20/20 to the detection of hand movement [2, 3]. Individuals with visual acuities of 20/30 or better are frequently asymptomatic and they are only identified as having features of a bilateral optic neuropathy at the time of contact tracing. On long-term follow-up, visual function was observed to deteriorate in 50% to 75% of patients with DOA but the rate of progression was highly variable, making genetic counseling difficult [2, 3]. Although a milder optic nerve disease compared with LHON, DOA still results in significant visual impairment with nearly half of all patients eventually registered blind.

As in LHON, the primary site of pathology in DOA is the papillomacular bundle and central, centrocecal, and

Table 2 Nuclear mitochondrial disorders with prominent optic nerve involvement

Inheritance	Locus	Gene	OMIM	Phenotypes
Dominant	1p36.2	*MFN2*	601152	Hereditary motor and sensory neuropathy type 6 (HMSN-6, CMT2A)
	3q28–q29	*OPA1*	165500	Isolated optic atrophy and syndromal dominant optic atrophy (DOA+)
	19q13.2–q13.3	*OPA3*	165300	Autosomal-dominant optic atrophy and early-onset cataracts (ADOAC)
Recessive	9q13–q21.1	*FXN*	229300	Friedreich's ataxia (FRDA)
	11q14.1–q21	*TMEM126A*	612989	Optic atrophy ± auditory neuropathy
	16q24.3	*SPG7*	607259	Hereditary spastic paraplegia type 7 (HSP-7)
	19q13.2–q13.3	*OPA3*	258501	Type III 3-methylglutaconic aciduria (Costeff syndrome)

(Adapted from Yu-Wai-Man et al. [2, 5])

paracentral scotomas are the most common visual field defects. The degree of dyschromatopsia is commensurate with the level of vision and pure tritanopia, once considered a pathognomonic feature of DOA, is only rarely seen. Histopathological studies of a postmortem eye retrieved from one patient showed relative preservation of melanopsin-containing RGCs, accounting for the lack of an afferent pupillary defect in DOA—another peculiarity shared with LHON [6••]. The optic nerve head in DOA can look diffusely pale or it can have a characteristic temporal wedge, especially in patients with early disease where RGC loss remains mostly localized to the papillomacular bundle [2, 3].

The Expanding Phenotypic Spectrum

Up to 20% of patients harboring *OPA1* mutations will develop a syndromal form of the disease (DOA+) marked by significant neurological complications [22•]. The most common extraocular feature observed in this group is sensorineural hearing loss, which usually manifests itself in the second and third decades of life after visual failure has become apparent. A proportion of *OPA1* carriers will progress to a more debilitated state with variable combinations of ataxia, peripheral neuropathy, myopathy, and progressive external ophthalmoplegia in later life. From a mechanistic perspective, it is also revealing that some patients with DOA+ can present with clinical features indistinguishable from other neurodegenerative disorders such as multiple sclerosis, hereditary spastic paraplegia (HSP), and the inherited spinocerebellar degenerations. The phenotypic spectrum of *OPA1* disease is likely to expand even further with greater clinical awareness and easier access to molecular genetic testing.

Other Nuclear Mitochondrial Optic Neuropathies

The nuclear defects underlying several common neuromuscular disorders have been clarified. A remarkable element has been the increasing realization that mitochondrial dysfunction plays a central role in the pathophysiology of disease groups as diverse as Charcot-Marie-Tooth (CMT) disease, HSP, and the inherited spinocerebellar ataxias—reflecting to a certain extent the broader phenotypic spectrum recently described for *OPA1* disease [2]. Mutations in *MFN2*, which codes for a critical mitochondrial outer membrane protein, have been identified in patients with hereditary motor and sensory neuropathy type 6 (HMSN-6), an autosomal-dominant axonal CMT subtype (Table 2) [23]. Affected individuals develop an early-onset peripheral neuropathy with a progressive bilateral optic atrophy in later childhood. Optic neuropathy also features prominently in Friedreich ataxia and HSP type 7 (HSP-7), caused by nuclear mutations in *FXN* and *SPG7*, respectively [2]. Frataxin is essential for the assembly of the iron-sulfur clusters embedded within the mitochondrial respiratory chain complexes, whereas paraplegin is a key mitochondrial protease involved in the proteolytic processing of *OPA1* [24, 25]. All these disease pathways are likely interrelated, and disturbance in one element will set into motion a vicious cycle, which eventually disturbs mitochondrial homeostasis triggering neuronal cell loss. As the molecular basis of other inherited human diseases is uncovered, it will be interesting to note whether optic atrophy is present in those cases where the genetic defect is ultimately revealed to affect mitochondrial function. A recent example is the identification of *TMEM126A* mutations among patients with autosomal-recessive optic atrophy, with or without an associated auditory neuropathy [26]. Although its exact functions still remain to be determined, fascinatingly, TMEM126A is a mitochondrial transmembrane protein present at high levels within the RGC layer and the optic nerve head [26].

Mechanisms Contributing to RGC Loss

The final pathological outcome in mitochondrial optic neuropathies is apoptotic RGC loss and several disease pathways can contribute to this irreversible process. Although a greater emphasis has been placed on the experimental data obtained for LHON and DOA, similar mechanisms have also been shown to operate in other mitochondrial cytopathies.

Bioenergetic Failure

Mitochondria are the cell's powerhouses providing most of its adenosine triphosphate (ATP) requirements through the tight control of mitochondrial respiratory chain activity. All three primary LHON mutations—m.3460 G>A, m.11778 G>A, and m.14484 T>C—disrupt key polypeptide subunits of complex I. Similarly, *OPA1* mutations have a detrimental impact on mitochondrial oxidative output by impairing the assembly and stability of the respiratory chain complexes [27]. Most studies, based on in vitro or in vivo assays, indicate a significant impairment in complex I activity, leading to a reduction in mitochondrial membrane potential and overall ATP synthesis (reviewed in [5] and [15]). Although this bioenergetic deficit is bound to impact negatively on RGCs, by itself, this cannot account for their selective vulnerability. Photoreceptors, for example, have a much higher energetic demand and outer retinal function is usually preserved in both LHON and DOA.

ROS and Excitotoxicity

The disrupted flow of high-energy electrons along the respiratory chain leads to free radical production and increased

ROS levels have been consistently observed in transmitochondrial LHON cybrids (reviewed in [5] and [15]). The efficient reuptake of glutamate is also disrupted in these cellular models due to the downregulation of excitatory amino acid transporter (EAAT1) activity. A *drosophila Opa1* (*dOpa1*) model has recently been established and homozygous mutant flies developed a rough and glossy eye phenotype due to the loss of hexagonal lattice cells, with decreased lens and pigment deposition. This genetically engineered *dOpa1* mutation led to a dramatic increase in ROS levels, which could be partially rescued with dietary antioxidant supplementation or overexpression of *SOD1* [28]. Heterozygous adult flies were phenotypically normal but similar to the homozygotes, ROS levels were elevated with clear evidence of cellular oxidative stress. Increased ROS levels and glutamate excitotoxicity clearly represent a toxic combination, sufficiently potent to initiate the apoptotic cascade.

Disturbed Calcium Handling

Besides its localization to the mitochondrial outer membrane, MFN2 is also associated with the endoplasmic reticulum (ER), resulting in a close communication between the mitochondrial and ER membranes [29••, 30]. When the MFN2 protein is disrupted or absent, as in CMT-2A this tethering effect is lost with dramatic consequences on cellular calcium homeostasis. The ER and mitochondrial network are important calcium stores and the dynamic flux between these two compartments buffers against cytosolic calcium spikes, which can sensitize the cell to various pro-apoptotic signals such as glutamate [29••, 30]. Mirroring the pathomechanism of *MFN2* mutations, mtDNA point mutations involving complex I and complex IV subunits have also been directly linked with disturbed calcium handling in neuronal populations [31]. Although speculative, it is likely that a similar process is operating in LHON and DOA, contributing to RGC dysfunction and ultimately disease conversion among at-risk mutational carriers [32]. The emerging links between calcium homeostasis and mitochondrial dysfunction are an exciting new development, highlighting potential disease pathways amenable to therapeutic intervention.

Mitochondrial Network Dynamics

Cytochrome *c* is a powerful pro-apoptotic mediator and as a protective mechanism, high concentrations of these molecules are carefully sequestered within the mitochondrial cristae. Irrespective of the mtDNA mutation involved, the dissipation of the mitochondrial membrane potential accelerates the cytosolic release of these cytochrome *c* molecules, precipitating an irreversible commitment toward programmed cell death [33]. The identification of *OPA1* and *MFN2* mutations in DOA and CMT-2A has provided further insights into this key disease mechanism. OPA1 ensures the integrity of the mitochondrial cristae's tight junctions, preventing cytochrome *c* from leaching out into the cytosolic space. In addition, OPA1 and MFN2 both belong to the dynamin superfamily of mechanoenzymes, sharing considerable structural similarities, including a highly conserved catalytic GTPase domain [24]. These two proteins have important pro-fusional properties and by working closely together, they maintain a highly-interconnected mitochondrial network throughout the cell's structure [24, 33]. Unsurprisingly, the pathological hallmark of *OPA1*- and *MFN2*-mutant fibroblasts is mitochondrial network fragmentation, which not only impairs mitochondrial oxidative phosphorylation, but also leads to the uncontrolled release of calcium and cytochrome *c* into an already compromised cellular environment [27, 34, 35••].

Somatic mtDNA Defects

Pathological levels of cytochrome *c* oxidase–negative fibers have been identified in skeletal muscle biopsies from patients with DOA+ [35••, 36••]. The underlying biochemical defect in these muscle fibers is secondary to the accumulation of high levels of somatic mtDNA deletions, which have clonally expanded during the patient's lifetime, partly accounting for the delayed onset of these extraocular features [37••]. Intriguingly, the risk of developing DOA+ is three times higher with missense mutations targeting the functional GTPase domain, consistent with a dominant-negative mutational effect [22•]. OPA1 is clearly involved in preserving the integrity of the mitochondrial genome and recent studies have provided some tantalizing insights into the mechanisms that contribute to mtDNA instability [38], [39••, 40••]. OPA1 is thought to anchor the mtDNA replicative machinery, known as nucleoids, to the mitochondrial inner membrane and a dominant-negative mutation could plausibly upset this delicate balance, leading to mtDNA deletion formation [40••]. Why is this relevant to our understanding of RGC loss? Patients with DOA+ have worse visual acuities and significantly thinner RNFL thickness compared with those who only develop isolated optic atrophy [41]. The accumulation of these somatic mtDNA deletions is therefore clearly having an incremental effect on the other deleterious consequences linked to *OPA1* mutations.

Why Are RGCs Selectively Vulnerable?

One factor that could explain this tissue-specific vulnerability is the rather unusual anatomical peculiarity encountered at the lamina cribrosa, where RGC axons first acquire their

myelin sheaths. This transition is marked by a sharp differential gradient, with a much higher density of mitochondria and voltage-gated sodium channels in the pre-laminar unmyelinated segment of the optic nerve [42, 43]. These physiological adaptations facilitate the efficient propagation of action potentials in the absence of an insulating myelin covering. The pre-laminar region therefore represents a weak link, significantly more exposed to the disadvantageous consequences of, even subtle, mitochondrial biochemical defects.

Histopathological studies of optic nerves retrieved from two patients with LHON, one harboring the m.3460 G>A mutation and the other the m.11778 G>A mutation, have revealed some interesting observations on the susceptibility of specific RGC populations (reviewed in [2] and [15]). A prominent loss of smaller-caliber axons was observed, corresponding to the parvocellular RGC population, whereas the larger-caliber magnocellular RGCs were relatively preserved. These ultrastructural findings were subsequently confirmed with higher-resolution transmission electron microscopy. Parvocellular RGCs are a major component of the papillomacular bundle and this greater vulnerability to impaired mitochondrial oxidative phosphorylation could be related to their relatively smaller cross-sectional areas, the latter further exacerbating axonal stasis in conditions of sustained metabolic stress.

The maintenance of a higher mitochondrial concentration in the pre-laminar region also highlights the central role played by the cytoskeleton, especially the microtubule network, in channeling mitochondria to their appropriate cellular locations. Axonal transport in highly specialized neuronal populations such as RGCs is critically dependent on these mitochondrial-cytoskeletal interactions (reviewed in [2] and [15]). These can be adversely affected either by an underlying mitochondrial respiratory chain defect, or by a primary disturbance in microtubule assembly—the pathological hallmark of the HSP group of disorders [2]. Optic atrophy is well described in HSP-7 and it is likely that optic nerve involvement remains an under-reported feature in other HSP genetic subtypes.

Therapeutic Interventions

Visual Rehabilitation

The majority of patients with mitochondrial optic neuropathies are severely visually impaired and the sudden onset of visual loss in otherwise healthy individuals carries a significant psychological and socioeconomic burden. Therefore, clinicians have an important role to play in facilitating access to rehabilitative services such as low visual aids and occupational therapy.

Clinical Surveillance

It is essential to screen for associated systemic complications, such as diabetes and cardiomyopathy, among patients with mitochondrial cytopathies. The development of diabetic peripheral neuropathy and cardiac-related exertional dyspnea can further compound the physical difficulties faced by patients with poor vision, and they should be aggressively managed as part of a multidisciplinary team. As a general health measure, patients with mitochondrial disease should be advised not to smoke and to moderate their alcohol intake. Furthermore, in LHON, smoking, and to a lesser extent excessive binge drinking, have been linked with an increased risk of visual loss [16•].

Pharmacological Agents

Various pharmacological agents with putative neuroprotective properties have been used to mitigate the deleterious consequences of mitochondrial dysfunction and to prevent further RGC loss (reviewed in [44••]). The most promising agent to date is idebenone (2,3-dimethoxy-5-methyl-6-[10-hydroxydecyl]-1,4-benzoquinone), a short-chain synthetic benzoquinone analogue, which promotes mitochondrial ATP synthesis in addition to having antioxidant properties. Coenzyme Q10 (CoQ_{10}) is a longer-chain quinone analogue and based on limited evidence, CoQ_{10} supplementation is often used to treat patients with mitochondrial cytopathies. Idebenone is thought to have some advantageous properties over CoQ_{10}, both in terms of its bioavailability and its mode of action. Unlike CoQ_{10}, idebenone is able to bypass complex I inhibition by shuttling electrons directly from the cytosol to complex III, thereby restoring ATP production and decreasing lactate levels [45].

The results of a multicenter randomized placebo-controlled trial (RHODOS [Rescue of Hereditary Optic Disease Outpatient Study]) of idebenone in LHON have recently been released. Idebenone was well tolerated at a dose of 900 mg per day and no adverse drug-related events were reported. The visual outcome data indicate that patients with discordant visual acuities (LogMAR>0.2), and thus at highest risk of further deterioration in the least affected eye, were more likely to benefit from treatment with idebenone [44••]. The findings from the RHODOS trial are promising and for the first time, they offer the hope of preserving vision for affected LHON carriers who are still at an early stage of the disease process.

Looking into the Future: Gene Therapy

Gene therapy for primary mitochondrial cytopathies poses several discrete challenges; the mitochondrial inner membrane is a relatively impermeable membrane that needs to be

bypassed, and a highly efficient vector is needed to transfect a sufficient number of mitochondria per cell to achieve the desired effect. A possible solution is to bypass the mitochondrial genome using an allotopic approach. Instead, the gene of interest is transfected into the nuclear genome and the protein product is engineered with a specific targeting sequence that facilitates its uptake into the mitochondrial compartment, thereby compensating for the mtDNA mutation. Proof of principle has been demonstrated in experimental LHON models where adeno-associated virus vectors have been used to successfully transfect cells with a replacement wild-type mtDNA allele or neuroprotective genes such as *SOD2* [46–48]. These results are encouraging and allotopic rescue could be easily applied to the RGC layer which is easily accessible. However, key issues of safety and efficacy need to be further addressed before their application to human clinical trials can be advocated [2].

Preventing Disease Transmission

Several strategies are currently being explored to prevent the transmission of pathogenic mitochondrial and nuclear mutations among women of child-bearing age. The difficult technical and ethical issues raised by preimplantation genetic testing and new in vitro fertilization techniques such as pronuclear transfer are outside the scope of this review, and these have been detailed elsewhere [2, 49].

Conclusions

A number of recurring disease mechanisms have been identified that contribute to RGC loss in mitochondrial optic neuropathies. These provide a unique opportunity for targeted therapeutic interventions aimed not only at improving visual function, but also the neurological deficits seen in the more severe mitochondrial cytopathies. However, despite these major advances, the risk factors underpinning the selective vulnerability of RGCs have yet to be clarified. Research in this area has been severely limited by the lack of diseased human optic nerves but hopefully, with the development of faithful animal models and more advanced biotechnological tools, we will soon be in a position to disentangle these fundamental research questions both at the structural and molecular levels.

Acknowledgments P. Yu-Wai-Man is a Medical Research Council (MRC, UK) Clinician Scientist in Neuro-Ophthalmology and P.F. Chinnery is a Wellcome Trust Senior Fellow in Clinical Science. P.F. Chinnery also receives funding from Parkinson's UK, the MRC Translational Muscle Centre, and the UK NIHR Biomedical Research Centre in Ageing and Age-related Disease.

Disclosure No potential conflicts of interest relevant to this article were reported.

References

Papers of particular interest, published recently, have been highlighted as:
- • Of importance
- •• Of major importance

1. McFarland R, Taylor RW, Turnbull DM. The neurology of mitochondrial DNA disease. Lancet Neurol. 2002;1(6):343–51.
2. Yu-Wai-Man P, Griffiths PG, Chinnery PF. Mitochondrial optic neuropathies—Disease mechanisms and therapeutic strategies. Progress in Retinal and Eye Research. 2011;30(2):81–114.
3. Fraser JA, Biousse V, Newman NJ. The Neuro-ophthalmology of Mitochondrial Disease. Surv Ophthalmol. 2010;55(4):299–334.
4. Man PY, Griffiths PG, Brown DT, et al. The epidemiology of Leber hereditary optic neuropathy in the North East of England. Am J Hum Genet. 2003;72(2):333–9.
5. Yu-Wai-Man P, Griffiths PG, Hudson G, Chinnery PF. Inherited mitochondrial optic neuropathies. Journal of Medical Genetics. 2009;46(3):145–58.
6. •• La Morgia C, Ross-Cisneros FN, Sadun AA, et al.: Melanopsin retinal ganglion cells are resistant to neurodegeneration in mitochondrial optic neuropathies. Brain. 2010;133:2426–38. *This paper describes the preservation of a special class of melanopsin-containing RGCs in LHON and DOA, providing for the first time a neuroanatomical basis for the relatively spared pupillary light reflexes in these two disorders.*
7. Chinnery PF, Andrews RM, Turnbull DM, Howell NN. Leber hereditary optic neuropathy: Does heteroplasmy influence the inheritance and expression of the G11778A mitochondrial DNA mutation? American Journal of Medical Genetics. 2001;98(3):235–43.
8. Hudson G, Carelli V, Spruijt L, et al. Clinical expression of Leber hereditary optic neuropathy is affected by the mitochondrial DNA-haplogroup background. Am J Hum Genet. 2007;81(2):228–33.
9. Ji YL, Zhang AM, Jia XY, et al. Mitochondrial DNA Haplogroups M7b1 ′ 2 and M8a Affect Clinical Expression of Leber Hereditary Optic Neuropathy in Chinese Families with the m.11778 G -> A Mutation. Am J Hum Genet. 2008;83(6):760–8.
10. Bu XD, Rotter JI: X chromosome-linked and mitochondrial gene control of Leber hereditary optic neuropathy: evidence from segregation analysis for dependence on X chromosome inactivation. Proceedings of the National Academy of Sciences of the United States of America. 1991;88(18):8198–202.
11. Hudson G, Keers S, Man PYW, et al. Identification of an X-chromosomal locus and haplotype modulating the phenotype of a mitochondrial DNA disorder. Am J Hum Genet. 2005;77(6):1086–91.
12. Shankar SP, Fingert JH, Carelli V, et al. Evidence for a novel x-linked modifier locus for leber hereditary optic neuropathy. Ophthalmic Genetics. 2008;29(1):17–24.

13. Ji YL, Jia XY, Li SQ, et al. Evaluation of the X-linked modifier loci for Leber hereditary optic neuropathy with the G11778A mutation in Chinese. Mol Vis. 2010;16(47):416–24.
14. • Giordano C, Montopoli M, Perli E, et al.: Oestrogens ameliorate mitochondrial dysfunction in Leber's hereditary optic neuropathy. Brain. 2011;134:220–34. *This paper describes an elegant series of experiments showing that estrogens help protect LHON cybrids against the deleterious consequences of the three primary mtDNA mutations. These results support a hormonal component to the reduced disease penetrance observed among female LHON carriers.*
15. Carelli V, Ross-Cisneros FN, Sadun AA. Mitochondrial dysfunction as a cause of optic neuropathies. Progress in Retinal and Eye Research. 2004;23(1):53–89.
16. • Kirkman MA, Yu-Wai-Man P, Korsten A, et al.: Gene-environment interactions in Leber hereditary optic neuropathy. Brain. 2009;132:2317–26. *This is the largest epidemiological study to investigate the role of environmental factors in influencing LHON penetrance. A strong association was identified between the risk of visual loss and smoking. This effect showed a dose–response relationship with heavy smokers being more likely to be affected than light smokers. A trend toward increased visual failure was also noted among LHON carriers with heavy alcohol consumption.*
17. Schapira AHV. Mitochondrial disease. Lancet. 2006;368 (9529):70–82.
18. Gronlund MA, Honarvar AKS, Andersson S, et al. Ophthalmological findings in children and young adults with genetically verified mitochondrial disease. Br J Ophthalmol. 2010;94(1):121–7.
19. Anikster Y, Kleta R, Shaag A, et al. Type III 3-methylglutaconic aciduria (optic atrophy plus syndrome, or Costeff optic atrophy syndrome): Identification of the OPA3 gene and its founder mutation in Iraqi Jews. Am J Hum Genet. 2001;69(6):1218–24.
20. Reynier P, Amati-Bonneau P, Verny C, et al. OPA3 gene mutations responsible for autosomal dominant optic atrophy and cataract. Journal of Medical Genetics. 2004;41(9):e110.
21. Ryu SW, Jeong HJ, Choi M, et al. Optic atrophy 3 as a protein of the mitochondrial outer membrane induces mitochondrial fragmentation. Cellular and Molecular Life Sciences. 2010;67 (16):2839–50.
22. • Yu-Wai-Man P, Griffiths PG, Gorman GS, et al.: Multi-system neurological disease is common in patients with *OPA1* mutations. Brain. 2010;133:771–86. *This large multicenter study expands the phenotypic spectrum associated with OPA1 mutations. Up to 20% of mutational carriers developed a more severe disease variant (DOA+) characterized by prominent neuromuscular features such as deafness, myopathy, peripheral neuropathy, ataxia, and chronic progressive external ophthalmoplegia. Interestingly, there was a threefold increased risk of developing DOA+ with missense OPA1 mutations involving the GTPase domain compared with other mutational subgroups.*
23. Zuchner S, De Jonghe P, Jordanova A, et al. Axonal neuropathy with optic atrophy is caused by mutations in mitofusin 2. Ann Neurol. 2006;59(2):276–81.
24. Lenaers G, Reynier P, Elachouri G, et al. OPA1 functions in mitochondria and dysfunctions in optic nerve. Int J Biochem Cell Biol. 2009;41(10):1866–74.
25. Stemmler TL, Lesuisse E, Pain D, Dancis A. Frataxin and Mitochondrial FeS Cluster Biogenesis. J Biol Chem. 2010;285 (35):26737–43.
26. Hanein S, Perrault I, Roche O, et al. TMEM126A, Encoding a Mitochondrial Protein, Is Mutated in Autosomal-Recessive Nonsyndromic Optic Atrophy. Am J Hum Genet. 2009;84 (4):493–8.
27. Zanna C, Ghelli A, Porcelli AM, et al. OPA1 mutations associated with dominant optic atrophy impair oxidative phosphorylation and mitochondrial fusion. Brain. 2008;131:352–67.
28. Tang S, Le PK, Tse S, et al. Heterozygous Mutation of Opa1 in Drosophila Shortens Lifespan Mediated through Increased Reactive Oxygen Species Production. PLoS One. 2009;4(2): e4492.
29. •• de Brito OM, Scorrano L: Mitofusin 2 tethers endoplasmic reticulum to mitochondria. Nature. 2008;456(7222):605–10. *This seminal work describes how MFN2 tethers the ER to the mitochondrial network, thereby regulating calcium flux between these two compartments.*
30. de Brito OM, Scorrano L. Mitofusin-2 regulates mitochondrial and endoplasmic reticulum morphology and tethering: The role of Ras. Mitochondrion. 2009;9(3):222–6.
31. Trevelyan AJ, Kirby DM, Smulders-Srinivasan TK, et al. Mitochondrial DNA mutations affect calcium handling in differentiated neurons. Brain. 2010;133:787–96.
32. Dayanithi G, Chen-Kuo-Chang M, Viero C, et al. Characterization of Ca2+ signalling in postnatal mouse retinal ganglion cells: involvement of OPA1 in Ca2+ clearance. Ophthalmic Genet. 2010;31(2):53–65.
33. Westermann B. Mitochondrial fusion and fission in cell life and death. Nat Rev Mol Cell Biol. 2010;11(12):872–84.
34. Chevrollier A, Guillet V, Loiseau D, et al. Hereditary optic neuropathies share a common mitochondrial coupling defect. Ann Neurol. 2008;63(6):794–8.
35. •• Amati-Bonneau P, Valentino ML, Reynier P, et al.: OPA1 mutations induce mitochondrial DNA instability and optic atrophy plus phenotypes. Brain. 2008;131:338–51. *This study established OPA1 as a novel mtDNA maintenance disorder. Skeletal muscle biopsies from these patients revealed high levels of cytochrome c oxidase negative fibers, secondary to the accumulation of clonally expanded mtDNA deletions.*
36. •• Hudson G, Amati-Bonneau P, Blakely EL, et al.: Mutation of OPA1 causes dominant optic atrophy with external ophthalmoplegia, ataxia, deafness and multiple mitochondrial DNA deletions: a novel disorder of mtDNA maintenance. Brain. 2008;131:329–37. *This study established OPA1 as a novel mtDNA maintenance disorder. Skeletal muscle biopsies from these patients revealed high levels of cytochrome c oxidase negative fibers, secondary to the accumulation of clonally expanded mtDNA deletions*
37. •• Yu-Wai-Man P, Sitarz KS, Samuels DC, et al.: *OPA1* mutations cause cytochrome *c* oxidase deficiency due to loss of wild-type mtDNA molecules. Human Molecular Genetics. 2010;19 (15):3043–52. *This study established OPA1 as a novel mtDNA maintenance disorder. Skeletal muscle biopsies from these patients revealed high levels of cytochrome c oxidase negative fibers, secondary to the accumulation of clonally expanded mtDNA deletions.*
38. Chen HC, McCaffery JM, Chan DC. Mitochondrial fusion protects against neurodegeneration in the cerebellum. Cell. 2007;130 (3):548–62.
39. •• Chen HC, Vermulst M, Wang YE, et al.: Mitochondrial Fusion Is Required for mtDNA Stability in Skeletal Muscle and Tolerance of mtDNA Mutations. Cell. 2010;141(2):280–9. *This important study explores the fundamental roles played by mitofusins and OPA1 in both mtDNA maintenance and mitochondrial network stability. Loss of mitochondrial fusion was found to exacerbate mitochondrial dysfunction, with the induction of a compensatory mitochondrial proliferative response, and an increased rate of mtDNA mutagenesis.*
40. •• Elachouri G, Vidoni S, Zanna C, et al.: OPA1 links human mitochondrial genome maintenance to mtDNA replication and distribution. Genome Research. 2011;21(1):12–20. *This study provides strong evidence that the peptide segment encoded by exon 4b*

likely plays a crucial role in physically anchoring nucleoids to the mitochondrial inner membrane.

41. Yu-Wai-Man P, Bailie M, Atawan A, et al.: Pattern of retinal ganglion cell loss in dominant optic atrophy due to *OPA1* mutations. Eye. 2011; *Epub ahead of print*.
42. Andrews RM, Griffiths PG, Johnson MA, Turnbull DM. Histochemical localisation of mitochondrial enzyme activity in human optic nerve and retina. Br J Ophthalmol. 1999;83(2):231–5.
43. Bristow EA, Griffiths PG, Andrews RM, et al. The distribution of mitochondrial activity in relation to optic nerve structure. Arch Ophthalmol. 2002;120(6):791–6.
44. •• Klopstock K, Yu-Wai-Man P, Dimitriadis K, et al.: A randomized placebo-controlled trial of idebenone in Leber's hereditary optic neuropathy. Brain. 2011; 134(9): 2677–86. *This is the first adequately powered treatment trial for LHON, highlighting the benefit of a multinational approach and the need to develop global registries to support patient recruitment for relatively rare genetic diseases. High-dose idebenone is safe and it holds therapeutic potential for affected LHON carriers at highest risk of further visual loss.*
45. Haefeli RH, Erb M, Gemperli AC, Robay D, et al. NQO1-dependent redox cycling of idebenone: effects on cellular redox potential and energy levels. PLoS One. 2011;6(3): e17963.
46. Qi XP, Lewin AS, Sun L, et al. SOD2 gene transfer protects against optic neuropathy induced by deficiency of complex I. Ann Neurol. 2004;56(2):182–91.
47. Qi XP, Sun L, Hauswirth WW, et al. Use of mitochondrial antioxidant defenses for rescue of cells with a Leber hereditary optic neuropathy-causing mutation. Arch Ophthalmol. 2007;125(2):268–72.
48. Ellouze S, Augustin S, Bouaita A, et al. Optimized allotopic expression of the human mitochondrial ND4 prevents blindness in a rat model of mitochondrial dysfunction. Am J Hum Genet. 2008;83(3):373–87.
49. Brown DT, Herbert M, Lamb VK, et al. Transmission of mitochondrial DNA disorders: possibilities for the future. Lancet. 2006;368(9529):87–9.
50. Schaefer AM, McFarland R, Blakely EL, et al. Prevalence of mitochondrial DNA disease in adults. Ann Neurol. 2008;63 (1):35–9.

Human Molecular Genetics, 2010, Vol. 19, No. 15 **3043–3052**
doi:10.1093/hmg/ddq209
Advance Access published on May 18, 2010

OPA1 mutations cause cytochrome *c* oxidase deficiency due to loss of wild-type mtDNA molecules

Patrick Yu-Wai-Man[1,2], Kamil S. Sitarz[1], David C. Samuels[3], Philip G. Griffiths[1,2], Amy K. Reeve[1], Laurence A. Bindoff[4,5], Rita Horvath[1] and Patrick F. Chinnery[1,6,*]

[1]Mitochondrial Research Group, Institute for Ageing and Health, The Medical School, Newcastle University, Newcastle upon Tyne NE2 4HH, UK, [2]Department of Ophthalmology, Royal Victoria Infirmary, Newcastle upon Tyne, UK, [3]Department of Molecular Physiology and Biophysics, Center for Human Genetics Research, Vanderbilt University Medical Center, Nashville, TN, USA, [4]Department of Clinical Medicine, University of Bergen, Bergen, Norway, [5]Department of Neurology, Haukeland University Hospital, Bergen, Norway and [6]Institute of Human Genetics, Newcastle University, Newcastle upon Tyne, UK

Received March 16, 2010; Revised April 23, 2010; Accepted May 13, 2010

Pathogenic *OPA1* mutations cause autosomal dominant optic atrophy (DOA), a condition characterized by the preferential loss of retinal ganglion cells and progressive optic nerve degeneration. Approximately 20% of affected patients will also develop more severe neuromuscular complications, an important disease subgroup known as DOA$^+$. Cytochrome *c* oxidase (COX)-negative fibres and multiple mitochondrial DNA (mtDNA) deletions have been identified in skeletal muscle biopsies from patients manifesting both the pure and syndromal variants, raising the possibility that the accumulation of somatic mtDNA defects contribute to the disease process. In this study, we investigated the mtDNA changes induced by *OPA1* mutations in skeletal muscle biopsies from 15 patients with both pure DOA and DOA$^+$ phenotypes. We observed a 2- to 4-fold increase in mtDNA copy number at the single-fibre level, and patients with DOA$^+$ features had significantly greater mtDNA proliferation in their COX-negative skeletal muscle fibres compared with patients with isolated optic neuropathy. Low levels of wild-type mtDNA molecules were present in COX-deficient muscle fibres from both pure DOA and DOA$^+$ patients, implicating haplo-insufficiency as the mechanism responsible for the biochemical defect. Our findings are consistent with the 'maintenance of wild-type' hypothesis, the secondary mtDNA deletions induced by *OPA1* mutations triggering a compensatory mitochondrial proliferative response in order to maintain an optimal level of wild-type mtDNA genomes. However, when deletion levels reach a critical level, further mitochondrial proliferation leads to replication of the mutant species at the expense of wild-type mtDNA, resulting in the loss of respiratory chain COX activity.

INTRODUCTION

Pathogenic mutations in the *OPA1* gene (OMIM 605290) account for ~60% of all cases of autosomal dominant optic atrophy (DOA), and the carrier rate in the general population is estimated to be at least 1 in 50 000 (1). The majority of patients are mono-symptomatic, with the onset of progressive central visual loss in early childhood invariably resulting in significant visual morbidity (2–4). Although optic nerve dysfunction is the pathognomonic feature of DOA, we have recently established that up to 20% of *OPA1* carriers will experience a more complicated disease course (5). These syndromal DOA$^+$ variants show a remarkable degree of phenotypic variability, but sensorineural deafness is a frequent neurological deficit,

*To whom correspondence should be addressed. Tel: +44 1912824375; Fax: +44 1912824373; Email: P.F.Chinnery@ncl.ac.uk

which develops from late childhood to early adulthood, followed by a combination of ataxia, myopathy, peripheral neuropathy and progressive external ophthalmoplegia (PEO) from the third decade of life onwards (5–9). These clinical observations are of major pathophysiological importance, as they highlight the deleterious consequences of *OPA1* mutations not only for retinal ganglion cells, whose axons constitute the optic nerve, but also for other central neuronal populations, peripheral nerves and skeletal muscle.

The marked inter- and intra-familial variability in disease severity seen in DOA is likely to be a reflection of the multiple, distinct roles played by the Opa1 protein in normal cellular function (10,11). Following proteolytic cleavage by various proteases (12), Opa1 assembles as polymeric structures within the inner mitochondrial membrane. As a result of its pro-fusion dynamin-like GTPase properties, Opa1 actively maintains a highly interconnected mitochondrial network and sequesters pro-apoptotic cytochrome *c* molecules within the mitochondrial cristae spaces (13,14). Opa1 is also thought to regulate oxidative phosphorylation by stabilizing the mitochondrial respiratory chain complexes and by facilitating the effective coupling of electron transport with ATP synthesis (15,16). In addition to these essential biological functions, there is now growing evidence supporting a novel role for Opa1 in mitochondrial DNA (mtDNA) maintenance. Central to this argument is the characteristic histochemical finding of cytochrome *c* oxidase (COX)-negative fibres in skeletal muscle biopsies from *OPA1*-positive patients, together with the presence of multiple mtDNA deletions on long-range PCR analysis of homogenate skeletal muscle DNA (5–8). Different mechanisms have been postulated to account for the formation of these deleted mtDNA species, including an imbalance of the intra-mitochondrial nucleotide pool, and the impaired interaction of the N-terminal domain of Opa1 with mtDNA nucleoids, which are anchored in close physical proximity to the inner mitochondrial membrane (6,7,17). Interestingly, the level of COX-deficient muscle fibres was found to be over four times higher in the DOA^{+} group compared with the pure optic atrophy group (5). Importantly, COX-deficient fibres were also significantly more frequent among patients with pure DOA compared with age-matched healthy controls (5). These observations strongly implicate a contributory role for these secondary mtDNA defects in triggering multi-system cellular dysfunction among affected *OPA1* carriers. However, the mechanisms involved have not been defined and the nature of the mtDNA deletions induced by *OPA1* mutations still remains to be clarified. To explore these fundamental research questions and how they relate to disease severity, we performed a quantitative and qualitative study of the mtDNA changes present in single skeletal muscle fibres from patients harbouring *OPA1* mutations.

RESULTS

MtDNA copy number density varies in normal control skeletal muscle fibres

The normal control muscles studied were collected from a 1-year-old female (C-1F), a 22-year-old female (C-22F), a 31-year-old female (C-31F), a 35-year-old male (C-35M) and a 52-year-old female (C-52F). The mtDNA copy number density was measured as the total number of mtDNA molecules in a muscle fibre section, divided by the fibre's cross-sectional area. There was a statistically significant variation in mtDNA copy number density among Type I skeletal muscle fibres from the five controls, except for C-1F versus C-22F (C-1F: mean = 3.20, SD = 1.67, $n = 18$; C-22F: mean = 2.50, SD = 0.87, $n = 24$; C-31F: mean = 5.62, SD = 1.97, $n = 19$; C-35M: mean = 10.63, SD = 3.22, $n = 17$; C-52F: mean = 4.36, SD = 0.92, $n = 21$) (Fig. 1A, Supplementary Material, Table S1A). Similarly, mtDNA copy number density varied significantly among Type II skeletal muscle fibres, except for C-1F versus C-31F, and C-1F versus C-52F (C-1F: mean = 2.62, SD = 0.98, $n = 13$; C-22F: mean = 1.57, SD = 0.60, $n = 24$; C-31F: mean = 2.96, SD = 0.85, $n = 17$; C-35M: mean = 4.13, SD = 1.54, $n = 14$; C-52F: mean = 2.45, SD = 0.50, $n = 22$) (Fig. 1B, Supplementary Material, Table S1B).

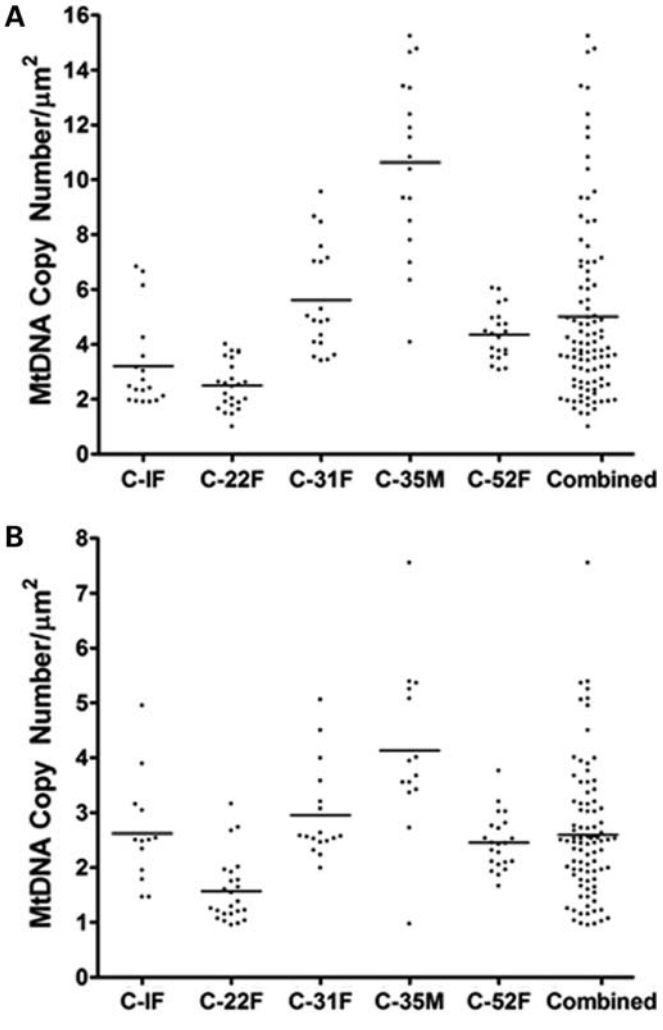

Figure 1. Total mtDNA content of single skeletal muscle fibres from normal controls: (**A**) Type I fibres, (**B**) Type II fibres.

Table 1. Clinical phenotype and *OPA1* mutational spectrum of our study cohort

Patient	Age (years)	Sex	Onset[a] (years)	*OPA1* mutation cDNA	AA change	Clinical phenotype Optic atrophy	Deafness	Ataxia	Myopathy	Neuropathy	PEO	Others
A	31	M	11	c.876-878del	p.V294fsX667	+						
B	59	M	5	c.876-878del	p.V294fsX667	+				+		HSP
C	44	M	2	c.1198C>T	p.P400S	+	+				+	
D	54	M	5	c.1212+3a>t	Splice defect	+	+					
E	43	M	5	c.1334G>A	p.R445H	+	+		+		+	
F	43	F	5	c.1334G>A	p.R445H	+	+			+	+	
G	54	M	–	c.1516+1g>t	Splice defect	+						
H	39	M	15	c.1516+1g>t	Splice defect	+						
I	58	F	–	c.2613+1g>a	Splice defect	+		+				MS-like illness
J	50	M	8	c.2613+1g>a	Splice defect	+						
K	43	M	5	c.2708_2711del	p.V903fsX3	+						
L	60	F	16	c.2713C>T	p.R905X	+						
M	40	F	15	c.2713C>T	p.R905X	+						
N[b]	60	M	–	c.768C>G c.854A>G	p.S256R p.Q285R	+		+	+	+		Spasticity
O[b]	64	F	–	c.768C>G c.854A>G	p.S256R p.Q285R	+		+	+	+		Spasticity

AA, amino acid; F, female; HSP, hereditary spastic paraparesis; M, male; MS, multiple sclerosis; PEO, progressive external ophthalmoplegia.
[a]Age of onset of visual failure.
[b]Norwegian siblings compound heterozygous for two novel *OPA1* mutations (5).

Table 2. Histochemical and mtDNA defects identified in skeletal muscle biopsies from our *OPA1*-positive patients

Patient	Skeletal muscle biopsy analysis Fibres (n)[b]	COX −ve (%)	RRF (%)	Long PCR[c]	Real-time PCR analysis Type I (*n*)[d]	Type II (*n*)[d]	COX −ve (*n*)	COX −ve single-fibre analysis[a] Deletion <70% (*n*)	(%)	Deletion ≥70% (*n*)	(%)
A	2826	0.1	0.0	+	15	14	2	1	50.0	1	50.0
B	482	2.1	0.6	++	14	14	8	3	37.5	5	62.5
C	1980	1.6	0.6	++	14	22	12	3	25.0	9	75.0
D	786	0.3	0.0	+	24	23	2	1	50.0	1	50.0
E	1272	3.1	0.7	++	19	12	20	3	15.0	17	85.0
F	1186	13.9	1.3	++	13	21	13	2	15.4	11	84.6
G	674	1.8	0.9	++	19	17	16	7	43.8	9	56.3
H	762	0.0	0.0	+	19	23	0	N/A	N/A	N/A	N/A
I	1304	1.4	0.3	++	21	21	15	1	6.7	14	93.3
J	848	0.0	0.0	–	14	19	0	N/A	N/A	N/A	N/A
K	832	0.6	0.1	+	14	13	6	2	33.3	4	66.7
L	1100	3.0	0.8	++	10	10	14	3	21.4	11	78.6
M	1126	0.5	0.1	+	14	15	6	0	0.0	6	100.0
N	1058	17.7	3.3	++	22	17	16	4	25.0	12	75.0
O	968	21.2	5.8	++	15	28	15	2	13.3	13	86.7

COX, cytochrome *c* oxidase; MtDNA, mitochondrial DNA; N/A, not applicable; PCR, polymerase chain reaction; RRF, ragged-red fibres.
[a]Level of mtDNA deletion detected in single COX-negative muscle fibres using our quantitative real-time PCR assay.
[b]Total number of muscle fibres present in the stained cryostat sections.
[c]Long PCR analysis of homogenate skeletal muscle DNA: (i) no deletion bands (−), (ii) smaller deletion bands in addition to the wild-type PCR fragment (+), and (iii) multiple deletion bands with no wild-type PCR fragment (++).
[d]Number of Type I and II COX-positive muscle fibres laser microdissected from 20 μm thick membrane sections.

OPA1 mutations lead to the accumulation of high levels of somatic mtDNA deletions in skeletal muscle fibres

The mean frequency of COX-negative fibres present in cryostat muscle sections from 15 *OPA1*-positive patients was 4.49% (SD = 7.00%, range = 0–21.20%, n = 15), with two patients, H and J, not harbouring any COX-negative fibres (Table 1). The presence and level of mtDNA deletion were determined for a total of 333 single skeletal muscle fibres from 15 patients: (i) Type I COX positive, $n = 94$; (ii) Type II COX positive, $n = 94$; and (iii) COX-negative, $n = 145$ (Table 2). The majority of COX-positive fibres harboured low deletion levels <30% (179/188, 95.2%), and there was no significant difference in mean deletion levels between Type I and II fibres (Type I: mean = 11.60%, SD = 7.99%; Type II: mean = 14.58%, SD = 11.51%, $P = 0.0723$). Among COX-negative fibres, 113 of 145 (77.9%) had deletion levels ≥70%, and the mean deletion level was significantly

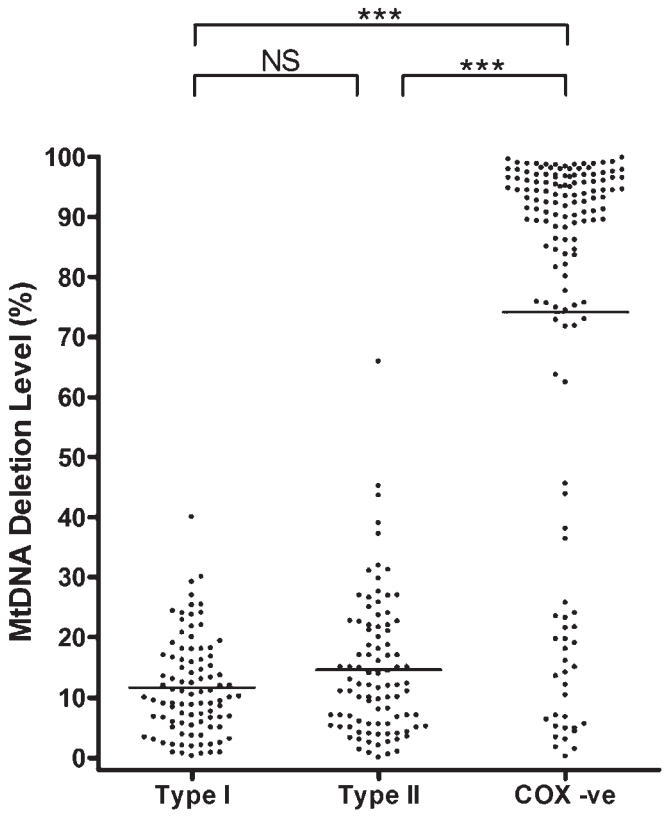

Figure 2. Level of mtDNA deletion in COX-positive and COX-negative single muscle fibres from *OPA1*-positive patients. NS at *P*-value = 0.0723; ***P-value <0.0001. Type I and Type II refer to COX positive fibres.

higher compared with both Type I and II COX-positive fibres (mean = 74.16%, SD = 33.04%, $P < 0.0001$) (Fig. 2).

COX-negative but not COX-positive muscle fibres are associated with significant mtDNA proliferation

There was no significant difference in mtDNA copy number density between COX-positive fibres from *OPA1*-positive patients and the combined control data set for both Type I fibres (*OPA1*: mean = 4.37, SD = 2.23; controls: mean = 4.91, SD = 3.17, $P = 0.0743$), and Type II fibres (*OPA1*: mean = 2.39, SD = 1.03; controls: mean = 2.60, SD = 1.20, $P = 0.1095$) (Fig. 3). However, there was evidence of significant mtDNA proliferation in COX-negative fibres when compared with adjacent COX-positive fibres from the same patient (Table 3, Supplementary Material, Fig. S1A–O), and COX-positive fibres from the combined control data set (Fig. 4). There was no significant difference in mean mtDNA copy number density between COX-negative fibres with mtDNA deletion levels ≥70% (mean = 11.55, SD = 8.83, $n = 113$) and <70% (mean = 9.10, SD = 5.32, $n = 32$, $P = 0.1385$). Of the 145 COX-negative fibres analysed, 44 were from patients with pure DOA (mean mtDNA proliferation ratio = 2.02, SD = 1.31, 95% confidence interval (CI) = 1.63–2.42) and 141 were from patients with DOA$^+$ phenotypes (mean mtDNA proliferation ratio = 2.66, SD = 1.52, 95% CI = 2.36–2.96), the difference being statistically significant ($P = 0.0172$) (Fig. 5).

MtDNA proliferation in COX-negative muscle fibres fails to maintain normal levels of wild-type mtDNA molecules

The mean wild-type mtDNA ratio was significantly lower for the COX-negative group (mean = 0.20, SD = 0.19, 95% CI = 0.17–0.24, $n = 112$) compared with the COX-positive group (mean = 1.00, SD = 0.32, 95% CI = 0.95–1.05, $n = 188$, $P < 0.0001$) (Fig. 6A). The relationship between the wild-type mtDNA ratio and the deletion level for COX-negative muscle fibres was in agreement with our previously established *in silico* model of mtDNA replication ($R^2 = 0.68$), and gave a predicted maximum mitochondrial proliferation factor (α) of 3.40 (95% CI = 2.60–4.80) (Fig. 6B).

COX-negative muscle fibres from *OPA1* patients harbour clonally expanded deleted mtDNA species

Deleted mtDNA species were detected in 31 COX-negative muscle fibres using our two-step long-range PCR protocol, and in none of them was the full-length 10 843 base pairs PCR product obtained. MtDNA deletions levels <30% were measured in 6 of 31 (19.4%) of these COX-negative fibres with our differential *MTND1–MTND4* real-time PCR assay. The deletion sizes ranged from 1.0 to 8.0 kb (mean = 5.2 kb, SD = 2.0 kb, $n = 33$), and two different deletions were amplified from the lysate of 2 of 31 (6.5%) COX-negative fibres. All these deletions were located within the major arc of the mitochondrial genome and they were predicted to result in the loss of critical segments containing both transfer RNA and protein-encoding genes.

DISCUSSION

Our study has revealed marked mtDNA proliferation in skeletal muscle from patients harbouring a range of pathogenic *OPA1* mutations. This observation is entirely compatible with the reported detrimental effect of *OPA1* mutations on mitochondrial oxidative phosphorylation (15,16,18), with the increased mtDNA copy number acting as a compensatory mechanism to maintain an adequate level of ATP for normal cellular function. COX-negative fibres were present in muscle biopsies from 13 *OPA1*-positive patients, and there was a consistent finding of mtDNA proliferation in these fibres, irrespective of disease severity. However, patients with DOA$^+$ phenotypes had significantly higher proliferation ratios in COX-negative muscle fibres when compared with those with isolated optic nerve involvement, indicating a possible important disease mechanism. Although we did not make any direct measurements of apoptotic markers in this study, mtDNA proliferation is linked with an increased susceptibility to undergo apoptosis in mitochondrial myopathies (19,20), and it is biologically plausible to postulate that such an effect would not be limited to muscle fibres, but would also extend to other post-mitotic tissues commonly affected in mitochondrial disorders. The relevance to *OPA1* disease becomes even more apparent in view of the fact that the level of COX deficiency in skeletal muscle is over four times higher in patients with DOA$^+$ compared with pure DOA (5). Even though the frequency of COX-negative fibres is lower among DOA patients with clinical features limited to the

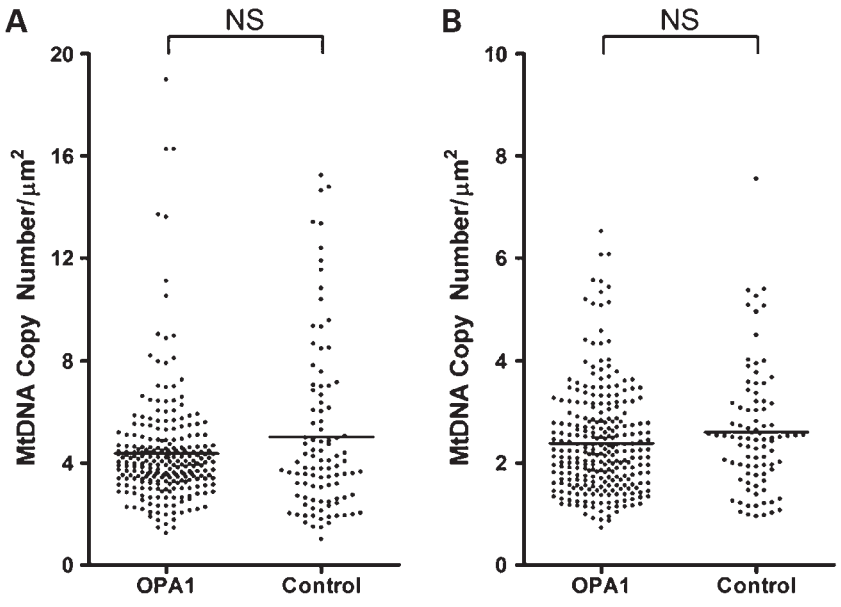

Figure 3. Comparison of total mtDNA copy number in single muscle fibres from *OPA1*-positive patients with normal controls. (**A**) Type I COX-positive fibres (NS at *P*-value = 0.0743), (**B**) Type II COX-positive fibres (NS at *P*-value = 0.1095). The control values represent the combined data set for C-1F, C-22F, C-31F, C-35M, and C-52F.

Table 3. Relative level of mtDNA proliferation seen in COX-negative muscle fibres

Patient	COX −ve fibres (n)[a]	MtDNA proliferation ratio[b]		
		Mean	95% confidence interval	
A	2	2.68	0.00	16.28
B	8	2.32	1.45	3.18
C	12	1.92	1.28	2.56
D	2	2.49	0.00	16.14
E	20	3.72	2.94	4.49
F	13	2.21	1.36	3.06
G	16	1.90	1.31	2.50
H	0	N/A	N/A	N/A
I	15	2.76	2.07	3.44
J	0	N/A	N/A	N/A
K	6	3.11	1.23	4.98
L	14	1.75	1.07	2.44
M	6	1.68	0.34	3.02
N	16	3.24	2.25	4.22
O	15	1.73	1.26	2.21

[a]Total number of COX-negative muscle fibres studied for each patient.
[b]The proliferation ratio for each COX-negative fibre was determined in relation to the mean mtDNA copy number (/μm^2) for COX-positive fibres from the same patient, with a value >1 indicating relative mtDNA proliferation (Supplementary Material, Fig. S1A–O).

optic nerve, this group still has significantly higher levels of COX-deficiency compared with age-matched healthy controls (5). The secondary mtDNA abnormalities, which precipitate this biochemical COX defect are therefore clearly linked to the underlying *OPA1* disease process. Although additional confirmatory studies are required, it is tempting to speculate that some *OPA1* mutations lead to multi-systemic manifestations and more severe visual failure as a result of their more pronounced effects on mtDNA deletion formation, and thus proliferation, with the consequent increase in apoptotic cell loss. The degree of mitochondrial network instability induced by different *OPA1* mutations also deserves further investigation, as the extent of fragmentation could have a crucial influence on the rate at which these somatic deletions become fixed at supra-threshold levels (21–23).

Our *in silico* model of mtDNA replication suggests that mitochondrial proliferation serves a useful biological purpose by maintaining wild-type mtDNA copy number at an optimal level (21,22). However, this compensatory mechanism only operates effectively up to a certain mutational load, beyond which it fails to prevent the loss of wild-type mtDNA genomes, and eventually becomes detrimental to cellular survival. The relationship observed in COX-negative *OPA1* muscle fibres between the level of wild-type and deleted mtDNA species is in agreement with our *in silico* prediction, and provides additional experimental evidence that the maintenance of wild-type mtDNA genomes is crucial for normal mitochondrial oxidative function. We previously showed that this was also the case in skeletal muscle fibres from a patient with PEO and mild proximal myopathy due to a 4.9 kb single deletion (23).

MtDNA copy number was determined at the single-fibre level for five normal control skeletal muscle samples, and a wide variation was observed for both Type I and II fibres. A likely confounding variable is the level of physical activity, which was not documented for the individuals from whom the biopsies were taken. Skeletal muscle is a highly adaptable tissue and it is capable of pronounced metabolic and morphological changes in response to endurance training or disuse (24,25). It is well established that physical exercise enhances mitochondrial oxidative capacity *in vivo* (26–28), and this beneficial adaptation has been linked to an increase in mtDNA density (29,30). The regulatory pathways involved are complex but an important element is the up-regulation in the level of *TFAM* expression (31,32), which encodes for a

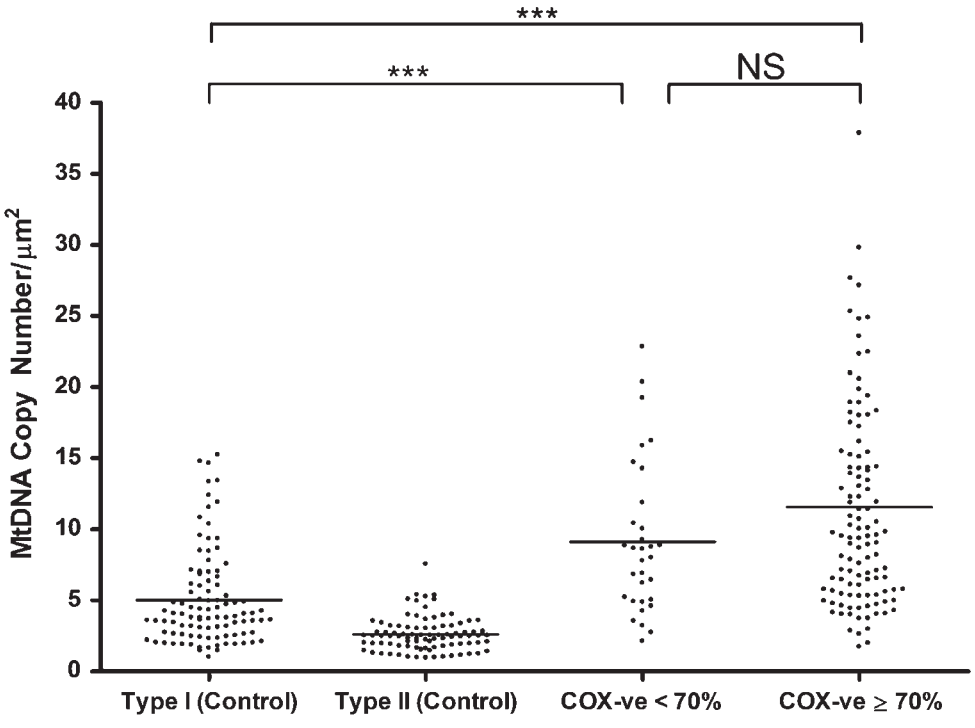

Figure 4. Comparison of total mtDNA copy number in COX-negative muscle fibres from *OPA1*-positive patients with COX-positive muscle fibres from the combined control data set. MtDNA deletion levels in COX-negative muscle fibres: low (<70%) and high (≥70%); NS at *P*-value = 0.1385; ***P-value <0.0001.

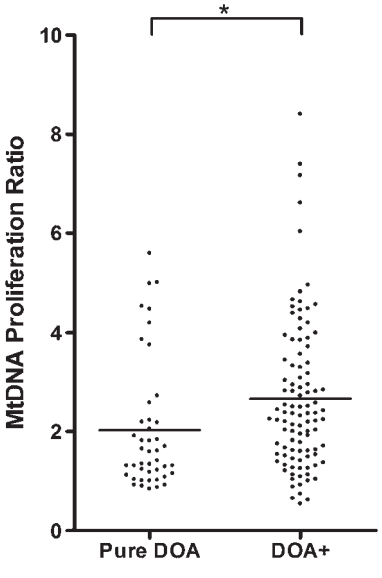

Figure 5. MtDNA proliferation ratio for COX-negative fibres from patients with pure DOA and DOA$^+$ phenotypes. The proliferation ratio for each COX-negative fibre was determined in relation to the mean mtDNA copy number ($/\mu m^2$) for COX-positive fibres from the same patient, with a value >1 indicating relative mtDNA proliferation. *P-value = 0.0172.

key activator of mtDNA transcription and replication (33,34). Our finding therefore highlights the need for caution when comparisons are made between individual patient muscle biopsies and controls, as erroneous conclusions could easily be reached, especially if only limited numbers are analysed. For this reason, we combined Type I and II fibres from our control data set, and used this normative range to interpret the results obtained from *OPA1*-positive muscle biopsies included in this study.

The majority of COX-positive muscle fibres from *OPA1*-positive patients had sub-threshold deletion levels <30% (179/188, 95.2%), i.e. within the detection limit of our quantitative real-time PCR assay (23,35,36). The mtDNA deletion level required to precipitate an overt biochemical defect at the cellular level is typically ≥70% in skeletal muscle (23,35,36), and using this threshold value, the histochemical status for over three-quarters of COX-negative muscle fibres could be accounted for (113/145, 77.9%). By applying a two-step long-range PCR strategy, clonal expansion of a single deleted mtDNA species was demonstrated for 29 of 31 (93.5%) COX-negative fibres, with the remaining fibres each harbouring two different deleted mtDNA species. Although long-range PCR is not quantitative, these results suggest that more than one deleted mtDNA species can propagate and reach high levels within a cell independently of each other. We recently reported the same observation in single substantia nigra neurones from three different groups: controls, patients with sporadic Parkinson's disease, and a patient with a heterozygous *POLG1* mutation leading to parkinsonism in association with PEO and multiple mtDNA deletions (37). It is also noteworthy that 6 of 31 (19.4%) COX-negative muscle fibres had mtDNA deletions levels <30% with our real-time PCR assay, which was designed primarily to detect deletions encompassing *MTND4* but not *MTND1* (23,38). It is therefore likely that

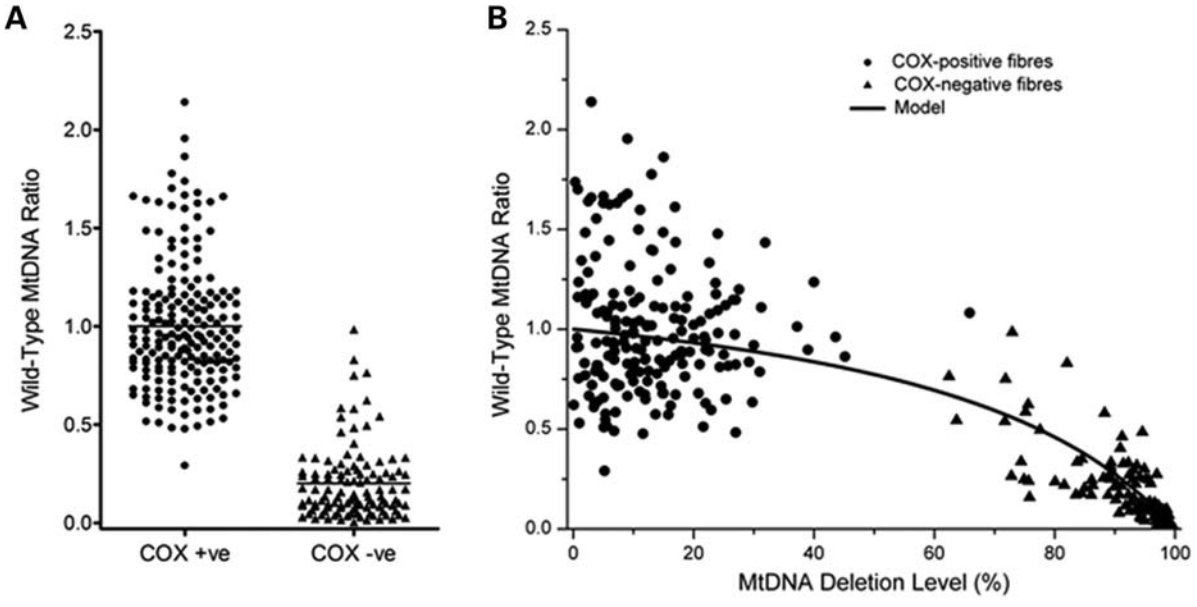

Figure 6. (**A**) Wild-type mtDNA ratio in single muscle fibres from *OPA1*-positive patients analysed according to COX status ($P < 0.0001$), (**B**) Variation in wild-type mtDNA ratio for COX-negative muscle fibres according to mtDNA deletion level. The simulated curve describes the relationship predicted by our *in silico* model, which is based upon the maintenance of wild-type mtDNA genomes ($R^2 = 0.68$). Circles indicate COX-positive fibres and triangles COX-negative fibres.

most of the COX-negative fibres with low deletion levels (32/145, 22.1%) in our study actually harboured smaller deletions, which spared both *MTND1* and *MTND4*, and therefore remained undetected. In support of this argument, Bua *et al*. (39) sequenced the breakpoints for 48 mtDNA deletions identified in aged normal skeletal muscle, and of these, 8 of 48 (16.7%) did not include *MTND1* and *MTND4*. We have not excluded the possibility that *OPA1* mutations could trigger COX deficiency via the accumulation of high levels of somatic mtDNA point mutations, but the evidence for this is weak, especially in post-mitotic tissues (40,41). Furthermore, previous studies of other mitochondrial maintenance disorders due to *POLG1* and *PEO1* mutations have only identified an increased burden of somatic mtDNA point mutations in the non-coding D-loop region (42–44). The significance of these mtDNA variants remains unclear but they would not be predicted to directly cause COX deficiency.

In summary, our study has provided some important insights into the consequences of *OPA1* mutations at the cellular level and has revealed possible important disease mechanisms. The accumulation of somatic, clonally expanded mtDNA deletions is a key pathological player, and the resulting mtDNA proliferation is likely to be an important mediator of apoptotic cell loss and disease severity. However, several intriguing features of *OPA1* disease remain to be clarified – its wide phenotypic spectrum, the marked variability seen within families segregating the same pathological variant, and the greater susceptibility of retinal ganglion cells. Dissecting the complex pathophysiological pathways involved will represent a major challenge, and future experimental paradigms will require the development of more sophisticated functional systems, such as animal models replicating the features seen in patients with DOA^+ phenotypes.

MATERIALS AND METHODS

Patients and controls

Quadriceps or tibialis anterior muscle biopsies from 15 *OPA1*-positive patients (mean age = 49.5 years, SD = 9.8 years, range = 31.0–64.0 years) (Table 1), and five normal controls with no evidence of ocular or neuromuscular pathologies (mean age = 28.2 years, SD = 18.7 years, range = 1.0–52.0 years) (Fig. 1) were included in this study. Among the DOA group, seven patients had isolated optic nerve involvement whereas eight patients manifested additional neuromuscular features. The clinical descriptions of these patients have been detailed previously (5), and muscle biopsies were obtained at the time of their initial diagnostic investigations. This study had the relevant institutional approval and complied with the Declaration of Helsinki.

Mitochondrial histochemistry

Skeletal muscle samples were snap frozen in melting liquid isopentane (−150°C) within 6 h of the biopsy being taken and then stored at −80°C. The specimens were mounted on OCT (VWR BDH Prolabo, UK) before being sectioned at 20 μm thickness onto glass and membrane slides using a Microm™ HM560 cryostat (Thermo Fisher, Germany). The serial muscle sections were then stained for COX, succinate dehydrogenase (SDH), and sequential COX-SDH activities, using standard histochemical protocols (45).

Single-muscle fibre analysis

Individual skeletal muscle fibres were cut using an LMD 6000™ laser dissecting microscope (Leica Microsystems, Germany) and collected into a 0.5 ml microcentrifuge cap

(Eppendorf, UK). Cross-sectional fibre area (μm^2) was recorded from the LMD 6000^{TM} operating software (Leica Microsystems) prior to laser microdissection. The fibres were incubated overnight in a 30 μl lysis solution containing proteinase K at 55°C for 16 h, followed by heat inactivation at 95°C for 10 min (23). The molecular investigations described below were then performed on the single-fibre lysate on the following day.

Quantitative real-time PCR

Our quantitative real-time PCR assay for single muscle fibres was originally designed based upon the fact that the *MTND1* gene is only rarely involved in large-scale rearrangements, whereas the *MTND4* gene is removed in the majority of reported mtDNA deletions (38,46). Absolute quantification of mtDNA content was performed on the MyiQ^{TM} real-time PCR detection system (Biorad, USA), with iQ SYBR Green and primers pairs designed to amplify short fragments spanning *MTND1* and *MTND4* (23). The primer sequences for the various real-time PCR templates used have been provided in the online Supplementary Material (Table S2). The total number of mtDNA molecules (total copy number) present in muscle fibre sections was determined from the *MTND1* Ct values, and the number of wild-type mtDNA molecules (wild-type copy number) from the *MTND4* Ct values, using the linear regression equations generated by serial dilutions of the relevant standards. Both assays were optimized and confirmed to be linear over an appropriate concentration range by the standard curve method, and all single-fibre lysates were measured in triplicates. The mtDNA deletion level was calculated with the $2^{-\Delta Ct}$ method from the obtained *MTND1*–*MTND4* ΔCt value.

Long-range PCR

Multiple mtDNA deletions in homogenate skeletal muscle DNA was investigated with either southern blot and/or long-range PCR (6,7). The detection of deleted mtDNA species in single skeletal muscle fibres was achieved using a previously optimized two-step long-range PCR strategy (37). Two rounds of PCR were required to achieve adequate amplification from the single-fibre lysate, and the primer pairs were specifically designed to allow the identification of large-scale rearrangements in the mutational hotspots along the major arc of the mitochondrial genome (Supplementary Material, Table S3). The Expand Long Template PCR System^{TM} (Roche, UK) was used with the following cycling procedures for both the first and second rounds of PCR: 3 min at 93°C; 10 cycles of 93°C for 30 s, 58°C for 30 s, 68°C for 12 min; 20 cycles of 93°C for 30 s, 58°C for 30 s, 68°C for 12 min + 5 s per additional cycle; and a final extension step of 11 min at 68°C. The PCR products were electrophoresed in a 0.7% agarose gel containing ethidium bromide at 40 V for 3 h, before being visualized under ultra-violet light.

Wild-type mtDNA ratio

For each patient, the mean wild-type mtDNA copy number density for COX-positive muscle fibres was determined by averaging the values obtained for all Type I and II fibres separately. To remove the variation among individuals, the wild-type mtDNA ratios for COX-positive and COX-negative fibres were normalized to each patient's mean wild-type mtDNA copy number density. The wild-type mtDNA ratio for each fibre was calculated by dividing the copy number density for that fibre with the patient's mean value for COX-positive fibres, either Type I or II.

In silico modelling

Our mathematical simulation of mtDNA replication is based upon recessive loss-of-function mutations, with the total amount of wild-type mtDNA being the primary determinant of mitochondrial function (21,22). Our modelling equation predicts that the wild-type mtDNA copy number (w) is a function of the mutation level (m) within a cell, and the mtDNA proliferation parameter (α):

$$w = \frac{1 - m}{1 - (\alpha - 1/\alpha)m}$$

The proliferation parameter (α) was determined from the wild-type and mutant copy number data by a non-linear least squares fitting routine using the Levenberg–Marquardt algorithm in Origin 7^{TM} (Northampton, MA). The proliferation parameter (α) represents the maximum proliferation that should be observed when the mutation level approaches 100%. The actual proliferation level observed will be smaller than the predicted α value.

Statistical analysis

Groups were compared using an independent sample *t*-test with GraphPad^{TM} v.4 statistical software (San Diego, CA).

SUPPLEMENTARY MATERIAL

Supplementary Material is available at *HMG* online.

ACKNOWLEDGEMENTS

We are grateful to the NHS National Commissioning Group service for "Rare Mitochondrial Disease of Adults and Children" who performed some of the diagnostic evaluations prior to this study, and particularly to Professor Rob Taylor who facilitated access to some of the research samples.

Conflicts of Interest statement. None declared.

FUNDING

This work was supported by a Medical Research Council (MRC, UK) Clinical Research Fellowship to P.Y.W.M. (G0701386). P.F.C. is a Wellcome Trust Senior Fellow in Clinical Science, and also receives funding from the Parkinson's Disease Society (UK), the Medical Research Council Translational Muscle Centre and the UK NIHR Biomedical Research Centre in Ageing and Age related disease. D.C.S.

is supported by an NIH/NIGMS grant R01GM073744. L.A.B. receives funding from Helse Vest (RHF) and the Norwegian Research Council. R.H. is supported by the Academy of Medical Sciences and the Deutsche Forschungsgemeinschaft (HO 2505/2-1). Funding to pay the Open Access Charge was provided by the Wellcome Trust.

REFERENCES

1. Yu-Wai-Man, P., Griffiths, P.G., Burke, A., Sellar, P.W., Clarke, M.P., Gnanaraj, L., Ah-Kine, D., Hudson, G., Czermin, B., Taylor, R.W. *et al.* (2010) The prevalence and natural history of dominant optic atrophy due to *OPA1* mutations. *Ophthalmology* April 22, 2010. [Epub ahead of print].
2. Newman, N.J. and Biousse, V. (2004) Hereditary optic neuropathies. *Eye*, **18**, 1144–1160.
3. Amati-Bonneau, P., Milea, D., Bonneau, D., Chevrollier, A., Ferre, M., Guillet, V., Gueguen, N., Loiseau, D., de Crescenzo, M.A.P., Verny, C. *et al.* (2009) OPA1-associated disorders: phenotypes and pathophysiology. *Int. J. Biochem. Cell Biol.*, **41**, 1855–1865.
4. Yu-Wai-Man, P., Griffiths, P.G., Hudson, G. and Chinnery, P.F. (2009) Inherited mitochondrial optic neuropathies. *J. Med. Genet.*, **46**, 145–158.
5. Yu-Wai-Man, P., Griffiths, P.G., Gorman, G.S., Lourenco, C.M., Wright, A.F., Auer-Grumbach, M., Toscano, A., Musumeci, O., Valentino, M.L., Caporali, L. *et al.* (2010) Multi-system neurological disease is common in patients with *OPA1* mutations. *Brain*, **133**, 771–786.
6. Amati-Bonneau, P., Valentino, M.L., Reynier, P., Gallardo, M.E., Bornstein, B., Boissiere, A., Campos, Y., Rivera, H., de la Aleja, J.G., Carroccia, R. *et al.* (2008) OPA1 mutations induce mitochondrial DNA instability and optic atrophy plus phenotypes. *Brain*, **131**, 338–351.
7. Hudson, G., Amati-Bonneau, P., Blakely, E.L., Stewart, J.D., He, L.P., Schaefer, A.M., Griffiths, P.G., Ahlqvist, K., Suomalainen, A., Reynier, P. *et al.* (2008) Mutation of OPA1 causes dominant optic atrophy with external ophthalmoplegia, ataxia, deafness and multiple mitochondrial DNA deletions: a novel disorder of mtDNA maintenance. *Brain*, **131**, 329–337.
8. Ferraris, S., Clark, S., Garelli, E., Davidzon, G., Moore, S.A., Kardon, R.H., Bienstock, R.J., Longley, M.J., Mancuso, M., Rios, P.G. *et al.* (2008) Progressive external ophthalmoplegia and vision and hearing loss in a patient with mutations in POLG2 and OPA1. *Arch. Neurol.*, **65**, 125–131.
9. Spinazzi, M., Cazzola, S., Bortolozzi, M., Baracca, A., Loro, E., Casarin, A., Solaini, G., Sgarbi, G., Casalena, G., Cenacchi, G. *et al.* (2008) A novel deletion in the GTPase domain of OPA1 causes defects in mitochondrial morphology and distribution, but not in function. *Hum. Mol. Genet.*, **17**, 3291–3302.
10. Davies, V. and Votruba, M. (2006) Focus on molecules: the OPA1 protein. *Exp. Eye Res.*, **83**, 1003–1004.
11. Lenaers, G., Reynier, P., ElAchouri, G., Soukkarieh, C., Olichon, A., Belenguer, P., Baricault, L., Ducommun, B., Hamel, C. and Delettre, C. (2009) OPA1 functions in mitochondria and dysfunctions in optic nerve. *Int. J. Biochem. Cell Biol.*, **41**, 1866–1874.
12. Martinelli, P. and Rugarli, E.L. (2010) Emerging roles of mitochondrial proteases in neurodegeneration. *Biochim. Biophys. Acta*, **1797**, 1–10.
13. Frezza, C., Cipolat, S., de Brito, O.M., Micaroni, M., Beznoussenko, G.V., Rudka, T., Bartoli, D., Polishuck, R.S., Danial, N.N., De Strooper, B. *et al.* (2006) OPA1 controls apoptotic cristae remodeling independently from mitochondrial fusion. *Cell*, **126**, 177–189.
14. Olichon, A., Landes, T., Arnaune-Pelloquin, L., Emorine, L.J., Mils, V., Guichet, A., Delettre, C., Hamel, C., Amati-Bonneau, P., Bonneau, D. *et al.* (2007) Effects of OPA1 mutations on mitochondrial morphology and apoptosis: relevance to ADOA pathogenesis. *J. Cell Physiol.*, **211**, 423–430.
15. Chevrollier, A., Guillet, V., Loiseau, D., Gueguen, N., de Crescenzo, M.A., Verny, C., Ferre, M., Dollfus, H., Odent, S., Milea, D. *et al.* (2008) Hereditary optic neuropathies share a common mitochondrial coupling defect. *Ann. Neurol.*, **63**, 794–798.
16. Zanna, C., Ghelli, A., Porcelli, A.M., Karbowski, M., Youle, R.J., Schimpf, S., Wissinger, B., Pinti, M., Cossarizza, A., Vidoni, S. *et al.* (2008) OPA1 mutations associated with dominant optic atrophy impair oxidative phosphorylation and mitochondrial fusion. *Brain*, **131**, 352–367.
17. Zeviani, M. (2008) OPA1 mutations and mitochondrial DNA damage: keeping the magic circle in shape. *Brain*, **131**, 314–317.
18. Amati-Bonneau, P., Guichet, A., Olichon, A., Chevrollier, A., Viala, F., Miot, S., Ayuso, C., Odent, S., Arrouet, C., Verny, C. *et al.* (2005) OPA1 R445H mutation in optic atrophy associated with sensorineural deafness. *Ann. Neurol.*, **58**, 958–963.
19. Mirabella, M., Di Giovanni, S., Silvestri, G., Tonali, P. and Servidei, S. (2000) Apoptosis in mitochondrial encephalomyopathies with mitochondrial DNA mutations: a potential pathogenic mechanism. *Brain*, **123**, 93–104.
20. Aure, K., Fayet, G., Lacene, E., Romero, N.B. and Lombes, A. (2006) Apoptosis in mitochondrial myopathies is linked to mitochondrial proliferation. *Brain*, **129**, 1249–1259.
21. Chinnery, P.F. and Samuels, D.C. (1999) Relaxed replication of mtDNA: a model with implications for the expression of disease. *Am. J. Hum. Genet.*, **64**, 1158–1165.
22. Capps, G.J., Samuels, D.C. and Chinnery, P.F. (2003) A model of the nuclear control of mitochondrial DNA replication. *J. Theor. Biol.*, **221**, 565–583.
23. Durham, S.E., Samuels, D.C., Cree, L.M. and Chinnery, P.F. (2007) Normal levels of wild-type mitochondrial DNA maintain cytochrome c oxidase activity for two pathogenic mitochondrial DNA mutations but not for m.3243A -> G. *Am. J. Hum. Genet.*, **81**, 189–195.
24. Holloszy, J.O. (2008) Regulation by exercise of skeletal muscle content of mitochondria and GLUT4. *J. Physiol. Pharmacol.*, **59** (Suppl. 7), 5–18.
25. Ljubicic, V., Joseph, A.M., Saleem, A., Uguccioni, G., Collu-Marchese, M., Lai, R.Y., Nguyen, L.M. and Hood, D.A. (2009) Transcriptional and post-transcriptional regulation of mitochondrial biogenesis in skeletal muscle: effects of exercise and aging. *Biochim. Biophys. Acta*, **1800**, 223–234.
26. Bengtsson, J., Gustafsson, T., Widegren, U., Jansson, E. and Sundberg, C.J. (2001) Mitochondrial transcription factor A and respiratory complex IV increase in response to exercise training in humans. *Pflugers Arch.*, **443**, 61–66.
27. Taivassalo, T., Shoubridge, E.A., Chen, J., Kennaway, N.G., DiMauro, S., Arnold, D.L. and Haller, R.G. (2001) Aerobic conditioning in patients with mitochondrial myopathies: physiological, biochemical, and genetic effects. *Ann. Neurol.*, **50**, 133–141.
28. Murphy, J.L., Blakely, E.L., Schaefer, A.M., He, L., Wyrick, P., Haller, R.G., Taylor, R.W., Turnbull, D.M. and Taivassalo, T. (2008) Resistance training in patients with single, large-scale deletions of mitochondrial DNA. *Brain*, **131**, 2832–2840.
29. Menshikova, E.V., Ritov, V.B., Fairfull, L., Ferrell, R.E., Kelley, D.E. and Goodpaster, B.H. (2006) Effects of exercise on mitochondrial content and function in aging human skeletal muscle. *J. Gerontol. Series A Biol. Sci. Med. Sci.*, **61**, 534–540.
30. Adhihetty, P.J., Taivassalo, T., Haller, R.G., Walkinshaw, D.R. and Hood, D.A. (2007) The effect of training on the expression of mitochondrial biogenesis- and apoptosis-related proteins in skeletal muscle of patients with mtDNA defects. *Am. J. Physiol. Endocrinol. Metab.*, **293**, E672–E680.
31. Gordon, J.W., Rungi, A.A., Inagaki, H. and Hood, D.A. (2001) Effects of contractile activity on mitochondrial transcription factor A expression in skeletal muscle. *J. Appl. Physiol.*, **90**, 389–396.
32. Norrbom, J., Wallman, S.E., Gustafsson, T., Rundqvist, H., Jansson, E. and Sundberg, C.J. (2010) Training response of mitochondrial transcription factors in human skeletal muscle. *Acta Physiol.*, **198**, 71–79.
33. Larsson, N.G., Wang, J.M., Wilhelmsson, H., Oldfors, A., Rustin, P., Lewandoski, M., Barsh, G.S. and Clayton, D.A. (1998) Mitochondrial transcription factor A is necessary for mtDNA maintenance and embryogenesis in mice. *Nature Genet.*, **18**, 231–236.
34. Ekstrand, M.I., Falkenberg, M., Rantanen, A., Park, C.B., Gaspari, M., Hultenby, K., Rustin, P., Gustafsson, C.M. and Larsson, N.G. (2004) Mitochondrial transcription factor A regulates mtDNA copy number in mammals. *Hum. Mol. Genet.*, **13**, 935–944.
35. Shoubridge, E.A., Karpati, G. and Hastings, K.E.M. (1990) Deletion mutants are functionally dominant over wild-type mitochondrial genomes in skeletal-muscle fiber segments in mitochondrial disease. *Cell*, **62**, 43–49.
36. Bua, E.A., McKiernan, S.H., Wanagat, J., McKenzie, D. and Aiken, J.M. (2002) Mitochondrial abnormalities are more frequent in muscles undergoing sarcopenia. *J. Appl. Physiol.*, **92**, 2617–2624.

37. Reeve, A.K., Krishnan, K.J., Elson, J.L., Morris, C.M., Bender, A., Lightowlers, R.N. and Turnbull, D.M. (2008) Nature of mitochondrial DNA deletions in substantial nigra neurons. *Am. J. Hum. Genet.*, **82**, 228–235.
38. He, L.P., Chinnery, P.F., Durham, S.E., Blakely, E.L., Wardell, T.M., Borthwick, G.M., Taylor, R.W. and Turnbull, D.M. (2002) Detection and quantification of mitochondrial DNA deletions in individual cells by real-time PCR. *Nucleic Acids Res.*, **30**.
39. Bua, E., Johnson, J., Herbst, A., Delong, B., McKenzie, D., Salamat, S. and Aiken, J.M. (2006) Mitochondrial DNA-deletion mutations accumulate intracellularly to detrimental levels in aged human skeletal muscle fibers. *Am. J. Hum. Genet.*, **79**, 469–480.
40. Reeve, A.K., Krishnan, K.J. and Turnbull, D. (2008) Mitochondrial DNA mutations in disease, aging, and neurodegeneration. *Ann. N. Y. Acad. Sci.*, **1147**, 21–29.
41. Reeve, A.K., Krishnan, K.J., Taylor, G., Elson, J.L., Bender, A., Taylor, R.W., Morris, C.M. and Turnbull, D.M. (2009) The low abundance of clonally expanded mitochondrial DNA point mutations in aged substantia nigra neurons. *Aging Cell*, **8**, 496–498.
42. Del Bo, R., Bordoni, A., Sciacco, M., Di Fonzo, A., Galbiati, S., Crimi, M., Bresolin, N. and Comi, G.P. (2003) Remarkable infidelity of polymerase gamma A associated with mutations in POLG1 exonuclease domain. *Neurology*, **61**, 903–908.
43. Wanrooij, S., Luoma, P., van Goethem, G., van Broeckhoven, C., Suomalainen, A. and Spelbrink, J.N. (2004) Twinkle and POLG defects enhance age-dependent accumulation of mutations in the control region of mtDNA. *Nucleic Acids Res.*, **32**, 3053–3064.
44. Chinnery, P.F. and Zeviani, M. (2008) 155th ENMC workshop: polymerase gamma and disorders of mitochondrial DNA synthesis, 21–23 September 2007, Naarden, The Netherlands. *Neuromuscul. Disord.*, **18**, 259–267.
45. Johnson, M.A. and Barron, M.J. (1996) Muscle biopsy analysis. In Lane, R.J.M. (ed.), *Handbook of Muscle Disease*, 1st edn. Marcel Dekker, New York, USA, pp. 61–79.
46. Brandon, M.C., Lott, M.T., Nguyen, K.C., Spolim, S., Navathe, S.B., Baldi, P. and Wallace, D.C. (2005) MITOMAP: a human mitochondrial genome database. *Nucleic Acids Res.*, **33**, D611–D613.

Biochimica et Biophysica Acta 1812 (2011) 321–325

Contents lists available at ScienceDirect

Biochimica et Biophysica Acta

journal homepage: www.elsevier.com/locate/bbadis

POLG mutations cause decreased mitochondrial DNA repopulation rates following induced depletion in human fibroblasts

Joanna D. Stewart [a,1], Susanne Schoeler [b,1], Kamil S. Sitarz [a], Rita Horvath [a], Kerstin Hallmann [b], Angela Pyle [a], Patrick Yu-Wai-Man [a], Robert W. Taylor [a], David C. Samuels [c], Wolfram S. Kunz [b], Patrick F. Chinnery [a,*]

[a] Mitochondrial Research Group, Institute of Human Genetics, Newcastle University, Central Parkway, Newcastle upon Tyne, NE1 3BZ, UK
[b] Departments of Epileptology and Life & Brain Center, University Bonn, Sigmund-Freud-Str. 25, D-53105 Bonn, Germany
[c] Center for Human Genetics Research, Vanderbilt University, Nashville, TN, 37232, USA

ARTICLE INFO

Article history:
Received 13 June 2010
Received in revised form 9 November 2010
Accepted 29 November 2010
Available online 5 December 2010

Keywords:
Mitochondria
Mitochondrial DNA
Depletion
Ethidium bromide

ABSTRACT

Disorders of mitochondrial DNA (mtDNA) maintenance have emerged as an important cause of human genetic disease, but demonstrating the functional consequences of *de novo* mutations remains a major challenge. We studied the rate of depletion and repopulation of mtDNA in human fibroblasts exposed to ethidium bromide in patients with heterozygous *POLG* mutations, *POLG2* and *TK2* mutations. Ethidium bromide induced mtDNA depletion occurred at the same rate in human fibroblasts from patients and healthy controls. By contrast, the restoration of mtDNA levels was markedly delayed in fibroblasts from patients with compound heterozygous *POLG* mutations. Specific *POLG2* and *TK2* mutations did not delay mtDNA repopulation rates. These observations are consistent with the hypothesis that mutations in *POLG* impair mtDNA repopulation within intact cells, and provide a potential method of demonstrating the functional consequences of putative pathogenic alleles causing a defect of mtDNA synthesis.

1. Introduction

Mitochondria contain multiple copies of mitochondrial DNA (mtDNA), which codes for 13 essential components of the mitochondrial respiratory chain which are essential for aerobic metabolism in all nucleated mammalian cells. The efficient synthesis of adenosine triphosphate (ATP) is critically dependent on the amount and quality of mtDNA within single cells. Pathogenic mutations of mtDNA can affect the structure of respiratory chain subunits, or affect the intra-mitochondrial protein synthetic machinery. Likewise, a drastic reduction in mtDNA levels also leads to a decrease in intra-mitochondrial protein synthesis, compromising cellular function through a relative deficiency of available ATP. Unlike nuclear DNA, mitochondrial DNA (mtDNA) is continually copied and degraded, independent of the cell cycle (so called "relaxed replication") [1]. This means that any disruption of the mtDNA replication machinery can have almost immediate effects on cellular function.

Nuclear gene mutations causing secondary defects of mitochondrial DNA (mtDNA) are a major cause of human genetic disease [2]. An overlapping spectrum of dominantly-inherited neuromuscular phenotypes have been described in families transmitting mutations in *POLG* and *POLG2* [3,4], *PEO1* [5], *ANT1* [6], and *OPA1* [7]. These genes code for proteins that are intimately involved in mtDNA synthesis (reviewed comprehensively in [8]). *POLG* codes for polγ, the only DNA polymerase within mitochondria. *POLG2* codes for the accessory (or p55) subunit of polγ, which binds to the linker region of the catalytic subunit and promotes processivity during mtDNA synthesis. *PEO1* codes for the mtDNA helicase Twinkle, and *ANT1* codes for the adenine nucleotide translocase, which maintains intra-mitochondrial nucleoside levels. *OPA1* codes for the mitochondrial fusion–fission protein *Opa1*, which also plays a role in apoptosis. Mutations in the genes encoding these proteins lead to secondary mtDNA mutations which accumulate in post-mitotic tissues and cause progressive multisystem neurological disease. The mtDNA mutations affect the synthesis or structure of respiratory chain proteins, leading to a biochemical defect of oxidative phosphorylation and a deficiency of ATP synthesis [9,10]. On the other hand, recessive mutations in *POLG* and *PEO1* also cause a loss of mtDNA (depletion) and a more severe childhood disorder with encephalopathy and liver failure, including the Alpers-Huttenlocher syndrome (AHS) [11,12]. Several other recessive mtDNA depletion syndromes have been described [2], many due to mutations affecting proteins that regulate intra-mitochondrial nucleoside levels, such as *TK2* encoding thymidine kinase 2 [13]. The loss of mtDNA also leads to a decrease in intra-mitochondrial protein synthesis, which compromises oxidative phosphorylation and leads to a decrease in ATP synthesis [14].

POLG remains the major identified cause of autosomal mitochondrial disease, with an exponential growth in the number of new *POLG* substitutions identified in patients with secondary mtDNA defects.

* Corresponding author. Institute of Human Genetics, Central Parkway, Newcastle upon Tyne, NE1 3BZ, UK. Tel.: +44 191 222 3009; fax: +44 191 222 8553.
E-mail address: p.f.chinnery@ncl.ac.uk (P.F. Chinnery).
[1] These authors contributed equally to this work.

0925-4439/$ – see front matter © 2010 Elsevier B.V. All rights reserved.
doi:10.1016/j.bbadis.2010.11.012

Despite its importance, *POLG* is highly polymorphic in the general population, and there have been several cases where putative pathogenic alleles were later described in control subjects. Proving the pathogenic nature of novel *POLG* mutations is a major challenge facing the field. Several groups have established an in vitro method of studying the biochemical consequences of different alleles by isolating recombinant proteins over-expressed in baculovirus-infected cells [2]. Although this has shown that several potentially pathogenic alleles compromise catalytic activity, proof-reading and processivity of the enzyme [2], technical limitations restrict this approach to specific regions of the protein, excluding some known and putative pathogenic alleles from analysis. In addition, the in vitro approaches to measure mtDNA replication are not all applicable when studying the potential effects of additional proteins that affect intra-mitochondrial nucleotide pools, or proteins thought to interact with the mtDNA replisome [15]. An alternative approach involves the measurement of polγ activity in cell extracts [16]. Although this enables the evaluation of the intact enzyme, even with the optimal enrichment through mitochondrial fractionation, there is inevitable contamination with nuclear DNA polymerase and RNase activity, limiting the sensitivity of the assay for mildly deleterious *POLG* mutations. To address these issues we developed a simple kinetic assay for mtDNA replication in intact primary human cells by depleting cell lines of mtDNA by treatment with ethidium bromide (EtBr) and comparing the rate of repopulation in patient cell lines to controls. Ethidium bromide is a known inhibitor of mitochondrial transcription and replication processes but with no effect on nuclear DNA [17,18]. This double stranded DNA intercalating drug has effectively been used to reduce the copy number of mtDNA in proliferating cells [19]. The effect of the drug is reversible; so that once EtBr is removed from the culture media, cells are able to repopulate their mtDNA [20]. This approach has been used to investigate the mechanisms regulating mtDNA copy number within cells [18,21]. It has also been used to show that deleted smaller mtDNA molecules repopulate cells faster than wild-type molecules [22]. Here we applied a similar approach to cell lines with a genetically determined mtDNA replication defect for the first time.

2. Methods

Primary human fibroblasts were cultured from seven patients available to us in our laboratories (P1–P7) and seven healthy control subjects (C1–C7). Patients 1, 4, and 5 (P1, P4, and P5) had AHS caused by compound heterozygous mutations in *POLG* P1:p.W748S and p.G848S; P4: p.W748S and c.3600delT; and P5: p.G737R and p.A767N [23,24] with mtDNA depletion in liver and/or muscle. Patients 2 and 3 (P2, P3) had AHS caused by homozygous mutations in *POLG* P2:p.R1096C; and P3:homozygous p.T251I, p587L. Patient 6 (P6) had a recessive mitochondrial DNA depletion myopathy due to a homozygous deletion of exons 1 and 2 of *TK2*: −270 + 2561del-ins; 7287–7335inv, with mtDNA depletion in the skeletal muscle. Patient 7 (P7) had autosomal dominant chronic progressive external ophthalmoplegia due to a heterozygous *POLG2* substitution (c.1352G>A/p.G451E) with multiple mtDNA deletions in the skeletal muscle [4].

Clinical descriptions of patients 1, 4, 5 and 7 have been published previously [3,15,16], but the clinical features of patients 2, 3, and 6 have not been described before.

Patient 2 was a one-year-old boy of Arabic ethnic origin, having first grade cousins as parents. He suffered from multifocal therapy-refractory epilepsy. At the age of one year and three months MRI showed a global supratentorial reduction of brain volume with a discrete signal-increased hippocampus in the FLAIR sequence, which was interpreted as a probable right-sided hippocampal sclerosis. Skeletal muscle biopsy was taken at the age of one year. In the biopsy COX-negative fibers, reduced mtDNA copy number (863 +/− 101) in contrast to controls (16045 +/− 8817), and multiple deletions were detected. Genetic characterization showed the homozygous R1096C mutation in *POLG1*.

Patient 3 was a 26-year-old woman, whose symptoms first appeared at age 16 as mainly nocturnal nausea followed by loss of consciousness without motor relinquishing (no tongue bite). In ten years eight attacks were reported since the first seizure. These were triggered by stress, but she could prevent the loss of consciousness by learned strategies in two cases. Furthermore obsessive–compulsive disorder was diagnosed at the age of 24 and she was treated in the psychiatry. The electroencephalogram (EEG) at this time showed fronto-temporal-parietal accented deceleration. Clear spike-wave and sharp-wave could not be ascertained. EEG a year before showed repeated high-tension potentials in theta band bifrontally. Genetic characterization showed a pathogenic homozygous T251I/P587L mutation combination in *POLG1*.

Patient 6 was a 2-month-old boy. His Turkish parents are second grade consanguineous, without any known familiar disorders. The baby was prematurely delivered at the 36 + 2 week of pregnancy. Fetal hypokinesia with dysmorphic signs at a normal fetal karyotype (46XY) were noted. Further features included: lissencephaly/pachygyria, microecephaly, bilateral optic atrophy, severe peripartal asphyxia, respiratory insufficiency, arterial hypotonia, low T3/T4 syndrome, anemia, electrolytic dysfunction, thrombosis, capillary-leak syndrome, bilateral chylothorax, and occipital skin necrosis. EEG at the second day of life was extremely low-strained, no epileptic activity was detected. Skeletal muscle biopsy by the age of one month revealed fiber atrophy, fiber destruction and almost complete COX-deficiency. MtDNA copy number in skeletal muscle was reduced to 92 +/− 6 (controls: 16045 +/− 8817). Genetic characterization showed a homozygous mutation in TK2 (−270 + 2561del-ins; 7287–7335inv). At the age of 56 days the baby died from multi-organ dysfunction.

Cells were grown in MEM Earles media (GIBCO) supplemented with 10% fetal bovine serum, 0.1 mg/ml sodium pyruvate, 2 mM L-glutamine and 0.05 mg/ml uridine. All cells were grown in a humidified atmosphere with 5% CO_2 at 37 °C. MtDNA depletion was induced by the addition of 50 ng/ml ethidium bromide (EtBr) to the culture medium for either 7 days (experiment 1) or 16 days (experiment 2) before a return to normal media. Untreated cell lines were studied in parallel, and all cells were kept between 50 and 80% confluence with excess fresh medium to ensure exponential growth. We did not observe differences in the cell doubling times between the patient and control cell lines during ethidium bromide treatment, nor during the repopulation phase of the experiment. All cell culture studies were done in three independent experiments.

The amount of mtDNA in the patient P4, P5, P7 and control C3–C7 fibroblasts was measured in duplicate by real-time PCR using iQ™ Sybr Green on the BioRad ICycler (BioRad, CA) to a target template spanning from nt3459 to nt3569 of the *MTND1* gene as described [25,26], normalized using a nuclear-encoded template for the beta microglobulin (*B2M*) gene spanning from nucleotide 4146 to nucleotide 4376 (NCBI, AC025270). Relative copy number was calculated from the threshold cycle value, ΔCt value, where the mean amount of mtDNA/cell = $2(2^{-\Delta Ct})$, to account for the two copies of *B2M*. The percentage difference in the mtDNA copy number for the untreated and treated arms of the study were compared on each analysis day.

MtDNA copy numbers in patient P1–P3, P6 and control C1-C2 fibroblasts were determined using the primers MT16520F and MT35R used together with probe MT16557TM to detect mitochondrial DNA [24]. Nuclear DNA content was estimated by amplifying a fragment from the single-copy gene Kir4.1 with primers KIR835F and KIR903R in the presence of probe KIR857TM. The quantitative PCR was performed on the MyiQ Real-Time PCR System (Bio-Rad, Munich, Germany). The exact cycle number values were calculated as $\ln(c)/b$, which corresponds to the inflection point of non-linear fitted

regression of the sigmoidal amplification curves applying the following equation: $y = y_0 + a\ (1 - e^{-bx})^c$ (y_0, background fluorescence intensity; y, measured fluorescence intensity; x, cycle number; and a, b, c, curve parameters to be fitted). Calculations were performed using the SigmaPlot 2001 statistical analysis software. For each value three independent experiments were carried out with different concentrations of template DNA, each experiment in triplicates, and primer efficiencies were calculated.

For patients P4, P5, P7 and control C3–C7 fibroblasts multiple mtDNA deletions were investigated using a long range polymerase chain reaction (PCR) assay which amplifies a ~10 kb fragment across the major arc of mtDNA genome using a pair of primers (L6249 (nucleotides 6249–6265) and H16215 (nucleotides 16225–16196)).

The potential presence of large mitochondrial DNA deletions was investigated for patient P1–P3, P6 and control C1-C2 fibroblasts by amplifying overlapping PCR products of 9.5–12.7 kb size using a JumpStart AccuTaq DNA polymerase (Sigma-Aldrich, Steinheim, Germany) and the following primer pairs: MT2623F with MT14695R, MT3922F with MT45R, MT16520F with MT10673R, MT5462F with MT16084R, and MT7027F with MT45R. The mtDNA deletion was quantified by a modified version of the single-molecule PCR method [27]. Primers MT3922F and MT45R were used in 42 cycles of the previously described long PCR program to amplify a 12.7-kb-long part of the mitochondrial genome. DNA samples were diluted to a degree such that after amplification, in addition to the long wild-type product, only 1 or 2 deletion specific (i.e. shorter) or no products were detectable in each lane. We assume that under these circumstances, each deletion-specific band is derived from a single deleted mtDNA molecule. Deletion-specific bands were then counted in all lanes, and this number was compared with total mtDNA copy numbers determined in a similar manner but using a higher dilution of the DNA sample (i.e. on average, less than 1 copy of mtDNA per reaction). In the latter reaction, a primer pair (primers MT16520F and MT1144R) was used that spanned the D-loop region and part of the small arc that are very rarely deleted. This gave an amplification product from all types of mtDNA molecules irrespective of whether they were deleted.

3. Results

The absolute amount of mtDNA in the untreated fibroblasts from four of the *POLG* patients was significantly less than in the controls (P1, $P = 1.75 \times 10^{-9}$; P2, $P = 2.27 \times 10^{-8}$; P3, $P = 5.83 \times 10^{-6}$; and P5, $P = 0.028$), but no different to controls for one *POLG* patient (P4), and no different to controls for the *POLG2* and *TK2* patients. There was no significant change in the level of mtDNA in untreated fibroblasts from patients and controls (C1–C7 and P1–P7) when these were cultured through multiple passages in parallel with the treated cells (Supplementary Table 1). Treatment with EtBr caused significant depletion of mtDNA in control and patient cell lines. Both control and patient fibroblasts developed mtDNA depletion at the same rate, falling to <15% of the untreated steady state within 10 days exposure. After removal of the EtBr on day 7, the mtDNA copy number increased to pre-treatment levels, reaching normal levels within 10 days in control cell lines and in the cell line of the *TK2* patient (Fig.1A, B and C and Supplementary Table 2a). The mtDNA content for the *POLG* fibroblasts was significantly less than the controls at all time points in patients P2 and P3, but patient P1 returned to normal levels 12 days after withdrawal of EtBr (Fig. 1B). By contrast, the fibroblasts from the patient with a homozygous deletion of two *TK2* exons (P6) showed repopulation profiles faster than that observed in the controls (Fig. 1C). We therefore carried out further experiments with a longer period of exposure to EtBr in order to demonstrate more dramatic effects in fibroblasts with *POLG* mutations.

The remaining patient (P4, P5, and P7) and control cell lines (C3–C7) were treated with EtBr for 16 days (Fig. 2). As before, both patient and control cell lines developed the mtDNA depletion at the same rate (Fig. 2A, B and C and Supplementary Table 2b). The control cell lines exposed to EtBr for 16 days showed a similar rate of repopulation to control cell lines exposed to EtBr for 7 days (Figs. 1A and 2A). By contrast, the three patient fibroblast cell lines showed different rates of repopulation with mtDNA. MtDNA levels in fibroblasts from the two *POLG* patients (P4 and P5) never reached pre-treatment levels 29 days after removal of EtBr (P4 = 28.1% ± 19.4, $P = 0.034$ compared to the controls, P5 = 7.87% ± 7.13, $P = 0.003$ compared to the controls; Fig. 2B). By contrast, fibroblasts from the patient with a heterozygous *POLG2* substitution (P7) showed repopulation profiles similar to that observed in the controls at all time points (Fig. 2C). To confirm our findings, we repeated the entire experiment for one cell line (P4) and obtained identical results (Fig. 2D).

No rearrangements of mtDNA were detected in the treated or untreated cell fibroblasts from the controls and from P2-P7. In the

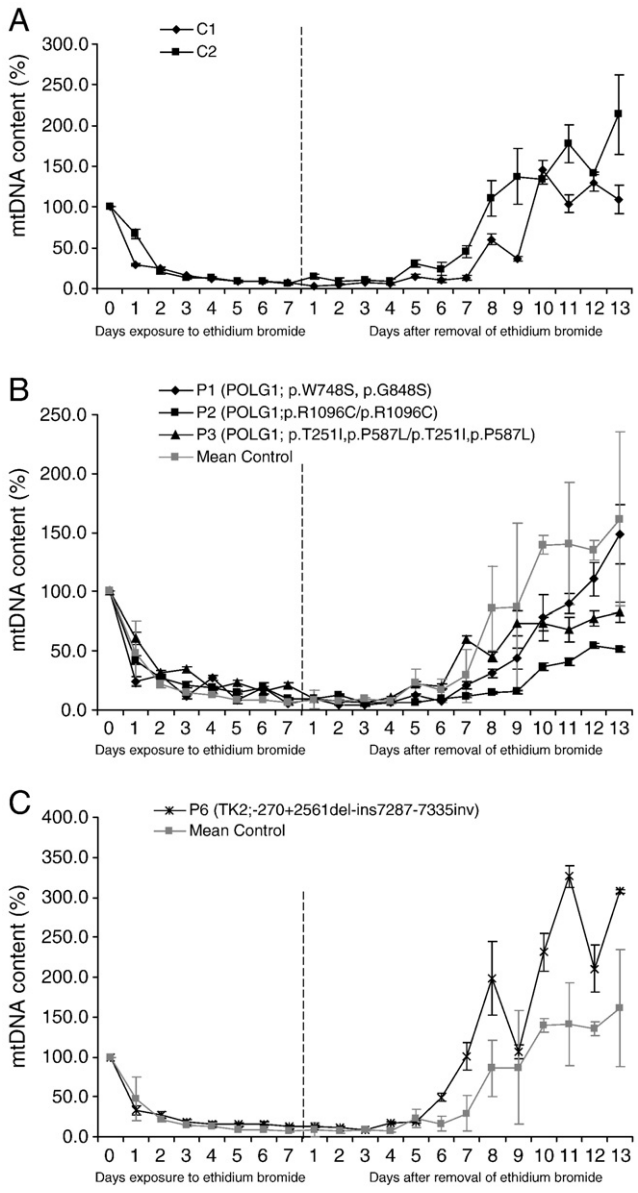

Fig. 1. MtDNA depletion and repopulation in control human fibroblasts and fibroblasts from three *POLG* patients and a *TK2* patient after 7 days of treatment with 50 ng/ml ethidium bromide. (A) Controls C1 & C2 (B) Patient P1:p.W748S and p.G848S in *POLG*; P2:p.R1096C/p.R1096C in *POLG*; P3:p.T251I, p587L/p.T251I, p587L in *POLG*. (C) Patient 6 (P6): homozygous deletion of exons 1 and 2 of *TK2* −270 + 2561del-ins; 7287–7335inv. Data points show the mean of three independent experiments +/−SD values.

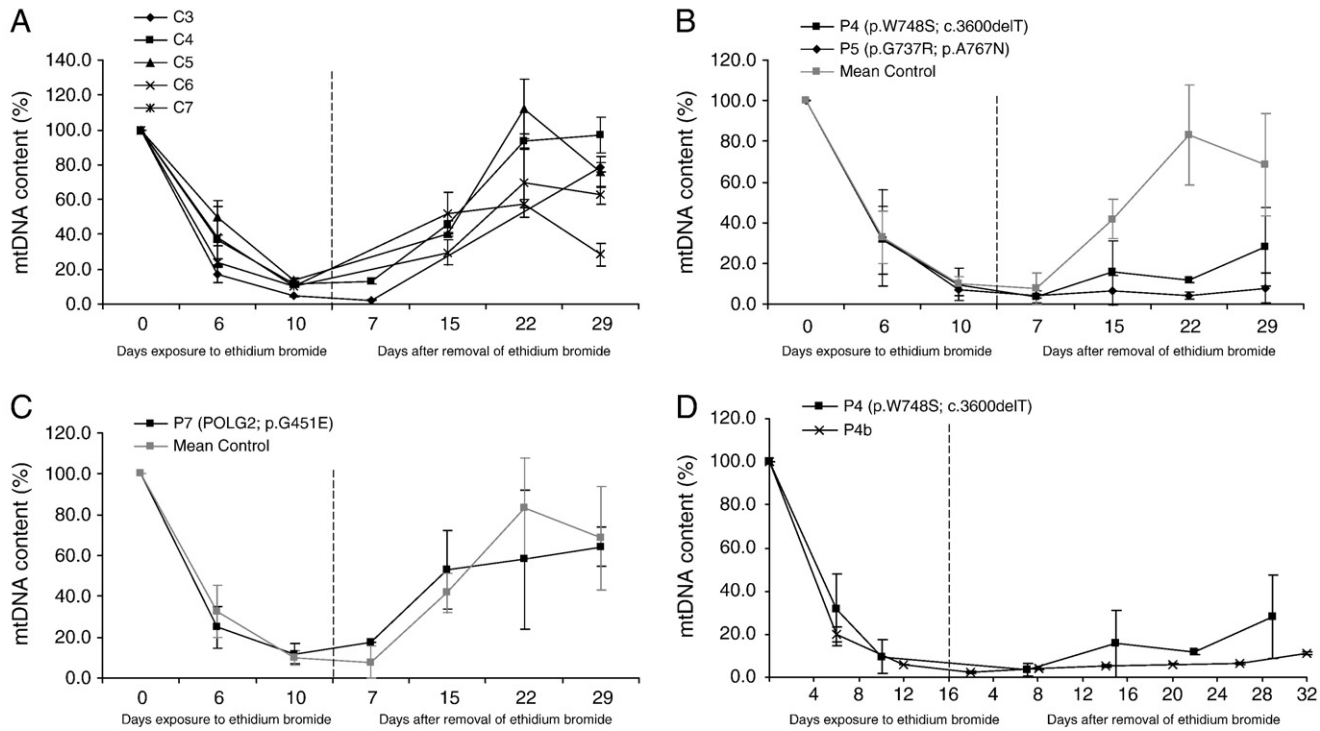

Fig. 2. MtDNA depletion and repopulation in control human fibroblasts and patients with a mtDNA maintenance disorder after 16 days of treatment with 50 ng/ml ethidium bromide. (A) Controls C3–C7. (B) Patients P5: p.G737R and p.A767N in *POLG*; P4: p.w748S and c.3600delT in *POLG*. (C) P7: c.1352 G>A/p.G451E in *POLG2*. (D) Reproducibility data for Patient P4: p.W748S and c.3600delT in *POLG*. Data points show the mean of three independent experiments +/−SD values.

fibroblasts of patient P1, a deletion between nt 2887 and 14567 with an inverted insertion 7395–9299 was detected, both in the untreated and the EtBr treated cells. The proportion of deleted mtDNA did not change during or after treatment with EtBr (Fig. 3). The percentage level of mutated mtDNA before EtBr treatment was 0.37% ± 0.03%. The percentage level of mutated mtDNA immediately after EtBr treatment was 1.44 ± 0.09%. The percentage level of mutated mtDNA after repopulation was 0.20 ± 0.02%.

4. Discussion

Here we show that specific *POLG* mutations can delay the rate of repopulation of mtDNA in human fibroblasts exposed to EtBr. Given that we did not observe any difference between control and patient cell doubling times before or after EtBr treatment, these findings are consistent with the notion that pathogenic *POLG* mutations can directly influence mtDNA maintenance within intact human cells, and are in keeping with in vitro data showing reduced catalytic activity and processivity for several pathogenic *POLG* alleles [2].

Intriguingly, the steady-state level of mtDNA in untreated fibroblasts from one *POLG* patient (P4) was no different to controls.

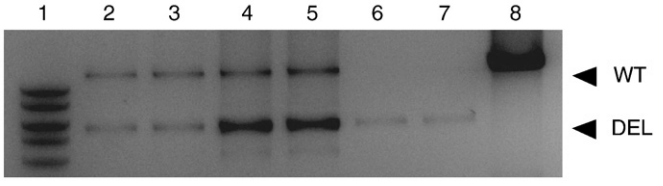

Fig. 3. Percentage level of deleted mtDNA before, during and after EtBr treatment in patient 1. Long range PCR products were separated on an agarose gel. Uppermost bands represent non-deleted mitochondrial genomes (WT); lower bands show the presence of shorter DNA molecules with deletions (DEL). Lanes: 1—marker; 2, 3—after repopulation; 4, 5—before EtBr treatment; 6, 7—after EtBr treatment; and 8—undeleted control.

This has been observed before [28], and suggests that the capacity for adequate mtDNA turnover in quiescent fibroblasts is not compromised by some pathogenic *POLG* alleles. However, in contrast to the previous study, where depletion was only observed in cells harbouring two mutations affecting either the polymerase or exonuclease catalytic domain [28], we also observed depletion in one patient (P5) with two linker-region mutations (p.G737R and p.A767N). This provides further evidence of the crucial role played by the linker region in mtDNA replication, probably through the direct interaction with the p55 accessory subunit which promotes processive polymerase activity [4].

Notably, EtBr caused the loss of mtDNA at remarkably similar rates in patient and control fibroblast cell lines. This suggests that 50 ng/ml EtBr effectively terminates mtDNA synthesis, and the loss of mtDNA during EtBr exposure is likely to be due to the natural destruction of mtDNA as part of the mtDNA turnover during relaxed replication. By inference, in the steady state, this must be matched by equivalent rates of mtDNA synthesis to maintain the constant amount of mtDNA we observed in the untreated cells. Thus, if mtDNA replication is suddenly abolished by EtBr treatment, then the loss of mtDNA will occur through the same endogenous destruction mechanism that occurs in the steady state. In this context, the rate of mtDNA depletion during EtBr exposure will provide one estimate of the steady-state turnover of mtDNA by relaxed replication. The time course we observed is in keeping with previous measurements of mtDNA turnover using a different approach [29,30].

Since the steady state mtDNA content of a cell is determined by the balance between replication and degradation, it would be reasonable to expect a cell to compensate for the mtDNA replication defect by slowing down mtDNA degradation. However, the same rates of ethidium-bromide induced mtDNA depletion that we observed in patient and control cell lines suggest that the presence of *POLG*, *POLG2*, and *TK2* mutations does not lead to a slower degradation of mtDNA in an attempt to compensate for the mtDNA maintenance defect. The cellular mtDNA content therefore is likely to be regulated solely through the mechanism controlling mtDNA replication.

By contrast, after withdrawal of the EtBr, the rates of repopulation of the individual cell lines were less consistent. This may reflect differences in the dynamics of cell proliferation between different sub-clones, cell–cell mosaicism in mtDNA levels previously observed in *POLG* fibroblasts [28], or it may reflect differences in mtDNA replication rates at different stages of the cell cycle [31]. Despite this variation, we observed clear differences between mutated *POLG* fibroblasts, and fibroblasts with the heterozygous *POLG2* and homozygous *TK2* mutations, although this must be interpreted with caution because we only studied one cell line in each case. Given that the same *POLG2* mutation (c.1352G>A/p.G451E) compromised polymerase activity through impaired subunit interaction in the recombinant in vitro system [4], it seems unlikely that the absence of a repopulation defect in fibroblasts reflects the non-pathogenic nature of this allele. It is possible, that the defect caused by a heterozygous *POLG2* mutation is more subtle compared to the compound heterozygous *POLG* cell lines. Alternatively, the normal rates of repopulation could either reflect the relative insensitivity of the assay we present here, or be due to compensatory mechanisms within the intact organelle that are not at play in the in vitro assay, which is based on short strands of mtDNA synthesis using limited components of the replisome under idealized experimental conditions [4]. The absence of an effect of the *TK2* mutations on mtDNA repopulation rates in fibroblasts is in keeping with the well-known tissue-specificity of this particular mtDNA depletion disorder, where the major phenotype is limited to skeletal muscle. Tissue-specific compensatory mechanisms in fibroblasts probably stabilise the mitochondrial dTTP pool, as recently reported in fibroblasts from two patients with different deleterious *TK2* mutations [32]. These mechanisms could account for the rapid repopulation and supra-normal mtDNA levels seen >5 days after the withdrawal of EtBr (Fig. 1C). Further work will clarify the extent and magnitude of these effects for the range of different mutations in different genes known to be involved in mtDNA maintenance, and the sensitivity and specificity of the repopulation assay.

Acknowledgements

PFC is a Wellcome Trust Senior Fellow in Clinical Science who also receives funding from the Medical Research Council (UK), the UK Parkinson's Disease Society, and the UK NIHR Biomedical Research Centre for Ageing and Age-related disease award to the Newcastle upon Tyne Foundation Hospitals NHS Trust. RWT is supported by a Wellcome Trust Programme Grant (074454/Z/04/Z) and the UK National Commissioning Group for Rare Mitochondrial Disorders of Adults and Children. RH is supported by the Deutsche Forschungsgemeinschaft HO 2505/2-1 and the Newcastle upon Tyne Hospitals NHS Charity (RES0211/7262) and the Academy of Medical Sciences (UK, BH090164). WSK was supported by grants of the Deutsche Forschungsgemeinschaft (KU-911/15-1, TR3-A11 and TR3-D12) and the BMBF (01GZ0704 and 01GM0868).

Appendix A. Supplementary data

Supplementary data to this article can be found online at doi:10.1016/j.bbadis.2010.11.012.

References

[1] C.W. Birky, Relaxed and stringent genomes: why cytoplasmic genes don't obey Mendel's laws, J. Hered. 85 (1994) 355–365.
[2] W.C. Copeland, Inherited mitochondrial diseases of DNA replication, Annu. Rev. Med. 59 (2008) 131–146.
[3] G. Van Goethem, B. Dermaut, A. Lofgren, J.-J. Martin, C. Van Broeckhoven, Mutation of *POLG* is associated with progressive external ophthalmoplegia characterized by mtDNA deletions, Nat. Genet. 28 (2001) 211–212.
[4] M.J. Longley, S. Clark, C. Yu Wai Man, G. Hudson, S.E. Durham, R.W. Taylor, S. Nightingale, D.M. Turnbull, W.C. Copeland, P.F. Chinnery, Mutant POLG2 disrupts DNA polymerase gamma subunits and causes progressive external ophthalmoplegia, Am. J. Hum. Genet. 78 (2006) 1026–1034.
[5] J.N. Spelbrink, F.Y. Li, V. Tiranti, K. Nikali, Q.P. Yuan, S. Wanrooij, N. Garrido, G.P. Comi, L. Morandi, L. Santoro, A. Toscano, G.M. Fabrizi, H. Somer, R. Croxen, D. Beeson, J. Poulton, A. Suomalainen, H.T. Jacobs, M. Zeviani, C. Larsson, Human mitochondrial DNA deletions associated with mutations in the gene encoding Twinkle, a phage T7 gene 4-like protein localised in mitochondria, Nat. Genet. 28 (2001) 223–231.
[6] J. Kaukonen, J.K. Juselius, V. Tiranti, A. Kyttala, M. Zeviani, G.P. Comi, S. Keranen, L. Peltonen, A. Suomalainen, Role of adenine nucleotide translocator 1 in mtDNA maintenance, Science 289 (2000) 782–785.
[7] G. Hudson, P. Amati-Bonneau, E.L. Blakely, J.D. Stewart, L. He, A.M. Schaefer, P.G. Griffiths, K. Ahlqvist, A. Suomalainen, P. Reynier, R. McFarland, D.M. Turnbull, P.F. Chinnery, R.W. Taylor, Mutation of OPA1 causes dominant optic atrophy with external ophthalmoplegia, ataxia, deafness and multiple mitochondrial DNA deletions: a novel disorder of mtDNA maintenance, Brain 131 (2007) 329–337.
[8] M.A. Graziewicz, M.J. Longley, W.C. Copeland, DNA polymerase gamma in mitochondrial DNA replication and repair, Chem. Rev. 106 (2006) 383–405.
[9] E.A. Schon, E. Bonilla, S. DiMauro, Mitochondrial DNA mutations and pathogenesis, J. Bioenerg. Biomembr. 29 (1997) 131–149.
[10] R.W. Taylor, D.M. Turnbull, Mitochondrial DNA mutations in human disease, Nat. Rev. Genet. 6 (2005) 389–402.
[11] R.K. Naviaux, K.V. Nguyen, POLG mutations associated with Alpers' syndrome and mitochondrial DNA depletion, Ann. Neurol. 55 (2004) 706–712.
[12] A.H. Hakonen, P. Isohanni, A. Paetau, R. Herva, A. Suomalainen, T. Lonnqvist, Recessive Twinkle mutations in early onset encephalopathy with mtDNA depletion, Brain 130 (2007) 3032–3040.
[13] A. Saada, A. Shaag, H. Mandel, Y. Nevo, S. Eriksson, O. Elpeleg, Mutant mitochondrial thymidine kinase in mitochondrial DNA depletion myopathy, Nat. Genet. 29 (2001) 342–344.
[14] M. Zeviani, S. Di Donato, Mitochondrial disorders, Brain 127 (2004) 2153–2172.
[15] S. Wanrooij, S. Goffart, J.L. Pohjoismaki, T. Yasukawa, J.N. Spelbrink, Expression of catalytic mutants of the mtDNA helicase Twinkle and polymerase POLG causes distinct replication stalling phenotypes, Nucleic Acids Res. 35 (2007) 3238–3251.
[16] J.W. Taanman, S. Rahman, A.T. Pagnamenta, A.A. Morris, M. Bitner-Glindzicz, N.I. Wolf, J.V. Leonard, P.T. Clayton, A.H. Schapira, Analysis of mutant DNA polymerase gamma in patients with mitochondrial DNA depletion, Hum. Mutat. 30 (2009) 248–254.
[17] R.D. Leibowitz, The effect of ethidium bromide on mitochondrial DNA synthesis and mitochondrial DNA structure in HeLa cells, J. Cell Biol. 51 (1971) 116–122.
[18] B.L. Seidel-Rogol, G.S. Shadel, Modulation of mitochondrial transcription in response to mtDNA depletion and repletion in HeLa cells, Nucleic Acids Res. 30 (2002) 1929–1934.
[19] M.P. King, G. Attardi, Isolation of human cell lines lacking mitochondrial DNA, Methods Enzymol. 264 (1996) 304–313.
[20] M.P. King, G. Attardi, Human cells lacking mtDNA: repopulation with exogenous mitochondria by complementation, Science 246 (1989) 500–503.
[21] C.T. Moraes, L. Kenyon, H. Hao, Mechanisms of human mitochondrial DNA maintenance: the determining role of primary sequence and length over function, Mol. Biol. Cell 10 (1999) 3345–3356.
[22] F. Diaz, M.P. Bayona-Bafaluy, M. Rana, M. Mora, H. Hao, C.T. Moraes, Human mitochondrial DNA with large deletions repopulates organelles faster than full-length genomes under relaxed copy number control, Nucleic Acids Res. 30 (2002) 4626–4633.
[23] R. Horvath, G. Hudson, G. Ferrari, N. Fütterer, S. Ahola, E. Lamantea, H. Prokisch, H. Lochmüller, R. McFarland, V. Ramesh, T. Klopstock, P. Freisinger, F. Salvi, J.A. Mayr, R. Santer, M. Tesarova, J. Zeman, B. Udd, R.W. Taylor, D. Turnbull, M. Hanna, D. Fialho, A. Suomalainen, M. Zeviani, P.F. Chinnery, Phenotypic spectrum associated with mutations of the mitochondrial polymerase gamma gene, Brain 129 (2006) 1674–1684.
[24] G. Zsurka, M. Baron, J.D. Stewart, C. Kornblum, M. Bos, R. Sassen, R.W. Taylor, C.E. Elger, P.F. Chinnery, W.S. Kunz, Clonally expanded mitochondrial DNA mutations in epileptic individuals with mutated DNA polymerase gamma, J. Neuropathol. Exp. Neurol. 67 (2008) 857–866.
[25] S.E. Durham, E. Bonilla, D.C. Samuels, S. DiMauro, P.F. Chinnery, Mitochondrial DNA copy number threshold in mtDNA depletion myopathy, Neurology 65 (2005) 453–455.
[26] S.E. Durham, D.T. Brown, D.M. Turnbull, P.F. Chinnery, Progressive depletion of mtDNA in mitochondrial myopathy, Neurology 67 (2006) 502–504.
[27] Y. Kraytsberg, K. Khrapko, Single-molecule PCR: an artifact-free PCR approach for the analysis of somatic mutations, Expert Rev. Mol. Diagn. 5 (2005) 809–815.
[28] N. Ashley, A. O'Rourke, C. Smith, S. Adams, V. Gowda, M. Zeviani, G.K. Brown, C. Fratter, J. Poulton, Depletion of mitochondrial DNA in fibroblast cultures from patients with POLG1 mutations is a consequence of catalytic mutations, Hum. Mol. Genet. 17 (2008) 2496–2506.
[29] N.J. Gross, G.S. Getz, M. Rabinowitz, Apparent turnover of mitochondrial deoxyribonucleic acid and mitochondrial phospholipids in the tissues of the rat, J. Biol. Chem. 244 (1969) 1552–1562.
[30] C.F. Emmerson, G.K. Brown, J. Poulton, Synthesis of mitochondrial DNA in permeabilised human cultured cells, Nucleic Acids Res. 29 (2001) E1.
[31] J.W. Taanman, J.R. Muddle, A.C. Muntau, Mitochondrial DNA depletion can be prevented by dGMP and dAMP supplementation in a resting culture of deoxyguanosine kinase-deficient fibroblasts, Hum. Mol. Genet. 12 (2003) 1839–1845.
[32] M. Frangini, C. Rampazzo, E. Franzolin, M.C. Lara, M.R. Vila, R. Marti, V. Bianchi, Unchanged thymidine triphosphate pools and thymidine metabolism in two lines of thymidine kinase 2-mutated fibroblasts, FEBS J. 276 (2009) 1104–1113.